Topology in Physics

Proseminar
in Theoretical Physics

Institut für theoretische Physik
ETH Hönggerberg
CH-8093 Zürich
Switzerland

July 31, 2006

Contents

1 Lie Algebras: a crash course

Cyril Stark
Supervisor: Urs Wenger

The goal of this paper is to give an introduction to the representation theory of Lie algebras. In the first part, the fundamentals of Lie groups and their Lie algebras are presented in a very compact form. In the second and the third part, the representations of $\mathfrak{su}(2)$ and $\mathfrak{su}(3)$ are discussed and basic terms are introduced. In the forth part follows the generalization of the machinery introduced in the analysis of $\mathfrak{su}(2)$ and $\mathfrak{su}(3)$. The last part is related to the classification of complex simple Lie algebras. Most of the proofs are omitted in the first, the forth and the fifth part.

1 Introduction

Lie algebras are closely connected to *symmetries*. Their use in the description of physical systems allows to apply *algebraical* methods to get further insight. Concrete applications of Lie theory appear in the description of atomic, molecular and nuclear spectra or in gauge theories. Furthermore, Lie algebras are related to several algebraical structures like group algebras, Hopf algebras, quantum groups and vertex operator algebras which are used in mathematical physics. The goal of this paper is to provide an informal introduction to Lie theory. A detailed presentation of the subject is given in [1, 2].

2 Fundamentals

Definition of a Lie Group

Definition (Lie Group). A *Lie group* G is a set G that has two structures that are compatible to each other: the structure of a group and the structure of a C^∞-manifold. 'Compatible' means that the operations 'multiplication' and 'inverse' associated to the group structure of G are differentiable maps (C^∞).

Definition 1. Let G and H be two Lie groups. A *homomorphism between Lie groups* is a group homomorphism which is differentiable. In the remainder of this section we will simply write 'homomorphism' instead of 'homomorphism between Lie groups'.

Definition 2. Let G be a Lie group. A *representation* of G is a homomorphism between Lie groups from G to $GL(V)$.

The matrix group $GL_n(\mathbb{R})$ is a basic example for a Lie group. This group is an open subset of the vector space of all $n \times n$ matrices and therefore a C^∞-manifold. Obviously, the multiplication is differentiable as well as the inverse-operation (compare Cramer's rule).
Whenever no basis is specified, the maps corresponding to the matrices in $GL_n(\mathbb{R})$ must be considered as automorphisms. The set of all automorphisms $V \to V$ is denoted by $GL(V)$.

Definition 3. A *complex Lie group* is a complex manifold endowed with a group structure in such a way that the operations 'product' and 'inverse' associated to the group structure are holomorphic maps.

A complex manifold is a smooth manifold of dimension $2n$ such that the local charts $(U_\eta,\ \phi_\eta)$ have the property that the change-of-coordinate map $\phi_\alpha \circ \phi_\beta$ are holomorphic.

Definition and basic properties of Lie Algebras

The ultimate goal is the study of representations of Lie groups. For that purpose one makes use of the differentiable structure of the Lie group. More precisely, we will try to determine a characterization of $\rho : \ G \to \ H$ being a Lie group homomorphism expressed by maps between tangent spaces of G and H.

The right idea is to look at the automorphisms of G given by *conjugation*:

$$\begin{array}{rcccl} \Psi_g & : & G & \to & G \\ & & \text{h} & \to & \Psi_g(h) := g \cdot h \cdot g^{-1}, \end{array}$$

i.e.,

$$\Psi : \ G \ \to \ GL(G), \tag{1.1}$$

where $GL(G)$ denotes the set of all automorphisms on G. We observe

$$\rho \ group \ homomorphism \ \Rightarrow \ \rho \circ \psi_g = \psi_{\rho(g)} \circ \rho, \tag{1.2}$$

since

$$\rho \circ \psi_g(h) = \rho(g)\rho(h)\rho^{-1}(g) = \psi_{\rho(g)} \circ \rho(h).$$

We are going to differentiate (at the identity) two times, i.e., we use that ρ is differentiable. After the second differentiation we will deduce an identity based on

the assumption that ρ is a group homomorphism that involves only the differential of ρ.
Differentiation at the identity of (1.2) yields

$$d\rho_e \circ d(\psi_g)_e = d(\psi_{\rho(g)})_e \circ d\rho_e.$$

We define a new map to reformulate this result.

Definition 4. The adjoint map Ad is defined as

$$\begin{array}{rccl} Ad & : & G & \to & GL(T_eG) \\ & & \mathrm{g} & \mapsto & Ad(g) := d(\Psi_g)_e : \ T_eG \ \to \ T_eG. \end{array}$$

Thus, the adjoint map Ad realizes a representation of G called the *adjoint representation* of the Lie group G.

Therefore,

$$\rho \textit{ group homomorphism } \Rightarrow \ d\rho_e \circ Ad(g) = Ad(\rho(g)) \circ d\rho_e. \tag{1.3}$$

This identity still explicitly depends on $\rho(g)$. Thus, we differentiate a second time to get

$$d\rho_e \circ d(Ad)_e(X)(Y) = d(Ad)_e(d\rho_e(X), d\rho_e(Y)). \tag{1.4}$$

Definition 5. One defines $ad := d(Ad)_e$. The tangent space at $GL(T_eG)$ can be identified with the entire space $End(T_eG)$. Thus,

$$\begin{array}{rccl} ad & : & T_eG & \to & End(T_eG) \\ & & X & \mapsto & ad(X) := d(Ad)_e(X) : \ T_eG \ \to \ T_eG. \end{array}$$

Therefore, we can consider the map ad to be a bilinear map

$$T_eG \times T_eG \ \to \ T_eG.$$

Notation:

$$[X, Y] := ad(X)(Y).$$

Using this definition in identity (1.4) yields the following important identity (Assumption: ρ is a homomorphism)

$$d\rho_e([X, Y]) = [d\rho_e(X), d\rho_e(Y)]. \tag{1.5}$$

We can even state the following two assertions which are much stronger (without proof):

Theorem 1. *Let G and H be two Lie groups, with G connected. Then: Each homomorphism $\rho : \ G \ \to \ H$ is uniquely determined by its differential $d\rho_e : \ T_eG \ \to \ T_eH$ at the identity.*

Theorem 2. *Let G and H be two Lie groups, with G connected and simply connected. Then: A linear map $L: T_eG \to T_eH$ is the differential of a homomorphism $\rho: G \to H$ iff it preserves the bracket operation, i.e.,*

$$L([X,Y]) = [L(X), L(Y)].$$

Observation 1. *Properties of the bracket operation $[,]$ on T_eG:*

1. Skew-symmetry*, i.e.,*
$$[X,Y] = -[Y,X].$$
2. *Satisfaction of the* Jacobi identity*, i.e.,*
$$[X,[Y,Z]] + [Z,[X,Y]] + [Y,[Z,X]] = 0.$$

A general vector space with such a structure is called a Lie algebra:

Definition (Lie Algebra). A vector space V together with a skew-symmetric bilinear form
$$[\cdot,\cdot]: V \times V \to V$$
which satisfies the Jacobi identity is called a *Lie algebra* (usually denoted $\mathfrak{g}$).

One can also show that the 'contrary' is true as well, i.e., that the tangent space at a Lie group has exactly the structure of a Lie algebra. That's the reason why the tangent space T_eG of a Lie group G is called the *Lie algebra $\mathfrak{g}$ of the Lie group G*.
An even stronger assertion is (without proof)...

Proposition 1. *Every finite-dimensional (abstract) Lie algebra is the Lie algebra of a Lie group.*

A real (complex) Lie algebra is a Lie algebra whose vector space is a real (complex) vector space.

Definition 6. A *homomorphism $L: \mathfrak{g}_1 \to \mathfrak{g}_2$ between Lie Algebras* $\mathfrak{g}_1$ and $\mathfrak{g}_2$ is a linear map of vector spaces which preserves the bracket operation, i.e.,

$$L([X,Y]_{\mathfrak{g}_1}) = [L(X), L(Y)]_{\mathfrak{g}_2}.$$

Definition 7. A *Lie subalgebra* is a linear subspace which is closed under the bracket.

Let us try to explicitly compute the bracket operation for $G = GL_n\mathbb{R}$.

The Lie group $GL_n(\mathbb{R})$ is an open subset of the space $End(\mathbb{R}^n)$. Thus, we can identify $End(\mathbb{R}^n)$ with the tangent space $T_eGL_n(\mathbb{R})$ and the conjugation Ψ_g on $GL_n(\mathbb{R})$ extends naturally to $End(\mathbb{R}^n) = T_eGL_n(\mathbb{R})$, i.e.,

$$Ad(g)(X) \equiv d(\Psi_g)_e(X) = g \cdot X \cdot g^{-1},$$

for all $X \in T_eGL_n(\mathbb{R}) = End(\mathbb{R}^n)$.
Let X and Y be two tangent vectors to $GL_n(\mathbb{R})$ and let $\gamma : I \subset \mathbb{R} \rightarrow GL_n(\mathbb{R})$ be a curve such that $\gamma(0) = e$ and such that $\gamma'(0) = X$. Then

$$\begin{aligned}
[X, Y] &\equiv ad(X)(Y) \\
&= \frac{d}{dt} |_{t=0} \, Ad(\gamma(t))(Y) \\
&= \frac{d}{dt} |_{t=0} \, (\gamma(t) Y \gamma^{-1}(t)) \\
&= \gamma'(0) \cdot Y \cdot \gamma^{-1}(0) + \gamma(0) \cdot Y \cdot (-\gamma(0)) \cdot \gamma'(0) \\
&= X \cdot Y - Y \cdot X. \qquad (1.6)
\end{aligned}$$

Definition (Representation). A representation of a Lie algebra $\mathfrak{g}$ on a vector space V is a homomorphism between Lie algebras

$$\pi : \mathfrak{g} \rightarrow \mathfrak{gl}(V) = End(V),$$

i.e., π is a linear map form the vector space corresponding to $\mathfrak{g}$ to the vector space corresponding to $\mathfrak{gl}(V)$such that

$$\pi([X, Y]_{\mathfrak{g}}) = [\pi(X), \pi(Y)]_{\mathfrak{gl}(V)} = \pi(X) \circ \pi(Y) - \pi(Y) \circ \pi(X),$$

for all $X, \ Y \in \mathfrak{g}$.

The last equation follows from our discussion about $GL_n(\mathbb{R})$ with the only difference that this time $\mathfrak{gl}(V)$ is considered to be the space of automorphisms and not to be a space of matrices (i.e., no basis has been specified).

As corollaries of theorem 1 and theorem 2 we can state the following crucial observation.

Crucial Observation. *The representations of a connected and simply connected Lie group are in one-to-one correspondence to the representations of its Lie algebra.*

Definition 8. Let V be a finite-dimensional real vector space. Then the *complexification* $V_{\mathbb{C}}$ *of the vector space* V is the space of formal combinations

$$v_1 + iv_2,$$

with v_1, $v_2 \in V$. This is a *real* vector space and becomes a *complex* vector space, if we define

$$i(v_1 + iv_2) \equiv iv_1 - v_2.$$

Proposition 2. *Let $\mathfrak{g}$ be a finite-dimensional real Lie algebra and $\mathfrak{g}_{\mathbb{C}}$ its complexification to a complex vector space. Then there exists a* unique *extension of the bracket operation of the Lie algebra $\mathfrak{g}$ to the vector space $\mathfrak{g}_{\mathbb{C}}$ which becomes a Lie algebra.*

Proof. Since the extension of the bracket must still be bilinear, we have that

$$[X_1 + iX_2, Y_1 + iY_2] = ([X_1, Y_1] - [X_2, Y_2]) + i([X_1, Y_2] + [X_2, Y_1]).$$

Therefore the extension is unique. To proof the existence of the extension of the Lie bracket we must check that the new bracket fulfills the demands in the definition of a Lie bracket. The extension is obviously skew symmetric and real bilinear since this is true for the bracket on $\mathfrak{g}$.
To check *complex* bilinearity we only have to check (think of skew-symmetry) that the new bracket is complex-linear in one argument:

$$\begin{aligned}
[i(X_1 + iX_2), Y_1 + iY_2] &= [iX_1 - X_2, Y_1 + iY_2] \\
&= (-[X_1, Y_2] - [X_2, Y_1]) + i([X_1, Y_1] - [X_2, Y_2]) \\
&= i(([X_1, Y_1] - [X_2, Y_2]) + i([X_1, Y_2] + [X_2, Y_1])) \\
&= i[X_1 + iX_2, Y_1 + iY_2].
\end{aligned}$$

What is left to check is the Jacobi identity. We first observe (using bilinearity) that

$$[X, [Y, Z]] + [Z, [X, Y]] + [Y, [Z, X]] = 0,$$

for all $X \in \mathfrak{g}_{\mathbb{C}}$ and $Y, Z \in \mathfrak{g}$. The same argument applies to Y, Z and it follows that the Jacobi identity holds for the extended bracket on $\mathfrak{g}_{\mathbb{C}}$. □

Definition 9. The vector space $\mathfrak{g}_{\mathbb{C}}$ together with the unique extension of the bracket operation of a real Lie algebra $\mathfrak{g}$ is called the *complexification $\mathfrak{g}_{\mathbb{C}}$ of the real Lie algebra $\mathfrak{g}$*.

Proposition 3. *Let $\mathfrak{g}$ be a real Lie algebra and $\mathfrak{g}_{\mathbb{C}}$ its complexification. Then an arbitrary finite-dimensional complex representation $\tilde{\pi}$ of $\mathfrak{g}$ can be extended uniquely to a complex-linear representation of $\mathfrak{g}_{\mathbb{C}}$ given by*

$$\pi(X + iY) = \tilde{\pi}(X) + i\tilde{\pi}(Y)$$

for all $X, Y \in \mathfrak{g}$.
In addition we have that π is irreducible iff $\tilde{\pi}$ is irreducible.

Proof. Existence and uniqueness are trivial.
Let us prove the statement concerning the irreducibility.
"⇒": Let $\tilde{\pi}$ be irreducible and let W be a complex linear subspace invariant under π. This implies that W is invariant under $\tilde{\pi}$. Therefore W is equal to $\{0\}$ or to the whole representation space $\Rightarrow$ π is irreducible.

"$\Leftarrow$": Let π be irreducible and let W be a complex linear subspace invariant under $\tilde{\pi}$. We deduce that $\pi(W) \equiv \tilde{\pi}(W) + i\tilde{\pi}(W) \subset W$ since W is a complex vector space. Therefore W is equal to $\{0\}$ or is equal to the entire representation space $\Rightarrow \tilde{\pi}$ is irreducible. □

Lemma 1. $\mathfrak{su}(n)_{\mathbb{C}} \cong \mathfrak{sl}(n, \mathbb{C})$

Proof. The complexification $\mathfrak{su}(n)_{\mathbb{C}}$ of the real Lie algebra $\mathfrak{su}(n)$ and $\mathfrak{sl}(n;\mathbb{C})$ are subalgebras of the Lie algebra $\mathfrak{gl}(n;\mathbb{C})$ (compare the definition of the complexification). The Lie algebra $\mathfrak{sl}(n;\mathbb{C})$ is the space of complex and traceless $n \times n$-matrices. We can write each element X of $\mathfrak{sl}(n;\mathbb{C})$ (uniquely) in the form

$$X = \frac{X - X^*}{2} + i\frac{X + X^*}{2i},$$

where $(X - X^*)/2$ and $(X + X^*)/2i$ are both traceless and skew and are therefore elements of $\mathfrak{su}(n)$. This implies the claim. □

The Exponential Map

Let G be a Lie group with Lie algebra $\mathfrak{g}$, $X \in \mathfrak{g}$ and $g \in G$. The map $m_g : G \to G$ is the diffeomorphism defined by left-multiplication with g, i.e., $m_g(h) := g \cdot h$ for all $h \in G$.
Now we introduce a vector field on the Lie group G defined by

$$v_X(g) := (m_g)_*(X). \tag{1.7}$$

($(m_g)_*(X) \equiv d(m_g)_{m_{g^{-1}}} X$.) This is locally integrable. Thus, there exists $I \subset \mathbb{R}$, $\phi : I \to G$ differentiable with $\phi(0) = e$, such that

$$\phi'_X(t) = v_X(\phi_X(t)) \tag{1.8}$$

for all $t \in I$. Since $\phi(s+t) = \phi(s) \cdot \phi(t)$ and since ϕ is defined on a finite interval I, we can deduce that ϕ extends uniquely to all of $\mathbb{R}$:

$$\phi_X : \mathbb{R} \to G. \tag{1.9}$$

Definition 10. Let G be a Lie group with Lie algebra $\mathfrak{g}$. We define the *exponential map* by

$$\begin{array}{rccl} exp & : & \mathfrak{g} & \to & G \\ & & X & \mapsto & exp(X) := \phi_X(1). \end{array}$$

Properties of the exponential map:

1. Let ψ be a Lie group homomorphism. Then the following diagram commutes
$$\begin{array}{ccc} \mathfrak{g} & \xrightarrow{\psi_*} & \mathfrak{h} \\ \downarrow exp & & \downarrow exp \\ G & \xrightarrow{\psi} & H \end{array}$$

2. The exponential map is differentiable. Its derivative at the origin of $\mathfrak{g}$ is the identity map. Thus, the exponential map realizes a diffeomorphism from a neighborhood of the origin of $T_eG \cong \mathfrak{g}$ to a neighborhood of the identity element $e \in G$. Such a neighborhood of $e \in G$ generates the identity component of G.

3. Let G be a compact Lie group with Lie algebra $\mathfrak{g}$. Then: exponentiation of a representation of $\mathfrak{g}$ yields a representation of G.

4. $\phi_X(t) = exp(t \cdot X)$

5. $exp((t + t') \cdot X) = exp(t \cdot X) \cdot exp(t' \cdot X)$

6. $exp(-X) = (exp(X))^{-1}$

7. Let G be a matrix Lie group. Then: the exponential map is equal to the exponential map of matrices, i.e.,
$$exp(X) = \sum_{k=0}^{\infty} \frac{X^k}{k!}$$
for all $X \in G$.

First Classification of Lie Algebras

As it is usual in mathematics, we have started with the discussion of a certain mathematical structure (here the Lie algebra). Once one doesn't get any further in the general analysis, one tries to organize the different manifestations of the general structure, i.e., one tries to classify the original structure. The next step is the investigation of the different classes. The following classification reflects how much a Lie algebra fails to be Abelian.

Definition 11. Let $\mathfrak{g}$ be a Lie algebra and let $\mathfrak{h} \subset \mathfrak{g}$ be a subalgebra. The subalgebra is an *ideal* if
$$[X, Y] \in \mathfrak{h}$$
for all $X \in \mathfrak{h}$ and $Y \in \mathfrak{g}$.

The bracket operation on $\mathfrak{g}$ induces a bracket operation on the quotient space $\mathfrak{g}/\mathfrak{h}$ iff $\mathfrak{h}$ is an ideal of $\mathfrak{g}$.
Therefore, we make the next definition.

Definition 12. A Lie algebra is called *simple* if $dim\ \mathfrak{g} > 1$ and if it contains no nontrivial ideals.

Definition 13. The *lower central series* $\mathcal{D}_k\mathfrak{g}$ of subalgebras is defined by

$$\mathcal{D}_1\mathfrak{g} := [\mathfrak{g}, \mathfrak{g}], \qquad \mathcal{D}_k\mathfrak{g} := [\mathfrak{g}, \mathcal{D}_{k-1}\mathfrak{g}].$$

The subalgebras $\mathcal{D}_k\mathfrak{g}$ are ideals in $\mathfrak{g}$.

Definition 14. The *derived series* $\mathcal{D}^k\mathfrak{g}$ of subalgebras is defined by

$$\mathcal{D}^1\mathfrak{g} := [\mathfrak{g}, \mathfrak{g}], \qquad \mathcal{D}^k\mathfrak{g} := [\mathcal{D}^{k-1}\mathfrak{g}, \mathcal{D}^{k-1}\mathfrak{g}].$$

The subalgebras $\mathcal{D}^k\mathfrak{g}$ are ideals in $\mathfrak{g}$ and $\mathcal{D}^k\mathfrak{g} \subset \mathcal{D}_k\mathfrak{g}$ for all k.
Furthermore, $\mathcal{D}_1\mathfrak{g} = \mathcal{D}^1\mathfrak{g} =: \mathcal{D}\mathfrak{g}$.

Definition 15. Let $\mathfrak{g}$ be a Lie algebra. Then:

1. $\mathfrak{g}$ is called *nilpotent* if $\mathcal{D}_k\mathfrak{g} = 0$ for some k.
2. $\mathfrak{g}$ is called *solvable* if $\mathcal{D}^k\mathfrak{g} = 0$ for some k.
3. $\mathfrak{g}$ is called *perfect* if $\mathcal{D}\mathfrak{g} = \mathfrak{g}$.
4. $\mathfrak{g}$ is called *semisimple* if $\mathfrak{g}$ has no nonzero solvable ideals.

The term 'semisimple' will become clearer in the section about semisimple Lie algebras.
The sum of two solvable ideals of a Lie algebra $\mathfrak{g}$ is again solvable.

Definition 16. The sum of all solvable ideals of $\mathfrak{g}$ is a maximal solvable ideal, called the *radical* $Rad(\mathfrak{g})$ of $\mathfrak{g}$.

The following proposition can be used to determine the radical of $\mathfrak{g}$ (the definition of the Killing form follows in section 5).

Proposition 4. *Let $\mathfrak{g}$ be a Lie algebra. Then: the radical $Rad(\mathfrak{g})$ of $\mathfrak{g}$ is the orthogonal complement to $\mathcal{D}\mathfrak{g}$ with respect to the Killing form.*

The quotient $\mathfrak{g}/Rad(\mathfrak{g})$ is semisimple according to the definition of semisimplicity. A consequence of Lie's theorem (compare Fulton and Harris §9.2) is that any irreducible representation of a solvable Lie algebra is one-dimensional. One arrives at the following theorem which describes how to find irreducible representations of an arbitrary complex Lie algebra $\mathfrak{g}$.

Theorem 3. *Let $\mathfrak{g}$ be an arbitrary complex Lie algebra and let $\mathfrak{g}_{semisimple} = \mathfrak{g}/Rad(\mathfrak{g})$ be its semisimple component.*
Then: Every irreducible representation π of $\mathfrak{g}$ is of the form

$$\pi = \pi_{semisimple} \otimes L,$$

where $\pi_{semisimple}$ is an irreducible representation of $\mathfrak{g}_{semisimple}$ (i.e., a representation of $\mathfrak{g}$ that is trivial on $Rad(\mathfrak{g})$), and L is a one-dimensional representation.

Simple Lie Algebras

As we will see in section 6, every simple complex Lie algebra is either isomorphic to $\mathfrak{sl}_n(\mathbb{C})$, $\mathfrak{so}_n(\mathbb{C})$, $\mathfrak{sp}_{2n}(\mathbb{C})$ (the symplectic Lie algebra) or to one of the so called exceptional Lie algebras.

Semisimple Lie Algebras

There are two fundamental problems concerning the representations of general Lie groups and general Lie algebras: first, the complete reducibility property of representations is not valid and second, the action of an element in a Lie group or in a Lie algebra can be diagonalizable under one representation and not under another. This problems vanish immediately as soon as we pass to semisimple Lie algebras.

Theorem (Complete Reducibility). *Let $\mathfrak{g}$ be a semisimple Lie algebra and let π be an arbitrary representation of $\mathfrak{g}$ with representation space V. Assume that $W \subset V$ is an invariant subspace under the action of $\mathfrak{g}$.*
Then: there exists a subspace $W' \subset V$ complementary to W and invariant under the action of $\mathfrak{g}$.

Recall that we can write any endomorphism X of a complex vector space V in the form

$$X = X_s + X_n,$$

where X_s is diagonalizable and X_n is nilpotent.

Theorem (Preservation of Jordan Decomposition). *Let $\mathfrak{g}$ be a semisimple Lie algebra. Then there exist for any $X \in \mathfrak{g}$ elements $X_s \in \mathfrak{g}$ and $X_n \in \mathfrak{g}$ such that*

$$\pi(X)_s = \pi(X_s), \ \pi(X)_n = \pi(X_n)$$

for any representation π, where $\pi(X)_s$ is diagonalizable and where $\pi(X)_n$ is nilpotent.

In addition, the following proposition holds:

Proposition 5. *The following is equivalent:*

1. $\mathfrak{g}$ *is a semisimple Lie algebra.*
2. $\mathfrak{g}$ *is a direct sum of simple Lie algebras.*
3. *The Killing form is non-degenerate (i.e., the set* $\{x \in V | < x, y >_{Killing} = 0 \text{ for all } y \in V\}$ *is trivial).*
4. $\mathfrak{g}$ *has no nonzero Abelian ideals.*
5. *The radical of* $\mathfrak{g}$ *is zero.*

3 Representations of $\mathfrak{su}(2)$

The goal of this section is to analyze the irreducible complex representations of $\mathfrak{su}(2)$. Motivation: First, in the analysis of the representations of general semisimple Lie algebras one uses the representations of $\mathfrak{sl}(2,\mathbb{C}) \cong \mathfrak{su}(2)$, second, $\mathfrak{su}(2)$ is an easy example of how one uses commutation relations to get the representations of a Lie algebra and third, $\mathfrak{su}(2)$ is of physical importance.
In proposition 3 we saw that every finite-dimensional complex representation of $\mathfrak{su}(2)$ extends uniquely to a complex-linear representation of the complexification $\mathfrak{su}(2)_{\mathbb{C}}$. According to Lemma 1 this complexification is isomorphic to $\mathfrak{sl}(2,\mathbb{C})$. Therefore the extension of a representation π to $\mathfrak{sl}(2,\mathbb{C})$ is irreducible iff the representation π of $\mathfrak{su}(2)$ is irreducible.
We conclude that the study of the irreducible representations of $\mathfrak{su}(2)$ is equivalent to the study of the irreducible complex-linear representations of $\mathfrak{sl}(2,\mathbb{C})$.
We prefer the analysis of $\mathfrak{sl}(2,\mathbb{C})$ to the analysis of $\mathfrak{su}(2)$ since we can work with the following nice basis in the case of $\mathfrak{sl}(2,\mathbb{C})$ which will simplify our computations:

$$H = \begin{pmatrix} 1 & 0 \\ 0 & -1 \end{pmatrix};\ X = \begin{pmatrix} 0 & 1 \\ 0 & 0 \end{pmatrix};\ Y = \begin{pmatrix} 0 & 0 \\ 1 & 0 \end{pmatrix}, \tag{1.10}$$

with

$$[H, X] = 2X, \quad [H, Y] = -2Y, \quad [X, Y] = H. \tag{1.11}$$

Assume that π is an arbitrary irreducible finite-dimensional representation of $\mathfrak{sl}(2,\mathbb{C})$ on a vector space V.
As a first observation we have the following remark which is a result of the preservation of the Jordan decomposition under a representation (compare section 2):

Remark 1. $\pi(H)$ is diagonalizable and therefore

$$V = \bigoplus V_\alpha,$$

where the index α runs over the eigenvalues of $\pi(H)$ which are complex numbers.

With the decomposition of V into eigenspaces of $\pi(H)$ we have brought a first structure (wrt the action of $\pi(H)$) into the representation space V. As a result of the commutation relations (1.11) we will see in the following that this structure of V will be preserved under the action of $\pi(X)$ and $\pi(Y)$ ($\Rightarrow$ the structure will be preserved under the action of $\pi(\mathfrak{sl}(2,\mathbb{C}))$). This will equip us with much insight into representations of $\mathfrak{sl}(2,\mathbb{C})$.

After this outlook let us try to answer the following question: How do $\pi(X)$ and $\pi(Y)$ act on the decomposition in Remark 1?

Remark 2. Let $W = \bigoplus W_\alpha$ be a decomposition of a vectorspace W into eigenspaces W_α of a linear Operator L acting on W with eigenvalues $\alpha \in \mathbb{C}$. Whenever one wants to determine in which eigenspace the vector $K(w)$ ($w \in W$; K being another linear Operator on W) lies, we simply apply L:

$$L(K(w)) = \xi K(w), \quad \xi \in \mathbb{C} \;\Leftrightarrow\; K(w) \in W_\xi.$$

Therefore the answer to the question above is given by the following calculation using the commutation relations (1.11):

$$\begin{aligned} \pi(H)\circ\pi(X)(v) &= \pi(X)\circ\pi(H)(v) + [\pi(H),\pi(X)](v) \\ &= \pi(X)\circ\pi(H)(v) + 2\pi(X)(v) \\ &= (\alpha+2)\cdot\pi(X)(v), \qquad\qquad for\ v \in V_\alpha. \end{aligned} \tag{1.12}$$

Similarly,

$$\begin{aligned} \pi(H)\circ\pi(Y)(v) &= \pi(Y)\circ\pi(H)(v) + [\pi(H),\pi(Y)](v) \\ &= \pi(Y)\circ\pi(H)(v) - 2\pi(Y)(v) \\ &= (\alpha-2)\cdot\pi(Y)(v), \qquad\qquad for\ v \in V_\alpha. \end{aligned} \tag{1.13}$$

We summarize these results in the following

Lemma 2.

$$\pi(H) : V_\alpha \to V_\alpha \qquad \pi(X) : V_\alpha \to V_{\alpha+2} \qquad \pi(Y) : V_\alpha \to V_{\alpha-2}$$

From the 3 facts that

1. π is irreducible ($\Rightarrow$ the only invariant subspaces are V and $\{0\}$),
2. only those subspaces V_η and V_ξ are getting mapped into each other by the action of $\mathfrak{sl}(2,\mathbb{C})$ iff $\eta - \xi$ is an integer multiple of 2 and
3. only finitely many linear subspaces can contribute to a direct-sum-decomposition of V (since the vector space V is finite-dimensional)

we deduce that

Lemma 3. *There exists $\beta \in \mathbb{C}$ and $k \in \mathbb{Z}$, such that*

$$V = V_\beta \oplus V_{\beta+2} \oplus V_{\beta+4} \oplus ... \oplus V_{\beta+2k}.$$

Define $n := \beta + 2k \in \mathbb{C}$.

Lemma 4. *Let $v \in V_{n \equiv \beta+2k}$. Then*

$$V = span\{v,\ \pi(Y)(v),\ \pi(Y)^2(v),\ \pi(Y)^3(v),\ ...\}.$$

Proof. Define $W \equiv span\{v,\ \pi(Y)(v),\ \pi(Y)^2(v),\ \pi(Y)^3(v),\ ...\}$. Recall that the representation π is irreducible by assumption. This implies that it is sufficient to show that W is invariant under the action of X, Y and H. Again we will use the commutation relations (1.11).
W is preserved under the action of Y since $\pi(Y) \circ \pi(Y)^m(v) = \pi(Y)^{m+1}(v) \in W$ for all $m \in \mathbb{N}$.
W is preserved under the action of H since all the basis elements of W lie in different eigenspaces of $\pi(H)$ which are all preserved under the action of H.
It is left to show that

$$\pi(X) \circ \pi(Y)^m(v)) \in W, \quad \forall v \in W.$$

Consider the case $m = 0$:

$$\pi(X)(v) = 0$$

(compare Lemma 3).
Consider the case $m = 1$:

$$\begin{aligned} \pi(X) \circ \pi(Y)(v) &= \pi(Y) \circ \pi(X)(v) + [\pi(X), \pi(Y)](v) \\ &= 0 + \pi(H)(v) \\ &= nv. \end{aligned}$$

Consider the case $m = 2$:

$$\begin{aligned} \pi(X) \circ \pi(Y)(\pi(Y)(v)) &= \pi(Y) \circ \pi(X)(\pi(Y)(v)) + [\pi(X), \pi(Y)](\pi(Y)(v)) \\ &= \pi(Y) \circ (nv) + \pi(H)(\pi(Y)(v)) \\ &= n\pi(Y)(v) + (n-2)\pi(Y)(v) \\ &= (n + (n-2)) \cdot \pi(Y)(v). \end{aligned}$$

Repeating these calculations yields

$$\begin{aligned} \pi(X) \circ \pi(Y)^m(v)) &= [n + (n-2) + (n-4) + \ldots + (n-2(m-1))] \cdot \pi(Y)^{(m-1)}(v) \\ &= m(n-m+1) \cdot \pi(Y)^{(m-1)}(v). \end{aligned} \tag{1.14}$$

The last step can easily be proved by induction ($m \Rightarrow m+1$, the cases $m = 0,\ 1,\ 2$ have already been checked above):

$$\begin{aligned} n + (n-2) + (n-4) + \ldots + (n - 2(m+1-1)) &= n + (n-2) + (n-4) + \ldots \\ &\quad + (n - 2(m-1)) + n - 2m \\ &= m(n - m + 1) + n - 2m \\ &= mn - m^2 + m + n - 2m \\ &= (m+1)(n - (m+1) + 1) \Rightarrow \checkmark. \end{aligned}$$

We have shown that $\pi(Y)^m(v)$ is mapped to a multiple $\pi(Y)^{m-1}(v) \Rightarrow W$ is preserved under the action of X.
$\therefore W = V$ and $\{v,\ \pi(Y)(v),\ \pi(Y)^2(v),\ \pi(Y)^3(v),\ ...\}$ forms a basis of V. □

Corollary 1. *For each eigenspace V_α of $\pi(H)$ we have that*

$$dim\ V_\alpha = 1.$$

Since we know how the basis elements $H,\ X$ and Y act on the basis vector of each eigenspace V_α, we know how the representation π of $\mathfrak{sl}(2,\mathbb{C})$ acts on the vector space V_α as linear maps. Thus, we know how the representation π of $\mathfrak{sl}(2,\mathbb{C})$ acts on the whole vector space $V = \bigoplus V_\alpha$ and we arrive at the second corollary of lemma 4

Corollary 2. *Every irreducible representation π of $\mathfrak{sl}(2,\mathbb{C})$ is determined by the set $\{\alpha \in \mathbb{C} | V_\alpha$ is an eigenspace of $\pi(H)\}$.*

Let $m \in \mathbb{N}$ be the smallest non-negative *integer* such that $\pi(Y)^m(v) = 0$ with $v \in V_n$. We apply $\pi(X)$ and use identity (1.14) to get

$$0 = \pi(X) \circ \pi(Y)^m(v) = m(n - m + 1) \cdot \pi(Y)^{(m-1)}(v). \tag{1.15}$$

Since $\pi(Y)^{(m-1)}(v)$ is by assumption not equal to zero we get:

$$0 = (n - m + 1) \Leftrightarrow m = n + 1. \tag{1.16}$$

But the integer m is also equal to the dimension of V. Thus, we deduce, that the representation space V is $n+1$-dimensional (compare lemma 2, lemma 3 and corollary 1).
This implies that the direct decomposition $V = \bigoplus V_\alpha$ of V into one-dimensional eigenspaces V_α of $\pi(H)$ consists of $n+1$ terms. We deduce

$$\begin{aligned} V &= V_n \oplus V_{n-2} \oplus \ldots \oplus V_{n-2n} \\ &= V_n \oplus V_{n-2} \oplus \ldots \oplus V_{-n+2} \oplus V_{-n}. \end{aligned} \tag{1.17}$$

We can summarize the former results in the following theorem.

Theorem 4. *Let π be an irreducible representation of $\mathfrak{sl}(2,\mathbb{C})$ with representation space V. Then the spectrum of $\pi(H)$ is a subset of $\mathbb{Z}$ of the form*

$$\{-n,\ -n+2,\ -n+4,\ \ldots,\ -2,\ 0,\ 2,\ \ldots,\ n-2,\ n\}$$

or

$$\{-n,\ -n+2,\ -n+4,\ \ldots,\ -1,\ 1,\ \ldots,\ n-2,\ n\}.$$

Each irreducible representation of $\mathfrak{sl}(2,\mathbb{C})$ can be labeled by the largest eigenvalue n of $\pi(H)$. Each eigenspace of $\pi^{(n)}(H)$ is one-dimensional and $V^{(n)} = \bigoplus_{k\in\{-n,\ -n+2,\ \ldots,\ n-2,\ n\}} V_k^{(n)}$.

Corollary 3. *The number of irreducible factors in an arbitrary representation π of $\mathfrak{sl}(2,\mathbb{C})$ is equal to the multiplicities of 0 and 1 as eigenvalues of $\pi(H)$.*

4 Representations of $\mathfrak{su}(3)$

Definitions and first Observations

As in the case of $\mathfrak{su}(2)$ we observe that we are allowed to study the representations of $\mathfrak{sl}(3,\mathbb{C})$ instead of $\mathfrak{su}(3)$, since the representations of $\mathfrak{sl}(3,\mathbb{C})$ are in one-to-one correspondence with the complex-linear representations of the complexification $\mathfrak{su}_{\mathbb{C}}(3) \cong \mathfrak{sl}(3,\mathbb{C})$ (compare proposition 3 and lemma 1).
The main result of our discussion about the irreducible representation of $\mathfrak{su}(2)$ was that each irreducible representation π can be classified in term of the largest eigenvalue of $\pi(H)$.
Thus, it arises the natural question, which element in $\pi(\mathfrak{sl}(3,\mathbb{C}))$ will take over the role of $\pi(H)$. The answer is that there isn't any such element in $\pi(\mathfrak{sl}(3,\mathbb{C}))$. But instead we will use a whole subspace $\mathfrak{h}$ of $\pi(\mathfrak{sl}(3,\mathbb{C}))$.
The main goal of this section is to classify the irreducible representations of $\mathfrak{sl}(3,\mathbb{C})$ (as we have done it in the analysis of $\pi(\mathfrak{sl}(2,\mathbb{C}))$). We will prove that these representations are determined (up to equivalence) by their "highest weight" (to be defined later).
The study of $\mathfrak{sl}(3,\mathbb{C})$ will equip us with the concepts necessary to classify the finite-dimensional representations of all semisimple Lie algebras.

We define $\mathfrak{h} \subset \mathfrak{sl}(3,\mathbb{C})$ to be the *two-dimensional* subspace of all diagonal matrices in $\mathfrak{sl}(3,\mathbb{C})$ (this is the so called *Cartan subalgebra* for $\mathfrak{sl}(3,\mathbb{C})$).

$$\mathfrak{h} := \{ \begin{pmatrix} a_1 & 0 & 0 \\ 0 & a_2 & 0 \\ 0 & 0 & a_3 \end{pmatrix} | a_1 + a_2 + a_3 = 0\} \tag{1.18}$$

$$\mathfrak{h}^* = \{\mu_1 \cdot L_1 + \mu_2 \cdot L_2 + \mu_3 \cdot L_3 \mid \mu_1,\ \mu_2,\ \mu_3 \in \mathbb{C}\}/\{L_1 + L_2 + L_3 = 0\}, \tag{1.19}$$

with

$$L_i \begin{pmatrix} a_1 & 0 & 0 \\ 0 & a_2 & 0 \\ 0 & 0 & a_3 \end{pmatrix} := a_i. \tag{1.20}$$

Definition 17. Let π be an arbitrary representation of $\mathfrak{sl}(3,\mathbb{C})$ with representation space V. Then we define

1. A vector $v \in V$ is a *weight vector* if v is a simultaneous eigenvector for $\pi(H)$ for *each* $H \in \mathfrak{h}$.

2. Let v be a weight vector with corresponding eigenvalue $\alpha(H)$ for $H \in \mathfrak{h}$. This quantity $\alpha(H)$ is a complex number depending linearly on $H \in \mathfrak{h}$, i.e., $\alpha \in \mathfrak{h}^*$. The linear functional α is called a *weight* of the representation.

3. All the weight vectors corresponding to a weight α span a vector space V_α which is a so called *weight space*.

4. The dimension of the weight space V_α is called the *multiplicity* of the weight α.

According to the preservation of the Jordan decomposition (compare section 2) all elements in $\mathfrak{h}$ are diagonalizable in *any* representation of $\mathfrak{sl}(3,\mathbb{C})$. Additionally, all elements in $\mathfrak{h}$ commute in *any* representation of $\mathfrak{sl}(3,\mathbb{C})$ since they commute in $\mathfrak{sl}(3,\mathbb{C})$. Recall that commuting, diagonalizable matrices are *simultaneously diagonalizable*.

Remark 3. This implies that any finite-dimensional representation space V decomposes into a direct sum of weight spaces (i.e., simultaneous eigenspaces) V_α of *all* elements in $\mathfrak{h}$:

$$V = \bigoplus V_\alpha,$$

where $\alpha \in \mathfrak{h}^*$ ranges over a finite subset of $\mathfrak{h}^*$ since V is finite-dimensional by assumption.

Now that we know how to 'replace' the basis element H from the discussion of $\mathfrak{sl}(2,\mathbb{C})$ we should determine how to 'replace' the basis elements X and Y. Recall that

$$ad(H)(X) = [H,X] = 2X, \quad ad(H)(Y) = [H,Y] = -2Y, \tag{1.21}$$

i.e., the elements X and $Y \in \mathfrak{sl}(2,\mathbb{C})$ are eigenvectors for the adjoint action of $H \in \mathfrak{sl}(2,\mathbb{C})$. Thus, to replace X and $Y \in \mathfrak{sl}(2,\mathbb{C})$ we have to look for simultaneous eigenvectors for the adjoint action of $\mathfrak{h}$ (i.e., weight vectors in the case of the adjoint representation). This yields a decomposition

$$\mathfrak{sl}(3,\mathbb{C}) = \mathfrak{h} \oplus (\bigoplus \mathfrak{g}_\alpha), \tag{1.22}$$

where α ranges over a finite subset of $\mathfrak{h}^*$ as explained in remark 3. The subspaces $\mathfrak{g}_\alpha \subset \mathfrak{sl}(3,\mathbb{C})$ are the analogue of the subspaces V_α appearing in remark 3, i.e.,

$$ad(H)(X) = [H,X] = \alpha(H)\cdot X, \tag{1.23}$$

for every $H \in \mathfrak{h}$ and $X \in \mathfrak{g}_\alpha$.

Definition 18. In case of the adjoint representation weights are called *roots*, weight vectors are called *root vectors* and weight spaces are called *root spaces*. The finite set of all roots is denoted $R \subset \mathfrak{h}^*$.

The next goal is to determine the subspaces $\mathfrak{g}_\alpha \subset \mathfrak{sl}(3,\mathbb{C})$ and to explicitly write down the corresponding weight $\alpha \in \mathfrak{h}^*$.
To determine the $\mathfrak{g}_\alpha$'s observe that

$$[H,M]_{ij} = [\begin{pmatrix} a_1 & 0 & 0 \\ 0 & a_2 & 0 \\ 0 & 0 & a_3 \end{pmatrix}, \begin{pmatrix} m_{11} & m_{12} & m_{13} \\ m_{21} & m_{22} & m_{23} \\ m_{31} & m_{32} & m_{33} \end{pmatrix}]_{ij} = (a_i - a_j)\cdot m_{ij} \tag{1.24}$$

for every $H \in \mathfrak{h}$ and $M \in \mathfrak{sl}(3,\mathbb{C})$. Thus, $M \in \mathfrak{sl}(3,\mathbb{C})$ is a root vector iff all but one entry of M are zero. We deduce that the root spaces $\mathfrak{g}_\alpha$ are spanned by matrices $E_{i,j}$ which are defined to be the (3×3)-matrices whose (i,j)th entry is equal to 1 and whose other entries are equal to zero. In total we span six ($E_{i,j} \in \mathfrak{sl}(3,\mathbb{C})$) one-dimensional complex subspaces of $\mathfrak{sl}(3,\mathbb{C})$ (recall that $\mathfrak{sl}(3,\mathbb{C})$ is 8-dimensional, that $\mathfrak{h}$ is 2-dimensional and remember identity (1.22)).

Example 1. We apply the above thoughts to $E_{1,2}$, which spans a certain root space of $\mathfrak{sl}(3,\mathbb{C})$:

$$ad(H)(E_{1,2}) = \alpha(H)\cdot E_{1,2} = (a_1 - a_2)\cdot E_{1,2} \quad \Rightarrow \quad \alpha(H) = L_1 - L_2.$$

(Compare equation (1.20) for the last implication.)

Therefore we arrive at the

Observation 2. *The root of the root space spanned by the matrix $E_{i,j}$ is $L_i - L_j$.*

We have seen that the representation space V decomposes into a direct sum of weight spaces and that $\mathfrak{sl}(3,\mathbb{C}) = \mathfrak{h} \oplus (\bigoplus \mathfrak{g}_\alpha)$. The subspace $\mathfrak{h} \subset \mathfrak{sl}(3,\mathbb{C})$ acts on the different V_α's as scalar multiplication (by definition of the V_α's). To get more information about how the $\mathfrak{g}_\alpha$'s act on the V_α's, we proceed exactly as in (1.12): We use commutation relations. First, we have to consider the special case of the adjoint representation (recall the Jacobi identity):

$$\begin{aligned} ad(H)\circ ad(X)(Y) &\equiv [H,[X,Y]] \\ &= -[Y,[H,X]] - [X,[Y,H]] \\ &= [[H,X],Y] + [X,[H,Y]] \\ &= (\alpha(H) + \beta(H))\cdot ad(X)(Y), \end{aligned} \tag{1.25}$$

for every $H \in \mathfrak{h}$, $X \in \mathfrak{g}_\alpha$ and $Y \in \mathfrak{g}_\beta$. This crucial calculation proves the following fundamental observation.

Observation 3.

$$ad(\mathfrak{g}_\alpha): \quad \mathfrak{g}_\beta \to \mathfrak{g}_{\alpha+\beta}$$

Let us proceed to the general case (recall that the commutation relations are the same in every representation):

$$\begin{aligned} \pi(H)\circ\pi(X)(v) &= [\pi(H),\pi(X)](v) + \pi(X)\circ\pi(H)(v) \\ &= \beta(H)\cdot\pi(X)(v) + \alpha(H)\cdot\pi(X)(v) \\ &= (\alpha(H)+\beta(H))\cdot\pi(X)(v), \end{aligned} \tag{1.26}$$

for all $H \in \mathfrak{h}$, $X \in \mathfrak{g}_\alpha$ and $v \in V_\beta$. We deduce

Observation 4.

$$\pi(\mathfrak{g}_\alpha): \quad V_\beta \to V_{\alpha+\beta}$$

As a consequence, the weights of an arbitrary *irreducible* representation differ only by integral linear combinations of $L_i - L_j$, i.e., linear combinations with integer coefficients (recall that there must not exists any other invariant subspace than V or $\{0\}$).

Definition 19. The integral linear combinations of $L_i - L_j$ generate a lattice Λ_R called the *root lattice*.

Consider again the adjoint representation. From the structure of the roots (i.e., the weights for the adjoint representation) one can deduce much knowledge about the Lie algebra. Thus, we introduce the following diagrammatical method: Draw the six roots $L_i - L_j \in \mathfrak{h}^*$ lying in the real subspace $\tilde{\mathfrak{h}}^*$ with two real dimensions as in figure 1.1.

The points symbolize the root space corresponding to each specific root. The '0' in the middle should be considered as the Cartan subalgebra $\mathfrak{h}$ (which corresponds to the root '0' since its elements commute). The irreducibility of the adjoint representation implies that the subspace $\mathfrak{h}$ and all the $\mathfrak{g}_\alpha$'s get mapped into each other under the action of $\mathfrak{sl}(3,\mathbb{C}) = \mathfrak{h} \oplus (\bigoplus \mathfrak{g}_\alpha)$ (recall that there must not be any invariant subspace different from $\{0\}$ and the representation space $V = \mathfrak{sl}(3,\mathbb{C})$). We deduce that the only possibility to draw the six roots $L_i - L_j$ is the one shown in figure 1.1 (compare also observation 3). The locations of L_1, L_2 and L_3 follow.

In the discussion of $\mathfrak{sl}(2,\mathbb{C})$ we discovered an 'extremal' eigenspace V_n for the action of H (by 'extremal' we mean that V_n is sent to $\{0\}$ under the action of X, i.e. V_n is sent to $\{0\}$ by *half* of the roots).
To deduce an analog statement for the present discussion, we have to explain what we mean by 'extremal' in the context of $\mathfrak{sl}(3,\mathbb{C})$.
Seen from another point of view, the extremal eigenspace V_n of $\mathfrak{sl}(2,\mathbb{C})$ is the eigenspace corresponding to the root n lying farthest away from the origin of

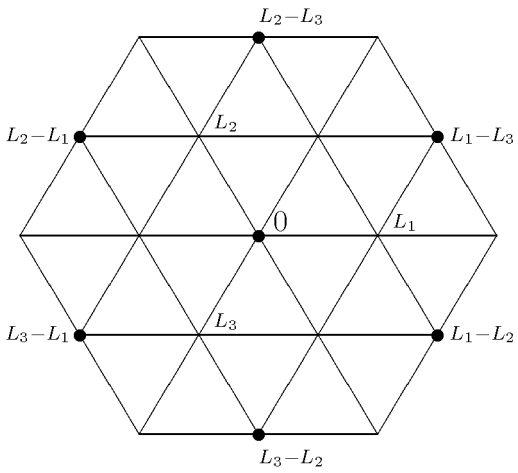

Figure 1.1: Root diagram for $\mathfrak{sl}(3,\mathbb{C})$

the one-dimensional vector space $\mathfrak{h}^*_{\mathfrak{sl}(2,\mathbb{C})}$. In the present circumstances we are dealing with a 2-dimensional Cartan subalgebra $\mathfrak{h}^*$. Thus, we first have to define a specific direction (we will see that the specific choice doesn't affect the result). More concretely, we define a linear functional

$$l: \quad \Lambda_R \to \mathbb{C}, \tag{1.27}$$

such that l never vanishes on Λ_R, i.e., the kernel of l doesn't intersect any lattice point of Λ_R so that

$$\Lambda_R = R^+ \cup R^- \tag{1.28}$$

(disjoint) with $l(\beta) > 0$ for all $\beta \in R^+$ and $l(\gamma) < 0$ for all $\gamma \in R^-$. A specific example of the present circumstances is shown in figure 1.2 (the thick line visualizes the kernel of l).

We call a root space $\mathfrak{g}_\alpha$ extremal, if α is the farthest root in the chosen specific direction.

Observation 5. *The extremal root space $\mathfrak{g}_{L_1-L_3}$ (in case of the specific example shown in the figure above) is sent to $\{0\}$ under the action of $R^+ = \{L_2-L_3,\ L_1-L_3,\ L_1-L_2,\}$. I.e., the elements in $\mathfrak{g}_{L_1-L_3}$ are simultaneous eigenvectors for all elements in $\mathfrak{h}$ and get killed by the action of half of the roots. Thus, we have arrived at a situation which is completely analogue to the one discussed in the case of $\mathfrak{sl}(2,\mathbb{C})$.*

The explicit expression of l from our specific example is of the form

$$l(\lambda_1 L_1 + \lambda_2 L_2 + \lambda_3 L_3) = \lambda_1 a + \lambda_2 b + \lambda_3 c \tag{1.29}$$

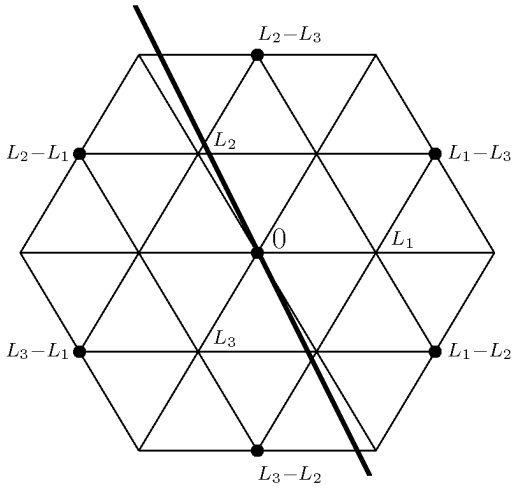

Figure 1.2: Visualization of a specific kernel

with $a+b+c=0$ and $a>b>c$ and $\lambda_1,\ \lambda_2,\ \lambda_3 \in \mathbb{C}$.
Note that the positive root spaces are generated by the matrices $E_{i,j}$ for $i<j$ and that the negative root spaces are generated by the matrices $E_{i,j}$ for $i>j$.

Let us pass over to the analysis of an arbitrary finite-dimensional representation π of $\mathfrak{sl}(3,\mathbb{C})$ with representation space V. We summarize the observations above in the following lemma wrt the general irreducible representation.

Lemma 5. *One can always find a vector $v \in V$, such that*

1. *v is a simultaneous eigenvector for all elements in $\mathfrak{h}$ and such that*
2. *v gets killed by the application $\pi(E_{2,3})$, $\pi(E_{1,3})$ or $\pi(E_{1,2})$ (i.e, by the action of all elements corresponding to the roots in R^+).*

The vector $v \in V$ in the lemma is called a *highest weight vector*.
In the analysis of $\mathfrak{sl}(2,\mathbb{C})$ we proceeded at this point by claiming that the vectors $v,\ Y(v),\ Y^2(v),\ Y^3(v),\ldots$ (with v being a highest weight vector) would generate the whole representation.

Claim 1. *Let π be an irreducible representation of $\mathfrak{sl}(3,\mathbb{C})$ with representation space V and highest weight vector v. Then the representation is generated by the successive application of $\pi(E_{2,1})$, $\pi(E_{3,1})$ and $\pi(E_{3,2})$ (which correspond to the roots in R^-) on v.*

Proof. Let W be the subspace generated by the images of the highest weight vector v under the application of $\pi(E_{2,1})$, $\pi(E_{3,1})$ and $\pi(E_{3,2})$. We are going to show that W is invariant under the action of $\mathfrak{sl}(3,\mathbb{C})$. Then: irreducibility of π

will imply that $V = W$.
The short calculation $[E_{2,1}, E_{3,2}] = -E_{3,1}$ verifies that W is spanned by the images of successive applications of $\pi(E_{2,1})$ and $\pi(E_{3,2})$. Recall that

$$\mathfrak{sl}(3,\mathbb{C}) = \mathfrak{h} \oplus \mathbb{C}\cdot E_{1,2} \oplus \mathbb{C}\cdot E_{1,3} \oplus \mathbb{C}\cdot E_{2,3} \oplus \mathbb{C}\cdot E_{2,1} \oplus \mathbb{C}\cdot E_{3,1} \oplus \mathbb{C}\cdot E_{3,2}.$$

The vector space W is obviously invariant under $\pi(\mathfrak{h})$ (the operators $\pi(E_{2,1})$, $\pi(E_{3,2})$ transform weight spaces into weight spaces; compare observation 4) and $\mathbb{C}\cdot\pi(E_{2,1})$, $\mathbb{C}\cdot\pi(E_{3,1})$, $\mathbb{C}\cdot\pi(E_{3,2})$(true according to the definition of W).
It is left to check the invariance under the application of $\mathbb{C}\cdot\pi(E_{1,2})$, $\mathbb{C}\cdot\pi(E_{1,3})$ and $\mathbb{C}\cdot\pi(E_{2,3})$:
Since $[E_{1,2}, E_{2,3}] = E_{1,3}$ it is enough to show that W is invariant under the successive application of $\pi(E_{1,2})$ and $\pi(E_{2,3})$. We prove this by induction over the number of factors $\pi(E_{1,2})$ and $\pi(E_{2,3})$ applied to the highest weight vector v.
We start with only one factor: First, we show that the vector $\pi(E_{2,1})(v)$ stays in W after the application of $\pi(E_{1,2})$ and $\pi(E_{2,3})$. We begin with the action of $\pi(E_{1,2})$:

$$\begin{aligned}\pi(E_{1,2})\circ\pi(E_{2,1})(v) &= [\pi(E_{1,2}),\pi(E_{2,1})](v) + \pi(E_{2,1})\circ\pi(E_{1,2})(v)\\ &= [\pi(E_{1,2}),\pi(E_{2,1})](v) + 0\\ &= \alpha([\pi(E_{1,2}),\pi(E_{2,1})])\cdot v \in W.\end{aligned}$$

We have used that $E_{1,2}(v) = 0$ (by definition of v) and that $[\pi(E_{1,2}),\pi(E_{2,1})] \in \mathfrak{h}$.
On the other hand: the action of $\pi(E_{2,3})$:

$$\begin{aligned}\pi(E_{2,3})\circ\pi(E_{2,1})(v) &= [\pi(E_{2,3}),\pi(E_{2,1})](v) + \pi(E_{2,1})\circ\pi(E_{2,3})(v)\\ &= 0.\end{aligned}$$

We have used that $E_{2,3}(v) = 0$ (by definition of v) and that $[\pi(E_{2,3}),\pi(E_{2,1})] = 0$.
An analogue statement proves that $\pi(E_{3,2})(v)$ is invariant under the action of $\pi(E_{1,2})$ and $\pi(E_{2,3})$.
For the remainder of this proof we define $w_n(v)$ to be the image of v under an action which consists of a sequence of factors $\pi(E_{2,1})$ and $\pi(E_{3,2})$ with length n or less. Additionally, we define W_n to be the vector space spanned by all possible vectors w_n. Thus, $W = \bigcup W_n$.
Claim: $\pi(E_{1,2})$ and $\pi(E_{2,3})$ map W_n into W_{n-1}.
Proof of the claim: Each w_n is equal to $\pi(E_{2,1})(w_{n-1})$ or $\pi(E_{3,2})(w_{n-1})$.
'Induction-step': Assume that $\pi(E_{1,2})$ and $\pi(E_{2,3})$ map W_{n-1} into W_{n-2}. Note that w_{n-1} is a weight vector with some weight ξ.
Case 1: $w_n = \pi(E_{2,1})(w_{n-1})$:

$$\begin{aligned}\pi(E_{1,2})(w_n(v)) &= \pi(E_{1,2})\circ\pi(E_{2,1})(w_{n-1}(v))\\ &= [\pi(E_{1,2}),\pi(E_{2,1})](w_{n-1}(v)) + \pi(E_{2,1})\circ\pi(E_{1,2})(w_{n-1}(v))\\ &= \xi([\pi(E_{1,2}),\pi(E_{2,1})])\cdot w_{n-1}(v) + \pi(E_{2,1})(w_{n-2}(v))\\ &= \subset W_{n-1},\end{aligned}$$

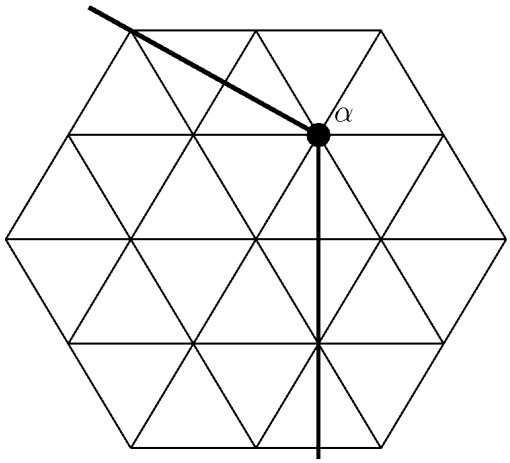

Figure 1.3: 120°-sector which contains all weights.

since $[\pi(E_{1,2}), \pi(E_{2,1})] \in \mathfrak{h}$. On the other hand we have that

$$\begin{aligned} \pi(E_{2,3})(w_n(v)) &= \pi(E_{2,3}) \circ \pi(E_{2,1})(w_{n-1}(v)) \\ &= [\pi(E_{2,3}), \pi(E_{2,1})](w_{n-1}(v)) + \pi(E_{2,1}) \circ \pi(E_{2,3})(w_{n-1}(v)) \\ &= 0 + \pi(E_{2,1})(w_{n-2}(v)) \\ &= \subset W_{n-1}, \end{aligned}$$

since $[E_{2,3}, E_{2,1}] = 0$.
Case 2: $w_n = \pi(E_{3,2})(w_{n-1})$: Analogue calculation.
This finishes the proof of the claim.
Since the case '$n = 1$' has been verified above the proof of the original claim is concluded. □

Corollary 4. *1. All the weights of an irreducible representation lie in* 120°*-sector* $\subset \mathfrak{h}^*$ *with vertex* α *(the highest weight). Compare the figure below.*

2. dim $W_\alpha = 1$. *Thus all the other weight spaces (generated as in claim 1) are at most one-dimensional.*

Proposition 6. *Let* π *be an arbitrary representation of* $\mathfrak{sl}(3, \mathbb{C})$ *with representation space* V *and highest weight vector* v. *Let* W *denote the vector space spanned by the images of* v *under the successive applications of the operators* $\pi(E_{2,1})$, $\pi(E_{3,1})$ *and* $\pi(E_{3,2})$ *(which correspond to the roots in* R^-*). Then:* W *is the representation space of an irreducible subrepresentation* $\tilde{\pi}$.

Proof. Let α denote the so called 'highest weight' corresponding to the highest weight vector v. The proof of Claim 1 shows that W is the representation space

of a subrepresentation $\tilde{\pi}$ (i.e., W is closed under the action of $\mathfrak{sl}(3,\mathbb{C})$). We have to show that this subrepresentation is irreducible.
Let us assume the contrary, i.e., let us assume that $\tilde{\pi}$ is not irreducible. Therefore, $\tilde{\pi} = \tilde{\pi}' \oplus \tilde{\pi}''$ for some representations $\tilde{\pi}'$ and $\tilde{\pi}''$ with representation spaces W' and W'' ($W = W' \oplus W''$). The operations 'projection to W' or W''' and 'action of $\mathfrak{h}$' have simultaneous eigenspaces, since they commute. The eigenspaces of the projections are W' and W''. Therefore, we arrive at the following decomposition of W:

$$\begin{aligned} W &= W' \oplus W'' \\ &= W_\alpha \oplus W_{\alpha_1} \oplus W_{\alpha_2} \oplus \dots \quad (\textit{decomposition into weight spaces}) \\ &= W'_\alpha \oplus W''_\alpha \oplus W'_{\alpha_1} \oplus W''_{\alpha_1} \oplus \dots \end{aligned}$$

Claim 1 implies that W_α is one-dimensional. Thus, all the eigenspaces W_{α_i} are at most one-dimensional. We deduce that at least one of the spaces W'_{α_i} or W''_{α_i} is equal to $\{0\}$ for each weight space 'i'. Let us assume without loss of generality that $W''_\alpha = \{0\}$. Therefore, $\pi(\textit{successive applications of } \mathfrak{sl}(3,\mathbb{C}))(W_\alpha = W'_\alpha)$ must reach the whole space W (compare the definition of W). Since the representations $\tilde{\pi}'$ and $\tilde{\pi}''$ are not allowed to mix under the successive action of $\mathfrak{sl}(3,\mathbb{C})$, this action applied to W'_α can't reach any subspace of W''.
I.e., W is spanned without any elements in $W'' \subset W \Rightarrow W'' = \{0\}$ and $W' = W$.
$\therefore$ The representation $\tilde{\pi}$ is irreducible. □

The Appearance of the Weight Diagram

The next natural question we try to answer is: How does a concrete weight diagram of $\mathfrak{sl}(3,\mathbb{C})$ look like?
We will proceed as follows: First, we try to determine the explicit form of the convex hull of the weights and second, we try to determine the interior of this convex hull.

The convex Hull

Let us have a second look at figure 1.3 to recall that there aren't any weights above the line 'generated' by the dots representing the weight spaces $\mathfrak{g}_\alpha$, $\mathfrak{g}_{\alpha+L_2-L_1}$, $\mathfrak{g}_{\alpha+2(L_2-L_1)}$, ... and that there aren't any weights to the right of the line 'generated' by the dots representing the weight spaces $\mathfrak{g}_\alpha$, $\mathfrak{g}_{\alpha+L_3-L_2}$, $\mathfrak{g}_{\alpha+2(L_3-L_2)}$, ...
We first consider the line which is the upper boundary for the finite set of weights. Finite dimensionality of V implies that there exists an integer m, such that $\mathfrak{g}_{\alpha+k(L_2-L_1)} = \{0\}$ for all $k \geq m$ (compare figure 1.4). To determine m we make the following important observation: The elements $E_{1,2}$, $E_{2,1}$ and $H_{1,2} \equiv [E_{1,2}, E_{2,1}]$ span a subalgebra (denoted $\mathfrak{s}_{L_1-L_2}$) of $\mathfrak{sl}(3,\mathbb{C})$ which is isomorphic to $\mathfrak{sl}(2,\mathbb{C})$.

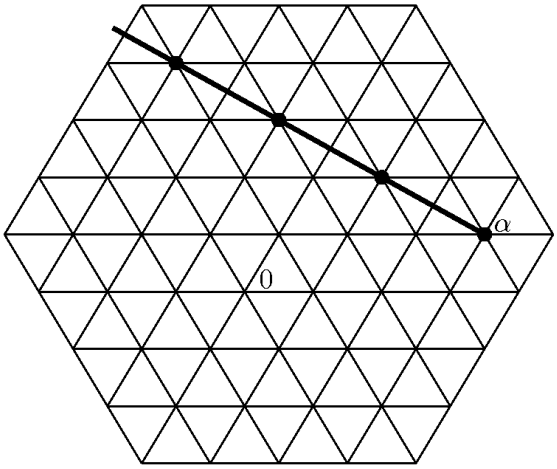

Figure 1.4: Upper boundary

Observation 6. *Let $i \neq j$. Then the elements $E_{i,j}$, $E_{j,i}$ and $H_{i,j} := [E_{i,j}, E_{j,i}]$ span a subalgebra (denoted $\mathfrak{s}_{L_i - L_j}$) of $\mathfrak{sl}(3,\mathbb{C})$ which is isomorphic to $\mathfrak{sl}(2,\mathbb{C})$.*

The subalgebra $\mathfrak{s}_{L_1-L_2}$ shifts the weight spaces V_β parallel and antiparallel to the direction $L_1 - L_2$. Obviously, the subspace

$$W := \bigoplus_k V_{\alpha + k(L_2 - L_1)}$$

is preserved under the action of $\mathfrak{s}_{L_1-L_2}$. Thus, W is a representation space of a representation ρ of $\mathfrak{s}_{L_1-L_2} \cong \mathfrak{sl}(2,\mathbb{C})$. This representation is irreducible, since there are no invariant subspaces. We deduce that the eigenvalues of $\rho(H_{12})$ are integer-valued and the spectrum of $\rho(H_{12})$ is symmetric about the origin of $\mathbb{Z}$ (compare theorem 4). This implies that the dots representing the spaces $V_{\alpha+k(L_2-L_1)}$ are symmetric to the line $\{L \in \mathfrak{h}^* | < L, H_{1,2} >= 0\}$, where '$<,>$' denotes the pairing between space and dual space. I.e., the dots representing the weight spaces $V_{\alpha+k(L_2-L_1)}$ are preserved under reflection in the line $\{L \in \mathfrak{h}^* | < L, H_{1,2} >= 0\}$. See section 5 for the explicit proof.
Exactly the same consideration applies to the analysis of $\mathfrak{s}_{L_2-L_3}$. The result is shown in figure 1.5.

The weight α is the highest weight wrt the linear functional l given in equation (1.29). But this specific definition was arbitrary. We could have also defined l, such that $b > a > c$. As a consequence, the weight β (compare figure 1.5) would have been the highest weight instead of α. Under this circumstances, the same considerations would have been applicable. Thus, we can update the line which will enclose all the weights: compare figure 1.6.

Now, we continue to apply these considerations for other definitions of the linear functional l (totally 6 possibilities), until the line forms a closed boundary.

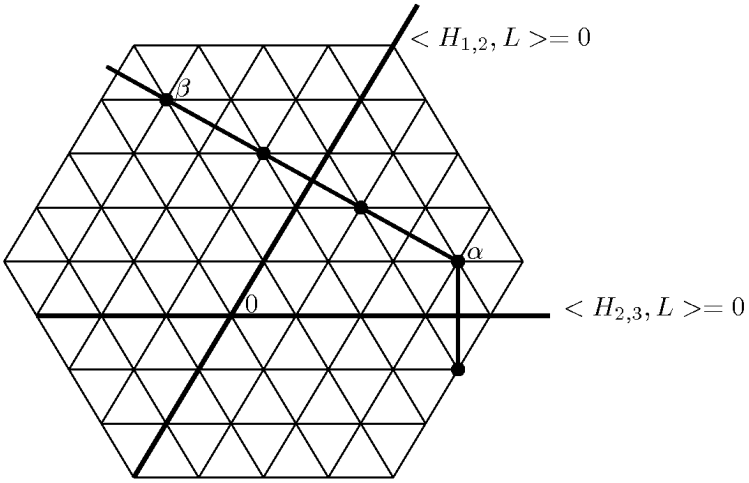

Figure 1.5: Upper and right boundary

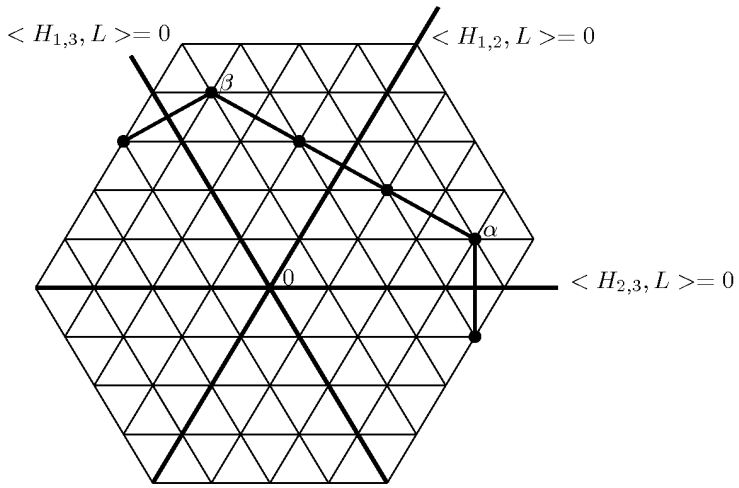

Figure 1.6: Upper, right and left boundary

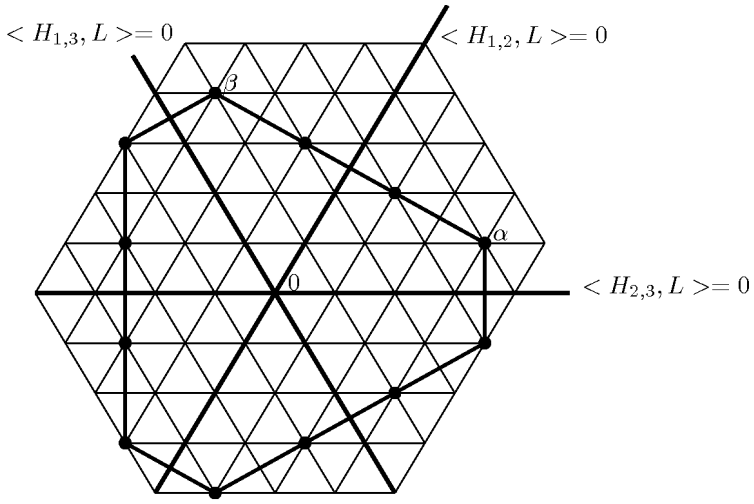

Figure 1.7: Convex hull

Observation 7. *Let π be a representation of $\mathfrak{sl}(3,\mathbb{C})$ with representation space V and highest weight α. Then: the vertices of the convex hull of the weights are exactly the images of α under the reflections in the three lines $\{L \in \mathfrak{h}^* | < H_{i,j}, L >= 0\}$ (compare figure 1.7). Thus, the convex hull forms a hexagon (if $\alpha \notin$ one of the three reflection-lines) or a triangle (if $\alpha \in$ one of the three reflection-lines).*

Claim 2. *Every weight γ is a linear combination of L_2 and L_3 (or equivalently of L_1 and L_3 or L_1 and L_2) with integer coefficients.*

Proof. Observe that from theorem 4 we deduce that all the eigenvalues of $\pi(H_{i,j})$ must be integer-valued, and that $\mathfrak{h} = \mathbb{C} \cdot H_{1,2} \oplus \mathbb{C} \cdot H_{1,3}$. Consider the arbitrary weight $\gamma = \lambda_1 L_1 + \lambda_2 L_2 + \lambda_3 L_3 \in \mathfrak{h}^*$ together with a vector $v \in V_\gamma$.

$$\begin{aligned}
\pi(H_{1,2})(v) &= \gamma(H_{1,2}) \cdot v \\
&= [\lambda_1 L_1(H_{1,2}) + \lambda_2 L_2(H_{1,2}) + \lambda_3 L_3(H_{1,2})] \cdot v \qquad (\lambda_i \in \mathbb{C}) \\
&= (\lambda_1 - \lambda_2) \cdot v \\
\pi(H_{1,3})(v) &= (\lambda_1 - \lambda_3) \cdot v \\
\pi(H_{2,3})(v) &= (\lambda_2 - \lambda_3) \cdot v
\end{aligned}$$

Thus, $(\lambda_1 - \lambda_2) \in \mathbb{Z}$, $(\lambda_1 - \lambda_3) \in \mathbb{Z}$ and $(\lambda_2 - \lambda_3) \in \mathbb{Z}$ and therefore $\lambda_2 = \lambda_1 + a$, $\lambda_3 = \lambda_1 + b$, with $a,\ b \in \mathbb{Z}$. We deduce

$$\begin{aligned}
\gamma &= \lambda_1 L_1 + \lambda_2 L_2 + \lambda_3 L_3 \\
&= \lambda_1 \cdot (L_1 + L_2 + L_3) + a \cdot L_2 + b \cdot L_3 \qquad (a,\ b \in \mathbb{Z}) \\
&= a \cdot L_2 + b \cdot L_3.
\end{aligned}$$

In the last step we have used identity (1.19). □

Here we see explicitly that the weights lie in a real subspace in $\mathfrak{h}$.
The linear combinations of the L_i's with integer coefficients form a lattice $\Lambda_W \subset \mathfrak{h}^*$ which is the so called *weight lattice*.
In the case of irreducible representations we can state the following proposition as a consequence of the claim above.

Proposition 7. *All weights of an irreducible representation of $\mathfrak{sl}(3,\mathbb{C})$ are elements of the weight lattice Λ_W and are congruent modulo the root lattice Λ_R (i.e., they differ by an integral linear combination of $L_i - L_j$).*

The Interior of the convex Hull

Let us reveal the interior of the convex hull enclosing all weights of a certain representation.
The subspace

$$W := \bigoplus_{k\in\mathbb{Z}} V_{\gamma+k(L_i-L_j)}$$

of V is a representation space of a representation of $\mathfrak{s}_{L_1-L_2} \cong \mathfrak{sl}(2,\mathbb{C})$. According to theorem 4, there exists an upper and lower bound k_1 and k_2 of $k \in \mathbb{Z}$, such that $V_{\gamma+k(L_i-L_j)} \neq \{0\}$ for all $k \in \{k_1,\ k_1+1,\ \ldots,\ k_2-1,\ k_2\}$. If we choose γ on the boundary of the convex hull, we recognize that there is a corresponding weight 'on the other side' of the convex hull (this is meant wrt. an arbitrary (i,j)-direction). It follows from the main theorem in the discussion of $\mathfrak{sl}(2,\mathbb{C})$ that the weights of a representation of $\mathfrak{sl}(2,\mathbb{C})$ form an *unbroken* string. The space in between of these two 'boundary-weights' has to be filled up with other weights (according to the remark before) such that the weights are congruent modulo Λ_R. We get the complete weight diagram (shown in figure 1.8) if we repeat this procedure for every 'boundary-weight' and every direction parallel to the lattice Λ_W.
Thus, we have proven the following proposition.

Proposition 8. *Let π be an arbitrary irreducible representation of $\mathfrak{sl}(3,\mathbb{C})$. Let $\alpha \in \mathfrak{h}^*$ be an 'extremal weight' ('extremal' means that $|l(\alpha)|$ is maximal with l denoting an arbitrary linear functional as in (1.29)). Then: all the weights lie in Λ_W, are congruent modulo Λ_R and are enclosed by the convex hull whose vertices are the images of α under the reflections at the three lines $\{L \in \mathfrak{h}^* | < H_{i,j}, L >= 0\}$.*

The Highest Weight Theorem

Assume that we are working with the specific form of the linear functional l given in (1.29). From the observation in the last subsection about the shape of

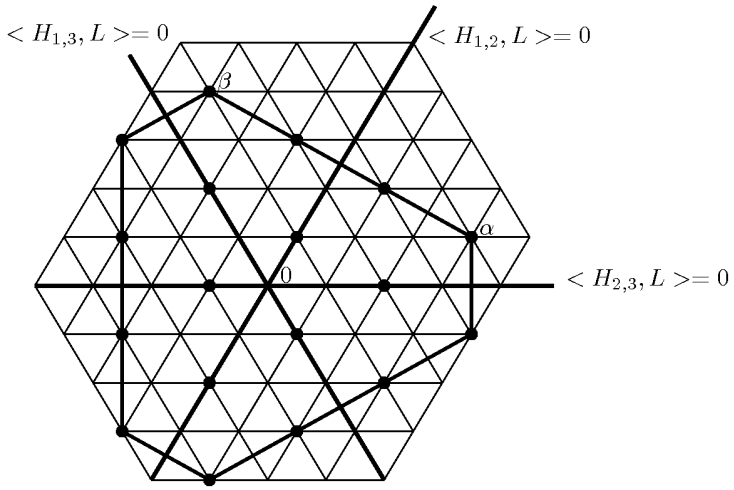

Figure 1.8: Complete weight diagram

the convex hull enclosing all weights (compare observation 7), we know that all possible highest weights must lie in the 60°-sector shown in figure 1.9. Thus,

Observation 8. *Every highest weight must be of the form (note that* $L_2 = -L_1 - L_3$*)*

$$(a+b)L_1 + bL_2 = aL_1 - bL_3$$

for a, b *being non-negative integers.*

Before we continue, we have to state a basic proposition about products of representations of Lie algebras and about the dual representation of a Lie algebra.

Proposition 9. *Let* π_1, π_2 *and* π *be representations of a Lie algebra* $\mathfrak{g}$ *with representation space* V*. Then:*

- $(\pi_1 \otimes \pi_2)(g) = \pi_1(g) \otimes 1 + 1 \otimes \pi_2(g)$ *(representation space:* $V \otimes V$*),*
- $(\pi_1 \wedge \pi_2)(g) = \pi_1(g) \wedge 1 + 1 \wedge \pi_2(g)$ *(representation space:* $V \wedge V$*),*
- $(\pi_1 \otimes_{sym} \pi_2)(g) = \pi_1(g) \otimes_{sym} 1 + 1 \otimes_{sym} \pi_2(g)$ *(representation space:* $V \otimes_{sym} V$*)*
- $\pi^*(g) = -\pi^T(g)$ *(representation space:* V^**),*

for all $g \in \mathfrak{g}$*.*

This proposition is proven in the appendix.

Corollary 5. *Let* π_1, π_2 *and* π *be representations of a Lie algebra* $\mathfrak{g}$ *with representation space* V*. Then:*

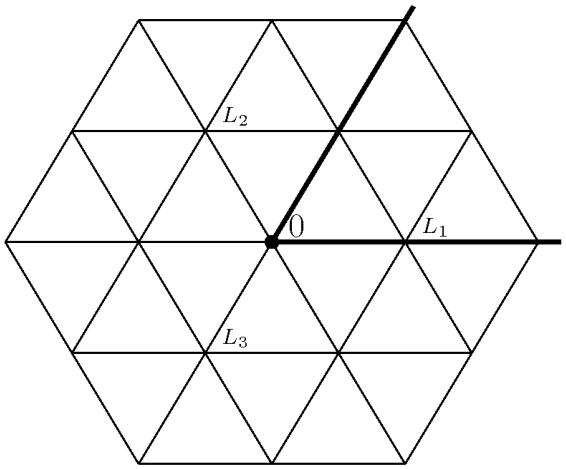

Figure 1.9: Locus of the highest weight vectors

- *The weights of the representation $\pi_1 \otimes \pi_2$ are the pairwise sum of the weights of the representations π_1 and π_2.*
- *The weights of the representation $\pi_1 \wedge \pi_2$ are the pairwise sum of distinct weights of the representations π_1 and π_2.*
- *The weights of the representation $\pi_1 \otimes_{sym} \pi_2$ are the pairwise sum of the weights of the representations π_1 and π_2.*
- *The weights of the representation π^* are the negative weights of the representation π.*

Proof. We confine us to the proof of the second assertion. Let w_1 be an eigenvector for $\pi_1(g)$ with eigenvalue γ and let w_2 be an eigenvector for $\pi_2(g)$ with eigenvalue ϵ. Then:

$$\begin{aligned}(\pi_1 \wedge \pi_2)(g)(w_1 \wedge w_2) &= (\pi_1(g) \wedge 1)(w_1 \wedge w_2) + (1 \wedge \pi_2(g))(w_1 \wedge w_2) \\ &= [\pi_1(g)(w_1)] \wedge w_2 + w_1 \wedge [\pi_2(g)(w_2)] \\ &= \gamma \cdot w_1 \wedge w_2 + \epsilon \cdot w_1 \wedge w_2 \\ &= [\gamma + \epsilon] \cdot w_1 \wedge w_2.\end{aligned}$$

Assume $w_2 = \lambda \cdot w_2 \Rightarrow\ w_1 \wedge w_2 = \lambda \cdot w_1 \wedge w_1 = 0$. Thus, the weights of the representation $\pi_1 \wedge \pi_2$ are the pairwise sum of *distinct* weights of the representations π_1 and π_2. □

Corollary 6. *Let π_1 and π_2 be two representations of $\mathfrak{sl}(3, \mathbb{C})$. Let v_1 and v_2 be the highest weight vectors with corresponding highest weights α_1 and α_2. Then: $v_1 \otimes v_2$ is a highest weight vector for $\pi_1 \otimes \pi_2$ with highest weight $\alpha_1 + \alpha_2$.*

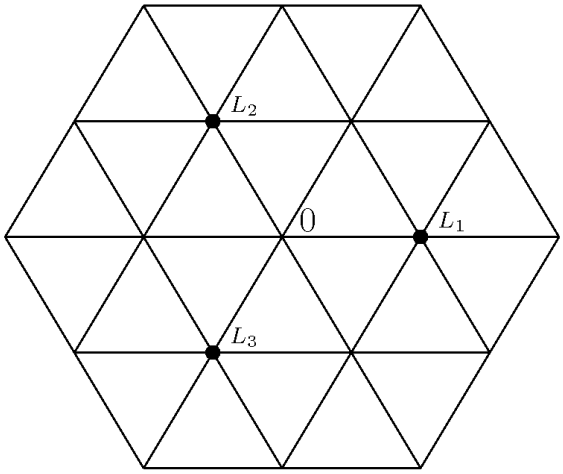

Figure 1.10: Weight diagram for the standard representation Σ

Let us examine the consequences for some specific representations which will be useful later on.
Let Σ be the standard representation of $\mathfrak{sl}(3,\mathbb{C})$ on $\mathbb{C}^3$. Since $\mathfrak{h}$ is the space of diagonal matrices given in (1.19), the weight vectors are the standard basis vectors e_1, e_2 and e_3 with corresponding weights L_1, L_2 and L_3. This yields the diagram given in figure 1.10.

The diagram for the dual representation Σ^* is shown in figure 1.11 (compare the corollary 5).

We immediately deduce the form of the diagrams corresponding to $Sym^2(\Sigma)$, $Sym^2(\Sigma^*)$, $Sym^3(\Sigma)$, $Sym^3(\Sigma^*)$, ... (compare figure 1.12, figure 1.13, figure 1.14 and 1.15). We recognize that the symmetric powers $Sym^n(\Sigma)$ and $Sym^m(\Sigma^*)$ yield exactly the triangular diagrams discussed in observation 7. Thus, $Sym^n(\Sigma)$ and $Sym^m(\Sigma^*)$ are *irreducible*, since all the weights have multiplicity 1 (i.e., they can't be a sum of irreducible diagrams).
Furthermore, $Sym^n(\Sigma)$ has highest weight $n \cdot L_1$ and $Sym^m(\Sigma^*)$ has highest weight $(-m) \cdot L_3$.
This enables us to construct representations of $\mathfrak{sl}(3,\mathbb{C})$ with arbitrary highest weight $aL_1 - bL_3$ by tensor products between $Sym^n(\Sigma)$ and $Sym^m(\Sigma^*)$ (compare observation 8 and corollary 6).
We are ready now to state the following important theorem.

Theorem (Highest Weight Theorem). *Let a and b be two non-negative integers. Then there exists a unique irreducible, finite-dimensional representation $\Gamma_{a,b}$ of $\mathfrak{sl}(3,\mathbb{C})$ with highest weight $aL_1 - bL_3$.*

Proof. We have to prove the existence and the uniqueness of the irreducible representation $\Gamma_{a,b}$.

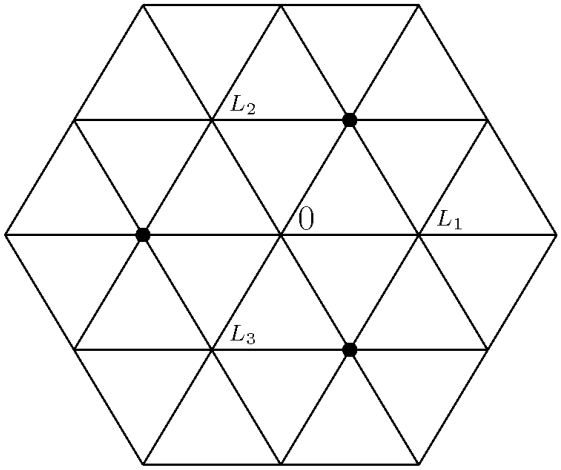

Figure 1.11: Weight diagram for Σ^*

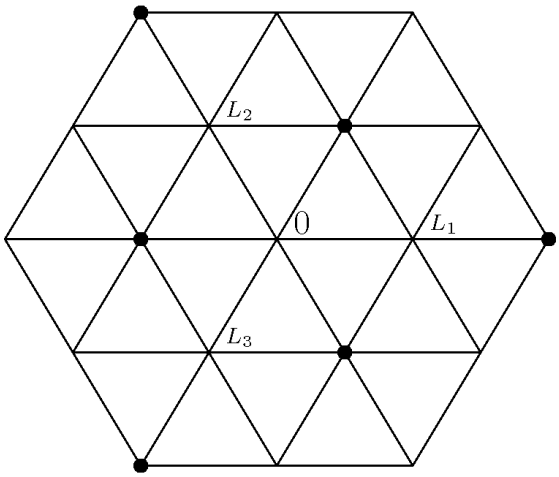

Figure 1.12: Weight diagram for $Sym^2(\Sigma)$

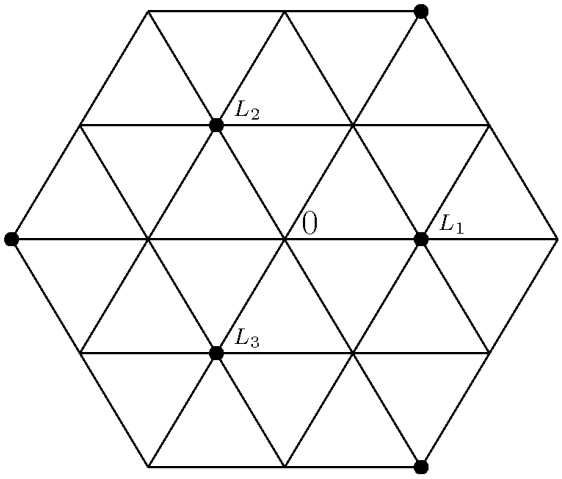

Figure 1.13: Weight diagram for $Sym^2(\Sigma^*)$

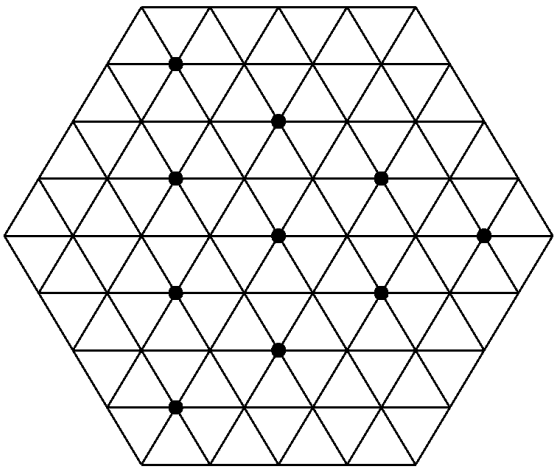

Figure 1.14: Weight diagram for $Sym^3(\Sigma)$

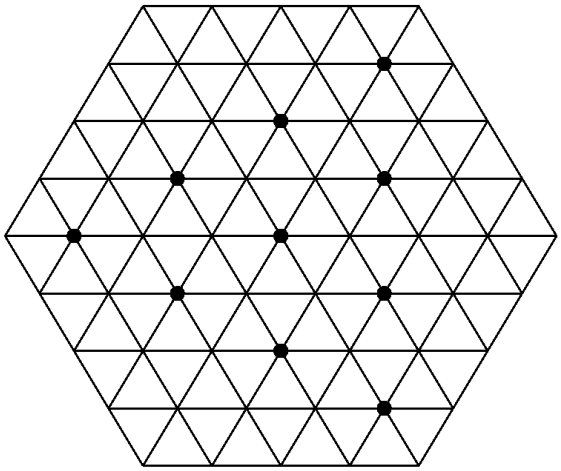

Figure 1.15: Weight diagram for $Sym^3(\Sigma^*)$

Existence: We have just learned that $Sym^a(\Sigma) \otimes Sym^b(\Sigma^*)$ has the desired highest weight. According to proposition 6, $Sym^a(\Sigma) \otimes Sym^b(\Sigma^*)$ contains an irreducible subrepresentation with the desired highest weight.
Uniqueness: Assume that there would exist another irreducible representation $\tilde{\Gamma}_{a,b}$ with the same highest weight. Let v and $\tilde{v}$ denote the highest weight vectors of $\Gamma_{a,b}$ and $\tilde{\Gamma}_{a,b}$ respectively and with representation spaces V and $\tilde{V}$ respectively. Then $(v, \tilde{v})$ is a highest weight vector of $\Gamma_{a,b} \oplus \tilde{\Gamma}_{a,b}$ with highest weight $aL_1 - bL_3$. Let $\Xi \subset \Gamma_{a,b} \oplus \tilde{\Gamma}_{a,b}$ be the irreducible representation with a representation space U generated by the highest weight vector $(v, \tilde{v})$ (compare proposition 6). The projections $\pi_1 : U \to V$ and $\pi_2 : U \to \tilde{V}$ are non-zero linear maps. Furthermore, $\pi_1 \circ \Xi = \Gamma_{a,b} \circ \pi_1$ and $\pi_2 \circ \Xi = \tilde{\Gamma}_{a,b} \circ \pi_2$. Therefore, we can apply Schur's lemma to get that π_1 and π_2 are isomorphisms which implies that $\Gamma_{a,b} \cong \tilde{\Gamma}_{a,b}$ (compare section 7). □

Corollary 7. *The irreducible representation $\Gamma_{a,b}$ is an irreducible subrepresentation of $Sym^a(\Sigma) \otimes Sym^b(\Sigma^*)$.*

Let us now describe the relation between $\Gamma_{a,b}$ and $Sym^a(\Sigma) \otimes Sym^b(\Sigma^*)$.

Proposition 10. *Assume that $b \leq a$. Then:*

$$Sym^a(\Sigma) \otimes Sym^b(\Sigma^*) = \bigoplus_{i=0}^{b} \Gamma_{a-i,b-i}.$$

Observation 9. *The multiplicities of $\Gamma_{a,b}$ increase by one on each hexagon of the weight diagram and are constant on each triangle (without proof).*

To finish this section we state an algorithm to decompose an arbitrary representation π of $\mathfrak{sl}(3, \mathbb{C})$ into irreducible representations:

1. Determine the decomposition of π into weight spaces.
2. Find the highest weight $\alpha = aL_1 - bL_3$ of π.
3. Define $\tilde{\pi}$ such that $\pi \cong \tilde{\pi} \oplus \Gamma_{a,b}$. The weight diagram of π 'minus' the weight diagram of $\Gamma_{a,b}$ is the weight diagram of $\tilde{\pi}$.
4. Repeat this process for $\tilde{\pi}$.

5 The Analysis of General Simple Lie Algebras

The procedure carried out in the last section to analyze $\mathfrak{sl}(3,\mathbb{C})$ can be generalized to an algorithm for the analysis of general complex semisimple Lie algebras. Each of the following subsections (until the subsection about the Killing form) stands for one step in the general algorithm. We will omit the general proofs.

Verification of the semisimplicity of the Lie algebra

Semisimplicity is crucial for the following discussion. If the Lie algebra $\mathfrak{g}$ is not semisimple, one can restrict the analysis to the semisimple part of $\mathfrak{g}$ to get the irreducible representations of $\mathfrak{g}$ (compare theorem 3).

Determination of the Cartan subalgebra $\mathfrak{h} \subset \mathfrak{g}$

Definition (Cartan Subalgebra). Let $\mathfrak{g}$ be a complex semisimple Lie algebra. Then a *Cartan subalgebra* $\mathfrak{h} \subset \mathfrak{g}$ is a complex subalgebra which is maximally commuting and whose action is diagonalizable in an arbitrary faithful representation.
The dimension of $\mathfrak{h}$ is the so called *rank* of $\mathfrak{g}$.

'Maximally commuting' means: if we add only one element in $\mathfrak{g} \setminus \mathfrak{h}$ to $\mathfrak{h}$ we loose the commutativity of $\mathfrak{h}$.
A representation is called 'faithful', if its homomorphism is one-to-one. From the Jordan decomposition theorem in section 2 we deduce that the Cartan subalgebra is diagonalizable in every faithful representation. Especially, the action of $\mathfrak{h}$ is diagonalizable in the adjoint representation.
All elements in $\mathfrak{h}$ are simultaneously diagonalizable since they commute.

Decomposition of $\mathfrak{g}$ into a direct sum of root spaces

Compare definition 17 and definition 18 for the terms 'weight', 'weight space', 'multiplicity', 'root', 'root space'.

In regard of the adjoint representation:

The adjoint action of $\mathfrak{h}$ on $\mathfrak{g}$ is diagonalizable. Thus, $\mathfrak{g}$ decomposes into the direct sum of its root spaces:

$$\begin{aligned} \mathfrak{g} &= \mathfrak{h} \oplus (\bigoplus \mathfrak{g}_\alpha) \\ ad(H)(X) &= \alpha(H) \cdot X, \end{aligned} \tag{1.30}$$

for all $H \in \mathfrak{h}$ and $X \in \mathfrak{g}_\alpha$. The index α in the direct sum ranges over the finite set $R \subset \mathfrak{h}^*$ of all roots. Note that $\mathfrak{h} = \mathfrak{g}_0$.
The calculation (1.25) proves that

$$ad(\mathfrak{g}_\alpha): \quad \mathfrak{g}_\beta \to \mathfrak{g}_{\alpha+\beta}. \tag{1.31}$$

We state without general proof the following properties of the configuration of the roots in $\mathfrak{h}^*$:

Observation 10. *1. Every root space $\mathfrak{g}_\alpha$ is one-dimensional.*

2. The rank of the root lattice $\Lambda_R \subset \mathfrak{h}^*$ generated by the roots is equal to the dimension of $\mathfrak{h}^*$.

3. The set R of all roots is symmetric about the origin, i.e. $\alpha \in R \Rightarrow -\alpha \in R$.

In regard of a general representation:

Let π be an arbitrary representation of a Lie algebra $\mathfrak{g}$ with representation space V. Then the representation space V decomposes into a direct sum of weight spaces V_α:

$$\begin{aligned} V &= \bigoplus V_\alpha \\ \pi(H)(v) &= \alpha(H) \cdot v, \end{aligned} \tag{1.32}$$

for all $H \in \mathfrak{h}$ and all $v \in V_\alpha$.
The fundamental calculation (1.26) proves that

$$\pi(\mathfrak{g}_\alpha): \quad V_\beta \to V_{\alpha+\beta}. \tag{1.33}$$

Let us assume that π is *irreducible*. Thus, there must not be any invariant subspace wrt. the action of $\mathfrak{g}$. Together with (1.26) we deduce that *the weights of an irreducible representation are congruent modulo the root lattice Λ_R.*
Like in the discussion of $\mathfrak{sl}(3,\mathbb{C})$ we can draw the so called *weight diagram* (compare for example figure 1.8).

Determination of subalgebras isomorphic to $\mathfrak{sl}(2,\mathbb{C}$

An important step in the discussion of $\mathfrak{sl}(3,\mathbb{C})$ was the discovery of subalgebras of $\mathfrak{sl}(3,\mathbb{C})$ which were isomorphic to $\mathfrak{sl}(2,\mathbb{C})$. Define

$$\mathfrak{s}_\alpha := \mathfrak{g}_\alpha \oplus \mathfrak{g}_{-\alpha} \oplus [\mathfrak{g}_\alpha, \mathfrak{g}_{-\alpha}]. \tag{1.34}$$

Then: $\mathfrak{s}_\alpha$ is a subalgebra of $\mathfrak{g}$ which is isomorphic to $\mathfrak{sl}(2,\mathbb{C})$ (without proof). Note that $\mathfrak{g}_\alpha$, $\mathfrak{g}_{-\alpha}$ are one-dimensional and that $[\mathfrak{g}_\alpha, \mathfrak{g}_{-\alpha}]$ is at most one-dimensional (compare observation 10).
We can chose a basis $X_\alpha \in \mathfrak{g}_\alpha$, $Y_\alpha \in \mathfrak{g}_{-\alpha}$ and $H_\alpha \in [\mathfrak{g}_\alpha, \mathfrak{g}_{-\alpha}]$ satisfying the commutation relations of $\mathfrak{sl}(2,\mathbb{C})$. This determines H_α (it must take the eigenvalues 2 and (-2) on $\mathfrak{g}_\alpha$ and $\mathfrak{g}_{-\alpha}$ respectively, i.e., $\alpha(H_\alpha) = 2$).

The weight lattice Λ_W

In the discussion of $\mathfrak{sl}(2,\mathbb{C})$ we learned that the eigenvalues of H are integer-valued in any representation. In the present case of $\mathfrak{s}_\alpha$ this means that the eigenvalues of the action H_α are integer-valued in any representation of $\mathfrak{s}_\alpha$.
In particular, the eigenvalues of the action of all elements $H_\alpha \in \mathfrak{h}$ found in subsection 5 must be integer-valued in any representation of $\mathfrak{g}$.
Therefore, every weight $\beta \in \mathfrak{h}^*$ of every representation of $\mathfrak{g}$ must yield integers when evaluated on any of the H_α's. The weights with this property form a lattice in $\mathfrak{h}^*$ called the *weight lattice* Λ_W of $\mathfrak{g}$.
Note: First, all weights of all representations of $\mathfrak{g}$ lie in Λ_W and second, $R \in \Lambda_W \;\Rightarrow\; \Lambda_R \subset \Lambda_W$.

Symmetry under the Weyl group

The pairing $< H_\alpha, \beta > \equiv \beta(H_\alpha)$ between elements in $\mathfrak{h}$ and elements in $\mathfrak{h}^*$ can be considered as a scalar product between α, $\beta \in \mathfrak{h}^*$.
We define the reflections $W_\alpha(\beta)$ in the plane $\Omega_\alpha := \{\beta \in \mathfrak{h}^* | < H_\alpha, \beta >= 0\}$ parallel to α:

$$\begin{aligned} W_\alpha(\beta) &:= \beta - 2 \cdot \frac{< H_\alpha, \beta >}{< H_\alpha, \alpha >} \cdot \alpha \\ &= \beta - 2 \cdot \frac{\beta(H_\alpha)}{\alpha(H_\alpha)} \cdot \alpha \\ &= \beta - \beta(H_\alpha) \cdot \alpha. \end{aligned} \tag{1.35}$$

(Recall from subsection 5 that $\alpha(H_\alpha) = 2$.)

Definition (Weyl Group). Let α be a weight of an arbitrary representation of $\mathfrak{g}$. Then: all the reflections

$$W_\alpha(\beta) := \beta - \beta(H_\alpha) \cdot \alpha$$

generate a group of reflections in $\mathfrak{h}^*$ called the *Weyl group* $\mathfrak{W}$.

Let us break up the set of weights into equivalence classes

$$[\beta]_\alpha = \{\text{weights } \gamma \mid \gamma = \beta + n \cdot \alpha,\ n \in \mathbb{Z}\}. \tag{1.36}$$

Similarly,

$$V_{[\beta]_\alpha} := \bigoplus_{n\in\mathbb{Z}} V_{\beta+n\alpha}. \tag{1.37}$$

Each of these spaces $V_{[\beta]_\alpha}$ realizes a representation of the subalgebra $\mathfrak{s}_\alpha \subset \mathfrak{g}$ when we restrict the original representation space V to $V_{[\beta]_\alpha}$, since $V_{[\beta]_\alpha}$ is closed under the action of $\mathfrak{s}_\alpha$ (compare (1.33)).

Proposition 11. *The set of weights of any representation of* $\mathfrak{g}$ *is invariant under the Weyl group* $\mathfrak{W}$.

Proof. It is possible to explicitly write down the whole string of weights that correspond to nonzero summands in (1.37)...
When we shift the representant β of the equivalence class to 'the boundary' $\tilde{\beta}$ of the string and write down the whole string as

$$\tilde{\beta},\ \tilde{\beta}+\alpha,\ \tilde{\beta}+2\alpha,\ \ldots\ ,\ \tilde{\beta}+m\alpha$$

for an integer $m \geq 0$. Then we arrive at the following string of integers

$$\tilde{\beta}(H_\alpha),\ (\tilde{\beta}+\alpha)(H_\alpha) = \tilde{\beta}(H_\alpha)+2,\ \ldots\ ,\ (\tilde{\beta}+m\alpha)(H_\alpha) = \tilde{\beta}(H_\alpha)+2m.$$

According to theorem 4, this string of integers has to be symmetric about the origin of $\mathbb{Z}$, i.e.,

$$\tilde{\beta}(H_\alpha) = -(\tilde{\beta}(H_\alpha)+2m) \Rightarrow \tilde{\beta}(H_\alpha) = -m \in \mathbb{Z}. \tag{1.38}$$

Thus, the whole string of weights corresponding to nonzero summands in (1.37) is

$$\tilde{\beta},\ \tilde{\beta}+\alpha,\ \tilde{\beta}+2\alpha,\ \ldots\ ,\ \tilde{\beta}-\tilde{\beta}(H_\alpha)\alpha. \tag{1.39}$$

In particular,

$$\begin{aligned} W_\alpha(\beta + k\cdot\alpha) &\equiv \beta + k\alpha - (\beta+k\alpha)(H_\alpha)\cdot H_\alpha \\ &= \beta + (m-k)\cdot\alpha. \end{aligned}$$

The same consideration shows that the multiplicities are symmetric wrt. the action of the Weyl group. This implies that the set of weights is invariant under the Weyl group. □

At this point we can introduce the so called *Killing form* on $\mathfrak{g}$. The Killing form on $\mathfrak{g}$ is an inner product on $\mathfrak{h}^*$ with the characteristic property that it is the unique inner product on $\mathfrak{h}^*$ which is preserved under the action of the Weyl group $\mathfrak{W}$ (i.e., the Weyl group acts as a group of orthogonal transformations). Equivalently, we could say that the Killing form is the unique inner product for which the line in $\mathfrak{h}^*$ spanned by α is perpendicular to the plane Ω_α. Thus, *the Weyl group is the group of transformations generated by the reflections in the planes* Ω_α *perpendicular to the root* α.

Ordering of the roots; the highest weight vector

As in the discussion of $\mathfrak{sl}(3,\mathbb{C})$ we define a linear functional l, such that its kernel doesn't intersect the root lattice Λ_R. This yields a decomposition

$$R = R^+ \cup R^-,$$

where $R^+ := \{roots\ \alpha \mid l(\alpha) > 0\}$ and $R^- := \{roots\ \alpha \mid l(\alpha) < 0\}$.

Definition 20. Let π be an arbitrary representation of $\mathfrak{g}$ with representation space V. Then a vector $v \in V$ is called a *highest weight vector* if v is simultaneously a weight vector and gets killed by the action of $\pi(\mathfrak{g}_\alpha)$ for all $\alpha \in R^+$. The weight α corresponding to v is called the *highest weight*.

Proposition 12. *Let $\mathfrak{g}$ be a complex semisimple Lie algebra.*

1. *There exists a highest weight vector for every finite-dimensional representation π of $\mathfrak{g}$.*
2. *Let π be a finite-dimensional representation of $\mathfrak{g}$ with representation space V and let $W \subset V$ denote the vector space generated by the images of the highest weight vector v under successive application of $\pi(\mathfrak{g}_\alpha)$ for all $\alpha \in R^-$. Then: the restriction of the original representation π to the representation space $W \subset V$ is an irreducible subrepresentation of $\mathfrak{g}$.*
3. *The highest weight vector of an irreducible representation is unique (up to multiplication with scalars).*

A root α is called *primitive* of *simple*, if it can't be written as a sum of two positive (respectively negative) roots.

Let us go over to the appearance of weight diagrams. As in the case of $\mathfrak{sl}(3,\mathbb{C})$ we make the following observation:

Observation 11. *The weights of a representation π are*

1. *congruent to the highest weight α modulo the root lattice Λ_R and*
2. *they lie in the convex hull with vertices being the images of α under the Weyl group.*

From what we have learned in (1.39) we deduce that the highest weight of a representation is a weight satisfying $\alpha(H_\gamma) \geq 0$ for all $\gamma \in R^+$.

Definition 21. The set of points in the real span of the roots which satisfy the inequalities $\alpha(H_\gamma) \geq 0$ for every $\gamma \in R^+$ is called the *Weyl chamber* $\mathcal{W}$ associated to the specific ordering of the roots.
In terms of the Killing form, this is the set of points making an angle between 0 and 90 degrees with *each* positive root.

Classification of the irreducible representations

We arrive at the fundamental theorem which we won't prove in general but it should be evident after what we have done so far.

Theorem (Highest Weight Theorem). *Let $\alpha \in \mathfrak{h}^*$ be a point in the intersection between the Weyl chamber $\mathcal{W}$ (which is associated to a specific ordering of the roots) and the weight lattice Λ_W.*
Then: there exists a unique irreducible, finite-dimensional representation Γ_α of $\mathfrak{g}$ with highest weight α.
The weights of Γ_α are the elements of Λ_W congruent to α modulo the root lattice Λ_R which are enclosed by the convex hull generated by the images of α under the action of the Weyl group.

There always exist so called *fundamental weights* $\omega_1,\ \omega_2,\ \ldots\ \omega_n$, such that every highest weight can be expressed as a linear combination of the fundamental weights with non-negative, integer-valued coefficients. (Geometrically these are the weights on the edges of the Weyl chamber.) One usually writes $\Gamma_{a_1,\ \ldots\ ,\ a_n}$ instead of Γ_α if $\alpha = a_1\omega_1 + \ \ldots\ + a_n\omega_n$.
Before we finish this section, we should say a few words about the Killing form which we introduced in section 5.

The Killing Form

There are several different ways to define the Killing form. We mention two possibilities.

Definition (Killing Form (version 1)). The *Killing form* $(\cdot,\cdot)$ on $\mathfrak{g}$ is the symmetric bilinear form (hence an inner product) on $\mathfrak{g}$ defined by

$$(X, Y) := tr(ad(X) \circ ad(Y) :\ \mathfrak{g} \to \mathfrak{g}),$$

for all X and Y in $\mathfrak{g}$. This induces inner products on $\mathfrak{h}$ and $\mathfrak{h}^*$ respectively which are denoted in the same way.

Definition (Killing Form (version 2)). The *Killing form* $(\cdot,\cdot)$ on $\mathfrak{g}$ is the symmetric bilinear form (hence an inner product) on $\mathfrak{g}$ defined by the characteristic property that the Killing form is invariant under the group of automorphisms on $\mathfrak{g}$.

Note that the decomposition

$$\mathfrak{g} = \mathfrak{h} \oplus (\bigoplus_{\alpha \in R} \mathfrak{g}_\alpha)$$

is *orthogonal* according to the first definition, since $ad(\mathfrak{g}_\alpha) :\ \mathfrak{g}_\beta \to \mathfrak{g}_{\alpha+\beta}$.
One reason why we introduce the Killing form is the following proposition:

Proposition 13. *The line in $\mathfrak{h}^*$ spanned by a root α is perpendicular (wrt. the Killing form $(\cdot,\cdot)$) to the hyperplane Ω_α.*

From this proposition one can deduce that the Weyl chamber is the set of vectors in $\mathfrak{h}^*$ which form an acute angle (wrt. $(\cdot,\cdot)$) with all positive roots.

Now we state an explicit isomorphism between $\mathfrak{h}$ and $\mathfrak{h}^*$ which is determined by the Killing form.

Proposition 14. *The isomorphism between $\mathfrak{h}^*$ and $\mathfrak{h}$, which is determined by the Killing form, maps an element α to*

$$T_\alpha := \frac{2}{(H_\alpha, H_\alpha)} \cdot H_\alpha.$$

Conversely, the inverse isomorphism maps

$$H_\alpha \;\to\; \frac{2}{(\alpha,\alpha)} \cdot \alpha.$$

Using this notation, we define the induced *Killing form on* $\mathfrak{h}^*$:

$$(\alpha,\beta) := (T_\alpha, T_\beta). \tag{1.40}$$

From the orthogonality of the action of the Weyl group and (1.38) one can deduce the next proposition.

Proposition 15. *Let α and β be two roots. Then:*

$$2 \cdot \frac{(\beta,\alpha)}{(\alpha,\alpha)} = \beta(H_\alpha)$$

is an integer.

6 The Classification of Complex Semisimple Lie Algebras

In the first part of this section, we introduce and classify all Dynkin diagrams whereas in the second part, we try to recover the Lie algebra from its corresponding Dynkin diagram.

Dynkin Diagrams and their Classification

As we have already indicated, the roots span a real subspace of the Cartan subalgebra $\mathfrak{h}^*$. On this space the Killing form is positive definite (without proof). This real vector space together with the Killing form $(\cdot,\cdot)$ yields a Euclidean space $\mathbb{E}$. A positive root is called *simple* if it is not the sum of two other positive roots. We list the central properties of a root system:

Proposition 16. *Let R be a root system. Then:*

1. *The root system R is a finite set and its elements span the Euclidean space $\mathbb{E}$.*
2. *$\alpha \in R \;\Rightarrow\; -\alpha \in R$.*
3. *$k \cdot \alpha \notin R$ for all $k \in \mathbb{Z} \setminus \{\pm 1\}$*
4. *The root system R is invariant under the action of the Weyl group $\mathfrak{W}$.*
5. *The quantity*
$$n_{\beta\alpha} := 2 \cdot \frac{(\beta, \alpha)}{(\alpha, \alpha)}$$
is an integer for every $\alpha,\ \beta \in R$.
6. *Let α and β be two roots such that $\beta \neq \pm\alpha$. Then: the α-string through β (i.e., $\beta - p\alpha, \ldots, \beta, \ldots, \beta + q\alpha$) consists of at most four elements. Additionally, $p - q = n_{\beta\alpha}$.*
7. *Let α and β be two roots such that $\beta \neq \pm\alpha$. Then:*
$$\begin{aligned} (\beta, \alpha) > 0 \;&\Rightarrow\; \alpha - \beta \text{ is a root}, \\ (\beta, \alpha) < 0 \;&\Rightarrow\; \alpha + \beta \text{ is a root}. \end{aligned}$$
If $(\beta, \alpha) = 0$, then $\alpha - \beta$ and $\alpha + \beta$ are both roots or both aren't roots.
8. *The angle between distinct simple roots cannot be acute.*
9. *The simple roots are linearly independent.*
10. *The number of simple roots is equal to $n = dim_{\mathbb{C}}\ \mathfrak{h} = dim_{\mathbb{R}}\ \mathbb{E}$.*
11. *Every positive root can be written uniquely as a non-negative integral combination of simple roots.*

The integer n is called the rank of the Lie algebra or the root system.

The fifth property implies a strong restriction on the possible geometric configurations of the roots:
Let θ be the angle (wrt. the Killing form) between two arbitrary roots α and β. We deduce that
$$n_{\beta\alpha} = 2 \cdot \frac{(\beta, \alpha)}{(\alpha, \alpha)} = 2\cos(\theta) \cdot \frac{\|\beta\|}{\|\alpha\|}. \tag{1.41}$$
Thus,
$$n_{\beta\alpha} n_{\alpha\beta} = 4\cos^2(\theta) \tag{1.42}$$

θ	$\pi/6$	$\pi/4$	$\pi/3$	$\pi/2$	$2\pi/3$	$3\pi/4$	$5\pi/6$
$\frac{\|\beta\|}{\|\alpha\|}$	$\sqrt{3}$	$\sqrt{2}$	1	*	1	$\sqrt{2}$	$\sqrt{3}$

Table 1.1: The geometry of the root system

is an integer between 0 and 4. All possible configurations are shown in the following table.

We list all possible root systems of rank 1 and 2.

Rank 1. The only possible root system is the root system corresponding to $\mathfrak{sl}(2,\mathbb{C})$:

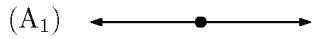

Rank 2. The root system for $\mathfrak{sl}(2,\mathbb{C}) \times \mathfrak{sl}(2,\mathbb{C}) \cong \mathfrak{so}_4(\mathbb{C})$ is $A_1 \times A_1$. The root system for $\mathfrak{sl}(3,\mathbb{C})$ is A_2. The root system for $\mathfrak{so}_5(\mathbb{C}) \cong \mathfrak{sp}_4(\mathbb{C})$ is B_2. The root system for the exceptional Lie algebra $\mathfrak{g}_2$ is G_2.

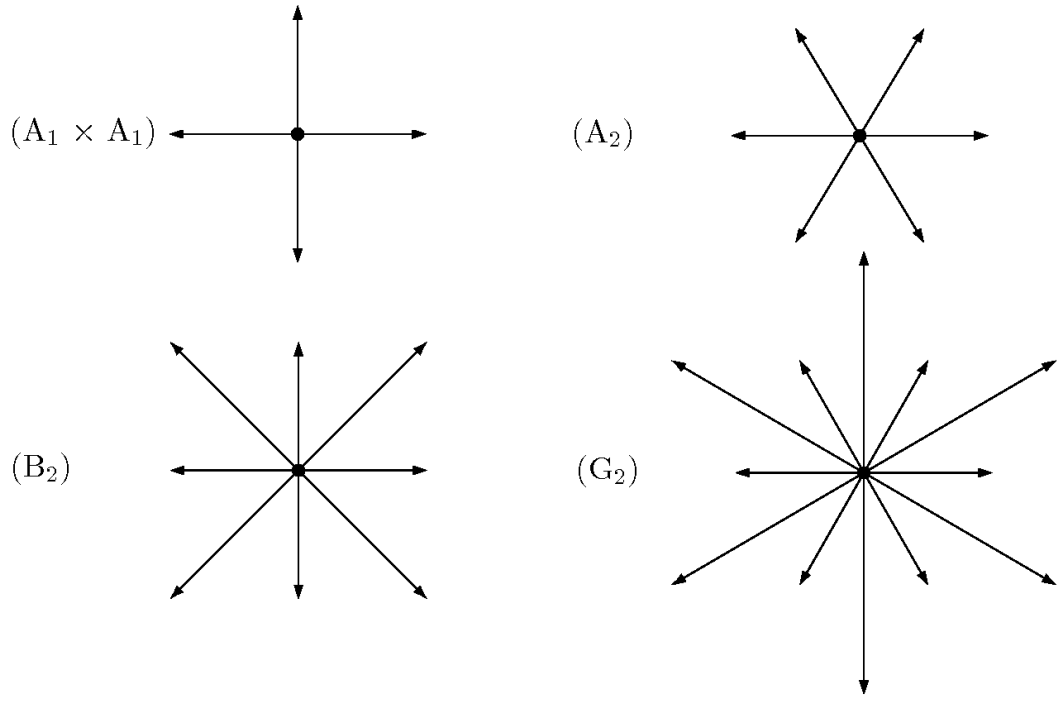

Definition 22. The direct sum of two root systems is a root system. A root system is called *irreducible* if it is not a direct sum of two other root systems.

Dynkin Diagrams. The Dynkin diagram for a certain root system is a diagram consisting of nodes ◯ for each *simple* root and lines joining them. The number of lines between the nodes is defined by the angle θ between the specific simple roots. When there is more than one line joining two nodes then the corresponding simple roots can have different length. In this case one includes an arrow into the diagram pointing from the longer to the shorter simple root.

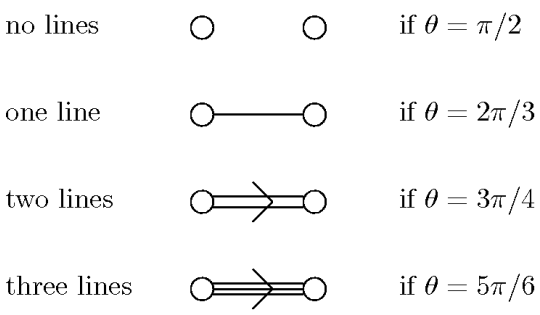

Note that a Dynkin diagram contains the knowledge of (α_i, α_j) for all $i \neq j$.

Two Dynkin diagrams are *isomorphic* if there exists a one-to-one onto map of the nodes such that the number of lines between the nodes and such that the direction of the arrows are preserved. The root diagrams are independent of the specific ordering of the roots.

Now we state the crucial classification theorem which classifies every irreducible root system. Its proof is completely based on Euclidean geometry (compare table 1.1).

Theorem (Classification of Dynkin Diagrams). *The Dynkin diagrams given in figure 1.16 are all possible Dynkin diagrams of irreducible root systems. With the correspondences*

$$\begin{array}{lcl} (A_n) & \leftrightarrow & \mathfrak{sl}_{n+1}(\mathbb{C}) \\ (B_n) & \leftrightarrow & \mathfrak{so}_{2n+1}(\mathbb{C}) \\ (C_n) & \leftrightarrow & \mathfrak{sp}_{2n}(\mathbb{C}) \\ (D_n) & \leftrightarrow & \mathfrak{sl}_{2n}(\mathbb{C}) \end{array}$$

To complete the classification of complex simple Lie algebras, we would have to prove the following theorem:

Theorem 5. *1. Let R_1 and R_2 be two root systems for two different Cartan subalgebras of the same complex semisimple Lie algebra. Then: R_1 and R_2 are isomorphic.*

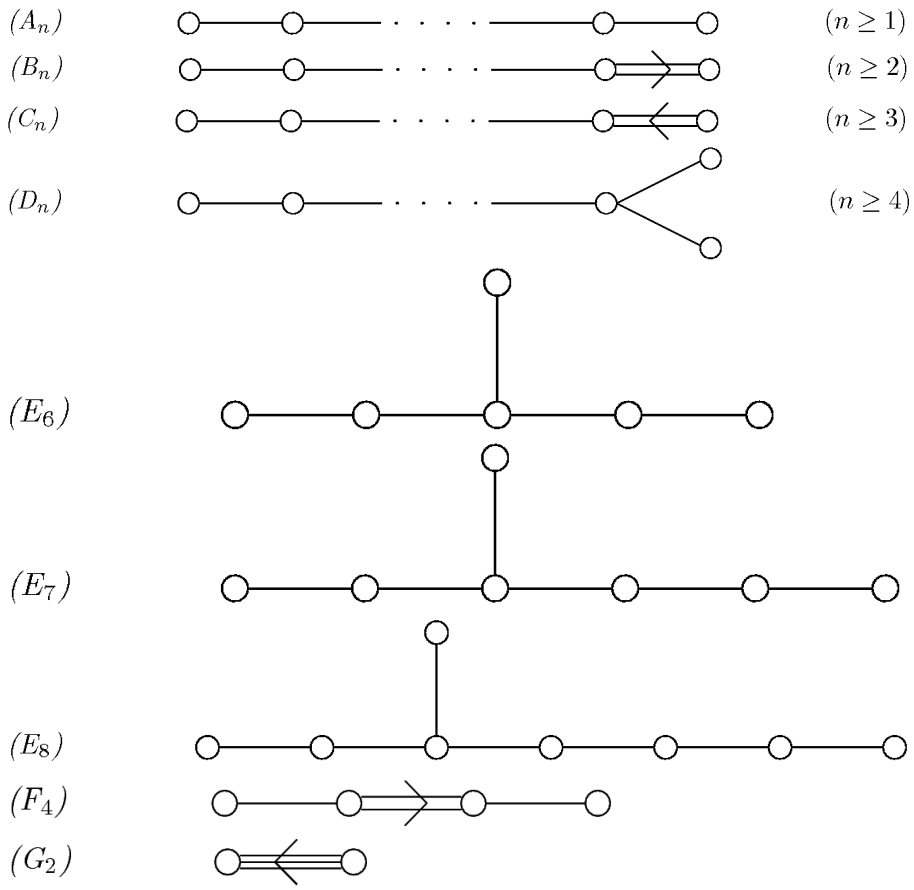

Figure 1.16: All irreducible Dynkin diagrams.

2. *A complex semisimple Lie algebra is simple iff its root system is irreducible.*

3. *Complex semisimple Lie algebras which have isomorphic root systems are isomorphic.*

4. *Every root system arises as the root system of a complex semisimple Lie algebra.*

A semisimple Lie algebra is determined (up to isomorphisms) by the specification of its simple summands.

Reconstruction of a Lie Algebra from its Dynkin Diagram

This section consists of two parts: first, we learn how to get the root system of a given Dynkin diagram and second, we learn how to recover the Lie algebra from its root system. Therefore, we will be able to reconstruct the Lie algebra from its Dynkin diagram.

Reconstruction of the root system from its Dynkin Diagram

The *simple* roots follow directly from the diagram; we denote them $\alpha_1, \ldots, \alpha_n$. According to 11th property of proposition 16, all positive roots can be written as an integral linear combination with non-negative coefficients. In the following, we will try to answer the question: Which non-negative integral linear combinations $\sum_{i=0}^{n} m_i\alpha_i$ are roots? The answer to this question determines all the positive roots and therefore the entire root system.
Let $\beta = \sum_{i=0}^{n} m_i\alpha_i$ be any positive root. Then: $\sum_{i=0}^{n} m_i$ is the so called *level* of β.

Claim 3. *1. Every positive root γ can be written in the form*

$$\gamma = \beta + \alpha_j,$$

where β is a root or 0 and α_j is a simple root.

2. Let $\beta = \sum_{i=0}^{n} m_i\alpha_i$ be a positive root and let α_j be a simple root. Then: $\beta + \alpha$ is a root iff

$$p > n_{\beta\alpha_j} \equiv 2 \cdot \frac{(\beta, \alpha_j)}{(\alpha_j, \alpha_j)} = \sum_{i=0}^{n} m_i \cdot n_{\alpha_i\alpha_j},$$

where p is the lower bound for the α_j-string, i.e.,

$$\beta - p\alpha, \ldots, \beta, \ldots, \beta + q\alpha.$$

Furthermore, $p \leq m_j$.

Proof. Let $\gamma = \sum_{i=1}^{n} r_i\alpha_i$ be a positive root with level $m + 1$. Since the Killing form is positive definite on the root system, we have

$$0 < (\gamma, \gamma) = \sum r_i \cdot (\gamma, \alpha_i).$$

Thus, $(\gamma, \alpha_i) > 0$ for some i with $r_i > 0$ (if all quantities (γ, α_i) and r_i were negative, level $m + 1$ of γ wouldn't be possible). Using the 7th property of proposition 16, we deduce that $\gamma - \alpha_i$ is a root. Therefore, γ was of the form $\beta + \alpha_j$. This proves the first statement.
Assume we would know all positive roots with level $\leq m$ and let β be any *positive* root with level m. Question: Is $\beta + \alpha_j$ a root?
If $\beta + \alpha_j$ is a root it has to be contained in the α_j-string

$$\beta - p\alpha_j, \ldots, \beta, \ldots, \beta + q\alpha_j$$

through β, i.e., we have to demand $q_{\alpha_j - string} > 0$. This is equivalent to $p > n_{\beta\alpha_j}$ (compare the 6th property of proposition 16).
property 11 of proposition 16 says that no root can be written as a linear combination with mixed signs. β is a positive root by assumption. Therefore, $\beta - p\alpha$ is a positive root $\Rightarrow$ $p \leq m_j$ □

Reconstruction of the simple Lie Algebra from its root system

The process of the reconstruction of the simple Lie Algebra from its root system can be divided into three steps:

1. Define a basis of the Lie algebra.
2. Compute the entire multiplication table of all elements in the basis.
3. Check that the structure we have gotten (i.e., the vector space spanned by the basis together with the multiplication table) really defines a simple Lie algebra.

What one would have to prove is the following

1. The multiplication table is determined by the Dynkin diagram.
2. Existence: There exists a simple Lie algebra for each Dynkin diagram.
3. Uniqueness: The simple Lie algebra corresponding to a certain Dynkin diagram is unique up to isomorphisms.

Now, we describe, how one can find a basis of $\mathfrak{g}$.
Let $\alpha_1, \ldots, \alpha_n$ denote the simple roots which follow directly from the root system. These simple roots realize a basis in $\mathfrak{h}^*$. After the discussion in the last subsection we know how to get the entire root system from the set of simple roots.
Let $\gamma \in R^+$ be an arbitrary positive root. The goal is to find a basis for the Cartan subalgebra $\mathfrak{h}$ and every root space $\mathfrak{g}_\gamma$ (which are one-dimensional), since

$$\mathfrak{g} = \mathfrak{h} \oplus (\bigoplus \mathfrak{g}_\epsilon).$$

We need two ingredients to construct the basis. The first one is the following lemma.

Lemma 6. *Let α, $\beta \neq \pm\alpha$ and $\alpha + \beta$ be roots. Then:*

$$[\mathfrak{g}_\alpha, \mathfrak{g}_\beta] = \mathfrak{g}_{\alpha+\beta}.$$

Proof. We have already seen that $[\mathfrak{g}_\alpha, \mathfrak{g}_\beta] \subset \mathfrak{g}_{\alpha+\beta}$ and that all root spaces are one-dimensional. What is left to show is that $[\mathfrak{g}_\alpha, \mathfrak{g}_\beta] \neq 0$.
Consider the α-string

$$\bigoplus_{k\in\mathbb{Z}} \mathfrak{g}_{\beta+k\cdot\alpha}.$$

If $\beta \neq \pm\alpha$ the α-string realizes an irreducible representation of $\mathfrak{sl}(2,\mathbb{C})$, since all the root spaces in the string are one-dimensional.
Assume that $[\mathfrak{g}_\alpha, \mathfrak{g}_\beta] = 0$. Then: the following two parts of the string

$$\bigoplus_{n\geq 2} \mathfrak{g}_{\beta+n\cdot\alpha} \qquad \bigoplus_{l\geq 0} \mathfrak{g}_{\beta-l\cdot\alpha}$$

wouldn't mix under the action of $ad(\mathfrak{g}_\alpha)$, i.e., they would realize subrepresentations which is a contradiction to the observation of irreducibility above. □

The second ingredient is the observation we made in the last subsection that we can write the arbitrary positive root γ in the form (compare claim 3)

$$\gamma = \alpha_{i_1} + \ \ldots \ + \alpha_{i_r}, \tag{1.43}$$

such that

$$\alpha_{i_1} + \ \ldots \ + \alpha_{i_s} \tag{1.44}$$

is a root for every $s \in \{1, \ \ldots \ , \ r\}$.
From these two ingredients we deduce the following:
Once we have found the basis elements for all root spaces corresponding to simple roots and for $\mathfrak{g}_{\alpha_{i_1}+\ \ldots\ +\alpha_{i_{r-1}}}$, the basis element for $\mathfrak{g}_\gamma \equiv \mathfrak{g}_{\alpha_{i_1}+\ \ldots\ +\alpha_{i_r}}$ follows directly by the application of '$ad(basis\ of\ \mathfrak{g}_{\alpha_{i_r}})$', since

$$ad(\mathfrak{g}_{\alpha_{i_r}}): \quad \mathfrak{g}_{\alpha_{i_1}+\ \ldots\ +\alpha_{i_{r-1}}} \ \rightarrow \ \mathfrak{g}_{\alpha_{i_1}+\ \ldots\ +\alpha_{i_r}} \equiv \mathfrak{g}_\gamma.$$

Thus, to begin, we have to determine the basis for $\mathfrak{h}$ and for all the simple root spaces $\mathfrak{g}_{\alpha_i}$:
Choose $X_i \in \mathfrak{g}_{\alpha_i}$ and $Y_i \in \mathfrak{g}_{-\alpha_i}$ arbitrarily. Define $H_i := [X_i, Y_i]$. Adjust Y_i, such that

$$[H_i, X_i] = 2 \cdot X_i \ and \ [H_i, Y_i] = -2 \cdot Y_i.$$

Therefore, $span\{H_i, \ X_i, \ Y_i\} = \mathfrak{s}_{\alpha_i} \cong \mathfrak{sl}(2,\mathbb{C})$.
We repeat this procedure for every simple root α_i. We finally get a basis for $\mathfrak{g}_{\alpha_i}$ and $\mathfrak{g}_{-\alpha_i}$ for every $1 \leq i \leq n$ and a basis for $\mathfrak{h}$ (since $dim\ \mathfrak{h} = dim\ \mathfrak{h}^*$). Then we can complete the basis of $\mathfrak{g}$ as described above.

7 Appendix

Products of representations and dual representations

Definition 23. Let G be a Lie group and let Π_1 and Π_2 be representations of G on vector spaces V_1 and V_2. Then:

- $\Pi_1 \otimes \Pi_2(g) := \Pi_1(g) \otimes \Pi_2(g)$
- $\Pi_1 \wedge \Pi_2(g) := \Pi_1(g) \wedge \Pi_2(g)$

- $\Pi_1 \otimes_{sym} \Pi_2(g) := \Pi_1(g) \otimes_{sym} \Pi_2(g)$
- $\Pi_1^*(g) := \Pi^T(g^{-1})$

for all $g \in G$.

Proposition 17. *Let π_1, π_2 and π be representations of a Lie algebra $\mathfrak{g}$ with representation space V. Then:*

- $(\pi_1 \otimes \pi_2)(g) = \pi_1(g) \otimes 1 + 1 \otimes \pi_2(g)$ *(representation space: $V \otimes V$),*
- $(\pi_1 \wedge \pi_2)(g) = \pi_1(g) \wedge 1 + 1 \wedge \pi_2(g)$ *(representation space: $V \wedge V$),*
- $(\pi_1 \otimes_{sym} \pi_2)(g) = \pi_1(g) \otimes_{sym} 1 + 1 \otimes_{sym} \pi_2(g)$ *(representation space: $V \otimes_{sym} V$)*
- $\pi^*(g) = -\pi^T(g)$ *(representation space: V^*),*

for all $g \in \mathfrak{g}$.

Proof. We only prove the second assertion, because the proofs of the others follow in an analogue way.
Let $u(t)$ and $v(t)$ be two general curves in a vector space V. Then:

$$\begin{aligned}
& \frac{d}{dt}(u(t) \wedge v(t)) = \lim_{h \to 0} \frac{u(t+h) \wedge v(t+h) - u(t) \wedge v(t)}{h} \\
= & \lim_{h \to 0} \frac{u(t+h) \wedge v(t+h) - u(t+h) \wedge v(t)}{h} + \frac{u(t+h) \wedge v(t) - u(t) \wedge v(t)}{h} \\
= & \lim_{h \to 0} u(t+h) \wedge \frac{v(t+h) - v(t)}{h} + \frac{u(t+h) - u(t)}{h} \wedge v(t) \\
= & u(t) \wedge \frac{d}{dt} v(t) + \frac{d}{dt} u(t) \wedge v(t).
\end{aligned}$$

Let $\mathfrak{g}$ be the Lie algebra of G, let $X \in \mathfrak{g}$ and let $u,\ v \in V$. Then:

$$\begin{aligned}
& \pi_1 \wedge \pi_2(X)(u \wedge v) \equiv \frac{d}{dt}|_{t=0} (\Pi_1 \wedge \Pi_2)(e^{tX})(u \wedge v) \\
= & \frac{d}{dt}|_{t=0} (\Pi_1(e^{tX}) \wedge \Pi_2(e^{tX}))(u \wedge v) \\
= & (\frac{d}{dt}|_{t=0} \Pi_1(e^{tX})) \wedge \Pi_2(e^{tX})(u \wedge v) + \Pi_1(e^{tX}) \wedge (\frac{d}{dt}|_{t=0} \Pi_2(e^{tX}))(u \wedge v) \\
= & (\pi_1(X) \wedge 1)(u \wedge v) + (1 \wedge \pi_2(X))(u \wedge v).
\end{aligned}$$

□

Schur's Lemma

Theorem (Schur's Lemma). *1. Let π and π' be two irreducible representations of a group G with representation spaces V and V'. Assume that $L \cdot \pi(g) = \pi'(g) \cdot L$ for a linear map $L: V \to V'$ and all $g \in G$.*
Then: either $L \equiv 0$ or L is a vector space isomorphism.

2. Let π be a finite-dimensional irreducible representation of a group G with representation space V, let L be a linear map $L: V \to V$ such that $L \cdot \pi(g) = \pi(g) \cdot L$ for all $g \in G$.
Then: $L = \lambda \cdot 1$ on V with $\lambda \in \mathbb{C}$.

3. Let π be a finite-dimensional irreducible and Abelian representation of a group G with representation space V.
Then: V is one-dimensional.

2 Goldstone bosons and the Higgs mechanism

Stefan Pfenninger
Supervisor: Stefan Fredenhagen

Starting with the fact that the Lagrangian of electrodynamics is locally invariant under the transformation group $U(1)$, i.e. $\phi \to \exp(i\alpha(x))\phi$, $\mathcal{A}_\mu \to \mathcal{A}_\mu + ie\partial_\mu\alpha(x)$, the first part of this report will consider the opposite question of how possible Lagrangians that have such an invariance might look like in general. Astonishingly, we get quite similar results by replacing the Abelian group $U(1)$ with a general non-Abelian group G. Using these experiences, in the second part we will consider the concept of spontaneous symmetry breaking again in two parts. Firstly we will look at the case of a global symmetry to be broken what leads us to Goldstone's theorem and secondly we consider the case of a local symmetry breaking, what leads us to the Higgs mechanism. This important concept appears in many real physical problems and we discuss briefly this appearance in the electroweak theory and in superconductivity. Write here a short summary of your talk. It should contain all important informations and catch the readers attention.

1 Non-Abelian gauge invariance

Motivation and conventions

Considering the Lorentz invariant Lagrangian density for scalar electrodynamics[1], one can see that it is locally gauge invariant under the group $U(1)$, whereby local gauge invariance means that the transformation can depend on the space-time point x, and global invariance would mean invariance under a constant transformation.
In the first section, we will derive the rather astonishing result that one can also "derive" the Lagrangian density for scalar electrodynamics by only assuming this local gauge invariance under $U(1)$. This leads us to the idea that we might create other interesting theories by using more general groups. So we will first have a look at the group $SU(2)$ and then generalize the methods to a general symmetry group.
We will use natural units ($\hbar = 1 = c$) and Einstein's sum convention in which Greek indices run from $(0, .., 3)$ and roman indices from $(1, .., 3)$. In this section, we follow [3] and [4].

Abelian gauge invariance - U(1) gauge theory

Starting with the complex-valued scalar field ϕ, we assume that our theory has to be invariant under the transformation

$$\phi(x) \to V(x)\phi(x) \qquad , \qquad V(x) := e^{i\alpha(x)} \in U(1). \tag{2.1}$$

The phase rotation $\alpha(x)$ is an arbitrary real function, depending on the point of space-time, since we want to discuss a local gauge invariance. If we want to find out what kind of Lagrangian matches our requirement of local $U(1)$ invariance, we simply consider the different transformation behaviors of the possible terms that a Lagrangian can have. Of course, if we only take $U(1)$ invariant terms to build a Lagrangian, we can ensure its local $U(1)$ invariance.
First, we consider a mass term

$$m\phi^*\phi(x). \tag{2.2}$$

We see that such terms are invariant under both global and local $U(1)$ transformation and do not need further considerations.

[1]

$$\begin{aligned} \mathcal{L}(\phi, \mathcal{D}_\mu\phi) &= -\frac{1}{4}\mathcal{F}_{\mu\nu}\mathcal{F}^{\mu\nu} + \frac{1}{2}(\mathcal{D}_\mu\phi)^*\mathcal{D}^\mu\phi - V(\phi^*\phi) \quad \text{where} \\ \mathcal{D}_\mu &:= \partial_\mu\phi + i\mathcal{A}_\mu\phi \quad \text{and} \quad \mathcal{A} \quad \text{the Lorentz covariant potential.} \end{aligned}$$

It becomes more interesting when we have a look at terms including derivatives of ϕ. While the behavior under a global transformation is

$$\partial^\mu \phi(x) \to V \partial^\mu \phi(x),$$

the one under a local transformation is

$$\partial^\mu \phi(x) \to V(x)\partial^\mu \phi(x) + \phi(x)\partial^\mu V(x).$$

The reason of the appearance of a second term becomes more clear if we have a look at the definition of the derivative in a given direction n,

$$n^\mu \partial_\mu \phi(x) := \lim_{\epsilon \to 0} \frac{1}{\epsilon}[\phi(x + \epsilon n) - \phi(x)]. \tag{2.3}$$

We can see that, since the transformation (2.1) depends on the point in space-time, both summands have a completely different transformation under (2.1). One idea to solve this problem is to introduce a factor $U(y, x)$ called *comparator* that compensates the difference in phase transformations from one point to the next with the transformation law

$$U(y, x) \to V(y)U(y, x)V(x)^{-1}. \tag{2.4}$$

This ensures that $\phi(x)$ and $U(x, y)\phi(y)$ transform in the same way. Of course, the comparator has to ensure $U(x, x) = 1$. We can now define an operator $\mathcal{D}$ called *covariant derivative*:

$$n^\mu \mathcal{D}_\mu \phi(x) := \lim_{\epsilon \to 0} \frac{1}{\epsilon}[\phi(x + \epsilon n) - U(x + \epsilon n, x)\phi(x)]. \tag{2.5}$$

Using the expansion for the two points to be close together, we get

$$U(x + \epsilon n, x) = 1 - ie\epsilon n^\mu \mathcal{A}_\mu(x) + O(\epsilon^2), \tag{2.6}$$

in which the $\mathcal{A}_\mu$ is a new real vector field called *gauge field* or *connection*. Thus, the covariant derivative takes the form

$$\mathcal{D}_\mu \phi(x) = \partial_\mu \phi(x) + ie\mathcal{A}_\mu(x)\phi(x), \tag{2.7}$$

and by inserting(2.6) into (2.4) and comparing the ϵ-coefficients:

$$\begin{aligned}
U(x + \epsilon n, x) &\to e^{i\alpha(x+\epsilon n)}(1 - ie\epsilon n^\mu \mathcal{A}_\mu(x) + O(\epsilon^2))e^{-i\alpha(x)} \\
&= e^{i\alpha(x)+i\partial_\mu \alpha(x)\epsilon n^\mu + O(\epsilon^2)} e^{-i\alpha(x)}(1 - ie\epsilon n^\mu \mathcal{A}_\mu(x) + O(\epsilon^2)) \\
&= (1 + i\partial_\mu \alpha(x)\epsilon n^\mu)(1 - ie\epsilon n^\mu (A)_\mu(x)) + O(\epsilon^2) \\
&= 1 - ie\epsilon n^\mu \mathcal{A}_\mu + i\partial_\mu \alpha(x)\epsilon n^\mu + O(\epsilon^2) \\
\Rightarrow \mathcal{A}_\mu(x) &\to \mathcal{A}_\mu(x) - \frac{1}{e}\partial_\mu \alpha(x).
\end{aligned} \tag{2.8}$$

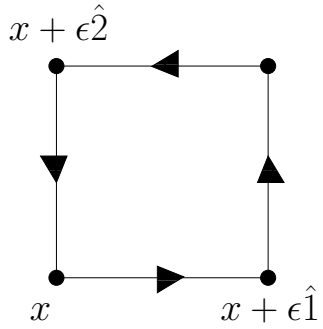

Figure 2.1: square in the (1,2)-plane of space-time, used for the construction of a field strength

If we check the behavior of $\mathcal{D}$ under the local symmetry transformation (2.1) we find

$$\begin{aligned} \mathcal{D}_\mu\phi(x) &\rightarrow e^{(i\alpha(x))}\partial_\mu\phi(x) + \phi(x)\partial_\mu e^{(i\alpha(x))} + (ie\mathcal{A}_\mu(x) - i\partial_\mu\alpha(x))e^{(i\alpha(x))}\phi(x) \\ &= e^{(i\alpha(x))}[\partial_\mu + ie\mathcal{A}_\mu]\phi(x), \end{aligned}$$

hence

$$\mathcal{D}_\mu\phi(x) \rightarrow e^{i\alpha(x)}\mathcal{D}_\mu\phi(x). \tag{2.9}$$

Note that the definition of the covariant derivative as well as the existence and the transformation law of the gauge field $\mathcal{A}_\mu$ are a direct consequence of the condition of the local symmetry. Without these constructs we would not be able to write an invariant Lagrangian.

To complete the construction, we also need to find locally invariant terms that depend on $\mathcal{A}_\mu$ and its derivatives, but not on $\phi(x)$ itself. Once again, we consider the comparator $U(y,x)$. To simplify we make some assumptions about $U(y,x)$; it should be a pure phase $U(y,x) = e^{i\beta(y,x)}$ with $\beta(y,x)$ an arbitrary real function, and $U(x,y)^\dagger = U(y,x)$. For ϵ small, this leads to an approximation [2]

$$U(x+\epsilon n, x) = e^{-ie\epsilon n^\mu \mathcal{A}_\mu(x+\frac{\epsilon}{2}n)+O(\epsilon^3)}. \tag{2.10}$$

Now consider a small square lying in the (1,2)-plane of the space-time with unit vectors $\hat{1}$ and $\hat{2}$ (see Fig. 2.1). Define $\mathbb{U}(x)$ as the product of four $U(y,x)$ - functions so that the new function $\mathbb{U}(x)$ is invariant under (2.1):

$$\mathbb{U}(x) := U(x, x+\epsilon\hat{2})U(x+\epsilon\hat{2}, x+\epsilon\hat{1}+\epsilon\hat{2})U(x+\epsilon\hat{1}+\epsilon\hat{2}, x+\epsilon\hat{1})U(x+\epsilon\hat{1}, x). \tag{2.11}$$

[2] Consider the equation $U(y,x) = e^{-ie\int_{P_{xy}} d\tilde{x}^\mu \mathcal{A}_\mu(\tilde{x})}$ which accomplish all the conditions on a comparator and this for any line P_{xy} (*"Wilson line"*) running from x to y. Now $\int_x^{x+\epsilon n} \mathcal{A}_\mu(\tilde{x})d\tilde{x}n^\mu = \epsilon n^\mu \mathcal{A}_\mu(x+\frac{\epsilon n}{2}) + O(\epsilon^3)$ can be proved by integrating the well known equation $f(x+\epsilon) = f(x+\frac{\epsilon}{2}) + \frac{\epsilon}{2}\frac{\partial}{\partial\epsilon}f(x+\frac{\epsilon}{2}) + O(\epsilon^2)$ over ϵ using the boundaries $[0,\epsilon]$.

Because $\mathbb{U}(x)$ is invariant under (2.1) even for $\epsilon \to 0$, and by using (2.10) we get a locally invariant function of $\mathcal{A}_\mu$:

$$\begin{aligned}\mathbb{U}(x) &= \exp(-ie\epsilon[-\mathcal{A}_2(x+\frac{\epsilon}{2}\hat{2}) \\ &\quad -\mathcal{A}_1(x+\frac{\epsilon}{2}\hat{1}+\epsilon\hat{2})+\mathcal{A}_2(x+\epsilon\hat{1}+\frac{\epsilon}{2}\hat{2})+\mathcal{A}_1(x+\frac{\epsilon}{2}\hat{1})]+O(\epsilon^3)),\end{aligned}$$

and expanded:

$$\mathbb{U}(x) = 1 - ie\epsilon^2[\partial_1\mathcal{A}_2(x) - \partial_2\mathcal{A}_1(x)] + O(\epsilon^3). \tag{2.12}$$

Since $\mathbb{U}(x)$ is locally invariant, $\mathcal{F}_{\mu\nu} := \partial_\mu\mathcal{A}_\nu(x) - \partial_\nu\mathcal{A}_\mu(x)$ is so as well. $\mathcal{F}_{\mu\nu}$ is called *field strength tensor*. If we think of the Lagrangian of electrodynamics, we can see that $\mathcal{F}_{\mu\nu}$ corresponds to the electromagnetic field tensor.

A shorter approach of finding the invariance of $\mathcal{F}_{\mu\nu}$ starts with the covariant derivative: since $\mathcal{D}_\mu\phi(x) \to V(x)\mathcal{D}_\mu\phi(x) : [\mathcal{D}_\mu, \mathcal{D}_\nu]\phi(x) \to V(x)[\mathcal{D}_\mu, \mathcal{D}_\nu]\phi(x)$, what implies that $[\mathcal{D}_\mu, \mathcal{D}_\nu]$ is invariant under (2.1) [3]. A closer look at the commutator $[\mathcal{D}_\mu, \mathcal{D}_\nu]$ shows that it is not a derivative at all:

$$\begin{aligned}[\mathcal{D}_\mu, \mathcal{D}_\nu]\phi(x) &= [\partial_\mu, \partial_\nu]\phi(x) + ie([\partial_\mu, \mathcal{A}_\nu] - [\partial_\nu, \mathcal{A}_\mu])\phi(x) \\ &\quad -e^2[\mathcal{A}_\mu, \mathcal{A}_\nu]\phi(x) \\ &= ie(\partial_\mu\mathcal{A}_\nu(x) - \partial_\nu\mathcal{A}_\mu(x))\phi(x),\end{aligned}$$

and that with the definition of $\mathcal{F}_{\mu\nu}$ we can write

$$[\mathcal{D}_\mu, \mathcal{D}_\nu] = ie\mathcal{F}_{\mu\nu} \tag{2.13}$$

and that it is thus invariant.
We can now create a Lagrangian out of ϕ, $\mathcal{D}\phi$ and of $\mathcal{F}_{\mu\nu}$ and its derivatives. When we assume that operators with dimension not larger than 4 make sure that the theory keeps renormalizable, only 5 terms can appear:

$$\mathcal{L} = (\mathcal{D}_\mu\phi)^*\mathcal{D}^\mu\phi - \frac{1}{4}(\mathcal{F}_{\mu\nu})^2 - ic\epsilon^{\alpha\beta\mu\nu}\mathcal{F}_{\alpha\beta}\mathcal{F}_{\mu\nu} - m\phi^*\phi + a(\phi^*\phi)^2, \tag{2.14}$$

where the $-\frac{1}{4}$ in the second term is just conventional. The U(1) group, which was a global symmetry has become a local symmetry group and is now called *gauged*.
Note that we achieved this result only by assuming a local symmetry; furthermore, the existence of an electromagnetic vector potential appears naturally. If we insist on having a Lagrangian $\mathcal{L}$ that is also invariant under time reversal or parity, the third term disappears and our construction remind us on the Lorentz invariant Lagrangian density for scalar electrodynamics.

[3] this argument is only true when V(x) and $[\mathcal{D}_\mu, \mathcal{D}_\nu]$ do commute. In the $U(1)$ case this is of course the case since V(x) is a scalar function. In the next section though, we will see that this invariance is no more true.

Non-Abelian Gauge Theory and the Yang-Mills Lagrangian

In this section, we want to generalize the methods of the previous section in which we assumed the symmetry group to be the Abelian Group $U(1)$. We now want to consider a general group G as a symmetry group which is in particular non-Abelian. Before we start to generalize the results from the previous section, we first write down some conditions on the general group and very briefly some facts about Lie algebras.

Mathematical concepts As we have seen in the last section, our gauge theory is related to a symmetry group, which we had to gauge. In order to use similar methods like we did in the Abelian case, the symmetry group G must be at least a *continuous* group. We actually focus our attention only on *continuously generated groups*, which means that the group contains elements arbitrarily close to the identity. This condition allows us to write an infinitesimal group element g in the form of

$$g(\alpha) = 1 + i\alpha^a X^a + O(\alpha^2) \qquad , \qquad X^a \in Lie(G). \tag{2.15}$$

The set of *generators* X^a span a vector space[4], and so the commutator of generators X^a is a linear combination of generators,

$$[X^a, X^b] = i\mathfrak{f}^{abc} X^c \tag{2.16}$$

in which the $\mathfrak{f}^{abc}$ are called *structure constants*.
We can choose X^a to be a set of hermitian generators [5] and because of the *Jacobi identity* of the X^a , $[X^a, [X^b, X^c]] + [X^b, [X^c, X^a]] + [X^c, [X^a, X^b]] = 0$ we get

$$\mathfrak{f}^{ade}\mathfrak{f}^{bcd} + \mathfrak{f}^{bde}\mathfrak{f}^{cad} + \mathfrak{f}^{cde}\mathfrak{f}^{abd} = 0, \tag{2.17}$$

where it can be proved that $\mathfrak{f}^{abc}$ are totally antisymmetric.

Another nice concept we will use is the irreducible representation *ad* of a Group G, called the *adjoint representation* whose definition is

$$G \to Aut(V) \qquad , \qquad g \mapsto (v \mapsto gvg^{-1}). \tag{2.18}$$

The representation matrices of the associated representation of the Lie algebra of G are given by the structure constants,

$$(\rho^*(X^b))_{ac} = i\mathfrak{f}^{abc} \qquad , \qquad X^b \in Lie(G). \tag{2.19}$$

[4]Note that the definition of a generator A of a group element a is here the equation $a = e^{iA}$ and not e^A.

[5]We know that there is a scalar product in the representational vector space for every representation of the group G such that the representational matrix is unitary. According to this fact, the generators of G can be represented by hermitian matrices X^a.

Methods of generalization illustrated by the group SU(2) We are now ready to generalize the methods to a general symmetry group G. Because $SU(2)$ is a well known example for such a group, we will apply the results to this group to illustrate the effect more concretely.

We start now with the more general situation using a set of N fields instead of a single field:

$$\psi(x) = \begin{pmatrix} \psi_1(x) \\ \vdots \\ \psi_N(x) \end{pmatrix} \tag{2.20}$$

For the $SU(2)$ case, it is enough to have $N = 2$,

$$\psi(x) = \begin{pmatrix} \psi_1(x) \\ \psi_2(x) \end{pmatrix}. \tag{2.21}$$

$\psi(x)$ transforms analogously to the Abelian case,

$$\psi(x) \to V(x)\psi(x) \quad , \quad V(x) := \exp(i\alpha^a(x)X^a) \in G \tag{2.22}$$

where X^a are the hermitian generators of the group G and the index a goes from $1, .., dim(G)$.
For $G = SU(2)$, we have $X^a = \frac{\sigma^a}{2}$ with $\sigma^j, (j = 1, 2, 3)$ the hermitian Pauli spin matrices. Expanding $V(x)$ for a small α yields

$$V(x) = 1 + i\alpha^a(x)X^a + O(\alpha^2). \tag{2.23}$$

Now we want to gauge the group by changing (2.22) into a local symmetry group. This can be ensured by insisting on the condition that the Lagrangian should be invariant under (2.22) for $\alpha = \alpha(x)$ an arbitrary function of x. We will now try to use the same methods as in the previous section, in which our symmetry group was $U(1)$. One fundamental difference is that the generators X^a do not have to commute as in the Abelian case. For $G = SU(2)$ this is the case since the Pauli matrices do not commute.
In general, the field theory with a non-commuting local symmetry is called a *non-Abelian gauge theory.*
Exactly as in the Abelian case, we introduce a comparator $U(y, x)$, but since ψ is a N component object, $U(y, x)$ has to be a $N \times N$ matrix. Again we claim $U(x, x) = \mathrm{id}$ and the transformation law to be

$$U(y, x) \to V(y)U(y, x)V(x)^\dagger. \tag{2.24}$$

Assuming $U(y, x)$ to be a unitary matrix, we can expand $U(y, x)$ in terms of the hermitian generators of G, and for a small distance between the two points x and y, we have

$$U(x + \epsilon n, x) = \mathrm{id} + ig\epsilon n^\mu \mathcal{A}_\mu{}^a X^a + O(\epsilon^2). \tag{2.25}$$

The constant g is extracted and we will use it later. As one can see, the new fields $\mathcal{A}_\mu$ are elements of the Lie algebra $Lie(G)$,

$$\mathcal{A}_\mu = \mathcal{A}_\mu{}^a X^a \tag{2.26}$$

and the $\mathcal{A}_\mu{}^a$ are called *Yang-Mills fields*. For $G = SU(2)$ we get analogously $\mathcal{A}_\mu = \mathcal{A}_\mu{}^j \frac{\sigma^j}{2}$. If we write the new expansion (2.25) in the old definition (2.5), then we get a new expression for the covariant derivative:

$$\mathcal{D}_\mu = \partial_\mu - ig\mathcal{A}_\mu{}^a X^a \tag{2.27}$$

Now we want to find the gauge transformation law of the Yang-Mills fields $\mathcal{A}_\mu$. Inserting (2.25) in (2.24):

$$1 + ig\epsilon n^\mu \mathcal{A}_\mu{}^a X^a \to V(x+\epsilon n)(1 + ig\epsilon n^\mu \mathcal{A}_\mu{}^a X^a)V^\dagger(x) \tag{2.28}$$

Using $V(x+\epsilon n) = (1+\epsilon n^\mu \partial_\mu)V(x) + O(\epsilon^2)$ and $\partial_\mu V(x) = -\partial_\mu V^\dagger(x)$ one obtains by comparing the terms proportional to $ig\epsilon n^\mu$:

$$\mathcal{A}_\mu{}^a(x) X^a \to V(x)[\mathcal{A}_\mu{}^a(x) X^a + \frac{i}{g}\partial_\mu]V^\dagger(x). \tag{2.29}$$

The infinitesimal transformation laws for ψ and $\mathcal{A}_\mu{}^a$ are:

$$\begin{aligned} \psi &\to (1 + i\alpha^a X^a)\psi \qquad \text{and} \\ \mathcal{A}_\mu{}^a(x) &\to \mathcal{A}_\mu{}^a(x) + \frac{1}{g}\partial_\mu \alpha^a + f^{abc}\mathcal{A}_\mu{}^b(x)\alpha^c \end{aligned} \tag{2.30}$$

In order to check that the new covariant derivative transforms as

$$\mathcal{D}_\mu \psi(x) \to V(x)\mathcal{D}_\mu \psi(x) \tag{2.31}$$

one might use (2.29) and show it in a straight forward way. This calculation is not so easy, because there are lots of matrices that do not commute with each other. Since our construction (2.5) does not need such a verification, we leave the calculation to those who do not believe [6].

Again, we need to find gauge-invariant terms that depend only on $\mathcal{A}_\mu$. Inspired by the Abelian case, we consider the commutator of covariant derivatives and its transformation

$$[\mathcal{D}_\mu, \mathcal{D}_\nu]\psi(x) \to V(x)[\mathcal{D}_\mu, \mathcal{D}_\nu]\psi(x). \tag{2.32}$$

Just as in the Abelian case, we can show that $[\mathcal{D}_\mu, \mathcal{D}_\nu]$ is not a differential operator anymore but only a multiplicative factor in form of a $N \times N$ matrix which does not commute with the matrix $V(x)$ anymore:

$$[\mathcal{D}_\mu, \mathcal{D}_\nu] = -ig\mathcal{F}_{\mu\nu}{}^a X^a \tag{2.33}$$

[6] For $G = SU(2)$, this calculation is done in [3] but only for a small α.

where

$$\mathcal{F}_{\mu\nu}{}^a X^a = \partial_\mu \mathcal{A}_\nu{}^a X^a - \partial_\nu \mathcal{A}_\mu{}^a X^a - ig[\mathcal{A}_\mu{}^a X^a, \mathcal{A}_\nu{}^a X^a]. \tag{2.34}$$

This expression can be simplified if we remember the commutation relations (2.16) of the generators X^a,

$$\mathcal{F}_{\mu\nu}{}^a X^a = \partial_\mu \mathcal{A}_\mu{}^a X^a - \partial_\nu \mathcal{A}_\nu{}^a X^a + g\mathfrak{f}^{abc} \mathcal{A}_\mu{}^b \mathcal{A}_\nu{}^c \mathcal{X}^a. \tag{2.35}$$

In the $SU(2)$ case, we remember the commutation relations of the Pauli matrices, $[\frac{\sigma^j}{2}, \frac{\sigma^k}{2}] = i\epsilon^{jkl}\frac{\sigma^l}{2}$, with the antisymmetric structure constants ϵ^{jkl}. As usual, the equation (2.35) for the $SU(2)$ case looks the same, we only have to replace X^a by $\frac{\sigma^j}{2}$.
From the equations (2.24) (2.32) and (2.33) we can conclude that the new field strength tensor transforms according to the adjoint representation

$$\mathcal{F}_{\mu\nu}{}^a X^a \to V(x)\mathcal{F}_{\mu\nu}{}^a X^a V(x)^\dagger, \tag{2.36}$$

or in the infinitesimal form

$$\begin{aligned} \mathcal{F}_{\mu\nu}{}^a X^a &\to \mathcal{F}_{\mu\nu}{}^a X^a + [i\alpha^a X^a, \mathcal{F}_{\mu\nu}{}^b X^b] \qquad \Leftrightarrow \\ \mathcal{F}_{\mu\nu}{}^a &\to \mathcal{F}_{\mu\nu}{}^a - \mathfrak{f}^{abc}\alpha^b \mathcal{F}_{\mu\nu}{}^c \end{aligned} \tag{2.37}$$

Note that the field strength tensor is no longer gauge-invariant, since the factors (matrices!) in equation (2.36) do not commute anymore. However, in an appropriate normalization, we can still find gauge-invariant terms out of the field strength tensor, for example the term

$$tr[(\mathcal{F}_{\mu\nu}{}^a X^a)^2] = \frac{1}{2}(\mathcal{F}_{\mu\nu}{}^a)^2. \tag{2.38}$$

Such a term in a Lagrangian would describe a nontrivial, interacting field theory, because it contains cubic and quartic terms in $\mathcal{A}_\mu{}^a$. Such a theory is called *Yang-Mills theory*.
Using the equations (2.30) and (2.37), it is possible to show that any globally symmetric function of ψ , $\mathcal{F}_{\mu\nu}{}^a$ and their covariant derivatives is also locally symmetric, and might possibly appear in a Lagrangian.
However, as we have already seen in equation (2.14), in a renormalizable theory, not so many terms are possible, and under the assumption that our Lagrangian preserves time reversal and parity, only four terms are allowed:

$$\mathcal{L} = \mathcal{D}_\mu \phi^* \mathcal{D}^\mu \phi - \frac{1}{4}(\mathcal{F}_{\mu\nu}{}^a)^2 - m\phi^*\phi + a(\phi^*\phi)^2. \tag{2.39}$$

Using the Euler-Lagrange equations

$$\partial_\mu \frac{\partial \mathcal{L}}{\partial(\partial_\mu \phi^\alpha)} - \frac{\partial \mathcal{L}}{\partial \phi^\alpha} = 0, \tag{2.40}$$

the corresponding classical equations of motion follow,

$$\partial^\mu \mathcal{F}_{\mu\nu}{}^a + g\mathfrak{f}^{abc}\mathcal{A}^{b\mu}\mathcal{F}^c_{\mu\nu} = -gj_\nu{}^a \tag{2.41}$$

where

$$j_\nu{}^a = -i[(\mathcal{D}_\nu\phi)^* X^a\phi - \phi^* X^a(\mathcal{D}_\nu\phi)]. \tag{2.42}$$

Now we want to adjust the covariant derivative on the adjoint representation, that means if a field $\xi(x)$ does not transform the way equation (2.1) shows, but in the adjoint representation, we want $\mathcal{D}$ acting on $\xi(x)$ to respect that, in the way that the second term of $\mathcal{D}$ should act on the field $\xi(x)$ according to the adjoint representation and its corresponding Lie algebra representation ρ^* respectively,

$$(\mathcal{D}_\mu\xi)_a \quad = \quad \partial_\mu\xi_a - ig\mathcal{A}_\mu{}^b(\rho^*(X^b))_{ac}\xi_c \quad = \quad \partial_\mu\xi_a + g\mathfrak{f}^{abc}\mathcal{A}_\mu{}^b\xi_c, \tag{2.43}$$

where we used equation (2.19). Together with equation (2.43) we can write equation (2.30) in the new form

$$\mathcal{A}_\mu{}^a \to \mathcal{A}_\mu{}^a + \frac{1}{g}(\mathcal{D}_\mu\alpha)^a \tag{2.44}$$

and equation (2.37) becomes

$$(\mathcal{D}^\mu\mathcal{F}_{\mu\nu})^a = -gj_\nu{}^a. \tag{2.45}$$

One can see that with this generalization of the covariant derivative - now it respects the transformation behaviors of the fields it acts on - the strange-looking terms involving $\mathfrak{f}^{abc}$ are gone and even for a general symmetry group G we receive the same results as in the previous sections only by generalizing the covariant derivative.

To finish this section, we want to show that there is, of course, an analogue of the homogeneous Maxwell equations in electrodynamics[7] . We first consider the antisymmetric double commutator of covariant derivatives

$$\epsilon^{\mu\nu\lambda\sigma}[\mathcal{D}_\nu, [\mathcal{D}_\lambda, \mathcal{D}_\sigma]] = 0. \tag{2.46}$$

The term vanishes because of its total antisymmetry[8]. Since we know that $[\mathcal{D}_\lambda, \mathcal{D}_\sigma] = -ig\mathcal{F}_{\lambda\sigma}{}^a X^a$, equation (2.46) can be reduced to

$$\epsilon^{\mu\nu\lambda\sigma}(\mathcal{D}_\nu\mathcal{F}_{\lambda\sigma})^a = 0 \tag{2.47}$$

which is the equation corresponding to the homogeneous Maxwell equation.

[7] Remember that also in the classical electrodynamic theory, the homogeneous Maxwell equation do not follow from the Euler-Lagrange equations. Because the field strength tensor $\mathcal{F}_{\mu\nu}$ is defined by the Lorentz invariant potential $\mathcal{A}_\mu$, the homogeneous Maxwell equation follows automatically.

[8] Since $\epsilon^{\mu\nu\lambda\sigma}$ is a total antisymmetric tensor with $\epsilon^{1234} = 1$, only 3! terms are non-zero when the first component is fixed. If for example we fix the 4^{th} coefficient,

$$\epsilon^{4123} = \epsilon^{4231} = \epsilon^{4312} = -1 \quad , \quad \epsilon^{4213} = \epsilon^{4132} = \epsilon^{4321} = 1 \quad \text{, and the rest all zero.}$$

2 Goldstone bosons and the Higgs mechanism

Everything in this chapter will be done for classical field theory except for the particle interpretation out of a Lagrangian density. Our results are therefore not completely correct, but one might see that what we derive can be interpreted as the first terms in a quantum expansion. A discussion of quantum corrections is done in [4].

Spontaneous symmetry breaking

In the context of Lagrangians with scalar potentials, spontaneous symmetry breakdown is defined as follows:
Given that we have a rigid group G and a potential $V(\phi)$ that is group invariant under this group, i.e.

$$V(U(g)\phi) = V(\phi) \tag{2.48}$$

for $U(g)$ a unitary, continuous representation of G. If the point $\phi(x) = \phi_0$ where $V(\phi)$ takes its minimum is not G invariant, i.e.

$$U(g)\phi_0 \neq \phi_0 \qquad \text{for} \qquad g \in G, \tag{2.49}$$

then the symmetry is said to be *spontaneously broken*.
A visual example of the spontaneous breaking of a symmetry is given in [6]:
Imagine an infinite crystalline array of spin-$\frac{1}{2}$ magnetic dipoles that are interacting with their nearest neighbors. Even though the Hamiltonian is rotationally invariant, the ground state is not because it is a state in which all the dipoles are aligned in some arbitrary direction and is infinitely degenerate for an infinite ferromagnet [9] . Now imagine a little (i.e. $< \infty$) man living inside this huge crystal. He would definitely have a hard time to find out that the laws of nature are rotational invariant. As long as his experiments interact even just a little bit with the background field, he might detect rotational invariance only as an approximate symmetry. He would have no reasons to suspect that it was in fact an exact symmetry. The idea that the little man could check that he lives in a infinitely degenerated ground state and therefore misses a symmetry is good but an impossible task for a little man, since he had to change the directions of infinitely many spins at the time.

Therefore

$$\begin{aligned}\epsilon^{4\nu\lambda\sigma}[\mathcal{D}_\nu,[\mathcal{D}_\lambda,\mathcal{D}_\sigma]] &= -1\{[\mathcal{D}_1,[\mathcal{D}_2,\mathcal{D}_3]]_4+[\mathcal{D}_2,[\mathcal{D}_3,\mathcal{D}_1]]_4+[\mathcal{D}_3,[\mathcal{D}_1,\mathcal{D}_2]]_4\}\\ &\quad +\{[\mathcal{D}_2,[\mathcal{D}_1,\mathcal{D}_3]]_4+[\mathcal{D}_1,[\mathcal{D}_3,\mathcal{D}_2]]_4+[\mathcal{D}_3,[\mathcal{D}_2,\mathcal{D}_1]]_4\}\\ &= 0\end{aligned}$$

because of the Jacobi identity.

[9] Because the ferromagnet is infinite, there are no special directions for the spins to align. Every direction is possible and so, there are infinitely many ground states.

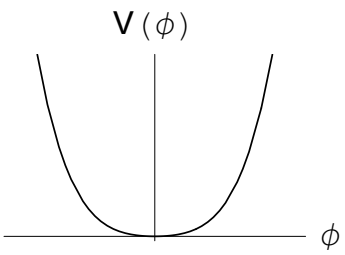

Figure 2.2: *potential for* $\mu^2 > 0$

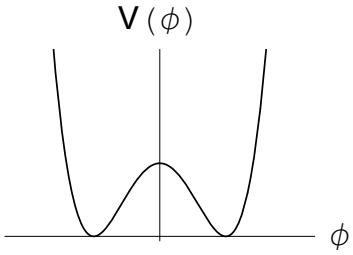

Figure 2.3: *potential for* $\mu^2 < 0$

Like the little man who lives in the crystal, missing the rotational symmetry, we assume that our laws of nature may possess symmetries which are not manifest to us because our vacuum state is not invariant under them. With *vacuum state* is meant the state of lowest energy, and we characterize the spectra of small oscillations around the vacuum as *particle masses*.
This idea that we might miss a symmetry is one of the main motivations for the further discussion.

Example: spontaneous symmetry breaking of a discrete symmetry group Consider the set of n real scalar fields $\phi(x)$, with the Lagrange density

$$\mathcal{L} = \frac{1}{2}(\partial_\mu \phi)(\partial^\mu \phi) - V(\phi). \tag{2.50}$$

The energy density corresponding to (2.50) is

$$\mathcal{H} = \frac{1}{2}(\partial_0 \phi)^2 + \frac{1}{2}(\nabla \phi)^2 + V(\phi). \tag{2.51}$$

We assume to have a potential

$$V(\phi) = \frac{\lambda}{4!}\phi^4 + \frac{\mu^2}{2}\phi^2, \tag{2.52}$$

where λ is a positive number and μ^2 might be positive or negative. We can easily see the symmetry

$$\phi \to -\phi. \tag{2.53}$$

If μ^2 is positive, then the potential looks like the one in Fig. 2.4. The vacuum is then at $\phi_0 = 0$ and the symmetry is not broken and the mass of the particle corresponding to the field ϕ is μ.
If μ^2 is negative (see Fig. 2.5), it is convenient to introduce a quantity

$$c^2 := -\frac{6\mu^2}{\lambda} \tag{2.54}$$

and the potential can be written as

$$V(\phi) = \frac{\lambda}{4!}(\phi^2 - c^2)^2 \tag{2.55}$$

plus an irrelevant constant. One can see from equation (2.55) that the potential has two minima, $\phi = \pm c$. Which one we choose does not matter, the symmetry is spontaneously broken anyway. So we choose $\phi = c$ and define a new, shifted field

$$\phi' := \phi - c. \tag{2.56}$$

In terms of this shifted field, the potential is

$$V(\phi) = \frac{\lambda}{4!}(\phi'^2 + 2c\phi')^2 = \frac{\lambda}{4!}\phi'^4 + \frac{\lambda c}{6}\phi'^3 + \frac{\lambda c^2}{6}\phi'^2 \tag{2.57}$$

We can see here, that the squared of the mass of the particle that corresponds to the field ϕ' is $\frac{\lambda c^2}{3}$ and not $\mu^2 = \frac{\lambda c^2}{6}$ as one might think by considering equation (2.50) and (2.52). Of course we have to be careful by interpreting particles out of a Lagrangian density, because our vacuum state might not be at $\phi_0 = 0$. In such a case we need to expand the Lagrangian around ϕ_0 because in our definition of particles we consider the neighborhood of the vacuum state, just the way we did it here.
Note also that a cubic ϕ term appears, which makes it hard to detect the hidden symmetry

$$\phi' \to -(\phi' + 2c). \tag{2.58}$$

So here we can see, that for such a system with spontaneous symmetry breaking, we might have two Lagrangians (here (2.50) and (2.57)) describing the same system, but in one we can see easily the symmetry and in one the particles.

Example: spontaneous symmetry breaking of a continuous symmetry group This time, we choose ϕ to be a complex scalar field defined by the Lagrangian

$$\mathcal{L}_0(\phi(x), \partial^\mu\phi(x)) = \partial_\mu\phi^*\partial^\mu\phi - V(\phi^*\phi) \tag{2.59}$$

and its classical Hamiltonian

$$\mathcal{H} = \int d^3x[\pi^*\pi + \nabla\phi^*\nabla\phi + V(\phi^*\phi)] \qquad , \qquad \pi := \frac{\partial\phi}{\partial t}. \tag{2.60}$$

$\mathcal{L}$ is invariant under the global gauge transformation

$$\phi(x) \to e^{-i\alpha}\phi(x). \tag{2.61}$$

One possible vacuum state is the constant $\phi(x) = \phi_0$, such that $V(\phi_0)$ is at its smallest value. If $\phi_0 \neq 0$, then ϕ_0 is not invariant under a global phase

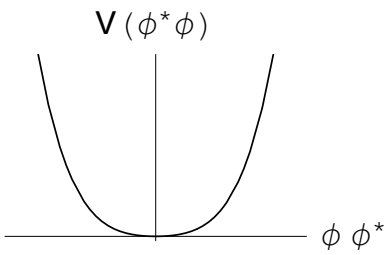

Figure 2.4: *potential for* $\mu^2 > 0$

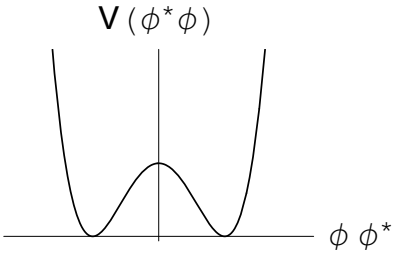

Figure 2.5: *potential for* $\mu^2 < 0$

transformation, hence the symmetry is spontaneously broken. The lowest state is again infinitely degenerated because the phase of ϕ_0 is arbitrary.
We want to fix a potential

$$V(\phi^*\phi) = \mu^2\phi^*\phi + \lambda(\phi^*\phi)^2 + const. \tag{2.62}$$

and get the equation of motion

$$(\partial_\mu\partial^\mu + \mu^2)\phi = -2\lambda\phi^*\phi^2 \tag{2.63}$$

by using the Euler-Lagrange equations.
If $\lambda = 0$ and $\mu^2 > 0$, the Lagrangian contains no terms representing interaction and we get the plane waves of wave vectors k^μ with $k^2 = \mu^2$ corresponding to a single-particle state of mass μ.
If $\lambda > 0$ and $\mu^2 > 0$ the potential looks like Fig. 2.2 and the lowest solution is $\phi(x) = 0$ what corresponds to no spontaneous symmetry breaking.
If $\lambda > 0$ and $\mu^2 < 0$ the potential looks like Fig. 2.3 and we can already see that the lowest solution $\phi(x) = \phi_0 \neq 0$ and so the symmetry is spontaneously broken. We want to study this case now.
The potential is defined only up to a constant, so that we can rewrite it in the form:

$$V(\phi^*\phi) = \lambda(\phi^*\phi - \phi_0^2)^2 + const. \qquad , \qquad \phi_0 \neq 0 \tag{2.64}$$

and the lowest state corresponds to $\phi^*\phi = \phi_0^2$, or

$$\phi(x) = \phi_0 e^{i\alpha_0} \tag{2.65}$$

with α_0 an arbitrary real constant.
We expand $\phi(x)$ around the vacuum solution ϕ_0

$$\phi(x) = (\phi_0 + \eta(x))e^{i\alpha(x)} \qquad , \qquad \alpha(0) = \alpha_0 \tag{2.66}$$

and the complex fields $\phi(x)$ and $\phi^*(x)$ are then replaced by real fields $\eta(x)$ and $\alpha(x)$. The Lagrange density changes to

$$\mathcal{L}_0 = \partial_\mu\eta\partial^\mu\eta - \lambda(2\phi_0 + \eta)^2\eta^2 + (\phi_0 + \eta)^2\partial_\mu\alpha\partial^\mu\alpha. \tag{2.67}$$

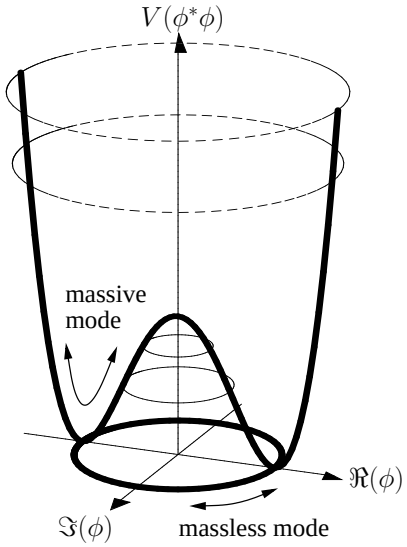

Figure 2.6: *Two possible modes in the scalar field if the potential V implies a vacuum state that is not invariant under the symmetry $U(1)$.*

Close to the vacuum state, η is small and we drop terms higher than second order in η [10] :

$$\mathcal{L}_0 = [\partial_\mu \eta \partial^\mu \eta - 4\lambda\phi_0^2\eta^2] + \phi_0^2 \partial_\mu \alpha \partial^\mu \alpha + O(\eta^3). \tag{2.68}$$

If we look at equation (2.68), we see that the terms in the brackets describe a particle of mass $2\phi_0\sqrt{\lambda}$. The next term describes a massless scalar particle because the α-field appears in the Lagrangian only by its derivatives. These modes are illustrated in Fig. 2.6.

There exists a nice way in which we could have seen purely geometrically that there must enter a massless particle term in the Lagrangian. If our vacuum is not invariant under the symmetry group $U(1)$ we have a curve in an abstract space of all states passing through all the possible vacuum states. In our case, the curve is a circle in the complex plane as drawn in Fig. 2.6. If we expand the potential around the vacuum, no terms involving the variable that measures displacement along this curve can appear, because the potential is constant along this curve. Since this curve is parametrized by the function $\alpha(x)$, and $\alpha(x)$ appears in the Lagrangian by its derivatives, we always have a massless particle.
Such a massless particle is called a *Goldstone boson*, what leads us to the next section.

[10] If we drop the second order term in η as well, we will loose the information how the system behaves around the vacuum solution since the Euler-Lagrange equations kill one η.

Goldstone's Theorem and Goldstone bosons

In the last example of the previous section, we have seen that the spontaneous breakdown of a global symmetry implies the existence of a massless particle called Goldstone boson. One should remember that the symmetry that is spontaneously broken is still a symmetry of the system. It is manifested not through the invariance of the lowest state, but in the *"Goldstone mode"* - through the existence of a Goldstone boson.
In this section we want to give an idea of the general version of that statement called *Goldstone's theorem*.

We start with a Lagrangian that is globally invariant under the symmetry group G and assume to have a set of N real fields, ψ and a potential $V(\psi)$ which is invariant under a group transformation

$$\psi(x) \to e^{i\alpha^a X^a}\psi(x) \qquad \text{and so} \qquad V(\psi) = V(e^{i\alpha^a X^a}\psi(x)), \tag{2.69}$$

where the X^a are a set of N hermitian matrices and the α^a are arbitrary real parameters.
Now we want to construct the subgroup H of G that contains all the elements of G that leave the vacuum state ψ_0 of the Lagrangian invariant [11] . H does of course depend on the potential $V(\phi)$ and may be anything from the trivial identity subgroup (all symmetries spontaneously broken) to the full group (no symmetries spontaneously broken). We want to choose the indices of the group generators so that this subgroup H is generated by the first $N-K$ generators where $N \geqslant N-K \geqslant 0$. Formally, this means

$$H = \{h \in G | h\psi_0 = \psi_0\} \qquad \text{and} \qquad X^a\psi_0 = 0 \qquad \forall a \leqslant N-K. \tag{2.70}$$

Now the K remaining generators do not leave ψ_0 invariant, and according to the discussion at the end of the previous chapter, in the abstract space of all states, we have a K-dimensional surface of constant potential $V(\psi)$. Thus, by the same geometrical arguments as before [12] , the theory must contain K massless particles, one for each spontaneously broken symmetry. As we said before, these particles are called *Goldstone Bosons* and the statement we just proved is a special case (the classical case) of *Goldstone's theorem*, that can be proved in much greater generality in quantum field theory[13] .

[11] It is easy to see that this is in fact a subgroup (see also chapter *little group*).
[12] A more mathematical proof is done in [7], p.93.
[13] See [6], p.120:
"given a field theory obeying the usual axioms (Lorentz invariance, locality, Hilbert space with positive-definite inner product, etc.), if there is a local conserved current (the axiomatic version of the statement that the Lagrangian is invariant under some continuous transformation) such that the space integral of its time component does not annihilate the vacuum state, then the theory necessarily contains a massless spinless meson, with the same internal symmetry and parity properties as the time component of the current".

Higgs mechanism

In the very beginning of this report, we have seen that there are certain Lagrangians that are invariant not only under a global symmetry transformation, but also under a local one. From the previous section we know that there are spontaneous symmetry breakings, but we discussed that phenomenon only in case of a global gauge invariance. In this section, we will discuss the case of a local gauge invariance in an Abelian and a non-Abelian example.

Higgs mechanism in an Abelian model Consider the following Lagrangian with the complex, scalar field ϕ, the covariant derivative $\mathcal{D}$ and the potential $V(\phi^*\phi)$:

$$\begin{aligned} \mathcal{L} &= -\frac{1}{4}\mathcal{F}^{\mu\nu}\mathcal{F}_{\mu\nu} + (\mathcal{D}^\mu\phi)^*\mathcal{D}_\mu\phi - V(\phi^*\phi), \\ \mathcal{D}_\mu\phi &= (\partial_\mu + ie\mathcal{A}_\mu)\phi \\ V(\phi^*\phi) &= \lambda(\phi^*\phi - \phi_0^2)^2 \quad , \quad \phi_0 \neq 0. \end{aligned} \tag{2.71}$$

The gauge field $\mathcal{A}^\mu$ transforms according to equation (2.8) and the field ϕ according to equation (2.1).
Using the Hamiltonian of the Lagrangian (2.71), it is possible to show [14] that a lowest energy solution is

$$\mathcal{A}^\mu(x) = 0 \qquad \text{and} \qquad \phi(x) = \phi_0 e^{i\alpha_0} \tag{2.72}$$

where α_0 is an arbitrary constant, and since $\phi_0 \neq 0$ we see that there is a spontaneous symmetry breaking for all α_0 and without loss of generality we choose $\alpha_0 = 0$.
Considering the close neighborhood of the vacuum state ϕ_0, we write $\phi(x) = \phi_0 + \theta(x)$ with $\theta(x) := \theta_1(x) + i\theta_2(x)$ and get the Lagrangian

$$\begin{aligned} \mathcal{L}(\mathcal{A}_\mu, \theta) &= -\frac{1}{4}\mathcal{F}^{\mu\nu}\mathcal{F}_{\mu\nu} + (\mathcal{D}^\mu\theta)^*\mathcal{D}_\mu\theta + \frac{1}{2}e^2\phi_0^2\mathcal{A}_\mu\mathcal{A}^\mu + e^2\phi_0\theta_1\mathcal{A}_\mu\mathcal{A}^\mu \\ &\quad -e\phi_0\theta_2(\partial_\mu\mathcal{A}_\mu) - \lambda(4\phi_0^2\theta_1^2 + 4\phi_0\theta_1|\theta|^2 + |\theta|^4), \end{aligned} \tag{2.73}$$

Now we take advantage of the fact that the Lagrangian is invariant under a local phase transformation and gauge away the phase of ϕ such that we can assume ϕ to be real,

$$\phi(x) = \rho(x) \qquad , \qquad \forall x \in \mathbb{R}^4 : \quad \rho(x) \in \mathbb{R}. \tag{2.74}$$

That leads us to the Lagrangian

$$\mathcal{L}(\mathcal{A}_\mu, \rho) = -\frac{1}{4}\mathcal{F}^{\mu\nu}\mathcal{F}_{\mu\nu} + (\partial_\mu\rho)^2 + e^2\mathcal{A}_\mu\mathcal{A}^\mu\rho^2 - \lambda(\rho^2 - \phi_0^2)^2. \tag{2.75}$$

[14] see [4], p.54

As in the previous section, we call the local gauge symmetry *spontaneously broken* when $\phi_0 \neq 0$. A vacuum solution is $\rho = \phi_0$ and $\mathcal{A}_\mu = 0$. This follows from the equations of motion (see equation (2.78)). Because $\phi_0 \neq 0$, we get a spontaneous symmetry breaking to discuss.
Again we consider the field $\rho(x)$ in a close neighborhood of the vacuum state ϕ_0,

$$\rho(x) = \phi_0 + \eta(x), \tag{2.76}$$

and the Lagrangian changes to the form

$$\begin{aligned} \mathcal{L}(\mathcal{A}_\mu, \eta) &= -\frac{1}{4}\mathcal{F}^{\mu\nu}\mathcal{F}_{\mu\nu} + (\partial_\mu \eta)^2 + e^2 \mathcal{A}_\mu \mathcal{A}^\mu \phi_0^2 \\ &\quad + e^2 \mathcal{A}_\mu \mathcal{A}^\mu \eta^2 - \lambda(4\phi_0^2\eta^2 + 4\phi_0\eta^3 + \eta^4). \end{aligned} \tag{2.77}$$

By comparing the two Lagrangians (2.73) and (2.77) we recognize that in (2.73), there appears a massless particle (Goldstone Boson) according to the field θ_2 but there is no such massless particle in (2.77) anymore. Since the second Lagrangian (2.77) is reached by a local gauge transformation, we can see that the Goldstone boson can be gauged away.
So the Goldstone Boson is just a so-called gauge phantom and by using the right gauge transformation, it disappears. Now we want to investigate the form of the gauge fields $\mathcal{A}_\mu$ in this gauge, because once we have chosen the gauge transformation for ϕ it is fixed for the fields $\mathcal{A}_\mu$ as well.
Using the Euler-Lagrange equations, we get the equations of motion

$$\partial_\mu \mathcal{F}^{\mu\nu} = -2e^2\rho^2\mathcal{A}^\nu \quad , \quad (\partial^\mu + ie\mathcal{A}^\mu)(\partial_\mu + ie\mathcal{A}_\mu)\rho = 2\lambda\rho(\phi_0^2 - \rho^2). \tag{2.78}$$

Expanding the equations of motion in the regime where η and $\mathcal{A}^\mu$ are small quantities leads us to the new equations of motion

$$\begin{aligned} (\partial^\mu\partial_\mu + 2e^2\phi_0^2)\mathcal{A}^\mu &= 0 \quad , \quad \partial^\mu \mathcal{A}_\mu = 0 \quad \text{and} \\ (\partial^\mu\partial_\mu + 4\lambda\phi_0^2)\eta &= 0 \end{aligned} \tag{2.79}$$

Here we can see that the massless particle appears no more but the gauge field $\mathcal{A}$ has become massive because of the non-zero coefficient $2e^2\phi_0^2$ that corresponds with the squared value of the mass. The conclusion can be shown in the following way: at the beginning we can choose a fixed gauge so that the original independent fields are $\mathcal{A}^1, \mathcal{A}^2$ and ϕ, ϕ^*. With the expansion around the vacuum state and using the gauge which changes the field ϕ into a real field ρ, we replace the original fields by $\mathcal{A}^1, \mathcal{A}^2, \mathcal{A}^3$ and η. Now we can see that the Goldstone boson, which is in fact just a gauge phantom, has been "eaten" by the gauge field and that one gets a massive gauge field. This magic trick was discovered by P.Higgs (and independently by other people) and it is called the *Higgs mechanism*. Some more discussion can be found at section 2 after we will have also considered the Higgs mechanism for a general non-Abelian gauge group.

The little group Before we have a look at one example of the Higgs mechanism of a non-Abelian local gauge transformation, we want to discuss briefly a useful concept called the little group.
We assume that only some spin-0 fields, *Higgs fields*, can have non-vanishing vacuum values, and therefore cause spontaneous symmetry breaking. The reason is that higher-spin fields which cause spontaneous symmetry breaking would spontaneously break the Lorentz invariance in contradiction to experimental evidence. We will use the same Lagrangian (2.71) and write ϕ for the Higgs fields. The potential $V(\phi)$ has its minimum at $\phi(x) = \phi_0$ with the minimum value zero:

$$V(\phi_0) = 0, \quad V'(\phi_0) = 0, \quad V''(\phi_0) > 0. \tag{2.80}$$

As we know, spontaneously symmetry breaking happens if $\phi_0 \neq 0$ and a vacuum solution is

$$\phi(x) = \phi_0 \quad \text{and} \quad \mathcal{A}_a{}^{\mu}(x) = 0 \quad (\Rightarrow \mathcal{D}_{\mu}\phi(x) = 0). \tag{2.81}$$

As we have seen earlier in the $U(1)$ case, ϕ_0 is not the only possible vacuum state because $e^{i\alpha}\phi_0$ for an arbitrary α would do it as well. The same happens for a spontaneously symmetry breaking in the non-Abelian gauge theory, and we want to discuss it the same way as in the Abelian case.
First, we specify that ϕ_0 is constant $\neq 0$, which means that all the components of ϕ_0 are independent of space-time points x. Since we assume the potential V to be independent of x, this is indeed possible. As we have seen in earlier sections, there might be certain elements $h \in G$ for that $h\phi_0$ builds another possible vacuum state. Consider now the elements $\tilde{h}$ of G, that leave ϕ_0 invariant, such that the two vacuum states ϕ_0 and $\tilde{h}\phi_0$ do not differ. Because we assume to have a spontaneous symmetry breakdown, this must not hold for all the elements g of the local gauge transformation Group G. We call the set of the elements that leave the vacuum state invariant the *little group*, and say that the symmetry G is *spontaneously broken down to* H [15] .
The Lie algebra of the little group is made of a subset of generators $\{x_\alpha\}$ of the generators $\{X_a\}$ of G. Since

$$e^{-iw^a x_a}\phi_0 = \phi_0 \tag{2.82}$$

for arbitrary w^a, all the generators of the little group must hold the equation

$$x_\alpha \phi_0 = 0. \tag{2.83}$$

[15] For an example take $G = SU(2)$, $\phi = (\phi_1, \phi_2, \phi_3)$ and $V(\phi) := \lambda(\phi_1^2 + \phi_2^2 + \phi_3^2 - a^2)^2$. We can see the vacuum solution $\phi_0 = (\phi_{01}, \phi_{02}, \phi_{03})$ with $\phi_{01}^2 + \phi_{02}^2 + \phi_{03}^2 = a^2$. If we fix a solution ϕ_0 pointing in the direction e_1, it follows that a $U\phi_0 = \phi_0$ for a rotation U with axis e_1. Since we can write every such U in the Form $U = \exp(-iwX_1)$ we see that $SU(2)$ is spontaneously broken down to $U(1)$.

Since the generators of G not in the set $\{x_\alpha\}$ cannot annihilate ϕ_0 we can divide the set $\{X_a\}$ into two disjoint subsets:

$$\begin{aligned} \{X_a\} = \{X_j, x_\alpha\} \quad , \quad X_j\phi_0 &\neq 0 \quad (j = 1, ..., K) \\ x_\alpha\phi_0 &= 0 \quad (\alpha = 1, .., N-K) \end{aligned} \tag{2.84}$$

For convenience, we choose real antisymmetric generators $\{T_j\}$ instead of the hermitian $\{X_j\}$,

$$\begin{aligned} T_j &:= -iX_j \quad (j = 1, .., K) \quad \text{and} \\ t_\alpha &:= -ix_\alpha \quad (\alpha = 1, .., N-K), \end{aligned} \tag{2.85}$$

and we assume ϕ_0 to be a real vector and therefore the representational vector space to be a real R-dimensional vector space.
We can show that the vectors $T_j\phi_0$, $(j = 1, .., K)$ are independent and therefore span a K-dimensional subspace of the R-dimensional representational vector space. For the little group to be non-empty, we need to satisfy the condition

$$R - K > 0. \tag{2.86}$$

We call the K-dimensional space spanned by $T_j\phi_0$ $(j = 1, .., K)$ the *Goldstone space* and its complement the $(R-K)$-dimensional space, the *Higgs space*.
It can be shown that for any vector ϕ in the representational vector space and for any gauge group G, there is always a gauge transformation $U_0 \in G$ such that $U_0\phi$ is orthogonal to the Goldstone space:

$$(T_j\phi_0, U_0\phi) = 0 \quad , \quad (j = 1, .., K), \tag{2.87}$$

where we use the standard scalar product $(f, g) := \sum_{n=1}^{R} f_n g_n$. This $U_0\phi$ is said to be in *unitary gauge* [16]. Therefore we have

$$\phi(x) \to U_0(x)\phi(x)$$

[16] Proof:
For fixed ρ and ϕ, consider the mapping

$$\begin{aligned} f : G &\to \mathbb{R} \\ f : U &\mapsto (\rho, U\phi) \end{aligned}$$

Since G is compact, the function f has an extrema, let's say at position U_0. A small variation of U around U_0 therefore gives

$$\delta f = f(U_0 + \delta U) - f(U_0) = 0.$$

By writing the element $\delta U = \omega_a T_a U_0$ and using the definition of f, we see

$$0 = \delta f = (\rho, \omega_a T_a U_0\phi) = \omega_a(\rho, T_a U_0\phi) = \omega_a(T_a\rho, U_0\phi).$$

Since the ω_a are arbitrary, the last scalar product has to be zero and therefore the statement follows.

$$U_0(x)\phi(x) = \begin{pmatrix} 0 \\ \tilde{\phi}(x) \end{pmatrix} \begin{matrix} \text{Goldstone space, } K\text{-dimensional} \\ \text{Higgs space, } (R-K)\text{-dimensional.} \end{matrix} \tag{2.88}$$

Higgs mechanism in a non-Abelian model Using the results of the previous section, the vacuum solution can be written in the unitary gauge and has then the form

$$\phi(x) = \phi_0 = \begin{pmatrix} 0 \\ \tilde{\phi}_0 \end{pmatrix} \quad , \quad \mathcal{A}_a{}^\mu = 0. \tag{2.89}$$

We expand around this vacuum solution:

$$\phi(x) = \begin{pmatrix} 0 \\ \tilde{\phi}_0 + \eta(x) \end{pmatrix} \quad , \quad \mathcal{A}_a{}^\mu \quad \text{small.} \tag{2.90}$$

From equation (2.80) we can expand the potential

$$V(\phi) \quad = \quad \frac{1}{2}\eta^\nu\eta^\mu\partial_\nu\partial_\mu V(\phi_0) \quad = \quad \frac{1}{2}(\eta, V''(\phi_0)\eta). \tag{2.91}$$

For the matter field current j of the Lagrangian

$$\mathcal{L} = -\frac{1}{4}\mathcal{F}_a{}^{\mu\nu}\mathcal{F}_{a\mu\nu} + (\mathcal{D}^\mu\phi)^*(\mathcal{D}_\mu\phi) - V(\phi) \tag{2.92}$$

is already known from equation (2.42) and we can also expand it to [17]

$$j_a{}^\mu = -g^2(T_a\phi_0, T_b\phi_0)\mathcal{A}_b{}^\mu. \tag{2.93}$$

Together with the following bloc matrices,

$$(\mu^2)_{rs} := \begin{bmatrix} 0 & 0 \\ 0 & V''(\phi_0) \end{bmatrix} \begin{matrix} \text{Goldstone space} \\ \text{Higgs space} \end{matrix} \quad , \quad \text{and} \tag{2.94}$$

$$(M^2)_{ab} := g^2(T_a\phi_0, T_b\phi_0) = \begin{bmatrix} (M^2)_{ij} & 0 \\ 0 & 0 \end{bmatrix} \begin{matrix} \text{Goldstone space} \\ \text{Higgs space,} \end{matrix} \tag{2.95}$$

the linearized equations of motion can be written in the form [18]

$$\partial_\mu\partial^\mu\eta_r + (\mu^2)_{rs}\eta_s \quad = \quad 0 \quad , \quad (r = 1, .., R-K) \tag{2.96}$$

$$\partial_\mu\partial^\mu\mathcal{A}_i{}^\nu + (M^2)_{ij}\mathcal{A}_j{}^\nu \quad = \quad 0 \quad , \quad (\partial_\nu\mathcal{A}_i{}^\nu = 0), \quad (i = 1, .., K) \tag{2.97}$$

$$\partial_\mu\partial^\mu\mathcal{A}_\alpha{}^\nu - \partial^\nu(\partial_\mu\mathcal{A}_\alpha{}^\mu) \quad = \quad 0 \quad , \quad (\alpha = 1, .., N-K). \tag{2.98}$$

The first equation describes massive particles called *Higgs bosons*, while the second one describes massive gauge bosons because the gauge fields of the spontaneously broken symmetry have eaten their Goldstone bosons. The third equation describes massless gauge bosons which are the gauge particles associated with the unbroken symmetry H.

[17] see [4], p.78
[18] see [4], p.78

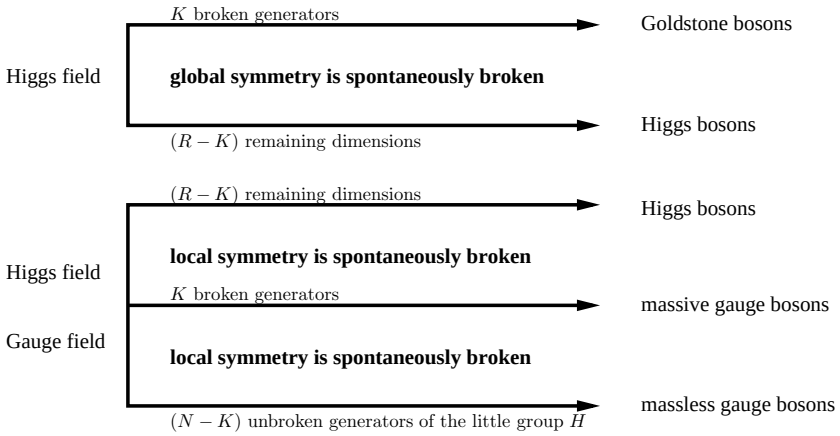

Figure 2.7: *Scheme of Goldstone's theorem and of the Higgs mechanism*

Conclusions

So far we have done a lot of very theoretical work that is schematically shown in Fig. 2.7. In the upper part, the spontaneous symmetry breaking of a global symmetry is considered. We have seen, that for those generators of the global symmetry group that do not leave the vacuum state invariant exist corresponding Goldstone bosons (Goldstone's thm). For the other generators that leave the vacuum state invariant, we get the same massive particles as in the case of no spontaneous symmetry breaking.
In the lower part of Fig. 2.7, we consider the case of spontaneous symmetry breaking of a local symmetry. As we have seen in the discussion of the Higgs mechanism, the Goldstone bosons associated to the K generators of the gauge group that do not leave the vacuum state invariant are only "gauge phantoms" , which means that they can be gauged away. Doing so, the same number of massless gauge bosons as the number of Goldstone bosons get massive. Considering the generators that leave the vacuum state invariant, as in the case of global symmetry breaking, they imply their Higgs bosons corresponding to them. When we have no Goldstone bosons to gauge away, the corresponding massless gauge bosons stay massless.

Until now, we have ignored the experimental results in our discussion about what kind of particles we have been able to detect. If we want to reduce all possible theories to those that contain only the particles already measured, we may not have any massless particles except one, the photon. To achieve this, the entire gauge group must be spontaneously broken, except for a one parameter subgroup. The gauge field corresponding to it remains then massless and we consider it to be corresponding with the electromagnetic potential that does indeed contain a massless particle, the photon.

It might be useful to remember historically that the spontaneous symmetry

breaking and the theory of non-Abelian gauge fields were considered to be independent. Since both of the theories contain massless particles, the Goldstone bosons and the massless gauge bosons, their physical relevance were thought to be little. It took some time (1959-1967) to realize, that these two problems cancel each other, in the way that the Goldstone bosons disappear and the massless gauge bosons gain mass.

Two physical applications

To see that the very theoretical work we have done until now has important applications in many experimentally "proved" theories, we want to have a look at two examples where our conclusions and the mechanisms we found are successfully used. Of course, we will discuss here only the very general results and give an idea how our results from the previous sections get important.

Electroweak theory The weak interaction acts between all particles and is for example responsible for the β-decay of certain particles. Its range is very small, i.e. much less than 1 fm and as the name says, it is weak compared to the other two fundamental interactions namely the strong and the electromagnetic interaction. The weak interaction is though stronger than the third fundamental interaction, the long ranged gravitation. However, it is possible to formulate a theory called *electroweak theory* that connects the electromagnetic and the weak interaction, thanks to the results of the gauge theory.

Summarized, the results of the theory of the weak interaction are the following. Three massive particles, the two bosons $W^{\pm}$ and the particle Z are responsible for the interaction and that the theory's symmetry group is SU(2). We also know that the massless photon is responsible for the electromagnetic interaction with its symmetry group U(1).
The idea of the electroweak theory is now to consider the symmetry group $SU(2) \times U(1)$ with the little group $U(1)$ for a certain vacuum state that is spontaneously broken. The existing massless gauge boson is identified as the photon from the electromagnetic theory. The other three gauge fields get massive and the appearing particles are identified with the three massive particles $W^{\pm}$ and Z. There also appears a massive Higgs field.
This method is exactly like the general one we described in the previous section. The results following from this theory do mostly agree very good with the results from experiments, except for the missing Higgs boson that has not been found yet.

Superconductor As a second example where the Higgs mechanism actually takes place we want to consider the phenomenon of superconductivity. Again, the exact mathematical formulation would take too much time to formulate here and we focus on the general procedures.

In the ground state of a material, under a critical temperature T_c an important process might happen: the condensation of the electrons to electron pairs called *cooper pairs*. This happens because of a small electron-electron attraction. The fermion property of one electron has disappeared because the cooper-pairs can be treated as spinless particles. Such a procedure does force the question if a symmetry of the system might be broken. To check that, we need some more mathematical formalism, which we can find in the Landau-Ginzburg theory of superconductivity.
The idea of the Landau-Ginzburg theory of superconductivity is to couple the Landau description of a (second order) phase transition to an external electromagnetic field. The Lagrangian of this theory is quite similar to the one we used in the section 2 where we discussed an example of the Abelian Higgs mechanism,

$$\mathcal{L}(x) = -\frac{1}{4}\mathcal{F}^{\mu\nu}\mathcal{F}_{\mu\nu} + (\mathcal{D}^{\mu}\phi)^{*}\mathcal{D}_{\mu}\phi - \lambda(\phi^{*}\phi - \phi_0^2)^2. \tag{2.99}$$

where the ϕ_0^2 is proportional to the term $(T - T_c)/T_c$. This Lagrangian is valid only for temperatures below the critical temperature T_c because only boson and no fermion fields appear. We also know already that this Lagrangian is invariant under the local $U(1)$ gauge transformation (see equation (2.1) and (2.8)) and that the vacuum state is spontaneously broken. One result we can use now is that the formerly massless gauge particle has got the mass $m_A^2 = 2e^2\phi_0^2$. Since we consider the gauge field $\mathcal{A}_\mu$ as corresponding to the vector potential from electrodynamics and the former massless particle to the photon, we see that the latter gets massive with the mass m_A. From the theory of electrodynamics we know that a mass term for the fields appearing in the Lagrangian leads to the Proca Lagrange density. This generates fields that vanish within the scale of $\frac{1}{m_A}$. This explains the *Meissner effect* that says that an external electromagnetic field penetrates a superconductor only to the depth $\frac{1}{m_A}$.

3 Magnetic monopoles: Dirac and Polyakov-t'Hooft

Philip Grech
Supervisor: Urs Wenger

Although not yet found in nature magnetic monopoles are of theoretical interest. In particular their existence would yield an explanation for the quantisation of electric charge.

We will consider two different constructions: The first one was given by Dirac in 1931, who examined the consequences of a magnetic monopole if a consistent description in electrodynamics and *quantum mechanics is required. We will use two approaches: The first one is based on the quantisation of the angular momentum in quantum mechanics, whereas the second uses gauge transformations of the electromagnetic field.*
The second construction will follow 't Hooft and Polyakov, who were able to show that magnetic monopole solutions can also arise in non-Abelian gauge theories. We will not quantise the fields. Furthermore, we try to illuminate the connection between the 't Hooft-Polyakov monopole and the Dirac monopole.

A lower bound on the monopole mass will be calculated and we see that under rather special assumptions the field equations for the 't Hooft-Polyakov monopole can be solved analytically. The so obtained solution will differ from the Dirac monopole fundamentally.

1 Dirac Monopole

Covariant Formulation of Electrodynamics

We will not deduce the fact that a covariant formulation of electrodynamics can be given, yet just repeat the principal results (for further information see [10] or [11]): The four-current and the four-potential

$$(j^\mu) = \begin{pmatrix} \rho_e \\ \vec{j} \end{pmatrix} \quad \text{and} \quad (A^\mu) = \begin{pmatrix} \phi \\ \vec{A} \end{pmatrix} \tag{3.1}$$

transform like four-vectors. ρ_e denotes the electric charge, $\vec{j}_e$ the corresponding current, ϕ the scalar and $\vec{A}$ the vector potential.

$$\partial_\mu j^\mu = 0 \tag{3.2}$$

is the continuity equation,

$$\Box A^\mu = j^\mu \tag{3.3}$$

is the wave equation for the potential. We use the signature (+ - - -) for the Minkowski metric ($\eta^{\mu\nu}$). $\Box = \eta^{\mu\nu}\partial_\mu\partial_\nu$ is the d'Alembert operator, a Lorentz scalar (Given that (j^μ) is a four-vector it follows from (3.3) that (A^μ) is a four-vector). The Lorentz gauge takes the form

$$\partial_\mu A^\mu = 0. \tag{3.4}$$

We define the antisymmetric field tensor:

$$(F^{\mu\nu}) = (\partial^\mu A^\nu - \partial^\nu A^\mu) = \begin{pmatrix} 0 & -E^1 & -E^2 & -E^3 \\ E^1 & 0 & -B^3 & B^2 \\ E^2 & B^3 & 0 & -B^1 \\ E^3 & -B^2 & B^1 & 0 \end{pmatrix} \tag{3.5}$$

and its dual tensor

$$\star F^{\mu\nu} = \frac{1}{2}\epsilon^{\mu\nu\lambda\rho}F_{\lambda\rho}. \tag{3.6}$$

Maxwell's equations now take the simple form:

$$\partial_\nu F^{\mu\nu} = j^\mu \tag{3.7}$$

$$\partial_\nu \star F^{\mu\nu} = 0 \tag{3.8}$$

Notice that the dual field tensor is obtained from the original tensor by applying the duality transformations $\vec{E} \to \vec{B}$ and $\vec{B} \to -\vec{E}$.

Consider now the gauge transformation $A'_\mu = A_\mu - \partial_\mu\chi$, where χ is an arbitrary function. Then we have

$$(F'^{\mu\nu}) = (\partial^\mu A^\nu - \partial^\mu\partial^\nu\chi - \partial^\nu A^\mu + \partial^\nu\partial^\mu\chi) = (F^{\mu\nu}).$$

Thus the electromagnetic field remains unchanged.

This formalism will be used to be able to illustrate certain parallels between the Abelian and the non-Abelian case. In this chapter we shall content ourselves with the usual Maxwell equations, since the covariant formulation is not really needed for the arguments given.

Generalised Duality in Electrodynamics

We contemplate Maxwell's equations but introduce as well magnetic charges ρ_m and currents $\vec{j_m}$:

$$\vec{\nabla} \cdot \vec{E} = \rho_e \qquad \vec{\nabla} \wedge \vec{E} + \partial_t \vec{B} = -\vec{j}_m \tag{3.9}$$

$$\vec{\nabla} \cdot \vec{B} = \rho_m \qquad \vec{\nabla} \wedge \vec{B} - \partial_t \vec{E} = \vec{j}_e \tag{3.10}$$

We assumed that the magnetic continuity equation has the same form as the one for the electric densities.[19] Consider now the generalised duality transformation which "rotates" the electromagnetic field and its charges and currents:

$$\begin{pmatrix} \vec{E}' \\ \vec{B}' \\ \rho_e' \\ \rho_m' \\ \vec{j_e'} \\ \vec{j_m'} \end{pmatrix} = \begin{pmatrix} \cos\alpha & -\sin\alpha & 0 & 0 & 0 & 0 \\ \sin\alpha & \cos\alpha & 0 & 0 & 0 & 0 \\ 0 & 0 & \cos\alpha & -\sin\alpha & 0 & 0 \\ 0 & 0 & \sin\alpha & \cos\alpha & 0 & 0 \\ 0 & 0 & 0 & 0 & \cos\alpha & -\sin\alpha \\ 0 & 0 & 0 & 0 & \cos\alpha & \cos\alpha \end{pmatrix} \begin{pmatrix} \vec{E} \\ \vec{B} \\ \rho_e \\ \rho_m \\ \vec{j_e} \\ \vec{j_m} \end{pmatrix}. \tag{3.11}$$

As an example we compute for the first Maxwell equation

$$\vec{\nabla} \cdot \vec{E'} = \vec{\nabla} \cdot (\cos\alpha \cdot \vec{E} - \sin\alpha \cdot \vec{B}) = \cos\alpha \cdot \rho_e - \sin\alpha \cdot \rho_m = \rho_e'.$$

It is easy to verify that also the other equations are invariant under the above transformation. Assume that $\frac{\rho_m}{\rho_e}$ is equal for every particle in nature. Then there is an $\alpha \in \mathbb{R}$ such that

$$\rho_m' = \rho_e(\sin\alpha + \frac{\rho_m}{\rho_e}\cos\alpha) = 0$$

and

$$\vec{j_m'} = 0$$

accordingly.

It is thus a *convention* when we choose $q_e = -|e|$ and $q_m = 0$ for an electron. Therefore the crucial question is not whether non-vanishing magnetic charge densities exist but whether there are two particles with different ratios $\frac{q_m}{q_e}$. We remark that when we talk about magnetic monopoles in this article, we always think of a particle which has a different ratio $\frac{q_m}{q_e}$ than what has been measured yet.

[19] Alternatively we could have written $\partial_\nu F^{\mu\nu} = j^\mu$ and $\partial_\nu \star F^{\mu\nu} = k^\mu$ with $(k^\mu) = (\rho_m, \vec{j}_m)$.

Angular Momentum Approach

For the further discussion of the Dirac Monopole we refer to [12] and [13]. Dirac discovered a quantisation condition for the electric charge by requiring a consistent description of magnetic monopoles in electrodynamics *and* quantum mechanics. In this chapter we show how we can connect the magnetic charge to a certain angular momentum. The quantisation of the electric charge will then follow directly from the quantum mechanical quantisation of this angular momentum.
Consider a particle at the point $\vec{r}$ with electric charge q and mass m in the field of a magnetic monopole with magnetic charge g placed at the origin ($r = |\vec{r}|$):

$$\vec{B} = \frac{g}{4\pi r^3}\vec{r} \tag{3.12}$$

$$m\ddot{\vec{r}} = q\dot{\vec{r}} \wedge \vec{B}. \tag{3.13}$$

Since this is no central force we cannot expect the orbital angular momentum to be preserved. Nevertheless $\vec{B}$ has a rotational symmetry and we may conjecture a conserved quantity. Thus compute

$$\begin{aligned}
\frac{d}{dt}(\vec{r} \wedge m\dot{\vec{r}}) &= \vec{r} \wedge m\ddot{\vec{r}} \\
&= \frac{qg}{4\pi r^3}\vec{r} \wedge (\dot{\vec{r}} \wedge \vec{r}) \\
&= \frac{qg}{4\pi r^3}\left[\dot{\vec{r}}r^2 - \vec{r}(\dot{\vec{r}} \cdot \vec{r})\right] \\
&= \frac{d}{dt}\left(\frac{qg}{4\pi}\hat{r}\right).
\end{aligned}$$

We set $\hat{r} := \frac{\vec{r}}{r}$ and used $\frac{d}{dt}\frac{\vec{r}}{r} = \frac{\dot{\vec{r}}}{r} - \frac{\vec{r}\cdot(\vec{r}\cdot\dot{\vec{r}})}{r^3}$. Now define the *total* angular momentum as

$$\vec{J} := \vec{r} \wedge m\dot{\vec{r}} - \frac{qg}{4\pi}\hat{r}, \tag{3.14}$$

which is indeed a conserved quantity. To understand the second term of $\vec{J}$ remember that the construction of the Maxwell torsion tensor yields the identification of the field momentum density with $\vec{E} \wedge \vec{B}$. This leads to an expression for the angular momentum of the electromagnetic field:

$$\vec{J}_{em} = \int d^3x(\vec{x} \wedge (\vec{E} \wedge \vec{B})). \tag{3.15}$$

$\vec{E}$ denotes the field of the electric charge q at $\vec{r}$, $\vec{B}$ is given by (3.12).

$$\begin{aligned} J^i_{em} &= \int d^3x E^j(\delta_{ij} - \hat{x}^i\hat{x}^j)\frac{g}{4\pi x} \\ &= \int d^3x E^j \frac{\partial}{\partial x^j}(\frac{g\hat{x}^i}{4\pi}) \\ &\overset{i.b.p}{=} -\int d^3x \vec{\nabla}\cdot\vec{E}\frac{g}{4\pi}\hat{x}^i. \end{aligned}$$

Using $\vec{\nabla}\cdot\vec{E} = q\cdot\delta(\vec{x}-\vec{r})$, $\delta(\vec{x})$ is the Dirac delta, we get the angular momentum of the electric field:

$$\vec{J}_{em} = -\frac{qg}{4\pi}\hat{r}. \tag{3.16}$$

Thus we can argue that the total angular momentum for which we derived conservation is nothing but the sum of the orbital angular momentum of the particle and the angular momentum of the electromagnetic field. Since

$$\hat{r}\cdot\vec{J} = -\frac{qg}{4\pi} \Rightarrow \cos\theta = -\frac{qg}{4\pi J} \tag{3.17}$$

we see that the trajectory of the particle lies on a cone around the negative $\vec{J}$-axis with semi-vertical angle $\arccos(\frac{qg}{4\pi J})$ and its apex at the monopole. The first equation in (3.17) will lead us to our goal: If we involve quantum mechanics it is reasonable to expect that the components of $\vec{J}$ will satisfy the commutation relations of the angular momentum algebra (see also chapter (1)) and have thus eigenvalues being integer multiples of $\frac{1}{2}\hbar$. We consider the component along the straight line connecting the monopoles and the charged particle and get

$$\frac{qg}{4\pi} = \frac{1}{2}n\hbar, \qquad n\in\mathbb{Z}, \tag{3.18}$$

which is the Dirac quantisation condition. This, of course, is not a rigorous derivation but at least it makes things plausible.

Quantisation of Charge

To see that (3.18) is equivalent to the fact that charge is quantised consider the case of many particles with either a magnetic charge g_i or an electric charge q_i. Get:

$$\frac{q_ig_j}{4\pi} = \frac{1}{2}n_{ij}\hbar \qquad n_{ij}\in\mathbb{Z}. \tag{3.19}$$

Fixing g_j we get

$$q_i = \frac{2\pi\hbar}{g_j}n_{ij}.$$

We calculate the highest common factor n_{0j} of the $\{n_{ij}\}$ and conclude that every electric charge is thus an integral multiple of $q_0 = \frac{2\pi\hbar}{g_j}n_{0j}$. By Euclid's algorithm

(see e.g. [14]) n_{0j} is a linear combination of the n_{ij} with integer coefficients, thus q_0 is a linear combination of the q_i with integer coefficients. Since the total charge of the system equals the sum of the charges of the involved particles, it is possible to really measure q_0. The same reflections lead to an elementary *magnetic* charge g_0. Nota bene: It suffices a single magnetic monopole in the whole universe to guarantee the quantisation of electric charge.

Forces

In analogy to the force law we have for electric charges, we can assume that two magnetic charges g_0 repel each other with $\frac{g_0^2}{4\pi r^2}$ and we can compare the magnitude of these forces:

$$\frac{F_m}{F_e} = \frac{g_0^2}{q_0^2} = \frac{n_0^2}{4}(\frac{q_0^2}{4\pi\hbar})^{-2} \approx 5 \cdot 10^3 n_0^2, \tag{3.20}$$

which is large even for $n_0 = 1$. It is therefore expected to be quite difficult to pair-produce magnetic monopoles and that they are much heavier than electrically charged particles (we will calculate a lower bound on the mass in chapter 2).

Quantisation of Motion

In this section we want to analyse more precisely the quantum mechanical behaviour of our system given in 1. The Lagrangian of a particle in an electromagnetic field is

$$L = \frac{1}{2}m\dot{\vec{r}}^2 + q\dot{\vec{r}} \cdot \vec{A} - q\phi \tag{3.21}$$

where $(A^\mu) = (\phi, \vec{A})$ is the electromagnetic four-potential ($\vec{\nabla} \wedge \vec{A} = \vec{B}$ and $-\nabla\phi = \vec{E}$), since this leads to the correct equations of motion:

$$\begin{aligned} \frac{\partial L}{\partial r_j} &= q\dot{r}_i \frac{\partial A_i}{\partial r_j} - q\frac{\partial \phi}{\partial r_j} \\ \frac{d}{dt}\frac{\partial L}{\partial \dot{r}_j} = \frac{d}{dt}(m\dot{r}_j + qA_j) &= m\ddot{r}_j + q\frac{\partial A_j}{\partial r_i}\dot{r}_i + q\frac{\partial A_j}{\partial t} \end{aligned}$$

$$\begin{aligned} \Rightarrow m\ddot{r}_j &= q\dot{r}_i(\frac{\partial A_i}{\partial r_j} - \frac{\partial A_j}{\partial r_i}) - q\frac{\partial \phi}{\partial r_j} - q\frac{\partial A_j}{\partial t} \\ &= q(\dot{\vec{r}} \wedge \vec{B})_j + qE_j. \end{aligned}$$

A Legendre transformation gives the Hamiltonian

$$H = \vec{p} \cdot \dot{\vec{r}} - L = \frac{1}{2m}(\vec{p} - q\vec{A})^2 + q\phi \tag{3.22}$$

with

$$\vec{p} = \frac{\partial L}{\partial \dot{\vec{r}}} = m\dot{\vec{r}} + q\vec{A}. \tag{3.23}$$

Note that this Hamiltonian can also be obtained by translating the four-momentum of the Hamiltonian $H = \frac{p^2}{2m}$ of a free particle: $p^\mu \to p^\mu + qA^\mu$. Since the magnetic field is not source-free, a vector potential $\vec{A}$ cannot exist everywhere. We will come back to this problem, yet ignore it for the moment.
We define the Poisson bracket by

$$\{\alpha, \beta\} := \sum_{i=1}^{3} \left(\frac{\partial \alpha}{\partial r^i}\frac{\partial \beta}{\partial p^i} - \frac{\partial \alpha}{\partial p^i}\frac{\partial \beta}{\partial r^i}\right) \tag{3.24}$$

and get

$$\{r^i, r^j\} = \{p^i, p^j\} = 0 \tag{3.25}$$
$$\{r^i, p^j\} = \{r^i, m\dot{r}^j\} = \delta_{ij} \tag{3.26}$$
$$\{m\dot{r}^i, m\dot{r}^j\} = -q(\partial^i A^j - \partial^j A^i) = q\epsilon_{ijk}B^k. \tag{3.27}$$

Using the product rule $\{\alpha\beta, \gamma\} = \alpha\{\beta, \gamma\} + \{\alpha, \gamma\}\beta$ we compute expressions for Poisson brackets with the angular momentum $\vec{L} = \vec{r} \wedge m\dot{\vec{r}}$:

$$\begin{aligned}
\{L^i, r^j\} &= \epsilon_{ijk} r^k \\
\{L^i, m\dot{r}^j\} &= \epsilon_{ijk} m\dot{r}^k + q(\delta_{ij}\vec{r}\cdot\vec{B} - B^i r^j) \\
&\overset{\text{in our case}}{=} \epsilon_{ijk} m\dot{r}^k + \frac{qg}{4\pi r}(\delta_{ij} - \hat{r}^i\hat{r}^j) \\
&= \epsilon_{ijk} m\dot{r}^k + \{\frac{qg}{4\pi}\hat{r}^i, m\dot{r}^j\},
\end{aligned}$$

where $\hat{r}^i$ denotes r^i/r. We are now ready to derive expressions for the *total* angular momentum $\vec{J} = \vec{r} \wedge m\dot{\vec{r}} - \frac{qg}{4\pi}\hat{r}$:

$$\{J^i, m\dot{r}^j\} = \epsilon_{ijk} m\dot{r}^k \tag{3.28}$$
$$\{J^i, r^j\} = \epsilon_{ijk} r^k \tag{3.29}$$
$$\{J^i, J^j\} = \epsilon_{ijk} J^k. \tag{3.30}$$

Since $H = \frac{1}{2}m\dot{\vec{r}}^2$ we can re-derive the conservation of $\vec{J}$ from the first equation. We perform the transition to quantum mechanics by applying the correspondence principle:

$$\{\alpha, \beta\} \to \frac{1}{i\hbar}[\alpha, \beta] \tag{3.31}$$

$$\vec{p} \to -i\hbar\vec{\nabla}. \tag{3.32}$$

Equation (3.30) confirms that the total angular momentum (operator) does indeed fulfill the requirements of an angular momentum algebra as we assumed in chapter 1.

We replace $m\dot{r}^i = p^i - qA^i$ by $-i\hbar\partial^i - qA^i = -i\hbar\mathcal{D}^i$. The operator

$$\mathcal{D}^\mu = \partial^\mu + ieA^\mu \tag{3.33}$$

($e := q/\hbar$) is called covariant derivative. We will see that this concept can be extended to the case of non-Abelian gauge theories. The gauge fields which form the connection of the covariant derivative are then Lie algebra-valued.

The Schrödinger equation for the wavefunction of a charged particle is

$$-\frac{\hbar^2}{2m}\mathcal{D}^2\psi + q\phi\psi = i\hbar\frac{\partial\psi}{\partial t} \tag{3.34}$$

where ψ denotes the wavefunction.

It can easily be shown that this equation is not invariant under a gauge transformation $A_\mu \to A'_\mu = A_\mu + \partial_\mu\chi$. However, we can guarantee that the equation is gauge-*covariant* if we specify that under a gauge transformation

$$\psi \to \psi' = e^{-ie\chi}\psi. \tag{3.35}$$

In this section we have fortified the assumption that we could assume an angular momentum algebra in section (1). Still it remains the problem that the existence of the vector potential $\vec{A}$ cannot be assumed. By using the covariance of Schrödinger's equation, we will see in the next section an approach which avoids these difficulties.

Vector Potential Approach

Construction of the Potential It is a classical theorem of vector analysis (named after Helmholtz) that if we have a vector field $\vec{B}$ with $\vec{\nabla}\cdot\vec{B} = 0$ then there exists another vector field $\vec{A}$ satisfying $\vec{\nabla}\wedge\vec{A} = \vec{B}$. $\vec{A}$ is the so called vector potential. Since in the case of magnetic monopoles the divergence of $\vec{B}$ is non-zero at the origin, it is not possible to find a vector potential that is defined on every point in $\mathbb{R}^3$. The best we can get is a vector potential being defined everywhere except on a line - the Dirac string $\mathcal{S}$ - from the origin to infinity. To be precise, we consider the magnetic field of the monopole and attach a solenoid along the negative z-axis, which corresponds to the Dirac string:

$$\vec{B}_{sol} = \frac{g}{4\pi r^2}\hat{r} + g\theta(-z)\delta(x)\delta(y)\hat{z} \tag{3.36}$$

where $\theta(x)$ denotes the Heaviside function. From electrostatics we know that the first term is the gradient of the fundamental solution for the Laplace operator. Therefore we can easily compute

$$\vec{\nabla}\cdot\vec{B}_{sol} = 0. \tag{3.37}$$

Thus by Helmholtz' theorem, $\vec{B}_{sol}$ can be represented by a vector potential $\vec{A}$ such that $\vec{B}_{sol} = \vec{\nabla} \wedge \vec{A}$. For the monopole field we find

$$\frac{g}{4\pi r^2}\hat{r} = \vec{\nabla} \wedge \vec{A} - g\theta(-z)\delta(x)\delta(y)\hat{z}. \tag{3.38}$$

We will now construct the vector potential explicitly. Since the magnetic field is radial, only the radial part of the rotation operator is of interest:

$$(\vec{\nabla} \wedge \vec{A})_r = \frac{1}{r\sin\theta}(\frac{\partial}{\partial\theta}(\sin\theta A_\phi) - \frac{\partial A_\theta}{\partial\phi}). \tag{3.39}$$

Thus by symmetry we can expect the vector potential to have the form $\vec{A}(\vec{r}) = A(r,\theta)\hat{\phi}$ where $\hat{\phi}$ denotes the vector $(\cos\phi, \sin\phi, 0)$. Consider a sphere with center at the origin. The magnetic flux through a circle C that intersects the sphere is spherically symmetric and is therefore proportional to the solid angle subtended by the circle C and the origin. This solid angle corresponds to the surface M of the sphere cap that has been cut off by C:

$$M = \pi(a^2 + h^2) = \pi(r^2\sin^2\theta + r^2 - 2r^2\cos\theta + r^2\cos^2\theta) = \pi(2r^2 - 2r^2\cos\theta)$$

where a is the radius of C and h is the height of the cap. The magnetic flux is

$$\frac{gM}{4\pi r^2} = \frac{g\cdot(\pi(2r^2 - 2r^2\cos\theta))}{4\pi r^2} = \frac{g}{2}(1-\cos\theta).$$

Finally, we get

$$\frac{g}{2}(1-\cos\theta) = \int \vec{B}\cdot d\vec{S} = \int \vec{\nabla}\wedge\vec{A}\cdot d\vec{S} = \int \vec{A}\cdot d\vec{l} = 2\pi A(r,\theta) r\sin\theta$$

and

$$\vec{A}(\vec{r}) = \frac{g}{4\pi r}\frac{(1-\cos\theta)}{\sin\theta}\hat{\phi}. \tag{3.40}$$

Notice that for $\theta = \pi$ the vector potential becomes singular. This is not surprising since we are then evaluating $\vec{A}$ on the Dirac string.

With the so obtained vector potential it is possible to describe a quantum mechanically behaving particle in a magnetic field $\vec{B}$. From the requirement that for different choices of the Dirac string, we should be led to equivalent equations, we can deduce Dirac's quantisation condition.

Gauge Transformation and Dirac Condition Imagining a Dirac string on the positive z-axis we can deduce – with the construction we used in the previous chapter – another expression for the vector potential:

$$\vec{A}_S = -\frac{g}{4\pi r}\frac{(1+\cos\theta)}{\sin\theta}\hat{\phi}. \tag{3.41}$$

$\vec{A}_S$ has a singularity on the north pole of the two-sphere S^2 of radius 1 with center at the origin. For clarity, we shall denote the field from equation (3.40) by $\vec{A}_N$.

On a region where both $\vec{A}_N$ and $\vec{A}_S$ are well defined and generate the same magnetic field, they may only differ by a gauge transformation. Such a region would be the equator E and there we have

$$\begin{aligned} \vec{A}_N - \vec{A}_S &= -\nabla\chi \\ &= \frac{g}{2\pi}\hat{\phi} \quad \Rightarrow \quad \chi = -\frac{g}{2\pi}\phi. \end{aligned} \tag{3.42}$$

The gauge function χ is *not* continuous. We could not avoid this fact as we see by a calculation of the enclosed magnetic charge (N: northern hemisphere $(0 \leqslant \theta \leqslant \pi/2)$; S: southern hemisphere $(\pi/2 \leqslant \theta \leqslant \pi)$):

$$\begin{aligned} g &= \int_{S^2} \vec{B}\cdot d\vec{S} = \int_N \vec{B}_N \cdot d\vec{S} + \int_S \vec{B}_S \cdot d\vec{S} \\ &\overset{Stokes}{=} \int_E (\vec{A}_N - \vec{A}_S)\cdot d\vec{l} = \chi(0) - \chi(2\pi) \end{aligned} \tag{3.43}$$

Reconsidering equations (3.34) and (3.35) we see that the only requirement for continuous physical quantities is the continuity of the phase factor $e^{-ie\chi}$. Thus:

$$e^{-ie\chi(0)} \overset{!}{=} e^{-ie\chi(2\pi)} \quad \Rightarrow \quad ge = 2\pi n \Leftrightarrow gq = 2\pi n\hbar. \tag{3.44}$$

So the more rigorous approach via the vector potential leads again to the Dirac condition (3.18).

2 't Hooft-Polyakov Monopole

Brief Review of General Gauge Theory Formalism

We follow the introduction into the matter of gauge theory given in [15] and [12]. Consider a Lie group $\mathcal{G}$ with Hermitian generators $\{T^a\}$. $L(\mathcal{G})$ is the Lie algebra of $\mathcal{G}$, the tangent space for the Lie group at the unit element. So, any C^1-curve $g(t)$ in $\mathcal{G}$ can be written as

$$g(t) = 1 + At + \mathcal{O}(t^2) \tag{3.45}$$

where 1 denotes the unity element of $\mathcal{G}$ and A is an element of $L(\mathcal{G})$. Let D be a representation of $\mathcal{G}$ and ϕ be a Lorentz scalar field transforming under D:

$$\phi \to D(g)\phi \quad \text{where } g \in \mathcal{G}. \tag{3.46}$$

If $g = g(x)$, this is a *local* gauge transformation. With D we can associate a representation of the Lie algebra which – since there cannot be any confusion – we will also denote by D:

$$D(1 + \epsilon A) = 1 + \epsilon D(A) \tag{3.47}$$

where ϵ is a small parameter. It is not too hard to show that D as a function on $L(\mathcal{G})$ preserves the Lie brackets and is linear.

We introduce Lie algebra-valued gauge fields ${W_a}^\mu$ such that

$$\mathbf{W}^\mu = {W_a}^\mu T^a. \tag{3.48}$$

The usual derivative does not transform properly, since

$$\partial^\mu \phi \to D(g)\partial^\mu \phi + \partial^\mu D(g)\phi, \tag{3.49}$$

and we replace it by the covariant derivative $\mathcal{D}^\mu$ for which we postulate that $\mathcal{D}^\mu\phi \to D(g)\mathcal{D}^\mu\phi$. Such a derivative indeed exists if we specify that the gauge fields transform according to

$$\mathbf{W}^\mu \to g\mathbf{W}^\mu g^{-1} + \frac{i}{e}(\partial^\mu g)g^{-1}, \tag{3.50}$$

because

$$\begin{aligned}
\mathcal{D}^\mu\phi &= \partial^\mu\phi + ieD(\mathbf{W}^\mu)\phi \\
&\to D(g)\partial^\mu\phi + \partial^\mu D(g)\phi + ieD(g\mathbf{W}^\mu g^{-1} + \frac{i}{e}(\partial^\mu g)g^{-1})D(g)\phi \\
&= D(g)\partial^\mu\phi + \partial^\mu D(g)\phi + ieD(g)D(\mathbf{W}^\mu)\phi - \partial^\mu D(g)\phi \\
&= D(g)\mathcal{D}^\mu\phi.
\end{aligned} \tag{3.51}$$

Here, we used the identities $D(\partial^\mu g g^{-1}) = \partial^\mu D(g)D(g^{-1})$, $D(g\mathbf{W}^\mu g^{-1}) = D(g)D(\mathbf{W}^\mu)D(g^{-1})$ and linearity of $D(\cdot)$ as a function on the Lie algebra. We compute the commutator of the covariant derivative and see that it is no differential operator:

$$\begin{aligned}
[\mathcal{D}^\mu, \mathcal{D}^\nu]\,\phi &= \dots \\
&= ie\{D(\partial^\mu \mathbf{W}^\nu) - D(\partial^\nu \mathbf{W}^\mu) + ieD([\mathbf{W}^\mu, \mathbf{W}^\nu])\}\phi
\end{aligned} \tag{3.52}$$

and define the antisymmetric gauge field tensor by

$$\mathbf{G}^{\mu\nu} = {G_a}^{\mu\nu}T^a = \partial^\mu \mathbf{W}^\nu - \partial^\nu \mathbf{W}^\mu + ie\,[\mathbf{W}^\mu, \mathbf{W}^\nu] \tag{3.53}$$

so that we have:

$$[\mathcal{D}^\mu, \mathcal{D}^\nu]\,\phi = ieD(\mathbf{G}^{\mu\nu})\phi. \tag{3.54}$$

This equation shows the behavior of $\mathbf{G}^{\mu\nu}$ under a gauge transformation:

$$\mathbf{G}^{\mu\nu} \to g\mathbf{G}^{\mu\nu}g^{-1}. \tag{3.55}$$

We conclude this chapter with some useful formulas: The covariant derivative obeys the Jacobi identity:

$$[\mathcal{D}^\lambda, [\mathcal{D}^\mu, \mathcal{D}^\nu]] + [\mathcal{D}^\mu, [\mathcal{D}^\nu, \mathcal{D}^\lambda]] + [\mathcal{D}^\nu, [\mathcal{D}^\lambda, \mathcal{D}^\mu]] = 0. \tag{3.56}$$

Applying this to an arbitrary ϕ and using equation (3.54) yields

$$\begin{aligned}[\mathcal{D}^\lambda,[\mathcal{D}^\mu,\mathcal{D}^\nu]]\phi &= ie[\mathcal{D}^\lambda, D(\mathbf{G}^{\mu\nu})]\phi \\ &= ieD(\mathcal{D}^\lambda \mathbf{G}^{\mu\nu})\phi \end{aligned} \tag{3.57}$$

where

$$\mathcal{D}^\lambda \mathbf{G}^{\mu\nu} = \partial^\lambda \mathbf{G}^{\mu\nu} + ie[\mathbf{W}^\lambda, G^{\mu\nu}] \tag{3.58}$$

is the covariant derivative for the adjoint representation $\xi \to g\xi g^{-1}$ ($g \in \mathcal{G}$), which has this form due to equation (3.55). The Jacobi identity produces the Bianchi identity:

$$\mathcal{D}^\lambda \mathbf{G}^{\mu\nu} + \mathcal{D}^\mu \mathbf{G}^{\nu\lambda} + \mathcal{D}^\nu \mathbf{G}^{\lambda\mu} \quad \Leftrightarrow \quad \mathcal{D}_\nu \star \mathbf{G}^{\mu\nu}. \tag{3.59}$$

The Georgi-Glashow Model

We follow [12] and [16]. Consider a $SO(3)$ gauge field interacting with a Higgs field $\mathbf{\Phi}$. The Lagrangian is

$$\mathcal{L} = -\frac{1}{4} G_a{}^{\mu\nu} G_{a\mu\nu} + \frac{1}{2}\mathcal{D}^\mu \mathbf{\Phi} \cdot \mathcal{D}_\mu \mathbf{\Phi} - V(\mathbf{\Phi}), \tag{3.60}$$

where

$$V(\mathbf{\Phi}) = \frac{1}{4}\lambda(\phi_1^2 + \phi_2^2 + \phi_3^2 - a^2). \tag{3.61}$$

The gauge field strength $G_a{}^{\mu\nu}$ is given by

$$G_a{}^{\mu\nu} = \partial^\mu W_a{}^\nu - \partial^\nu W_a{}^\mu - e\epsilon_{abc} W_b{}^\mu W_c{}^\nu. \tag{3.62}$$

$W_a{}^\mu$ is the gauge potential. We set $(T_a)^{ij} = -i\epsilon_{aij}$. The covariant derivative, $\mathcal{D}^\mu\phi := \partial^\mu\phi + ieD(\mathbf{W}^\mu)\phi$, of ϕ is then given by

$$(\mathcal{D}^\mu \mathbf{\Phi})_a = \partial^\mu \phi_a - e\epsilon_{abc} W_b{}^\mu \phi_c. \tag{3.63}$$

The conditions for the action $S = \int_{M^4} \mathcal{L} d^4x$ to be stationary are (we applied the Euler-Lagrange equations):

$$(\mathcal{D}_\nu G^{\mu\nu})_a = -e\epsilon_{abc}\phi_b (\mathcal{D}^\mu \mathbf{\Phi})_c \tag{3.64}$$

$$(\mathcal{D}^\mu \mathcal{D}_\mu \mathbf{\Phi})_a = -\lambda\phi_a(\phi^2 - a^2). \tag{3.65}$$

Furthermore, by construction the Bianchi identities are automatically valid:

$$\mathcal{D}_\mu \star \mathbf{G}^{\mu\nu} = 0. \tag{3.66}$$

The energy density corresponds to the (0,0)-component of the energy-momentum tensor for this theory:

$$\theta_{00} = \frac{1}{2}\{(\mathcal{E}_a{}^i)^2 + (\mathcal{B}_a{}^i)^2 + (\Pi_a)^2 + \left[\mathcal{D}^i\phi_a\right]^2\} + V(\mathbf{\Phi}) \tag{3.67}$$

where

$$G_a^{\ 0i} = -\mathcal{E}_a^{\ i}, \quad G_a^{\ ij} = -\epsilon_{ijk}\mathcal{B}_a^{\ k} \quad \text{and} \quad \Pi_a = (\mathcal{D}^0\mathbf{\Phi})_a. \tag{3.68}$$

We observe that θ_{00} vanishes if and only if:

$$G_a^{\ \mu\nu} = 0 \tag{3.69}$$

$$(\mathcal{D}^\mu\mathbf{\Phi})_a = 0 \tag{3.70}$$

$$V(\mathbf{\Phi}) = \frac{1}{4}\lambda(\phi^2 - a^2)^2 = 0. \tag{3.71}$$

A field configuration satisfying equations (3.69), (3.70) and (3.71) is called vacuum configuration. An example is:

$$\phi_a = a\delta_{a3} \quad W_a^{\ \mu} = 0, \tag{3.72}$$

where δ_{ab} denotes the Kronecker delta. A configuration satisfying equations (3.70) and (3.71) is called Higgs vacuum configuration. The introduction of a Higgs field is of great importance: To reach a state of finite energy, we have to ensure that our system reaches the Higgs vacuum state. The condition $V(\phi) = 0$ implies that $\phi_a\phi_a = a^2$. Alternatively stated:

$$\mathbf{\Phi} \in \mathcal{M}_0 \quad \text{where} \quad \mathcal{M}_0 = \{\mathbf{\Phi} : V(\mathbf{\Phi}) = 0\}. \tag{3.73}$$

$\mathcal{M}_0$ is a two-dimensional sphere of radius a. Since $\mathbf{\Phi}$ assumes a certain value in $\mathcal{M}_0$, it is not invariant under all rotations of $SO(3)$ but only under those around the $\mathbf{\Phi}$-axis. They form a subgroup $H_{\mathbf{\Phi}}$ of $SO(3)$. Of course, for each position of $\mathbf{\Phi}$ this group is isomorphic to SO(2), or equivalently U(1), and we will call it simply H. H is the exact symmetry group of the theory. By the introduction of the Higgs field $\mathbf{\Phi}$ the SO(3) symmetry of our model is spontaneously broken down to U(1).[20]

It is reasonable to identify H with the electromagnetic gauge group. The generator of this group is given by the orthogonal projection of a $SO(3)$ generator $\mathbf{T}$ onto the $\mathbf{\Phi}$-axis: $\mathbf{T} \cdot \mathbf{\Phi}/a$.

We will see that in the Higgs vacuum we can naturally obtain a correspondence with Maxwell's fields. If equations (3.70) and (3.71) do not hold, fundamentally new solutions can occur, such as magnetic monopoles.

From gauge field theory it is known that if we expand the Lagrangian about a vacuum configuration $\mathbf{\Phi}_0$, $(\mathbf{h}(x) = \mathbf{\Phi}_0 + \mathbf{\Delta}(x))$, the term in the Lagrangian that is proportional $\mathbf{\Delta}(x)^2$ corresponds to the square of the mass divided by $2\hbar$.

[20] In other words: Spontaneous symmetry breaking is the situation where the ground state of the theory has less symmetries than the Lagrangian itself.

Table 3.1: Particle Attributes

	Mass	Spin	Electric charge
Higgs particle	$\mu = a(2\lambda)^{1/2}\hbar$	0	0
Photon	0	$\hbar$	0
Massive gauge particles	$M = ae\hbar = aq$	$\hbar$	$\pm q = \pm e\hbar$

To obtain the electric charge, compare the covariant derivatives:

$$\partial^\mu + ieW_a{}^\mu T_a \quad \text{and} \quad \partial^\mu + i\frac{Q}{\hbar}A^\mu. \tag{3.74}$$

The second equation results from (3.33). This comparison can be done by performing a canonical projection for the connection of the $SO(3)$-covariant derivative:

$$ie\mathbf{W}^\mu \quad \rightarrow \quad ie(\frac{\mathbf{\Phi}}{a}\cdot\mathbf{W}^\mu)\cdot(\frac{\mathbf{\Phi}}{a}\cdot\mathbf{T}) \tag{3.75}$$

Taking the previously mentioned projection in $L(\mathcal{G})$, it is natural to identify A^μ with $\mathbf{\Phi}/a\cdot\mathbf{W}^\mu$. We find an electric charge operator

$$Q = e\hbar\frac{\mathbf{\Phi}}{a}\cdot\mathbf{T}. \tag{3.76}$$

This expression is valid in any representation. Let us quickly look at this more closely: In Maxwell's theory, the $U(1)$ generator is essentially given by the electric charge Q. A possible explanation for its quantisation would be that Q actually results from a larger gauge group, say $SO(3)$. Q is then also a generator of $SO(3)$ and element of the angular momentum algebra, so it has quantised eigenvalues.
Up to now, no magnetic monopoles are involved. Yet we need a mechanism, that tells us how to select the right directions within $so(3)$. This is given by the Higgs field (which cannot vanish in the vacuum in order to provide a distinct direction in the Lie algebra) and automatically yields magnetic monopoles. If extra fields are added to the model, T_a may even have any eigenvalue which is half an integer. Thus we are finally led to the condition that Q can only assume values that are integer multiples of $q_0 := \frac{1}{2}e\hbar$.

Monopole Solution

We are looking for simple –yet non-trivial – solutions for the model. A general solution for equations (3.64) and (3.65) is not known. We can expect the solution

with the lowest non-zero energy to be time-independent and highly symmetric. Several symmetry considerations lead to the ansatz (see [12]):

$$\phi_a(\vec{r}) = H(aer)r^a/ar^2 \quad W_a{}^0(\vec{r}) = 0 \tag{3.77}$$

$$W_a{}^i(\vec{r}) = -\epsilon_{aij}\frac{r^j}{er^2}\left[1 - K(aer)\right]. \tag{3.78}$$

To obtain finite energy we have to ensure that asymptotically, (3.71) is valid:

$$\phi_{\infty a}(\vec{r}) = \lim_{r\to\infty}\phi_{\mathbf{a}}(r\hat{r}) = a\hat{r}^a. \tag{3.79}$$

Thus $\mathbf{\Phi}$ defines a map from a two-sphere at spatial infinity to $\mathcal{M}_0$, which is essentially S^2:

$$\mathbf{\Phi} : S^2 \overset{homeo}{\cong} S^2_\infty \to \mathcal{M}_0 \overset{homeo}{\cong} S^2. \tag{3.80}$$

Note that it is impossible to transform configuration (3.79) into the vacuum configuration (3.72) in a continuous way: For every $\epsilon > 0$ there is a neighborhood U_ϵ of the south pole of S^2_∞, such that two values of $\mathbf{\Phi}$ that are assumed on U_ϵ exist that would have to be mapped by two rotations with rotation axis differing by $\pi/2$. Since this difference cannot be made arbitrarily small, the deformation is not continuous. Therefore we can expect the monopole to be stable in the sense that it will not fall into the vacuum state.

It exists a simpler way to obtain the equations of motion than to just plug our ansatz into equations (3.64) and (3.65). Faddeev ([17]) and Coleman ([18]) have found a principle which roughly states the following: Suppose we have a function (or as in our case: a functional) F defined on a set X. Let $\mathcal{G}_0$ be the group describing the symmetry operations of F on X. We denote the set of fixed points with respect to all symmetry operations by X_0. Then the stationary points of F over X_0 are also stationary points of F over X.

It is a fact that our ansatz (3.77) and (3.78) consists of those configurations which form the set X_0, since it was obtained by symmetry considerations.

We could also argue that we are looking for those configurations which minimize the energy ($\xi := aer$):

$$\begin{aligned} E &= -\int \mathcal{L}d^3r \\ &= \frac{4\pi a}{e}\int_0^\infty \frac{d\xi}{\xi^2}(\xi^2(\frac{dK}{d\xi})^2 + \frac{1}{2}(\xi\frac{dH}{d\xi} - H)^2 \\ &\quad + \frac{1}{2}(K^2-1)^2 + K^2H^2 + \frac{\lambda}{4e^2}(H^2-\xi^2)^2). \end{aligned} \tag{3.81}$$

Applying the Euler-Lagrange equations leads to:

$$\xi^2\frac{d^2K}{d\xi^2} = KH^2 + K(K^2-1) \tag{3.82}$$

$$\xi^2 \frac{d^2 H}{d\xi^2} = 2K^2 H + \frac{\lambda}{e^2} H(H^2 - \xi^2). \tag{3.83}$$

Since we require finite energy, equation (3.81) implies certain boundary conditions. As ξ goes to zero we should be able to compensate the divergence resulting from the pole of $1/\xi^2$. The first term of the integrand does not cause any problems. The second term gives the condition

$$H \leqslant \mathcal{O}(\xi) \quad (\xi \to 0). \tag{3.84}$$

For the third term:

$$K^2 - 1 = (K-1)(K+1) \Rightarrow K - 1 \leqslant \mathcal{O}(\xi) \quad (\xi \to 0). \tag{3.85}$$

These boundary conditions are also enough stringent for the two remaining terms. As ξ goes to infinity we need to ensure that the integrand vanishes fast enough:

$$K \to 0 \quad \text{and} \quad H \sim \xi \quad (\xi \to \infty). \tag{3.86}$$

The existence of solutions of (3.82) and (3.83) with boundary conditions (3.85)-(3.86) has been proven by Schwarz (see [19]) and was first conjectured by a numerical analysis.

Equations (3.77) and (3.78) will (in the regime where $\xi \to \infty$) asymptotically take the form:

$$\phi_a = \frac{r^a}{er^2} aer \quad \text{and} \quad W_a{}^i = -\epsilon_{aij} \frac{r^j}{er^2} \tag{3.87}$$

leading to a field strength tensor

$$\begin{aligned} G_a{}^{ij} &= \partial^i W_a{}^j - \partial^j W_a{}^i - e\epsilon_{abc} W_b{}^i W_c{}^j \\ &\sim \frac{1}{er^4} \epsilon_{ijk} r^a r^k \sim \frac{1}{aer^3} \epsilon_{ijk} r^k \phi_a. \end{aligned} \tag{3.88}$$

After a projection on the $\mathbf{\Phi}$-axis we obtain

$$F^{ij} = \frac{\mathbf{\Phi}}{a} \cdot \mathbf{G}^{ij} = \frac{1}{er^3} \epsilon_{ijk} r^k$$

$$\Rightarrow B^i = -\frac{r^i}{er^3}, \quad \text{since} \quad F^{ij} = -\epsilon_{ijk} B^k. \tag{3.89}$$

Comparing this result with equation (3.12) gives the magnitude of the magnetic charge:

$$g = -\frac{4\pi}{e} = -\frac{4\pi\hbar}{q}. \tag{3.90}$$

This is consistent with the Dirac condition (3.18). By (3.76) it follows that the smallest possible charge that may enter the theory is $q_0 = \frac{1}{2}q$ because the possible electric charges are related to the eigenvalues of $\mathbf{T}$. We get

$$\frac{q_0 g}{4\pi\hbar} = -\frac{1}{2} \tag{3.91}$$

and g assumes the smallest value allowed by the Dirac condition.

The set of equations (3.82) and (3.83) can be solved in the limit where $\xi \to \infty$. Thus we can make a statement of how fast the asymptotic values of the boundary conditions (3.85)-(3.86) are assumed. We expand (3.82):

$$\frac{d^2K}{d\xi^2} = K \underbrace{\frac{H^2}{\xi^2}}_{\approx 1} + \underbrace{\frac{K(K^2-1)}{\xi^2}}_{\approx 0} \approx K \tag{3.92}$$

and (3.83):

$$\begin{aligned} \frac{d^2H}{d\xi^2} &= \underbrace{\frac{1}{\xi^2}2K^2H}_{\approx 0} + \frac{1}{\xi^2}\frac{\lambda}{e^2}H(H^2-\xi^2) \approx \frac{\lambda}{e^2\xi}\underbrace{(H+\xi)}_{\approx 2\xi}(H-\xi). \\ &\approx \frac{2\lambda}{e^2}\overbrace{(H-\xi)}^{=:h} \qquad \Rightarrow \frac{d^2h}{d\xi^2} \approx \frac{2\lambda}{e^2}h. \end{aligned} \tag{3.93}$$

The equations of motion are now decoupled linear differential equations and as such easy to solve. Finally, we get

$$K = \mathcal{O}\left[\exp(-\xi)\right] = \mathcal{O}\left[\exp(-Mr/\hbar)\right] \tag{3.94}$$

$$H - \xi = \mathcal{O}\left[\exp(-\mu\xi/M\right] = \mathcal{O}\left[\exp(-\mu r/\hbar)\right] \tag{3.95}$$

where $\mu := (2\lambda)^{1/2}a\hbar$ and $M := ae\hbar$ are the masses of the Higgs and the massive gauge particles respectively as introduced in chapter (2). Thus by this result (i.e. by the at least exponential decay), we can consider the 't Hooft-Polyakov monopole to have finite size, principally determined by the Compton wavelengths $\hbar/M$ and $\hbar/\mu$:

Inside we have a smooth structure; outside we obtain a field configuration indistinguishable from that of the Dirac monopole.

Connection with Maxwell's Equations

In chapter 2 we have seen that outside a radius R_0, which is determined by the Compton wavelengths of the heavy particles in the theory, our field is exponentially close to the Higgs vacuum (3.70) & (3.71). This was based on an analysis

of the field configuration with the lowest non-zero energy.
We will now assume that *any* finite-energy solution will be very close to the Higgs vacuum except for a finite number of areas, which we will regard as monopoles. With a given $\mathbf{\Phi}$, the general form of $\mathbf{W}^\mu$ satisfying (3.70) and (3.71) is

$$\mathbf{W}^\mu = \frac{1}{a^2 e}\mathbf{\Phi} \wedge \partial^\mu \mathbf{\Phi} + \frac{1}{a}\mathbf{\Phi} A^\mu \tag{3.96}$$

where A^μ is an arbitrary smooth four-vector function (see [20]). We shall content ourselves with the following calculation, which shows that (3.96) is indeed in the Higgs vacuum:

$$\begin{aligned} \mathcal{D}^\mu \mathbf{\Phi} &= \partial^\mu \mathbf{\Phi} - (\frac{1}{a^2}\mathbf{\Phi} \wedge \partial^\mu \mathbf{\Phi}) \wedge \mathbf{\Phi} + (\frac{e}{a}\mathbf{\Phi} A^\mu) \wedge \mathbf{\Phi} \\ &= \partial^\mu \mathbf{\Phi} + \frac{1}{a^2}\mathbf{\Phi} \cdot (\mathbf{\Phi} \cdot \partial^\mu \mathbf{\Phi}) - \partial^\mu \mathbf{\Phi} \frac{1}{a^2} \cdot (\mathbf{\Phi} \cdot \mathbf{\Phi}) = 0. \end{aligned} \tag{3.97}$$

The second term in the second line vanishes due to the Leibniz rule:

$$0 = \partial^\mu (\mathbf{\Phi} \cdot \mathbf{\Phi}) = (\mathbf{\Phi} \cdot \partial^\mu \mathbf{\Phi}) + (\partial^\mu \mathbf{\Phi} \cdot \mathbf{\Phi}) = 2 \cdot (\partial^\mu \mathbf{\Phi} \cdot \mathbf{\Phi}).$$

Furthermore we get

$$\begin{aligned} \mathbf{G}^{\mu\nu} &= \frac{1}{a}\mathbf{\Phi} F^{\mu\nu} \\ &\quad \text{with} \quad F^{\mu\nu} = \frac{1}{a^3 e}\mathbf{\Phi} \cdot (\partial^\mu \mathbf{\Phi} \wedge \partial^\nu \mathbf{\Phi}) + \partial^\mu A^\nu - \partial^\nu A^\mu. \end{aligned} \tag{3.98}$$

This result is derived in the appendix. The field tensor points in the direction of $\mathbf{\Phi}$. So the only non-vanishing component of $\mathbf{G}^{\mu\nu}$ is exactly the one associated with the $U(1)$ gauge group of rotations about $\mathbf{\Phi}$, which we can identify with the electromagnetic field strength tensor.

$$\begin{aligned} 0 = \mathcal{D}_\nu \mathbf{G}^{\mu\nu} &= \partial_\nu \mathbf{G}^{\mu\nu} - e\mathbf{W}_\nu \wedge \mathbf{G}^{\mu\nu} \\ &= \partial_\nu (\frac{1}{a}\mathbf{\Phi} F^{\mu\nu}) - e(\frac{1}{a^2 e}\mathbf{\Phi} \wedge \partial_\nu \mathbf{\Phi} + \frac{1}{a}\mathbf{\Phi} A_\nu) \wedge (\frac{1}{a}\mathbf{\Phi} F^{\mu\nu}) \\ &= \frac{1}{a}\partial_\nu \mathbf{\Phi} F^{\mu\nu} + \frac{1}{a}\mathbf{\Phi}\ \partial_\nu F^{\mu\nu} + \frac{1}{a^3}\mathbf{\Phi} F^{\mu\nu} \wedge (\mathbf{\Phi} \wedge \partial_\nu \mathbf{\Phi}) \\ &= \frac{1}{a}\partial_\nu \mathbf{\Phi} F^{\mu\nu} + \frac{1}{a}\mathbf{\Phi} \partial_\nu F^{\mu\nu} - \frac{1}{a^3} F^{\mu\nu} \partial_\nu \mathbf{\Phi} a^2 \\ &= \frac{1}{a}\mathbf{\Phi} \partial_\nu F^{\mu\nu}. \end{aligned} \tag{3.99}$$

Since the modulus of $\mathbf{\Phi}$ is finite, this equation only holds if $\partial_\nu F^{\mu\nu} = 0$. Analogously, we can transform the Bianchi identity $\mathcal{D}_\nu \star \mathbf{G}^{\mu\nu} = 0$ into the homogeneous Maxwell equations $\partial_\nu \star F^{\mu\nu}$. So outside the monopole our $SO(3)$ theory coincides with Maxwell's $U(1)$ theory.

Generalised Quantisation Condition for the 't Hooft-Polyakov Monopole

We proceed with our analysis of a field in the Higgs vacuum by regarding the magnetic flux, g_Σ, through a surface Σ. Since outside the monopole the fields obey Maxwell's equations, it is only possible to receive a non-zero flux by integrating over a surface that surrounds a region where (3.70) and (3.71) are not satisfied, namely around a monopole region:

$$\begin{aligned} g_\Sigma &= \int_\Sigma \vec{B} \cdot d\vec{S} \\ &= \int_\Sigma -\frac{1}{2}\epsilon_{ijk} F^{jk} \cdot dS^i \\ &\overset{(3.98)}{=} \int_\Sigma -\frac{1}{2}\epsilon_{ijk} \frac{1}{a^3 e} \mathbf{\Phi} \cdot (\partial^j \mathbf{\Phi} \wedge \partial^k \mathbf{\Phi}) dS^i. \end{aligned} \tag{3.100}$$

The last term in equation (3.98) vanishes due to Stokes' theorem ($\partial S = \emptyset$). If Σ has the shape of a sphere (as we had it before: take e.g. S^2_∞) we see immediately that the derivatives $\partial^i \mathbf{\Phi}$ are tangential to S^2_a. Thus the magnetic charge only depends on the values that $\mathbf{\Phi}$ assumes on Σ.

Furthermore consider a variation of the field

$$\mathbf{\Phi} + \delta\mathbf{\Phi} \qquad \mathbf{\Phi} \cdot \delta\mathbf{\Phi} = 0. \tag{3.101}$$

The variation of the integrand is then given by

$$\begin{aligned} \delta\left[\mathbf{\Phi} \cdot (\partial^j \mathbf{\Phi} \wedge \partial^k \mathbf{\Phi})\right] &= 3\delta\mathbf{\Phi} \cdot (\partial^j \mathbf{\Phi} \wedge \partial^k \mathbf{\Phi}) + \partial^j \left[\mathbf{\Phi} \cdot (\delta\mathbf{\Phi} \wedge \partial^k \mathbf{\Phi})\right] \\ &\quad -\partial^k \left[\mathbf{\Phi} \cdot (\delta\mathbf{\Phi} \wedge \partial^j \mathbf{\Phi})\right] \end{aligned} \tag{3.102}$$

using $\delta\partial^i \mathbf{\Phi} = \partial^i \delta\mathbf{\Phi}$ and the cyclic permutations of $\vec{a} \cdot (\vec{b} \wedge \vec{c})$. As we consider three spatial dimensions, $\partial^j \mathbf{\Phi} \wedge \partial^k \mathbf{\Phi}$ is orthogonal to $\delta\mathbf{\Phi}$ and the first term vanishes. Again, we can apply Stokes' theorem and the last two terms vanish when integrated over Σ.

Thus the magnetic flux is stable against small deformations (*homotopies*) of the Higgs field. Physically, homotopies are generated by

- time development of $\mathbf{\Phi}$,
- continuous gauge transformations of $\mathbf{\Phi}$,
- deformations of the surface Σ within the Higgs vacuum.

Thus g_Σ is time- and gauge-independent and does not vary under continuous deformations of Σ. In particular, g is an additive 'quantum number' as made plausible in the figure 3.1:

$$g_{\Sigma_{12}} = g_{\Sigma_1} + g_{\Sigma_2}. \tag{3.103}$$

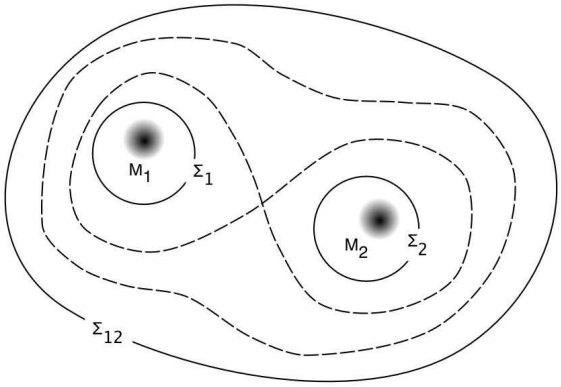

Figure 3.1: Continuous deformation of the surface Σ_{12} into the surfaces Σ_1 and Σ_2.

The quantisation comes from the fact that we can write $g_{_\Sigma} = -4\pi N$ where N indicates the so called Kronecker index of the map $\phi : \Sigma \to \mathcal{M}_0$. To be more precise, continue with (3.100):

$$g_{_\Sigma} = -\frac{1}{2a^3 e}\int_\Sigma \epsilon_{ijk}\phi_a\epsilon_{abc}\partial^j\phi_b\partial^k\phi_c dS^i \tag{3.104}$$

Σ is a two-manifold and can thus (locally) be parametrised by two parameters ξ_α ($\alpha \in \{1,2\}$):

$$x^i = x^i(\xi_\alpha).$$

With elementary calculus we derive

$$dS^i = \frac{1}{2}\epsilon_{imn}\frac{\partial x^m}{\partial\xi^\alpha}\frac{\partial x^n}{\partial\xi^\beta}\epsilon_{\alpha\beta}d^2\xi \quad \text{and} \quad \partial_j\phi_b = \frac{\partial\xi^\gamma}{\partial x^j}\frac{\partial\phi_b}{\partial\xi^\gamma}$$

and get:

$$\begin{aligned} g_{_\Sigma} &= -\frac{1}{2a^3e}\int_\Sigma \frac{1}{2}\epsilon_{ijk}\phi_a\epsilon_{abc}\epsilon_{\alpha\beta}\epsilon_{imn}\frac{\partial\xi^\gamma}{\partial x^j}\frac{\partial\phi_b}{\partial\xi^\gamma}\frac{\partial\xi^\lambda}{\partial x^k}\frac{\partial\phi_c}{\partial\xi^\lambda}\frac{\partial x^m}{\partial\xi^\alpha}\frac{\partial x^n}{\partial\xi^\beta}d^2\xi \\ &\quad \text{(using} \quad \epsilon_{ijk}\epsilon_{imn} = \delta_{jm}\delta_{kn} - \delta_{jn}\delta_{km} \quad \text{and the chain rule)} \\ &= -\frac{1}{a^3e}\int_\Sigma \frac{1}{2}\epsilon_{abc}\epsilon_{\alpha\beta}\phi_a\frac{\partial\phi_b}{\partial\xi^\alpha}\frac{\partial\phi_c}{\partial\xi^\beta}d^2\xi \\ &= -\frac{1}{2e}\int_\Sigma \epsilon_{abc}\epsilon_{\alpha\beta}\hat{\phi}_a\frac{\partial\hat{\phi}_b}{\partial\xi^\alpha}\frac{\partial\hat{\phi}_c}{\partial\xi^\beta}d^2\xi. \end{aligned} \tag{3.105}$$

For the square of the integrand we compute

$$\begin{aligned} (\epsilon_{abc}\epsilon_{\alpha\beta}\hat{\phi}_a\frac{\partial\hat{\phi}_b}{\partial\xi^\alpha}\frac{\partial\hat{\phi}_c}{\partial\xi^\beta})^2 &= (\epsilon_{\alpha\beta}\hat{\phi}_a(\hat{\phi_\alpha}\wedge\hat{\phi_\beta})_a)^2 \\ &= 4\mathbf{G}(\frac{\partial\hat{\mathbf{\Phi}}}{\partial\xi^\alpha},\frac{\partial\hat{\mathbf{\Phi}}}{\partial\xi^\beta}) \end{aligned} \tag{3.106}$$

where $\mathbf{G}$ denotes Gram's determinant (we used the fact that $\hat{\mathbf{\Phi}}$ has unit length and is parallel to $\frac{\partial \mathbf{\Phi}}{\partial \xi^\alpha} \wedge \frac{\partial \mathbf{\Phi}}{\partial \xi^\beta}$). Thus we are integrating over $\pm 2\sqrt{\mathbf{G}}$. While (ξ_α, ξ_β) covers the sphere S^2_∞ once, $\hat{\mathbf{\Phi}}$ covers S^2 N_+ times with the positive sign of $\sqrt{\mathbf{G}}$ and N_- times with the negative sign. Since the ϕ_a are supposed to be single-valued functions the difference $N_+ - N_-$ has to be an integer N, thus

$$g_\Sigma = -\frac{4\pi N}{e}. \tag{3.107}$$

Considering the map

$$\mathbf{\Phi}_N(\vec{r}) = a(\cos N\chi \sin\theta, \sin N\chi \sin\theta, \cos\theta), \tag{3.108}$$

we see immediately that indeed every N can be realised. We obtain the beautiful result that the magnetic charge is quantised by topological reasons. The smallest electric charge entering the theory is $q_0 = \frac{1}{2}e\hbar$ and we deduce

$$\frac{gq_0}{4\pi\hbar} = -\frac{1}{2}N, \tag{3.109}$$

which is identical to the Dirac quantisation condition (3.18)!

Topological Aspects

In what comes next, we will see three further approaches to characterise a smooth map $\hat{\mathbf{\Phi}}$ between two spheres (see [21], [22] or [16]), that emerges from the map $\mathbf{\Phi}$ induced by the Higgs field. In the end of this section we will see the implications of these three viewpoints.

Brouwer Degree Reconsider the mapping induced by the Higgs field $\hat{\mathbf{\Phi}} : S^2_\infty \to S^2$ and introduce also in the target space local coordinates, say ϕ_α ($\alpha \in \{1, 2\}$), such that $\phi_\alpha = \phi_\alpha(\xi_\beta)$. Fix a regular value $\psi = (\psi_1, \psi_2)$ (i.e. the Jacobian of $\hat{\mathbf{\Phi}}$ does not vanish at any point in $\hat{\mathbf{\Phi}}^{-1}(\psi)$).

The Brouwer degree of the map $\hat{\mathbf{\Phi}}$ at the point ψ is defined as

$$d(\hat{\mathbf{\Phi}}; \psi) = \sum_{\xi \in \phi^{-1}(\psi)} \operatorname{sgn}\det\left(\frac{\partial \phi_\alpha}{\partial \xi^\beta}\right). \tag{3.110}$$

It can be shown that d does not depend on the particular choice of a regular point in S^2. Thus we can write: $d(\hat{\mathbf{\Phi}}; \psi) = d(\hat{\mathbf{\Phi}})$.

Homotopy Classes A continuous map $\psi : X \to Y$, where X and Y are topological spaces, is called a *based* map, if we can identify two base points x_0, y_0

in X and Y respectively such that $\psi(x_0) = y_0$. Two based maps ψ_0 and ψ_1 are called *homotopic* if and only if there is a continuous map

$$\tilde{\psi} : X \times [0,1] \to Y \tag{3.111}$$

with a parameter $\tau \in [0,1]$, such that $\tilde{\psi}|_{\tau=0} = \psi_0$ and $\tilde{\psi}|_{\tau=1} = \psi_1$ and $\tilde{\psi}(x_0;\tau) = y_0 \ \forall \tau \in [0,1]$. It can be shown that "homotopic" defines an equivalence relation. For the special case where $X \cong S^n$ the set of homotopy classes of based maps $\psi : S^n \to Y$ is denoted by $\Pi_n(Y)$. For $n \geqslant 1$, Π_n forms a group, where the group multiplication of two equivalence classes is realised as follows: Consider a representative of a class. Due to the stereographic projection such a map can be characterised by $\psi_1 : (I^n, \partial I^n) \to (Y, y_0)$, where $I := [0,1]$ and the homotopies $\psi_{1\tau}$ are required to satisfy $\psi_{1\tau}(\partial I^n) = y_0 \ \forall \tau$. It can be shown that

$$\psi_1 \cdot \psi_2(s_1, s_2, \ldots, s_n) := \begin{cases} \psi_1(2s_1, s_2, \ldots, s_n) & s_1 \in [0, 1/2] \\ \psi_2(2s_1 - 1, s_2, \ldots, s_n) & s_1 \in [1/2, 1] \end{cases} . \tag{3.112}$$

does indeed define a group operation.

An interesting result of algebraic topology is

$$\Pi_n(S^n) = \mathbb{Z} \quad \forall n \geqslant 1. \tag{3.113}$$

Thus in our case, every homotopy class is uniquely characterised by an integer number.

Poincaré-Hopf Index Let $\vec{x}_0$ be an isolated zero of the Higgs field $\mathbf{\Phi}$. Introduce a small two sphere S^2_ϵ with center $\vec{x}_0$. The Brouwer index of the normalized field $\hat{\tilde{\mathbf{\Phi}}} : S^2_\epsilon \to S^2$ is called Poincaré-Hopf index i of the zero $\vec{x}_0$.

Implications Now we illuminate the connections between these three definitions: Firstly, it is a special case of a general theorem of Hopf that two smooths maps ψ_0 and ψ_1 are homotopic if and only if they have the same Brouwer degree. Secondly, if $\mathbf{\Phi}$ has only nondegenerate zeros, the Brouwer degree of $\hat{\mathbf{\Phi}}$ equals the sum of the Poincaré-Hopf indices of all zeros of $\mathbf{\Phi}$. Thirdly, the Brouwer degree $d(\hat{\mathbf{\Phi}})$ is equal to the Kronecker index $N_{\hat{\mathbf{\Phi}}}$.

These facts enable us to determine the magnetic charge of a field configuration by topological analysis of the Higgs field.

Relation between the Dirac and the 't Hooft-Polyakov Monopole

See also [16] and [13]. It seems rather amazing that we receive the same quantisation condition for the Dirac and for the 't Hooft-Polyakov monopole. There is indeed a connection between these two.

Notwithstanding certain technical assumptions, we can write $M_H = G/H$ where M_H is the vacuum manifold, G the original gauge group and H the gauge group after symmetry breaking. Thus the magnetic charge can by the previous chapter be characterised by $\Pi_2(G/H)$.

Furthermore, in the case of the Dirac monopole, the gauge transformations $e^{-ie\chi(\phi)}$ between the gauge fields on the two hemispheres of S^2 (see chapter (1)) are paths in $U(1) \cong S^1$ and can be classified by $\Pi_1(U(1)) = \Pi_1(S^1) = \Pi_1(H)$. The integer n has again the meaning of a winding number in this context.

It is a remarkable result of algebraic topology that

$$\Pi_2(G/H) = \Pi_1(H), \tag{3.114}$$

or in our special case:

$$\Pi_2(SO(3)/U(1)) = \Pi_2(S^2) = \Pi_1(S^1). \tag{3.115}$$

This corresponds with equation (3.113) and yields a link between the Dirac and the 't Hooft-Polyakov point of view.

To be more concrete, let us try to gauge $\hat{\mathbf{\Phi}}$ such that it points in the direction of T^3. Of course, if $\hat{\mathbf{\Phi}}$ has a non-vanishing winding number, we cannot transform it smoothly into the constant map. However, this can be done on the northern (we denote the group element of the associated gauge transformation by $g^{(1)}$) and southern hemisphere ($g^{(2)}$) of S^2 respectively. On the overlap region (=equator), $g^{(1)}{g^{(2)}}^{-1}$ preserves $\hat{\mathbf{\Phi}}' = T^3$ and therefore lies in the $U(1)$ subgroup of $SU(2)$ generated by T^3: $g^{(1)}{g^{(2)}}^{-1} = \exp(i\alpha(\phi)T^3)$.

The gauge transformations $g^{(1)}$ and $g^{(2)}$ are well defined on their respective regions: $\alpha(2\pi) = \alpha(0) + 2\pi\tilde{N}$, $\tilde{N} \in \mathbb{Z}$. Consider now the two abelianised gauge fields that we get after the transformation (which, for the Higgs field, looks as follows: $\hat{\mathbf{\Phi}}^{(1)} = D(g^{(1)}{g^{(2)}}^{-1})\hat{\mathbf{\Phi}}^{(2)} = g^{(1)}{g^{(2)}}^{-1}\hat{\mathbf{\Phi}}^{(2)}$):

$$\mathbf{A}^{(1)} - \mathbf{A}^{(2)} = -\frac{1}{e}\vec{\nabla}\alpha. \tag{3.116}$$

Since the Higgs field is now constant, equation (3.98) exactly simplifies to the case of the Dirac monopole: the total magnetic flux is determined in the same way and does only depend on the amount by which α increases around the equator. One can show that $\tilde{N} = N$.

Bogomolny Bound on the Monopole Mass

In the remaining part of this article we refer to [12]. Contrary to the Dirac monopole, which we have to regard as an external source and for which it is therefore impossible to calculate the mass, we can give an estimate for the lower bound on the mass of the 't Hooft-Polyakov monopole.

From differential geometry we have the following formula holding for covariant derivatives:

$$X \cdot \langle Y, Z\rangle = \langle \mathcal{D}_X Y, Z\rangle + \langle Y, \mathcal{D}_X Z\rangle$$

where the connection of $\mathcal{D}$ is compatible with $\langle\ ,\ \rangle$ and X,Y,Z denote smooth vector fields. Thus (without proving the compatibility of $\mathcal{D}$ with $\langle\ ,\ \rangle$), it follows that

$$\partial_k(\mathcal{B}_a^k \phi_a) = \underbrace{\mathcal{D}^k \mathcal{B}_a{}^k}_{=0} \phi_a + \mathcal{B}_a{}^k (\mathcal{D}^k \mathbf{\Phi})_a. \tag{3.117}$$

The first term vanishes due to the Bianchi identity. We compute the magnetic charge:

$$\begin{aligned} g &= \int_{S^2_\infty} \vec{B} \cdot d\vec{S} = \int \partial_k B^k d^3 r = \frac{1}{a} \int \partial_k (\mathcal{B}_a{}^k \phi_a) d^3 r \\ &= \frac{1}{a} \int \mathcal{B}_a{}^k (\mathcal{D}^k \mathbf{\Phi})_a d^3 r. \end{aligned} \tag{3.118}$$

Similarly we receive an expression for the electric charge

$$q = \int_{S^2_\infty} \vec{E} \cdot d\vec{S} = \frac{1}{a} \int \mathcal{E}_a{}^k (\mathcal{D}^k \mathbf{\Phi})_a d^3 r \tag{3.119}$$

using the equations of motion (3.64). Consider the center-of-mass frame of the monopole. Einstein's relation $E^2 = M^2 + \vec{p}^2$ (E is the energy and $\vec{p}$ the momentum) simplifies to $E = M$ and we get

$$\begin{aligned} M = E &= \int d^3 r \{ \frac{1}{2} \left[(\mathcal{E}_a{}^k)^2 + (\mathcal{B}_a{}^k)^2 + (\mathcal{D}^0 \mathbf{\Phi})^2 + (\mathcal{D}^i \mathbf{\Phi})^2 \right] + V(\phi) \} \\ &\geqslant \int d^3 r \frac{1}{2} \{ (\mathcal{E}_a{}^k)^2 + (\mathcal{B}_a{}^k)^2 + (\mathcal{D}^i \mathbf{\Phi})^2 \} \\ &= \frac{1}{2} \int d^3 r \{ \mathcal{E}_a{}^k - (\mathcal{D}^k \mathbf{\Phi})_a \sin\theta \}^2 + \frac{1}{2} \int d^3 r \{ \mathcal{B}_a{}^k - (\mathcal{D}^k \mathbf{\Phi})_a \cos\theta \}^2 \\ &\quad + a(q \sin\theta + g \cos\theta) \\ &\geqslant a(q \sin\theta + g \cos\theta) \end{aligned} \tag{3.120}$$

where the non-trivial step is the third equality. The estimate holds for any $\theta \in \mathbb{R}$ and we can interpret the last line as the standard scalar product of the vector $\vec{\gamma} = (aq, ag)$ and the unit vector $\vec{e}_\theta = (\cos\theta, \sin\theta)$. Since θ is arbitrary, we choose $\vec{e}_\theta$ parallel to $\vec{\gamma}$. The last line then equals the norm of $\vec{\gamma}$ and we get the most stringent inequality, the Bogomolny bound on the monopole mass:

$$M \geqslant a(q^2 + g^2)^{1/2}. \tag{3.121}$$

For the 't Hooft-Polyakov monopole (equation (3.119) would not have been needed):

$$M \geqslant a|g|. \tag{3.122}$$

Choosing the smallest possible magnetic charge $|g| \overset{(3.107)}{=} 4\pi/e$ we can compare the monopole mass M_g with the mass $M_q = ae\hbar = qa$ of the heavy gauge bosons in the theory (see table 3.1):

$$M_g \geqslant \frac{4\pi\hbar}{q^2} M_q = \frac{\nu}{\alpha} M_q. \tag{3.123}$$

$\nu \in \{1, 1/4\}$ depending on whether the electron charge is q or $q/2$ and α is the fine-structure constant. In any case, M_g is is much larger than M_q. This makes it impossible to observe magnetic monopoles with contemporary technologies.

Bogomolny-Prasad-Sommerfield (BPS-) Monopole

In this chapter we will see that for the special case of a vanishing potential $V(\mathbf{\Phi})$ analytic solutions of our problem exist, which saturate the bound (3.122). Thus the inequalities in the Bogomolny estimate have to become equalities. This implies the following conditions (q=0):

$$\mathcal{D}^0 \mathbf{\Phi} = 0 \qquad \mathcal{E}_a{}^i = 0 \tag{3.124}$$

$$\mathcal{B}_a{}^i = \pm(\mathcal{D}^i \phi)_a \qquad \text{as} \qquad g \gtrless 0 \tag{3.125}$$

$$V(\mathbf{\Phi}) = 0. \tag{3.126}$$

These equations can only be simultaneously realised in the limit $\lambda \to 0^+$ for the proportionality constant of the potential V.

Although V vanishes ultimately, we will keep the boundary condition

$$|\mathbf{\Phi}| \to a \qquad \text{as} \qquad r \to \infty. \tag{3.127}$$

such that the charges are still defined and quantised. The equations of motion now take the form

$$\mathcal{D}_\nu G^{\mu\nu} = e\mathbf{\Phi} \wedge \mathcal{D}^\mu \mathbf{\Phi} \qquad \mathcal{D}_\mu \mathcal{D}^\mu \mathbf{\Phi} = 0. \tag{3.128}$$

Equation (3.125) is called the Bogomolny equation and is a first order differential equation. While the equations of motion give a condition for stationary points of the energy, the Bogomolny equation yields a global minimum of the energy for a given N. With a straightforward computation, it can be shown that such a minimum is indeed a stationary point.

Using our ansatz (3.77) & (3.78) we get:

$$\xi \frac{dK}{d\xi} = -KH \qquad \xi \frac{dH}{d\xi} = H - (K^2 - 1). \tag{3.129}$$

By differentiating the one and substituting it into the other equation we would get the original equations (3.82) and (3.83). The change of variables $H = -1-\xi h$ and $K = \xi k$ yields the equations (' denotes the derivative)

$$k' = hk \qquad \text{and} \qquad h' = k^2. \tag{3.130}$$

This system can be decoupled:

$$h'' = 2kk' = 2hk^2 = 2hh' = (h^2)' \Rightarrow h' = h^2 + A, \quad A \in \mathbb{R}. \tag{3.131}$$

The boundary conditions (3.85)-(3.86) yield that $h \to -1$ and $h' \to 0$. This leads –by substitution in the differential equation– to $A = -1$. So we can integrate equation (3.131):

$$\xi + B = -\int dh \frac{1}{1-h^2} = -\coth^{-1}(h), \quad B \in \mathbb{R}$$

$$\Rightarrow h = -\coth(\xi + B). \tag{3.132}$$

B has to be zero since this is the only value for which $H = -\xi h - a$ is continuous (only then the divergence of $\coth(\xi + B)$ at $\xi = -B$ can be compensated) and k is now easily obtained:

$$k = \pm\sqrt{h'} = \pm\frac{1}{\sinh\xi}. \tag{3.133}$$

Since $K - 1 \overset{!}{\leqslant} \mathcal{O}(\xi)$ as $\xi \to 0$ we choose the positive sign and finally obtain a solution in terms of elementary functions:

$$H(\xi) = \xi\coth\xi - 1 \tag{3.134}$$

$$K(\xi) = \frac{\xi}{\sinh\xi} \tag{3.135}$$

The massless Higgs field is now long range because as $r \to \infty$:

$$\phi_a \to a\hat{r}^a - \frac{\hat{r}^a}{er} \tag{3.136}$$

With "long range" we mean that in addition to the previously derived exponential decay we have a much slower algebraic decay. Due to the Bogomolny equation the contribution of the gauge and the Higgs field to the mass density are equal. This results in a twice as big density in the tail of the monopole as we had it in the constructions by 't Hooft-Polyakov (for $\lambda > 0$) or Dirac. This should yield observable consequences if we analyse interactions with a gravitational field.
Furthermore, the long range force exerted by the Higgs field is always attractive and has been found to be equal in magnitude (see [23]) to the magnetic force

law induced by equation (3.12): Oppositely charged monopoles experience an enforcement of the attraction but in the case of equally charged monopoles the two forces exactly cancel. We conclude with the remark that the BPS-monopole shows that the 't Hooft-Polyakov construction can differ essentially from the one given by Dirac and that it is therefore more general.

3 Appendix

Field Strength Tensor in the Higgs Vacuum

We obtain this form by straightforward computation:

$$
\begin{aligned}
\mathbf{G}^{\mu\nu} &= \partial^\mu \mathbf{W}^\nu - \partial^\nu \mathbf{W}^\mu + ie\,[\mathbf{W}^\mu, \mathbf{W}^\nu] \\
&= \frac{1}{a^2 e}(\partial^\mu \mathbf{\Phi} \wedge \partial^\nu \mathbf{\Phi} + \mathbf{\Phi} \wedge \partial^\mu \partial^\nu \mathbf{\Phi}) + \frac{1}{a}\partial^\mu \mathbf{\Phi} A^\nu + \frac{1}{a}\mathbf{\Phi}\partial^\mu A^\nu \\
&\quad -\frac{1}{a^2 e}(\partial^\nu \mathbf{\Phi} \wedge \partial^\mu \mathbf{\Phi} + \mathbf{\Phi} \wedge \partial^\nu \partial^\mu \mathbf{\Phi}) - \frac{1}{a}\partial^\nu \mathbf{\Phi} A^\mu - \frac{1}{a}\mathbf{\Phi}\partial^\nu A^\mu \\
&\quad +ie\left[\frac{1}{a^2 e}\mathbf{\Phi} \wedge \partial^\mu \mathbf{\Phi} + \frac{1}{a}\mathbf{\Phi} A^\mu, \frac{1}{a^2 e}\mathbf{\Phi} \wedge \partial^\nu \mathbf{\Phi} + \frac{1}{a}\mathbf{\Phi} A^\nu\right] \\
&= \frac{2}{a^2 e}\partial^\mu \mathbf{\Phi} \wedge \partial^\nu \mathbf{\Phi} + \frac{1}{a}\mathbf{\Phi}(\partial^\mu A^\nu - \partial^\nu A^\mu) + \frac{1}{a}(\partial^\mu \mathbf{\Phi} A^\nu - \partial^\nu \mathbf{\Phi} A^\mu) \\
&\quad +ie\left[\frac{1}{a^2 e}\mathbf{\Phi} \wedge \partial^\mu \mathbf{\Phi}, \frac{1}{a^2 e}\mathbf{\Phi} \wedge \partial^\nu \mathbf{\Phi}\right] + ie\left[\frac{1}{a^2 e}\mathbf{\Phi} \wedge \partial^\mu \mathbf{\Phi}, \frac{1}{a}\mathbf{\Phi} A^\nu\right] \\
&\quad +ie\left[\frac{1}{a}\mathbf{\Phi} A^\mu, \frac{1}{a^2 e}\mathbf{\Phi} \wedge \partial^\nu \mathbf{\Phi}\right] + ie\left[\frac{1}{a}\mathbf{\Phi} A^\mu, \frac{1}{a}\mathbf{\Phi} A^\nu\right] \\
&= \frac{2}{a^2 e}\partial^\mu \mathbf{\Phi} \wedge \partial^\nu \mathbf{\Phi} + \frac{1}{a}\mathbf{\Phi}(\partial^\mu A^\nu - \partial^\nu A^\mu) + \frac{1}{a}(\partial^\mu \mathbf{\Phi} A^\nu - \partial^\nu \mathbf{\Phi} A^\mu) \\
&\quad +\frac{-1}{a^4 e}(\mathbf{\Phi} \wedge \partial^\mu \mathbf{\Phi}) \wedge (\mathbf{\Phi} \wedge \partial^\nu \mathbf{\Phi}) + \frac{-1}{a^3}(\mathbf{\Phi} \wedge \partial^\mu \mathbf{\Phi}) \wedge (\mathbf{\Phi} A^\nu) \\
&\quad +\frac{-1}{a^3}\mathbf{\Phi} A^\mu \wedge (\mathbf{\Phi} \wedge \partial^\nu \mathbf{\Phi}) \\
&= \frac{2}{a^2 e}\partial^\mu \mathbf{\Phi} \wedge \partial^\nu \mathbf{\Phi} + \frac{1}{a}\mathbf{\Phi}(\partial^\mu A^\nu - \partial^\nu A^\mu) + \frac{1}{a}(\partial^\mu \mathbf{\Phi} A^\nu - \partial^\nu \mathbf{\Phi} A^\mu) \\
&\quad -\frac{1}{a^2 e}(\partial^\mu \mathbf{\Phi} \wedge \partial^\nu \mathbf{\Phi}) - \frac{1}{a}\partial^\mu \mathbf{\Phi} A^\mu + \frac{1}{a}\partial^\nu \mathbf{\Phi} A^\mu \\
&= \frac{1}{a^2 e}\partial^\mu \mathbf{\Phi} \wedge \partial^\nu \mathbf{\Phi} + \frac{1}{a}\mathbf{\Phi}(\partial^\mu A^\nu - \partial^\nu A^\mu) \\
&= \frac{1}{a}\mathbf{\Phi} F^{\mu\nu} \\
&\quad \text{with} \quad F^{\mu\nu} = \frac{1}{a^3 e}\mathbf{\Phi} \cdot (\partial^\mu \mathbf{\Phi} \wedge \partial^\nu \mathbf{\Phi}) + \partial^\mu A^\nu - \partial^\nu A^\mu. \qquad (3.137)
\end{aligned}
$$

4 Dislocations in crystals

David Gablinger
Supervisor: Urs Aeberhard

In this proseminar talk we deal with crystal dislocations, which are a sort of topological defect. Basically, they can be divided into screw and edge dislocations. We will then treat some of their elastic properties, in particular a general formula for the displacement of dislocations, forces on dislocations and the interaction between dislocation loops. We will also look at their movement and discover properties that allow analogies to particle physics.

1 Dislocations Inside Solid State Physics

At first, it might be interesting to see where dislocations occur inside the vast world of solid state physics. Dislocations are a type of crystalline defect, so let us start with an overview of crystalline defects: Basically they can be divided into five categories, of which two are effects from solid-state physics, so only three are considered defects in the classical crystallographical sense. Furthermore, they can be ordered by their dimensionality:

Different Kinds of Defects

- 0D: Point Defects
  Point defects can be divided into defects due to an additional atom in the lattice, and defects with a missing atom. This can be more complicated by having a ionic crystal. These defects always occur, due to thermodynamical reasons: they raise both the inner energy U and entropy S. In the Equilibrium, the free energy $F = U - TS$ will be minimized. With $S = k \cdot \ln W$, the concentration of such defects can be calculated as $c_{def} = \frac{N_{def}}{N} = \exp(\frac{-E_d}{kT})$. This is done in detail for example in [24].

- 1D: Line Defects (Dislocations)
  These are basically the defects we will deal with in this proseminar. There are different possible defects that go along an axis or line and do not end inside a crystal:

  - singularities in liquid crystals
    The polarization behavior of liquid crystals permits some experiments with nice pictures investigating these singularities.
  - rotation dislocations
    These are dislocations where the "dislocated" part of the crystal gets bigger with increasing distance to the dislocation line. These dislocations can lead to crystallites with additional faces.
  - translation dislocations
    These are the line defects that occur most often, and furthermore we will mainly deal with them. In principle, a dislocation is an "ordered" lattice mismatch, in the sense that the mismatch continues to some direction. Translation dislocations shift the lattice by one lattice constant, such that very far away from the dislocation, the lattice looks exactly like the perfect lattice, but the closer we come to the dislocation line, the more we can see its

- 2D: Grain Boundaries
  Grain boundaries are the "borders" where two different crystallites of the same type meet. An example for such a border can be described when there is a small angle between the two crystallites. In that case, the border can be made out of a series of dislocations. Then the angle between the two lattices is $\theta = \frac{b}{h}$, where b is the burgers vector of the edge dislocation and h is the distance between two neighboring dislocations.

- 3D: Volume Defect: Thermal Movement
  As known from the solid-state physics course, phonons can change physical properties of a crystal. For example as known from the solid state physics course, they can lower the reflexes of an x-ray diffraction experiment by the Debye-Waller factor. In a completely different manner, thermal movement can also be crucial for the study of movement of dislocations, as for certain kinds of dislocation motion there is a minimum temperature.

- ∂3D: Surface Defect: Finite Crystal size
  The finite size of any crystal is an imperfection in the sense that any finite crystal is not periodical. As we will see, dislocations can not end inside the crystal, so this means that dislocations either are closed loops, or start (and end) at a surface.

Applications of Dislocations

As dislocations in general, and especially translation dislocations are very physical objects, that is they are not hypothetical in any sense, and not theoretical constructs, but real-world objects instead, it is interesting to look at applications.

Perhaps the most obvious application of past dislocation research is chip industry. The miniaturization of electronics has made it impossible to use crystals that have dislocations inside, as they alter the physical properties of the crystal too much. Today, it is possible to grow crystals without dislocations inside.

Another obvious application is the so-called work hardening, which has been used throughout at least two thousand years: Iron becomes much harder by adding a few weight percents of carbon, i.e. it becomes steel. However a rigorous explanation for this property could only be given in the last century, that is after studying dynamic properties of dislocations: the carbon in the steel provides pinning centers for the dislocation, which "fixes" the dislocation in its position.

From an experimental physics point of view, the whole field of dislocations is much larger, for example, singularities in liquid crystals are treated as dislocations too. In that sense there are many phenomena which are well understood today, but which we will not treat.

Today, another application is, that dislocations provide a physical object to which different new theories can be applied, that means dislocations should provide an example for a new theory with a mathematically similar behavior. The most prominent example is maybe the analogy to vortices in a topological treatment of physics.

general assumptions

The study of dislocations can be done very rigorously, down to using quantum mechanics, lattices and so on. However, before starting the next section, it is maybe important to note that for the rest of this proseminar, we will restrict ourselves only to the simplest cases. That means in particular:

- In particular, we do not include properties that come from the crystal lattice and its periodicity, this means our medium will be homogeneous and continuous.
- We treat dislocations only inside elasticity theory, that means in a purely classical theory.
- We look at dislocations from a distance, that means we only work within a linearized theory
- We only consider isotropic media
- usually assume an infinite crystal size, in particular avoid surfaces whenever possible.

Since the reader might not be too familiar with elasticity theory, it is maybe worthwhile to note some definitions and properties. I have tried to keep the same notion than Prof. Sigrist in his script about continuum mechanics, so every reader familiar with that script may omit the next section.

2 Introduction to Elasticity

Basic Definitions

In the following, we will always assume Einstein convention, unless explicitly noted otherwise.

- displacement and strain tensor
  The strain tensor describes a deformation of a medium in the following sense: Let us describe every position inside the undeformed medium by using the position vector r. When we start to deform the medium, we need an additional position dependent vector field that describes the difference to the original position. We call this vector field **the displacement** u_i.

$$r_i' = r_i + u_i(r) \tag{4.1}$$

  Now we look at the change of distance between two nearby points $(r, r+dr)$.

$$\begin{aligned} \mathrm{d}r'^2 - \mathrm{d}r^2 &= \mathrm{d}x_i'\mathrm{d}x_i' - \mathrm{d}x_i\mathrm{d}x_i && (4.2)\\ &= (\mathrm{d}x_i + \mathrm{d}u_i)(\mathrm{d}x_i + \mathrm{d}u_i) - \mathrm{d}x_i\mathrm{d}x_i && (4.3)\\ &= \left(\mathrm{d}x_i + \frac{\partial u_i}{\partial x_l}\mathrm{d}x_l\right)\left(\mathrm{d}x_i + \frac{\partial u_i}{\partial x_j}\mathrm{d}x_j\right) - \mathrm{d}x_i\mathrm{d}x_i && (4.4)\\ &= \mathrm{d}x_i\frac{\partial u_i}{\partial x_l}\mathrm{d}x_l + \mathrm{d}x_i\frac{\partial u_i}{\partial x_j}\mathrm{d}x_j + \frac{\partial u_i}{\partial x_l}\mathrm{d}x_l\frac{\partial u_i}{\partial x_j}\mathrm{d}x_j && (4.5) \end{aligned}$$

  At this point, we can assume that the deformation and thus the first derivative of the displacement is small, such that the last term drops away. Since we sum over both j and l, we can rename both to j. Then we get the usual definition of **the strain tensor** :

$$\epsilon_{ij} = \frac{1}{2}\left(\frac{\partial u_i}{\partial x_j} + \frac{\partial u_j}{\partial x_i}\right) \tag{4.6}$$

$$\mathrm{d}r'^2 - \mathrm{d}r^2 = 2\epsilon_{ij}\mathrm{d}x_i\mathrm{d}x_j \tag{4.7}$$

- definition of the stress tensor
  Usually a body in an equilibrium situation, in particular without outer forces acting on it is called undeformed. When deforming the body, there

are stresses acting inside, that is there are forces acting between neighboring volume elements. The Force on such a part of the volume then is:

$$F_{\Delta V} = \int_{\Delta V} F \mathrm{d}V = \oint_{\partial \Delta V} \sigma_{ik} \mathrm{d}f_k \tag{4.8}$$

where σ is called **stress tensor**

- deformations and energy
  It is now interesting to find an expression for the elastic energy of a deformed body in terms of the new quantities σ and ϵ, because in the end this will allow to find a relation between stress and strain. Now let us consider an infinitesimal deformation:

$$\delta W = \int \delta w \mathrm{d}V = \int F_i \delta u_i \mathrm{d}V = \int \frac{\partial \sigma_{ij}}{\partial x_j} \delta u_i \mathrm{d}V \tag{4.9}$$

  After integrating by parts and neglecting the surface term and using that the strain tensor is symmetric, we get **the elastic energy**:

$$I = -\frac{1}{2} \int \sigma_{ij} \epsilon_{ij} \mathrm{d}V \tag{4.10}$$

  Similarly, the **free energy density** functional is

$$\mathcal{F}(u) = \int_V \underbrace{\left(\frac{1}{2} \sigma_{ij} \epsilon_{ij} - \rho_0 F_i u_i \right)}_{F^{\mathrm{vol}}} \mathrm{d}V - \oint_{\partial V} \underbrace{u_i P_i}_{F^{\mathrm{su}}} \mathrm{d}S \tag{4.11}$$

  Where ρ_0 is the mass density. with the inner energy being proportional to

$$U = T\mathrm{d}S - I \qquad F = -S\mathrm{d}T + I \tag{4.12}$$

$$\sigma_{ij} = \left(\frac{\partial U}{\partial \epsilon_{ij}} \right) \qquad \Longleftrightarrow \qquad \sigma_{ij} = \left(\frac{\partial F}{\partial \epsilon_{ij}} \right) \tag{4.13}$$

  the last equality can be used to derive a relation between stress and strain

- relations between stress and strain
  Furthermore, we assume a particular free energy, where F_0 is the free energy density without deformation, and λ and μ are the **Lamé coefficients**:

$$F = F_0 + \frac{\lambda}{2} \epsilon_{ii}^2 + \mu \epsilon_{ij} \epsilon_{ij} \tag{4.14}$$

If we now apply the above expression for the free energy into the relation between stress and strain (4.13), we get

$$\sigma_{ij} = 2\mu\epsilon_{ij} + \lambda\delta_{ij}\epsilon_{kk} \tag{4.15}$$

This relation is also known as **Hooke's law**. Formally, this relation can be written as:

$$\sigma_{ij} = c_{ijlm}\epsilon_{lm} \tag{4.16}$$

With c being the modulus of elasticity. For our special case of a homogeneous, isotropic, elastic body, it is

$$c_{ijlm} = \lambda\delta_{ij}\delta_{lm} + \mu\left(\delta_{il}\delta_{jm} + \delta_{im}\delta_{jl}\right) \tag{4.17}$$

Using the above Lamé coefficients, we can define ν **Poisson's module of contraction** ν by:

$$\nu = \frac{\lambda}{2(\lambda+\mu)} \tag{4.18}$$

We can also solve Hook's law for ϵ:

$$\epsilon_{ij} = \frac{1}{2\mu}\sigma_{ij} + \frac{-\lambda}{2\mu(2\mu+3\lambda)}\delta_{ij}\sigma_{kk} = \frac{1}{2\mu}\left(\sigma_{ij} - \frac{\nu}{\nu+1}\delta_{ij}\sigma_{kk}\right) \tag{4.19}$$

Equations of Motion

In this section, we want to derive the equations of motion for elasticity, because they will be used throughout the rest of this paper.

$$S = \int \mathrm{d}tL = \int \mathcal{L}\mathrm{d}^4x \tag{4.20}$$

$$= \int \left(\frac{\rho_0}{2}\left(\partial_t u_i\right)^2 - F^{\mathrm{vol}}\right)\mathrm{d}V\mathrm{d}t - \oint \mathrm{d}t\mathrm{d}SF^{\mathrm{su}} \tag{4.21}$$

$$= \int \left(\frac{\rho_0}{2}\left(\partial_t u_i\right)^2 - \left(\epsilon_{ij}\sigma_{ij} - u_i\rho_0 F_i\right)\right)\mathrm{d}V\mathrm{d}t + \int \left(u_i P_i\right)\mathrm{d}S\mathrm{d}t \tag{4.22}$$

$$\tag{4.23}$$

After integration by parts in the first term of (4.22), we have

$$S = \int \left(\frac{\rho_0}{2}\left(\partial_t u_i\right)^2 + u_i\partial_j\sigma_{ij} + u_i\rho_0 F_i\right)\mathrm{d}V\mathrm{d}t \tag{4.24}$$

With the Euler-Lagrange equations,

$$\frac{\partial\mathcal{L}}{\partial u} - \partial_\mu\left(\frac{\partial\mathcal{L}}{\partial(\partial_\mu u)}\right) = 0 \tag{4.25}$$

we get

$$\frac{\partial \mathcal{L}}{\partial u} = \partial_j \sigma_{ij} + \rho_0 F_i \tag{4.26}$$

$$\partial_\mu \left(\frac{\partial \mathcal{L}}{\partial(\partial_\mu u)} \right) = \partial_t \left(\frac{\partial \mathcal{L}}{\partial(\partial_t u)} \right) = \rho_0 \partial_t^2 u_i \tag{4.27}$$

So finally, we have the following equations of motion.

$$\rho_0 \partial_t^2 u_i = \partial_j \sigma_{ij} + \rho_0 F_i \tag{4.28}$$

$$\Leftrightarrow \quad \rho_0 \partial_t^2 u_i = (\lambda + \mu) \nabla (\nabla \cdot u) + \mu (\Delta u) + \rho_0 F_i \tag{4.29}$$

The second term in (4.22) could be used to find the boundary condition:

$$\sigma_{ij} n_j = P_i \tag{4.30}$$

Most of the time, we will not need the full equations of motion (4.29), so there are simplifications

Note that for the **static case**, the equations of motion simplify to

$$0 = (\lambda + \mu) \nabla (\nabla \cdot u) + \mu (\Delta u) + \rho_0 F_i \tag{4.31}$$

and for the case with **no external forces** acting on the body to

$$0 = (\lambda + \mu) \nabla (\nabla \cdot u) + \mu (\Delta u) \ . \tag{4.32}$$

Elastic waves inside the free medium are described by

$$\rho_0 \partial_t^2 u_i = (\lambda + \mu) \nabla (\nabla \cdot u) + \mu (\Delta u) \ . \tag{4.33}$$

3 Basic Dislocation Properties

Volterra Construction And General Properties

The Volterra construction is covered in a number of textbooks, such as [25], [26], [27]. Let us now take a closer look at translation dislocations: Take a hollow cylinder made of our elastic medium. Then let us cut the cylinder along a surface parallel to the rotation axis. We can now shift the opened cylinder along the two cut surfaces in by an arbitrary vector b, which is called **Burgers vector**. For this shifting vector, there are two instructive cases:

- The vector points upwards, i.e. along the cylinder axis, so the cylinder looks now like a screw, hence the name **screw dislocation**. If we look at the crystal lattice level by level, we can also make the comparison to a parking lot with rising levels.

- Or we can shift perpendicular to the cylinder axis, so the cylinder looks now a bit like a slug. This dislocation is an **edge dislocation**. If we look at the crystal lattice case, we can construct that dislocation by taking a perfect lattice, and insert an additional crystal plane.

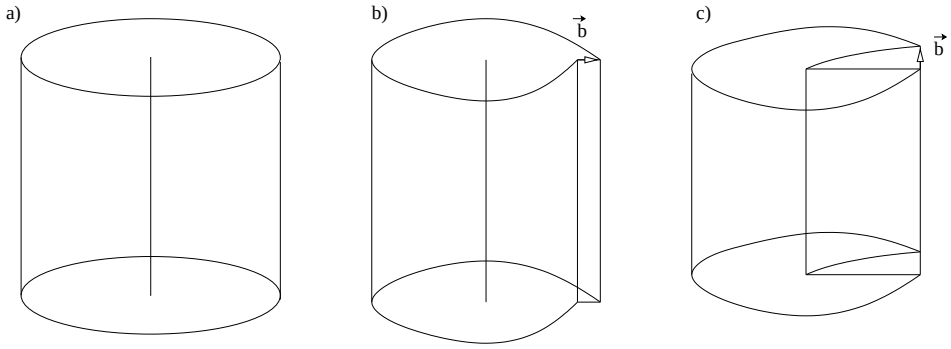

Figure 4.1: a) the undeformed cylinder b)an edge dislocation c)a screw dislocation

The hole in the center of the cylinder must contain a singularity of the displacement field u. This construction of a line defect is called Volterra construction.
To see the properties of this Volterra construction more formally, we can trace the displacement vector u along any path Γ around the line defect l and note this as

$$\oint_\Gamma \mathrm{d}u_i = \oint_\Gamma \frac{\mathrm{d}u_i}{\mathrm{d}x_k}\mathrm{d}x_k = \int_{S_\Gamma} \underbrace{\epsilon_{kmj}\frac{\mathrm{d}^2 u_i}{\mathrm{d}x_j \mathrm{d}x_m}}_{\text{dislocation density}} \mathrm{d}A_k = b_i \tag{4.34}$$

Where we applied Stokes theorem. As this path Γ can be arbitrary, the vector b is a conserved quantity for the singularity, in a way a "topological quantum number". The line defect thus cannot end just somewhere in the crystal, but instead must either go from surface to surface, or along a grain boundary, or be closed loops.

We can rewrite the dislocation density, by using that the surface integral yields the burgers vector, and then write the burgers vector as the result of an integration over an area delta function. Omitting the integral gives:

$$\epsilon_{kmj}\frac{\mathrm{d}^2 u_i}{\mathrm{d}x_j \mathrm{d}x_m} = b_i l_k \delta(\rho) = \alpha_{ik} \tag{4.35}$$

with ρ being the radial distance in the surface perpendicular to the dislocation line. Note that this is an approximation, where we go around the dislocation

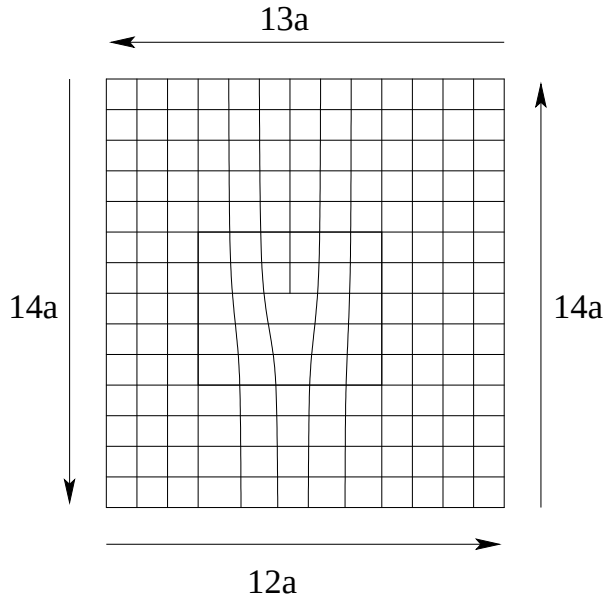

Figure 4.2: we can now choose an arbitrary path around this dislocation, as long as we stay away from its core, but there will be one remaining burgers vector with the length of one lattice constant

with a certain radius greater than the lattice parameter a, i.e. the delta function is an approximation. With that particular dislocation density, we can find four properties of the Burgers vector:

- b is independent of the cut surface, and of the path chosen around the dislocation line. With the dislocation density, this can be seen directly out of the property of the delta function.
- b adds like an ordinary vector, that means especially that the Burgers vector enclosing multiple dislocations is equal to the sum of the Burgers vectors of the dislocations. These two properties can be seen with the surface integral over the dislocation density: If we have there a sum of delta functions, the integration of each delta function gives a burgers vector.
- and it also means that at any node, where dislocation lines cross, the sum of all incoming Burgers vectors must equal the sum of all outgoing Burgers vectors: $\sum b_{in} = \sum b_{out}$. This can be seen with an argument similar to the one above.
- dislocation lines cannot end inside the crystal, this can be seen with the fact that the derivation of the dislocation density with respect to x_m gives 0.

Now we take a closer look at screw and edge dislocations.

Displacement of the Screw Dislocation

When we look back to the Volterra construction, we can note that for the screw dislocation only the z-component of u is non-vanishing, but only dependent of x and y. The trace of the strain tensor, as well as all diagonal components are zero for that reason, as can be seen in the figure.

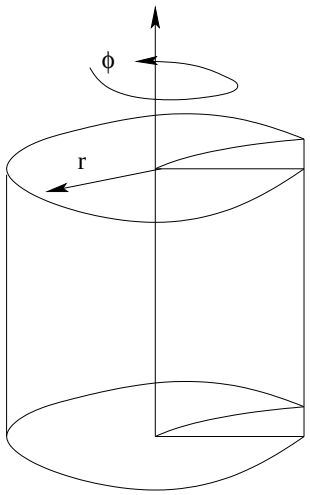

Figure 4.3: cylinder coordinates for the screw dislocation

$$\epsilon_{kk} = \nabla \cdot u = 0 \tag{4.36}$$

the elastostatic field equation without external forces (4.32)

$$\partial_j \sigma_{ij} = 0 = 2\mu \partial_j \epsilon_{ij} + \lambda \partial_i \epsilon_{kk} \tag{4.37}$$

then becomes

$$0 = \frac{\partial}{\partial x_j} \frac{\partial u_z}{\partial x_j} = \partial_x^2 u_z + \partial_y^2 u_z = \frac{1}{r} \frac{\partial}{\partial r} \left(r \frac{\partial u_z}{\partial r} \right) + \frac{1}{r^2} \frac{\partial^2 u_z}{d\theta^2} \tag{4.38}$$

together with the condition for the Burgers vector, there is a trivial solution

$$u_z(r, \phi) = \frac{b\phi}{2\pi} \qquad \Leftrightarrow \qquad u_z(x, y) = \frac{b}{2\pi} \arctan\left(\frac{y}{x}\right) \tag{4.39}$$

Strain and Stress Tensor of Screw Dislocations

With the definition of the strain tensor (4.6) we have

$$\epsilon_{zx} = \frac{1}{2} \underbrace{\frac{\partial u_x}{\partial z}}_{=0} + \frac{\partial u_z}{\partial_x} = \frac{b}{4\pi} \left(\frac{-y}{x^2 + y^2} \right) = -\frac{b}{4\pi} \frac{\sin\theta}{r} \tag{4.40}$$

$$\epsilon_{zy} = \frac{1}{2}\underbrace{\frac{\partial u_y}{\partial z}}_{=0} + \frac{\partial u_z}{\partial_y} = \frac{b}{4\pi}\left(\frac{x}{x^2+y^2}\right) = -\frac{b}{4\pi}\frac{\cos\theta}{r} \tag{4.41}$$

with $\sigma_{ij} = 2\mu\epsilon_{ij} + \lambda\delta_{ij}\epsilon_{kk}$ (4.15) and because all ϵ_{kk} are zero, the stress tensor $\sigma_{ij} = 2\mu\epsilon_{ij}$ has the same two components. If we change coordinates, only $\sigma_{z\theta}$ is non-zero:

$$\sigma_{z\theta} = \frac{\mu b}{4\pi}\frac{1}{r} \tag{4.42}$$

Stress Tensor of Edge Dislocations

Now: Burgers vector along x or y-direction. If we look back to the Volterra construction, then $u_z = 0$, and also $\frac{\partial u_i}{\partial z} = 0$, that is we have a plane deformation. In such a plane deformation. Then the only stresses we need to determine are the normal stresses σ_{xx}, σ_{yy}, and $\sigma_{xy} = \sigma_{yx}$. Note also that $\sigma_{zz} = \nu(\sigma_{xx} + \sigma_{yy})$, from the relations between stress and strain.

Now we define an additional function Ξ, by

$$\sigma_{xx} = \frac{\partial^2\Xi}{\partial y^2}\,, \quad \sigma_{yy} = \frac{\partial^2\Xi}{\partial x^2}\,, \quad \sigma_{xy} = \frac{\partial^2\Xi}{\partial x\partial y} \tag{4.43}$$

We can also transform this definition to cylindrical coordinates:

$$\sigma_{rr} = \frac{1}{r}\frac{\partial\Xi}{\partial r} + \frac{1}{r^2}\frac{\partial^2}{\partial\theta^2}\,, \quad \sigma_{\theta\theta} = \frac{\partial^2\Xi}{\partial r^2}\,, \quad \sigma_{r\theta} = -\frac{\partial}{\partial r}\left(\frac{1}{r}\frac{\partial\Xi}{\partial\theta}\right) \tag{4.44}$$

Now we look again with the static equation (4.32) ,

$$\partial_j\sigma_{ij} = 0 = 2\mu\partial_j\epsilon_{ij} + \lambda\partial_i\epsilon_{kk} \tag{4.45}$$

With our definition, we can note that the static equation for a plane deformation is satisfied by any solution for the biharmonic equation

$$\nabla^4\Xi = 0 \tag{4.46}$$

We can now make an ansatz of separation of variables,

$$\Xi = R(r)\Theta(\theta) \tag{4.47}$$

Then we can solve the resulting differential equations by trying first to find a solution for Θ, where for example a $\sin\theta$ is a possible solution. Then we can solve the differential equation for $R(r)$ and see that one solution is

$$\Xi_0 = -\frac{\mu b}{2\pi(1-\nu)} r\ln r\sin\theta = -\frac{\mu b}{2\pi(1-\nu)} y\ln(x^2+y^2)^{\frac{1}{2}} \tag{4.48}$$

Now we can insert this solution back into the definition for Ξ and get the stress tensor elements:

$$\sigma_{rr} = D\frac{\sin\theta}{r} \tag{4.49}$$

$$\sigma_{\theta\theta} = D\frac{\sin\theta}{r} \tag{4.50}$$

$$\sigma_{r\theta} = \sigma_{\theta r} = D\frac{\cos\theta}{r} \tag{4.51}$$

$$\sigma_{zz} = 2D\nu\frac{\sin\theta}{r} \tag{4.52}$$

Note that $D = \frac{\mu b}{2\pi(1-\nu)}$. In Cartesian coordinates, σ becomes:

$$\sigma_{xx} = -D\frac{y(3x^2+y^2)}{(x^2+y^2)^2} \tag{4.53}$$

$$\sigma_{yy} = D\frac{y(x^2-y^2)}{(x^2+y^2)^2} \tag{4.54}$$

$$\sigma_{xy} = \sigma_{yx} = D\frac{x(x^2-y^2)}{(x^2+y^2)^2} \tag{4.55}$$

$$\sigma_{zz} = 2D\nu\frac{-y}{(x^2+y^2)} \tag{4.56}$$

Displacement of Edge Dislocations

From the stress tensor elements, we can get the strain with $\sigma = 2\mu\epsilon$, and then the displacement with $\epsilon_{ij} = \frac{1}{2}(\partial_i u_j + \partial_j u_i)$ where u_z is zero:

$$u_x = \frac{-b}{2\pi}\left(\theta + \frac{\sin 2\theta}{4\,(1-\nu)}\right) \tag{4.57}$$

$$u_y = \frac{-b}{2\pi}\left(\frac{1-2\nu}{2\,(1-\nu)}\ln r + \frac{\cos 2\theta}{4\,(1-\nu)}\right) \tag{4.58}$$

$$u_z = 0 \tag{4.59}$$

Dislocations and Vortices

Here we will look for a sort of a formal relation between dislocations and classical vortices.

vortices

As can be seen in a textbook about fluid dynamics, the circulation Γ around a point in the medium is given by

$$\Gamma = \oint_{\partial S} v\mathrm{d}l = \iint_S (\nabla \times v)\,\mathrm{d}f = \iint \Omega \mathrm{d}f \tag{4.60}$$

where v is the velocity field. Consider the case of a vortex with $v = \frac{1}{2\pi r^2}(\omega \times r)$, then

$$\Gamma = \oint_{\partial S} v \mathrm{d}l = \oint r \mathrm{d}\phi \frac{\omega}{2\pi r} = \omega \tag{4.61}$$

dislocations

Formally, we can set up the same equations for dislocations (note that $\beta_{ij} := \frac{\partial u_i}{\partial x_j}$)

$$b = \int_{\mathrm{d}C} \beta \mathrm{d}l = \iint_C (\nabla \times \beta)\, \mathrm{d}f = \iint \alpha \mathrm{d}f \tag{4.62}$$

For a screw dislocation, the analogy can be seen quite directly: take the displacement $u_z = \frac{b\theta}{2\pi}$, which we calculated previously, then $\beta_{zx} = b\frac{-y}{x^2+y^2}$ and $\beta_{zy} = b\frac{x}{x^2+y^2}$ Then formally, β can be written in the following form

$$\beta_{zi} = \frac{1}{2\pi(x^2+y^2)} \begin{pmatrix} 0 \\ 0 \\ b_z \end{pmatrix} \times \begin{pmatrix} x \\ y \\ z \end{pmatrix}$$

From that we can see that the Burgers vector b is similar to the circulation of a vortex. Note that this is only valid for screw dislocations, i.e. dislocations have tensorial quantities, where vortices have vectorial ones.

$$\beta = \frac{1}{2\pi r^2}(b \times r) \tag{4.63}$$

4 Static Properties of Dislocations

The General Formula for the Displacement of a Dislocation

We will now look at a more general formula for the displacement which is valid for a closed dislocation loop.

- dislocation density, strain tensor
  First we look again at the α and β tensors which are the dislocation density and the displacement derivative with respect to x_j. These definitions allow to formulate the strain tensor in terms of the dislocation density.

  As seen from the figures for the Volterra construction, there is a discontinuity of the displacement at some point, i.e. it suddenly "jumps" from one value to another value, like a step function, with the difference between the two values equal to the Burgers vector, i.e. $u \equiv \Theta(x)$. If we then are interested in the local strain at the discontinuity, we get the following expression:

$$\frac{1}{2}(n_l b_m + n_m b_l)\delta(\zeta) = \epsilon_{lm} \tag{4.64}$$

where ζ is a coordinate taken from the surface S along the normal to the surface. We will use that later.

- static equation
  We start with a static equation, i.e. Strain must be proportional to applied force. In the end, this gives nothing else but the already known static equations of motion (4.31), this time formulated using the c_{ijlm} tensor :

$$F_i = -\frac{\partial \sigma_{ij}}{\partial x_k} = -c_{iklm}\frac{\partial \epsilon_{lm}}{\partial x_k} = \frac{1}{2}c_{iklm}\left(\partial_k\partial_m u_l + \partial_k\partial_l u_m\right) \tag{4.65}$$

  this equation can be solved for the displacement using Greens formalism with the fundamental equation

$$\delta(x) = -c_{iklm}(\partial_k\partial_l\mathcal{G}_{im} + \partial_k\partial_m\mathcal{G}_{il}) \tag{4.66}$$

  where c_ijklm is the modulus of elasticity, where we are interested in the isotropic case. with the Green's tensor, u comes out of the convolution of $\mathcal{G}$ with F :

$$u_i(r) = \int \mathcal{G}_{ik}(r - r')F_k \mathrm{d}^3 r \tag{4.67}$$

  The Greens tensor for the isotropic case is then

$$\mathcal{G}_{ik}(r) = \frac{1}{8\pi\mu}\left(\frac{2\delta_{ik}}{r} - \frac{\lambda+\mu}{\lambda+2\mu}\frac{\partial^2 r}{\partial x_i \partial x_k}\right) , \tag{4.68}$$

  with $r = |\vec{r}| = \sqrt{x^2+y^2+z^2}$.
  To justify this, consider the derivatives of r:

$$\Delta r = \frac{2}{r} \qquad \text{and} \qquad \Delta\frac{1}{r} = 4\pi\delta \tag{4.69}$$

- the displacement
  Now we plug into the convolution of Greens tensor with the force again the other side of the static equation. We use the discussed dislocation strain at the discontinuity to get an explicit expression for the force:

$$u_i(r) = \int \mathcal{G}_{ij}(r - r') \cdot -c_{jklm}\partial_k \epsilon_{lm} \mathrm{d}^3 r \tag{4.70}$$

$$= \int \mathcal{G}_{ij}(r - r') \cdot -c_{jklm}\partial_k \frac{1}{2}(l_l b_m + l_m b_l)\delta(\zeta)\mathrm{d}^3 r \tag{4.71}$$

$$= -c_{jklm}b_m \int l_l \partial_k \mathcal{G}_{ij}(r - r')\mathrm{d}S' \tag{4.72}$$

Here, we insert the exact Greens tensor and write out the isotropic c_{jklm} and get six terms. By using Stokes theorem and (4.69), one obtains the following expression:

$$u(r) = \frac{\Omega b}{4\pi} + \frac{b}{4\pi} \times \oint_L \frac{\mathrm{d}r'}{\rho} + \frac{1}{8\pi(1-\nu)} \nabla \oint_L (b \times (r - r')) \frac{\mathrm{d}r'}{\rho} \tag{4.73}$$

with

$$\rho = |r - r'| \tag{4.74}$$

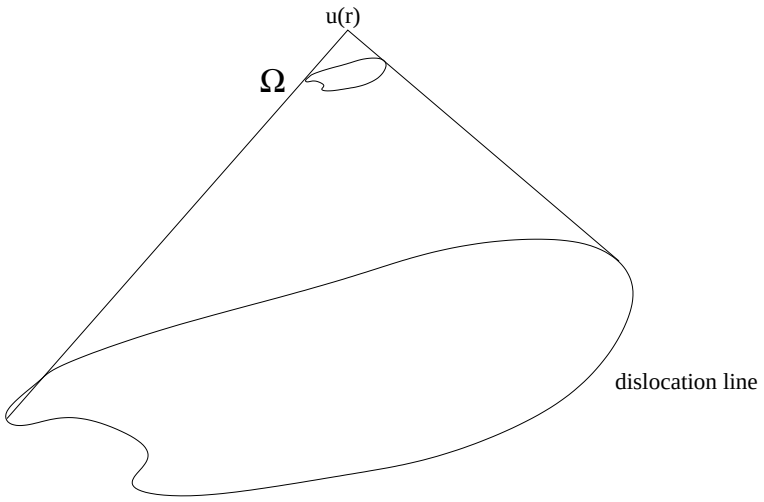

Figure 4.4: the displacement at a point r distant from the dislocation loop

simple example

We can now check whether this formula makes sense with the simplest example, that is the screw dislocation: assume the dislocation parallel to the z-axis, with the burgers vector in the same direction. Then the formula should yield the already known displacement in z-direction:

$$u_z(r) = \frac{\Omega b_z}{4\pi} + \underbrace{\epsilon_{zij} \frac{b_i}{4\pi} \oint_L \frac{\mathrm{d}l_j}{\rho}}_{\epsilon_{zzi}=0,\ \text{only}\ b_z \neq 0} + \frac{1}{8\pi(1-\nu)} \nabla_z \underbrace{\oint_L (\epsilon_{ijk} b_j \times (r_k - l_k)) \frac{\mathrm{d}l}{\rho}}_{\Xi := \oint_L (\epsilon_{izk} b_z (r_k - l_k)) \frac{\mathrm{d}l}{\rho}} \tag{4.75}$$

$\Rightarrow \Xi$ is $\neq 0$ only for $i \neq z$, so ∇_z yields 0

$$u_z = \frac{\Omega b_z}{4\pi} = \frac{b_z}{2\pi} \theta \tag{4.76}$$

Energy of Screw Dislocations

It requires energy to create dislocations, because a dislocation is a permanent displacement of the crystal lattice. If we assume the crystal size and the dislocation length to be infinite, then the elastic energy of the dislocation will be divergent, analogous to the divergence of global vortex energy. However, it is possible and meaningful to define an energy per length.

From elasticity we have the following relations:

$$E = -\frac{1}{2}\int \sigma_{ij}\epsilon_{ij}\mathrm{d}V \tag{4.77}$$

$$\frac{\partial E}{\partial l} = -\frac{1}{2}\int (\frac{1}{2\mu}\sigma_{ij}\sigma_{ij} - \frac{\lambda}{2\mu(2\mu+3\lambda)}\sigma_{ii}\sigma_{kk})\mathrm{d}S \tag{4.78}$$

$$:= E_{\text{all}} - E_{\text{diag}} \tag{4.79}$$

$\Longrightarrow$ Use this to calculate the elastic energy of screw/edge dislocation

For the screw dislocation, all diagonal entries of the stress must be zero, as discussed above, so the diagonal energy part vanishes.

$$E_{\text{diag}} = 0 \tag{4.80}$$

With the note that in cylindrical coordinates, $\sigma_{z\theta} \neq 0$

$$E_{\text{all}} = \frac{1}{2\mu}\int_{r_0}^{r} \left(\sigma_{3\theta}^2 + \sigma_{\theta 3}^2\right) 2\pi r \mathrm{d}r \tag{4.81}$$

$$= \frac{1}{2\mu}\int_{r_0}^{r} \left(\frac{\mu^2 b^2}{(4\pi)^2 r^2} + \frac{\mu^2 b^2}{(4\pi)^2 r^2}\right) 2\pi r \mathrm{d}r \tag{4.82}$$

$$= \frac{\mu b^2}{4\pi}\left(\ln\left(\frac{r}{r_0}\right)\right) + 0 = \frac{\partial E}{\partial l} \tag{4.83}$$

where r_0 is the core radius

Energy of Edge Dislocations

With the calculated stress and strain from the previous sections, we can calculate the energy of an edge dislocation:

$$\frac{\partial E}{\partial l} = \frac{1}{2}\int \left(\sigma_{rr}\epsilon_{rr} + \sigma_{\theta\theta}\epsilon_{\theta\theta} + 2\sigma_{r\theta}\epsilon_{r\theta}\right) r \mathrm{d}r\mathrm{d}\theta \tag{4.84}$$

$$= \frac{\pi}{\mu} D^2 \ln\left(\frac{r}{r_0}\right)(1-\nu) \tag{4.85}$$

$\Rightarrow$ So the expression shows the same logarithmic dependence on the radius!

Forces Acting on Dislocations

We want to look at the force on a dislocation in an external stress field. This treatment was first given by [28], and is also covered in many books, for example in [29]. Then the interaction energy of the dislocation loop is as given by (4.9) . However in our case, we look at an infinitesimal translation of the dislocation loop, so then with $\frac{\partial \sigma_{ij}}{\partial x_j} = F_j$, and integration by parts (omitting surface terms), we get

$$\delta I = \oint_L F_i \delta x_i \, \mathrm{d}l = \int_S \sigma_{ik} \delta u_{ik} \mathrm{d}S \tag{4.86}$$

Using Gauss' law, one can transform the surface integral with differential element S_i to a volume integral.

$$\int_S \sigma_{ik} \delta u_{ik} \, \mathrm{d}S_i = \int_V \partial_i \left(\sigma_{ik} \delta u_{ik} \right) \, \mathrm{d}V \tag{4.87}$$

$$= \int_V \partial_i \sigma_{ik} \delta u_{ik} \, \mathrm{d}V + \int_V \sigma_{ik} \delta \epsilon_{ik} \, \mathrm{d}V \tag{4.88}$$

Since we assumed an external, constant stress field, i.e. $\partial_i \sigma_{ik} = 0$, the first term vanishes.

For an infinitesimal displacement of an element of the dislocation line, the change of the according surface area is

$$\delta S_i = \epsilon_{ikm} \delta x_k t_m \mathrm{d}l \tag{4.89}$$

With the note that the inelastic volume change becomes

$$\delta \epsilon_{kk} = \delta x_i \epsilon_{ilm} b_l t_m \delta(\xi) \mathrm{d}V \tag{4.90}$$

$$\delta \epsilon_{kk} \mathrm{d}V \longrightarrow \epsilon_{ilm} b_l t_m \delta x_i \mathrm{d}l \tag{4.91}$$

Then we can write the following

$$F_i = \epsilon_{ilm} t_l \sigma_{mk} b_k \tag{4.92}$$

Note that the formula we just derived is analogous to the Biot-Savart formula from electrodynamics, where the Force on a conductor is :

$$\mathrm{d}F_i = \mathcal{I} \epsilon_{ijk} \mathrm{d}l_j B_k \tag{4.93}$$

Note however that our case is more complex, as the stress field σ which corresponds to the magnetic field B is a tensor, and the burgers vector corresponds to the (scalar) current $\mathcal{I}$.

Mirror Charges and Dislocations

In this section we will try to see what happens when we give up on the idea of an infinite medium, meaning we now have an elastic medium at the lower half and a vacuum at the upper half with one boundary plane.

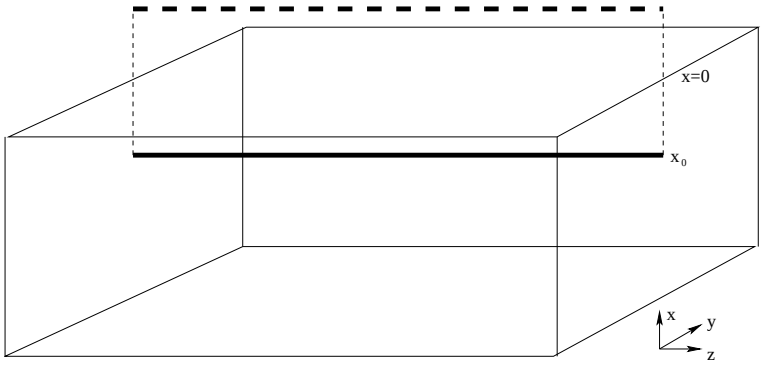

Figure 4.5: the dislocation and its mirrored version

For that we take the case of a screw dislocation parallel to the surface. The boundary condition of a strain free surface should still be satisfied, so $P_i = \sigma_{ij} n_j = 0$, where n is a vector normal to the surface. For simplicity, we assume the following coordinates: the boundary between free space and our elastic medium is the $x = 0$ plane, with the dislocation being located at $x = -x_0$ and $y = 0$, the line being along the z-axis. The condition of a stress free surface is then $\sigma_{xz}\big|_{x=0} = 0$. The stress induced by the dislocation is:

$$\sigma_{xz} = \left(\frac{-y}{(x+x_0)^2 + y^2} \right) \qquad \sigma_{yz} = \left(\frac{(x+x_0)}{(x+x_0)^2 + y^2} \right) \tag{4.94}$$

By introducing a mirror dislocation with opposite sign, we can gain a strain free surface:

$$P_x = \frac{\mu b}{2\pi} \left(\frac{-y}{(x+x_0)^2 + y^2} \right) - \left(\frac{-y}{(x-x_0)^2 + y^2} \right) \Big|_x = 0 \tag{4.95}$$

However, $P_y \neq 0$, and thus there is an attractive net force on the dislocation, i.e. the dislocation is forced to the surface because of the mirror dislocation:

$$F_i = \epsilon_{ilm} t_l \sigma_{mk} b_k = \epsilon_{izm} t_z \sigma_{mz} b_z \tag{4.96}$$

$$F_x = -t_z \sigma_{yz} b_z = \frac{\mu b_1 b_2}{4pi} \left(\frac{-x_0}{x_0^2} \right) \tag{4.97}$$

Interaction Between Dislocation Loops

simple example

We can first look at a simple example, that is the interaction energy between two parallel screw dislocations. We start by assuming two screw dislocations along the z-axis, and calculate the force the two exert on each other:

$$F_i = \epsilon_{ilm} t_l \sigma'_{mk} b_k = \epsilon_{izm} t_z \sigma'_{mz} b_z \tag{4.98}$$

Then we assume both of them are at $y = const.$ So x-component of the force is:

$$F_x = \epsilon_{xzy} t_z \sigma'_{yz} b_z \tag{4.99}$$

Now we are only interested in the x-coordinate, so we transform to radial coordinates,

$$F_x = b_1 \frac{\mu b_2}{4\pi} \frac{1}{r} \tag{4.100}$$

The interaction energy is then obtained by using $\int F \mathrm{d}x = I$, and it gives with the core radius r_0

$$I = \frac{\mu b_1 b_2}{4\pi} \ln(\frac{r}{r_0}) \tag{4.101}$$

Now we want to look at a more general formula for the interaction energy of two dislocation loops.

additional definitions

Before starting with the derivation, we need to note some additional formalisms

- we denote Kroener's incompatibility tensor as

$$\eta_{ik} = \epsilon_{ilm} \epsilon_{kpq} \partial_l \partial_p \epsilon_{mq} \tag{4.102}$$

- similarly, Kroener's stress function χ is defined by

$$\sigma_{ik} = \epsilon_{ilm} \epsilon_{kpq} \partial_l \partial_p \chi_{mq} \tag{4.103}$$

- we can define the modified stress function χ'

$$2\mu \chi'_{ik} = \chi_{ik} - \frac{\nu + 2}{\nu} \chi_{nn} \delta_{ik} \tag{4.104}$$

- then the biharmonic equation holds

$$\nabla^4 \chi' = \eta \tag{4.105}$$

- the Green's function for the biharmonic equation is

$$\chi' = \frac{1}{8\pi} \int \eta(r')|r - r'|\mathrm{d}^3 r' \tag{4.106}$$

- for our usual dislocations, the Green's function becomes, when inserting the exact η

$$\chi' = \frac{1}{16\pi} b_l \partial_m \int |r - r'|(\epsilon_{ilm}\mathrm{d}l_k + \epsilon_{klm}\mathrm{d}l_i) \tag{4.107}$$

- Lastly, the stress function for such a dislocation then is

$$\sigma_{ik} = 2\mu \left(\Delta\chi'_{ik} + \frac{1}{1-\nu} \left(\partial_i \partial_k \chi'_{nn} - \delta_{ik} \Delta \chi'_{nn} \right) \right) \tag{4.108}$$

Interaction between two loops Let us start with two dislocation loops s_1 and s_2.

- Their interaction energy then can be obtained by looking at the stress field generated by one loop acting on the other:

$$I = \int_{s1} b_1 \sigma_{s2} \mathrm{d}S_1 \tag{4.109}$$

- Now we insert the solution for the stress function in terms of χ'

$$I = \int b_1 \left(\Delta\chi'_{ik} + \frac{1}{1-\nu} \left(\frac{\partial \chi'_{nn}}{\partial x_i \partial x_k} \right) - \delta_{ik} \Delta \chi'_{nn} \right) \mathrm{d}S_1 \tag{4.110}$$

- Inserting the Green's function for χ' into this expression again gives four terms, which by using Stokes theorem give Blin's formula:

$$\begin{aligned} I = -\frac{2\mu}{4\pi} \int_{L_1} \int_{L_2} (b_1 \times b_2) \frac{\mathrm{d}l_1 \times \mathrm{d}l_2}{\rho} \\ + \frac{\mu}{4\pi} \int_{L_1} \int_{L_2} \frac{(b_1 \mathrm{d}l_1)(b_2 \mathrm{d}l_2)}{\rho} \\ - \frac{\mu}{4\pi(1-\nu)} \int_{L_1} \int_{L_2} (b_1 \times \mathrm{d}l_1) \nabla\nabla\rho (b_2 \times \mathrm{d}l_2) \end{aligned} \tag{4.111}$$

with

$$\rho = |l_1 - l_2| \tag{4.112}$$

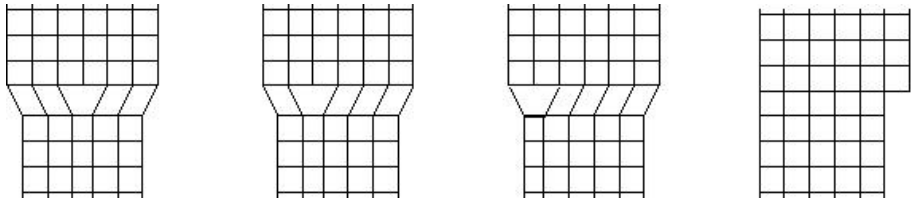

Figure 4.6: a dislocation gliding along a plane needs to overcome a periodic stress

5 Dynamic Properties of Dislocations

Introductory note: As a real translation dislocation occurs only in real crystals, that is within an atomic lattice, the motion of dislocations is step-wise in the sense that the lattice periodicity provides also a stress field which the dislocation needs to overcome. the full treatment of dislocation motion requires integral equations, because:

- Consider Peierls Nabarro model: gliding dislocation needs to overcome periodic stress generated by the lattice, the easiest possible function is of course a sinus.

$$\sigma_{zy}(x)\Big|_{y=\text{const}} = \mu \frac{\partial u_z}{\partial y}\Big|_{y=\text{const}} = \frac{\mu\beta}{\pi} \int_{-\infty}^{\infty} \frac{1}{\xi - x} \frac{\mathrm{d}u_z(\xi, y)}{\mathrm{d}\xi} \mathrm{d}\xi \tag{4.113}$$

$$-\frac{\mu b}{2\pi a} \sin \frac{4\pi u_z(x)}{b} \tag{4.114}$$

- Note that this is an approximation outside of our purely elastic approach!

Motion of Dislocations

If we stay in our narrow set of assumptions, we can note that the fast movement of dislocations resembles the relativistic movement of a massive particle. For that we start with the equation of motion (4.29) for elasticity, which describe both and note that dislocations move within the same framework

relativistic motion

$$\rho_0 \partial_t^2 u_i = (\lambda + \mu) \nabla (\nabla \cdot u) + \mu (\Delta u) + \rho_0 F_i \tag{4.115}$$

If we now consider the motion of a screw dislocation, then

$$\left(\frac{\partial^2}{\partial x^2} + \frac{\partial^2}{\partial y^2} + \frac{1}{c^2} \frac{\partial^2}{\partial t^2} \right) u_z = 0$$

with $c = \frac{\mu}{\rho_0}$

transforming the equation with $x' = \gamma(x - vt)$ yields again the equation for the static case

$$\partial_{x'}^2 u' + \partial_{y'}^2 u' = 0 \tag{4.116}$$

- the solution for the screw dislocation is still applicable

$$u_z = \frac{b}{2\pi} \arctan\left(\frac{y'}{x'}\right) \tag{4.117}$$

- transformation to original coordinates gives that the displacement of the moving dislocation becomes narrower (as to be expected)

$$u_z(x, y, t) = \frac{b}{2\pi} \arctan\left(\frac{y}{\gamma(x - vt)}\right) \tag{4.118}$$

- Note for the next section: Solution can of course be built using elementary solutions of the form

$$u_z = \exp\left(i(x - vt) \mp i\zeta y\right) \tag{4.119}$$

  where $\zeta := i\gamma^{-1} = (\frac{v^2}{c^2} - 1)^{1/2}$ and $i\zeta = (1 - \beta^2)^{1/2}$

'mass' of a dislocation If we look at dislocations analogous to particles, then the energy required to build a dislocation could be seen as its mass, similarly. As the energy of a moving dislocation increases, we see that the analogy to particle physics is still valid, as the mass of the dislocation increases by a factor of γ.

$$E_0 = E_{\text{elast},0} = \int \mathrm{d}V \left[\left(\frac{\partial u_z}{\partial x}\right)^2 + \left(\frac{\partial u_z}{\partial y}\right)^2\right] = \frac{\mu b^2}{2\pi}\left(\ln\left(\frac{r}{r_0}\right)\right) \tag{4.120}$$

$$E_{\text{tot}} = E_{\text{elast,mov}} + E_{kin} = \int \mathrm{d}x\mathrm{d}y \left[\left(\frac{\partial u_z}{\partial x}\right)^2 + \left(\frac{\partial u_z}{\partial y}\right)^2 + \left(\frac{\partial u_z}{\partial t}\right)^2\right] \tag{4.121}$$

$$= \gamma E_0 \tag{4.122}$$

$\Rightarrow$ With $E_0 = m_0 c^2$, the dislocation can be considered as having a mass!

Supersonic Dislocations

Supersonic dislocations are still being researched, both from an experimental and a theoretical point of view,for example [30], [31]. In this section, we will follow one of the first papers on the topic from J.D. Eshelby who treated the case of

a screw dislocation moving faster than the speed of elastic waves in a dispersive medium in [32].

When the dislocation is faster than sound, the wave equation becomes hyperbolic (denote $\zeta := i\gamma^{-1} = (\frac{v^2}{c^2} - 1)^{1/2}$)

$$\frac{\partial^2 u_z}{\partial y^2} - \zeta^2 \frac{\partial^2 u_z}{(x - vt)^2} = 0 \tag{4.123}$$

Note again that for screw dislocations, $\sigma_{zy} = 2\mu\epsilon_{zy} = \partial_z u_y + \partial_y u_z = \partial_y u_z$ Now the hyperbolic wave equation together with σ_{zy} gives a relation that makes Peierls-Nabarro equation unnecessary:

$$\sigma_{zy} = \mu \frac{\partial u_z}{\partial y} = \mu\zeta \frac{\partial u_z}{\partial x'} \tag{4.124}$$

Now we look at a dispersive medium, i. e. $c(k) = \omega(k)/k$, and look at the Fourier transform of the displacement:

$$u_z = \int_{-\infty}^{\infty} \hat{u_z}(k) \exp\left(ik(x - vt)\right) \mathrm{d}k \tag{4.125}$$

The stress can also be Fourier transformed and be expressed in terms of the displacement.

$$\widehat{\frac{\mathrm{d}u_z}{\mathrm{d}t}}(-k) = -vik\widehat{u_z}(k) \tag{4.126}$$

$$\widehat{\sigma_{zy}}(k) = -\mu(k)ki\zeta(k)\widehat{u_z}(k) \tag{4.127}$$

Then we have an energy flux density out of the slip plane, namely

$$E = -2\int \sigma_{zy}\frac{\mathrm{d}u_z}{\mathrm{d}t}\mathrm{d}x = -4\pi \int \hat{\sigma_{zy}}(k)\frac{\mathrm{d}\hat{u}_z}{\mathrm{d}t}(-k)\mathrm{d}k \tag{4.128}$$

Where the last equation comes with Perceval's theorem.

Using that the lattice provides a maximum $k = k_m$, and the above Fourier transforms, we can simplify the energy flux density integral:

$$E = 8\pi v \int_{k'}^{k_m} \mu(k)k^2\zeta(k)\hat{u_z}(k)\hat{u_z}(-k)\mathrm{d}k \tag{4.129}$$

When we now assume additionally

- that the subsonic components vanish
- and that we are only slightly above v_m, so ζ is the only quantity over which integration is performed, all other values are replaced by k_m

- furthermore, ζ can be expressed in terms of $\omega(k)/k$; using that

$$\gamma = (v/c(k)+1)^{\frac{1}{2}}\,(v/c(k)-1)^{\frac{1}{2}} \approx \frac{2^{\frac{1}{2}}(k-k')^{\frac{1}{2}}}{k_m} \tag{4.130}$$

These properties then give

$$E = (16\pi 2^{1/2}/3)v\mu(k_m)k_m^2\widehat{u_z}(k_m)\widehat{u_z}(-k_m)\frac{(k_m-k')^{3/2}}{k_m^{3/2}} \tag{4.131}$$

When we now assume that a solution to the wave equation for u_z is still proportional to

$$u_z = \frac{b}{2\pi}\arctan(x/\kappa) \tag{4.132}$$

then we have the following identities

1. due to the proportionality of stress and strain, and the simple form of the strain for a screw dislocation, together with the Fourier transform property of the derivative, we have that
   $\widehat{\sigma_{yz}}(k) = k * u_z(k)$
2. note that the Fourier transform of σ is symmetric
   $\widehat{\sigma_{yz}}(k) = \widehat{\sigma_{yz}}(-k)$
3. $\widehat{\sigma_{yz}}(k) = \frac{b}{2\pi}\exp(-\kappa|k|)$

This gives then approximately with $k_m = \frac{\pi}{a}$ and $\mu(k_m) = \frac{4\mu}{\pi^2}$

$$\sigma^a \approx (\frac{\Delta v}{v_m})^{3/2}\exp(-2\kappa\frac{\pi}{b}) \tag{4.133}$$

Which means, this is the stress required to keep the dislocation in motion, otherwise it gets damped. Note that this effect bears some analogy to Cherenkov radiation!

Conclusion

We have now seen in this proseminar both some static properties of dislocations including general formulas for displacement and interaction energy, and some dynamic properties including an analogy to Cherenkov radiation. What remains to say, is what these statements are good for:

First of all, we notice, that we have only done the simplest elastic treatment. There are many ways to build up more complicated, improved models, and it is still possible to do active research.

Second, we have seen that dislocations are experimentally accessible, so if there is any new model that can be applied to dislocations, then in principle it can also be verified in experiments.

And third, we have seen that it is actually possible to make analogies between dislocations and other fields of physics.

5 Solitons

Sämi Lang
Supervisor: Ilka Brunner

This text is about solitons. Solitons are particle-like objects occurring in classical field theories. There is a special focus on kinks, which are solitons corresponding to one space dimension. The first chapter will give a general introduction on solitons, while the second chapter is mostly concerned with the topological classification and the existence of solitons. In chapter 3 explicit kink solutions will be discussed, namely the ϕ^4 kinks and the sine-Gordon kinks.

1 Introduction

What is a soliton?

Before we start to investigate solitons, we must clarify what a soliton actually is. There is no commonly used "definition" of a soliton, some authors require more features for an object to be called a soliton and some less. Nevertheless, in this text we shall have a clear notion of what we call a soliton. There are classical field theories, which have interesting, particle-like solutions to their fully nonlinear field equations. By "particle-like" we mean that these solutions are smooth-structured and stable, and that they have a finite mass as well as an energy density, which is localized on some finite region of space. But the real distinctive property of these "new particles" is, that the have a topological structure that differs from the vacuum. The topological character of a field configuration is often captured by a simple integer N, called the *topological charge*. This topological charge remains constant under time evolution, since time evolution is assumed to be an example for a continuous deformation and an integer simply can't change under a continuous deformation. This really is the reason for the stability of the new particles. Although they are often of large energy, they remain stable, since they cannot change their topological charge. The integer N can be interpreted

as the net number of new particles, with the energy increasing as $|N|$ increases. The vacuum has $N = 0$. The *minimal* energy field configuration with $N = 1$ is particle-like in the sense we mentioned above (if its energy density is localized). It is called a *topological soliton* or just *soliton*. The analogue configuration with $N = -1$ is an *antisoliton* (usually a reflection symmetry reverses the sign of N). Soliton-antisoliton pairs can annihilate or be pair-produced. Field configurations with $N > 1$ are interpreted as multi-soliton states. Depending on what is energetically more favourable such a state can relax to a N-soliton bound-state or decay into N well separated charge 1 solitons.

The depending of the interaction energy of two well separated solitons on their separation is completely determined by the linearized, asymptotic field of the solitons and is therefore usually rather simple. The force between two solitons is identified with the derivative of the interaction energy with respect to the separation.

Static soliton solutions

As we mentioned, solitons are solutions of the fully nonlinear field equations of a theory. These nonlinear partial differential equations (PDE's) are of second order and in general very hard to solve. But Bogomolny showed, that in many theories it is possible to reduce the second order PDE's to first order PDE's. These first order PDE's are generally called Bogomolny equations. Bogomolny equations never involve time derivatives and hence their solutions are static soliton or multi-soliton configurations.

Bogomolny found out that in these theories the energy of a field configuration is bounded from below by a numerical multiple of the modulus of the topological charge N, with equality if the field satisfies the Bogomolny equation. Therefore solutions of the Bogomolny equation *minimize* the energy within a given topological class of fields (defined by N) and are indeed (static) solitons in our sense.

As we will see, kinks in one space dimension are solutions of a Bogomolny equation.

Soliton dynamics

We have already stated, that there is interaction between solitons. It is therefore important to understand this interaction and the dynamics of solitons. If a theory is relativistic, a static soliton solution can be boosted to move with an velocity less than the speed of light.

If solitons are well separated they can be treated as point-like objects carrying charges (or even more complicated inner structure) and there are usually parameters that can be naturally interpreted as the locations of the solitons. The forces between the solitons can directly be calculated by considering integrals of

the energy-momentum tensor. Given these forces, one can compute the relative motion of the solitons and interpret the result in terms of charges.

But if the solitons come closer together the picture of them being point-like objects breaks down. The treatment of the scattering can become very complicated and only numerical methods can help.

2 Classification and existence of solitons

In this section we will make some rather general statements on solitons. Admittedly we will restrict ourselves mostly to the case of one space dimension, since our main task in the following sections is to discuss kinks, which are objects corresponding to one space dimension. We shall first discuss the topological structure and classification of solitons. As a consequence of these considerations, there will be some conditions on the topological structure of a particular Lagrangian field theory for solitons to exist. After that we will present another statement on the existence or non-existence of solitons, the so called Derrick's scaling argument.

For the purpose of classification of solitons, we have to review some notions of topology. That's what we do next.

Some topology and notation

For our discussion, we will need the following definitions.

Definition 1. Let X and Y be two manifolds without boundary. Consider continuous maps $\Psi_1, \Psi_2 : X \to Y$ between them. Ψ_1 is said to be *homotopic to* Ψ_2, $\Psi_1 \simeq \Psi_2$, if there exist a continuous map $\tilde{\Psi} : X \times [0,1] \to Y$ with τ parameterizing the interval [0,1], such that $\tilde{\Psi}|_{\tau=0} = \Psi_1$ and $\tilde{\Psi}|_{\tau=1} = \Psi_2$. $\tilde{\Psi}$ is called a *homotopy between* Ψ_1 *and* Ψ_2.

Definition 2. Let $A \subset X$ be a submanifold. Let $\Psi_1, \Psi_2 : X \to Y$ be continuous maps with $\Psi_1|_A = \Psi_2|_A$. A *homotopy relative to A between* Ψ_1 *and* Ψ_2 is a homotopy $\tilde{\Psi}$ between Ψ_1 and Ψ_2 with the further property: $\forall a \in A, \forall t \in [0,1] : \tilde{\Psi}(a,t) = \Psi_1(a) = \Psi_2(a)$. One writes: $\Psi_1 \simeq \Psi_2$ rel. A.

Often A consists only of a single point, say $\mathbf{x}_0$. We call continuous maps Ψ from X to Y, which send $\mathbf{x}_0$ to some fixed point $\mathbf{y}_0$ in Y, $\Psi(\mathbf{x}_0) = \mathbf{y}_0$, *based maps*. Homotopy is an equivalence relation and therefore maps can be classified into homotopy classes. A case of interest is when X is a sphere. The n-sphere S^n is the set of points in $\mathbb{R}^{n+1}$ at unit distance from the origin. The north pole (NP) is the point $(0, ..., 1) \in S^n$. For $n \geq 1$, we denote the set of homotopy classes rel. NP of based maps $f : S^n \to Y$, which send NP to some fixed $\mathbf{y}_0 \in Y$, by $\pi_n(Y, \mathbf{y}_0)$. One can define a composition for elements of $\pi_1(Y, \mathbf{y}_0)$ and verify that this defines a group structure on $\pi_1(Y, \mathbf{y}_0)$. The composition of equivalence classes is just the composition of paths for some representatives of the equivalence classes. The group $\pi_1(Y, \mathbf{y}_0)$ is called the *fundamental group of* Y *with base point* $\mathbf{y}_0$. One can show that $\pi_1(S^1, \mathbf{y}_0) = \mathbb{Z}$.

The set of homotopy classes of (unbased) maps $f : S^n \to Y$ we denote by $\pi_n(Y)$. For $n = 0$ we regard S^0 as consisting of just one single point (not of the two points ± 1). Thus the classes $\pi_0(Y)$ are then maps from a single point to Y, up to homotopy equivalence. Since maps with image points in the same connected component of Y are homotopic, $\pi_0(Y)$ is the set of distinct connected components of Y.

Topology and solitons

Here we want to elucidate the topological aspects of scalar fields defined on flat space $\mathbb{R}^d$ (mostly $d = 1$). In the last section we introduced the notion of homotpy. Homotopy theory is one of the two basic techniques for classifying solitons in theories with scalar fields. The other is topological degree theory, which we will not discuss. Homotopy theory is more general and more distinctive, on the other hand topological degree theory is a more refined tool. Also the topological charge of a field configuration (which in the end is the relevant physical quantity) is more closely linked to the topological degree of the field than to its homotopy class. This is because the topological charge often is nothing but the topological degree of the field. But in the examples, that we will discuss in chapter 3, there is always a physically natural way to define the topological charge of a field, if one knows in which homotopy class it lies.

One essential point in the topological classification of fields is, that we'll have to combine topological and energetic considerations in order to make some interesting statements. For example it is not sufficient, just to assume the fields are continuous. If there are no further restrictions, linear fields are topologically trivial: Any field configuration $\phi(x)$ can be replaced by $(1-\tau)\phi(x)$ and if τ runs from 0 to 1 this is a homotopy taking $\phi(x)$ to the trivial field, $\phi \equiv 0$.

The nonlinear case, where ϕ is a map from $\mathbb{R}^d$ to a manifold Y, is a bit different. Since $\mathbb{R}^d$ is contradictable to a point, every field configuration is homotopic to a constant map: $\phi((1-\tau)x)$ is a homotopy taking $\phi(x)$ to the constant map $\phi \equiv \phi(0)$. Therefore field configurations are classified by $\pi_0(Y)$.

But if we require that the energy density is zero at infinity (note that this condition is necessary to have finite energy but not sufficient) the topological classification becomes more interesting (at least for linear fields).

Consider a multiplet of n scalar fields $\phi = (\phi_1, ..., \phi_n)$ with an energy functional of the form

$$E = \int \frac{1}{2} \nabla\phi_l \cdot \nabla\phi_l + U(\phi_1, ..., \phi_n)\, d^d x. \tag{5.1}$$

If the fields are time independent, then E is the total energy. Assume the potential $U(\phi_1, ..., \phi_n)$ has minimal value $U_{min} = 0$ (this can in general be arranged by adding a constant to U, which doesn't alter the field equations). The set $\mathcal{V} \subset \mathbb{R}^n$, where U takes its minimal value, is called the vacuum manifold of the theory.

At spatial infinity ϕ must take its values in $\mathcal{V}$, in order to have zero energy density there. The values may be different in different directions. Thus a field configuration defines a map

$$\phi^\infty : S^{d-1} \to \mathcal{V}$$
$$\hat{e} \mapsto \lim_{\lambda\to\infty} \phi(\lambda\hat{e}).$$

In a linear theory we lose no topological information, if we only keep track of these asymptotic data: Two field configurations with the same asymptotic data are homotopic. Moreover, field configurations ϕ, $\tilde{\phi}$ with the asymptotic data ϕ^∞, $\tilde{\phi}^\infty$, are still homotopic if ϕ^∞ is homotopic to $\tilde{\phi}^\infty$. Therefore the topological character of a field configuration $\phi(x)$ is captured the homotopy class of ϕ^∞, which is an element of $\pi_{d-1}(\mathcal{V})$.

As we mentioned before, we are interested in the case $d = 1$. Here $S^{d-1} = \{\pm 1\} \subset \mathbb{R}$. Hence ϕ^∞ is a map from two points to $\mathcal{V}$. The set of topologically distinct vacua is the set of distinct connected components of $\mathcal{V}$, which we denoted by $\pi_0(\mathcal{V})$. Since $\pi_0(\mathcal{V})$ is the set of topologically distinct vacua, an element v_1 of $\pi_0(\mathcal{V})$ is a homotopy class of vacuum solutions. But sometimes we will write $\phi_1 \in \pi_0(\mathcal{V})$, where ϕ_1 is a vacuum configuration and identify the homotopy class with its representative. The topological class of a field configuration $\phi(x)$ is defined by an element (v_1, v_2) of $\pi_0(\mathcal{V}) \times \pi_0(\mathcal{V})$. If, for example, $\mathcal{V}$ consists of p points in $\mathbb{R}^n$ then there are p^2 topologically different types of fields. If $v_1 = v_2$ then the field lies in the class of the vacuum solution, $\phi \equiv v_1$. If $v_1 \neq v_2$ then the field is said to be *kink-like* and interpolates between different vacua v_1 (at $-\infty$) and v_2 (at $+\infty$). If there is only one scalar field in the theory (i.e $n = 1$) then the topological solitons (if they exist) are called *kinks*. We will see explicit kink-solutions in chapter 3.

Now lets turn to nonlinear scalar fields $\phi : \mathbb{R} \to Y$, where Y is a closed manifold. A topological soliton on $\mathbb{R}$, taking its values on a closed manifold Y, is called a *nonlinear kink*. There may be a potential $U(\phi)$, taking its minimal value on some submanifold $\mathcal{V} \in Y$. We still require that $\phi(\pm\infty) \in \mathcal{V}$, but in the nonlinear case it's not useful to look at the homotopy class of the map ϕ^∞, since it does not fully determine the topological character of the field configuration $\phi(x)$. Nevertheless, if we insist that $\phi(+\infty) = \phi(-\infty) = \mathbf{y_0}$, or if the potential $\mathcal{V}$ consists only of the point $\mathbf{y_0}$, then ϕ^∞ is a constant map with value $\mathbf{y_0}$. This boundary condition allows a topological compactification of space $\mathbb{R}$ to S^1. We add a single point at spatial infinity and identify it with NP (this can be achieved by stereographic projection). $\phi : \mathbb{R} \to Y$ then extends to a continuous map $\phi : S^1 \to Y$, taking NP to $\mathbf{y_0}$. The topological class of ϕ is therefore an element of $\pi_1(Y, \mathbf{y_0})$. But if $\phi(+\infty) \neq \phi(-\infty)$, then the topological classification is a bit more complicated. As we shall see, the sine-Gordon kink has also an interpretation as a nonlinear kink: Usually the field is regarded as linear and the potential U as periodic. But it is also possible to force the field to take its values on a circle and then the potential has unique minimum on this circle.

If $d \geq 2$, the topological classification of nonlinear scalar fields is a bit different. One requires *finite* energy of the fields in order to make a reasonable classification. But we will not discuss this here.

In summary we have the following: Possible (linear) kinks are classified by an element of $\pi_0(\mathcal{V}) \times \pi_0(\mathcal{V})$, where $\mathcal{V}$ is the vacuum manifold of the theory, and possible nonlinear kinks are classified by an element of $\pi_1(Y, \mathbf{y_0})$, where Y is the target manifold of the theory. It is therefore clear, that for topological solitons to exist, these sets have to consist of more than one element.

Derrick's theorem

In this section we consider only static field configurations with finite energy. We've seen that such configurations are characterized by their homotopy class. The vacuum solution, which is spatially constant and minimizes the energy within all possible fields, lies in the trivial class. But since we are interested in solitons, we are interested in fields, that minimize the energy within a given homotopy class, other than the trivial one. Such minima are usually stable solitons. What we would like to know is: Are there any minima of the energy within other homotopy classes than the trivial one? This question is hard to answer but more generally we can ask: Are there any stationary points of the energy other than the vacuum?

A simple *non-existence* theorem is the so called Derrick's theorem. It applies for theories defined in $\mathbb{R}^d$. Derrick made the observation that in many theories, the energy functional for static fields has the following property: If you take *any* non-vacuum field configuration, subject it to a spatial rescaling (see below) and compute the variation of the energy with respect to this rescaling, then it will never be zero. But since a stationary point of the energy must be stationary against all variations, including spatial rescalings, such theories can have no static finite energy solutions in any homotopy class other than the trivial one.

To be more precise: In $\mathbb{R}^d$ a spatial rescaling is a map $\mathbf{x} \mapsto \mu\mathbf{x}$, with $\mu > 0$. Let $\Psi(\mathbf{x})$ be a finite energy field configuration, with Ψ any kind of fields, or multiplet of fields, and let $\Psi^{(\mu)}(\mathbf{x})$, $0 < \mu < \infty$, be the 1-parameter family of field configurations obtained from $\Psi(x)$, if one applies the map $\mathbf{x} \mapsto \mu\mathbf{x}$. We shall clarify how $\Psi^{(\mu)}(\mathbf{x})$ is related to $\Psi(\mathbf{x})$ below. Let

$$e(\mu) = E(\Psi^{(\mu)}) \tag{5.2}$$

denote the energy of the field configuration $\Psi^{(\mu)}(\mathbf{x})$, as a function of μ. Then we have Derrick's theorem:

Suppose that for an arbitrary, finite energy field configuration $\Psi(\mathbf{x})$, which is not the vacuum, the function $e(\mu)$ has no stationary point. Then the theory has no static solutions of the field equation with finite energy, other than the vacuum.

The theorem is only useful, if we define $\Psi^{(\mu)}$ in an appropriate way so that it

is easy to compute $e(\mu)$. For a scalar field configuration $\phi(\mathbf{x})$ one simply defines

$$\phi^{(\mu)}(\mathbf{x}) = \phi(\mu\mathbf{x}) \tag{5.3}$$

For a vector field $\mathbf{V}$ one defines

$$\mathbf{V}^{(\mu)}(\mathbf{x}) = \frac{1}{\mu}\mathbf{V}(\mu\mathbf{x}). \tag{5.4}$$

Note that the rescaling is done in an appropriate way, depending on the geometrical meaning of the fields. In the same sense all other kinds of fields are rescaled. Furthermore, under these rescaling rules the boundary condition $\phi \in \mathcal{V}$ at spatial infinity is preserved; also if ϕ is a nonlinear scalar field, the rescaling is consistent: if $\phi \in Y$, then $\phi^{\mu} \in Y$.

Assume we are dealing with a theory involving just a scalar field ϕ with an energy of the form

$$\begin{aligned} E(\phi) &= \int W(\phi)\nabla\phi\cdot\nabla\phi + U(\phi)\, d^d x \\ &\equiv E_2 + E_0 \end{aligned} \tag{5.5}$$

where we have decomposed the energy into its component parts. The explicit powers of μ, occurring when the integrand is rescaled, are indicated by the subscripts. Then

$$\begin{aligned} e(\mu) = E(\phi^{\mu}) &= \int W(\phi^{\mu})\nabla\phi^{\mu}\cdot\nabla\phi^{\mu} + U(\phi^{\mu})\, d^d x \\ &= \int \mu^2 W(\phi(\mu\mathbf{x}))(\nabla\phi)(\mu\mathbf{x})\cdot(\nabla\phi)(\mu\mathbf{x}) + U(\phi(\mu\mathbf{x}))\, d^d x \\ &= \mu^{2-d}E_2 + \mu^{-d}E_0, \end{aligned} \tag{5.6}$$

where the last step follows by a change of variables from $\mathbf{x}$ to $\mu\mathbf{x}$. Therefore $e(\mu)$ is a simple algebraic function of μ, with coefficients E_2 and E_0, that depend on the initial choice of a field configuration $\phi(\mathbf{x})$.

E_2 and E_0 are in general both positive. In this case the characteristics of $e(\mu)$ are widely determined by the spatial dimension d. If $d = 3$ or $d = 2$,

$$e(\mu) = \begin{cases} \frac{1}{\mu}E_2 + \frac{1}{\mu^3}E_0 & d = 3 \\ E_2 + \frac{1}{\mu^2}E_0 & d = 2 \end{cases} \tag{5.7}$$

so $e(\mu)$ decreases monotonically as μ increases. There is no stationary point and therefore there exist no non-vacuum solutions of the field equation with finite energy. In other terms, there exist no finite energy solitons. If $d = 1$,

$$e(\mu) = \mu E_2 + \frac{1}{\mu}E_0, \tag{5.8}$$

which is stationary at $\mu = \sqrt{E_0/E_2}$. So in this case finite energy soliton solutions are not ruled out. Thus, in a purely scalar theory, that has an energy of the form (5.5), finite energy solitons are only possible in one dimension, but not in higher dimensions. In chapter 3 we will see, that in one dimension finite energy solitons are not only possible, but do indeed exist.

Note that for the vacuum $E_2 = E_0 = 0$ and therefore the vacuum evades Derrick's theorem in all dimensions.

Another way to make use of the condition that the energy of a solution is stationary under rescaling, is the following. Suppose that $d = 1$, and let $\phi(x)$ be a *solution* of the field equation of a theory with an energy of the form (5.5). Then

$$e(\mu) = \mu E_2 + \frac{1}{\mu} E_0, \tag{5.9}$$

so

$$\frac{de}{d\mu} = E_2 - \frac{1}{\mu^2} E_0. \tag{5.10}$$

Since $\phi(x)$ is a solution of the field equation, the derivative must be zero at $\mu = 1$. Therefore E_2 must equal E_0, and that means that if the gradient term and the potential term are integrated over $\mathbb{R}$, they each contribute half of the total energy. This relation is called a *virial theorem*.

3 Kinks

Bogomolny bounds

The simplest examples of topological solitons occur in one space dimension and involve a single real valued scalar field $\phi(x,t)$. Consider the Lagrangian density

$$\mathcal{L} = \partial_\mu \phi \partial^\mu \phi - U(\phi), \tag{5.11}$$

where U is a real valued non-negative function of ϕ. The field equation, that follows from this density is

$$\partial_\mu \partial^\mu \phi + \frac{dU}{d\phi} = 0 \tag{5.12}$$

Let U_{min} be the global minimum of U, which we will from now on assume to be equal to zero, $U_{min} = 0$. As before $\mathcal{V}$ will denote the set of constant vacuum fields, i.e. $\mathcal{V} = \{\phi_0 \in \mathbb{R}, \text{ such that } U(\phi_0) = U_{min} = 0\}$. The potential energy is given by

$$V = \int \frac{1}{2}\phi'^2 + U(\phi)\, dx, \tag{5.13}$$

where ϕ' is the gradient of the field, $\phi' = \frac{\partial \phi}{\partial x}$. The kinetic energy is

$$T = \int \frac{1}{2}\dot{\phi}^2\, dx, \tag{5.14}$$

where $\dot{\phi}$ is the time derivative of the field, $\dot{\phi} = \frac{\partial \phi}{\partial t}$. The total energy is $T + V$.

We know from the last chapter, that finite energy field configurations of such a theory are classified by an element (ϕ_-, ϕ_+) of $\pi_0(\mathcal{V}) \times \pi_0(\mathcal{V})$, where $\phi_\pm = \lim_{x \mapsto \pm\infty} \phi(x)$. We also know, that in order to have solitons, $\pi_0(\mathcal{V})$ needs to be non-trivial. That is the case, if we assume $\mathcal{V}$ to consist of several isolated points. Solutions, which interpolate between different vacua, that is $\phi_+ \neq \phi_-$, are called kinks. Kinks lie in different homotopy classes than the vacuum solutions, and therefore they cannot be continuously deformed to a constant zero energy solution by deformations which keep the energy finite, i.e. deformations which preserve the boundary condition $\phi(\pm\infty) \in \mathcal{V}$. This really is, where the stability of a kink solution comes from, because time evolution is an example for a continuous deformation, that keeps the energy finite.

Recall from the last section, that we are now in a situation ($d = 1$, combination in V of a potential term and a term quadratic in the field gradient), where Derrick's theorem allows static soliton solutions. Also, for these solutions the virial theorem

$$\int_{-\infty}^{\infty} \frac{1}{2}\phi'^2 \, dx = \int_{-\infty}^{\infty} U(\phi) \, dx \tag{5.15}$$

holds.

We will now show that it is possible to derive a lower bound on the energy E of any field configuration with the bound only depending on (ϕ_-, ϕ_+). This means, that the bound is actually given in terms of solely topological data. We start with the simple inequality

$$(\frac{1}{\sqrt{2}}\phi' \pm \sqrt{U(\phi)})^2 \geq 0. \tag{5.16}$$

Expanding this on both sides and integrating over space, we obtain

$$\int_{-\infty}^{\infty} \frac{1}{2}\phi'^2 + U(\phi) \, dx \geq \pm \int_{-\infty}^{\infty} \sqrt{2U(\phi)}\phi' \, dx. \tag{5.17}$$

Therefore, for static fields

$$E \geq \mid \int_{-\infty}^{\infty} \sqrt{2U(\phi)}\phi' \, dx \mid = \mid \int_{\phi_-}^{\phi_+} \sqrt{2U(\phi)} \, d\phi \mid . \tag{5.18}$$

Since T is positive, this bound also holds for time dependent fields. We assumed that $U(\phi) \geq 0$ and this allows us to introduce a superpotential $W(\phi)$, that satisfies $U(\phi) = \frac{1}{2}(\frac{dW}{d\phi})^2$. If we substitute this, then the right-hand side of (5.18) can be integrated and the bound takes the form

$$E \geq \mid W(\phi_+) - W(\phi_-) \mid . \tag{5.19}$$

Bounds of this general form, where the energy is bounded from below in terms of solely topological data, are known as *Bogomolny bounds*.

For our purposes such a bound is extremely useful. We are interested in fields, that minimize the energy within a given topological class of fields. Such a topological class is completely determined by the topological data that occur in the bound. So the only thing we have to do, is to look for fields, which attain equality in the bound and of course check, that they also satisfy the field equation. To attain equality in the Bogomolny bound the field must be time independent, $\dot{\phi} = 0$, and satisfy one of the first order Bogomolny equations

$$\phi' = \pm\sqrt{2U(\phi)}, \tag{5.20}$$

where solutions of the equation with the + sign (if they exist) are called kinks and those with the - sign antikinks. For these solutions, the gradient term and the potential term of the energy density, $\frac{1}{2}\phi'^2$ and $U(\phi)$, are pointwise the same, which is a stronger statement than the virial theorem (5.15).

It is easy to check, that solutions of the Bogomolny equations (5.20) satisfy the field equation: Differentiating (5.20) yields

$$\phi'' = \pm\frac{1}{\sqrt{2U}}\frac{dU}{d\phi}\phi' = \frac{dU}{d\phi}.$$

One could have also argued in an other way: Since solutions of (5.20) are global minima of the energy within the topological class of fields defined by (ϕ_-, ϕ_+), they are critical points of the energy and therefore automatically static solutions of the second order field equation (5.12).

ϕ^4 kinks

In this section we start to be concrete and make a detail discussion of the simplest model with kinks, where there are two topologically different vacua, that is $\pi_0(\mathcal{V})$ consists of two elements. A potential which satisfies $U(\phi) \geq 0$ and attains global minima $U_{min} = 0$ at two distinct points is for example

$$U(\phi) = \lambda(m^2 - \phi^2)^2 \tag{5.21}$$

where m and λ are positive real constants, $m,\ \lambda > 0$.

Obviously, the global minima is degenerated and is attained at the two points $\phi = \pm m$. Thus there are two vacua, which we denote by $\mathcal{V}_+$ and $\mathcal{V}_-$. This model is known as the *ϕ^4-model*. Its full Lagrangian density is given by

$$\mathcal{L} = \frac{1}{2}\partial_\mu\phi\partial^\mu\phi - \lambda(m^2 - \phi^2)^2 \tag{5.22}$$

and the corresponding field equation reads as

$$\partial_\mu\partial^\mu\phi - 4\lambda(m^2 - \phi^2)\phi = 0. \tag{5.23}$$

Finite energy configurations are classified by an element (ϕ_-, ϕ_+) of $\pi_0(\mathcal{V}) \times \pi_0(\mathcal{V})$, but we can capture the topological content of a given field in a even more compact notation, if we define the *topological charge*

$$N = \frac{\phi_+ - \phi_-}{2m}, \tag{5.24}$$

where $\phi_\pm = \lim_{x \mapsto \pm\infty} \phi(x)$. The possible values of N are $\{0, 1, -1\}$. If $N = 0$, then the field lies in the same homotopy class as one of the vacuum solutions, $\phi(x) = \pm m$, to which it may be continuously deformed. The kink is the minimal energy solution with $N = 1$ and interpolates between the vacua $\mathcal{V}_-$ and $\mathcal{V}_+$ as x increases from $-\infty$ to ∞. The antikink is the corresponding solution with $N = -1$, which is obtained by making the replacement $\phi \mapsto -\phi$ in the kink solution.

We know that these kink solutions are given by the solutions of the Bogomolny equations. The Bogomolny energy bound for the ϕ^4 model is

$$E \geq |\int_{\phi_-}^{\phi_+} \sqrt{2\lambda}(m^2 - \phi^2)\, d\phi| = |\sqrt{2\lambda}[m^2\phi - \frac{1}{3}\phi^3]_{\phi_-}^{\phi_+}| = \frac{4}{3}m^3\sqrt{2\lambda}|N|. \tag{5.25}$$

Since $|N| = 1$ for both the kink and antikink, the bound in these sectors is $E \geq \frac{4}{3}m^3\sqrt{2\lambda}$. To attain equality, one of the first order Bogomolny equations (5.20) has to be satisfied, which in the ϕ^4 model takes the form

$$\phi' = \pm\sqrt{2\lambda}(m^2 - \phi^2). \tag{5.26}$$

The + sign gives a kink, the - sign an antikink. This equation (with the + sign) can be integrated to yield the kink solution

$$\phi(x) = m \tanh(\sqrt{2\lambda}m(x - a)), \tag{5.27}$$

where a is an arbitrary constant of integration. This solution has the energy density

$$\mathcal{E} = \frac{1}{2}\phi'^2 + \lambda(m^2 - \phi^2)^2 = 2\lambda m^4 \operatorname{sech}^4(\sqrt{2\lambda}m(x - a)). \tag{5.28}$$

And the total energy of the kink therefore is $E = \int_{-\infty}^{\infty} \mathcal{E}\, dx = \frac{4}{3}m^3\sqrt{2\lambda}$, as it should be. Since the solution is static, the total energy E is also the rest mass M of the kink. Note that at the point $x = a$, $\phi(x)$ is equal to zero, the value mid-way between the asymptotic values $\pm m$. The point $x = a$ is also the point, where the energy density is maximal, and equal to $2\lambda m^4$. It is therefore natural to interpret the point a as the position of the kink. It is a free parameter of the solution, corresponding to the translation invariance of the Lagrangian density. In figure (5.1) we plot the kink solution (5.27) and its energy density (5.28) for the choice of parameters $\lambda = \frac{1}{2}$, $m = 1$ and $a = 0$.

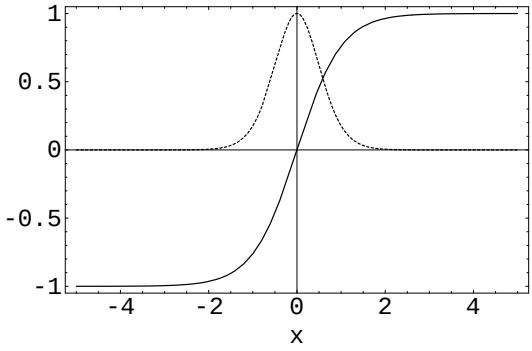

Figure 5.1: The kink solution (solid curve) and its energy density (dashed curve)

Since the Lagrangian density (5.22) is relativistic, we can get a moving kink solution by simply applying a Lorentz boost

$$\phi(t,x) = m\tanh(\sqrt{2\lambda}m\gamma(x-vt-a)), \tag{5.29}$$

where $-1 < v < 1$ is the velocity of the kink and $\gamma = 1/\sqrt{1-v^2}$ is the Lorentz factor. The energy of the moving kink is $E = \frac{4}{3}\gamma m^3\sqrt{2\lambda}$.

The possible values of the topological charge N are 0 and ± 1, so there are no multi-kink solutions with $N > 1$. However, it is possible to have a field configuration with a finite mixture of kinks and antikinks. As an example and to conclude this section we compute the interaction energy of a well separated kink-antikink pair, and show that there is an attractive force between the two. To simplify the analysis we set $\lambda = \frac{1}{2}$ and $m = 1$, since by a simple redefinition of the field and length units, the constants λ and m can always be scaled to equal any given positive values.

We will derive the interaction energy by identifying the force produced on one soliton by the other with the rate of change of momentum. For a general theory of the form (5.11), the momentum on the semi-finite interval $(-\infty, b]$ is

$$P = -\int_{-\infty}^{b} \dot{\phi}\phi'\,dx. \tag{5.30}$$

The force on this interval is then

$$F = \dot{P} = -\int_{-\infty}^{b} \ddot{\phi}\phi' + \dot{\phi}\dot{\phi}'\,dx = [-\frac{1}{2}(\dot{\phi}^2 + \phi'^2) + U(\phi)]_{-\infty}^{b}. \tag{5.31}$$

The final expression is obtained by using the field equation (5.12) and integrating over the total time derivative terms.

Now consider a kink-antikink pair, with the antikink at position $-a$ and the kink at position a, where $a \gg 1$, so that they are well separated. A field

configuration, that describes such a situation, is for example

$$\phi(x) = \phi_1(x) + \phi_2(x) + 1, \tag{5.32}$$

where $\phi_1(x)$ is the antikink and $\phi_2(x)$ is the kink, given explicitly by

$$\phi_1(x) = -\tanh(x+a), \;\; \phi_2(x) = \tanh(x-a). \tag{5.33}$$

Let the endpoint of the interval, b, lie between the kink and antikink, and far from each, that is, $-a \ll b \ll a$. Then throughout the interval the terms $(\phi_2 + 1)$ and ϕ_2' are both close to zero, so we can linearize in these terms. To first order this yields the result

$$F = [-\frac{1}{2}\phi_1'^2 + U(\phi_1) - \phi_1'\phi_2' + (1+\phi_2)\frac{dU}{d\phi}(\phi_1)]_{-\infty}^{b} = [-\phi_1'\phi_2' + (1+\phi_2)\phi_1'']_{-\infty}^{b}, \tag{5.34}$$

where, to obtain the second expression, we have used the fact that the antikink solves the Bogomolny equation (5.20) to cancel the first two terms in the first expression and replaced the last term, using the static version of the field equation (5.12). Our field configuration has the property, that its spatial derivatives fall of exponentially fast at infinity, and so there is clearly no contribution from the lower limit in the expression (5.34). Since the point b is far from both the kink and antikink, we may evaluate the contribution from the upper limit, using the asymptotic forms

$$\phi_1(x) \sim -1 + 2e^{-2(x+a)}, \qquad \phi_2(x) \sim -1 + 2e^{2(x-a)}. \tag{5.35}$$

So the expression for the force asymptotically reads as

$$F = 32e^{-2R} = \frac{dE_{int}}{dR}, \tag{5.36}$$

where we have defined the kink-antikink separation $R = 2a$, and equated the force with the derivative of the interaction energy E_{int}. The force F is independent of b, as it should be since b has non physical significance and was only introduced to perform the analysis. Thus we can indeed identify F with the force on the antikink, produced by the kink. Finally, we have the following asymptotic interaction energy

$$E_{int} = -16e^{-2R}. \tag{5.37}$$

which is negative and decreases as the separation decreases. This indicates that the force between the kink and antikink is attractive.

Numerical simulations of the full time-dependent field equation, starting with a well separated kink-antikink pair at rest, confirm this picture of the kink-antikink interaction: The kink and the antikink move toward each other and annihilate into radiation.

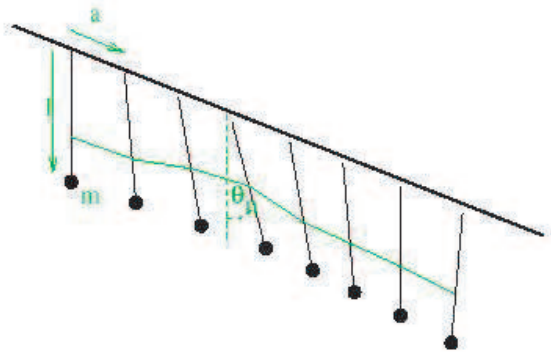

Figure 5.2: A physical system described by the sine-Gordon model

Sine-Gordon kinks

In the ϕ^4 model we have not seen multi-kink solutions, since they were not consistent with the finite energy boundary condition. A model, where multi-kink solutions exist, is the sine-Gordon model, which is defined by the Lagrangian density

$$\mathcal{L} = \partial_\mu \phi \partial^\mu \phi - (1 - \cos\phi) \tag{5.38}$$

with corresponding field equation

$$\partial_\mu \partial^\mu \phi + \sin(\phi) = 0. \tag{5.39}$$

We can visualize a physical model, which would be described by such an equation. Consider a long straight, horizontal 'clothesline' with identical pendula of mass m and length l attached at equal distance along its length. The whole system lies in an elastic with coefficient of force k and the masses are acted on by gravity. If θ_n is the angle of the nth pendulum, then the nth mass has the following Lagrangian

$$L = \frac{m}{2} l^2 \dot{\theta_n}^2 - mgl(1 - \cos(\theta_n)) - \frac{k}{2a}(\theta_{n+1} - \theta_n)^2 - \frac{k}{2a}(\theta_{n-1} - \theta_n)^2, \tag{5.40}$$

the equation of motion therefore reads

$$ml^2 \ddot{\theta_n} = -mgl \sin(\theta_n) + \frac{k}{a}(\theta_{n+1} + \theta_{n-1} - 2\theta_n). \tag{5.41}$$

Let the x direction be along the clothesline and $x_n = na$, then if a is small we can approximate

$$\frac{k}{a}(\theta_{n+1} + \theta_{n-1} - 2\theta_n) = ka \frac{(\theta_{n-1} - \theta_n)/a - (\theta_n - \theta_{n-1})/a}{a} \approx ka\theta''(x_n). \tag{5.42}$$

So the equation of motion becomes

$$ml^2\ddot{\theta} = -mgl\sin(\theta) + ka\theta''. \tag{5.43}$$

Now let $a \mapsto 0$ and $k \mapsto \infty$, such that $ka \mapsto ml^2$ is finite. Then

$$\ddot{\theta} - \theta'' = -\frac{g}{l}\sin(\theta), \tag{5.44}$$

which is the sine-Gordon equation, if units are suitably chosen.

It is obvious that the vacuum configurations of the sine-Gordon model are given by the constant solutions $\phi = 2\pi n$, where $n \in \mathbb{Z}$ is any integer, so

$$\pi_0(\mathcal{V}) = 2\pi\mathbb{Z}. \tag{5.45}$$

Once again finite energy solutions are classified by an element $(\phi_+, \phi_-) \in \pi_0(\mathcal{V}) \times \pi_0(\mathcal{V})$. But since the Lagrangian density (5.38) is invariant under 2π shifts of the fields, $\phi \mapsto \phi \pm 2\pi$, these can equivalently be classified by the topological charge

$$N = \frac{\phi_+ - \phi_-}{2\pi}, \tag{5.46}$$

which is an integer and counts the net number of solitons.

The Bogomolny bound for the sine-Gordon model is

$$E \geq \int_{\phi_-}^{\phi_+} 2|\sin(\frac{\phi}{2})|\,d\phi = \int_0^{2\pi N} 2|\sin(\frac{\phi}{2})|\,d\phi = 4|N|[-\cos(\frac{\phi}{2})]_0^{2\pi} = 8|N|, \tag{5.47}$$

where we have used the periodicity of the integrand and the fact that the range of integration is an N-fold cover of the interval $[0, 2\pi]$, to evaluate the integral. Equality in the bound is attained by solutions of one of the first order Bogomolny equations

$$\phi' = \pm 2\sin(\frac{\phi}{2}). \tag{5.48}$$

If we restrict ourselves to kink solutions, by choosing the + sign, this can be integrated directly to yield

$$\phi(x) = 4\tan^{-1}(e^{x-a}), \tag{5.49}$$

where a is an arbitrary constant of integration. We see that $\phi_- = 0$ and $\phi_+ = 2\pi$, so this solution has topological charge $N = 1$ and describes a single kink. The energy density of the kink is

$$\mathcal{E} = 4\,\mathrm{sech}^2(x - a), \tag{5.50}$$

which is maximal at the point $x = a$. This is also the point, where ϕ has value π, the value half-way between the vacuum values 0 and 2π. Thus a can be

interpreted as the position of the sine-Gordon kink - just as in the case of the ϕ^4-kink. From the expression of the energy density it is easy to confirm that $E = \int_{\infty}^{\infty} \mathcal{E}\, dx = 8$.

The general solution of the Bogomolny equations is a kink of unit charge, and therefore there are no multi-kink solutions of the Bogomolny equations. From this we can conclude that there is a repulsive force between two kinks: Any field configuration with $N = 2$ has to obey the strict Bogomolny bound $E > 16$, but in the limit in which two kinks are infinitely separated, the energy must be equal to the sum of the energies of the two individual kinks, that is $E = 16$. So the potential energy of two kinks decreases as they separate, and this indicates that there is a repulsive force between them. In the last section we computed the asymptotic kink-antikink interaction energy in the ϕ^4 model. We cam do an analogue calculation to find the asymptotic interaction energy of two sine-Gordon kinks. We start from (5.31) and consider the two kink field

$$\phi(x) = \phi_1(x) + \phi_2(x), \tag{5.51}$$

where $\phi_1(x)$ is a kink at position $-a$ and $\phi_2(x)$ is a kink at position a and $a \gg 0$. We assume also that $-a \ll b \ll a$. Then throughout the interval $(-\infty, b]$ the terms ϕ_2 and ϕ_2' are both close to zero and we can linearize in this terms. This yields the result

$$F = [-\frac{1}{2}\phi_1'^2 + U(\phi_1) - \phi_1'\phi_2' + \phi_2 \frac{dU}{d\phi}(\phi_1)]_{-\infty}^{b} = [-\phi_1'\phi_2' + \phi_2\phi_1'']_{-\infty}^{b}, \tag{5.52}$$

where, to obtain the second expression, we have used (5.20) and (5.12) - just as in (5.34). Again, there is no contribution from the lower limit in the expression (5.52), since the derivatives fall off rapidly. Because b is far from both kinks, we may use the asymptotic expressions of ϕ_1 and ϕ_2 to evaluate the contribution from the upper limit. These asymptotic forms are

$$\phi_1(x) \sim 4(\frac{\pi}{2} - e^{-(x+a)}), \qquad \phi_2(x) \sim 4e^{x-a}. \tag{5.53}$$

Therefore the asymptotic expression for the force is

$$F = -32e^{-R}, \tag{5.54}$$

where $R = 2a$ is the kink-kink separation. Thus the asymptotic interaction energy is

$$E_{int} = 32e^{-R}. \tag{5.55}$$

The fact that there is a repulsive force between two kinks implies that there are no static multi-kink solutions of sine-Gordon equation. But all the same, there exist time dependent solutions, that describe multi-kink states and in particular

the scattering of two or more kinks. As a simple example we will now explicitly construct a two-kink solution of the sine-Gordon equation using so called Baecklund transformations.

If we introduce lightcone coordinates, $x_\pm = \frac{1}{2}(x \pm t)$, with corresponding derivatives, $\partial_\pm = \frac{\partial}{\partial_{x_\pm}}$, the sine-Gordon field equation (5.39) becomes

$$\partial_-\partial_+\phi = \sin(\phi). \tag{5.56}$$

The following pair of equations is known as a *Baecklund transformation*

$$\partial_+\psi = \partial_+\phi - 2\beta\sin(\frac{\phi+\psi}{2}), \qquad \partial_-\psi = \partial_-\phi + \frac{2}{\beta}\sin(\frac{\phi-\psi}{2}), \tag{5.57}$$

where β is a non-zero constant and is called the *Baecklund parameter*. The Baecklund transformation (5.57) may be thought of as determining the field ψ, given the field ϕ, ore vice versa. Since partial derivatives commute, one can subject (5.57) to the compatibility condition $\partial_-\partial_+\psi = \partial_+\partial_-\psi$, which implies that

$$\partial_-\partial_+\phi - \beta\cos(\frac{\phi+\psi}{2})(\partial_-\phi+\partial_\psi) = -\partial_+\partial_-\phi + \frac{1}{\beta}\cos(\frac{\phi-\psi}{2})(\partial_+\phi-\partial_+\psi). \tag{5.58}$$

And this reduces to the sine-Gordon equation, $\partial_-\partial_+\phi = \sin(\phi)$, if we eliminate the first derivative terms using equations (5.57). Of course one can also subject the Baecklund transformation (5.57) to the compatibility condition $\partial_-\partial_+\phi = \partial_+\partial_-\phi$, which gives the sine-Gordon equation for ψ, that is, $\partial_-\partial_+\psi = \sin(\psi)$. Thus, if ϕ and ψ satisfy the equations (5.57) and are enough 'regular' (i.e the compatibility conditions hold), each of them automatically satisfies the sine-Gordon equation. But we are not interested in finding general functions ψ and ϕ, that satisfy equations (5.57). We will think of the Baecklund transformation as a map between solutions of the sine-Gordon equation. That is, we start with a known solution ϕ of the sine-Gordon equation and generate a new solution ψ via the Baecklund transformation. Since the Baecklund transformation contains a free parameter β, this extra parameter is introduced into the new solution, in addition to a constant of integration.

As an example, if we start with the trivial vacuum solution $\phi = 0$, then equations (5.57) take the simplified form

$$\partial_+\psi = -2\beta\sin(\frac{\psi}{2}), \qquad \partial_-\psi = -\frac{2}{\beta}\sin(\frac{\psi}{2}). \tag{5.59}$$

These equations are integrated to give the solution

$$\psi(x_+, x_-) = 4\tan^{-1}(e^{-\beta x_+ - x_-/\beta + \alpha}), \tag{5.60}$$

where α is a constant of integration. If we make the identifications

$$v = \frac{1-\beta^2}{1+\beta^2}, \quad \gamma = \frac{1}{\sqrt{1-v^2}} = -\frac{1+\beta^2}{2\beta}, \quad a = \frac{2\beta\alpha}{1+\beta^2}, \tag{5.61}$$

where $\beta < 0$, this solution can be written as

$$\psi(t,x) = 4\tan^{-1}(e^{\gamma(x-vt-a)}), \tag{5.62}$$

which we recognize as the Lorentz boosted version of the one-kink solution (5.49).

Now we use the Baecklund transformation to construct a two-kink solution in a purely algebraic way, evading the task of having to explicitly integrate equations (5.57), which could be very hard for a complicated seed solution ϕ. If we start with the seed solution $\phi = \phi_0$, we can generate two new solutions ψ_1 and ψ_2, using different Baecklund parameters β_1 and β_2. One can show, that the following theorem of permutability holds: With an appropriate choice of integration constants, the solution ψ_{12}, obtained by applying the Baecklund transformation with parameter β_2 to the seed solution ψ_1, is equal to the solution ψ_{21}, obtained by applying the Baecklund transformation with parameter β_1 to the seed solution ψ_2. The consistency condition $\psi_{12} = \psi_{21}$ yields the relation

$$\psi_{12} = \psi_{21} = 4\tan^{-1}[(\frac{\beta_1+\beta_2}{\beta_2-\beta_1})\tan(\frac{\psi_1-\psi_2}{4})] - \psi_0, \tag{5.63}$$

which gives a new solution ψ in terms of the triplet of known solutions ψ_0, ψ_1, ψ_2.

We have seen, that if we start with the vacuum solution $\psi_0 = 0$, we can obtain the one-kink solutions $\psi_j = 4\tan^{-1}(e^{\theta_j})$ $(j = 1, 2)$, where $\theta_j = -\beta_j x_+ - x_-/\beta_j + \alpha_j$. So we can get another solution, by substituting these into equation (5.63)

$$\psi(x_+, x_-) = 4\tan^{-1}[(\frac{\beta_1+\beta_2}{\beta_2-\beta_1})\frac{\sinh(\frac{\theta_1-\theta_2}{2})}{\cosh(\frac{\theta_1+\theta_2}{2})}]. \tag{5.64}$$

For simplicity, set $\beta_1 = -1/\beta_2 \equiv \beta$, and $\alpha_1 = \alpha_2 = 0$. Then (5.64) becomes

$$\psi(t,x) = 4\tan^{-1}[\frac{v\sinh(\gamma x)}{\cosh(\gamma v t)}], \tag{5.65}$$

where we made the same identifications (5.61) as before. This solution has topological charge $N = 2$, since it interpolates between the vacua -2π and 2π. It therefore describes a time dependent two-kink field.

We can interpret this solution, if we write it in the form

$$\tan(\frac{\psi}{4}) = e^{\gamma(x-a)} - e^{-\gamma(x+a)}, \tag{5.66}$$

where $a > 0$ is the time dependent function

$$a(t) = \frac{1}{\gamma} \log(\frac{2}{v} \cosh(\gamma v t)). \tag{5.67}$$

If $|vt| \gg 1$, then $\cosh(\gamma v t) \sim \frac{1}{2} e^{\gamma |vt|}$ and therefore $a \sim |vt| - \log(v)/\gamma \equiv |vt| + \delta$ is also large. In this limit, near the point a, the second term on the right-hand side of (5.66) is exponentially small and can be neglected. The remaining term describes a single kink, located at $x = a \sim |vt| + \delta$ and moving with speed v. Similarly, near $x = -a$, one can neglect the first term and the remaining term describes a kink at position $x = -a \sim -(|vt| + \delta)$ and moving with speed v. Thus this solution indeed describes a two-kink state. If $|t|$ is large, the two kinks are well separated and both move toward the origin at speed v for $t < 0$ and away from the origin at the same speed for $t > 0$. This is consistent with our statement that there is a repulsive force between two kinks: When they come closer together, they feel the repulsive force and smoothly bounce back off each other. The motion is symmetric about $t = 0$, since the solution is an even function of t. The time of closest approach is $t = 0$. The interpretation of a as half the separation of the two kinks is only valid, when a is large, so we should not use it near $t = 0$ to estimate the distance of closest approach. In figure (5.3) we plot the energy density at various times for the two-kink solution (5.65) with $v = 0.2$. The total energy is 16γ.

We can validate the expression (5.55) for the asymptotic interaction energy, if we compare the exact two kink solution to the approximate motion one would predict using the equation of motion, that follows from (5.55). For two kinks at positions $\pm a$, the approximate equation of motion reads as

$$\ddot{a} = 4e^{-2a}, \tag{5.68}$$

where we have equated the force $F = 32e^{-2a}$ with the product of the kink acceleration $\ddot{a}$ and its mass, which is 8. Using the conditions $\dot{a}(-\infty) = -v$ and $\dot{a}(0) = 0$, so that the kinks each have initial speed v and the time of closest approach is at $t = 0$, then (5.68) has the solution

$$a(t) = \log(\frac{2}{v} \cosh(vt)). \tag{5.69}$$

This is the non-relativistic limit of the exact expression (5.67), which is obtained by replacing the Lorentz factor γ by 1. So for low speeds $v \ll 1$, the asymptotic force law yields a very good approximation for the true dynamics. One source of the error for high speeds is that when the two kinks come closer together, the terms neglected in the asymptotic expression become relevant.

Figure (5.4) shows the exact kink trajectories given by the expression (5.67) and the approximate trajectories obtained form (5.69), for speeds $v = 0.2$ and $v = 0.6$.

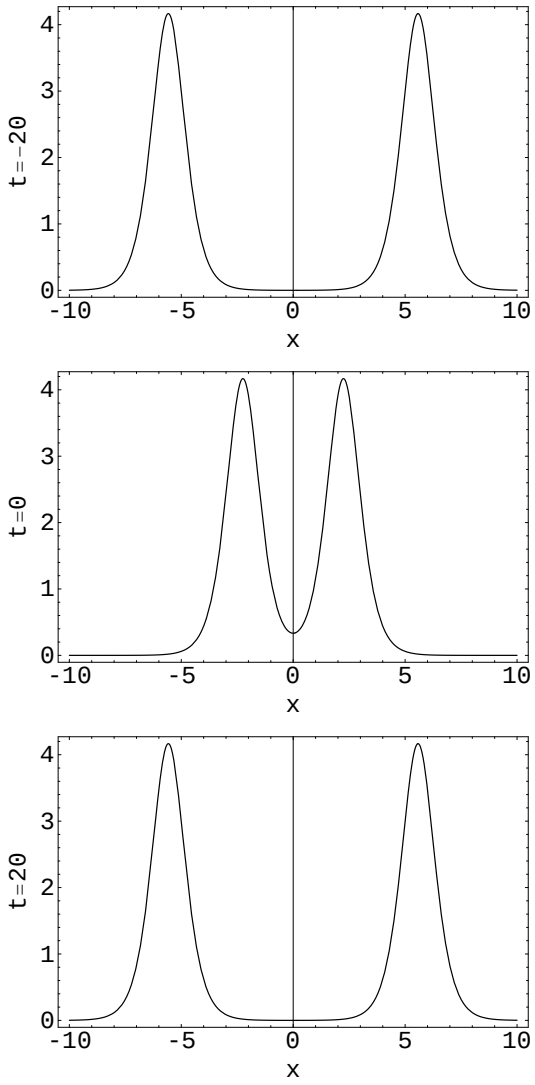

Figure 5.3: The energy density of the two kink solution at various times

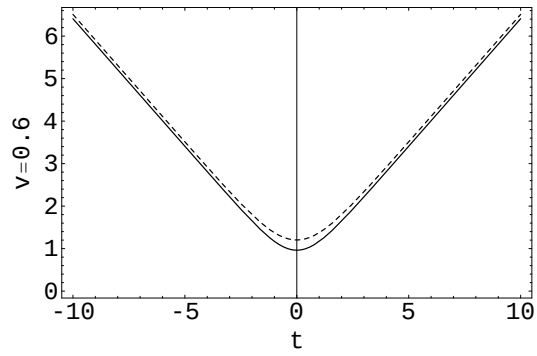

Figure 5.4: Exact solution for $a(t)$ (solid curve) versus asymptotic force solution for $a(t)$ (dashed line) at various speeds

In Chapter 2 we mentioned, that the sine-Gordon kink has also an interpretation as a nonlinear kink. To see this, we need to formulate the sine-Gordon model as a nonlinear scalar field model. For that purpose we introduce the two-component unit vector

$$\phi = (\phi_1, \phi_2) = (\sin(\phi), \cos(\phi)). \tag{5.70}$$

In terms of this field the sine-Gordon Lagrangian density (5.38) becomes

$$\mathcal{L} = \frac{1}{2}\partial_\mu \phi \cdot \partial^\mu \phi - (1 - \phi_2) + \nu(1 - \phi \cdot \phi), \tag{5.71}$$

where we introduced the Lagrange multiplier ν to constrain ϕ to lie on the circle S^1. To ensure finite energy, the field must attain the (unique) vacuum value $\phi = (0, 1)$ at spatial infinity, which corresponds in the previous formulation to the field ϕ being an integer multiple of 2π at infinity. Therefore the vacuum manifold consists only of one singly point, which - as we mentioned - allows us to compactify space $\mathbb{R}$ to S^1. The field is therefore a map $\phi : S^1 \to S^1$ and is classified by an element N of $\pi_1(S^1) = \mathbb{Z}$. The integer N is the winding number of the map and can be computed as

$$N = \frac{1}{2\pi} \int_{-\infty}^{\infty} \epsilon_{ab} \phi'_a \phi_b \, dx, \tag{5.72}$$

where ϵ_{ab} is the alternating tensor in two dimensions, with $\epsilon_{12} = -\epsilon_{21} = 1$, and all other components zero. One can easily check, that this is equal to the topological charge (5.46), which we defined previously.

6 Solitons in density wave systems

Mathias Ritzmann
Supervisor: Urs Aeberhard

We treat the formation of the charge density wave ground state in a 1D mean-field framework. We analyse solitons in trans-polyacetylene with half band-filling, deriving charge, spin, and charge distribution of the soliton. An extension to third band-filling is discussed briefly. For the half-filled band case, the soliton has unusual charge-spin relations whereas for the third-filled case, the soliton has fractional charge.

1 Introduction

Some materials with a highly anisotropic band structure have a ground state called charge-density wave in which the crystal lattice is deformed periodically. We treat the formation of the charge density wave ground state due to electron-phonon interaction in a one-dimensional model using the nearly-free electron approximation and linear response theory for the electron gas.
Solitons in polyacetylene with a half-filled pi band are investigated, charge, spin, and charge distribution are calculated using Green's Functions. Extensions to the case of a third-filled pi band are discussed briefly.

Experimental Signature

In Figure 6.1, one can see that the material is a metal at temperatures above T_2, the resistance gets lower as the temperature decreases, whereas below T_2 the resistance increases with decreasing temperature, as it is characteristic for a semiconductor. The same metal-semiconductor transition can be seen for potassium molybdenum blue bronze in Figure 6.2, above the phase transition temperature,

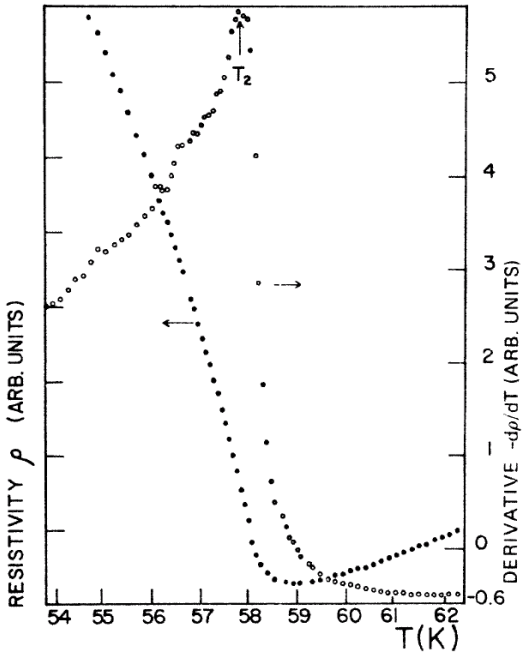

Figure 6.1: Resistivity measurements for $NbSe_3$ taken from [35]. Solid circles denote resistivity, open circles its derivative with respect to temperature.

the conductivity increases with decreasing temperature, below it decreases with decreasing temperature.

Figure 6.3 shows a divergence in the derivative of the thermal conductivity of rubidium blue bronze at the temperature where the charge density wave forms, which indicates a second order phase transition.

2 The Formation of the Charge Density Wave

We discuss the formation of a charge density wave in a one-dimensional free electron gas coupled to the underlying lattice, following [38] very closely.
The Hamiltonian of the electrons is

$$\mathbf{H}_{el} = \sum_k \epsilon_k a_k^\dagger a_k, \tag{6.1}$$

where the electron energy ϵ_k equals $\frac{\hbar^2 k^2}{2m}$, m denoting the effective electron mass. a_k is the annihilation operator for an electron with momentum k, $a_k^\dagger$ the corresponding creation operator.
Our considerations are always for one spin direction, we will sum over spins at the end of the calculation.

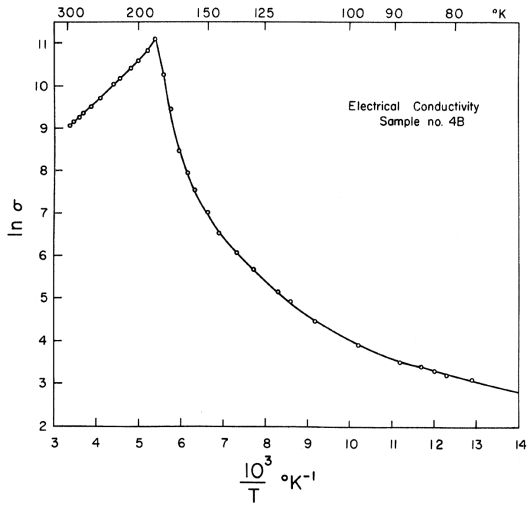

Figure 6.2: Natural logarithm of the conductivity as a function of inverse temperature for potassium molybdenum blue bronze. Image from [36]
.

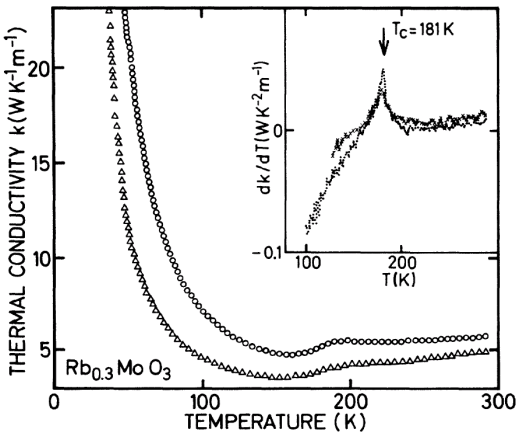

Figure 6.3: Thermal conductivity as a function of temperature measured for two samples of rubidium blue bronze. In the inset the temperature derivative of the thermal conductivity near the phase transition is shown. Image from [37].

The Hamiltonian of the lattice vibrations is

$$\mathbf{H}_{ph} = \sum_q \left(\frac{P_q P_{-q}}{2M} + \frac{M\omega_q^2}{2} Q_q Q_{-q} \right), \tag{6.2}$$

where Q_q is the normal coordinate for the oscillator normal mode with wavevector q, P_q is the associated momentum, ω_q the normal mode frequency, M the mass of the ion.
We write the harmonic oscillator with creation and annihilation operators for phonons with wavevector q,

$$\mathbf{H}_{ph} = \sum_q \hbar\omega_q (b_q^\dagger b_q + \frac{1}{2}), \tag{6.3}$$

where

$$Q_q = \left(\frac{\hbar}{2M\omega_q} \right)^{\frac{1}{2}} \left(b_q + b_{-q}^\dagger \right), \tag{6.4}$$

$$P_q = \left(\frac{\hbar M\omega_q}{2} \right)^{\frac{1}{2}} \left(-b_{-q} + b_q^\dagger \right), \tag{6.5}$$

which gives for the lattice displacement at a point

$$u(x) = \sum_q \sqrt{d} \left(\frac{\hbar}{2M\omega_q} \right)^{\frac{1}{2}} \left(b_q + b_{-q}^\dagger \right) e^{iqx} \quad x = n \cdot d, \tag{6.6}$$

with d denoting the distance between two ions in equilibrium position.
We assume that the potential depends on the position of the ions only (which is technically an approximation because the ions are moving charges), therefore

$$\mathbf{H}_{el-ph} = \sum_{k,k',n} \langle k \left| V(r - n \cdot d - u) \right| k' \rangle \, a_k^\dagger a_{k'} \tag{6.7}$$

$$= \sum_{k,k',n} e^{i(k'-k)(n\cdot d+u)} V_{k-k'} a_k^\dagger a_{k'}, \tag{6.8}$$

where n counts through the lattice positions, u is the displacement from the equilibrium position, $V_{k-k'}$ is the $k-k'$-component of the Fourier transform of $V(r)$, the potential of a single ion.
We assume small displacement from the equilibrium position, enabling us to linearise the exponential

$$e^{i(k'-k)u} \approxeq 1 + i(k'-k)u = 1 + i(k'-k)\sqrt{d} \sum_q u_q e^{iqn\cdot d}, \tag{6.9}$$

by inserting the definition of u. The electron-phonon interaction Hamiltonian is then

$$\mathbf{H}_{el-ph} = \sum_{k,k',n} e^{i(k'-k)n\cdot d}\left(1 + i(k'-k)\sqrt{d}\sum_q u_q e^{iqn\cdot d}\right) V_{k-k'} a_k^\dagger a_{k'} \tag{6.10}$$

$$= \sum_{k,k',n} e^{i(k'-k)n\cdot d} V_{k-k'} a_k^\dagger a_{k'} + i\sqrt{d}\sum_{k,k'}(k'-k)V_{k-k'}a_k^\dagger a_{k'}\sum_q \underbrace{\sum_n e^{in\cdot d(k'-k+q)}}_{=\frac{1}{d}\delta_{q-k+k'}} u_q \tag{6.11}$$

$$= \sum_{k,k',n} e^{i(k'-k)n\cdot d} V_{k-k'} a_k^\dagger a_{k'} + i\frac{1}{\sqrt{d}}\sum_{k,k'}(k'-k)u_{k-k'}V_{k-k'}a_k^\dagger a_{k'}, \tag{6.12}$$

where the first term describes the interaction between the electrons and the ions in the equilibrium position. It leads to the formation of Bloch states from the free electron states. The effect on the dispersion relation is strongest close to the Brillouin zone edge. Since we are interested in materials where the Fermi wavevector is far away from the zone edge, we will not treat this term explicitly, instead we will just assume that our index k counts through Bloch states in the following. The second term, describing the interaction between the electrons and the phonons, can be written out using phonon creation and annihilation operators,

$$\mathbf{H}_{el-ph} = i\sum_{k,k'}(k'-k)\left(\frac{\hbar}{2M\omega_{k-k'}}\right)^{\frac{1}{2}}\left(b_{k-k'} + b_{k'-k}^\dagger\right)V_{k-k'}a_k^\dagger a_{k'} \tag{6.13}$$

$$= \sum_{(k-k'),k'} \underbrace{\left[-i(k-k')V_{k-k'}\left(\frac{\hbar}{2M\omega_{k-k'}}\right)^{\frac{1}{2}}\right]}_{g_{k-k'}}\left(b_{k-k'} + b_{k'-k}^\dagger\right)a^\dagger_{(k-k')+k'}a_{k'} \tag{6.14}$$

$$= \sum_{q,k'} g_q\left(b_q + b_{-q}^\dagger\right)a^\dagger_{q+k'}a_{k'}, \tag{6.15}$$

where we have introduced the electron-phonon coupling constant g_q.
The full model Hamiltonian is called Fröhlich Hamiltonian:

$$\mathbf{H} = \sum_k \epsilon_k a_k^\dagger a_k + \sum_q \hbar\omega_q b_q^\dagger b_q + \sum_{k,q} g_q a_{k+q}^\dagger a_k\left(b_q + b_{-q}^\dagger\right). \tag{6.16}$$

We now assume that the electron-phonon coupling $g_q = g$ is independent of q. The equation of motion for the normal coordinates is

$$\ddot{Q}_q = \frac{-i}{\hbar}\left[\dot{Q}_q, \mathbf{H}\right] = \frac{-1}{\hbar^2}\left[\left[Q_q, \mathbf{H}\right], \mathbf{H}\right], \tag{6.17}$$

which we compute using $[Q_q, P_{q'}] = i\hbar\delta_{q,q'}$.

$$[Q_q, \mathbf{H}] = \left[Q_q, \sum_r \frac{P_r P_{-r}}{2M}\right] \tag{6.18}$$

$$= \sum_r \frac{[Q_q, P_r P_{-r}]}{2M} \tag{6.19}$$

$$= \sum_r \frac{[Q_q, P_r]\, P_{-r} + P_r\, [Q_q, P_{-r}]}{2M} \tag{6.20}$$

$$= 2i\hbar P_{-q} \frac{1}{2M} \tag{6.21}$$

$$[P_{-q}, \mathbf{H}] = \sum_r \frac{M\omega_r^2}{2}\, [P_{-q}, Q_r Q_{-r}] + \sum_r \left(\sum_k a^\dagger_{k+r} a_k\right) g \left(\frac{2M\omega_r}{\hbar}\right)^{\frac{1}{2}} [P_{-q}, Q_r] \tag{6.22}$$

$$= \frac{M\omega_q^2}{2}(-2i\hbar Q_q) - i\hbar \left(\sum_k a^\dagger_{k-q} a_k\right) g \left(\frac{2M\omega_q}{\hbar}\right)^{\frac{1}{2}} \tag{6.23}$$

$$= i\hbar \left(-M\omega_q^2 Q_q - g \left(\frac{2M\omega_q}{\hbar}\right)^{\frac{1}{2}} \left(\sum_k a^\dagger_{k-q} a_k\right)\right) \tag{6.24}$$

$$\ddot{Q}_q = \frac{-1}{\hbar^2}\frac{i\hbar}{M} i\hbar \left(-M\omega_q^2 Q_q - g \left(\frac{2M\omega_q}{\hbar}\right)^{\frac{1}{2}} \left(\sum_k a^\dagger_{k-q} a_k\right)\right) \tag{6.25}$$

$$= -\omega_q^2 Q_q - g \left(\frac{2\omega_q}{M\hbar}\right)^{\frac{1}{2}} \rho_q, \tag{6.26}$$

where ρ_q denotes the q-Fourier coefficient of the electronic density,

$$\rho_{-q} = \rho_q^\dagger = \left(\sum_k a^\dagger_{k+q} a_k\right)^\dagger = \left(\sum_k a^\dagger_k a_{k-q}\right)^\dagger = \sum_k a^\dagger_{k-q} a_k. \tag{6.27}$$

We can write the effective force on Q_q in the form of an ionic potential

$$V(Q_q) = g \left(\frac{2M\omega_q}{\hbar}\right)^{\frac{1}{2}} Q_q, \tag{6.28}$$

writing

$$M\ddot{Q}_q = -M\omega_q^2 Q_q - \rho_q \frac{\partial}{\partial Q_q} V(Q_q). \tag{6.29}$$

We use the ionic potential only to calculate the charge density ρ_q. The relation between the ionic potential and the induced charge density is given in linear response theory by

$$\rho_q^{ind} = \chi(q, T) V_q, \tag{6.30}$$

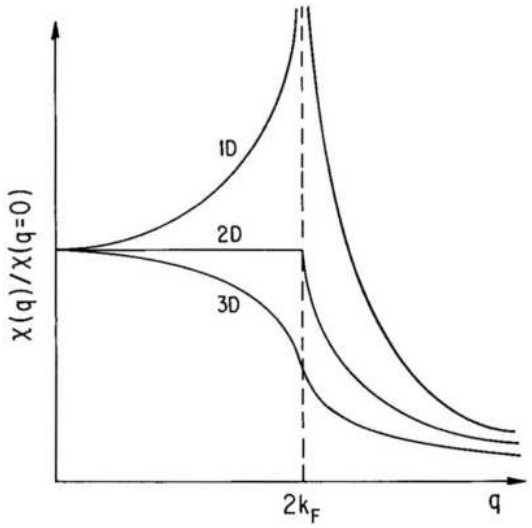

Figure 6.4: Lindhard response function at $T = 0$, normalised to its (negative) value at $q = 0$ as a function of wavevector q. Drawn for different dimensionalities. Image taken from [38]

where $\chi(q, T)$ is the wavevector- and temperature-dependent Lindhard response function. It is given in d dimensions by

$$\chi(q, T) = \int \frac{dk}{(2\pi)^d} \frac{f(E_k, T) - f(E_{k+q,T})}{E_k - E_{k+q}}, \tag{6.31}$$

where E_k denotes the energy of the electron with wavevector k, $f(E, T)$ is the Fermi function. In Figure 6.4 the Lindhard response function at $T = 0$ is drawn for different dimensions. Considering that for $T = 0$ and $d = 1$ the Lindhard response function goes to $-\infty$ as $q \mapsto 2f_F$, we are most interested in its behaviour at this point. Linearising the dispersion relation around $2k_F$ as shown in Figure 6.5, we have

$$\chi(2k_F, T) = -e^2 n(\epsilon_F) \int_0^{\frac{\epsilon_0}{2k_B T}} \frac{tanh(x)}{x} dx, \tag{6.32}$$

where ϵ_0 is a cutoff energy (usually one takes $\epsilon_0 = \epsilon_F$) which is made necessary by our introduction of a linearised dispersion that is only valid near k_F. $n(\epsilon_F)$ is the density of states at the Fermi surface. This leads us to

$$\chi(2k_F, T) = -e^2 n(\epsilon_F) \ln \frac{1.14\epsilon_0}{k_B T}, \tag{6.33}$$

which is drawn for various temperatures in figure 6.6. Using the above calcula-

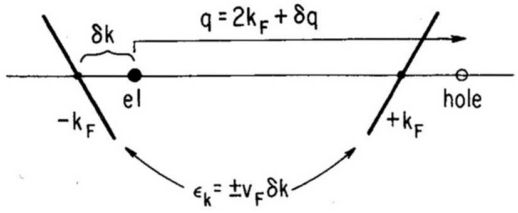

Figure 6.5: Linearised dispersion relation around $2k_F$ taken from [38]. Drawn into the figure is the scattering of an occupied state near $-k_F$ into an empty state near k_F that does hardly change the energy of the system.

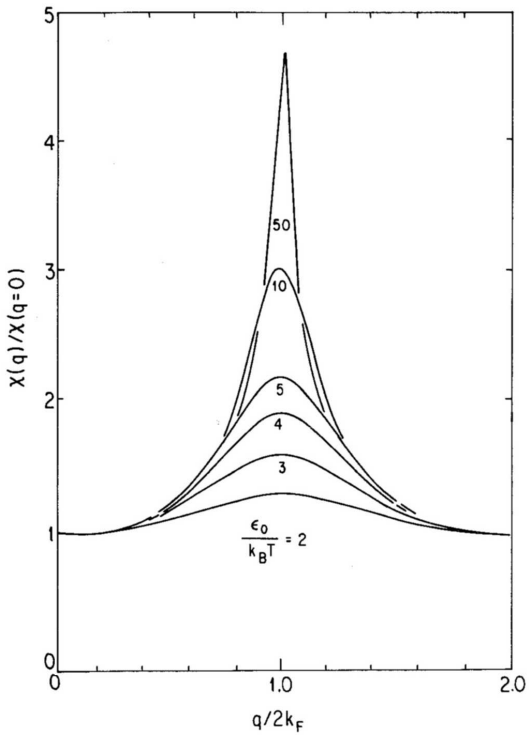

Figure 6.6: $\chi(k_F, T)$, drawn for various temperatures T as a function of wavevector. Illustration from [38]

tions for $\chi(2k_F, T)$ we can write the equation of motion for Q_q as

$$\ddot{Q}_q = -\left[\omega_q^2 + g\left(\frac{2\omega_q}{M\hbar}\right)^{\frac{1}{2}}\chi(q,T)g\left(\frac{2M\omega_q}{\hbar}\right)^{\frac{1}{2}}\right]Q_q \tag{6.34}$$

$$= -\left[\omega_q^2 + \frac{2g^2\omega_q}{\hbar}\chi(q,T)\right]Q_q, \tag{6.35}$$

which makes it evident that we have a new, smaller phonon frequency

$$\left(\omega_q^{new}\right)^2 = \omega_q^2 + \frac{2g^2\omega_q}{\hbar}\chi(q,T). \tag{6.36}$$

The effect is most prominent at $q = 2k_F$, we have

$$\left(\omega_{2k_F}^{new}\right)^2 = \omega_{2k_F}^2 - \frac{2g^2 n(\epsilon_F)\omega_{2k_F}}{\hbar}\ln\left(\frac{1.14\epsilon_0}{k_B T}\right). \tag{6.37}$$

This equation defines a (mean field) transition temperature where the phonon mode $2k_F$ freezes in,

$$k_B T^{MF} = 1.14\epsilon_0 e^{-\frac{\hbar\omega_{2k_F}}{2g^2 n(\epsilon_F)}}. \tag{6.38}$$

We have to add for completeness that the use of a one-dimensional model for studying the transition to the CDW ground state is somewhat problematic. In a one-dimensional world, fluctuations strongly suppress the transition to the CDW ground state (see for example [39]), the phase transition measured in the laboratory is the "locking in" of the phase of neighbouring chains (see [38]).

3 Soliton Excitations in Polyacetylene

This section is based on [40] and [41].
Trans-Polyacetylene has a twofold-degenerate ground state, as can be seen in Figure 6.7. Therefore, one can at least intuitively expect that there exist solitons, excitations corresponding to a moving domain wall between the two ground states.

We use the following approximations to simplify the treatment of polyacetylene

- neglect interactions between chains,
- treat the σ electrons only in the form of a spring constant,
- treat only displacements of CH groups along the chain direction,
- treat the π electrons in tight-binding approximation, expand nearest-neighbour hopping to first order around the equilibrium position (see Figure 6.8),

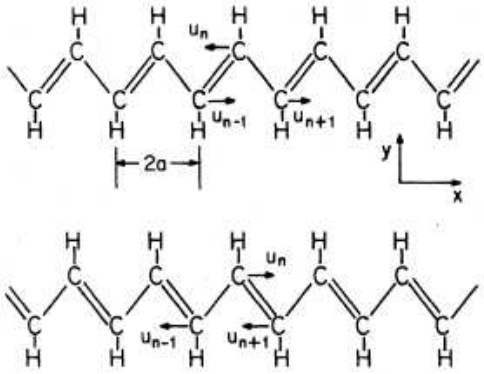

Figure 6.7: The two ground states of trans-polyacetylene, u_n is the dimerisation coordinate used in the model Hamiltonian. Above the A phase, below the B phase. Image from [40].

- neglect Coulomb interactions between electrons.

We have therefore for the σ bonding energy

$$E_\sigma = \frac{1}{2}\sum_n K\left(u_{n+1} - u_n\right), \tag{6.39}$$

where K is the effective spring constant. The chain has N atoms (we will refer to the CH groups as atoms since their structure is ignored) on it, we use periodic boundary conditions for simplicity.
We expand the hopping integral for the π electrons as

$$t_{n+1} = t_0 - \alpha\left(u_{n+1} - u_n\right), \tag{6.40}$$

where t_0 is the hopping integral for the undimerised chain, α is the electron-lattice displacement coupling constant. The above equation is the standard form for electron-phonon interaction in metals.

The kinetic energy of the CH groups, each with mass M, is given by

$$E_{kin} = \frac{1}{2}\sum_n M\dot{u}_n. \tag{6.41}$$

We have therefore the complete model Hamiltonian

$$\mathbf{H} = -\sum_{n,s} t_{n+1,n}\left(c^\dagger_{n+1,s}c_{n,s} + h.c.\right) + \frac{1}{2}\sum_n K\left(u_{n+1} - u_n\right) + \frac{1}{2}\sum_n M\dot{u}_n, \tag{6.42}$$

with $c^\dagger_{n,s}$ ($c_{n,s}$) denoting the creation (annihilation) operator for a π electron with spin s on the CH group number n. Of course, c and $c^\dagger$ satisfy anticommutation

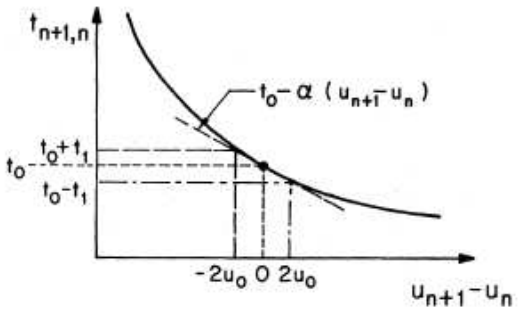

Figure 6.8: Nearest-neighbour hopping integral as a function of dimerisation coordinate difference (from [40]).

relations whereas u_n and p_n satisfy commutation relations. The system is spin degenerate, therefore we will not write out sums over spin explicitly in the following.
Given a perfectly dimerised chain, means $u_n = (-1)^n u$, the model Hamiltonian without the kinetic energy term reduces to

$$\mathbf{H}^d(u) = \sum_n \left[t_0 + (-1)^n 2\alpha u\right]\left(c_{n+1}^\dagger c_n + h.c.\right) + 2NKu^2. \tag{6.43}$$

We make use of the $2a$ periodicity of the problem by introducing a reduced zone scheme with a zone boundary $\pm\frac{\pi}{2a}$ and summing over two states per k value, one in the valence band and one in the conduction band. Figure 6.9 shows the $u = 0$ bands where

$$\begin{aligned} E_k^{0,v} &= -2t_0\cos(ka) = -\epsilon_k, \\ E_k^{0,c} &= 2t_0\cos(ka) = \epsilon_k. \end{aligned} \tag{6.44}$$

The operators c_k^v and c_k^c for valence- and conduction band states are given by

$$\begin{aligned} c_k^v &= \frac{1}{\sqrt{N}}\sum_n e^{ikan} c_n, \\ c_k^c &= \frac{-i}{\sqrt{N}}\sum_n e^{i(ka+\pi)n} c_n \end{aligned} \tag{6.45}$$

which enables us to write the Hamiltonian as

$$\mathbf{H}^d = \sum_k \epsilon_k\left(c_k^{c\dagger}c_k^c - c_k^{v\dagger}c_k^v\right) + 4\alpha u\sin(ka)\left(c_k^{c\dagger}c_k^v + c_k^{v\dagger}c_k^c\right) + 2NKu^2. \tag{6.46}$$

We arrive at the expression for the Hamiltonian in the k representation

$$\mathbf{H}^d = \sum_k \epsilon_k\left(c_k^{c\dagger}c_k^c - c_k^{v\dagger}c_k^v\right) + 4\alpha u\sin(ka)\left(c_k^{c\dagger}c_k^v + c_k^{v\dagger}c_k^c\right) + 2NKu^2. \tag{6.47}$$

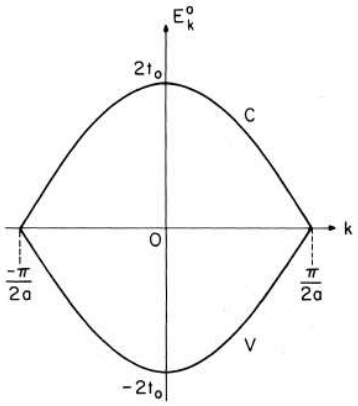

Figure 6.9: Brillouin zone scheme for the π electron band in the undimerised state. The unit cell is assumed to have two CH groups here to account for the dimerisation that will be included later, leading to the opening of gaps at the zone boundary. Then, the band denoted C will be the conduction band of a semiconductor, whereas the band denoted V will be the valence band. Taken from [40].

We are going to diagonalise this Hamiltonian by an $SU(2)$ transformation in the operators, the rotated operators are

$$\begin{pmatrix} a_k^v \\ a_k^c \end{pmatrix} = \begin{pmatrix} \alpha_k & -\beta_k \\ \beta_k^* & \alpha_k^* \end{pmatrix} \begin{pmatrix} c_k^v \\ c_k^c \end{pmatrix}, \quad |\alpha_k|^2 + |\beta_k|^2 = 1. \tag{6.48}$$

We write the Hamiltonian in equation (6.46) in terms of the new operators, using

$$\begin{pmatrix} c_k^v \\ c_k^c \end{pmatrix} = \begin{pmatrix} \alpha_k^* & \beta_k \\ -\beta_k^* & \alpha_k \end{pmatrix} \begin{pmatrix} a_k^v \\ a_k^c \end{pmatrix} \tag{6.49}$$

to get

$$\begin{aligned} \mathbf{H}^d = & \sum_k \epsilon_k \left[\left(-\beta_k a_k^{v\dagger} + \alpha_k^* \alpha_k^{c\dagger}\right) \left(-\beta_k^* a_v^k + \alpha_k a_k^c\right) - \left(\alpha_k a_k^{v\dagger} + \beta_k^* a_k^{c\dagger}\right) \left(\alpha_k^* a_k^v + \beta_k a_k^c\right) \right] \\ & + 4\alpha u \sin(ka) \left[\left(-\beta_k a_k^{v\dagger} + \alpha_k^* a_k^{c\dagger}\right) \left(\alpha_k^* a_k^v + \beta_k a_k^c\right) \left(\alpha_k a_k^{v\dagger} + \beta_k^* a_k^{c\dagger}\right) \left(-\beta_k^* a_k^v + \alpha_k a_k^c\right) \right] \\ & + 2NKu^2. \end{aligned} \tag{6.50}$$

We simplify the notation using the number operator $n = a^\dagger a$ giving us the

form

$$\begin{aligned}\mathbf{H}^d = \sum_k & n_k^v \left(\epsilon_k \left|\beta_k\right|^2 - \epsilon_k \left|\alpha_k\right|^2 + 4\alpha u \sin(ka) \left(-\alpha_k^* \beta_k\right) + 4\alpha u \sin(ka) \left(-\alpha_k \beta_k^*\right)\right) \\ & + n_k^c \left(\epsilon_k \left|\alpha_k\right|^2 - \epsilon_k \left|\beta_k\right|^2 + 4\alpha u \sin(ka) \left[\alpha_k^* \beta_k + \alpha_k \beta_k^*\right]\right) \\ & + \left[a_k^{v\dagger} a_k^c \left(-2\alpha_k \beta_k \epsilon_k + \left(\alpha_k^2 - \beta_k^2\right) 4\alpha u \sin(ka)\right) + h.c.\right] + 2NKu^2.\end{aligned} \tag{6.51}$$

For having a diagonal Hamiltonian in the rotated creation and annihilation operators we require $-2\epsilon_k \alpha_k \beta_k + 4\alpha u \sin(ka) \left(\alpha_k^2 - \beta_k^2\right) = 0$. We choose to have α_k real and positive, giving us

$$-\epsilon_k \alpha_k \beta_k + 2\alpha u \sin(ka)(\alpha_k^2 - \beta_k^2) = 0. \tag{6.52}$$

Inserting our choices $\alpha_k = |\alpha_k|$, $\beta_k = \pm |\beta_k|$, and $\beta_k^2 = 1 - \alpha_k^2$ we have

$$\epsilon_k^2 \alpha_k^2 (1 - \alpha_k^2) = 4\alpha_k^2 u^2 \sin^2(ka)(2\alpha_k^2 - 1)^2, \tag{6.53}$$

$$\epsilon_k^2 \alpha_k^2 - \epsilon_k^2 \alpha_k^4 = 16\alpha^2 u^2 \sin^2(ka)\alpha_k^4 - 16\alpha^2 u^2 \sin^2(ka)\alpha_k^2 + 4\alpha^2 u^2 \sin^2(ka), \tag{6.54}$$

$$\alpha_k^4(-\Delta_k^2 - \epsilon_k^2) + \alpha_k^2(\epsilon_k^2 + \Delta_k^2) - \frac{1}{4}\Delta_k^2 = 0, \tag{6.55}$$

where we have introduced $\Delta_k = 4\alpha u \sin(ka)$. We solve the equation for α_k^2, giving

$$\alpha_k^2 = \frac{-E_k^2 \pm \sqrt{E_k^4 - \Delta_k^2 E_k^2}}{-2E_k^2} \tag{6.56}$$

$$= \frac{1}{2} \pm \sqrt{\frac{E_k^4 - \Delta_k^2 E_k^2}{4E_k^4}} \tag{6.57}$$

$$= \frac{1}{2}\left(1 \pm \frac{\epsilon_k}{E_k}\right) \tag{6.58}$$

with $E_k^2 = \epsilon_k^2 + \Delta_k^2$. Because of $\alpha_k^2 + \beta_k^2 = 1$ the $\pm$ does only switch the roles of α_k and β_k, we can choose

$$\alpha_k^2 = \frac{1}{2}\left(1 + \frac{\epsilon_k}{E_k}\right), \quad \beta_k^2 = \frac{1}{2}\left(1 - \frac{\epsilon_k}{E_k}\right), \tag{6.59}$$

without loss of generality.
We have therefore $\alpha_k^2 - \beta_k^2 = \frac{\epsilon_k}{E_k} > 0$. Using this inequality we see in equation (6.52) that β_k has positive sign for $k > 0$, negative for $k < 0$, namely

$$\alpha_k = \left[\frac{1}{2}\left(1 + \frac{\epsilon_k}{E_k}\right)\right]^{\frac{1}{2}}, \quad \beta_k = \operatorname{sgn}(k)\left[\frac{1}{2}\left(1 - \frac{\epsilon_k}{E_k}\right)\right]^{\frac{1}{2}}. \tag{6.60}$$

We write the nonvanishing part of equation (6.51) as

$$\sum_k (n_k^c - n_k^v)\left(\epsilon_k(\alpha_k^2 - \beta_k^2) + 2\Delta_k\alpha_k\beta_k\right) + 2NKu^2. \tag{6.61}$$

Inserting $\epsilon_k(\alpha_k^2 - \beta_k^2) = \frac{\epsilon_k^2}{E_k}$ and $2\alpha_k\beta_k\Delta_k = \Delta_k\sqrt{1 - \frac{\epsilon_k^2}{E_k^2}} = \sqrt{\Delta_k^2 - \frac{\Delta_k^2\epsilon_k^2}{E_k^2}} = \sqrt{\frac{\Delta_k^4 + \epsilon_k^2\Delta_k^2 - \epsilon_k^2\Delta_k^2}{E_k^2}} = \frac{\Delta_k^2}{E_k}$ we have the diagonalised Hamiltonian

$$\mathbf{H}^d = \sum_k E_k\,(n_k^c - n_k^v) + 2NKu^2. \tag{6.62}$$

The ground state energy is obtained from equation (6.62) by setting $n_k^v = 1$ and $n_k^c = 0$ (we have N π atoms, the sum over k has $\frac{N}{2}$ terms, and the system is spin degenerate) giving

$$E_0(u) = -2\sum_k E_k + 2NKu^2. \tag{6.63}$$

We recall $E_k = \sqrt{\epsilon_k^2 + \Delta_k^2}$, $\epsilon_k = 2t_0\cos(ka)$, $\Delta_k = 4\alpha u\sin(ka)$ and we replace the sum by an integral, the normalisation is

$$\frac{L}{2\pi}\int_{-\frac{\pi}{2a}}^{\frac{\pi}{2a}} dk = \frac{N}{2}\frac{a}{\pi}\int_{-\frac{\pi}{2a}}^{\frac{\pi}{2a}} dk = \sum_k, \tag{6.64}$$

where $L = Na$ denotes the chain length. The integral expression for the ground state energy as a function of the dimerization u is therefore

$$E_0(u) = \frac{-L}{\pi}\int_{-\frac{\pi}{2a}}^{\frac{\pi}{2a}} E_k dk + 2NKu^2. \tag{6.65}$$

We make use of the inversion symmetry, $E_k = E_{-k}$ to get

$$\begin{aligned} E_0(u) &= \frac{-2L}{\pi}\int_0^{\frac{\pi}{2a}} E_k dk + 2NKu^2 \\ &= \frac{-2L}{\pi}\int_0^{\frac{\pi}{2a}} \sqrt{\left(2t_0\cos(ka)\right)^2 + \left(4\alpha u\sin(ka)\right)^2}dk + 2NKu^2, \end{aligned} \tag{6.66}$$

where we substitute $q = ak$, $k = \frac{\pi}{2a} \iff q = \frac{\pi}{2a}$, $dk = \frac{1}{a}dq$ to get

$$\begin{aligned} E_0(u) &= \frac{-2L}{a\pi}\int_0^{\frac{\pi}{2}} \sqrt{\left(2t_0\cos(q)\right)^2 + \left(4\alpha u\sin(q)\right)^2}dq \\ &= \frac{-4L}{a\pi}\int_0^{\frac{\pi}{2}} \sqrt{\left(t_0\cos(q)\right)^2 + \left(2\alpha u\sin(q)\right)^2}dq. \end{aligned} \tag{6.67}$$

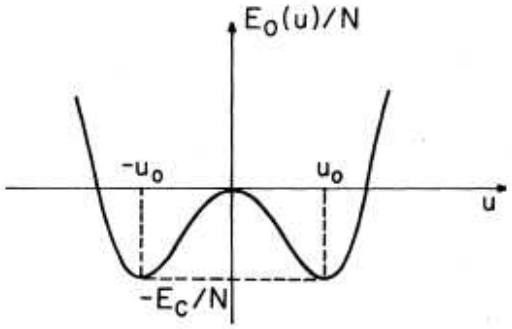

Figure 6.10: Energy per CH group as a function of dimerisation, the two stable minima are the A and B phase. Illustration from [40]

We replace cosine by sine,

$$\begin{aligned}(t_0\cos(q))^2+(2\alpha u\sin(q))^2 &= t_0^2+\sin^2(q)(-t_o^2+4\alpha^2u^2)\\ &= t_0^2\left(1-(1-\frac{4\alpha^2u^2}{t_0^2})\sin^2(q)\right),\end{aligned} \tag{6.68}$$

and we introduce the shorthand $z=\frac{t_1}{t_0}=\frac{2\alpha u}{t_0}$to get to

$$\begin{aligned}E_0(u) &= \frac{-4Nt_0}{\pi}\int_0^{\frac{\pi}{2}}\sqrt{\left(1-(1-z^2)\sin^2(q)\right)}dq+\frac{NKt_0^2z^2}{2\alpha^2}\\ &= \frac{-4Nt_0}{\pi}E(1-z^2)+\frac{NKt_0^2z^2}{2\alpha^2}\end{aligned} \tag{6.69}$$

where E denotes the complete elliptic integral of the first kind. If z is small (which is simply restating the condition that the hopping integral can be linearised) we can use the approximation

$$E(1-z^2)\approxeq 1+\frac{1}{2}\left(\frac{\ln 4}{|z|}-\frac{1}{2}\right)z^2+\ldots, \tag{6.70}$$

which shows us that the energy has a local maximum at $u=0$ and two global minima at u_0 (see Figure 6.10). We can use equation (6.69) to calculate the density of states per spin direction

$$\rho_0(E)=\frac{L}{2\pi\left|\frac{dE_k}{dk}\right|}=\begin{cases}\left(\frac{N}{\pi}\right)\frac{|E|}{\left[(4t_0^2-E^2)(E^2-\Delta^2)\right]^{\frac{1}{2}}} & |E|\in[\Delta,2t_0]\\ 0 \quad \text{otherwise}\end{cases}, \tag{6.71}$$

where $\Delta=\Delta_{\frac{\pi}{2a}}=4\alpha u_0=2t_1$.

Calculations Using Green's Functions

We are calculating various Green's functions which we are going to need later on for our treatment of the soliton. We use the eigenfunction expansion

$$G^d_{n,m}(E) = \left\langle \phi_n \left| \sum_k \frac{|\psi^c_k\rangle \langle\psi^c_k|}{E + i0^+ - E^c_k} + \frac{|\psi^v_k\rangle \langle\psi^v_k|}{E + i0^+ - E^v_k} \right| \phi_n \right\rangle, \tag{6.72}$$

to get

$$G^d_{n,m}(E) = \begin{cases} \frac{1}{N}\sum_k \frac{2Ee^{ika(n-m)}}{(E+i0^+)^2 - E_k^2} & n-m \quad \text{even} \\ \frac{-1}{N}\sum_k \frac{2E_k[\alpha_k + i\beta_k(-1)^n]^2 e^{ika(n-m)}}{(E+i0^+)^2 - E_k^2} & n-m \quad \text{odd}, \end{cases} \tag{6.73}$$

for the off diagonal elements and

$$G^d_{n,n}(E) = \begin{cases} \frac{-iE}{\left[(4t_0^2 - E^2)(E^2 - \Delta^2)\right]^{\frac{1}{2}}} & |E| \in [\Delta, 2t_0] \\ \frac{-E}{\left[(4t_0^2 - E^2)(\Delta^2 - E^2)\right]^{\frac{1}{2}}} & |E| \in (0, \Delta) \\ \frac{E}{\left[(E^2 - 4t_0^2)(E^2 - \Delta^2)\right]^{\frac{1}{2}}} & |E| \in (2t_0, \infty) \end{cases} \tag{6.74}$$

for the diagonal elements ($\Delta = 4\alpha u_0$). The expression for the diagonal elements can be checked using the density of states already calculated because we have

$$\rho^d(E) = \frac{-\operatorname{sgn} E}{\pi} \sum_n \Im G^d_{n,n}(E). \tag{6.75}$$

Soliton Excitations

The classical ground state is twofold degenerate, therefore there exists an excitation corresponding to a soliton. To get rid of the sign of the displacement u_n, we define the order parameter

$$\psi_n := (-1)^n u_n. \tag{6.76}$$

The two ground states are then

$$\psi_{0n} = \begin{cases} -u_0 & \text{A phase} \\ u_0 & \text{B phase} \end{cases}. \tag{6.77}$$

We are doing all of our calculations assuming a widely separated soliton-antisoliton pair in a ring , with the order parameter as in figure 6.11. This circumvents boundary effects caused by the shift of the order parameter at one end of the chain. If we started with a chain in a perfect B phase and introduced a soliton, one end of the chain would end up being in the A phase, needing energy for the switch.

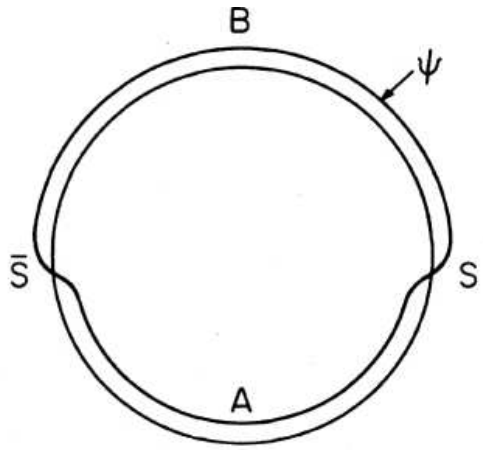

Figure 6.11: A soliton S and an antisoliton $\bar{S}$ in a ring of $(CH)_x$. The order parameter ψ is plotted radially, A and B denote the two ground states of the dimerised chain. Image from [40]

Because of the symmetry of soliton and antisoliton, we can just work with a chain approaching perfect B phase as $n \mapsto \infty$ and perfect A phase as $n \mapsto -\infty$. We are determining the minimum energy configuration for this chain by isolating a segment from $n = -\nu$ to $n = \nu$ of the chain surrounding the soliton (which is centered at $n = 0$). We decompose our Born-Oppenheimer model Hamiltonian as

$$\mathbf{H} = \mathbf{H}_0 + \hat{\mathbf{V}} \tag{6.78}$$

where $\mathbf{H}_0$ describes a chain with perfect B phase displacements for $n \leq -\nu$ and perfect A phase displacements for $n \geq \nu$. The hopping between groups in $-\nu \leq n \leq \nu$ is defined to be zero. Written out, the hopping integrals defining $\mathbf{H}_0$ are

$$t^0_{n+1,n} = \begin{cases} t_0 - (-1)^{n-\nu} t_1, & n < -\nu \\ 0, & -\nu \leq n < \nu \\ t_0 + (-1)^{n-\nu} t_1, & n \geq \nu. \end{cases} \tag{6.79}$$

where ν is taken to be odd.
The perturbation $\hat{\mathbf{V}}$ provides the missing hopping integrals, it is therefore defined by

$$-\hat{\mathbf{V}}_{n+1,n} = t_0 + (-1)^n \alpha(\psi_{n+1} + \psi_n), \quad -\nu \leq n < \nu \tag{6.80}$$

where the ψ_n will be minimising the total energy.
We are using the formula for calculating the energy difference due to a localised potential derived in the appendix, namely

$$\Delta E = \frac{2}{\pi} \int_{-\infty}^{E_F} \Im \ln \det \left(\mathbf{1} - G^0 \hat{\mathbf{V}} \right) dE. \tag{6.81}$$

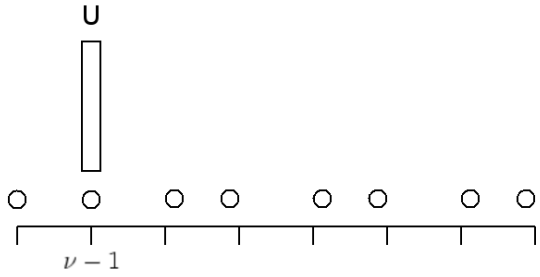

Figure 6.12: Schematic representation of the isolating potential used to get the Green's Function for the perfectly dimerised chain with neighbouring isolated atoms from the Green's Function for the infinite perfectly dimerised chain.

For carrying out that calculation, we first need the Green's function G^0 in the absence of the potential $\hat{\mathbf{V}}$, which is close to the Green's function G^d for the perfectly dimerized chain but not identical. We break the chain into three segments where G^0 is block diagonal, these are

$$A \quad n \geq \nu \tag{6.82}$$

$$S \quad -\nu < n < \nu \tag{6.83}$$

$$B \quad n \leq -\nu. \tag{6.84}$$

In the S segment, we have $G^0_{n,m}(E) = \frac{1}{E}\delta_{n,m}$ because there is no coupling between atoms. For the A segment, we decouple by introducing an artificial potential U placed on the group $\nu - 1$ as depicted in Figure 6.12. We consider $U \mapsto \infty$ to arrive at the decoupled case. We have in segment A the following equation for G^0:

$$G^0_{n,m} = G^d_{n,m} + G^d_{n,\nu-1} U G^0_{\nu-1,m} \tag{6.85}$$

which gives for $U \mapsto \infty$ in the A segment

$$G^0_{n,m} = G^d_{n,m} - \frac{G^d_{n,\nu-1} G^d_{\nu-1,m}}{G^d_{n,n}} \tag{6.86}$$

and in analogy for the B segment

$$G^0_{n,m} = \bar{G}^d_{n,m} - \frac{\bar{G}^d_{n,-\nu+1} \bar{G}^d_{-\nu+1,m}}{\bar{G}^d_{n,n}} \tag{6.87}$$

where $\bar{G}$ is G with t_1 replaced by $-t_1$.
Now we have the integrand in (6.81), we can carry out the integration numerically using the trial function

$$\psi_n = \begin{cases} u_0, & n \leq -\nu \\ -u_0 \tanh\left(\frac{n}{l}\right), & -\nu < n < \nu \\ -u_0, & n \geq \nu \end{cases} \tag{6.88}$$

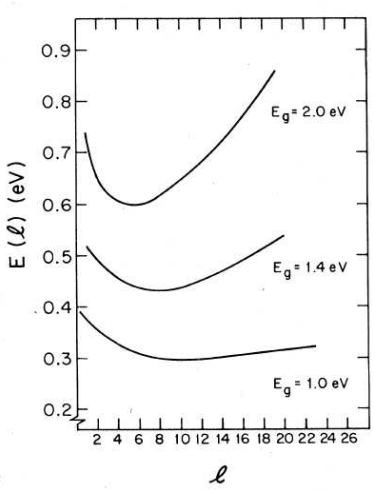

Figure 6.13: Soliton energy $E(l)$ as a function of an assumed half-width l. Shown for various values of the energy gap E_g. Taken from [40].

where l denotes the half-width of the soliton. The energy as a function of the half-width is plotted for three different gap energies in Figure 6.13. The half-width is determined by finding the minimum energy of the soliton.
The use of trial functions other than tanh does not result in considerable differences in the numerical results.

The Electronic Structure of the Soliton

We calculate the change in the density of states due to a soliton by using the formula

$$\frac{-1}{\pi}\partial_E \ln\det\left(\mathbf{1} - G^0\hat{\mathbf{V}}\right) = \rho(E) - \rho_0(E), \tag{6.89}$$

depicted in Figure 6.14. Together with the conservation of electrons, $\int_{-\infty}^{\infty}\Delta\rho(E)dE = 0$ and the symmetry of $\Delta\rho(E)$ we can see that the valence band and the conduction band each have a deficit of one-half state for each spin. Therefore, since the valence band is fully occupied whereas the conduction band is empty, the missing electron occupies the state ϕ_0 in the middle of the gap. Therefore a neutral soliton has spin one-half. A low energy charged soliton state corresponds to removing the unpaired soliton from ϕ_0 or adding a second electron (which might for example stem from doping the material). Therefore a charged soliton has spin zero. We have therefore the following unusual charge-spin relations:

$$Q_0 = 0, \quad s_0 = \frac{1}{2} \tag{6.90}$$

$$Q_\pm = \pm e, \quad s_\pm = 0. \tag{6.91}$$

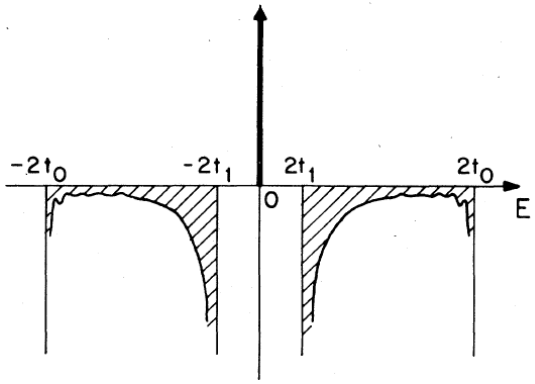

Figure 6.14: Change of density of states due to the presence of a soliton. The gap center state is a δ function of strength unity. Illustration of [40].

The missing electron density at each site is compensated by the electronic density $|\phi_0(n)|^2$. To see this we use the fact that the local density of states $\rho_{n,n}(E)$ satisfies the sum rule

$$\int_{-\infty}^{\infty} \rho_{n,n}(E)dE = 1 \tag{6.92}$$

We have also the symmetry $\Delta\rho_{n,n}(E) = \Delta\rho_{n,n}(-E)$ which leads us to the local compensation formula

$$2\int_{-\infty}^{-\Delta} \Delta\rho_{n,n}(E)dE + |\phi_0(n)|^2 = 0. \tag{6.93}$$

Because the distribution of the electronic density is not influenced by the occupancy of the state, we have also that the charge distribution of the charged soliton is $\pm|\phi_0(n)|^2$.
Numerical calculations for $\Delta\rho_{n,n}(E)$ are shown for $n = 0, 6, 12$ and $n = 1, 5, 11$ in Figure 6.15 for a soliton centered at $n = 0$. We see that the density of states vanishes for n odd.

This is an exact result and can be shown by considering $E_0 = 0$ which reads, written out,

$$\mathbf{H}\phi_0 = \begin{pmatrix} \ddots & \ddots & 0 & & \\ t_{n-1,n} & 0 & t_{n+1,n} & 0 & \\ 0 & t_{n,n+1} & 0 & t_{n+2,n+1} & 0 \\ 0 & 0 & \ddots & \ddots & \ddots \end{pmatrix} \begin{pmatrix} \vdots \\ \phi_0(n) \\ \phi_0(n+1) \\ \vdots \end{pmatrix} = 0. \tag{6.94}$$

In this form we can see that we have two uncoupled recursive equations for $\phi_0(odd)$ and $\phi_0(even)$. For the center at even n, only $\phi_0(even)$ is normalizable, and vice

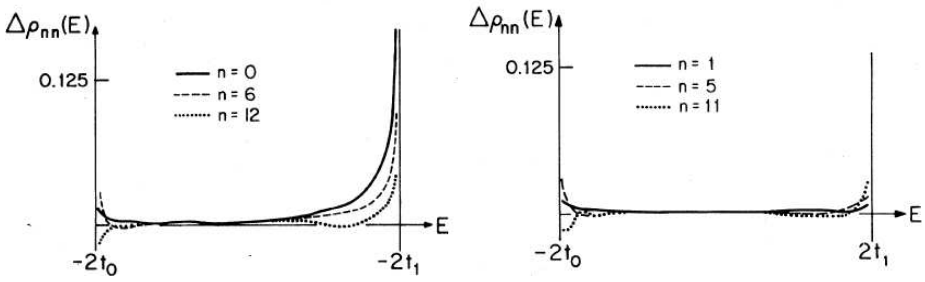

Figure 6.15: Change of local density of states due to the presence of a soliton for various distances from the soliton, even left, odd right. Both pictures from [40].

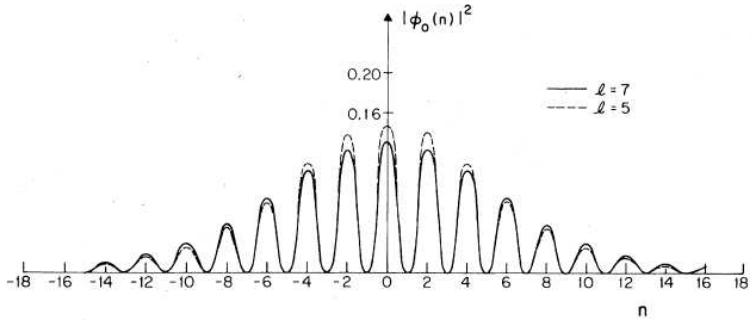

Figure 6.16: Shape of a soliton centered at $n = 0$, illustration from [40].

versa.
The shape of the soliton for an even center is

$$\phi_0(n) \approxeq \frac{1}{l} \operatorname{sech}\left(\frac{n}{l}\right) \cos\left(\frac{1}{2}\pi n\right), \tag{6.95}$$

which is depicted in Figure 6.16.

Third-filled band case

This section draws from [42].
We assume now a third-filled band in polyacetylene, reusing the concepts from above. The ground state of this system is threefold degenerate, shown diagrammatically in Figure 6.17. We have now two types of kinks, type I from A phase to B phase (and from B to C or C to A respectively) and type II from B to A (and from A to C or from C to B). We can calculate the charge of a type I kink using the fact that the chain gets shorter by a type I kink (see Figure 6.18). Since the phase shift is 2π in total a charge of $+2|e|$ flows into the region where the three kinks have been formed, therefore each type I kink has a charge of $+\frac{2}{3}|e|$ due to symmetry. This result can be checked by Green's function calculations

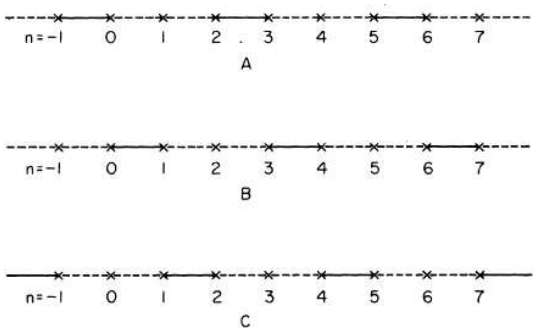

Figure 6.17: Three degenerate ground states for a trimerised chain, long bonds are dotted. Image from [42]

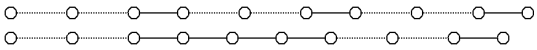

Figure 6.18: Above: Standard trimerised chain. Below: Trimerised chain with three type I kinks (each contracted to a single point for the illustration).

or numerical calculations. By the same argument as before one can see that a type II kink has a charge of $-\frac{2}{3}|e|$. Naturally, one identifies the type II kinks as the antiparticles of the respective type I kinks. In surprising analogy with hadron and quark structure, one can then see that either three (anti)solitons or a soliton and an antisoliton can be created without disturbing the ground state of the chain far away.

Appendix: Green's Functions – Introduction and Some Useful Formulas

This section derives some formulas used in [40], using [43] referenced therein.

Green's Function for $t > 0$

We set the starting time $t_0 = 0$ and define the Green's function as

$$\hat{G}(t) = -ie^{-i\mathbf{H}t} \quad t > 0 \tag{6.96}$$

and we set $\hat{G}(t) = 0$ for $t < 0$.
This definition corresponds to a definition using time-ordered creation and annihilation operators. We take the momentum basis:

$$\left\langle p_1 \left| \hat{G}(t) \right| p_2 \right\rangle = -i \left\langle 0 \left| T\left(\tilde{a}_{p_1}(t)\tilde{a}^\dagger_{p_2}(0)\right) \right| 0 \right\rangle \tag{6.97}$$

where T is the time-ordering operator. Therefore for $t > 0$:

$$\left\langle p_1 \left| \hat{G}(t) \right| p_2 \right\rangle = -i \left\langle 0 \left| e^{i\mathbf{H}t} a_{p_1} e^{-i\mathbf{H}t} a_{p_2}^\dagger \right| 0 \right\rangle = -i \left\langle p_1 \left| e^{-i\mathbf{H}t} \right| p_2 \right\rangle \tag{6.98}$$

and for $t < 0$:

$$i \left\langle 0 \left| a_{p_2}^\dagger e^{i\mathbf{H}t} a_{p_1} e^{-i\mathbf{H}t} \right| 0 \right\rangle = i \left\langle 0 \left| a_{p_2}^\dagger e^{i\mathbf{H}t} a_{p_1} \right| 0 \right\rangle = \left\langle 0 \left| e^{i\mathbf{H}t} \right| 0 \right\rangle = 0 \tag{6.99}$$

We define the Fourier transform as

$$f(\omega) = \int_{-\infty}^{\infty} f(t) e^{i\omega t} dt. \tag{6.100}$$

We recall that $\hbar = 1$ in our units, in particular $\omega = E$, therefore the Fourier transform of the Green's function $\hat{G}(E + i\delta)$, $\delta = 0^+$ is

$$\hat{G}(E + i\delta) = \int_{-\infty}^{\infty} \hat{G}(t) e^{i(E+i\delta)t} \tag{6.101}$$

$$= \int_{-\infty}^{\infty} -ie^{-i(\mathbf{H}-(E+i\delta))t} dt \tag{6.102}$$

$$= \int_{0}^{\infty} -ie^{-i(\mathbf{H}-(E+i\delta))t} dt \tag{6.103}$$

$$= \left[\mathbf{H} - (E + i\delta)\right]^{-1} e^{-i(\mathbf{H}-E)t} e^{-\delta t} \Big|_0^\infty \tag{6.104}$$

$$= \left[\mathbf{H} - (E + i\delta)\right]^{-1}. \tag{6.105}$$

We also note that if we write out the Hamiltonian in terms of eigenfunctions, $\mathbf{H} = \sum_k E_k \left|\psi_k\right\rangle \left\langle\psi_k\right|$ we immediately see that

$$\hat{G}(E + i\delta) = \left[\mathbf{H} - (E + i\delta)\right]^{-1} = \sum_k \left[E_k - (E + i\delta)\right]^{-1} \left|\psi_k\right\rangle \left\langle\psi_k\right|. \tag{6.106}$$

We make use of the distribution equation

$$\lim_{\eta \to 0, \eta > 0} \frac{1}{x + i\eta} = \text{principal part} \left(\frac{1}{x}\right) - i\pi\delta(x) \tag{6.107}$$

to see that

$$\frac{-1}{\pi} \Im \left(\text{Tr}(\hat{G}(E + i\delta)) \right) = \frac{-1}{\pi} \Im \left(\sum_k \left[E_k - (E + i\delta)\right]^{-1} \right) = \sum_k \delta\left(E_k - E\right) \tag{6.108}$$

which is the one-electron density of states $\rho(E)$ for the Hamiltonian $\mathbf{H}$.

Gap energy ΔE (eq. 6.81)

We have the unperturbed Hamiltonian $\mathbf{H}_0$ with eigenvalues ϵ_j. The perturbed Hamiltonian $\mathbf{H} = \mathbf{H}_0 + \hat{\mathbf{V}}$ has eigenvalues E_j.
We use the replacement of the energy E by $E - i\delta$, $\delta = 0^+$.
The Green's Function of the unperturbed Hamiltonian $\mathbf{H}_0$ is defined as $[E - i\delta - \mathbf{H}_0]^{-1}$

$$\det\left(\left[E - i\delta - \mathbf{H}_0\right]^{-1}\left[E - i\delta \ - \mathbf{H}\right]\right) = \prod_j \frac{E - i\delta - E_j}{E - i\delta - \epsilon_j} \tag{6.109}$$

$$= \det\left(\left[E - i\delta - \mathbf{H}_0\right]^{-1}\left[E - i\delta \ - \mathbf{H}_0 - \hat{\mathbf{V}}\right]\right) \tag{6.110}$$

$$= \det\left(1 - G^0(E)\hat{\mathbf{V}}\right) \tag{6.111}$$

which gives us

$$\frac{1}{\pi}\Im\left(\partial_E \ln\det\left(1 - G^0(E)\hat{\mathbf{V}}\right)\right) = \frac{1}{\pi}\Im\left(\partial_E\left[\sum_j \ln(E - i\delta - E_j) - \sum_j \ln(E - i\delta - \epsilon_j)\right]\right) \tag{6.112}$$

$$= \frac{1}{\pi}\Im\left(\sum_j \frac{1}{(E - i\delta - E_j)} - \sum_j \frac{1}{(E - i\delta - \epsilon_j)}\right) \tag{6.113}$$

$$= \rho(E) - \rho_0(E) \tag{6.114}$$

where $\rho(E)$ is the density of states with the full Hamiltonian $\mathbf{H}$, $\rho_0(E)$ with the unperturbed Hamiltonian $\mathbf{H}_0$.

We choose the energy eigenvectors ψ^0 of $\mathbf{H}_0$ as a basis, therefore $G^0(E)$ will be diagonal and if $\hat{\mathbf{V}}$ does only have matrix elements between some eigenvectors, means $\left\langle \psi_n^0 \middle| \hat{\mathbf{V}} \middle| \psi_m^0 \right\rangle \neq 0 \quad \text{iff} \quad n, m \in [n_{min}, n_{max}]$, $1 - G^0(E)\hat{\mathbf{V}}$ has nondiagonal elements only in the submatrix $[n_{min}, n_{max}]$, therefore the determinant is that of the submatrix.
We assume conservation of electrons, therefore we have

$$\int_{-\infty}^{E_F} \rho(E)dE = \int_{-\infty}^{E_F^0} \rho_0(E)dE. \tag{6.115}$$

If we assume $E_F < E_F^0$ ($E_F^0 > E_F$ is analogous), then we have

$$\int_{-\infty}^{E_F} \left(\rho(E) - \rho_0(E)\right) dE = \int_{E_F}^{E_F^0} \rho_0 dE \approx (E_F^0 - E_F)\rho_0(E_F), \tag{6.116}$$

because we take the system to be large and the potential not too big, which implies that $E_F - E_F^0$ will be small compared with E_F.

We write down the energy difference, inserting a spin factor of 2,

$$\frac{\Delta E}{2} = \int_{-\infty}^{E_F} E \cdot \rho(E) dE - \int_{-\infty}^{E_F^0} E \cdot \rho_0(E) dE \tag{6.117}$$

$$= \int_{-\infty}^{E_F} E \cdot \rho(E) dE - \int_{-\infty}^{E_F^0} E \cdot \rho_0(E) dE - \int_{E_F}^{E_F^0} E \cdot \rho_0(E) dE \tag{6.118}$$

$$= \int_{-\infty}^{E_F} E(\rho(E) - \rho_0(E)) dE - \underbrace{\int_{E_F}^{E_F^0} E \cdot \rho_0(E) dE}_{\approx E_F \int_{E_F}^{E_F^0} \rho_0(E) dE = E_F \int_{-\infty}^{E_F} (\rho(E) - \rho_0(E)) dE} \tag{6.119}$$

$$= \int_{-\infty}^{E_F} (E - E_F)(\rho(E) - \rho_0(E)) dE \tag{6.120}$$

$$= \int_{-\infty}^{E_F} (E - E_F) \frac{1}{\pi} \Im \left(\partial_E \ln \det(1 - G^0(E)\hat{\mathbf{V}}) \right) dE, \tag{6.121}$$

where we integrate by parts to eliminate the partial derivative with respect to energy, the boundary term vanishes at $E = -\infty$ because $G^0(E)$ is suppressed as E^{-1} for large energy:

$$\frac{\Delta E}{2} = (E - E_F) \frac{1}{\pi} \Im \ln \det(1 - G^0(E)\hat{\mathbf{V}}) \Big|_{-\infty}^{E_F} - \int_{-\infty}^{E_F} \frac{1}{\pi} \Im \ln \det(1 - G^0(E)\hat{\mathbf{V}}) dE \tag{6.122}$$

$$\Rightarrow \ \Delta E = \frac{-2}{\pi} \int_{-\infty}^{E_F} \Im \ln \det(1 - G^0(E)\hat{\mathbf{V}}) dE. \tag{6.123}$$

7 Vortices

Thomas Eggel
Supervisor: Stefan Fredenhagen

The topological structure of solutions of the Ginzburg-Landau equations is the main concern of this report. A brief introduction is to serve as a physical orientation of where the investigations are to take place. The GL energy functions will be discussed in the global and gauged theory. The topological possibilities in both cases are examined and a scaling argument is shown to provide useful information in the global theory. By the virtue of the Principle of Symmetric Criticality invariant solutions under a combined $SO(2)$ action in the gauged theory are shown to exhibit interesting behaviour. In the end interaction between vortices and a possible extension to a dynamic theory are investigated.

1 Introduction

The Landau theory of second order phase transitions is based on the assumptions that a phase transition can be characterized by some kind of order parameter and by a simple postulated dependence of the free energy on this order parameter. The crucial insight concerning superconductors was made by Ginzburg and Landau in 1950 [44] as they stated :

" We shall start from the idea that Ψ (the order parameter) represents some "effective" wave function of the "superconducting electrons". "

This implies that the order parameter is complex and is generally varying in space.

The free energy was then postulated to be of the form

$$f(\mathbf{x}) = f_n + \alpha|\phi(\mathbf{x})|^2 + \frac{1}{2}\beta|\phi(\mathbf{x})|^4$$

to which a gradient term is added to account for energy arising due to the

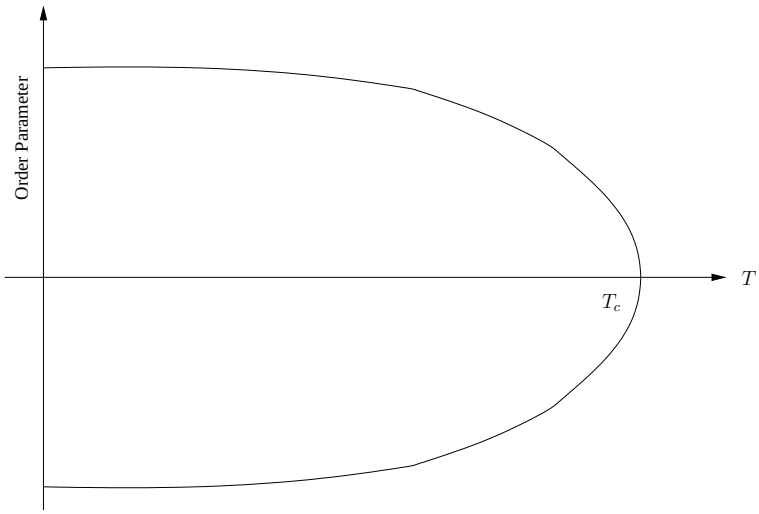

Figure 7.1: Order parameter close to T_c

spatial variation of the field, which reads

$$f(\mathbf{x}) = f_n + \alpha|\phi(\mathbf{x})|^2 + \frac{1}{2}\beta|\phi(\mathbf{x})|^4 + \frac{\hbar^2}{2m}|\nabla\phi(\mathbf{x})|^2,$$

see [45]. Vortices are now, heuristically speaking, soliton solutions of the field equations obtained by variation of an energy functional in which the above form of the free energy (1) is incorporated, which exhibit a certain behaviour. Namely a field configuration ϕ is considered to contain a vortex at a point $\mathbf{x}$ if

- $\mathbf{x}$ is an isolated point where ϕ vanishes
- along a small circle enclosing $\mathbf{x}$ counterclockwise, the phase of ϕ increases by $2\pi N$, $N \in \mathbb{Z} \setminus \{0\}$.

N is then called the multiplicity of the vortex. To get a geometrical idea of what a vortex field configuration looks like, one might find it useful to consider figure 7.2 as a first, heuristic indication of the form of a vortex.

2 The Ginzburg-Landau energy functions

Vortices are soliton solutions of the Ginzburg-Landau equations. These are the equations one obtains by variation of the Ginzburg-Landau energy functions

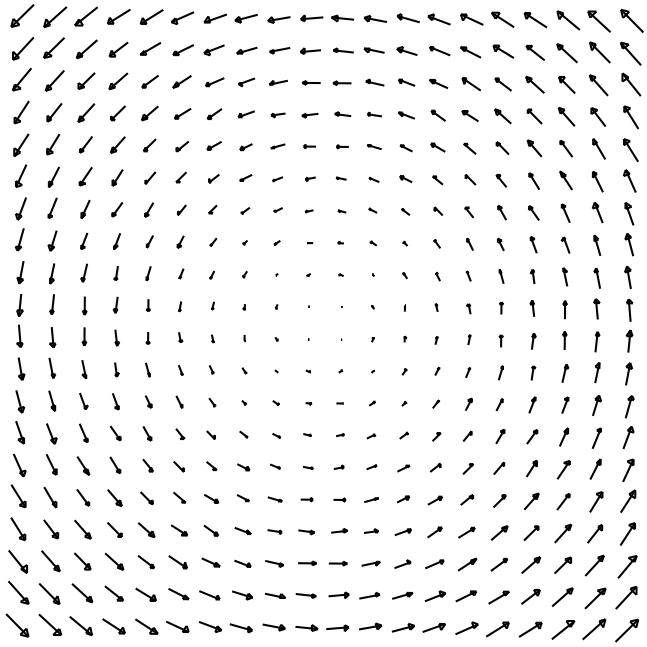

Figure 7.2: The winding of a field around a zero (vortex)

which are as a matter of fact functionals defined on the space of all field configurations. There are two types of field theories to be discussed: a global theory in which there is only the scalar field $\phi(x)$ present and the local theory in which the the scalar field $\phi(x)$ couples to an electromagnetic field with gauge group $U(1)$. The scalar field ϕ, which is a complex quantity, shall be written as

$$\phi(x) = \phi_1(x) + i\phi_2(x).$$

The Global Theory

In the global theory, the GL energy function is given by the following expression

$$V \equiv V(\phi) = \int \left(\frac{1}{2} \nabla \bar{\phi} \cdot \nabla \phi + U(\bar{\phi}.\phi) \right) d^2x \tag{7.1}$$

where U denotes the part of (1) that depends on $|\phi|$. For further investigation it will prove useful to chose the following form for U

$$U = \mu + \nu \bar{\phi}\phi + \frac{\lambda}{8}(\bar{\phi}\phi)^2, \qquad \mu, \nu, \lambda \in \mathbb{R}. \tag{7.2}$$

The functional (7.1) is invariant under a global $U(1)$ phase rotation

$$\phi(x) \mapsto e^{i\alpha}\phi(x), \tag{7.3}$$

If we require that a lower bound for the energy exist, λ must be chosen such that $\lambda > 0$. The coefficient μ can be adjusted such that the minimal value of U, $U_{\min}$ is zero. If furthermore ν is chosen < 0, equation (7.2) can be written in the following form

$$U = \frac{\lambda}{8}(m^2 - \bar{\phi}\phi)^2 \tag{7.4}$$

and the GL energy function reads

$$V = \int \left(\frac{1}{2}\nabla\bar{\phi}\cdot\nabla\phi + \frac{\lambda}{8}(m^2 - \bar{\phi}\phi)^2.\right) d^2x \tag{7.5}$$

We shall denote the vacuum manifold by $\mathcal{V}$ and thus, in the present case the vacuum manifold is just the circle $|\phi(x)| = m$. Thus

$$\pi_1(\mathcal{V}) = \pi_1(\mathcal{S}^1) = \mathbb{Z}, \tag{7.6}$$

which, we will find out, will give rise to the possibility of existence of vortices. Variation of (7.1) with respect to $\bar{\phi}$ yields the following field equation

$$\nabla^2\phi + \frac{\lambda}{2}(m^2 - \bar{\phi}\phi)\phi = 0. \tag{7.7}$$

The vacuum solutions are of the form $\phi(x) = me^{i\chi}$ and since the gradient energy has to vanish, $\chi =$ constant and thus the choice of χ spontaneously breaks the global $U(1)$ symmetry.

The Gauged Theory

In the gauged theory, the scalar field couples to the electromagnetic field and the GL energy function reads

$$V = \frac{1}{2}\int \left(B^2 + \overline{D_i\phi}D_i\phi + \frac{\lambda}{4}(m^2 - \bar{\phi}\phi)^2\right) d^2x, \tag{7.8}$$

where $B = f_{12} = \partial_1 a_2 - \partial_2 a_1$ is the magnetic field and $D_i\phi = \partial_i\phi - ia_i\phi$ the covariant derivatives.

The GL energy (7.8) is invariant under the following gauge transformation

$$\phi(x) \mapsto e^{i\alpha(x)}\phi(x) \tag{7.9}$$

$$a_i(x) \mapsto a_i(x) + \partial_i\alpha(x). \tag{7.10}$$

$e^{i\alpha(x)}$ is a spatially varying phase rotation. Variation of (7.8) with respect to ϕ,a_i yields the following field equations

$$D_i D_i \phi + \frac{\lambda}{2}(m^2 - \bar{\phi}\phi)\phi = 0 \tag{7.11}$$

$$\epsilon_{ij}\partial_j B + \frac{i}{2}(\bar{\phi} D_i \phi - \phi \overline{D_i \phi}) = 0 \tag{7.12}$$

We note that equation (7.12) has the form of Ampère's equation in two dimensions, with the quantity $j_i = \frac{i}{2}(\bar{\phi} D_i \phi - \phi \overline{D_i \phi})$ being interpreted as the electric current in the plane.

In order that a solution be a vacuum solution, the components of the integrand of (7.8) need to vanish separately. Thus the energy is minimized if

$$|\phi(x)| = m \tag{7.13}$$

$$B = 0 \tag{7.14}$$

$$D_i \phi = 0. \tag{7.15}$$

This requires that

$$\phi(x) = m e^{i\chi(x)} \quad \text{from (7.13)} \tag{7.16}$$

$$a_i(x) = \partial_i \alpha(x) \quad \text{from (7.15)} . \tag{7.17}$$

$D_i \phi$ vanishes if

$$(\partial_i \chi - \partial_i \alpha) e^{i\chi} \tag{7.18}$$

i.e. $\alpha(x) = \chi(x) +$ constant . The vacuum is thus of the following form

$$\phi(x) = m e^{i\chi(x)}, \; a_i(x) = \partial_i \chi(x), \tag{7.19}$$

which, by the gauge transformation $e^{i\chi}$, can be transformed to the simple vacuum $\phi = m, \; a_i = 0$.

Derrick's Theorem

In [46] G.H. Derrick noted that in many theories that have an energy functional of the form

$$E(\phi) = \int (\nabla \phi)^2 + f(\phi) \tag{7.20}$$

for any $f(\phi)$, the equations derived from the variation of the energy functional have no stable, time-independent, localized solutions. By localized it is meant that the integral (7.20) converges when taken over all space. This is shown as follows: Suppose ϕ is a localized solution in 3 dimensions of the variation $\delta E = 0$. Define the scaled field configuration $\phi^{(\mu)}(x) = \phi(\mu x)$ with μ some arbitrary constant and write $E_0 = \int f(\phi) d^3x$ and $E_2 = \int (\nabla \phi)^2 d^3x$ and write

$$e(\mu) = \int \left((\nabla \phi^\mu)^2 + f(\phi^\mu) \right) d^3x = \frac{1}{\mu} E_2 + \frac{1}{\mu^3} E_0 \tag{7.21}$$

where the second identity is obtained by a simple change of variables. Therefore

$$\left.\frac{de(\mu)}{d\mu}\right|_{\mu=1} = -E_2 - 3E_0 \tag{7.22}$$

$$\left.\frac{d^2e(\mu)}{d\mu^2}\right|_{\mu=1} = 2E_2 + 12E_0. \tag{7.23}$$

Now since ϕ^μ is a solution of the variation $\delta E = 0$ for $\mu = 1$, it follows that

$$\left.\frac{de(\mu)}{d\mu}\right|_{\mu=1} = 0 \tag{7.24}$$

$$E_0 = -\frac{1}{3}E_2 \tag{7.25}$$

$$\left.\frac{d^2e(\mu)}{d\mu^2}\right|_{\mu=1} = -2E_2 < 0 \tag{7.26}$$

Hence $\phi^{(\mu)}$ is not stable with respect to rescaling since the second variation is always negative and thus ϕ is unstable. If, as it occurs in our case, $f(\phi) \geq 0$, then the variation $\delta E = 0$ has no nontrivial localized solutions, be it stable or unstable, at all, for in this case both quantities E_0 and E_2 are non-negative and thus have to vanish separately which then yields $\phi \equiv 0$.

3 Application of Derrick's Theorem

In this subsection we will apply Derrick's Rescaling Theorem to the global and the local theory. We will see that in the global theory, Derrick's Theorem provides us with useful nonexistence information whereas in the local theory, the theorem will not prove so useful. Note that we are working in two spatial dimension which is different to the framework in which we have introduced the theorem, but this will not give rise to any significant changes.

The usefulness of Derrick's Theorem depends crucially on the way the rescaled quantities are defined. For the scalar field we define

$$\phi^{(\mu)}(x) = \phi(\mu x), \tag{7.27}$$

which means that the gradient takes the following form

$$\nabla\phi^{(\mu)}(x) = \nabla(\phi(\mu x)) = \mu\nabla\phi(\mu x). \tag{7.28}$$

For the gauge potential we will chose a form that ensures that the covariant derivative behaves similarly under spatial rescaling as the gradient. Thus we define

$$A^{(\mu)}(x) = \mu A(\mu x) \tag{7.29}$$

and therefore

$$D^{A^{(\mu)}}\phi^{(\mu)}(x) = \mu D^A \phi(\mu x) \tag{7.30}$$

and the field strength tensor acquires a second order term

$$F^{(\mu)}(x) = \mu^2 F(\mu x). \tag{7.31}$$

Derrick's Theorem in the Global Theory

We have seen that the vacuum solutions are of the form $\phi(x) = e^{i\chi}$ with χ constant. The question that is now arising is if there is other finite energy solutions not identical to the vacuum. The answer will be no and this will be shown using Derrick's Theorem.

Consider equation (7.5) and write

$$E_0 = \frac{\lambda}{8}\int (m^2 - \bar{\phi}\phi)^2 d^2x \tag{7.32}$$

and

$$E_2 = \int \left(\frac{1}{2}\nabla\bar{\phi}\cdot\nabla\phi\right) d^2x \tag{7.33}$$

and thus

$$e(\mu) = E_2 + \frac{1}{\mu^2}E_0. \tag{7.34}$$

If finite energy non-vacuum solutions existed, they would need to satisfy

$$E_0 = \frac{\lambda}{8}\int (m^2 - \bar{\phi}\phi)^2 d^2x = 0, \tag{7.35}$$

so $|\phi| = m$ everywhere. Let $\phi = me^{i\chi}$ and substitution into (7.7) yields

$$\nabla^2\chi = 0 \text{ and } \nabla\chi\cdot\nabla\chi = 0, \tag{7.36}$$

therefore $\chi =$ constant and thus ϕ is a vacuum.

Derrick's Theorem in the Local Theory

In the gauged theory, Derrick's Theorem does not rule out finite energy solutions other than the vacuum. Write (7.8) as

$$V = \frac{1}{2}\int \left(B^2 + \overline{D_i\phi}D\phi + \frac{\lambda}{4}(m^2 - \bar{\phi}\phi)^2\right) d^2x = E_4 + E_2 + E_0. \tag{7.37}$$

Hence the energy as a function of μ reads

$$e(\mu) = \mu^2 E_4 + E_2 + \mu^{-2}E_0. \tag{7.38}$$

Differentiation with respect to μ yields

$$\frac{d}{d\mu}e(\mu) = 2\mu E_4 - 2\mu^{-3}E_0. \tag{7.39}$$

Taking this expression at $\mu = 1$ yields

$$E_0 = E_4 \Leftrightarrow \frac{1}{2}\int B^2 d^2x = \frac{\lambda}{8}\int (m^2 - \bar{\phi}\phi)^2 d^2x, \tag{7.40}$$

the two contributions to the energy are equal. But this is by no means as restricting a condition as (7.35).

4 Topological Structures

Both in the global and local theory topological structure can be found. In the global theory the requirement of finite energy will show to be too strict for vortices to be allowed, whereas in the local theory there will be vortex solutions that are of finite energy.

Topology in the Global Theory

It is convenient to express (7.5) in polar coordinates $x^1 = \rho\cos\theta$ and $x^2 = \rho\sin\theta$:

$$V = \frac{1}{2}\int_0^\infty \int_0^{2\pi} \left(\partial_\rho\bar{\phi}\partial_\rho\phi + \frac{1}{\rho^2}\partial_\theta\bar{\phi}\partial_\theta\phi + \frac{\lambda}{4}(m^2 - \bar{\phi}\phi)^2\right)\rho d\rho d\theta. \tag{7.41}$$

Consider a field configuration whose energy density approaches 0 rapidly as $|x| \to \infty$. Thus

$$|\phi| \to m \text{ and } \partial_\rho\phi \to 0 \quad \text{as } \rho \to \infty \tag{7.42}$$

Assume the limit $\lim\limits_{\rho\to\infty}\phi(\rho,\theta)$ exists and denote it by

$$\phi^\infty(\theta) = me^{i\chi^\infty(\theta)}. \tag{7.43}$$

The map

$$\phi^\infty : S^\infty \longrightarrow S^1 \tag{7.44}$$

is a map from the circle at infinity to S^1. Since $S^1 = \mathcal{V}$, ϕ^∞ is a map from the circle at infinity to the vacuum manifold. Since we assume ϕ^∞ to be single valued, χ^∞ must satisfy

$$\chi^\infty(2\pi) = \chi^\infty(0) + 2\pi N \quad N \in \mathbb{N} \tag{7.45}$$

Let us now have a closer look at the contribution of χ^∞ to the energy density. The term in $\frac{1}{\rho^2}\partial_\theta\bar{\phi}\partial_\theta\phi$ is $\mathcal{O}(\frac{1}{\rho^2})$ provided $\chi^\infty(\theta)$ is differentiable. Let ρ_0 be sufficiently large, so that $\phi(\rho,\theta)$ can be approximated by

$$\phi^\infty(\rho,\theta) = me^{i\chi^\infty}. \tag{7.46}$$

Since $\partial_\theta \phi^\infty = i \cdot m \partial_\theta \chi^\infty e^{i\chi^\infty}$ and $\overline{\partial_\theta \phi^\infty} \partial_\theta \phi^\infty = m^2 (\partial_\theta \chi^\infty)^2$ the contribution to the energy outside of circle of radius ρ_0, denoted by E_{χ,ρ_0} is given by

$$E_{\chi,\rho_0} = \frac{1}{2} m^2 \int_{\rho_0}^{\infty} \int_0^{2\pi} \frac{1}{\rho} (\partial_\theta \chi^\infty)^2 d\rho d\theta. \tag{7.47}$$

The integrals in E_{χ,ρ_0} separate and the radial integral is logarithmically divergent unless $\partial_\theta \chi^\infty = 0$. In this case the field configuration would have a limit that is of the form

$$\phi^\infty(\theta) = m e^{i\chi^\infty} \quad \text{with } \chi = \text{const.} \tag{7.48}$$

For this field configuration with constant phase the winding number satisfies $N = 0$. Thus the requirement of finite energy does not allow for solutions that are topologically distinct to the vacuum. We would like to mention that if we were prepared to relax the condition of finite energy and allow solutions with logarithmically divergent energies, the radial part in (7.47) would not have to vanish and neither would N. Solutions with $N \neq 0$ do have a topological structure that is distinct to the topological structure of the vacuum and thus allowing for solutions with logarithmically divergent energies in the global theory leads to vortex solutions.

Topology in the Local Theory

Again we consider the GL energy in polar coordinates $x^1 = \rho \cos\theta$ and $x^2 = \rho \sin\theta$ and (7.8) becomes

$$V = \frac{1}{2} \int_0^{\infty} \int_0^{2\pi} \left(\frac{1}{\rho^2} f_{\rho\theta}^2 + \overline{D_\rho \phi} D_\rho \phi + \frac{1}{\rho^2} \overline{D_\theta \phi} D_\theta \phi + \frac{\lambda}{4} (m^2 - \bar{\phi}\phi)^2 \right) \rho d\rho d\theta. \tag{7.49}$$

The covariant derivatives are given by

$$D_\rho \phi = \partial_\rho \phi - i a_\rho \phi \tag{7.50}$$

$$D_\theta \phi = \partial_\theta \phi - i a_\theta \phi. \tag{7.51}$$

We will now seek to find a limiting form of an arbitrary finite energy field configuration ϕ. Let $\{\phi(x), a_i(x)\}$ be a finite energy field configuration. The requirement of finite energy, $V < \infty$, imposes the boundary condition

$$|\phi| \to m \text{ as } |x| \to \infty. \tag{7.52}$$

The different terms in the integrand of (7.49) have to vanish separately, so it follows that

$$D_\rho \phi \to 0 \quad \text{as} \quad |x| \to \infty. \tag{7.53}$$

Let us now fix an angle θ and move out on a radial line $0 \leq \rho \leq \infty$ and suppose ρ is large. Asymptotically $\phi = me^{i\chi}$ and thus

$$D_\rho \phi = im \cdot (\partial_\rho \chi - a_\rho) e^{i\chi} = 0. \tag{7.54}$$

The term in parentheses has to vanish and therefore $a_\rho = \partial_\rho \chi$. We now transform the field to the radial gauge $a_\rho = 0$ by a suitable gauge transformation.[21]

In the new gauge, $\partial_\rho \phi \to 0$ as $|x| \to \infty$, so

$$\lim_{\rho \to \infty} \phi(\rho, \theta) = \phi^\infty(\theta) = me^{i\chi^\infty(\theta)}, \tag{7.55}$$

which then defines ϕ on the circle at infinity i.e. a limiting form of ϕ along each radial line. Furthermore, the two quantities

$$c_1 = \int\int \frac{1}{\rho^2} \overline{D_\theta \phi} D_\theta \phi \rho d\rho d\theta \tag{7.56}$$

$$c_2 = \int\int \frac{1}{\rho^2} f_{\rho\theta}^2 \rho d\rho d\theta \tag{7.57}$$

need to satisfy $c_1 < \infty$ and $c_2 < \infty$. From the boundedness of c_1 it follows that

$$D_\theta \phi \to 0 \text{ as } \rho \to \infty \tag{7.58}$$

and from the boundedness of c_2 it follows that

$$f_{\rho\theta} \to 0 \text{ as } \rho \to \infty \tag{7.59}$$

Since $f_{\rho\theta} = \partial_\rho a_\theta - \partial_\theta a_\rho$, it follows from (7.59) that $\partial_\rho a_\theta = \partial_\theta a_\rho$ and since we are working in the radial gauge this is equivalent to $\partial_\rho a_\theta = 0$, so a_θ has a limit

$$\lim_{\rho \to \infty} a_\theta(\rho, \theta) = a_\theta^\infty(\theta). \tag{7.60}$$

This defines the gauge potential on the circle at infinity. Equation (7.58) implies

$$\partial_\theta \chi^\infty - a_\theta^\infty = 0. \tag{7.61}$$

So since the gauge potential is not necessarily vanishing on the circle at infinity, the derivative of the phase at infinity is not necessarily vanishing i.e. $\chi^\infty = \chi^\infty(\theta)$, not necessarily constant. This is a tremendous difference to the global theory in which under the requirement of finite energy, the phases of the field configurations need to be constant.

Again

$$\phi^\infty : S^1_\infty \longrightarrow S^1 \tag{7.62}$$

[21] Such a gauge transformation can always be found: if $a_\rho \neq 0$ then the gauge transformation $g(\rho, \theta) = exp\left(-i \int_0^\rho a_\rho(\rho', \theta) d\rho'\right)$ is an appropriate transformation.

is a map from the circle at infinity to the vacuum manifold $\mathcal{V} = S^1$ and the winding number N is an integer given by

$$N = \frac{1}{2\pi}\left(\chi^{\infty}(2\pi) - \chi^{\infty}(0)\right) \tag{7.63}$$

It is possible to uncover another nature of the quantity N which is often called the topological charge of the field configuration $\{\phi(x), a_i(x)\}$. The first Chern number c_1 is, in the framework of our theory, defined to be the following quantity

$$c_1 = \frac{1}{2\pi}\int_{-\infty}^{\infty}\int_{-\infty}^{\infty} f_{12}dx^1dx^2 \tag{7.64}$$

where $f_{12} = \partial_1 a_2 - \partial_2 a_1$ is the magnetic field in the plane. Now this can be written by Stokes' theorem for differential forms as a line integral along the circle at infinity

$$c_1 = \frac{1}{2\pi}\int_0^{2\pi} a_\theta d\theta|_{\rho=\infty} = \int_0^{2\pi} a^{\infty}(\theta)d\theta. \tag{7.65}$$

By the fundamental theorem of calculus, (7.63) can be written as

$$N = \frac{1}{2\pi}\int_0^{2\pi} \partial_\theta \chi^{\infty}(\theta)d\theta = \int_0^{2\pi} a^{\infty}(\theta)d\theta \tag{7.66}$$

where in the last identity equation (7.61) was used. From (7.65) it also becomes obvious that $2\pi N$ is the total flux of the magnetic field that traverses the whole plane. Thus we see that the magnetic flux is quantized in units of 2π.

There is also a third topological characterization of the winding number N. It can be regarded as the total vortex number in the plane, i.e. the total amount of points in the plane where the field vanishes with the respective multiplicities of the zeros taken into account. To see this we assume that the set of points where the field vanishes,

$$\{x|\phi(x) = 0\} \equiv \{A, B, C \ldots\} \tag{7.67}$$

is finite and that these zeros are isolated. We denote by $\{n_A, n_B, n_C, \ldots\}$ the multiplicities of the zeros. By the geometric argument provided by figure 7.3, it is obvious that the winding number of the field ϕ along the circle at infinity is the sum of the multiplicities

$$N = n_A + n_B + n_C + \ldots. \tag{7.68}$$

5 Vortex Solutions

All known finite energy, static solutions of the field equations have

- circular symmetry ($\lambda \neq 1$) about some point and

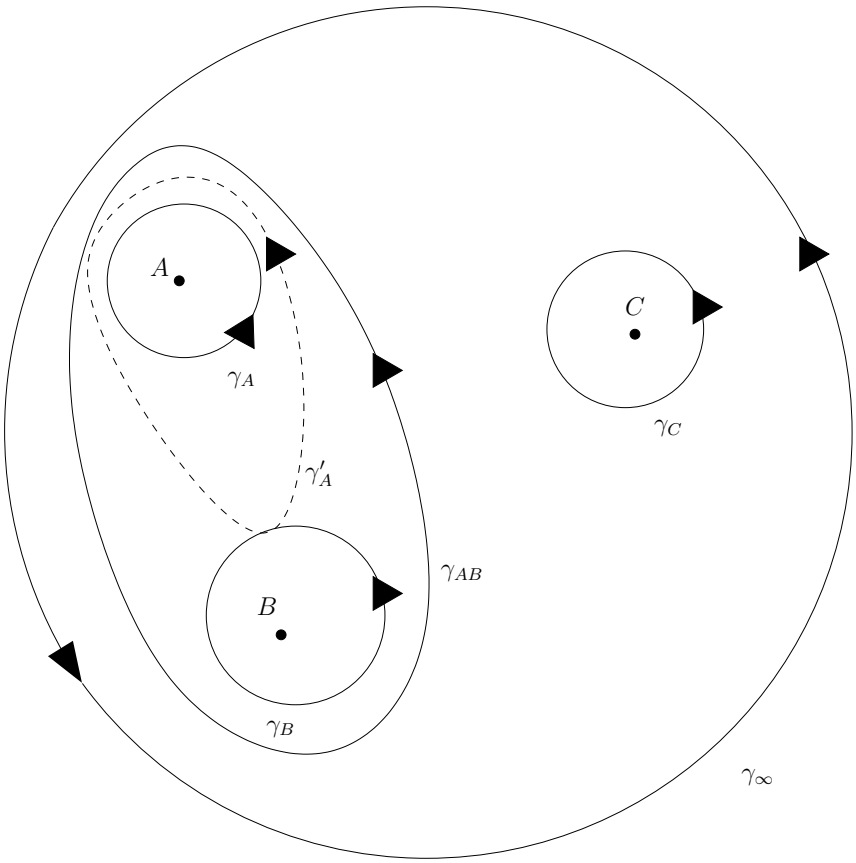

Figure 7.3: Zeros of ϕ and different paths

- a reflection symmetry .

In order to obtain information about the behaviour and the form of the fields and the energy density about a zero of ϕ, we will consider solutions that are invariant under a particular $SO(2)$ action. To ensure that the fields obtained in this way are really solutions, we will invoke the Principle of Symmetric Criticality.

Principle of Symmetric Criticality

The following principle allows one to conclude that if a variational principle is invariant under some symmetry group G, then to test if a field configuration that is invariant under a subgroup of the symmetry group is a stationary value it suffices to investigate the vanishing of the first variation of the action with respect to variations that are also symmetric, see [47] We will state it following [48]:

Let ϕ be the fields of some Lagrangian field theory with action $S(\phi)$ and let $\mathcal{C}$ denote the space of all field configurations ϕ. Let K be a subgroup of the symmetry group, and let $\mathcal{C}_K \subset \mathcal{C}$ denote the configuration space of all K-invariant fields, ie. fields ϕ such that

$$k(\phi) = \phi \quad \forall\, k \;\in\; K \tag{7.69}$$

Let denote $S_K(\phi)$ denote the action of the theory restricted to $\mathcal{C}_K$ and let $\phi_0(x) \in \mathcal{C}_K$ be a field configuration that extremizes S_K.

Then the Principle of Symmetric Criticality states that $\phi_0(x)$ is automatically a stationary point of the full action S

Solutions Invariant under Combined SO(2) Action

We will construct solutions that are invariant under a certain combined $SO(2)$ action. Consider the $SO(2)$ action by the combined rotations and phase rotations $(R(\beta), \tilde{R}(N\beta))$, $N \in \mathbb{Z}$ i.e.

$$\tilde{R}(\beta) : \phi \mapsto e^{i\beta}\phi \tag{7.70}$$

and $R(\beta)$ the usual rotation. Fix $m = 1$. Thus $(R(\beta), \tilde{R}(N\beta))$ is a phase rotation $e^{iN\beta}$ accompanying a rotation by β, which is a global transformation as it is independent of ρ, θ. This combined $SO(2)$ action leaves the field invariant, provided

$$\begin{array}{rcl} \phi(\rho,\theta) & = & e^{iN\theta}\phi(\rho) \\ a_\rho(\rho,\theta) & = & a_\rho(\rho) \\ a_\theta(\rho,\theta) & = & a_\theta(\rho) \end{array} \tag{7.71}$$

We now gauge transform $a_\rho \mapsto 0$. Because of the reflection symmetry $\phi(\rho,\theta) = \bar{\phi}(\rho,-\theta)$ we have that $\phi(\rho)$ is real.

The following boundary conditions ensure that at $\rho = 0$ ϕ is single valued and the gauge-potential non-singular and that at $\rho = \infty$ we have

$$D_\theta\phi = \partial_\theta\phi - ia_\theta\phi = (iN - iN)e^{iN\theta} = 0. \tag{7.72}$$

Since $\phi(0) = 0$ there is a vortex [22] located at the origin. Furthermore because of (7.71) the phase of ϕ increases by $2\pi N$ and since $a_\theta^\infty = N$ the total magnetic flux is given by

$$\int_0^{2\pi} a_\theta d\theta = \int_0^{2\pi} N d\theta = 2\pi N \tag{7.73}$$

We thus obtain a GL energy of the following form

$$V = \pi \int_0^\infty \left(\frac{1}{\rho^2}\left(\frac{da_\theta}{d\rho}\right)^2 + \left(\frac{d\phi}{d\rho}\right)^2 + \frac{1}{\rho^2}\left(N - a_\theta\right)^2\phi^2 + \frac{\lambda}{4}\left(1-\phi^2\right)^2 \right) \rho d\rho, \tag{7.74}$$

[22] or multivortex

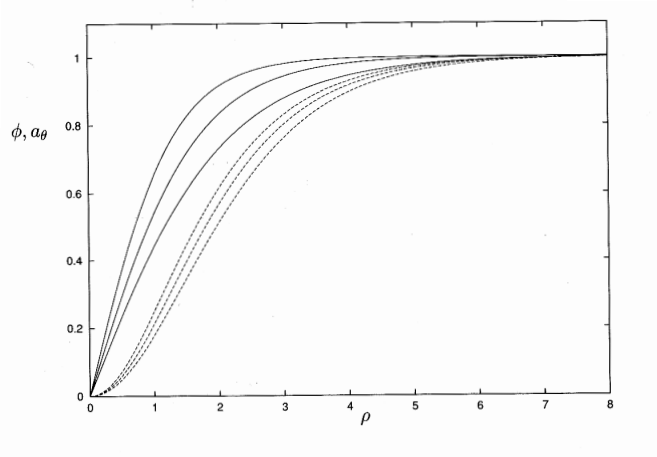

Figure 7.4: $\phi(\rho)$ (solid curves), $a_\theta(\rho)$ (dashed curves) for $N = 1$ with $\lambda = 0.5, 1.0, 2.0$. From [48].

which gives rise to the field equations

$$\frac{d^2\phi}{d\rho^2} + \frac{1}{\rho}\frac{d\phi}{d\rho} - \frac{1}{\rho^2}(N - a_\theta)^2\phi + \frac{\lambda}{2}(1 - \phi^2)\phi = 0 \tag{7.75}$$

$$\frac{d^2 a_\theta}{d\rho^2} - \frac{1}{\rho}\frac{da_\theta}{d\rho} + (N - a_\theta)\phi^2 = 0. \tag{7.76}$$

These equations have been solved numerically. Figure 7.4 shows the scalar field ϕ and the gauge field a_θ as functions of ρ for different values of λ. Figure 7.5 shows the energy density and the magnetic field for a $N = 1$ vortex with $\lambda = 1$. Note how the energy density as well as the magnetic field B are peaked about the location of a vortex. The existence of solutions of (7.75) and (7.76) has been proven for all $N \neq 0$ and all $\lambda > 0$.

6 Forces between Gauged Vortices

First we will give some general results concerning the forces that act between gauged vortices and then we will give an analytical expression for the forces between gauged vortices at large separation. We will assume in this subsection that λ is of the order of 1.

General Results

Generally one says that there is an attractive force acting between two vortices if the energy of the two-vortex field configuration increases as the separation between the vortices increases. Similarly, one says that there is a repelling force acting between two vortices if the energy of the two-vortex field configuration

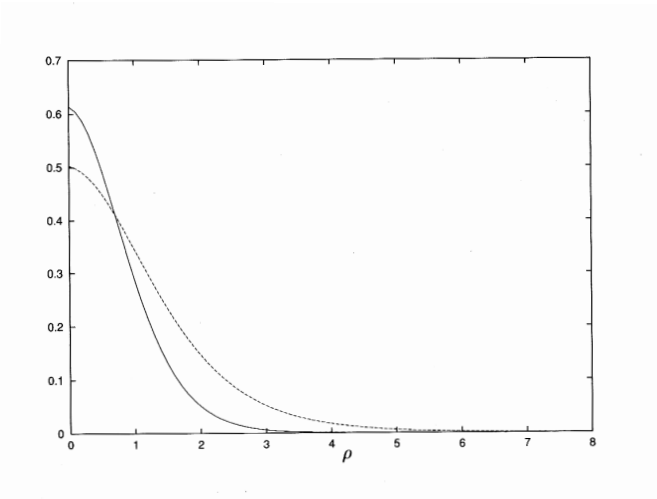

Figure 7.5: Energy density (solid curve) and magnetic field B (dashed curve) for the $N = 1$ vortex with $\lambda = 1$. From [48].

decreases as the separation between the vortices increases. From all the different ways of investigating the energy of multi-vortex configurations the following results emerge: For

$\lambda < \mathbf{1}$ Vortices attract

$\lambda > \mathbf{1}$ Vortices repel

$\lambda = \mathbf{1}$ Vortices are in a neutral equilibrium

In [49] the vortex interaction energy was calculated numerically for a two-vortex configuration as a function of the separation of the vortices. The results for $\lambda = 1.3, 1.0, 0.7$ are shown on figure 7.6

The different values for λ can be associated to the physical behaviour of a superconductor. Recall the magnetization curves of a type I/II superconductor as shown on figure . In a type I superconductor, the magnetic field is expelled until it reaches some critical value H_c. From this exterior field strength on, the magnetic field completely penetrates the superconductor, which leads to the dramatic discontinuity of the magnetization curve at $H = H_c$. This type of superconductor corresponds to $\lambda < 1$. The vortices attract and the overlapping of the vortices cause the magnetization to break down. A type II superconductor exhibits a different behaviour. Until the exterior field strength has attained some first critical value H_{c1}, a type II superconductor behaves like a type I superconductor. Once this first threshold value is surpassed, the magnetic field starts to penetrate the superconductor in flux quanta. This corresponds to $\lambda > 1$, i.e. to the case where the vortices repel. They arrange in a regular lattice since experimental superconductors are of finite size.

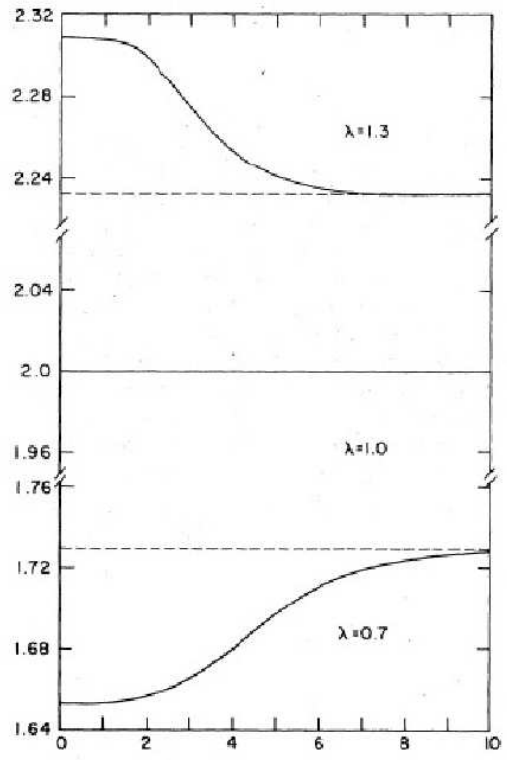

Figure 7.6: Energy of a two-vortex field configuration as a function of the vortex separation. From [49].

Forces between Gauged Vortices at large Separation

This case is interesting because there exist an analytic form for the asymptotic behaviour of the two vortex configuration. Let $E_{int}(s)$ denote the interaction energy between two $N = 1$ vortices at a separation $s >> 1$. This is given by the total energy minus twice the energy of infinitely separated vortices

$$E_{int}(s) = E_{tot} - 2E_1^{\infty}. \tag{7.77}$$

There is two contributions to the energy: A contribution due to the scalar field and a contribution coming from the magnetic field. The result is given by

$$E_{int}(s) = -\frac{A_s^2}{2\pi} K_0(\sqrt{\lambda}s) + \frac{A_m^2}{2\pi} K_0(s), \tag{7.78}$$

K_0 denoting the zeroth order modified Bessel function of the second kind and A_m and A_s coefficient that correspond to the magnetic and scalar field respectively. Figures 7.8 and 7.9 show plots of (7.78) for two different values of λ.

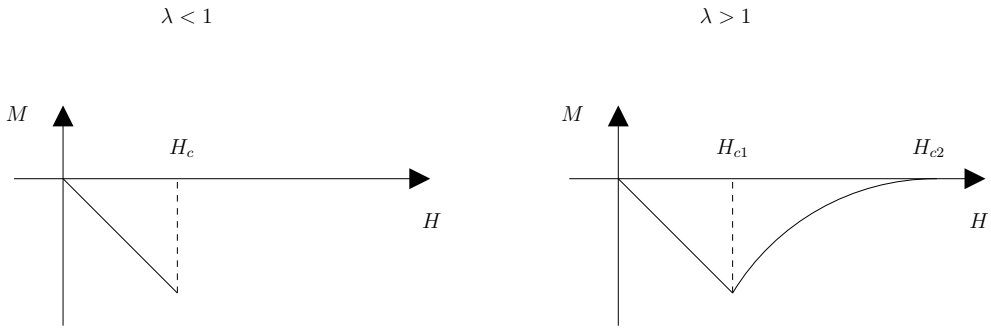

Figure 7.7: Magnetization curve of type I and II superconductors

7 Dynamics - Scalar Electrodynamics Model

The static GL equations determine how to energy of a configuration of several vortices depends on their separations. But this does not determine how the vortices will move. We will discuss a possible extension of the static gauged theory by the well known Abelian Higgs or Scalar Electrodynamics model. The Lagrangian of the Abelian Higgs model is given by

$$L = \int \left(-\frac{1}{4} f_{\mu\nu} f^{\mu\nu} + \frac{1}{2} \overline{D_\mu \phi} D^\mu \phi - \frac{\lambda}{8} (1 - \bar{\phi}\phi)^2 \right) d^2x. \tag{7.79}$$

We note that in addition to the gauged static GL energy as given in (7.8), with $m = 1$, we now consider also a kinetic energy part

$$T = \frac{1}{2} \int \left(e_1^2 + e_2^2 + \overline{D_0 \phi} D_0 \phi \right) d^2x \tag{7.80}$$

with e_1, e_2 components of the electric field and D_0 the time covariant derivative. The Euler-Lagrange field equations are given by

$$D_\mu D^\mu \phi - \frac{\lambda}{2} (1 - \bar{\phi}\phi)\phi = 0 \tag{7.81}$$

$$\partial_\mu f^{\mu\nu} + \frac{i}{2} (\bar{\phi} D^\nu \phi - \phi \overline{D^\nu \phi}) = 0. \tag{7.82}$$

The conserved quantities of the field configurations satisfying these field equations are the topological charge or winding number N and the conserved geometrical Noether charges. These include the momentum, the angular momentum and the energy. We will only discuss the momentum, for the other quantities we refer the reader to [48]. Momentum is associated with the translational invariance of the Lagrangian. An infinitesimal translation in the x^i direction combined with

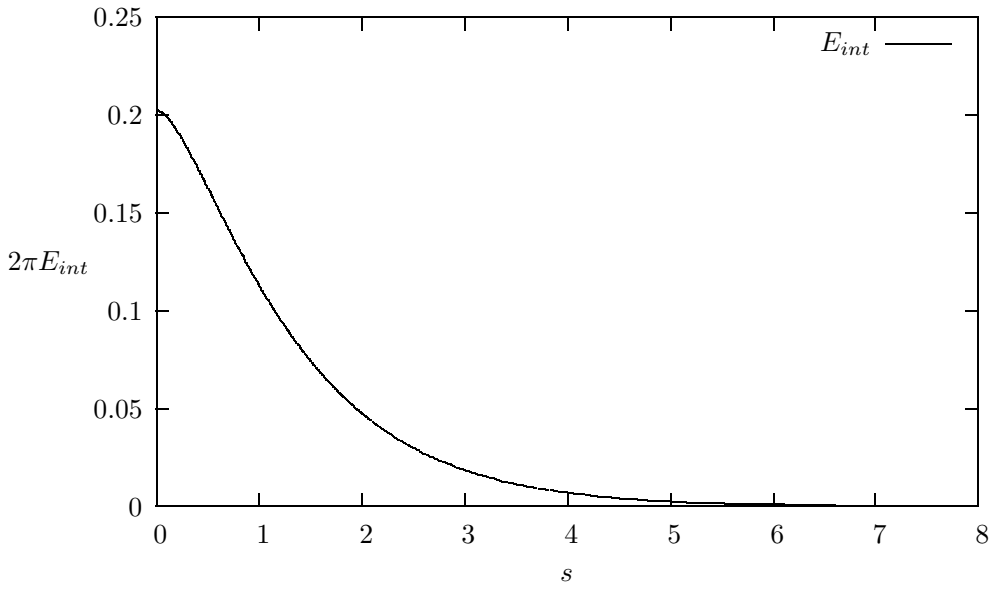

Figure 7.8: Asymptotic behaviour for $\lambda = 1.5$

an infinitesimal gauge transformation with parameter $-a_i$ yields the following gauge variations

$$\begin{array}{rcccl} \Delta\phi & = & \partial_i\phi - ia_i\phi & = & D_i\phi \\ \Delta\bar{\phi} & = & \partial_i\bar{\phi} + ia_i\bar{\phi} & = & \overline{D_i\phi} \\ \Delta a_j & = & \partial_i a_j - \partial_j a_i & = & \epsilon_{ij}B. \end{array} \tag{7.83}$$

This yields the following form for the conserved momentum

$$P_i = -\int \left(\frac{\partial\mathcal{L}}{\partial(\partial_0\phi)}\Delta\phi + \frac{\partial\mathcal{L}}{\partial(\partial_0\bar{\phi})}\Delta\bar{\phi} + \frac{\partial\mathcal{L}}{\partial(\partial_0 a_j)}\Delta a_j \right) d^2x \tag{7.84}$$

$$= -\int \left(\frac{1}{2}\overline{D_0\phi}D_i\phi + \frac{1}{2}D_0\phi\overline{D_i\phi} + \epsilon_{ij}e_jB \right) d^2x \tag{7.85}$$

where $\mathcal{L}$ denotes the Lagrangian density. The conserved electric charge is given by

$$Q = -\frac{i}{2}\int (\bar{\phi}D_0\phi - \phi\overline{D_0\phi})d^2x. \tag{7.86}$$

Withing this framework, an $N = 1$ vortex behaves like a particle whose rest-mass is given by the static GL energy. Solutions can be Lorentz boosted in order to obtain vortices moving at arbitrary speeds up to the speed of light. It is also possible to compose a superposition of such solutions and set vortices to collide. The geometrical quantities involved in a two vortex collision are indicated in figure 7.10

The 90^o scattering is the most interesting case. It shows that vortices are in a fundamental way non-Newtonian particles. Since vortices are indistinguishable,

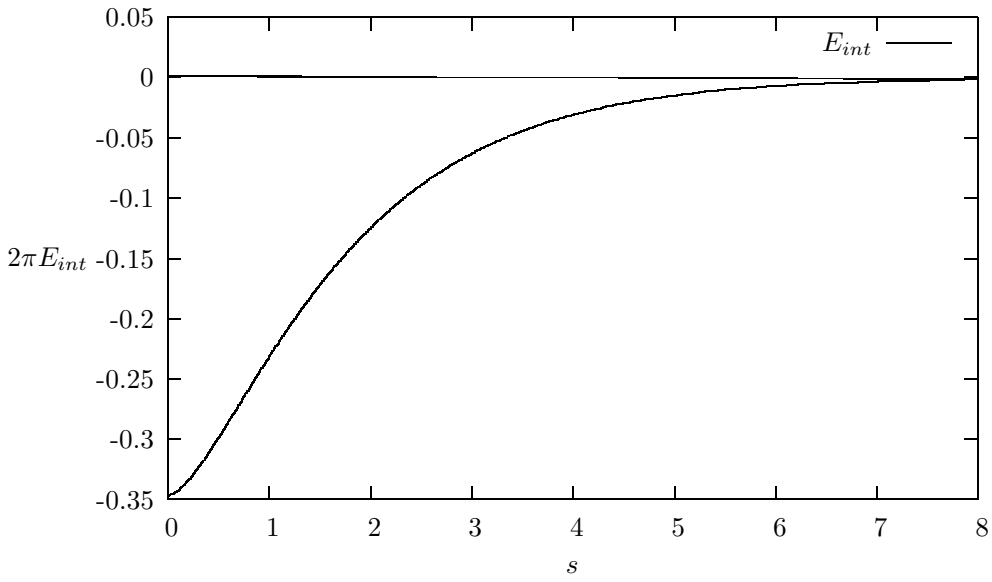

Figure 7.9: Asymptotic behaviour for $\lambda = 0.5$

because the fields are the fundamental objects and the vortex locations are simply the zeros of the scalar field, they can not be labeled. Thus two vortices can be followed until they collide but as the zeros emerge from the scattering location, it is no longer possible to tell which vortex, or which part of the outgoing vortices corresponds to a certain incoming vortex. For further information see [48].

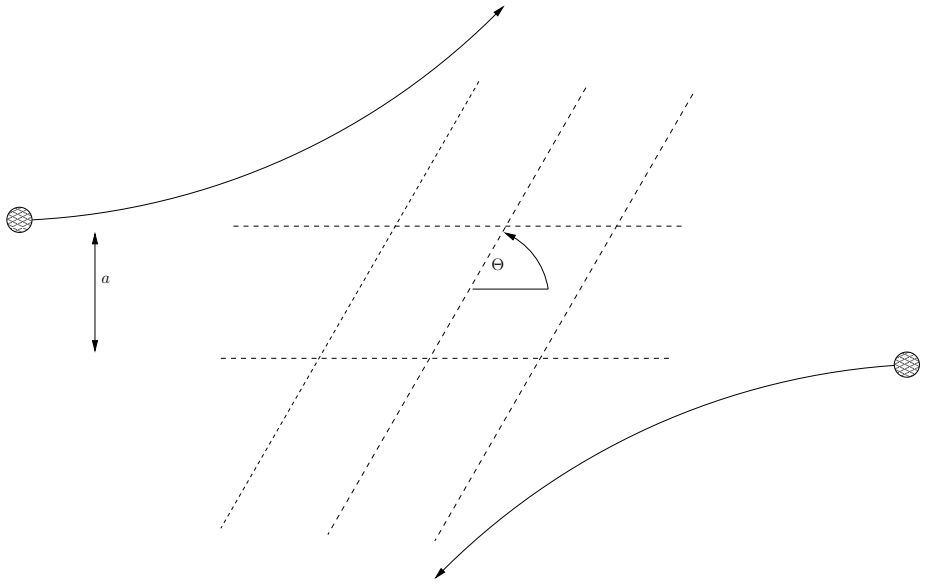

Figure 7.10: A two-vortex collision

8 Berezinskii Kosterlitz Thouless transition in spin systems

Lucas Lombriser
Supervisor: Munehisa Matsumoto

Spontaneous continuous symmetry breaking in two dimensions is not possible for non-zero temperatures. Therefore, common phase transitions are not expected in a two-dimensional xy-model. The appearance of vortices, however, induces the Berezinski-Kosterlitz-Thouless transition. The motivation of this chapter is to derive the arguments for such a transition and investigate some of its properties.

1 Introduction

Usually, one associates a phase transition to undergo spontaneous symmetry breaking when taking its disordered phase to the less symmetric ordered phase. We expect the several separate orientations of the order parameter below the critical temperature to be related by a symmetry operation with respect to the order parameter. The emergence of an exclusive orientation characterizes the spontaneous symmetry breaking. There, however, is a theorem by Mermin and Wagner, which states that there cannot be any spontaneous continuous symmetry breaking in dimension $d \leq 2$, provided a non-zero temperature. This implies absence of long-range order in a two-dimensional system with continuous symmetry. In a spin system described by a xy-model, which is of continuous symmetry, we, however, observe a phase transition which is known as the Berezinski-Kosterlitz-Thouless transition.

As we will see, at low temperatures, the spin interaction between nearest neighboring sites is subsiding algebraically, thus it is of quasi-long-range order.

For high temperatures, we, however, expect an exponential decay of the correlation, hence the spin interaction is short-ranged. Now, how can one explain this phenomenon without contradiction to the Mermin-Wagner theorem? As we will see, topological defects called vortices will make the phase transition possible, and thus we can elude a continuous symmetry breaking. But before we will get to that point, we will have to behold some more general concepts, such as the basics of statistical mechanics and renormalization group theory.

Statistical Mechanics

A classical system of N particles which is coupled to a reservoir of fixed temperature T, while its energy can fluctuate, is described by its canonical partition function

$$Z = \sum_{\phi} e^{-\beta H(\phi)}, \tag{8.1}$$

where H is the Hamiltonian and ϕ indicates a possible state. Further, we have $\beta = \frac{1}{k_B T}$, with k_B the Boltzmann constant and T the temperature. The exponential $e^{-\beta H}$ is also referred to as the Boltzmann weight. The probability that one particular state ϕ is occupied is then

$$P_\phi = \frac{e^{-\beta H(\phi)}}{Z}, \tag{8.2}$$

which is also called the canonical ensemble. This defines the entropy

$$S = k_B \ln\left(\frac{1}{P}\right), \tag{8.3}$$

where P is the probability of occurrence of a state when equally probable. S can, however, also be derived by thermodynamic means. All thermodynamic quantities can be determined by Eq. (8.1), starting with the free energy

$$F = -\frac{1}{\beta} \ln Z. \tag{8.4}$$

Furthermore, we obtain for the internal energy of a system

$$U = -T^2 \frac{\partial (F/T)}{\partial T} \tag{8.5}$$

and, by Legendre transformation of U with respect to S, we receive $-F$, thus

$$F = U - TS, \tag{8.6}$$

where the potential F is called the Helmholtz free energy. It describes a minimum in equilibrium, provided the temperature and the volume of the system are held

constant. The expectation value of a fluctuating quantity A is given by

$$\langle A\rangle = \sum_{\phi} A(\phi)P_{\phi} = \frac{\sum_{\phi} A(\phi)e^{-\beta H(\phi)}}{\sum_{\phi} e^{-\beta H(\phi)}}. \tag{8.7}$$

For the discussion of the Berezinski-Kosterlitz-Thouless transition, we have to adopt some general concepts about phase transitions. First, we introduce the order parameter, which is a non-zero value in the ordered phase. In the disordered phase, however, it is identically zero. The point at which the value of the order parameter becomes zero is the critical point, which defines the transition going from the ordered to the disordered phase. In a ferromagnet the order parameter is identified by the spontaneous magnetization. When a quantity σ exhibits correlation, the order of a system is indicated by the correlation function

$$G(\boldsymbol{x}) = \langle \sigma(\boldsymbol{x})\sigma(0)\rangle, \tag{8.8}$$

where $\boldsymbol{x}$ is the spatial distance. The order parameter will become zero for infinite system size, provided the correlation function tends to zero.

Another, general way of writing the correlation function is

$$G(\boldsymbol{x}) \approx \frac{e^{-r/\xi(T)}}{r^{d-2+\eta}}, \tag{8.9}$$

where η is a critical exponent and $\xi(T)$ is the correlation length, which is a measure of the length scale at which the behavior of a material begins to differ distinctly from its macroscopic properties.

For systems at thermal equilibrium, we observe a first-order transition when at the critical temperature T_c the first derivatives of the free energy with respect to a thermodynamic variable are discontinuous. If they are continuous, but the second derivatives exhibit discontinuity, it is termed a second-order phase transition. They are sometimes also called discontinuous and continuous phase transitions, respectively. In general, the correlation length of a first-order transition is finite, whereas for a second-order transition we expect infinite correlation length.

A very well known concept is the Ising model, which considers a lattice with classical spins $s_i = \pm 1$ attached to each lattice site i. The Hamiltonian is given by

$$H(s) = -\frac{1}{2}\sum_{i,k} J_{ik}s_i s_k - h\sum_i s_i, \tag{8.10}$$

where h indicates an external homogeneous field and the constant J describes the nearest neighbor interactions. Requiring $J > 0$, we obtain a model for a ferromagnet. For an Ising model with dimension $d \leq d_l$, where $d_l = 1$ is the lower critical dimension for discrete symmetries, there cannot be any phase transition.

The Renormalization Group

In renormalization group procedures, parameters defining the problem are re-expressed in terms of other parameters, without changing the physics in behind. This results in renormalization group flows in the parameter space, whose equations describe the physical problem and are the essence of renormalization group theory.

Consider real space renormalization in lattice spin systems, e.g. block spin transformations. Let us assume a two-dimensional Ising model which is not exposed to any magnetic field. Now we group the spins into squares of 3×3 spins and assign a new variable $s' = \pm 1$ to these blocks, where $s' = +1$ or $s' = -1$ if there are predominantly up spins or down spins, respectively, at hand. At the critical point, we observe a scale invariance, thus the configuration of the new variables s' and the one for the spins s are statistically the same. Starting above the critical point, the statistics change, but we find, assuming nearest neighbor interaction, that the dominant interactions will remain short-ranged, independent on the count of iterations of the transformation. Furthermore, the partition function, and thus thermodynamics, is not affected by the renormalization group procedure. Large distance behavior remains the same.

The renormalization group transformation can be understood as acting on the space of all possible couplings $\{K\}$, which is

$$\{K'\} = R\{K\}, \tag{8.11}$$

where R depends on the length rescaling parameter b. Suppose there is a fixed-point $K = K^*$ at which R is differentiable. Thus, by linearizing about the fixed-point, we obtain

$$K'_a - K^*_a \sim \sum_b T_{ab}(K_b - K_{b^*}), \tag{8.12}$$

where $T_{ab} = \partial K'_a / \partial K_b|_{K=K^*}$. Furthermore, retrieving the eigenvalues λ_i and the left eigenvectors $\{e^i\}$ of $\boldsymbol{T}$, we have

$$\sum_a e^i_a T_{ab} = \lambda^i e^i_b. \tag{8.13}$$

We assume the eigenvalues to be real. Near the fixed point, we observe

$$\begin{aligned} u'_i &= \sum_a e^i_a (K'_a - K^*_a) = \sum_{a,b} e^i_a T_{ab}(K_b - K^*_b) \\ &= \sum_b \lambda^i e^i_b (K_b - K^*_b) = \lambda^i u_i, \end{aligned} \tag{8.14}$$

where we have defined the scaling variables

$$u_i \equiv \sum_a e^i_a (K_a - K^*_a), \tag{8.15}$$

which describe linear combinations of the deviations from the fixed point, hence $K_a - K_a^*$. Furthermore, we can define the renormalization group eigenvalues y_i by $\lambda^i = b^{y_i}$. The scaling variables u_i are called relevant if $y_i > 0$ and irrelevant if $y_i < 0$. When $y_i = 0$, the scaling variables are marginal. A scaling variable that is relevant will, by repeated renormalization group iterations, drift off the fixed point, while in the irrelevant case, it will move toward zero, provided starting sufficiently close to the fixed point. When u_i is marginal, there can be made no predictions whether the fixed point is approached or u_i is driven away from it. From such renormalization group flows, we retrieve the physics of the system.

Suppose a n'-dimensional space describing the neighborhood of a fixed point with n relevant eigenvalues. Thus, ignoring marginal eigenvalues, there are $(n' - n)$ irrelevant eigenvalues and therefore an $(n' - n)$-dimensional hypersurface, whose points are attracted toward the fixed point. By continuity, we can expand this hypersurface to a finite region, which is called the critical surface and exhibits infinite correlation length. This surface can act as a separatrix when dividing points which tend to large values of K_a from those flowing toward $K_a = 0$.

The renormalization group is universal, thus possesses a universality class, which consists of all those critical models which flow into the same fixed point.

The xy-Model

Consider rotations in a two-dimensional plane of continuous symmetry, i.e. $U(1)$ or $O(2)$. We define θ as the angle indicating the direction of the order parameter, which is either a two-dimensional vector $\langle \boldsymbol{s} \rangle$ or a complex number $\langle \Psi \rangle$. The occurrence of an exclusive orientation of the order parameter is responsible for symmetry breaking. A two-dimensional lattice with a planar spin $\boldsymbol{s}(\boldsymbol{x}) = s(\cos\theta(\boldsymbol{x}), \sin\theta(\boldsymbol{x}))$ attached on each site $\boldsymbol{x}$ obeys the $O(2)$ symmetry. This is the so-called xy-model, where spin interactions are of nearest neighbor order. It can also be written in complex form, where the order parameter is replaced by $\langle \Psi \rangle = |\langle \Psi \rangle| e^{i\theta}$.

The Free Energy in the xy-Model

Considering Ginzburg-Landau theory, we find that, in the ordered phase of the xy-model, the free energy F has the shape of the bottom of a champagne bottle (Fig. 8.1). Its minimum is achieved on a circle on the base of the bottle. Points on this circle are depicted by the angle θ and the radius specified by the magnitude of the order parameter. Rotations around the circle correspond to spatially uniform changes in θ, and thus do not alter the free energy. However, spatially non-uniform changes in θ increase the free energy.

As long as there is no evidence for the contrary, we can assume the elastic free energy $F_{el} = F[\theta(\boldsymbol{x})] - F[\theta = \text{const.}]$ to be analytic in $\boldsymbol{\nabla}\theta$. Thus, the simplest

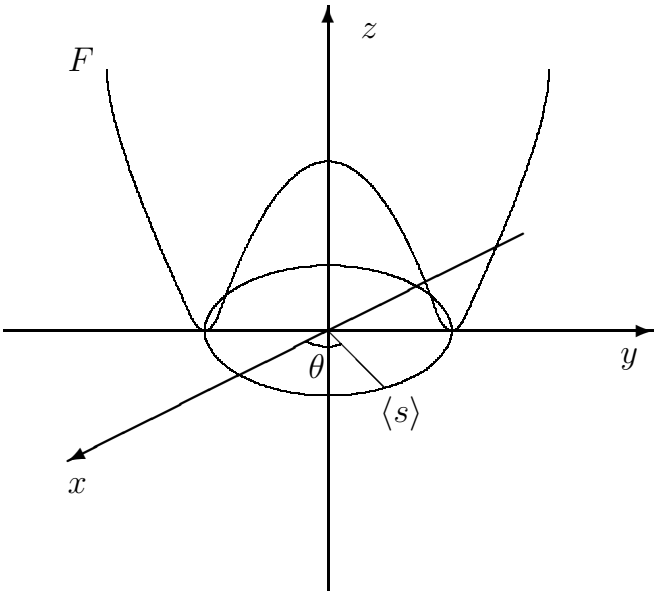

Figure 8.1: Free energy of the ordered phase. The horizontal is described by the order parameter of the xy-model. At temperatures lower than the critical temperature, the free energy takes the shape of a wine bottle. Sometimes it is also referred to as the Mexican hat potential.

form for F_{el} is

$$\frac{1}{2}\int d^d x \rho_s [\boldsymbol{\nabla}\theta(\boldsymbol{x})]^2 \tag{8.16}$$

when employing the absence of terms of linear dependence of $\boldsymbol{\nabla}\theta$ in the expansion of F_{el}, which follows from the fact that the uniform state is minimal with respect to any variations of the order parameter. Excitations of the order parameter are, in magnetism, called spin-waves. Such degrees of freedom are Goldstone modes that occur whenever a continuous symmetry is broken. The coefficient ρ_s is referred to as the spin-wave stiffness, helicity modulus, or simply as the rigidity. It can be thought of as the coefficient describing a parabolic dispersion relation. Lowest state in free energy is achieved when applying spatially uniform changes in θ. However, when imposing boundary conditions, we might want to consider non-uniform solutions for θ, e.g.

$$\theta = \theta_0 \frac{z}{L}, \tag{8.17}$$

$$F_{el} = \frac{1}{2}\rho_s L^{d-2}\theta^2, \tag{8.18}$$

when requiring $\theta = 0$ at $z = 0$ and $\theta = \theta_0$ at $z = L$. Therefore, we can define the spin-wave stiffness in the following way:

$$\rho_s = \lim_{L\to\infty} 2L^{2-d}\frac{F[\theta_0] - F[0]}{\theta_0^2}, \tag{8.19}$$

where the constraint for $F[0]$ is $\theta = 0$ at both $z = 0, L$ and $F[\theta_0]$ satisfies the conditions mentioned previously. In $d = 2$ dimensions, ρ_s has the units of energy and therefore is the characteristic temperature scale for the sample. At low temperatures, ρ_s is of order T_c. Eq. (8.16) is the simplest form consistent with the constraint of charge conservation and thus the invariance of the energy under continuous global $U(1)$ transformations. This can be perceived when taking into account the commutativity of the microscopic Hamiltonian H of a system with particle number N, i.e.

$$[H, N] = 0, \tag{8.20}$$

$$N \equiv \sum_{\sigma} \psi_{\sigma}^{\dagger} \psi_{\sigma}, \tag{8.21}$$

where the complex order parameter is

$$|\Psi| e^{i\vartheta(\boldsymbol{x})} \equiv \langle \psi_{\uparrow}^{\dagger} \psi_{\downarrow}^{\dagger} \rangle. \tag{8.22}$$

The unitary transformation $\mathcal{U} \in U(1)$, with

$$\mathcal{U} \equiv e^{\phi N}, \tag{8.23}$$

leaves the Hamiltonian invariant, i.e.

$$\mathcal{U} H \mathcal{U}^{\dagger} = H. \tag{8.24}$$

It can be shown that, in general, gauge transformations that leave the Hamiltonian invariant must conserve particle number, i.e. gauge invariance and charge conservation are equivalent. [50]

The free energy in Eq. (8.16) can also be derived from the Hamiltonian of a d-dimensional hypercubic lattice

$$H = -J \sum_{\langle ij \rangle} \boldsymbol{s}_i \cdot \boldsymbol{s}_j = -Js^2 \sum_{\langle ij \rangle} \cos(\theta_i - \theta_j), \tag{8.25}$$

where $\boldsymbol{s}_i$ and $\boldsymbol{s}_j$ are classical spins of magnitude s lying in the xy-plane. Their orientation with respect to the x-axis is indicated by θ_i, where $0 \leq \theta_i < 2\pi$ and $\langle ij \rangle$ indicates the summation over nearest neighbors. H exhibits a continuous symmetry, i.e. it is invariant under the transformation $\theta_i \rightarrow \theta_i + \theta_0$. We suppose $|\theta_i - \theta_j| << 2\pi$ at sufficiently low temperatures. Thus, we can use the Taylor expansion of the cosine,

$$\cos(\theta_i - \theta_j) = 1 - \frac{1}{2}(\theta_i - \theta_j)^2 + O[(\theta_i - \theta_j)^4], \tag{8.26}$$

to yield

$$H = -Js^2 \sum_{\langle ij \rangle} 1 + \frac{1}{2} Js^2 \sum_{\langle ij \rangle} (\theta_i - \theta_j)^2. \tag{8.27}$$

Replacing the first term by the ground state energy E_0 and writing the second term as the sum over $\boldsymbol{a}$ that runs over all nearest neighbors with lattice sites $\boldsymbol{x}$, we obtain

$$H = E_0 + \frac{Js^2}{4} \sum_{\boldsymbol{x},\boldsymbol{a}} [\theta(\boldsymbol{x}+\boldsymbol{a}) - \theta(\boldsymbol{x})]^2. \tag{8.28}$$

Furthermore, we assume $\theta(\boldsymbol{x})$ to vary little with $\boldsymbol{x}$. Hence, using Taylor expansion and the continuum model, we get

$$H = E_0 + \frac{Js^2}{2a^{d-2}} \int d^d x [\boldsymbol{\nabla}\theta(\boldsymbol{x})]^2, \tag{8.29}$$

with a being the distance between nearest neighbors. The second term of the expression above is equivalent to Eq. (8.16) as $\rho_s = \frac{Js^2}{a^{d-2}}$ in the d-dimensional hypercubic lattice.

Suppose now a spatially uniform external field $h_x(\boldsymbol{x})$ aligned along the x-axis. Then the additional term obtained in the Hamiltonian is

$$F_{ext} = -\int d^d x \; h_x \; \langle \boldsymbol{s}(\boldsymbol{x}) \rangle = -\int d^d x |\boldsymbol{s}(\boldsymbol{x})| \; h_x \; \cos\theta(\boldsymbol{x}). \tag{8.30}$$

The minimum energy state imposes $\theta = 0$ and $\langle \boldsymbol{s} \rangle = s\boldsymbol{e}_x$, i.e. the magnetization points also in x-direction. Thus, we observe a continuous symmetry breaking associated with the application of an external field.

Correlation and Order

The spin correlation function, following Eq. (8.8), is

$$\begin{aligned} G'(\boldsymbol{x}, 0) &= \langle \boldsymbol{s}(\boldsymbol{x}) \cdot \boldsymbol{s}(0) \rangle = s^2 \langle \cos[\vartheta(\boldsymbol{x}) - \vartheta(0)] \rangle \\ &= s^2 Re \langle e^{i(\vartheta(\boldsymbol{x}) - \vartheta(0))} \rangle = s^2 e^{-Re(g(\boldsymbol{x}))}. \end{aligned} \tag{8.31}$$

Note that ϑ is the phase of the fluctuating field, whereas θ indicated the phase of the average order parameter. Furthermore, $\boldsymbol{q}$ is a point of the reciprocal lattice and

$$g(\boldsymbol{x}) = T \int \frac{d^d q}{(2\pi)^d} \frac{1 - e^{i\boldsymbol{q}\cdot\boldsymbol{x}}}{\rho_s q^2}. \tag{8.32}$$

This expression can be derived in spin-wave approximation. We impose periodic boundary conditions and use Fourier representation to write

$$\vartheta(\boldsymbol{x}) = \frac{1}{\sqrt{N}} \sum_{\boldsymbol{q}} \vartheta_{\boldsymbol{q}} e^{i\boldsymbol{q}\cdot\boldsymbol{x}}. \tag{8.33}$$

Eq. (8.29) becomes

$$\begin{aligned} H &= E_0 + \frac{Js^2}{2a^{d-2}} \int d^d x \left(-\frac{1}{N}\right) \sum_{\boldsymbol{q},\boldsymbol{q}'} \boldsymbol{q}\boldsymbol{q}' \vartheta_{\boldsymbol{q}} \vartheta_{\boldsymbol{q}'} e^{i(\boldsymbol{q}+\boldsymbol{q}')\cdot\boldsymbol{x}} \\ &= E_0 - \frac{1}{N} \frac{Js^2}{2a^{d-2}} \sum_{\boldsymbol{q},\boldsymbol{q}'} \boldsymbol{q}\boldsymbol{q}' \vartheta_{\boldsymbol{q}} \vartheta_{\boldsymbol{q}'} \int d^d x e^{i(\boldsymbol{q}+\boldsymbol{q}')\cdot\boldsymbol{x}} \\ &= E_0 - \frac{Js^2 a^2}{2} \left(\frac{2\pi}{a}\right)^d \frac{1}{N} \sum_{\boldsymbol{q},\boldsymbol{q}'} \boldsymbol{q}\boldsymbol{q}' \vartheta_{\boldsymbol{q}} \vartheta_{\boldsymbol{q}'} \delta^{(d)}(\boldsymbol{q}+\boldsymbol{q}'), \end{aligned} \tag{8.34}$$

where, in Eq. (8.34), we have used the Dirac Delta function,

$$\delta^{(d)}(\boldsymbol{q}) = \left(\frac{1}{2\pi}\right)^d \int d^d x e^{i\boldsymbol{q}\cdot\boldsymbol{x}}. \tag{8.35}$$

Furthermore, we transform

$$\frac{1}{N} \sum_{\boldsymbol{q}'} \to \left(\frac{a}{2\pi}\right)^d \int d^d q' \tag{8.36}$$

and we obtain

$$\begin{aligned} H &= E_0 - \frac{Js^2 a^2}{2} N \sum_{\boldsymbol{q}} \boldsymbol{q} \vartheta_{\boldsymbol{q}} \int d^d q' \delta^{(d)}(\boldsymbol{q}+\boldsymbol{q}') \boldsymbol{q}' \vartheta_{\boldsymbol{q}'} \\ &= E_0 + \frac{Js^2 a^2}{2} \sum_{\boldsymbol{q}} q^2 \vartheta_{\boldsymbol{q}} \vartheta_{-\boldsymbol{q}} \\ &= E_0 + Js^2 a^2 {\sum_{\boldsymbol{q}}}' q^2 (\alpha_{\boldsymbol{q}}^2 + \gamma_{\boldsymbol{q}}^2), \end{aligned} \tag{8.37}$$

where $\vartheta_{\boldsymbol{q}} = \alpha_{\boldsymbol{q}} + i\gamma_{\boldsymbol{q}} = (\vartheta_{-\boldsymbol{q}})^*$ and $\sum'$ is the sum over half the Brillouin zone. Now we can evaluate the expectation value with methods of statistical mechanics, i.e. Eq. (8.7), explicitly

$$\langle e^{i(\vartheta(\boldsymbol{x})-\vartheta(0))} \rangle = \frac{\sum_{\vartheta_{\boldsymbol{q}}} e^{-\beta H} e^{i(\vartheta(\boldsymbol{x})-\vartheta(0))}}{\sum_{\vartheta_{\boldsymbol{q}}} e^{-\beta H}}, \tag{8.38}$$

where $\beta = \frac{1}{k_B T}$ and H is determined by Eq. (8.37). Furthermore, we define $\lambda = \beta J s^2 a^2$ and consider the transformation given in Eq. (8.36) as well as Gauss integration over the decoupled wave number space variables. Thus, for the de-

nominator, we find

$$\begin{aligned}
\sum_{\vartheta_{\boldsymbol{q}}} e^{-\beta H} &= e^{-\beta E_0} \sum_{\vartheta_{\boldsymbol{q}}} e^{-\frac{\lambda}{2}\sum_{\boldsymbol{q}} q^2 |\vartheta_{\boldsymbol{q}}|^2} \\
&= e^{-\beta E_0} \sum_{\vartheta_{\boldsymbol{q}}} \prod_{\boldsymbol{q}} e^{-\frac{\lambda}{2} q^2 |\vartheta_{\boldsymbol{q}}|^2} \\
&= \frac{1}{N'} \prod_{\boldsymbol{q}} \int d\vartheta_{\boldsymbol{q}} e^{-\frac{\lambda}{2} q^2 |\vartheta_{\boldsymbol{q}}|^2} \\
&= \frac{1}{N'} \prod_{\boldsymbol{q}} \int d\alpha_{\boldsymbol{q}} e^{-\frac{\lambda}{2} q^2 |\alpha_{\boldsymbol{q}}|^2} \int d\gamma_{\boldsymbol{q}} e^{-\frac{\lambda}{2} q^2 |\gamma_{\boldsymbol{q}}|^2} \\
&= \frac{1}{N'} \prod_{\boldsymbol{q}} \left(\frac{2\pi}{\lambda q^2} \right),
\end{aligned} \tag{8.39}$$

where N' is a constant, containing $e^{-\beta E_0}$ and the normalization factor of the continuity transform. The numerator is determined as follows:

$$\begin{aligned}
\sum_{\vartheta_{\boldsymbol{q}}} e^{-\beta H} e^{i(\vartheta(\boldsymbol{x}) - \vartheta(0))} &= e^{-\beta E_0} \sum_{\vartheta_{\boldsymbol{q}}} e^{-\frac{\lambda}{2} q^2 |\vartheta_{\boldsymbol{q}}|^2} e^{i \frac{1}{\sqrt{N}} \sum_{\boldsymbol{q}} \vartheta_{\boldsymbol{q}} (e^{i \boldsymbol{q} \boldsymbol{x}} - 1)} \\
&= e^{-\beta E_0} \sum_{\vartheta_{\boldsymbol{q}}} e^{-\frac{\lambda}{2} q^2 |\vartheta_{\boldsymbol{q}}|^2} e^{i \frac{1}{\sqrt{N}} \sum_{\boldsymbol{q}}' [\vartheta_{\boldsymbol{q}} (e^{i \boldsymbol{q} \boldsymbol{x}} - 1) + \vartheta^*_{\boldsymbol{q}} (e^{-i \boldsymbol{q} \boldsymbol{x}} - 1)]} \\
&= e^{-\beta E_0} \sum_{\vartheta_{\boldsymbol{q}}} e^{-\frac{\lambda}{2} q^2 |\vartheta_{\boldsymbol{q}}|^2} e^{i \frac{1}{2\sqrt{N}} \sum_{\boldsymbol{q}} [\vartheta_{\boldsymbol{q}} (e^{i \boldsymbol{q} \boldsymbol{x}} - 1) + \vartheta^*_{\boldsymbol{q}} (e^{-i \boldsymbol{q} \boldsymbol{x}} - 1)]} \\
&= \frac{1}{N'} \prod_{\boldsymbol{q}} \int d\alpha_{\boldsymbol{q}} e^{-\frac{\lambda}{2} q^2 |\alpha_{\boldsymbol{q}}|^2} e^{i \frac{1}{\sqrt{N}} \alpha_{\boldsymbol{q}} (\cos \boldsymbol{q} \cdot \boldsymbol{x} - 1)} \\
&\quad \cdot \int d\gamma_{\boldsymbol{q}} e^{-\frac{\lambda}{2} q^2 |\alpha_{\boldsymbol{q}}|^2} e^{i \frac{1}{\sqrt{N}} \alpha_{\boldsymbol{q}} \sin \boldsymbol{q} \cdot \boldsymbol{x}} \\
&= \frac{1}{N'} \prod_{\boldsymbol{q}} \left(\frac{2\pi}{\lambda q^2} \right) e^{-\frac{1}{2\lambda q^2} \frac{1}{N} [(\cos \boldsymbol{q} \cdot \boldsymbol{x} - 1)^2 + (\sin \boldsymbol{q} \cdot \boldsymbol{x})^2]} \\
&= \frac{1}{N'} \prod_{\boldsymbol{q}} \left(\frac{2\pi}{\lambda q^2} \right) e^{-\frac{1}{\lambda N} \sum_{\boldsymbol{q}} \frac{1 - \cos \boldsymbol{q} \cdot \boldsymbol{x}}{q^2}}.
\end{aligned} \tag{8.40}$$

Thus, Eq. (8.38) becomes

$$\langle e^{i(\vartheta(\boldsymbol{x}) - \vartheta(0))} \rangle = e^{-\frac{k_B T}{N J s^2 a^2} \sum_{\boldsymbol{q}} \frac{1 - \cos \boldsymbol{q} \cdot \boldsymbol{x}}{q^2}}. \tag{8.41}$$

Therefore, using Eqs. (8.31) and (8.36), we get

$$Re(g(\boldsymbol{x})) = \frac{k_B T a^{d-2}}{J s^2} \int \frac{d^d q}{(2\pi)^d} \frac{1 - \cos(\boldsymbol{q} \cdot \boldsymbol{x})}{q^2}, \tag{8.42}$$

which corresponds nicely to Eq. (8.32) as $\rho_s = \frac{Js^2}{a^{d-2}}$ and the Boltzmann constant is set $k_B = 1$. In $d = 2$ dimensions, $g(x)$ becomes

$$\begin{aligned} g(\boldsymbol{x}) &= \frac{T}{\rho_s}\int \frac{d^2Q}{(2\pi)^2}\frac{1-e^{i\boldsymbol{Q}\cdot\boldsymbol{x}}}{Q^2} \\ &= \frac{T}{2\pi\rho_s}\int \frac{dq\,d\theta}{2\pi}\frac{1-e^{iq|\boldsymbol{x}|\cos\theta}}{q}, \end{aligned} \tag{8.43}$$

where we have used $\boldsymbol{Q} = \boldsymbol{R}\boldsymbol{q}$, with $\boldsymbol{q} = (q\cos\theta, q\sin\theta)$, $\boldsymbol{R} \in SO(2)$, and $\boldsymbol{R}^T\boldsymbol{x} = (|\boldsymbol{x}|, 0)$, hence $\boldsymbol{Q}\cdot\boldsymbol{x} = (\boldsymbol{R}\boldsymbol{q})\cdot\boldsymbol{x} = \boldsymbol{q}\cdot(\boldsymbol{R}^T\boldsymbol{x}) = q|\boldsymbol{x}|\cos\theta$. Thus, Eq. (8.32) in $d = 2$ is written as

$$g(\boldsymbol{x}) = \frac{T}{2\pi\rho_s} I(|\boldsymbol{x}|), \tag{8.44}$$

$$I(|\boldsymbol{x}|) = \int_0^{\Lambda}\frac{dq}{q}\left[\frac{1}{2\pi}\int_0^{2\pi} d\theta\left(1-e^{iq|\boldsymbol{x}|\cos\theta}\right)\right], \tag{8.45}$$

where Λ is the high wave number cutoff. Using the Bessel function of order 0

$$J_0(q|\boldsymbol{x}|) = \frac{1}{2\pi}\int_{-\pi}^{\pi} e^{-iq|\boldsymbol{x}|\sin\theta} = \frac{1}{2\pi}\int_0^{2\pi} e^{iq|\boldsymbol{x}|\cos\theta}, \tag{8.46}$$

Eq. (8.45) becomes

$$I(|\boldsymbol{x}|) = \int \frac{1-J_0(q|\boldsymbol{x}|)}{q}dq, \tag{8.47}$$

which can be written in terms of $u = q|\boldsymbol{x}|$ and is broken into three parts,

$$\begin{aligned} I(|\boldsymbol{x}|) &= \int_0^1 \frac{1-J_0(u)}{u}du + \int_1^{\Lambda|\boldsymbol{x}|}\frac{du}{u} - \int_1^{\Lambda|\boldsymbol{x}|}\frac{J_0(u)}{u}du \\ &= \ln\Lambda|\boldsymbol{x}| + \tilde{\gamma} + O\left((\Lambda|\boldsymbol{x}|)^{-3/2}\right). \end{aligned} \tag{8.48}$$

For large $|\boldsymbol{x}|$, $\tilde{\gamma}$ becomes

$$\tilde{\gamma} = \int_0^1 \frac{1-J_0(u)}{u}du - \int_1^{\infty}\frac{J_0(u)}{u}du \approx -0.1159. \tag{8.49}$$

This quantity can be derived by evaluation of the following sums:

$$\int_0^1 \frac{1-J_0(u)}{u}du = \frac{1}{8}\sum_{k=0}^{\infty}\frac{k!}{[(1+k)!]^3}\left(-\frac{1}{4}\right)^k \approx 0.1212, \tag{8.50}$$

$$\begin{aligned} \int_1^{\infty}\frac{J_0(u)}{u}du &= \lim_{m\to\infty}\left(\sum_{k=1}^{m}\frac{1}{k} - \ln m\right) - \frac{1}{8}\sum_{k=0}^{\infty}\frac{k!}{[(1+k)!]^3}\left(-\frac{1}{4}\right)^k \\ &\quad - \ln 2 \\ &\approx 0.5772 - 0.1212 - 0.6931, \end{aligned} \tag{8.51}$$

where the Euler-Mascheroni constant, $\lim_{m\to\infty}\left(\sum_{k=1}^{m}\frac{1}{k}-\ln m\right)\approx 0.5772$, is also denoted as γ. In the case of a square lattice, $\tilde{\gamma}=\gamma+\frac{1}{2}\ln 8$, thus $\tilde{\gamma}\approx 1.6169$. For $d=2$ and $|x|$ large, using Eqs. (8.44) and (8.48),

$$\begin{aligned} g(\boldsymbol{x}) &= \frac{T}{2\pi\rho_s}I(|\boldsymbol{x}|)=\frac{T}{2\pi\rho_s}\left[\ln\left(\Lambda|\boldsymbol{x}|\right)+\tilde{\gamma}\right] \\ &= \frac{T}{2\pi\rho_s}\ln\left(\Lambda e^{\tilde{\gamma}}|\boldsymbol{x}|\right)=\frac{T}{2\pi\rho_s}\ln\left(\tilde{\Lambda}|\boldsymbol{x}|\right), \end{aligned} \tag{8.52}$$

where $\tilde{\Lambda}=\Lambda e^{\tilde{\gamma}}$. We perceive that $g(\boldsymbol{x})$ exhibits logarithmic divergence. Thus, Eq. (8.31) becomes

$$G'(\boldsymbol{x},0) = s^2 e^{-Re(g(\boldsymbol{x}))}=s^2 e^{-\frac{T}{2\pi\rho_s}\ln\left(\tilde{\Lambda}|\boldsymbol{x}|\right)} \tag{8.53}$$

$$= s^2(\tilde{\Lambda}|\boldsymbol{x}|)^{-\frac{T}{2\pi\rho_s}}. \tag{8.54}$$

This can be written as

$$G'(\boldsymbol{x},0) = s^2(\tilde{\Lambda}|\boldsymbol{x}|)^{-\eta}, \tag{8.55}$$

$$\eta = \frac{T}{2\pi\rho_s}, \tag{8.56}$$

which describes an algebraically decaying correlation for $|x|$ large. Such power-law decay in the order parameter correlation functions is referred to as quasi-long-range order (QLRO). Eq. (8.55) is in agreement with the Mermin-Wagner theorem and we observe that for $T>0$ the system appears to be in a critical phase. At high temperatures, however, we expect that

$$G(\boldsymbol{x})\sim\left(\frac{\rho_s}{2T}\right)^{|x|}\sim e^{-|\boldsymbol{x}|/\xi}, \tag{8.57}$$

where $\xi^{-1}=\ln(2T/\rho_s)$.

Thus, there must be a phase transition, despite the Mermin-Wagner theorem. It is carried out by topological defects called vortices. These are another kind of excitations, different from the spin-waves used above. They produce a phase transition that is independent of spontaneous symmetry breaking.

2 Vortices

Assume a d-dimensional space and consider the magnitude of the order parameter $\langle\boldsymbol{s}(\boldsymbol{x})\rangle=s(\cos\theta(\boldsymbol{x}),\sin\theta(\boldsymbol{x}))$ to be periodic in $\theta(\boldsymbol{x})$. We may encounter situations in which $\langle\boldsymbol{s}(\boldsymbol{x})\rangle$ is continuous everywhere but in a subspace of dimension d_s, with $d_s<d$, e.g. we suppose a singularity at the origin. This singularity can be removed by no longer defining the angle θ at this point and having the magnitude of the order parameter tend toward zero at the origin.

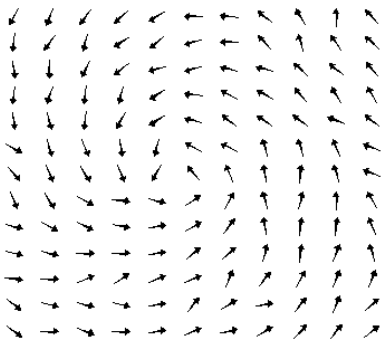

Figure 8.2: Vortex of unit strength in the xy-model. θ changes by 2π when encircling the singularity counterclockwise with a large closed curve. A closed curve, not containing the vortex core, exhibits no change in θ.

In $d = 2$, we can set $\theta(\boldsymbol{x}) = k\phi + \theta_0$, θ_0 being a constant, and we write $x = (r, \phi)$ in polar coordinates. Hence, $\langle \boldsymbol{s}(\boldsymbol{x}) \rangle$ will be continuous and we have a finite $\boldsymbol{\nabla}\theta = k/r$ everywhere but in the singularity. Therefore, one can extract the following conditions:

$$\oint \boldsymbol{\nabla}\theta(\boldsymbol{x}) \cdot d\boldsymbol{l} = 2k\pi, \tag{8.58}$$

where $\boldsymbol{l}$ is encircling the singularity, and

$$\oint \boldsymbol{\nabla}\theta(\boldsymbol{x}) \cdot d\boldsymbol{l} = 0, \tag{8.59}$$

where $\boldsymbol{l}$ is not encircling the singularity. In the two-dimensional xy-model, one can think of this as having the angle θ varying very little between neighboring sites. Following its behavior around a large closed curve, we find a change of θ by a non-zero multiple of 2π (Fig. 8.2). In spin configurations, such singularities are called vortices, and their winding number k is referred to as the vortex strength or vorticity. More generally speaking, such vortices belong to the class of topological defects. They have in common that they do not disappear under whatever continuous transformation of the order parameter. In $d = 3$, the vortices appear as lines, in analogy with charged wires. For reasons of simplicity, we shall predominantly suppose $d = 2$, as we are considering the Berezinski-Kosterlitz-Thouless transition in the xy-model.

Vortex Energy

The total energy of a vortex E_v in the two-dimensional xy-model with winding number k can be divided into two parts, the core energy E_c, arising with the destruction of the order parameter at the vortex core, and the elastic energy E_{el}, hence

$$E_v = E_c + E_{el}. \tag{8.60}$$

The free energy, Eq. (8.16), thus the elastic energy when neglecting entropy contributions, applied to vortex excitations satisfies

$$\oint d\theta = 2k\pi, \tag{8.61}$$

$$-\rho_s \nabla^2 \theta = 0, \tag{8.62}$$

where Eq. (8.61) is equivalent to Eq. (8.58). Requiring $\delta F_{el} = 0$, corresponding to ground state configuration of the spin system, produces Eq. (8.62),

$$\begin{aligned} \delta F_{el} &= \frac{\rho_s}{2}\delta \int d^d x [\boldsymbol{\nabla}\theta]^2 = \frac{\rho_s}{2}\int d^d x \frac{\partial}{\partial(\boldsymbol{\nabla}\theta)}[\boldsymbol{\nabla}\theta]^2 \delta(\boldsymbol{\nabla}\theta) \\ &= -\rho_s \int d^d x \; \nabla^2\theta \; \delta\theta = 0, \end{aligned} \tag{8.63}$$

when using partial integration. A solution to these constraints, excluding the origin, is the field

$$\theta = k\phi, \tag{8.64}$$

$$\boldsymbol{v}_s \equiv \boldsymbol{\nabla}\theta = \frac{k}{r}\boldsymbol{e}_\phi, \tag{8.65}$$

with $\phi = \tan^{-1}(y/x)$, $r = (x^2+y^2)^{1/2}$, and longitudinal superfluid velocity $\boldsymbol{v}_s$, since it is proportional to the gradient of a scalar function. Thus, the elastic energy, following Eq. (8.16), is

$$\begin{aligned} E_{el} &= \frac{1}{2}\rho_s \int d^2 x \boldsymbol{v}_s^2 = \frac{1}{2}\rho_s \int d^2 x \left(\frac{k}{r}\right)^2 \\ &= \frac{1}{2}\rho_s 2\pi k^2 \int_a^R dr \frac{r dr}{r^2} = \pi k^2 \rho_s \ln(R/a), \end{aligned} \tag{8.66}$$

with core radius a and linear dimension of the system R. The same result can be attained by a different calculation. Assuming a discontinuity of $2k\pi$ of the variable θ along a cut with surfaces Σ^- and Σ^+, while $\theta = 0$ on Σ^- and $\theta = 2k\pi$ on Σ^+, brings forth

$$\begin{aligned} E_{el} &= \frac{1}{2}\int d^2 x \rho_s (\boldsymbol{\nabla}\theta)^2 = \frac{1}{2}\int d^2 x \rho_s \left[\boldsymbol{\nabla}(\theta(\boldsymbol{\nabla}\theta)) - \theta(\nabla^2\theta)\right] \\ &= \frac{1}{2}\int d^2 x \rho_s \left[\boldsymbol{\nabla}(\theta(\boldsymbol{\nabla}\theta)) - \theta(\nabla^2\theta)\right] = \frac{1}{2}\int d^2 x \rho_s \boldsymbol{\nabla}(\theta \boldsymbol{v}_s) \qquad (8.67) \\ &= \frac{1}{2}\int \rho_s \theta \boldsymbol{v_s} \cdot d\boldsymbol{\Sigma} = \frac{1}{2}\int \theta \boldsymbol{h_s} \cdot d\boldsymbol{\Sigma} \qquad (8.68) \\ &= \frac{1}{2}\left(\int \theta^+ \boldsymbol{h_s} \cdot d\boldsymbol{\Sigma}^+ + \theta^- \boldsymbol{h_s} \cdot d\boldsymbol{\Sigma}^-\right) \\ &= \frac{1}{2}(\theta^+ - \theta^-)\int_a^R dr \rho_s |\boldsymbol{v}_s| = \pi k^2 \rho_s \ln(R/a), \qquad (8.69) \end{aligned}$$

where we have used Eq. (8.62) in Eq. (8.67), Gauss and $\boldsymbol{h}_s = \rho_s \boldsymbol{v}_s$ in Eq. (8.68). Furthermore, $\boldsymbol{e}_\phi$ and $-\boldsymbol{e}_\phi$ are the normals to Σ^+ and Σ^-, respectively. In the thermodynamic limit, Eq. (8.66) becomes infinite, thus we do not expect single vortices to appear. Since it is impossible to distort the spin configuration of a vortex into a completely aligned state, vortices are considered topologically stable, although single vortex excitations are located above ground state.

The core energy in two dimensions is depending linearly on the area of the defect and the condensation energy f_{cond} of the ordered state, which describes the increase in free energy per unit area originating from the destruction of the order parameter, hence

$$E_c = Aa^2 f_{\text{cond}}, \tag{8.70}$$

A being a numerical constant and a the core radius. We assume the total vortex energy in Eq. (8.60) to be minimized with respect to the parameter a. Therefore,

$$-\frac{\pi k^2 \rho_s}{a} = 2aAf_{\text{cond}} = 0, \tag{8.71}$$

$$a^2 = \frac{\pi k^2}{2} \frac{\rho_s}{Af_{\text{cond}}}, \tag{8.72}$$

and we obtain

$$E_c = \frac{\pi}{2} \rho_s k^2. \tag{8.73}$$

Consider two vortices which are separated by the distance r and at positions $\boldsymbol{x}_1$ and $\boldsymbol{x}_2$, respectively. Eq. (8.62) demands $\theta(\boldsymbol{x}) = \theta^{(1)} + \theta^{(2)}$, with $\theta^{(i)} = \tan^{-1}[(y - y_i)/(x - x_i)]$. Thus,

$$\begin{aligned} E_{el} &= \frac{1}{2} \int d^2x \rho_s (\boldsymbol{v}_s^{(1)} + \boldsymbol{v}_s^{(2)})^2 \\ &= E_1 + E_2 + \frac{1}{2} \int d^2x (\boldsymbol{h}_s^{(1)} \cdot \boldsymbol{v}_s^{(2)} + \boldsymbol{h}_s^{(2)} \cdot \boldsymbol{v}_s^{(1)}) \\ &= E_1 + E_2 + \frac{1}{2}(\theta_2^+ - \theta_2^-) \int_r^R \rho_s \frac{k_1}{r} dr + \frac{1}{2}(\theta_1^+ - \theta_1^-) \int_r^R \rho_s \frac{k_2}{r} dr \\ &= E_1 + E_2 + 2\pi \rho_s k_1 k_2 \ln(R/r), \end{aligned} \tag{8.74}$$

where $\boldsymbol{v}_s^{(i)} = \boldsymbol{\nabla} \theta^{(i)}$ and E_i are the energies of the isolated vortices,

$$E_i = \frac{1}{2} \int d^2x \rho_s (\boldsymbol{v}_s^{(i)})^2, \tag{8.75}$$

separated by the distance r. Hence, using $\ln(R/r) - \ln(R/a) = \ln(a/r)$,

$$\begin{aligned} E_{el} &= \pi \rho_s (k_1^2 + k_2^2) \ln(R/a) + 2\pi \rho_s k_1 k_2 \ln(R/r) \\ &= \pi \rho_s (k_1 + k_2)^2 \ln(R/a) + 2\pi \rho_s k_1 k_2 \ln(a/r). \end{aligned} \tag{8.76}$$

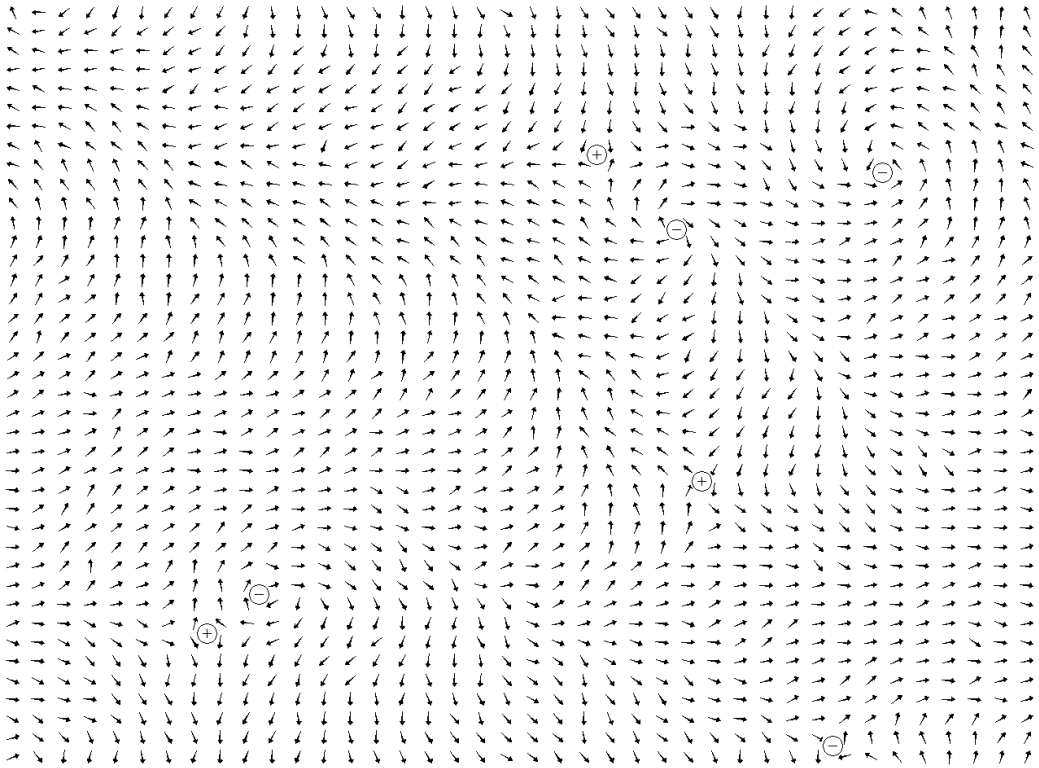

Figure 8.3: Multiple vortices in a finite xy-model. Vortices whose strengths have the same sign are repelling each other, whereas opposite signs lead to an attractive interaction.

Taking this to the general case of α vortices (Fig. 8.3), one observes that for $\sum_\alpha k_\alpha = 0$ the elastic energy does not diverge for infinite sample size. Such states will occur at $T > 0$ as thermal excitations. A pair of vortices with opposite strengths is topologically equivalent to the uniform state, i.e. they describe ground state excitations. The tightly bound configuration in which the vortices of such a pair are nearest neighbors is the state of minimal energy. Furthermore, one identifies easily the repulsive interaction of vortices of same sign, an attractive interaction for opposite signs, respectively. In the case of two vortices, we obtain

$$\begin{aligned} \boldsymbol{F}_{21} &= -\boldsymbol{\nabla}_2 E_v = 2\pi\rho_s k_1 k_2 \boldsymbol{\nabla}(\ln r) \\ &= 2\pi\rho_s k_1 k_2 \frac{(\boldsymbol{x}_2 - \boldsymbol{x}_1)}{|\boldsymbol{x}_2 - \boldsymbol{x}_1|^2}, \end{aligned} \tag{8.77}$$

which is the force exerted by vortex 1 on vortex 2.

Analogy in Magnetism

When considering loops of constant currents, we encounter a striking analogy between vortex interactions and magnetic interactions. We find that we can

apply the theory of magnetism to vortex theory in $d = 3$ when replacing the magnetic intensity $\boldsymbol{H}$ with $\boldsymbol{v}_s$ and the magnetic induction $\boldsymbol{B}$ with $\boldsymbol{h}_s$. These perceptions immediately impose further analogies, as

$$\int \boldsymbol{v}_s \cdot d\boldsymbol{l} = 2k\pi \quad \leftrightarrow \quad \int \boldsymbol{H} \cdot d\boldsymbol{l} = I, \tag{8.78}$$

$$\rho_s \nabla^2 \theta = \boldsymbol{\nabla} \cdot \boldsymbol{h}_s = 0 \quad \leftrightarrow \quad \boldsymbol{\nabla} \cdot \boldsymbol{B} = \mu \boldsymbol{\nabla} \cdot \boldsymbol{H} = 0. \tag{8.79}$$

Thus, it follows that the current I carried by the enclosed wire $I \leftrightarrow 2k\pi$ and the magnetic permeability $\mu \leftrightarrow \rho_s$. Now we introduce the field $\boldsymbol{m}$ as the analogy of the current density $\boldsymbol{J}$. For Γ encircling α vortex lines, we obtain

$$\oint_\Gamma \boldsymbol{v}_s \cdot d\boldsymbol{l} = \int \boldsymbol{\nabla} \times \boldsymbol{v}_s \cdot d\boldsymbol{S} = 2\pi \sum_\alpha k_\alpha = \int \boldsymbol{m} \cdot d\boldsymbol{S}. \tag{8.80}$$

Therefore, we have

$$\boldsymbol{\nabla} \times \boldsymbol{v}_s = \boldsymbol{m} \tag{8.81}$$

and we call $\boldsymbol{m}$ the vortex density. In case of a single vortex, we can write, in analogy with the current density of a wire,

$$\boldsymbol{m}(\boldsymbol{x}) = 2k\pi \boldsymbol{e}_z \delta^{(2)}(\boldsymbol{x}_\perp - \boldsymbol{x}), \tag{8.82}$$

where the vortex line at the core position $\boldsymbol{x} = (\boldsymbol{x}_\perp, 0)$ is parallel to $\boldsymbol{e}_z$. In case of α vortex lines with cores at $\boldsymbol{x} = (\boldsymbol{x}_\perp^\alpha, 0)$, Eq. (8.82) becomes

$$\boldsymbol{m}(\boldsymbol{x}) = 2\pi \boldsymbol{e}_z \sum_\alpha k_\alpha \delta^{(2)}(\boldsymbol{x}_\perp^\alpha - \boldsymbol{x}), \tag{8.83}$$

which for vortex loops with core position $\boldsymbol{x}^\alpha(\boldsymbol{l})$, as a function of arc length l, is

$$\boldsymbol{m}(\boldsymbol{x}) = 2\pi \sum_\alpha \int dl \frac{d\boldsymbol{x}^\alpha(\boldsymbol{l})}{dl} k_\alpha \delta^{(3)}(\boldsymbol{x}^\alpha(\boldsymbol{l}) - \boldsymbol{x}). \tag{8.84}$$

Furthermore, we have

$$\begin{aligned} \boldsymbol{\nabla} \times m &= \boldsymbol{\nabla} \times (\boldsymbol{\nabla} \times \boldsymbol{v}_s) \\ &= \boldsymbol{\nabla}(\boldsymbol{\nabla} \boldsymbol{v}_s) - \nabla^2 \boldsymbol{v}_s = -\nabla^2 \boldsymbol{v}_s, \end{aligned} \tag{8.85}$$

since $\nabla^2 \theta = 0$ by Eq. (8.62). This is compatible with

$$\boldsymbol{v}_s = \boldsymbol{\nabla} \times \int d^d x G(\boldsymbol{x} - \boldsymbol{x}') \boldsymbol{m}(\boldsymbol{x}'), \tag{8.86}$$

where $G(\boldsymbol{x} - \boldsymbol{x}')$ is the Laplacian Green function defined by

$$-\nabla^2 G(\boldsymbol{x} - \boldsymbol{x}') = \delta^{(d)}(\boldsymbol{x} - \boldsymbol{x}'), \tag{8.87}$$

which can also be written in the following form:

$$G(\boldsymbol{x}-\boldsymbol{x}') = \int \frac{d^d q}{(2\pi)^d} \frac{e^{i\boldsymbol{q}\cdot(\boldsymbol{x}-\boldsymbol{x}')}}{q^2}. \tag{8.88}$$

Moreover,

$$\boldsymbol{\nabla}\cdot\boldsymbol{m} = \boldsymbol{\nabla}(\boldsymbol{\nabla}\times\boldsymbol{v}_s) = \epsilon_{ijk}\partial_i\partial_j v_{s,k} = 0. \tag{8.89}$$

Therefore, Eq. (8.16) becomes

$$\begin{aligned}
E_{el} &= \frac{1}{2}\rho_s \int d^d x \boldsymbol{v}_s^2 = \frac{1}{2}\rho_s \int d^d x \left[\boldsymbol{\nabla}' \times \int d^d x' G(\boldsymbol{x}-\boldsymbol{x}')\boldsymbol{m}(\boldsymbol{x})\right]\boldsymbol{v}_s \\
&= \frac{1}{2}\rho_s \int d^d x (\boldsymbol{\nabla}'\times\boldsymbol{v}_s) \int d^d x' G(\boldsymbol{x}-\boldsymbol{x}')\boldsymbol{m}(\boldsymbol{x}) \\
&= \frac{1}{2}\rho_s \int d^d x \int d^d x' \boldsymbol{m}(\boldsymbol{x}) G(\boldsymbol{x}-\boldsymbol{x}')\boldsymbol{m}(\boldsymbol{x}') \\
&= \frac{1}{2}\rho_s \int \frac{d^d q}{(2\pi)^d}\frac{1}{q^2}\int d^d x\, \boldsymbol{m}(\boldsymbol{x}) e^{i\boldsymbol{q}\cdot\boldsymbol{x}} \int d^d x' \boldsymbol{m}(\boldsymbol{x}') e^{-i\boldsymbol{q}\cdot\boldsymbol{x}'} \\
&= \frac{1}{2}\rho_s \int \frac{d^d q}{(2\pi)^d}\frac{\boldsymbol{m}(\boldsymbol{q})\boldsymbol{m}(-\boldsymbol{q})}{q^2}.
\end{aligned} \tag{8.90}$$

3 Berezinski-Kosterlitz-Thouless Transition

Free Energy Argument

Suppose a two-dimensional lattice of linear dimension R with lattice parameter a. The vortex core can now be at $(R/a)^2$ different positions. Thus, in statistical mechanics, i.e. Eq. (8.3), the entropy of the system $S = \ln(R/a)^2 = 2\ln(R/a)$ when setting $k_B = 1$. The energy of a single vortex of unit strength ($k = 1$) is, using Eq. (8.66), $E = \pi\rho_s \ln(R/a)$. Therefore, a xy-system containing a single vortex of unit strength accomplishes a change in free energy, i.e.

$$F = E - TS = (\pi\rho_s - 2T)\ln(R/a), \tag{8.91}$$

where we have used Eq. (8.6). One can clearly identify the critical temperature $T_c = \pi\rho_s/2$. For temperatures lower than the critical temperature, $T < T_c$, the free energy finds its minimum only in case of absence of any isolated vortices. The contrary is true when $T > T_c$, and single vortices of unit strength will proliferate. Thus, T_c indicates the transition temperature from the algebraically ordered to the disordered phase.

Reduction in Spin-Wave Stiffness

In Sec. 2, we have seen that at the vortex core the magnitude of the order parameter tends to zero. But not only does this amplitude fluctuation reduce the

average magnitude of the order parameter, it diminishes the spin-wave stiffness as well. To see that, we first impose boundary conditions to $\vartheta(\boldsymbol{x})$, i.e. vanishing $\vartheta(\boldsymbol{x})$ at the edges of the sample. Hence, we want $\theta(\boldsymbol{x})$ to be spatially uniform. We expect the gradient of $\vartheta(\boldsymbol{x})$ averaged over the volume to be zero, since

$$\frac{1}{\Omega}\int d^dx\langle\boldsymbol{\nabla}\vartheta(\boldsymbol{x})\rangle = \frac{1}{\Omega}\int d\boldsymbol{S}\langle\vartheta(\boldsymbol{x})\rangle = 0, \tag{8.92}$$

S being the surface and Ω the volume of the sample. Now, let $\vartheta(\boldsymbol{x}) = \vartheta'(\boldsymbol{x})+\boldsymbol{v}\cdot\boldsymbol{x}$, with $\vartheta' = 0$ at the boundaries. Then we obtain a spatially uniform

$$\boldsymbol{\nabla}\theta = \frac{1}{\Omega}\int d^dx\langle\boldsymbol{\nabla}\vartheta'(\boldsymbol{x}) + \boldsymbol{v}\rangle = \boldsymbol{v}. \tag{8.93}$$

Furthermore, using Eq. (8.19), we write the renormalized spin-wave stiffness as

$$\rho_s^R = \frac{2}{v^2\Omega}[F(\boldsymbol{v}) - F(0)]. \tag{8.94}$$

We decompose ϑ into an analytic part $\vartheta_{\rm a}$ and a singular part $\vartheta_{\rm sing}$ caused by vortices. The Hamiltonian of the xy-model at low temperatures is a function of $\boldsymbol{v}_s = \boldsymbol{\nabla}\vartheta(\boldsymbol{x})$, which can be split into a longitudinal part $\boldsymbol{v}_s^{||} = \boldsymbol{\nabla}\vartheta_{\rm a}$ and a transverse part $\boldsymbol{v}_s^{\perp} = \boldsymbol{\nabla}\vartheta_{\rm sing}$. We have $\boldsymbol{\nabla}\times\boldsymbol{v}_s^{||} = 0$ and $\boldsymbol{\nabla}\cdot\boldsymbol{v}_s^{\perp} = 0$. The requirement of a spatially uniform gradient of the macroscopic phase leads to $\boldsymbol{v}_s = \boldsymbol{v}_s^{||} + \boldsymbol{v} + \boldsymbol{v}_s^{\perp}$, with $\vartheta_{\rm a} = 0$ on the boundaries. Thus, by Eq. (8.4),

$$F(\boldsymbol{v}) = -T\ \ln\mathrm{tr}\ \exp\left[-\frac{H(\boldsymbol{v})}{T}\right], \tag{8.95}$$

where $H(\boldsymbol{v}) = (\rho_s/2)\int d^dx(\boldsymbol{v}_s^{||} + \boldsymbol{v} + \boldsymbol{v}_s^{\perp})^2 + H'$ and H' is independent of $\boldsymbol{v}_s$. When only taking into account the first part of $H(\boldsymbol{v})$, we find by Eq. (8.95) and Taylor expansion,

$$\begin{aligned} F(\boldsymbol{v}) &= \frac{\Omega\rho_s v^2}{2} \\ &\quad - T\ln\mathrm{tr}\ \exp\left(-\frac{H(\boldsymbol{v}=0)}{T}\right)\exp\left(-\frac{\rho_s}{T}\int d^dx[\boldsymbol{v}\cdot\boldsymbol{v}_s(\boldsymbol{x})]\right) \\ &= \frac{\Omega\rho_s v^2}{2} - \frac{\rho_s^2}{2T}\int d^dxd^dx'\langle v_{si}(\boldsymbol{x})v_{sj}(\boldsymbol{x}'\rangle v_i v_j + F(0) + O(v^4). \end{aligned} \tag{8.96}$$

From Eqs. (8.94) and (8.96), one derives the following expression:

$$\rho_s^R = \rho_s - \frac{\rho_s^2}{(d-1)T}\int d^dx\langle\boldsymbol{v}_s^{\perp}(\boldsymbol{x})\cdot\boldsymbol{v}_s^{\perp}(0)\rangle. \tag{8.97}$$

Thus, we have a reduction in the macroscopic spin-wave stiffness ρ_s^R, caused by vortices. Rewriting this in terms of the vortex source function $\boldsymbol{m}$, we have

$$\rho_s^R = \rho_s - \left(\frac{1}{d-1}\right) \lim_{q\to 0} \frac{\rho_s^2}{q^2 T} \langle \boldsymbol{m}(\boldsymbol{q}) \cdot \boldsymbol{m}(-\boldsymbol{q}) \rangle, \tag{8.98}$$

which also corresponds to

$$\rho_s^R = \frac{1}{T} \int d^d x \left(\langle \boldsymbol{g}^{||}(\boldsymbol{x}) \cdot \boldsymbol{g}^{||}(0) \rangle - \frac{1}{d-1} \langle \boldsymbol{g}^{\perp}(\boldsymbol{x}) \cdot \boldsymbol{g}^{\perp}(0) \rangle \right), \tag{8.99}$$

using $\langle \boldsymbol{v}_s^{||}(\boldsymbol{q}) \cdot \boldsymbol{v}_s^{||}(-\boldsymbol{q}) \rangle = \frac{T}{\rho_s}$ and $\boldsymbol{g}(\boldsymbol{x}) \equiv \rho_s \boldsymbol{v}_s(\boldsymbol{x})$.

Renormalization Equations

We have contemplated, in analogy to the magnetic case, how vortex lines induce a vortex density, i.e. Eq. (8.83). The source function is normal to the xy-plane, $\boldsymbol{m}(\boldsymbol{x}) = 2\pi \boldsymbol{e_z} n_v(\boldsymbol{x})$, where $n_v(\boldsymbol{x})$ defines a scalar vortex density. In two dimensions, the correlation function will yield the expression given in Eq. (8.48). Similarly, we can now calculate the Laplacian Green function, Eq. (8.88), in two dimensions, hence

$$G(\boldsymbol{x}) = \int \frac{d^2 q}{(2\pi)^2} \frac{e^{i\boldsymbol{q}\cdot\boldsymbol{x}}}{q^2} = \frac{1}{2\pi} \int \frac{dq}{q} J_0(q|\boldsymbol{x}|). \tag{8.100}$$

When implying $I(|\boldsymbol{x}|)$ from Eq. (8.47), we can simplify the calculation and write

$$G(\boldsymbol{x}) = \frac{1}{2\pi} \ln(R/a) - \frac{1}{2\pi} I(|\boldsymbol{x}|). \tag{8.101}$$

Thus, using $\Lambda = 2\pi/a$, we obtain

$$G(\boldsymbol{x}) = \frac{1}{2\pi} \ln(R/a) - \frac{1}{2\pi} \ln(|\boldsymbol{x}|/a) + \text{const.} \tag{8.102}$$

By utilization of Eqs. (8.83) and (8.90), the contribution to E_{el} from the first term can be written as

$$\frac{\rho_s}{2} 2\pi \ln(R/a) \left(\int d^2 x n_v(\boldsymbol{x}) \right)^2 \sim \ln(R/a) \left(\sum_\alpha k_\alpha \right)^2. \tag{8.103}$$

For an infinite sample size, the total vorticity must equal zero. Else, Eq. (8.103) would lead to an infinite energy contribution. The Hamiltonian of the system is

$$H = H_{SW} + H_V, \tag{8.104}$$

where H_{SW} is the spin-wave part and H_V is the contribution from vortices, thus

$$\frac{H_{SW}}{T} = \frac{1}{2}K\int d^2x(\nabla\vartheta_a)^2, \tag{8.105}$$

$$\frac{H_V}{T} = -\pi K\int_{|\boldsymbol{x}-\boldsymbol{x}'|>a} d^2xd^2x' n_v(\boldsymbol{x})n_v(\boldsymbol{x}')\ln\left(\frac{|\boldsymbol{x}-\boldsymbol{x}'|}{a}\right) + \frac{E_c}{T}\sum_\alpha k_\alpha^2, \tag{8.106}$$

where $K = \rho_s/T$ is the reduced spin-wave stiffness and H_{SW} is emerging from the longitudinal part of $\boldsymbol{v}_s$. In Eq. (8.106), we integrate only over positions which are separated by a distance greater than the short distance cutoff a, such that no two vortices can occupy the same point in space. We can impose the vortices to lie on a lattice and consider a as lattice parameter, thus Eq. (8.106) becomes

$$\frac{H_V}{T} = -\pi K\sum_{\boldsymbol{l},\boldsymbol{l}'} k_{\boldsymbol{l}}k_{\boldsymbol{l}'}\ln\left(\frac{|\boldsymbol{R}_{\boldsymbol{l}}-\boldsymbol{R}_{\boldsymbol{l}'}|}{a}\right) + \frac{E_c}{T}\sum_{\boldsymbol{l}} k_{\boldsymbol{l}}^2, \tag{8.107}$$

where $\boldsymbol{l}$ indicates a vortex position and $\boldsymbol{R}_{\boldsymbol{l},\boldsymbol{l}'}$ are vectors in the lattice.

Often, it is useful to consider the analog case of a two-dimensional Coulomb gas with Hamiltonian H_C. Thus, H_V is identical to H_C up to core contributions. Therefore, the condition of having the total vorticity vanish is analog to the constraint of charge neutrality.

Furthermore, we rewrite Eq. (8.98) as

$$K_R = K - (2\pi)^2K^2\lim_{\boldsymbol{q}\to 0}\frac{\langle n_v(\boldsymbol{q})n_v(-\boldsymbol{q})\rangle}{q^2} \tag{8.108}$$

$$\equiv \lim_{\boldsymbol{q}\to 0} K_R(\boldsymbol{q}), \tag{8.109}$$

where $K_R = \rho_s^R/T$ is the renormalized spin rigidity. When considering low temperatures, thus $E_c >> T$, we can apply Taylor series expansion to the fugacity

$$y = e^{-E_c/T} \tag{8.110}$$

and, since constraining charge neutrality, which imposes $\lim_{q\to 0} n_v(\boldsymbol{q}) = 0$, we obtain for the vortex density correlation

$$\langle n_v(\boldsymbol{q})n_v(-\boldsymbol{q})\rangle = q^2C_2 + O(q^4), \tag{8.111}$$

where

$$C_2 = -\lim_{q\to 0}\frac{1}{4\Omega}\int d^2xd^2x'\langle n_v(\boldsymbol{x})n_v(\boldsymbol{x}')\rangle(\boldsymbol{x}-\boldsymbol{x}')^2$$

$$= -\frac{1}{4\Omega}\sum_{\boldsymbol{l},\boldsymbol{l}'}(\boldsymbol{R}_{\boldsymbol{l}}-\boldsymbol{R}_{\boldsymbol{l}'})^2\langle k_{\boldsymbol{l}}k_{\boldsymbol{l}'}\rangle. \tag{8.112}$$

To lowest order in y, we have

$$\langle k_l k_{l'} \rangle = -2y^2 \left(\frac{|\boldsymbol{R}_l - \boldsymbol{R}_{l'}|}{a} \right)^{-2\pi K} . \tag{8.113}$$

Considering only lowest order in K^{-1}, we obtain

$$K_R^{-1} = K^{-1} + 4\pi^3 y^2 \int_a^\infty \frac{dr}{a} \left(\frac{r}{a} \right)^{3-2\pi K} . \tag{8.114}$$

The integral converges for $3 - 2\pi K < -1$, hence $K > 2/\pi$, corresponding to low temperatures, while for $K \leq 2/\pi$ it diverges. Thus, perturbation theory does not hold at high temperatures. One relies upon renormalization group arguments to master this problem. The integral is divided into two components, where the first, converging component is incorporated into K^{-1},

$$\int_a^\infty \to \int_a^{ae^{\delta l}} + \int_{ae^{\delta l}}^\infty , \tag{8.115}$$

$$(K')^{-1} = K^{-1} + 4\pi^3 y^2 \int_a^{ae^{\delta l}} \frac{dr}{a} \left(\frac{r}{a} \right)^{3-2\pi K} . \tag{8.116}$$

Therefore,

$$\begin{aligned} K_R^{-1} &= (K')^{-1} + 4\pi^3 y^2 \int_{ae^{\delta l}}^\infty \frac{dr}{a} \left(\frac{r}{a} \right)^{3-2\pi K} \\ &= (K')^{-1} + 4\pi^3 y^2 e^{\delta l} e^{\delta l(3-2\pi K)} \int_a^\infty \frac{dr}{a} \left(\frac{r}{a} \right)^{3-2\pi K} \\ &= (K')^{-1} + 4\pi^3 (y')^2 \int_a^\infty \frac{dr}{a} \left(\frac{r}{a} \right)^{3-2\pi K} , \end{aligned} \tag{8.117}$$

where Eq. (8.117) was attained through rescaling the cutoff parameter,

$$ae^{\delta l} \to a, \tag{8.118}$$

and defining the rescaled fugacity

$$y' = e^{(2-\pi K)\delta l} y. \tag{8.119}$$

Taking into consideration y^4 corrections, Eq. (8.117) can be rewritten as

$$K_R^{-1} = (K')^{-1} + 4\pi^3 (y')^2 \int_a^\infty \frac{dr}{a} \left(\frac{r}{a} \right)^{3-2\pi K'} , \tag{8.120}$$

leading to a replacement of K by the shifted parameter K'. When rewriting Eq. (8.116) as

$$\frac{(K')^{-1} - K^{-1}}{\delta l} = 4\pi^3 y^2 \frac{1}{\delta l} \int_a^{ae^{\delta l}} \frac{dr}{a} \left(\frac{r}{a} \right)^{3-2\pi K} , \tag{8.121}$$

evaluating the integral,

$$\int_a^{ae^{\delta l}} \frac{dr}{a} \left(\frac{r}{a}\right)^{3-2\pi K} = \frac{1 - e^{(4-2\pi K)\delta l}}{2\pi K - 4}, \tag{8.122}$$

and letting $\delta l \to 0$, we obtain

$$\begin{aligned} \lim_{\delta l \to 0} \frac{(K')^{-1} - K^{-1}}{\delta l} &= 4\pi^3 y^2 \lim_{\delta l \to 0} \frac{1 - e^{(4-2\pi K)\delta l}}{(2\pi K - 4)\delta l} \\ &= 4\pi^3 y^2 \lim_{\delta l \to 0} e^{(4-2\pi K)\delta l} \qquad (8.123) \\ \frac{dK^{-1}}{dl} &= 4\pi^3 y^2, \qquad (8.124) \end{aligned}$$

where in Eq. (8.123) we have used de l'Hôpital's rule. The same procedure applied to Eq. (8.119) yields

$$\begin{aligned} \lim_{\delta l \to 0} \frac{y' - y}{\delta l} &= \lim_{\delta l \to 0} \frac{e^{(2-\pi K)\delta l} - 1}{\delta l} y \\ &= \lim_{\delta l \to 0} (2 - \pi K) e^{(2-\pi K)\delta l} y \\ \frac{dy}{dl} &= (2 - \pi K) y. \qquad (8.125) \end{aligned}$$

Thus, we have derived the differential renormalization equations, up to higher order correction terms,

$$\frac{dK^{-1}}{dl} = 4\pi^3 y^2(l) + O[y^4(l)], \tag{8.126}$$

$$\frac{dy(l)}{dl} = [2 - \pi K(l)] y(l) + O[y^3(l)]. \tag{8.127}$$

These two equations are often referred to as the Kosterlitz-Thouless recursion relations.

Vortex Unbinding

For $K(l) > 2/\pi$, one observes, by examination of the Kosterlitz-Thouless recursion relations, a decrease in the fugacity $y(l)$ with increasing arc length l. In case of $K(l) < 2/\pi$, the fugacity increases with growing l. This behavior is in perfect accordance to the occurrence of unbound vortices above the critical temperature T_c and their absence below T_c, as preliminarily deduced from an energy contemplation.

Another way of explaining this observation is derived from real space renormalization group discussed in Sec. 1. By an increase of the lattice parameter a, which also describes the minimum distance between vortices, closely bound

vortex-antivortex pairs separated by a distance less than a will disappear. The vortex density thus decreases. $K = K(l = 0)$ is a measure of the energy of angle variation between nearest neighboring sites at a distance a from each other. Therefore, the stiffness also decreases and $K^{-1}(l)$ will increase with increasing l. In contrary, when vortices are unbound, with rescaling of a, vortices persist.

In the analogy of the Coulomb gas, when replacing vortices with free charges, one can identify this transition with the unbinding of molecules at a condensed phase, while attaining a conducting plasma. The constraint of vanishing vorticity holds, hence charge neutrality of the plasma is required.

Integration of the Kosterlitz-Thouless Recursion Relations

Set $K^*(1 - x(l)) = K$, where $K = K^*$ and $y = y^*$ describe the fixed point of the recursion relations, Eqs. (8.126) and (8.127), which is $K^* = 2/\pi$, $y^* = 0$. For small deviations from the fixed point, one can consider only lowest order in x. Thus,

$$\begin{aligned} \frac{d}{dl}K^{-1} &= \frac{d}{dl}\frac{\pi}{2}(1-x)^{-1} \\ &= \frac{\pi}{2}(1-x)^{-2}\frac{dx}{dl} && (8.128) \\ &= 4\pi^3 y^2, && (8.129) \\ \frac{d}{dl}y &= \left[2 - \pi\frac{2}{\pi}(1-x)\right] y. && (8.130) \end{aligned}$$

Hence, to lowest order in x,

$$\begin{aligned} \frac{dx}{dl} &= 8\pi^2 y^2(1-x)^2 = 8\pi^2 y^2, && (8.131) \\ \frac{dy}{dl} &= 2xy, && (8.132) \end{aligned}$$

and

$$\begin{aligned} \frac{dx^2}{dl} &= 2x\frac{dx}{dl} = 16\pi^2 x y^2, && (8.133) \\ \frac{dy^2}{dl} &= 2y\frac{dy}{dl} = 4xy^2, && (8.134) \\ \frac{dx^2}{dy^2} &= \frac{dx^2}{dl}\frac{dl}{dy^2} = 4\pi^2. && (8.135) \end{aligned}$$

Solving the differential Eq. (8.135), one receives the hyperbolae

$$y^2 = \frac{1}{4\pi^2}(x^2 + C), \tag{8.136}$$

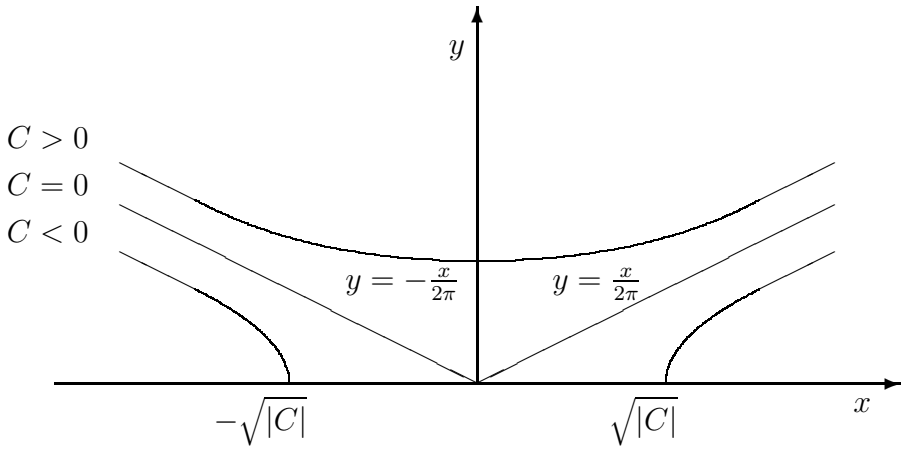

Figure 8.4: Hyperbolic solutions to Eq. (8.135). In case of $C = 0$, one obtains the asymptotes of the hyperbolae. The critical line $y = -x/(2\pi)$ ends in the critical fixed point $x^* = 0$, $y^* = 0$.

with C being a constant (Fig. 8.4). It is a measure for the distance from the critical point and can be written as

$$C = b^2(T - T_c). \tag{8.137}$$

Converting Eq. (8.131) in terms of x, one attains

$$\frac{dx}{dl} = 2(x^2 + C). \tag{8.138}$$

We see that, for $x \neq 0$, $x(l)$ increases with increasing l, i.e. x flows to the right. In case of low temperature, $T < T_c$, thus $C < 0$, when replacing $u(l) = x(l)/\sqrt{|C|}$, we obtain

$$\frac{du}{u^2 - 1} = 2\sqrt{|C|}dl. \tag{8.139}$$

Integration of the left hand side achieves

$$\begin{aligned}
\int_{u(0)}^{u(l)} \frac{du}{u^2 - 1} &= \frac{1}{2}\int_{u(0)}^{u(l)} du \left(-\frac{1}{u+1} + \frac{1}{u-1}\right) \\
&= -\frac{1}{2}\ln\left(\frac{u(l)+1}{u(0)+1}\right) + \frac{1}{2}\ln\left(\frac{u(l)-1}{u(0)-1}\right) \\
&= \frac{1}{2}\ln\left(\frac{1-u(l)}{1+u(l)}\frac{1+u(0)}{1-u(0)}\right).
\end{aligned} \tag{8.140}$$

The right hand side integrated is

$$\int_0^l 2\sqrt{|C|}dl = 2\sqrt{|C|}l. \tag{8.141}$$

Thus, one can write $u(l)$ as follows:

$$u(l) = -\frac{1 - D_0 e^{-4\sqrt{|C|}l}}{1 + D_0 e^{-4\sqrt{|C|}l}}, \tag{8.142}$$

where $D_0 = [1 + u(0)]/[1 - u(0)]$, while

$$\lim_{l\to\infty} x(l) = \lim_{l\to\infty} -\sqrt{|C|}\,\frac{1 - D_0 e^{-4\sqrt{|C|}l}}{1 + D_0 e^{-4\sqrt{|C|}l}} = -\sqrt{|C|}. \tag{8.143}$$

Furthermore, for $\rho_s^R(T_c)/T_c = 2/\pi$,

$$\begin{aligned} K_R &= \lim_{l\to\infty} K(l) = \lim_{l\to\infty} K^*(1 - x(l)) = K^*(1 + \sqrt{|C|}) \\ &= K^*(1 + b\sqrt{T - T_c}) = \frac{2}{\pi}[1 + b\sqrt{T - T_c}] \\ &= \frac{\rho_s^R(T_c)}{T_c}[1 + b\sqrt{T - T_c}], \end{aligned} \tag{8.144}$$

$$\rho_s^R(T) = \rho_s^R(T_c)[1 + b\sqrt{T - T_c}]. \tag{8.145}$$

Considering high temperatures, $T > T_c$, hence $C > 0$, the solution to Eq. (8.138) is

$$\int_{x(0)}^{x(l)} \frac{dx}{x^2 + C} = \frac{1}{\sqrt{C}}\left(\tan^{-1}\frac{x(l)}{\sqrt{C}} - \tan^{-1}\frac{x(0)}{\sqrt{C}}\right) = 2l. \tag{8.146}$$

For $T > T_c$, in the vicinity of the critical point, $x(0)$ is negative, and when $T \to T_c$, $\sqrt{|C|} \to 0$, while $|x(0)| >> \sqrt{|C|}$. Hence, $\tan^{-1}(x(0)/\sqrt{C}) \approx -\pi/2$. Let $x(l^*)$ be positive, thus $\tan^{-1}(x(l^*)/\sqrt{C}) \approx \pi/2$, and Eq. (8.146) becomes

$$2l^* = \frac{\pi}{\sqrt{C}}, \tag{8.147}$$

$$l^* = \frac{\pi}{2}\frac{1}{b\sqrt{T - T_c}} = \frac{b'}{\sqrt{T - T_c}}, \tag{8.148}$$

where $bb' = \pi/2$ is universal, although the coefficients b and b' are not. Thus, the correlation length in the neighborhood of the critical point, with the condition $T > T_c$, is

$$\frac{\xi}{a} = e^{l^*} = e^{b'/\sqrt{T - T_c}}. \tag{8.149}$$

Rewriting Eqs. (8.55) and (8.56) in terms of the renormalized parameters, one obtains

$$\bar{G}(\boldsymbol{x}) \sim |\boldsymbol{x}|^{-\eta(T)}, \tag{8.150}$$

$$\eta(T) = \frac{1}{2\pi K_R(T)}. \tag{8.151}$$

Thus, in the limit $T \to T_c^-$, the exponent $\eta(T)$ becomes

$$\lim_{T\to T_c^-} \eta(T) = \lim_{T\to T_c^-} \frac{1}{2\pi K_R(T)} = \frac{1}{4} \tag{8.152}$$

when taking into consideration

$$\lim_{T\to T_c^-} K_R(T) = \frac{2}{\pi}. \tag{8.153}$$

At exactly $T = T_c$, hence $C = 0$, Eq. (8.138) becomes

$$\frac{dx}{dl} = 2x^2, \tag{8.154}$$

which integrated delivers

$$x(l) = \frac{x(0)}{1 - 2lx(0)}. \tag{8.155}$$

For l large, we have $x(l) \approx -\frac{1}{2l}$, and thus $K_R^{-1} = \frac{\pi}{2}[1 + x(l)]$ to leading order in y. Applying the Josephson scaling relation to the reduced spin-wave stiffness, leads to

$$K_R(q) = e^{(d-2)l} K_R(e^l q). \tag{8.156}$$

Therefore, when setting $e^{l^*} q = 1$ or $x(l^*) = -(\ln q^{-1})/2$,

$$\begin{aligned} g(\boldsymbol{x}) &= \int \frac{d^2q}{(2\pi)^2} \frac{1 - e^{i\boldsymbol{q}\cdot\boldsymbol{x}}}{K_R(q)q^2} \\ &\sim \frac{1}{4} \int_{|\boldsymbol{x}|^{-1}}^{\Lambda} \frac{dq}{q} \left(1 - \frac{1}{2\ln q^{-1}}\right) \\ &\sim \frac{1}{4} \ln|\boldsymbol{x}| - \frac{1}{8} \ln(\ln|\boldsymbol{x}|), \end{aligned} \tag{8.157}$$

and

$$G(\boldsymbol{x}) = e^{-g(\boldsymbol{x})} \sim \frac{(\ln|\boldsymbol{x}|)^{1/8}}{|\boldsymbol{x}|^{1/4}}. \tag{8.158}$$

At high temperatures, $T > T_c$, we observe that

$$G(\boldsymbol{x}) \sim \left(\frac{K}{2}\right)^{|x|} \sim e^{-|\boldsymbol{x}|/\xi}, \tag{8.159}$$

with $\xi^{-1} = \ln(2/K)$.

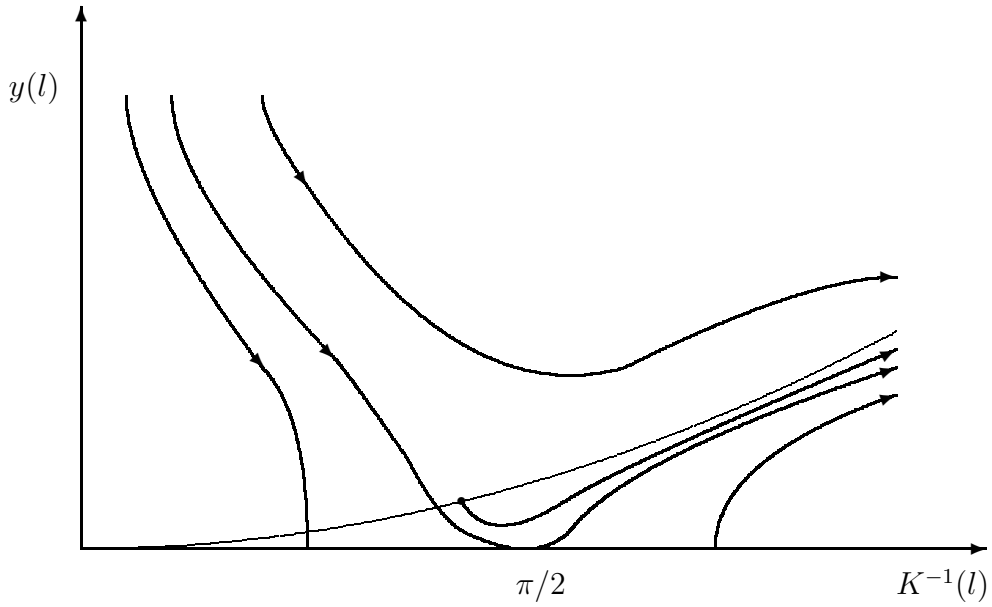

Figure 8.5: Renormalization flows of the recursion relations. The thin line represents initial conditions. The line originating at the dot applies to a temperature $T > T_c$.

Renormalization Analysis

One can now investigate the renormalization flows (Fig. 8.5) of the recursion relations, Eqs. (8.126) and (8.127). We find a separatrix, which passes through the critical point $y(l) = 0$, $K^{-1} = \pi/2$, indicated with $y_s(l)$, $K_s^{-1}(l)$. The initial conditions of a flow satisfy the fugacity term

$$y = e^{-E_c/T} = e^{-E_c K/\rho_s}, \tag{8.160}$$

and thus determine the transition temperature, which arises from intersection of the fugacity term with the separatrix y_s, K_s^{-1}. Furthermore, small y, with $K^{-1} < \pi/2$, i.e. points beneath the separatrix, flow toward $y(l) = 0$, with K^{-1} exhibiting a finite value. Thus, in the limit

$$K_R = \lim_{l\to\infty} K(l), \tag{8.161}$$

the renormalized rigidity will be finite, which induces the absence of any unbound vortices. Points above the separatrix will, however, tend to large y, with K^{-1} large, thus aim at a phase with unbound vortices and vanishing rigidity. For points that lie on the separatrix itself, having $K^{-1} < \pi/2$, the renormalization flow is toward the critical point.

Conclusion

Two-dimensional systems that exhibit $O(2)$ or $U(1)$ symmetry cannot undergo a phase transition based on spontaneous symmetry breaking. This is substantiated by the Mermin-Wagner theorem. However, a Berezinski-Kosterlitz-Thouless transition, which we have characterized as vortex unbinding phenomenon, is possible. It carries an algebraically ordered phase with power-law correlations to a disordered phase with exponential correlations.

More precisely, we have seen that for $T < T_c$ spin-wave theory applies and the system is of quasi-long-range order, namely

$$G(\boldsymbol{x}) \sim |\boldsymbol{x}|^{-\eta(T)}, \tag{8.162}$$

where $\eta(T) = 1/[2\pi K_R(T)]$. Located at the left-hand-side of the separatrix, the system aspires a state of vanishing fugacity, hence suppressed vortices, and finite rigidity. At $T = T_c$, vortices unbind and the correlation function becomes

$$G(\boldsymbol{x}) \sim \frac{[\ln(|\boldsymbol{x}|/a)]^{1/8}}{|\boldsymbol{x}|^{1/4}}. \tag{8.163}$$

The renormalization flow is toward the critical point. In the case of $T > T_c$, vortices are unbound and the system exhibits exponential correlations, i.e.

$$G(\boldsymbol{x}) \sim e^{-|\boldsymbol{x}|\xi^{-1}}, \tag{8.164}$$

where the inverse correlation length is $\xi^{-1} = \ln(2/K)$. Its flows head toward a state of vanishing rigidity.

4 Example in Condensed Matter Physics

Superfluid helium films exhibit proper xy-symmetry, thus one expects a Berezinski-Kosterlitz-Thouless transition, taking the superfluid to the normal fluid state. However, in this case we define

$$\boldsymbol{v}_s \equiv \frac{\hbar}{m}\boldsymbol{\nabla}\theta, \tag{8.165}$$

which has units of velocity. We therefore call $\boldsymbol{v}_s$ the superfluid velocity. The free elastic energy is then

$$F_{el} = \frac{1}{2}\int d^d x \rho_s v_s^2 = \frac{1}{2}\rho_s \left(\frac{\hbar}{m}\right)^2 \int d^d x (\boldsymbol{\nabla}\theta)^2. \tag{8.166}$$

Thus, the rigidity ρ_s is the mass density. When also replacing

$$\rho_s \to \left(\frac{\hbar}{m}\right)^2 \rho_s, \tag{8.167}$$

we can directly apply the results of Sec. 3 to two-dimensional superfluid helium films. Thus, for m being the mass of a helium core, we obtain

$$\begin{aligned} \lim_{T\to T_c^-} K(T) &= \lim_{T\to T_c^-} \frac{\rho_s}{T_c} = \lim_{T\to T_c^-} \frac{(m^2/\hbar)^2 \rho_s^R}{T_c} \\ &= \frac{2m^2 k_B}{\pi\hbar^2} \approx 3.4913 \times 10^{-9}\ \mathrm{g\ cm^{-2}\ K^{-1}} \end{aligned} \tag{8.168}$$

when considering Eq. (8.153) and reintroducing the Boltzmann constant k_B. Measurements of superfluid densities extrapolated to zero frequency yield for this value about 3.35×10^{-9} g cm^{-2} K^{-1}. [51]

Furthermore, one can also observe a large non-universal peak in the specific heat above T_c that is associated with the entropy liberated by the vortex unbinding and is characteristic for a Berezinski-Kosterlitz-Thouless transition.

9 Berry phase I: Mathematical concepts

Simon Wood
Supervisor: Sebastian Pilgram

Berry's geometric phase is a phenomenon encountered in periodic quantum-mechanical systems who's period is large. This report aims at giving a basic understanding of this phase and the mathematical tools required to determine it.

1 Introduction

In the quantum mechanical description of a physical system one has a finite or infinite dimensional Hilbert space $\mathcal{H}$ of state vectors and a set of linear operators acting on these state vectors. In a non isolated environment these operators depend on a set of (external) parameters $R = (R^1, R^2, \dots)$. Each R characterises a particular configuration of the environment and uniquely determines the operators. In particular, a changing environment is described by time-dependent parameters, $R = R(t)$.

For a quantum system in a classical environment, the parameters R label the points of a smooth manifold M. Every change of the environment is then described by a curve $\boldsymbol{C} : [0, T] \to M$, with points $R(t) \in \boldsymbol{C}$. The Manifold M is called the parameter space. The Hamiltonian operator is assumed to be a "smooth" single valued function of $R \in M$. Here smoothness of the Hamiltonians means that its eigenvalues and eigenvectors are smooth functions of R.

In a quantal environment the parameters are (generalised) eigenvalues of the operators of the of the quantal environment.

An example of a quantum mechanical system in a classical environment, that we will be looking at in detail later on is a magnetic moment $\boldsymbol{m}$ in a rotating (classical) magnetic field $\boldsymbol{B}$ of constant magnitude $B := |\boldsymbol{B}|$. The parameter-

dependent Hamiltonian is given by

$$H = H_0 - \boldsymbol{m} \cdot \boldsymbol{B} = H_0 - Bg\left(\frac{e}{2mc}\right)\hat{\boldsymbol{R}}\boldsymbol{J} = H_0 + b\hat{\boldsymbol{R}} \cdot \boldsymbol{J} \tag{9.1}$$

The parameter space of this Hamiltonian is

$$S^2 = \{\hat{R} \in \mathbb{R}^3 |\ |\hat{R}| = 1\}.$$

In general the evolution of the pure states of the quantum system in the external environment is described by the Schrödinger equation

$$i\frac{d\psi(t)}{dt} = H(R)\psi(t), \tag{9.2}$$

or

$$i\frac{d\psi(t)}{dt} = H(R(t))\psi(t) \tag{9.3}$$

for a changing environment. The general (mixed) states are described by the statistical operators $\rho(t) = |\psi(t)\rangle \langle\psi(t)|$ whose evolution is given by the Lioville von Neumann equation

$$i\frac{d\rho(t)}{dt} = [H(R(t)), \rho(t)]\,. \tag{9.4}$$

The space of physical states does not only contain the solutions of (9.3) for one given fixed value of the parameters R or for one given environmental process $t \mapsto R(t)$, but for all $R \in M$. This means that there is a single space of physical state vectors $\mathcal{H}$ for all values of R. For any given value of R, one may choose an orthonormal basis of eigenvectors $|n, R\rangle$ of the parameter-dependent Hamiltonian

$$\begin{aligned} H(R)\,|n, R\rangle &= E_n(R)\,|n, R\rangle \\ \langle m, R|n, R\rangle &= \delta_{mn} \end{aligned} \tag{9.5}$$

and write the Hamiltonian to its spectral resolution

$$H(R) = \sum_n E_n(R)\,|n, R\rangle \langle n, R|\,. \tag{9.6}$$

Given an environmental process along a time parametrisation $R(t)$, one can define a time dependent Hamiltonian as $H(t) := H(R(t))$ and the spectral resolution (9.6) changes to

$$H(t) := H(R(t)) = \sum_n E_n(R(t))\,|n, R(t)\rangle \langle n, R(t)|\,. \tag{9.7}$$

In general the projection operators

$$\Lambda_n(R(t)) := |n, R(t)\rangle \langle n, R(t)|\,, \tag{9.8}$$

corresponding to the eigenstates of $H(t)$ change with time, so the eigenstates themselves will also change.

We assume that the observables are single-valued functions of R over the whole parameter space of the environment. Single-valuedness of the observable means that if the same value of R occurs more than once (i.e., at different times) during a process, then the observables are the same at each occurrence. In particular, if the environmental process is periodic, i.e., if the environmental parameters $R(t)$ traverses a closed path $\boldsymbol{C}$ in M and return, after some period T, to their original values,

$$\boldsymbol{C} : R(0) \to R(t) \to R(T) = R(0), \tag{9.9}$$

then the Hamiltonian, its eigenvalues and the projection operators (9.8), which are uniquely defined by (9.6), are the same at $R(T)$ as they are at $R(0)$,

$$H(R(T)) = H(R(0)), \tag{9.10}$$

$$E_n(R(T)) = E_n(R(0)), \tag{9.11}$$

$$|n, R(T)\rangle \langle n, R(T)| = |n, R(0)\rangle \langle n, R(0)|\,. \tag{9.12}$$

It is important to note that though the observables are single-valued functions of R the basis vectors $|n, R\rangle$ themselves will in general not be single valued over the whole parameter space, but only on sufficiently small open subsets of M (called coordinate patches). In other words, in general it will not be possible to define smooth single-valued $|n, R\rangle$ for all $R \in M$. Thus (9.12) does *not* imply

$$|n, R(T)\rangle = |n, R(0)\rangle \quad \text{for } R(T) = R(0), \tag{9.13}$$

but *only*

$$|n, R(T)\rangle = e^{i\zeta_n} |n, R(0)\rangle \quad \text{for } R(T) = R(0), \tag{9.14}$$

where $e^{i\zeta_n}$ is a phase factor. This is a consequence of the Schrödinger equation (9.3) only defining its normalised eigenstates up to a complex phase $e^{i\zeta_n}$. Therefore the eigenstates $\{|n, R\rangle'\}$ gained from a phase transformation

$$|n, R\rangle \to |n, R\rangle' = e^{i\zeta_n(R)} |n, R\rangle \tag{9.15}$$

form just as valid a basis of eigenvectors of the Hamiltonian as $\{|n, R\rangle\}$ (where $\zeta_n(R)$ are arbitrary real phase angles).

Phase transformations for which the phase factors $e^{i\zeta_n(R(t))}$ are single-valued functions are called *gauge transformations*. In general, if we go from one patch $O_1 \subset M$ of the parameter space to a neighbouring patch $O_2 \subset M$ with a different parametrisation, then eigenvectors of $H(R)$ in the overlap region $R \in O_1 \cap O_2$ will be related by phase transformations of the form (9.15).

2 Berry's Geometric Phase and the Adiabatic Approximation

In this section we discuss an approximation for solving the Schrödinger equation (9.3). For a Hamiltonian $H(R(t))$ whose parameters change in time, the interaction with the environment can cause the physical system to evolve from the n-th eigenstate $|n, R(0)\rangle \langle n, R(0)|$ at $t = 0$ into any other eigenstate $|m, R(t)\rangle \langle m, R(t)|$, at a later time t. A very particular situation arises if this does not happen, i.e., when the state remains an eigenstate of $H(R(t))$ at all times t with the same energy quantum number n. The *adiabatic approximation* assumes that this is the case. This means that $|\psi(t)\rangle \langle \psi(t)|$ changes in such a way that at all times t

$$|\psi(t)\rangle \langle \psi(t)| \overset{\text{adiabatic}}{=} |n, R(t)\rangle \langle n, R(t)| = \Lambda_n(R(t)). \tag{9.16}$$

This time development is called *adiabatic time development*.

The dynamical equations (9.3),(9.4) and the equation for adiabatic time development (9.16) impose two separate conditions on the state $|\psi(t)\rangle \langle \psi(t)|$ and need not be generally compatible with each other. To see when they are compatible we insert (9.16) into (9.4). This yields

$$\begin{aligned} i\frac{d\rho(t)}{dt} &= [H(R(t)), \rho(t)] = [H(R(t)), \Lambda_n(R(t))] \\ &= \sum_m E_m(R(t)) \, [\Lambda_m(R(t)), \Lambda_n(R(t))] \\ &= E_n(R(t)) \, [\Lambda_n(R(t)), \Lambda_n(R(t))] = 0. \end{aligned} \tag{9.17}$$

Equation (9.17) means that $\rho(t)$ does not change in time,

$$W(t) = |\psi(t)\rangle \langle \psi(t)| = |\psi(0)\rangle \langle \psi(0)| = \rho(0), \quad \forall\, t. \tag{9.18}$$

Hence any adiabatically evolving state (9.16) (which obeys (9.4)) must be stationary. In particular it cannot have a non-trivial *cyclic evolution*

$$\rho(0) \to \rho(t) \to \rho(T) = \rho(0), \tag{9.19}$$

in which $\rho(t)$ changes in time. Therefore *exact adiabatic cyclic evolutions do not exist*. The adiabatic equality $\overset{\text{adiabatic}}{=}$ in (9.16) can only be an approximation.

Since we have shown that adiabatic development can only be an approximation, we must derive a condition of validity for the adiabatic approximation. First we express the evolving state vector $\psi(t)$ in the basis $\{|n, R(t)\rangle\}$,

$$\psi(t) = \sum_m c_m(t) \, |m, R(t)\rangle \, . \tag{9.20}$$

Suppose that initially $\psi(t)$ is an eigenvector of the initial Hamiltonian $H(0)$, then the adiabatic approximation is a valid approximation if and only if we can ignore all the coefficients $c_m(t)$ in (9.20) except $c_n(t)$, i.e.,

$$\psi(t) \overset{\text{adiabatic}}{=} c_n(t) \left| n, R(t) \right\rangle , \tag{9.21}$$

with $c_n(0) = 1$. The solutions of the Schrödinger equation (9.3) evolve unitarily, thus the coefficient $c_n(t)$ must be a phase factor (i.e., have modulus 1). Substituting the expression (9.21) for $\psi(t)$ in the Schrödinger equation (9.3) and using (9.5), we find

$$\left(\left(\frac{d}{dt} c_n(t) \right) \left| n, R(t) \right\rangle + c_n(t) \frac{d}{dt} \left| n, R(t) \right\rangle \right) = -iE_n(R(t)) c_n(t) \left| n, R(t) \right\rangle$$

$$\Rightarrow \left(\frac{d}{dt} c_n(t) + iE_n(R(t)) c_n(t) \right) \left| n, R(t) \right\rangle \overset{\text{adiabatic}}{=} -c_n(t) \frac{d}{dt} \left| n, R(t) \right\rangle . \tag{9.22}$$

The inner product of (9.22) with $|m, R(t)\rangle$ for $m \neq n$ in view of the orthogonality of the basis vectors yields

$$\begin{aligned} -c_n(t) \left\langle m, R(t) \right| \frac{d}{dt} \left| n, R(t) \right\rangle &= \left\langle m, R(t) \right| \left(\frac{d}{dt} c_n(t) + iE_n(R(t)) c_n(t) \right) \left| n, R(t) \right\rangle \\ &= \left(\frac{d}{dt} c_n(t) + iE_n(R(t)) c_n(t) \right) \delta_{mn} = 0 \end{aligned}$$

$$\Rightarrow \left\langle m, R(t) \right| \frac{d}{dt} \left| n, R(t) \right\rangle \overset{\text{adiabatic}}{=} 0, \quad \forall\, m \neq n. \tag{9.23}$$

This is the necessary and sufficient condition for the validity of the adiabatic approximation. We can express the left-hand side of this equation in terms of the matrix elements of the time derivative of the Hamiltonian. In order to show this, we take the differential of both sides of (9.5)

$$dH(R) \left| n, R \right\rangle + H(R) d \left| n, R \right\rangle = dE_n(R) \left| n, R \right\rangle + E_n(R) d \left| n, R \right\rangle ,$$

and compute the inner product of both sides of this equation with $|m, R\rangle$ for $m \neq n$. The left-hand side yields

$$\begin{aligned} \left\langle m, R \right| dH(R) \left| n, R \right\rangle + \left\langle m, R \right| H(R) d \left| n, R \right\rangle = &\left\langle m, R \right| dH(R) \left| n, R \right\rangle \\ &+ E_m(R) \left\langle m, R \right| d \left| n, R \right\rangle \end{aligned}$$

and the right-hand side

$$\begin{aligned} \left\langle m, R \right| dE_n(R) \left| n, R \right\rangle + \left\langle m, R \right| E_n(R) d \left| n, R \right\rangle = &dE_n(R) \delta_{mn} \\ &+ E_n \left\langle m, R \right| d \left| n, R \right\rangle \\ = &E_n(R) \left\langle m, R \right| d \left| n, R \right\rangle \end{aligned}$$

$$\Rightarrow \langle m,R|\, dH(R)\,|n,R\rangle + E_m(R)\,\langle m,R|\, d\,|n,R\rangle = E_n(R)\,\langle m,R|\, d\,|n,R\rangle$$
$$\Rightarrow \langle m,R|\, d\,|n,R\rangle = \frac{\langle m,R|\, dH(R)\,|n,R\rangle}{E_n(R)-E_m(R)} \tag{9.24}$$

For a given environmental process, $R = R(t)$, we can turn the differentials appearing in (9.24) into total time derivatives by dividing by dt. This leads to

$$\langle m,R(t)|\,\frac{d}{dt}\,|n,R(t)\rangle = \frac{\langle m,R(t)|\,\frac{d}{dt}H(R)\,|n,R(t)\rangle}{E_n(R(t))-E_m(R(t))}. \tag{9.25}$$

From the equation (9.25) combined with the condition (9.23) we can re-express the validity of the approximation in the form

$$\frac{\langle m,R(t)|\,\frac{d}{dt}H(R(t))\,|n,R(t)\rangle}{E_n(R(t))-E_m(R(t))} \overset{\text{adiabatic}}{=} 0, \quad \forall\, m\neq n. \tag{9.26}$$

The adiabatic approximation is a valid approximation if and only if the left-hand side of (9.26) can be neglected. It is important to note that the left-hand side of (9.26) has the dimension of frequency. This means that in order to decide whether it can be neglected, one must have an intrinsic frequency (or energy) scale for the quantum system. For our example of a magnetic moment interacting with a rotating magnetic field (9.1) the intrinsic frequency scale is given by b.

Calculating Berry's Geometric Phase

In the preceding section we showed that for a periodic Hamiltonian $H(t)$, an adiabatically evolving state $\rho(t) = |\psi(t)\rangle\langle\psi(t)|$ with the initial condition $\rho(0) = \Lambda_n(R(0))$ traverses a closed path $\mathcal{C}$ in the state space $\mathcal{P}(\mathcal{H})$. This does not imply that the normalised state vector $\psi(t)$ which fulfils the Schrödinger equation (9.3), also traverses a closed path in $\mathcal{H}$. In general the path

$$C : [0,T] \to \psi(t) \in \mathcal{H}, \quad \text{with } \langle\psi(t)|\psi(t)\rangle = 1, \tag{9.27}$$

is not closed in $\mathcal{H}$, but satisfies

$$C(T) = \psi(T) = e^{-i\alpha_\psi}\psi(0). \tag{9.28}$$

For the case of a time-independent Hamiltonian, the phase factor is

$$e^{-i\alpha_\psi} = e^{-iE_nT}, \text{ or } e^{-i\alpha_\psi} = e^{-i\int_0^T dt'\,E_n(t')}. \tag{9.29}$$

This is called the *dynamical phase factor*. For a general time-dependent Hamiltonian $H(R(t))$, there is an additional phase factor which is called the the *geometric phase* or *Berry phase*.

If the adiabatic approximation is valid, we can express the evolving state vector according to (9.21), where the coefficient c_n satisfies (9.22). We can obtain

the explicit formula for c_n by calculating the inner product of both sides of (9.22) with $|n, R(t)\rangle$. This yields

$$\left(\frac{d}{dt}c_n(t) + iE_n(R(t))c_n(t)\right)\delta_{nn} = -c_n(t)\,\langle n, R(t)|\,\frac{d}{dt}\,|n, R(t)\rangle\,,$$
$$\Rightarrow \frac{d}{dt}c_n(t) = -c_n(t)\left(iE_n(t) + \langle n, R(t)|\,\frac{d}{dt}\,|n, R(t)\rangle\right), \tag{9.30}$$

where $E_n(t) := E_n(R(t))$. This equation can be integrated to obtain

$$\frac{dc_n}{c_n} = -\left(iE_n(t) + \langle n, R(t)|\,\frac{d}{dt}\,|n, R(t)\rangle\right)dt,$$
$$\int_{c_n(0)}^{c_n(t)}\frac{dc_n}{c_n} = -i\int_0^t E_n(t')dt' - \int_0^t \langle n, R(t')|\,\frac{d}{dt'}\,|n, R(t')\rangle\,dt'. \tag{9.31}$$

In view of $c_n(0)$ being equal to 1, this leads to

$$\ln c_n|_{c_n(0)}^{c_n(t)} = -i\int_0^t E_n(t')dt' + i\gamma_n(t),$$
$$\Rightarrow c_n(t) = e^{-i\int_0^t E_n(t')dt'}e^{i\gamma_n(t)}, \tag{9.32}$$

where

$$e^{i\gamma_n(t)} := e^{i\int_0^t i\langle n,R(t')|\frac{d}{dt'}|n,R(t')\rangle dt'}. \tag{9.33}$$

Because the coefficient $c_n(t)$ in (9.22) has modulus 1 $\gamma_n(t)$ is a real phase angle.[23] It is important to note that $\gamma_n(t)$ is only defined up to an integer multiple of 2π.

A remarkable property of the phase angle $\gamma_n(t)$ is that it does not depend on the time dependence of the integrand in (9.33) but only on the path traced by $R(t)$ in the parameter space. In fact, it can be directly defined in terms of a curve integral

$$\gamma_n(t) = \int_0^t i\,\langle n, R(t')|\,\frac{d}{dt'}\,|n, R(t')\rangle\,dt'$$
$$= \int_{R(0)}^{R(t)} i\,\langle n, R|\,\frac{\partial}{\partial R^i}\,|n, R\rangle\,dR^i$$
$$= \int_{R(0)}^{R(t)} \boldsymbol{A}_i^n(R)dR^i \tag{9.34}$$

over a vector-valued function

$$\boldsymbol{A}^n := i\,\langle n, R|\,\nabla\,|n, R\rangle \tag{9.35}$$

[23] A more analytic proof will be supplied later in this section.

This vector-valued function is called the *Mead-Berry vector potential*. As can be seen in (9.35) it depends on single-valued basis eigenvectors $|n, R\rangle$ of $H(R)$. Since a smooth single-valued basis vector may in general not be found on the whole parameter space M, but only on its patches, the same is true for $\boldsymbol{A}^n$. This problem will be discussed in detail for the example (9.1) in section 3. Here we will assume that the curve $\boldsymbol{C}$ lies in a single patch over which a complete set of smooth and single-valued basis vectors $|n, R\rangle$ exists.

The Mead-Berry vector potential (9.35) may also be expressed as a (local) differential one-form,

$$A^n = A^n_i dR^i := \langle n, R| \frac{\partial}{\partial R^i} |n, R\rangle \, dR^i = i \langle n, R| \, d \, |n, R\rangle \,, \tag{9.36}$$

which is defined on the same patch as $|n, R\rangle$. Here the differentials dR^i are the basis differential one-forms (covariant vectors), and "d" is the exterior derivative operator. The one-form A^n is called the *Mead-Berry connection one-form*. It can be used to yield the following expression for the phase angle $\gamma_n(T)$ of (9.34),

$$\gamma_n(T) = \int_{R(0)}^{R(T)} i \langle n, R \, |d| \, n, R\rangle = \int_{\boldsymbol{C}} A^n, \tag{9.37}$$

where $\boldsymbol{C}$ is the curve traced by the parameters R in the parameter space M.

We shall now prove that $\gamma_n(t)$ is real. To do this, it suffices to show that $\langle n, R| \, d \, |n, R\rangle$ is purely imaginary. The proof requires the following identity

$$\begin{aligned} d \langle n, R|m, R\rangle &= d \, \delta_{nm} \\ (d \langle n, R|) \, |m, R\rangle + \langle n, R| \, d \, |m, R\rangle &= 0 \\ (d \langle n, R|) \, |m, R\rangle &= - \langle n, R| \, d \, |m, R\rangle \end{aligned} \tag{9.38}$$

Because the scalar product is a hermitian two-form and the identity (9.38) we receive

$$\begin{aligned} \langle n, R| \, d \, |n, R\rangle &= \overline{(d \langle n, R|) \, |n, R\rangle} \\ &= -\overline{\langle n, R| \, d \, |n, R\rangle}. \end{aligned} \tag{9.39}$$

So $\langle n, R| \, d \, |n, R\rangle$ is equal to the negative of its complex conjugate which can only be the case if it is purely imaginary.

Returning to equation (9.21) we now see that the state can be expressed as

$$\psi(t) \overset{\text{adiabatic}}{=} e^{-i \int_0^t E_n(t')dt'} e^{i\gamma_n(t)} \, |n, R(t)\rangle \,. \tag{9.40}$$

As can be seen in this equation in addition to the dynamical phase factor, there exists another phase factor which is given in terms of the eigenvectors $|n, R\rangle$ of $H(R)$ according to (9.37).

As we know from (9.15) the basis eigenvectors $|n, R(t)\rangle$ are only determined up to a phase factor. Thus, the additional phase factor in (9.40) can be transformed away by a phase transformation for non cyclic changes. In the following we will show that in general this is not possible for cyclic changes.

From the definition of the Mead-Berry vector potential (9.35), $\boldsymbol{A}^n(R)$ transforms according to

$$\begin{aligned}\boldsymbol{A}^n(R) \to \boldsymbol{A}'^n(R) &= \langle n, R|' \left(\nabla |n, R\rangle'\right) \\ &= i \langle n, R| e^{-i\zeta_n(R)} \left(\nabla e^{i\zeta_n(R)} |n, R\rangle\right) \\ &= i \langle n, R| \nabla |n, R\rangle + i e^{-i\zeta_n(R)} \left(\nabla e^{i\zeta_n(R)}\right). \\ &= \boldsymbol{A}^n(R) - \nabla\zeta_n(R). \end{aligned} \tag{9.41}$$

Alternatively we have the connection one-form

$$A^n(R) \to A'^n(R) = A^n(R) - d\zeta_n(R). \tag{9.42}$$

In view of (9.41), under a gauge transformation the phase angle $\gamma_n(t)$ transforms according to

$$\begin{aligned}\gamma_n(t) \to \gamma'_n(t) &= \int_{R(0)}^{R(t)} \boldsymbol{A}'^n(R) dR \\ &= \gamma_n(t) - \zeta_n(R(t)) + \zeta_n(R(0)). \end{aligned} \tag{9.43}$$

If we do the calculations that led to (9.40) using $|n, R\rangle'$ in place of $|n, R\rangle$, we obtain (9.40) with the primed quantities on the right-hand side. Using (9.21) we obtain for the primed quantities

$$e^{i\gamma'_n(t)} |n, R(t)\rangle' = e^{i\gamma'_n(t)} e^{i\zeta_n(R(t))} |n, R(t)\rangle . \tag{9.44}$$

If $\zeta_n(R(t))$ is an arbitrary single-valued function modulo 2π, we can choose it such that $\zeta_n(R(t)) = \gamma_n(t)$, thus the phase factor $e^{i\gamma'_n(t)} e^{i\zeta_n(R(t))}$ becomes unity and we find in place of (9.40)

$$\psi(t) = e^{-i\int_0^t E_n(t')dt'} |n, R(t)\rangle . \tag{9.45}$$

This also fulfils the initial condition

$$\rho(0) = |n, R(0)\rangle \langle n, R(0)| . \tag{9.46}$$

Since $|n, R\rangle'$ is just as a basis eigenvector as $|n, R\rangle$, we can use it to describe the time development of the state vector, i.e., use (9.45) which only involves the dynamical phase factor.

The above arguments made use of the fact that $\zeta_n(R(t))$ was arbitrary. If after some period T the environmental parameters return to their original values

as described by the closed path $\boldsymbol{C}$ of (9.9), then one cannot choose $\zeta_n(R(T))$ freely to remove $\gamma_n(T)$.

For $R(T) = R(0)$, the single valuedness of $e^{i\zeta_n(R)}$ implies

$$e^{i\zeta_n(R(T))} = e^{i\zeta_n(R(0))}, \text{ or } \zeta_n(R(T)) = \zeta_n(R(0)) + 2\pi k \quad k \in \mathbb{Z}. \tag{9.47}$$

Therefore according to (9.43)

$$\begin{aligned} \gamma_n(T) \to \gamma'_n(T) &= \oint_{\boldsymbol{C}} \boldsymbol{A}'^n(R)dR \\ &= \oint_{\boldsymbol{C}} \boldsymbol{A}(R)dR - 2\pi k \quad k \in \mathbb{Z} \\ &= \gamma_n(t) - 2\pi k \quad k \in \mathbb{Z}. \end{aligned} \tag{9.48}$$

Thus $\gamma_n(T)$ - which is only defined modulo 2π - is invariant under the gauge transformation (9.15) and cannot be removed. We therefore have

$$\psi(T) = e^{-i\int_0^T E_n(t')dt' + i\gamma_n(T)} |n, R(T)\rangle \tag{9.49}$$

with $\gamma_n(T)$ given by the loop integral over the closed path $\boldsymbol{C}$ of (9.9)

$$\begin{aligned} \gamma_n(\boldsymbol{C}) := \gamma_n(T) &= \oint_{\boldsymbol{C}} \boldsymbol{A}^n dR \qquad \text{modulo } 2\pi \\ &= \oint_{\boldsymbol{C}} A^n \qquad \text{modulo } 2\pi. \end{aligned} \tag{9.50}$$

Inserting the initial conditions we obtain

$$\psi(T) = e^{-i\int_0^T E_n(t)dt} e^{i\gamma_n(\boldsymbol{C})} \psi(0). \tag{9.51}$$

The phase angle $\gamma_n(\boldsymbol{C})$ is called the *Berry phase angle*, and $e^{i\gamma_n(\boldsymbol{C})}$ is called the *Berry phase factor*.

We have shown that for a closed path the extra phase factor cannot be transformed away. This does not mean that $\gamma_n(\boldsymbol{C})$ cannot be zero. Should this be the case, the vector potential $\boldsymbol{A}^n(R)$ (and the connection one-form $A^n(R)$) need not be zero but will be "trivial", which means

$$\boldsymbol{A}^n(R) = \nabla\zeta(R) \tag{9.52}$$

$$A^n(R) = d\zeta(R). \tag{9.53}$$

where $\zeta(R)$ is a well-defined function of R.[24] The cases that we are interested in are those for which the Berry phase angle is different from zero (or an integer

[24]Note that we still require the curve $\boldsymbol{C}$ to lie on a single patch of the parameter space. If this is not the case, then (9.52) may be satisfied on individual patches but since the curve $\boldsymbol{C}$ does not in general lie in one patch, the corresponding Berry phase may still be non-trivial. Such a phase is called a *topological phase* and subject of the Berry phase II: The Aharonov Bohm Effect presentation.

multiple of 2π). The Hamiltonian (9.1) provides an example of such a case. A detailed discussion of this system will be presented in the next section.

From (9.41) we see that the Mead-Berry vector potential satisfies the same gauge (phase) transformation rule, (9.41), as the vector potential of electromagnetism. The set of phase factors $e^{i\zeta_n(R)}$ form the group U(1) of unitary 1×1 matrices. We therefore have a gauge theory with gauge (symmetry) group U(1) and gauge potential $\boldsymbol{A}^n(R)$. This is the reason for which we call the phase transformation (9.15) a gauge transformation. Whereas $\boldsymbol{A}^n(R)$ is not an invariant quantity with respect to a gauge transformation (it transforms according to (9.41)), the Berry phase is gauge invariant. If the parameter space is three dimensional and the parameter R is a three dimensional vector $\boldsymbol{R} = (R^1, R^2, R^3)$, we have a complete analogy with electrodynamics. However, the physical meaning of the quantities associated with the Berry phase is different. The gauge potential (9.35) is defined in terms of the eigenvectors of the Hamiltonian and has nothing to do with electromagnetism. For an m-dimensional parameter space we again have a U(1)-gauge theory, but the gauge transformations and gauge potentials now depend on m parameters $R = (R^1, \ldots, R^m)$ and $\boldsymbol{A}^n(R)$ consists of m components $A_i^n(R)$, $i = 1, \ldots, m$. In this case we have a U(1) gauge theory over an m-dimensional parameter space.

In analogy to electrodynamics we can define a gauge field strength tensor F^n with the components

$$F_{ij}^n := \frac{\partial}{\partial R^i} A_j^n - \frac{\partial}{\partial R^j} A_i^n, \quad i, j = 1, 2, \ldots, m. \tag{9.54}$$

This is an antisymmetric covariant tensor field of rank two, i.e., it is a differential two-form

$$F^n = \frac{1}{2} F_{ij}^n dR^i \wedge dR^j = \frac{\partial A_j^n}{\partial R^i} dR^i \wedge dR^j = dA^n. \tag{9.55}$$

Here the antisymmetry of the wedge product $\wedge$ was used, and dA^n stands for the exterior derivative of the Mead-Berry connection one-form A^n given by (9.36). The two-form F^n is also called the *Mead-Berry curvature* two-form. It is given by

$$\begin{aligned} F^n &= d\left(i \langle n, R| \, d \, |n, R\rangle\right) \\ &= i \left(d \langle n, R|\right) \wedge d \, |n, R\rangle + i \langle n, R| \, d^2 \, |n, R\rangle \\ &= i \left(d \langle n, R|\right) \wedge d \, |n, R\rangle \end{aligned} \tag{9.56}$$

where we have used the identity $d^2 = 0$ of the exterior derivative.

An important property of the curvature two-form is that unlike the connection one-form, it is a gauge-invariant quantity. This follows directly from (9.42), (9.55), and the identity $d^2 = 0$,

$$F^n \to F'^n = dA'^n = dA^n - d^2\zeta_n = dA^n = dF^n. \tag{9.57}$$

The gauge invariance of F^n has two important consequences: F^n is a globally defined object over M, and it may be used to yield a direct formula for the Berry phase.

In order to obtain this formula, we assume that the curve $\boldsymbol{C}$ bounds a surface $S \subset M$, and use Stokes' theorem to convert the loop integral in (9.50) to a surface integral over S. The result is

$$\gamma_n(\boldsymbol{C}) = \oint_{\boldsymbol{C}} A^n = \int_S dA^n = \int_S F^n \quad \text{modulo } 2\pi. \tag{9.58}$$

The surface S can arbitrarily chosen as long as it is bounded by the closed curve $\boldsymbol{C}$.

Next we wish to use the manifestly gauge-invariant expression of the Berry phase angle (9.58), to investigate the consequences of a possible degeneracy of the energy eigenvalues. In order to see what happens when two energy levels become degenerate for some values of the parameters, we express the curvature two-form F^n in terms of the eigenvalues $E_n(R)$. Using the completeness of the basis $\{|m, R\rangle\}$,

$$\mathbf{1} = \sum_m |m, R\rangle \langle m, R| \,, \tag{9.59}$$

we can express (9.56) in the form

$$\begin{aligned} F^n &= i \sum_m \left[(d \langle n, R|) \, |m, R\rangle \right] \wedge \left[\langle m, R| \, d \, |n, R\rangle \right] \\ &= -i \sum_m \left[\langle n, R| \, d \, |m, R\rangle \right] \wedge \left[\langle m, R| \, d \, |n, R\rangle \right] \\ &= i \sum_{m \neq n} \left[\langle m, R| \, d \, |n, R\rangle \right] \wedge \left[\langle n, R| \, d \, |m, R\rangle \right] . \end{aligned} \tag{9.60}$$

In the second equality we used the identity (9.38) and the third equality follows from the antisymmetry of the wedge product of two one-forms. In particular, note that due to this antisymmetry the $m = n$ term in the sum is identically zero.

In order to show the dependence of F^n on the difference of the energy eigenvalues, we substitute (9.25) in the right-hand side of (9.60). This yields

$$F^n = i \sum_{m \neq n} \frac{\langle n, R| \left[dH(R) \right] |m, R\rangle \wedge \langle m, R| \left[dH(R) \right] |n, R\rangle}{\left[E_n(R) - E_m(R) \right]^2} \tag{9.61}$$

The form (9.61) does not depend on the phase factor of the basis vectors $|m, R\rangle$. Hence unlike the connection one-form (9.36), which is expressed in terms of the smooth single-valued $|n, R\rangle$ and can therefore be defined only on a patch

in the parameter space M where the latter exists, the curvature two-form (9.61) is globally defined on M. Therefore, (9.61) can be used to compute the geometric phase angle even for the cases where the curve $\boldsymbol{C}$ lies in a region in the parameter space where smooth single-valued $|n, R\rangle$ do not exist. The formula (9.61) also shows that the singularities of F^n occur at those values of $R = R_0$ where the eigenvalues are degenerate $E_n(R_0) = E_m(R_0)$.

From the above formulas we see that the Berry phase angle $\gamma_n(\boldsymbol{C})$ is independent of how the closed loop $\boldsymbol{C}$ is traversed (provided that the condition (9.26) for the validity of the adiabatic approximation is satisfied). This means that it is not sensitive to the details of the dynamics of the quantum system, it only depends upon the path $\boldsymbol{C}$ and is thus a geometric quantity.

3 Berry's Geometric Phase applied to a Precessing Magnetic Field

In this section we will take a closer look at the quantum system described by the equation (9.1), that of a quantum particle with magnetic moment $\boldsymbol{m} = \mu_B g \boldsymbol{J}$ in an external magnetic field $\boldsymbol{B}(t) = B\hat{\boldsymbol{R}}(t)$ whose direction $\hat{\boldsymbol{R}}(t)$ is changing periodically. In particular we will consider the case in which the direction of the magnetic field precesses around a fixed axis which we take as the 3-axis (z-axis) of our coordinate frame in space ($\mathbb{R}^3$). If the direction rotates slowly ("adiabatically") this system provides an application of the general ideas developed in Section 2. The Schrödinger equation for a magnetic moment in a precessing magnetic field has been solved exactly. Therefore we need not restrict ourselves to the adiabatic approximation and will also compute the non-adiabatic geometric phase. The latter is also known as the *Aharonov-Anandan phase*. With the help of this example we will then discover the non-adiabatic geometric phase for a general cyclic evolution.

In our example we are not interested in the dynamics of the particle in position space, but only in the dynamics of the spin in the magnetic field. So our Hamiltonian (9.1) reduces to

$$H(\hat{\boldsymbol{R}}(t)) = -\frac{Bge}{2mc}\hat{\boldsymbol{R}}(t) \cdot \boldsymbol{J} = b\hat{\boldsymbol{R}}(t) \cdot \boldsymbol{J} \tag{9.62}$$

where $\boldsymbol{J}$ is the angular momentum operator of the quantum system, $\hat{\boldsymbol{R}}(t)$ is the parameter that describes the changing environment, and $b = -\frac{Bge}{2mc}$ is a constant.

The Parameterisation of the Basis Vectors

For the system described by the Hamiltonian (9.62), the parameter space of the environment is the set of all unit vectors $\hat{\boldsymbol{R}}$ in $\mathbb{R}^3$. Therefore the parameter space of this system may be identified with the unit sphere S^2 embedded in $\mathbb{R}^3$. We

parametrise the points of S^2 by the polar and azimuthal angles (θ, φ) according to

$$\hat{\boldsymbol{R}} = \hat{\boldsymbol{R}}(\theta, \varphi) = \begin{pmatrix} \sin\theta\cos\varphi \\ \sin\theta\sin\varphi \\ \cos\theta \end{pmatrix}, \tag{9.63}$$

where

$$0 \leq \theta \leq \pi, \text{ and } 0 \leq \varphi < 2\pi.$$

This parametrisation associates unique values of the pair (θ, φ) to each unit vector $\hat{\boldsymbol{R}}$ except for the unit vector

$$\boldsymbol{e}_3 := \begin{pmatrix} 0 \\ 0 \\ 1 \end{pmatrix} \tag{9.64}$$

of the north pole $\mathcal{N}$ and the unit vector $-\boldsymbol{e}_3$ of the south pole $\mathcal{S}$. $\boldsymbol{e}_3$ and $-\boldsymbol{e}_3$ are given respectively, by $\theta = 0$ and $\theta = \pi$ for all values of φ; the value of φ is not determined when $\hat{\boldsymbol{R}} = \pm\boldsymbol{e}_3$.

The special case in which the magnetic field precesses uniformly about the 3-axis is described by

$$\boldsymbol{B}(t) = B(\sin\theta\cos\omega t, \sin\theta\sin\omega t, \cos\theta) = B\hat{\boldsymbol{R}}(\theta, \omega t), \tag{9.65}$$

with B, θ and $\omega = \varphi/t$ being constants. The precession of such a magnetic field is shown in Fig. 9.1.

The eigenvectors (9.5) for this example are defined by

$$H(R)\,|k, R\rangle = b\hat{\boldsymbol{R}} \cdot \boldsymbol{J}\,|k, R\rangle = bk\,|k, R\rangle\,. \tag{9.66}$$

They are eigenvectors of the operator $\hat{\boldsymbol{R}}(t) \cdot \boldsymbol{J}$. The place of the energy quantum number n in (9.5) is taken here by k which is the quantum number for the component of angular momentum along the (changing) direction of the external magnetic field.

For this example, the eigenvalues $E_k(R(t)) = bk$ of the time-dependent Hamiltonian $H(R(t))$ are constant, but the eigenvectors $|k, R(t)\rangle$ and the eigenprojectors $\Lambda_k(R(t)) = |k, R\rangle\langle k, R|$ change in time. The eigenvalue of the observable is constant but its physical interpretation changes in time; it is the eigenvalue of the observable $\hat{\boldsymbol{R}} \cdot \boldsymbol{J}$ where the direction $\hat{\boldsymbol{R}}(t)$ changes with respect to the laboratory frame.

The vectors of (9.66) are parameterised by the unit vector $\hat{\boldsymbol{R}}$ or by the polar and azimuthal angles (θ, φ). They can be obtained by applying (θ, φ)-dependent rotations to an eigenvector $|k, \boldsymbol{e}_3\rangle$ of the component of angular momentum in direction of the north pole, $J_3 = \boldsymbol{e}_3 \cdot \boldsymbol{J}$.

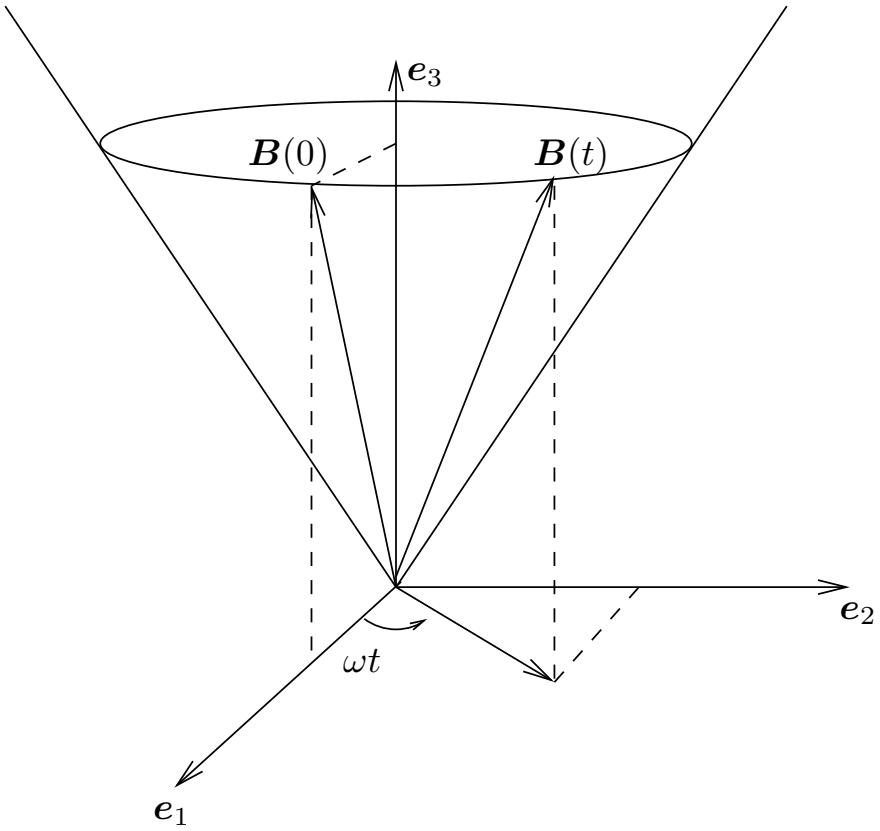

Figure 9.1: A quantal magnetic moment in an external magnetic field precesses uniformly around a cone of semi-angle θ with $\boldsymbol{e}_3$. (θ, φ) are the polar and azimuthal angles for the rotation of the external magnetic field.

There are many (θ, φ)-dependent rotations $\mathcal{R}(\theta, \varphi) \in \mathrm{SO}(3)$ which when applied to $\boldsymbol{e}_3$ give the unit vector $\hat{\boldsymbol{R}}(\theta, \varphi)$. We choose the following product of rotations.

$$\begin{aligned}\mathcal{R}(\theta, \varphi) &= \mathcal{R}_3(\varphi)\mathcal{R}_2(\theta)\mathcal{R}_3(-\varphi)\boldsymbol{e}_3 = \mathcal{R}_3(\varphi)\mathcal{R}_2(\theta)\boldsymbol{e}_3 \\ &= \mathcal{R}_3(\varphi)\hat{\boldsymbol{R}}(\theta, 0) = \hat{\boldsymbol{R}}(\theta, \varphi),\end{aligned} \tag{9.67}$$

where $\mathcal{R}_3(-\varphi)$ does *nothing* to the unit vector $\boldsymbol{e_3}$ and where $\mathcal{R}_2(\theta)$ produces the unit vector $\hat{\boldsymbol{R}}(\theta, 0)$ which lies in the 1-3 plane at an angle θ with respect to the $\boldsymbol{e_3}$-axis. The rotation $\mathcal{R}_3(-\varphi)$ has been included in the definition of $\mathcal{R}(\theta, \varphi)$ in order for the rotation $\mathcal{R}(0, \varphi)$ to be *independent* of φ.

Rotations, like any other continuous transformations, are represented in the space of quantum physical states by unitary operators (representing the group SU(2)). The unitary operators that represent the rotations $\mathcal{R}_3(\varphi)$ and $\mathcal{R}_2(\theta)$ are given by

$$U_3(\varphi) = e^{-i\varphi J_3}, \qquad U_2(\theta) = e^{-i\theta J_2}. \tag{9.68}$$

The product of two or more rotations is represented by the product of the corresponding operators. The rotation $\mathcal{R}(\theta, \varphi)$ of (9.67) is thus represented by the operator

$$U(\theta, \varphi) = U_3(\varphi)U_2(\theta)U_3(-\varphi) = e^{-i\varphi J_3}e^{-i\theta J_2}e^{i\varphi J_3}. \tag{9.69}$$

We now choose a fixed normalised eigenvector $|k, \boldsymbol{e}_3\rangle$ of $J_3 = \boldsymbol{e}_3 \cdot \boldsymbol{J} = \hat{\boldsymbol{R}}(0, 0) \cdot \boldsymbol{J}$ and transform it using the unitary operator $U(\theta, \varphi)$. The resulting state vector,

$$|k, \theta, \varphi\rangle := U(\theta, \varphi)\,|k, \hat{\boldsymbol{e}}_3\rangle = e^{-i\varphi J_3}e^{-i\theta J_2}e^{i\varphi J_3}\,|k, \hat{\boldsymbol{e}}_3\rangle\,, \tag{9.70}$$

is an eigenvector of the operator $\hat{\boldsymbol{R}}(\theta, \varphi) \cdot \boldsymbol{J}$ with eigenvalue k,

$$\hat{\boldsymbol{R}}(\theta, \varphi) \cdot \boldsymbol{J}\,|k, \theta\varphi\rangle = k\,|k, \theta, \varphi\rangle\,. \tag{9.71}$$

In order to prove (9.71), we use the following transformation property of the angular momentum operators J_i which follows from their commutation relations[25]

$$e^{-i\theta J_2}J_3e^{i\theta J_2} = J_3\cos\theta + J_1\sin\theta, \tag{9.72}$$

$$e^{-i\varphi J_3}J_1e^{i\varphi J_3} = J_1\cos\theta + J_2\sin\varphi, \tag{9.73}$$

$$e^{-i\varphi J_3}J_2e^{i\varphi J_3} = J_2\cos\varphi - J_1\sin\varphi. \tag{9.74}$$

[25]These properties can be verified using the Backer-Campbell-Hausdorff formula, $e^A B e^{-A} = B + \sum_{n=1}^{\infty} B_n/n!$, $B_0 := B$, $B_n := [A, B_{n-1}]$ and the commutation relations of the angular momentum operator.

Together with the fact that J_3 commutes with $e^{i\theta J_3}$, we receive

$$\begin{aligned}
\hat{\boldsymbol{R}}(\varphi,\theta)\cdot\boldsymbol{J}\,|k,\theta,\varphi\rangle &= (\sin\theta(J_1\cos\varphi + J_2\sin\varphi) + J_3\cos\theta)\,|k,\theta,\varphi\rangle \\
&= \left(e^{-i\varphi J_3}J_1 e^{i\varphi J_3}\sin\theta + J_3\cos\theta\right)|k,\theta,\varphi\rangle \\
&= \left(e^{-i\varphi J_3}J_1 e^{i\varphi J_3}\sin\theta + e^{-i\varphi J_3}J_3 e^{i\varphi J_3}\cos\theta\right)|k,\theta,\varphi\rangle \\
&= \left(e^{-i\varphi J_3}\left(J_1\sin\theta + J_3\cos\theta\right)e^{i\varphi J_3}\right)|k,\theta,\varphi\rangle \\
&= \left(e^{-i\varphi J_3}e^{-i\theta J_2}J_3 e^{i\theta J_2}e^{i\varphi J_3}\right)e^{-i\varphi J_3}e^{-i\theta J_2}e^{i\varphi J_3}\,|k,\hat{\boldsymbol{e}}_3\rangle \\
&= e^{-i\varphi J_3}e^{-i\theta J_2}e^{i\varphi J_3}k\,|k,\hat{\boldsymbol{e}}_3\rangle = k\,|k,\theta,\varphi\rangle
\end{aligned} \tag{9.75}$$

The state vector (9.70) is a smooth vector-valued function of (θ,φ). This vector-valued function gives a unique state vector for all $\hat{\boldsymbol{R}}$ except for the south pole $\hat{\boldsymbol{R}} = -\boldsymbol{e}_3$, where $\theta = \pi$ and (9.72) becomes

$$e^{-i\pi J_2}J_3 e^{i\pi J_2} = -J_3. \tag{9.76}$$

This implies

$$e^{-i\pi J_2}e^{-i\varphi J_3}e^{i\pi J_2} = e^{i\varphi J_3}, \tag{9.77}$$

$$e^{i\varphi J_3}e^{-i\pi J_2}e^{i\varphi J_3} = e^{-i\pi J_2} \tag{9.78}$$

which may be used to obtain

$$\begin{aligned}
|k,\pi,\varphi\rangle &= e^{-i\varphi J_3}e^{-i\pi J_2}e^{i\varphi J_3}\,|k,\hat{\boldsymbol{e}}_3\rangle \\
&= e^{-i\pi J_2}e^{2i\varphi J_3}\,|k,\hat{\boldsymbol{e}}_3\rangle \\
&= e^{-i\pi J_2}e^{2ik\varphi}\,|k,\hat{\boldsymbol{e}}_3\rangle\,.
\end{aligned} \tag{9.79}$$

This shows that at the south pole different normalised state vectors are obtained as φ varies in the range $0 \le \varphi < 2\pi$. φ also varies in the range $0 \le \varphi < 2\pi$ at the north pole but $|k,\theta,\varphi\rangle$ is single valued at the north pole because as a result of the inclusion of the rotation $\mathcal{R}_3(-\varphi)$ in the definition of $\mathcal{R}(\theta,\varphi)$, $|k,0,\varphi\rangle$ does not depend on φ. It is therefore a smooth single-valued vector function everywhere on S^2 except at the south pole.

A smooth vector-valued function which is well defined at the south pole but not at the north pole is obtained by a gauge transformation (9.15), namely

$$|k,\theta,\varphi\rangle' = e^{-i2k\varphi}\,|k,\theta,\varphi\rangle = e^{-i\varphi J_3}e^{-i\theta J_2}e^{i\varphi J_3}e^{-i2k\varphi}\,|k,0,0\rangle \tag{9.80}$$

$$= e^{-i\varphi J_3}e^{-i\theta J_2}e^{-i\varphi J_3}\,|k,0,0\rangle\,. \tag{9.81}$$

The new state vector $|k,\theta,\varphi\rangle'$ differs from $|k,\theta,\varphi\rangle$ by the phase factor $e^{i\zeta_k(\theta,\varphi)} = e^{-i2k\varphi}$. At the south pole $|k,\theta,\varphi\rangle'$ evaluates to a single vector

$$|k,\pi,\varphi\rangle = e^{-i\pi J_2}\,|k,\hat{\boldsymbol{e}}_3\rangle \tag{9.82}$$

but at the north pole it evaluates to many vectors

$$|k, 0, \varphi\rangle' = e^{-2ik\varphi} |k, \hat{\boldsymbol{e}}_3\rangle \,. \tag{9.83}$$

Hence $|k, \theta, \varphi\rangle$ can be used everywhere on S^2 except at the north pole. Either vector (9.70) or (9.80) can be used in the overlap region $O_1 \cap O_2$ of the two open patches

$$O_1 := S^2 \setminus \{\mathcal{S}\} \quad \text{and} \quad O_2 := S^2 \setminus \{\mathcal{N}\}, \tag{9.84}$$

of S^2.

The state vector $|k, \pi, \varphi\rangle'$ is an eigenvector of J_3 with eigenvalue $-k$ and an eigenvector of $\hat{\boldsymbol{R}}(\pi, \varphi) \cdot \boldsymbol{J} = -\boldsymbol{e}_3 \cdot \boldsymbol{J} = -J_3$ with eigenvalue k.

We thus see that two different parameterisations of $|k, \hat{\boldsymbol{R}}\rangle$ are needed. However, since $|k, \theta, \varphi\rangle$ and $|k, \theta, \varphi\rangle'$ differ only by the phase factor $e^{-i2k\varphi}$ the projection operators and corresponding subspaces rays in the Hilbert space coincide:

$$|k, \theta, \varphi\rangle \langle k, \theta, \varphi| = |k, \theta, \varphi\rangle' \langle k, \theta, \varphi|' \tag{9.85}$$

Calculating the Mead-Berry Connection and the Berry Phase for Adiabatic Evolutions

We next calculate the Mead-Berry connection one-form A^k for adiabatic evolution of the Hamiltonian (9.62) using the previously derived formula (9.36). By definition

$$A^k(R) = A^k_i dR^i = i \langle k, R| \frac{\partial}{\partial R^i} |k, R\rangle \, dR^i, \tag{9.86}$$

where $i = 1, 2$ correspond to the coordinates θ and φ of either of the patches O_1 or O_2 of the sphere S^2.

On the patch O_1 in which (9.70) holds, we have

$$\begin{aligned} A^k_\theta &= i \langle k, \theta, \varphi| \frac{\partial}{\partial \theta} |k, \theta, \varphi\rangle \\ &= \langle k, \hat{\boldsymbol{e}}_3| \, iU^\dagger(\theta, \varphi) \frac{\partial}{\partial \theta} U(\theta, \varphi) \, |k, \hat{\boldsymbol{e}}_3\rangle =: r \hat{A}_\theta, \end{aligned} \tag{9.87}$$

$$\begin{aligned} A^k_\varphi &= i \langle k, \theta, \varphi| \frac{\partial}{\partial \varphi} |k, \theta, \varphi\rangle \\ &= \langle k, \hat{\boldsymbol{e}}_3| \, iU^\dagger(\theta, \varphi) \frac{\partial}{\partial \varphi} U(\theta, \varphi) \, |k, \hat{\boldsymbol{e}}_3\rangle := r \sin\theta \hat{A}_\varphi, \end{aligned} \tag{9.88}$$

where $\hat{A}_\theta$ and $\hat{A}_\varphi$ are defined for future use. Next we compute

$$\begin{aligned} iU^\dagger(\theta,\varphi)\frac{\partial}{\partial\theta}U(\theta,\varphi) &= ie^{-i\theta J_3}e^{i\theta J_2}e^{i\varphi J_3}\frac{\partial}{\partial\theta}e^{-i\varphi J_3}e^{-i\theta J_2}e^{i\varphi J_3} \\ &= ie^{-i\theta J_3}e^{i\theta J_2}e^{i\varphi J_3}e^{-i\varphi J_3}(-iJ_2)e^{-i\theta J_2}e^{i\varphi J_3} \\ &= e^{-i\varphi J_3}J_2e^{i\varphi J_3} \\ &= J_2\cos\theta - J_1\sin\varphi, \end{aligned} \tag{9.89}$$

$$\begin{aligned} iU^\dagger(\theta,\varphi)\frac{\partial}{\partial\varphi}U(\theta,\varphi) &= ie^{-i\theta J_3}e^{i\theta J_2}e^{i\varphi J_3}\frac{\partial}{\partial\varphi}e^{-i\varphi J_3}e^{-i\theta J_2}e^{i\varphi J_3} \\ &= ie^{-i\theta J_3}e^{i\theta J_2}e^{i\varphi J_3}(-iJ_3)e^{-i\varphi J_3}e^{-i\theta J_2}e^{i\varphi J_3} \\ &\quad + ie^{-i\theta J_3}e^{i\theta J_2}e^{i\varphi J_3}e^{-i\varphi J_3}e^{-i\theta J_2}(iJ_3)e^{i\varphi J_3} \\ &= e^{-i\varphi J_3}(J_3\cos\theta - J_1\sin\theta)e^{i\varphi J_3} - J_3 \\ &= -\sin\theta(J_1\cos\varphi + J_2\sin\varphi) + J_3(cos\theta - 1). \end{aligned} \tag{9.90}$$

Substituting (9.89) and (9.90) in (9.87) and (9.88), we find

$$A^k_\theta(\theta,\varphi) = \langle k,\hat{\boldsymbol{e}}_3|\,(J_2\cos\varphi - J_1\sin\varphi)\,|k,\hat{\boldsymbol{e}}_3\rangle\,, \tag{9.91}$$

$$\begin{aligned} A^k_\varphi(\theta,\varphi) = \langle k,\hat{\boldsymbol{e}}_3| &- (J_1\cos\varphi + J_2\sin\varphi)\sin\theta \\ &+ J_3(\cos\theta - 1)\,|k,\hat{\boldsymbol{e}}_3\rangle\,. \end{aligned} \tag{9.92}$$

Leading us to

$$A^k_\theta(\theta,\varphi) = 0, \tag{9.93}$$

$$\begin{aligned} A^k_\varphi(\theta,\varphi) &= \langle k,\hat{\boldsymbol{e}}_3|\,J_3(\cos\theta - 1)\,|k,\hat{\boldsymbol{e}}_3\rangle \\ &= -k(1-\cos\theta), \quad \theta \neq \pi. \end{aligned} \tag{9.94}$$

Next we repeat the same calculation in the patch O_2 in which the basis vectors $|k,\theta,\varphi\rangle'$ of (9.80) are single valued. This leads to

$$A'^k_\varphi = \langle k,\hat{\boldsymbol{e}}_3|\,(J_2\cos\varphi - J_1\sin\varphi)\,|k,\hat{\boldsymbol{e}}_3\rangle\,, \tag{9.95}$$

$$\begin{aligned} A'^k_\varphi = \langle k,\hat{\boldsymbol{e}}_3| &- (J_1\cos\varphi + J_2\sin\varphi)\sin\theta \\ &+ J_3(\cos\theta - 1) + 2k\,|k,\hat{\boldsymbol{e}}_3\rangle\,. \end{aligned} \tag{9.96}$$

The components of the Mead-Berry connection one-form are then given by

$$A'^k_\theta = 0, \tag{9.97}$$

$$A'^k_\varphi = k(cos\theta + 1), \quad \theta \neq 0. \tag{9.98}$$

According to the general theory of Section 2 we expect A^k to transform according to (9.42). So with $\zeta = -2k\varphi$ we receive

$$A'^k - A^k = -d\zeta(\theta,\varphi) = d(2k\varphi) = 2kd\varphi. \tag{9.99}$$

Having obtained the expression for the Mead-Berry connection one-form, we next compute the corresponding curvature two-form. According to (9.55) this is given by

$$F^k = dA^k = \frac{\partial A^k_\theta}{\partial \varphi} d\varphi \wedge d\theta + \frac{\partial A^k_\varphi}{\partial \theta} d\theta \wedge d\varphi \tag{9.100}$$

In view of (9.93) and (9.94) we obtain

$$F^k = F^k_{\theta\varphi} d\theta \wedge d\varphi = -k \sin\theta d\theta \wedge d\varphi. \tag{9.101}$$

We can now use the formula (9.58) to calculate the Berry phase angle for a closed path $\boldsymbol{C}$,

$$\gamma_k(\boldsymbol{C}) = \int_S F^k = -k \int_S \sin\theta d\theta \wedge d\varphi = -k \int_S d\Omega \mod 2\pi, \tag{9.102}$$

where S is any surface, which has the closed curve $\boldsymbol{C}$ as its boundary, and where $d\Omega$ is the element of solid angle. Here we take the direction in which $\boldsymbol{C}$ is traversed, to be right handed with respect to the surface normal of S (see figure 9.2).

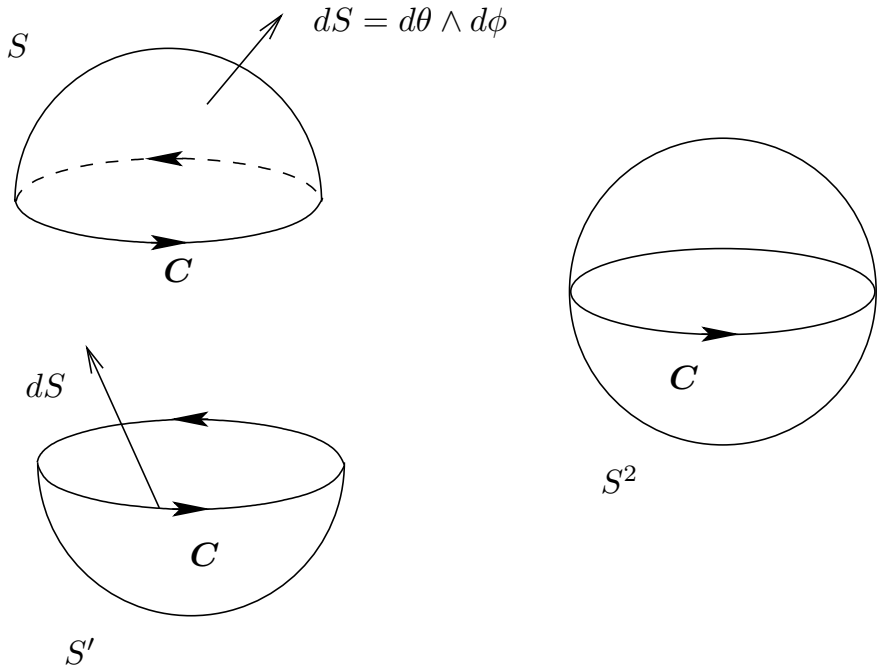

Figure 9.2: The difference of the line integrals of A and A' can transformed, using Stoke's theorem, into an integral over a closed 2-surface $S \cup S'$.

Denoting by $\Omega(\boldsymbol{C})$ the solid angle subtended by $\boldsymbol{C}$, i.e.,

$$\Omega(\boldsymbol{C}) := \int_S \sin\theta d\theta \wedge d\varphi, \tag{9.103}$$

we can write (9.102) in the form

$$\gamma_k(\boldsymbol{C}) = -k\Omega(\boldsymbol{C}) \qquad \text{mod } 2\pi. \tag{9.104}$$

As explained in section 2, unlike the single-valued basis vectors $|k, \theta, \varphi\rangle$ and the connection one-form A^k, the curvature two-form F^k is independent of the choice of local coordinates. Therefore in (9.102) we can use a surface $S \subset O_1$ or a surface $S' \subset O_2$, as long as both S and S' have $\boldsymbol{C}$ as their boundaries, i.e., $\partial S = \boldsymbol{C} = \partial S'$ (see figure 9.2). In order to investigate the consequences of this property of the curvature two-form, we next compute the Berry phase angle using S'. This yields

$$\gamma(\boldsymbol{C}) = \int_{S'} F^k = -k \int_{S'} \sin\theta d\theta \wedge d\varphi = k \int_{S^2 \setminus S} \sin\theta d\theta \wedge d\varphi, \tag{9.105}$$

$$= k \left(\int_{S^2} \sin\theta d\theta \wedge d\varphi - \int_S \sin\theta d\theta \wedge d\varphi \right). \tag{9.106}$$

where the direction of the normal of S' and the direction in which $\boldsymbol{C}$ is traversed are again given by the right-hand rule. This means that the normal of S' points into the sphere and the normal of S points out of the sphere. As the integral of $d\Omega$ over the whole unit sphere is 4π and the integral over S is given by (9.103) we obtain

$$\gamma_k(\boldsymbol{C}) = k(4\pi - \Omega(\boldsymbol{C})) \qquad \text{modulo } 2\pi. \tag{9.107}$$

Comparing (9.107) and (9.104), we find that

$$-k\Omega(\boldsymbol{C}) = 4\pi k - k\Omega(\boldsymbol{C}) \qquad \text{modulo } 2\pi, \tag{9.108}$$

which can only be satisfied if

$$k = 0, \pm\frac{1}{2}, \pm 1, \frac{3}{2}, \pm 2, \ldots \tag{9.109}$$

Thus we conclude that k must be an integer or a half-integer.

If the basis vectors (9.70) and (9.80) are also eigenvectors of $\boldsymbol{J}^2$ as they happen to be in our example, then the possible values of k must automatically be (9.109) But if these vectors are not $\boldsymbol{J}^2$eigenvectors - as is the case for a molecule - then (9.109) still holds.

So far $\boldsymbol{C}$ could have been any closed path on the unit sphere. We will now calculate the Berry phase for the special path $\boldsymbol{C}_1 : [0, T] \to S^2$

$$\boldsymbol{C}_1(t) := R(\theta(t), \varphi(t)) = R(\theta = \text{const}, \varphi = \omega t), \tag{9.110}$$

yielding the phase

$$\gamma_k(\boldsymbol{C}_1) = -k \int_0^{2\pi} \int_0^{\theta} \sin\theta' d\theta' d\varphi = -2\pi k(1 - \cos\theta). \tag{9.111}$$

Substituting (9.111) and (9.66) in (9.40) we obtain the expression for the adiabatically evolving state vector,

$$\psi(t) \overset{\text{adiabatic}}{=} e^{-ibtk} e^{i\gamma_k(t)} \left|k, \theta, \omega t\right\rangle, \tag{9.112}$$

$$\omega = \frac{2\pi}{T}, \quad \gamma_k(t) = \frac{t}{T}\gamma_k(\boldsymbol{C}). \tag{9.113}$$

In particular for $t = T$, we obtain from (9.51)

$$\psi(T) \overset{\text{adiabatic}}{=} e^{-i2\pi\frac{b}{\omega}k} e^{i\gamma_k(\boldsymbol{C})}\psi(0), \quad \psi(0) = \left|k, \theta, 0\right\rangle. \tag{9.114}$$

Using the fact that S^2 is a sub-manifold of $\mathbb{R}^3$ we re-express our results in terms of the Mead-Berry (three-)vector potential $\boldsymbol{A}^k$ (9.35) and the curvature (three-)vector of the field strength $\boldsymbol{F}^k$. To compute $\boldsymbol{A}^k$, we may view the connection one-form A^k as a one-form in $\mathbb{R}^3$, i.e.,

$$A^k = A^k_r dr + A^k_\theta d\theta + A^k_\varphi d\varphi,$$

where A^k_θ and A^k_φ are given by (9.93) and (9.94) and $A^k_r = 0$. Next we write A^k in a new (Cartesian) basis $(dr, rd\theta, r\sin\theta d\varphi)$:

$$A^k = \hat{A}^k_r dr + \hat{A}^k_\theta r d\theta + \hat{A}^k_\varphi r\sin\theta d\varphi.$$

The new components $\hat{A}^k_r = A^k_r = 0$, $\hat{A}^k_\theta = 0$, and $\hat{A}^k_\varphi$ are called the spherical components of A^k. They yield the components of the Mead-Berry vector potential in the spherical coordinates,

$$\boldsymbol{A}^k = \hat{A}^k_r \hat{\boldsymbol{e}}_r + \hat{A}^k_\theta \hat{\boldsymbol{e}}_\theta + \hat{A}^k_\varphi \hat{\boldsymbol{e}}_\varphi, \tag{9.115}$$

where $\hat{\boldsymbol{e}}_r$, $\hat{\boldsymbol{e}}_\theta$ and $\hat{\boldsymbol{e}}_\varphi$ are the unit vectors in $\mathbb{R}^3$ along the r, θ and φ directions, respectively. Leading us to

$$\boldsymbol{A}^k(\theta, \varphi) = \frac{k(cos\theta - 1)}{r\sin\theta}\hat{\boldsymbol{e}}_\varphi, \quad \theta \neq \pi. \tag{9.116}$$

Repeating the same computations in the coordinate patch O_2, we find

$$\boldsymbol{A}'^k = \frac{k(\cos\theta + 1)}{r\sin\theta}\hat{\boldsymbol{e}}_\varphi, \quad \theta \neq 0. \tag{9.117}$$

$\boldsymbol{A}'^k$ is related to $\boldsymbol{A}^k$ by the gauge transformation

$$\boldsymbol{A}'^k - \boldsymbol{A}^k = -\nabla\zeta = \frac{2k}{r\sin\theta}\hat{\boldsymbol{e}}_\varphi, \tag{9.118}$$

where $\zeta = -2k\varphi$.

More interestingly, we can compute the curvature three-vector,

$$\boldsymbol{F}^k = -\frac{k}{r^2}\hat{\boldsymbol{e}}_r = -\frac{k}{r^2}\hat{\boldsymbol{R}}(\theta,\varphi). \tag{9.119}$$

This can be obtained either by taking the curl of the vector potential or using the identity

$$F^k = F^k_{\theta\varphi} d\theta \wedge d\varphi = -k\sin\theta d\theta \wedge d\varphi = \hat{F}^k_r (r d\theta)(r\sin\theta d\varphi) = \boldsymbol{F}^k \cdot d\boldsymbol{S},$$

to read off $\boldsymbol{F}^k$ directly.

As seen from (9.119) the curvature three-vector (field strength) is directed along the radial direction $\hat{\boldsymbol{e}}_r = \hat{\boldsymbol{R}}(\theta,\varphi)$. It has the familiar form of the magnetic field of a monopole.

The Exact Solution of the Schrödinger Equation

In the preceding section we employed the results of section 2 to compute the Berry phase. Hence we used the adiabatic approximation in our computations without checking for the validity. In this section we shall explore the exact time-evolution of the state vector $\psi(t)$ which satisfies the Schrödinger equation

$$i\frac{\partial}{\partial t}\psi(t) = H(t)\psi(t), \text{ with } H(t) = b\hat{\boldsymbol{R}}(\theta,\omega t)\cdot\boldsymbol{J}. \tag{9.120}$$

In particular we are interested in the solutions of (9.120) which describe cyclic evolutions (9.18):

$$|\psi(\tau)\rangle\langle\psi(\tau)| = |\psi(0)\rangle\langle\psi(0)|. \tag{9.121}$$

In the adiabatic approximation the period τ is given by the period of the precession of the magnetic field, $\tau = T = \frac{2\pi}{\omega}$.

The expression (9.112) for the state vector is, as we showed in section 2, incompatible with the Schrödinger equation (9.120) and can only be approximations. For the example considered here, (9.120) can be exactly solved. In particular the cyclic solutions are known.

In order to find the exact solution of the Schrödinger equation (9.120), we proceed in the following way. The magnetic field (9.65) rotates counter-clockwise by an angle ωt about the $\boldsymbol{e}_3$ axis. Instead of rotating the observables (Hamiltonian, etc.) counterclockwise and keeping the state vector the same (in the laboratory frame) we can rotate the state vector $\psi(t)$ clockwise (by an angle $-\omega t$) about the $\boldsymbol{e}_3$ axis and keep the observables the same (view the magnetic field from a frame which rotates with the field, such that the field appears stationary). For the observable quantities (expectation values) these two points of view give the same result, e.g.,

$$\begin{aligned}\langle\psi(t)|H(t)|\psi(t)\rangle &= \langle\psi(t)|e^{-i\omega t J_3}H_0 e^{i\omega t J_3}|\psi(t)\rangle \\ &= \left\langle e^{i\omega t J_3}\psi(t)\right| H_0 \left|e^{i\omega t J_3}\psi(t)\right\rangle.\end{aligned} \tag{9.122}$$

This suggests the following unitary transformation of the state vector $\psi(t)$.

$$\psi(t) \to \psi'(t) := \tilde{U}(t)\psi(t) = e^{i\omega t J_3}\psi(t). \tag{9.123}$$

Inserting $\psi(t) = \tilde{U}^\dagger(t)\psi'(t)$ into the Schrödinger equation (9.120) for $\psi(t)$, we obtain the Schrödinger equation for $\psi'(t)$,

$$\begin{aligned} i\frac{\partial}{\partial t}e^{-i\omega t J_3}\psi'(t) &= H(t)e^{-i\omega t J_3}\psi'(t) \\ e^{-i\omega t J_3}i\frac{\partial}{\partial t}\psi'(t) &= (-\omega J_3 e^{-i\omega t J_3} + H(t)e^{-iwt J_3})\psi'(t) \\ i\frac{\partial}{\partial t}\psi'(t) &= (-\omega J_3 + e^{i\omega t J_3}H(t)e^{-i\omega t J_3})\psi'(t) := H'(t)\psi'(t). \end{aligned} \tag{9.124}$$

The state vector $\psi'(t)$ evolves in time according to the transformed Hamiltonian

$$H(t) := \tilde{U}H\tilde{U}^\dagger - i\tilde{U}\frac{\partial \tilde{U}^\dagger}{\partial t} = e^{i\omega t J_3}H(t)e^{-i\omega t J_3} - \omega J_3. \tag{9.125}$$

However the operator H' does not depend on time, for

$$H' = H_0 - \omega J_3 = b\left(\cos\theta J_3 + \sin\theta J_1 - \frac{\omega}{b}J_3\right) \tag{9.126}$$

This was to be expected since in the rotating frame $\boldsymbol{B}$ does not change. Because H' is time independent, (9.124) can be immediately integrated. The result is

$$\psi'(t) = e^{-itH'}\psi'(0). \tag{9.127}$$

The operator H' can also be related expressed as

$$H' = \Omega \boldsymbol{e}\cdot\boldsymbol{J}, \tag{9.128}$$

where

$$\boldsymbol{e} := \frac{b}{\Omega}\left(\cos\theta - \frac{\omega}{b}\right)\boldsymbol{e}_3 + \frac{b}{\Omega}\sin\theta\boldsymbol{e}_1, \tag{9.129}$$

$$\Omega := b\sqrt{1 + \frac{\omega}{b}\left(\frac{\omega}{b} - 2\cos\theta\right)}. \tag{9.130}$$

The unit vector $\boldsymbol{e}$ lies in the 1-3 plane. Therefore it can be written in the form

$$\boldsymbol{e} = \cos\tilde{\theta}\boldsymbol{e}_3 + \sin\tilde{\theta}\boldsymbol{e}_1 = \hat{\boldsymbol{R}}(\tilde{\theta}, 0), \tag{9.131}$$

where $\tilde{\theta}$ is the angle between $\boldsymbol{e}$ and $\boldsymbol{e}_3$, i.e.

$$\begin{aligned} \cos\tilde{\theta} &:= \frac{b}{\Omega}\left(\cos\theta - \frac{\omega}{b}\right) = \frac{\cos\theta - \nu}{\sqrt{1 - 2\nu\cos\theta + \nu^2}}, \\ \sin\tilde{\theta} &= \frac{b}{\Omega}\sin\theta = \frac{\sin\theta}{\sqrt{1 - 2\nu\cos\theta + \nu^2}}, \end{aligned} \tag{9.132}$$

and ν is a dimensionless parameter given by

$$\nu := \frac{\omega}{b}. \tag{9.133}$$

In view of (9.128), the time development given by (9.127) represents a 'rotation' of the state vector $\psi'(0)$ by an angle Ωt about the $\boldsymbol{e}$-axis,

$$\psi'(t) = e^{-i\Omega t\boldsymbol{e}\cdot\boldsymbol{J}}\psi'(0). \tag{9.134}$$

Having obtained the exact expression for $\psi'(t)$ we now transform back to the laboratory frame. Using (9.123) and (9.127), we find

$$\psi(t) = e^{-i\omega tJ_3}e^{-itH'}\psi(0). \tag{9.135}$$

Therefore the solution of the Schrödinger Equation (9.120) for arbitrary initial state vector $\psi(0)$ is given by

$$\psi(t) = e^{-i\omega tJ_3}e^{-i\Omega t\boldsymbol{e}\cdot\boldsymbol{J}}\psi(0) =: U^{\dagger}(t)\psi(0). \tag{9.136}$$

This means that the evolving state $\psi(t)$ is obtained from $\psi(0)$ by transforming $\psi(0)$ by the unitary time-evolution operator $U^{\dagger}(t)$ representing a rotation by Ωt along $\boldsymbol{e}$ followed by a rotation by ωt along $\boldsymbol{e}_3$.

The relation between (θ, φ) and $(\tilde{\theta}, \varphi)$, i.e., (9.132), involves the physical parameter ν. This relation can be expressed in terms of a function $F_\nu : M = S^2 \to S^2$ which (on the patch O_1 including the north pole) is given by

$$\begin{aligned} F_\nu(\hat{\boldsymbol{R}}(\theta,\varphi)) = F_\nu(\theta,\varphi) &= \left(\arccos\left(\frac{\cos\theta - \nu}{\sqrt{\nu^2 - 2\cos\theta\nu + 1}}\right), \varphi\right) \\ &= (\tilde{\theta}, \varphi) = \hat{\boldsymbol{R}}(\tilde{\theta}, \varphi). \end{aligned} \tag{9.137}$$

A global expression for F_ν may be obtained by viewing the sphere S^2 as embedded in $\mathbb{R}^3$. It is given by

$$F_\nu(x^1, x^2, x^3) = \frac{(x^1, x^2, x^3 - \nu)}{\sqrt{(x^1)^2 + (x^2)^2 + (x^3 - \nu)^2}}, \tag{9.138}$$

where $(x^1, x^2, x^3) \in \mathbb{R}^3$. For $\nu < 1$, the function F_ν is a smooth diffeomorphism of S^2 and consists of a translation in the $\boldsymbol{e}_3$ direction followed by a projection along $\boldsymbol{R}$ onto S^2.

Examining the condition (9.26) of validity of the adiabatic approximation it is not difficult to see that for our example (9.62), the left-hand side of (9.26) is proportional to the frequency ω of the precession of the magnetic field. since the intrinsic frequency scale of the system is given by b, the adiabatic approximation is valid if and only if $\nu = \omega/b \ll 1$.

The frequency b is the angular velocity with which the state vector $\psi(t)$ rotates about the direction of the magnetic field $\hat{\boldsymbol{R}}(\theta,0)$. For $\omega = 2\pi/T = 0$ ($\nu = 0$),

$$\psi(t) = e^{-itb\hat{\boldsymbol{R}}(\theta,0)\cdot\boldsymbol{J}}\psi(0). \tag{9.139}$$

This is most evident if we use (9.129) and (9.133) to rewrite (9.136) in the form

$$\begin{aligned}\psi(t) &= e^{-it\omega J_3}e^{-it\Omega\hat{\boldsymbol{R}}(\tilde{\theta},0)\cdot\boldsymbol{J}}\psi(0),\\ &= e^{-itb\nu J_3}e^{-itb(\hat{\boldsymbol{R}}(\theta,0)\cdot\boldsymbol{J}-\nu J_3)}\psi(0),\end{aligned} \tag{9.140}$$

and then specialise to the case $\nu = 0$. Equation (9.139) gives the time-evolution of a state vector $\psi(0)$ for the time-independent Hamiltonian

$$H = b\hat{\boldsymbol{R}}(\theta,0)\cdot\boldsymbol{J}, \quad \theta = \text{constant}. \tag{9.141}$$

Having obtained the exact solution (9.140) of the Schrödinger equation (9.120) we can identify the cyclic solutions, i.e., the solutions which satisfy (9.121). By definition the cyclic solutions with period τ are obtained by choosing the initial state vector $\psi(0)$ to be an eigenvector of the evolution operator

$$U^{\dagger}(\tau) = e^{-i\tau\omega J_3}e^{-i\tau\Omega\hat{\boldsymbol{R}}(\tilde{\theta},0)\cdot\boldsymbol{J}}. \tag{9.142}$$

The corresponding eigenvalue $e^{-i\alpha_\psi}$ is the total phase factor, for

$$\psi(\tau) = U^{\dagger}(\tau)\psi(0) = e^{-i\alpha_\psi}\psi(0). \tag{9.143}$$

In general, in order to find the cyclic states for arbitrary τ, one must find the (non-stationary) eigenstates of the evolution operator (9.142). This is quite easy if τ is chosen in such a way that the initial state is an eigenstate of both of the operators appearing on the right-hand side of (9.142). In this case

$$\left[e^{-i\tau\omega J_3}, e^{-i\tau\Omega\hat{\boldsymbol{R}}(\tilde{\theta},0)\cdot\boldsymbol{J}}\right]|\psi(0)\rangle = 0. \tag{9.144}$$

It is not difficult to see that this condition is satisfied for $\tau = T = 2\pi/\omega$. There are other possible values for τ, but we're merely interested in $\tau = T$ since that is the period of our adiabatic cyclic solutions.

Cyclic solutions with a period $\tau = T$ are obtained by finding the simultaneous eigenvectors of the operators $e^{-i2\pi J_3}, e^{-iT\Omega\hat{\boldsymbol{R}}(\tilde{\theta},0)\cdot\boldsymbol{J}}$, and therefore the evolution operator

$$U^{\dagger}(T) = e^{-i2\pi J_3}e^{-iT\Omega\hat{\boldsymbol{R}}(\tilde{\theta},0)\cdot\boldsymbol{J}}. \tag{9.145}$$

These eigenvectors which we shall denote by ϕ_k are consequently also eigenvectors of the operator

$$H(\tilde{\theta},0) := b\hat{\boldsymbol{R}}(\tilde{\theta},0)\cdot\boldsymbol{J}, \tag{9.146}$$

i.e., they satisfy

$$H(\tilde{\theta},0)\,|\phi_k\rangle = bk\,|\phi_k\rangle\,; \qquad \boldsymbol{e}\cdot\boldsymbol{J}\,|\phi_k\rangle = k\,|\phi_k\rangle\,. \tag{9.147}$$

From (9.70) and (9.71) with θ replaced by $\tilde{\theta}$ and ϕ by 0 it follows that ϕ_k is (up to a phase factor) given by

$$|\phi_k\rangle = |k,\tilde{\theta},0\rangle = U(\tilde{\theta},0)\,|k,\boldsymbol{e}_3\rangle = e^{-i\tilde{\theta}J_2}|k,\boldsymbol{e}_3\rangle. \tag{9.148}$$

to obtain eigenvalues of $e^{-i2\pi J_3}$ we proceed using (9.74) with $\varphi = 2\pi$. This yields

$$\begin{aligned} e^{-i2\pi J_3}\phi_k &= e^{-i2\pi J_3}|k,\tilde{\theta},0\rangle = e^{-i2\pi J_3}e^{-i\tilde{\theta}J_2}\,|k,0,0\rangle \\ &= e^{-i\tilde{\theta}J_2}e^{-i2\pi J_3}\,|k,0,0\rangle \\ &= e^{-i2\pi k}|k,\tilde{\theta},0\rangle. \end{aligned} \tag{9.149}$$

The initial state vectors which lead to a cyclic evolution with period $T = 2\pi/\omega$ are thus labelled by integers of half-integers k and given by (9.148),

$$|\psi(0)\rangle = |\phi_k\rangle = |k,\tilde{\theta},0\rangle, \tag{9.150}$$

(after an arbitrary phase factor has been fixed). The total phase of these cyclic evolutions, i.e., the eigenvalues $e^{-i\alpha_\psi}$ of (9.143) are also labelled by k and given by

$$\psi(T) = U^\dagger(T)\psi(0) = e^{-i\alpha_k}\psi(0) = e^{-i2\pi k}e^{-i2\pi\frac{\Omega}{\omega}k}\psi(0). \tag{9.151}$$

Thus, in this case, the possible initial states of an cyclic evolution are very similar to the initial states of an adiabatic evolution. The only difference is that the initial states of an adiabatic evolution are given by the eigenvectors $|k,\theta,0\rangle$ of the initial Hamiltonian $H(R(0)) = b\hat{\boldsymbol{R}}(\theta,0)\cdot\boldsymbol{J}$, whereas the initial states of the exact cyclic evolutions are given by the eigenvectors (9.148) of the operator

$$\tilde{H}(\theta,0) := H(\tilde{\theta},0) = b\hat{\boldsymbol{R}}(\tilde{\theta},0)\cdot\boldsymbol{J}, \tag{9.152}$$

which is different from $H(R(0))$.

The exact cyclic states are the states with the component k of angular momentum along the direction $\boldsymbol{e} = \hat{\boldsymbol{R}}(\tilde{\theta},0)$ rather than $\hat{\boldsymbol{R}}(\theta,0)$. For large values of ω ($\omega \approx b$) these to directions can be very different, but for $\nu = \omega/b \to 0$ they coincide.

We will next determine the analogue of the single-valued eigenvectors $|k,R(t)\rangle = |k,\theta(t),\varphi(t)\rangle$ which are used in the calculation of the Mead-Berry connection one-form and Berry phase. These vectors $\phi_k(t)$ lie on a curve "above" the closed curve

$$\mathcal{C} : t \to |\psi(t)\rangle\langle\psi(t)|; \qquad |\psi(T)\rangle\langle\psi(T)| = |\psi(0)\rangle\langle\psi(0)|. \tag{9.153}$$

in the state space $\mathcal{P}(\mathcal{H})$. This means that they fulfil

$$\phi_k(t) = \text{phase factor} \times \psi(t), \text{ and } \phi_k(T) = \phi_k(0). \tag{9.154}$$

There are many such vectors all differing by a phase transformation,

$$\phi_k(t) \to \phi'_k(t) = e^{i\zeta_k(t)}\phi_k(t), \quad \zeta_k(0) = \zeta_k(T) \qquad \text{modulo } 2\pi. \tag{9.155}$$

One and by far the most obvious choice for $\phi_k(t)$ is

$$\begin{aligned}\phi_k(t) &:= U(\tilde{\theta}, \omega t)|k, \boldsymbol{e}_3\rangle \\ &= e^{-i\omega t J_3} e^{-i\tilde{\theta} J_2} e^{i\omega t k}|k, \boldsymbol{e}_3\rangle =: |k, \tilde{\theta}, \omega t\rangle.\end{aligned} \tag{9.156}$$

These single-valued basis vectors $|k, \tilde{\theta}, \varphi = \omega t\rangle$ are eigenvectors of the operator

$$\tilde{H}(\theta, \varphi) := H(\tilde{\theta}, \varphi) = H(F_\nu(\theta, \varphi)) = b\hat{\boldsymbol{R}}(\tilde{\theta}, \varphi) \cdot \boldsymbol{J}, \tag{9.157}$$

where F_ν is the function given by (9.137). The operator $\tilde{H}(R) = H(F_\nu(R))$ is not the Hamiltonian but another parameter-dependent operator which can as well serve to define an orthonormal basis of the Hilbert space $\mathcal{H}$. In terms of the known vectors $|k, \tilde{\theta}, \varphi\rangle$, the cyclic solution of the Schrödinger equation (9.120) is given by

$$\psi(t) = e^{-i\omega t k} e^{-i\Omega t k}|k, \tilde{\theta}, \omega t\rangle. \tag{9.158}$$

This relation expresses the cyclically evolving state vector $\psi(t)$ in terms of the known quantities ω, Ω and $|k, \tilde{\theta}, \omega t\rangle$. It is the generalisation of the "adiabatic equality" (9.112). Similarly, (9.151) is the generalisation of (9.114). However the phase factor in (9.158) and (9.151) is not in the form of a product of the dynamical and the geometrical parts. Thus, in order to obtain an expression for each part, we must calculate at least on of them independently.

Dynamical and Geometrical Phase Factors for Non-Adiabatic Evolution

The splitting of the phase factor into a *dynamical* and a *geometrical* part can be performed in two different ways. Either one gives an argument why a certain part of the total phase is geometrical and obtains the dynamical part as the difference between the total and the geometrical part, or one defines the dynamical part and obtains the geometrical part as the difference between the total and the dynamical part. We will pursue the latter approach, namely define the dynamical phase angle α_k^{dyn} and obtain the geometrical phase angle α_k^{geom} as a derived quantity,

$$\alpha_k^{\text{geom}} = \alpha_k - \alpha_k^{\text{dyn}}. \tag{9.159}$$

The dynamical phase (angle) for general cyclic evolution is defined as

$$\alpha_k^{\rm dyn} := \int_0^T \langle\psi(t)|H(t)|\psi(t)\rangle dt, \tag{9.160}$$

the phase angle for the evolution of a stationary state as in (9.29).

We can easily calculate the dynamical phase (9.160) for the Hamiltonian (9.62),

$$\alpha_k^{\rm dyn} = k2\pi\left(\frac{\omega}{\Omega} + \cos\tilde{\theta}\right). \tag{9.161}$$

Using (9.159) and (9.151), we then find

$$\alpha_k^{\rm geom} = k2\pi(1-\cos\tilde{\theta}) = k2\pi\left(1+\frac{\omega}{\Omega} - \frac{b}{\Omega}\cos\theta\right). \tag{9.162}$$

This has the same form as (9.111) for the adiabatic case except that θ is replaced by $\tilde{\theta}$ of (9.132).

In the adiabatic approximation, $\nu = \omega/b \ll 1$, we can expand the expressions (9.130) and (9.132) with respect to ν. Up to first order in ν, we have

$$\frac{\omega}{b} \approx 1 - \nu\cos\theta, \tag{9.163}$$

$$\sin\tilde{\theta} \approx \sin\theta + \frac{\nu}{2}\sin 2\theta, \tag{9.164}$$

$$\cos\tilde{\theta} \approx \cos\theta + \frac{\nu}{2}(\cos 2\theta - 1) \tag{9.165}$$

From this we conclude that the adiabatic approximation of the geometrical phase angle for a general cyclic evolution (9.162) is identical with the Berry phase angle,

$$-\alpha_k^{\rm geom} \approx -2\pi k(1-\cos\theta) = \gamma_k^{\rm Berry}. \tag{9.166}$$

These results justify the choice of (9.159) as a definition of the geometrical phase for the general cyclic evolution. Next, we will show that the non-adiabatic geometric phase angle can be obtained from a connection one-form in the same way the Berry phase angle is obtained from the Mead-Berry connection one-form.

In analogy to (9.35) and (9.36), we define the following connection one-form

$$A^{\phi_k} := i\langle\phi_k|d|\phi_k\rangle, \tag{9.167}$$

and compute

$$\begin{aligned} A^{\phi_k} &= \langle k,\tilde{\theta},\varphi|d|k,\tilde{\theta},\varphi\rangle \\ &= \langle k,\tilde{\theta},\varphi|\frac{\partial}{\partial\tilde{\theta}}|k,\tilde{\theta},\varphi\rangle d\tilde{\theta} + \langle k,\tilde{\theta},\varphi|\frac{\partial}{\partial\varphi}|k,\tilde{\theta},\varphi\rangle d\varphi \\ &= \langle k,\tilde{\theta},\varphi|\frac{\partial}{\partial\tilde{\theta}}|k\tilde{\theta},\varphi\rangle\frac{\partial\tilde{\theta}}{\partial\theta}d\theta + \langle k,\tilde{\theta},\varphi|\frac{\partial}{\partial\varphi}|k,\tilde{\theta},\varphi\rangle d\varphi. \end{aligned} \tag{9.168}$$

Here we used the basis vectors given by (9.156), i.e., the eigenvectors of the operator $\tilde{H}(R)$. Comparing (9.168) with (9.86) and using (9.93) and (9.94), we conclude

$$A^{\phi_k} = -k(1-\cos\tilde{\theta})d\varphi = -k\left(1-\frac{b}{\Omega}\cos\theta+\frac{\omega}{\Omega}\right)d\varphi. \tag{9.169}$$

The curvature two-form (field strength) that follows from this connection one-form is given by

$$F^{\phi_k} = dA = -k\frac{1-\frac{\omega}{b}\cos\theta}{\left[1-\frac{\omega}{b}\cos\theta+\left(\frac{\omega}{b}\right)^2\right]^{3/2}}\sin\theta d\theta\wedge d\phi. \tag{9.170}$$

The component

$$F^{\phi_k}_{\theta\varphi} = -k\frac{1-\frac{\omega}{b}\cos\theta}{\left[1-\frac{\omega}{b}\cos\theta+\left(\frac{\omega}{b}\right)^2\right]^{3/2}}\sin\theta \tag{9.171}$$

of F^{ϕ_k} can be used to define the field strength (three-)vector

$$\boldsymbol{F}^{\phi_k} = -\frac{k}{r^2}\frac{1-\frac{\omega}{b}\cos\theta}{\left[1-\frac{\omega}{b}\cos\theta+\left(\frac{\omega}{b}\right)^2\right]^{3/2}}\hat{\boldsymbol{R}}(\theta,\varphi). \tag{9.172}$$

This is again a "monopole" type field similar to (9.119) but with modified "monopole strength". The connection one-form (9.169) has the same form as (9.94) for the Mead-Berry connection, except that here it depends on the angle $\tilde{\theta}$ which differs from the angle θ.

We can now use the analogue of (9.58) for the adiabatic approximation and define a geometric phase angle also for the general cyclic evolution by

$$\gamma_k := \oint_{\boldsymbol{C}} A^{\phi_k} = \oint i\langle\phi_k|d|\phi_k\rangle. \tag{9.173}$$

Then using (9.169), we obtain

$$\begin{aligned}\gamma_k &= -k\int_0^T(1-\cos\tilde{\theta})\omega dt\\ &= -2\pi k(1-\cos\tilde{\theta})\\ &= -2\pi k\left(1-\frac{b}{\Omega}\cos\theta+\frac{\omega}{\Omega}\right).\end{aligned} \tag{9.174}$$

This agrees with the result (9.166) obtained from (9.159) and (9.160).

With these results we can rewrite the cyclic solution (9.158) of the Schrödinger equation in a form which completely resembles the adiabatic approximation, i.e., (9.112),

$$\psi(t) = e^{-i\alpha_k^{\mathrm{dyn}}(t)} e^{i\gamma_k(t)} |k, \tilde{\theta}, \varphi\rangle, \tag{9.175}$$

where

$$\begin{aligned}
\alpha_k^{\mathrm{dyn}} &:= \int_0^t \langle\psi(t')|H(t')|\psi(t')\rangle dt' = \omega t k \left(\frac{\omega}{\Omega} + \cos\tilde{\theta}\right) \\
&= \frac{t\alpha_k}{T}, \\
\gamma_k(t) &:= \int_0^t i\langle\phi_k(t')|\frac{d}{dt'}|\phi_k(t')\rangle dt' \\
&= -k\int_0^t (1-\cos\tilde{\theta})\omega dt' = -\omega t k(1-\cos\tilde{\theta}) \\
&= \frac{t\gamma_k}{T}.
\end{aligned}$$

The concepts introduced in this section for the cyclic evolution, (9.153), are the analogues of the eigenvectors $|k, \theta, \varphi\rangle$ of the Hamiltonian. The connections A^{ϕ_k} of (9.169) are generalisations of the Mead-Berry phase (9.48).

The distinction between (9.175) and (9.112) is that in (9.175) we have an equality not an approximate one. This means that the pure state corresponding to $\psi(t)$ is indeed an exact cyclic evolution. If the frequency of the precession of the magnetic field ω is "small" enough, i.e., much smaller than the frequency b, then the curve (9.112) is "close enough" to (9.175), in order to provide an acceptable approximation for the geometric phase. Nevertheless an exact adiabatic cyclic evolution does not exist.

The geometrical phase (9.174) is not purely geometrical in the way that the Berry phase (9.166) is. Unlike the Berry phase that only depends on θ and is solely given by the path in the parameter space, the geometrical phase, for general cyclic evolution, also depends on the parameter $\nu = \omega/b$ of the Hamiltonian.

4 Experimental Verification of Berry's Phase

In 1986 Akira Tomita and Raymond Chiao [52] reported the first experimental verification of Berry's phase. The experiment consisted of a helically wound optical fibre inside which a linearly polarised photon could be adiabatically transported around a closed path in momentum space, with the polarisation of the photon being a direct measure for the Berry phase.

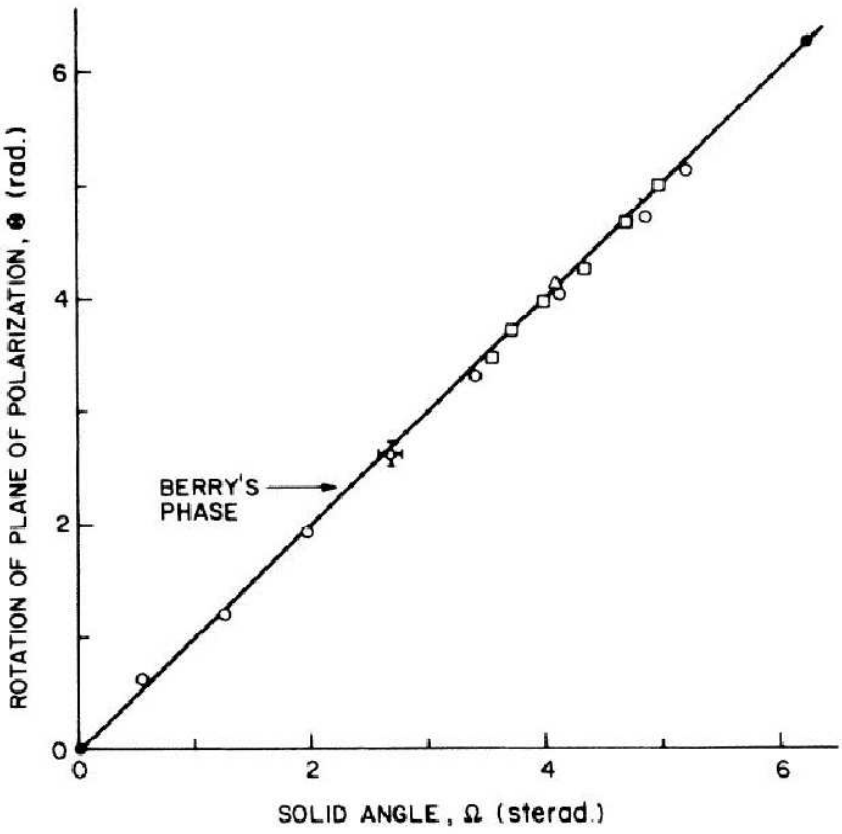

Figure 9.3: Measured angle of rotation of linearly polarised light vs calculated solid angle in momentum space. Open circles, the data for uniform helices; squares and triangle, nonuniform helices; solid circles, arbitrary planar paths. The solid line is the theoretical prediction.

The first Experiment

The parameter space of this system is the photon's momentum space, so in order to form a closed path in momentum or $\boldsymbol{k}$ space, the propagation directions of the input and output of the fibre were kept identical and the fibre was wound into a uniform helix, i.e., the pitch angle[26] θ was kept constant throughout the entire helix. Since the modulus of the photon's momentum k doesn't change as it propagates along the fibre, the parameter space reduces to the sphere S_k^2 with radius k. The constant pitch angle θ then corresponds to the photon tracing a

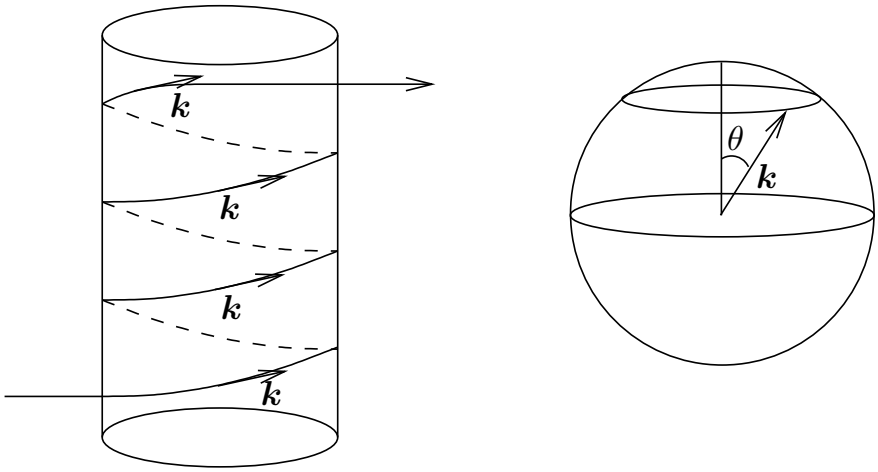

Figure 9.4: The momentum vector $\boldsymbol{k}$ of the photon traces a circle of constant longitude on the sphere S_k^2 in momentum space.

circle of constant longitude. So we have a situation that is very similar to what we encountered in section 3. Allowing us to reuse the formulae we computed. Formula (9.104) then go over to

$$\gamma(\boldsymbol{C}) = -\sigma\Omega(\boldsymbol{C}) = -2\pi\sigma(1-\cos\theta), \tag{9.176}$$

where $\sigma = \pm 1$ is the helicity quantum-number of the photon. Our previously formulated theory then predicts that $-\Omega(\boldsymbol{C})$ is the Berry phase for $\sigma = 1$, which corresponds to the angle φ of rotation of linear polarisation. As can be seen in the figure 9.3 the theory predicts the experimental results very accurately.

The second Experiment

In the second experiment the topological aspects[27] of the Berry phase were tested. The pitch angle θ was no longer kept constant. But as we can see in figure 9.3 these deviations from the uniform helix do not change the berry phase as long as the average pitch angle is the same as before.

[26] The angle between the local waveguide axis and the axis of the helix.
[27] These will be discussed in detail in the Berry Phase II talk.

5 The Aharonov-Anandan Lift of Cyclic States

In section 3 we examined the phenomenon of the geometric phase for a class of non-adiabatic cyclic evolution for the specific example of the time-dependent Hamiltonian (9.62). In this section we shall uncover the general pattern that underlies the results obtained in section 3.

In general we consider a time-dependent Hamiltonian $H(t) = H(R(t))$ whose time-dependence is given by a path $\boldsymbol{C}$ in a parameter space M

$$\boldsymbol{C} : R(0) \to R(t) \to R(\tau). \tag{9.177}$$

The time evolution of every pure physical state defines a curve in the space $\mathcal{P}(\mathcal{H})$ of all such states. In particular, a cyclic state $W(t) = |\psi(t)\rangle\langle\psi(t)|$ with period τ corresponds to a closed curve in $\mathcal{P}(\mathcal{H})$:

$$\mathcal{C} : W(0) \to W(t) \to W(\tau) = W(0). \tag{9.178}$$

In our example (9.62) the cyclic states are labelled by integers or half-integers k. They correspond to the closed paths

$$\mathcal{C}_k : W_k(0) \to W_k(t) = |\phi_k(t)\rangle\langle\phi_k(t)| \to W_k(T) = W_k(0), \tag{9.179}$$

in the state space $\mathcal{P}(\mathcal{H})$, where $\phi_k(t)$ is given by (9.156).

Consider an arbitrary cyclic evolution with period τ. Then associated with the corresponding closed curve $\mathcal{C}$ in $\mathcal{P}(\mathcal{H})$ are three different curves in the Hilbert space $\mathcal{H}$:

1. The curve

$$C : |\psi(0)\rangle \to |\psi(t)\rangle \to |\psi(\tau)\rangle = e^{-i\alpha_\psi}|\psi(0)\rangle, \tag{9.180}$$

   where $|\psi(t)\rangle$ is the solution of the Schrödinger equation with the initial state vector $|\psi(0)\rangle$ being cyclic.

2. The closed curve

$$C^{\text{closed}} : |\phi(R(0))\rangle \to |\phi(R(t))\rangle \to |\phi(R(T))\rangle = |\phi(R)\rangle, \tag{9.181}$$

   where $|\phi(R(t))\rangle$ is the generalisation of $|\phi_k(t)\rangle$ of (9.156), i.e., $|\phi(R)\rangle$ is a smooth single-valued function with values in $\mathcal{H}$ which has the property $W(t) = |\phi(R(t))\rangle\langle\phi(R(t))|$. $|\phi(R)\rangle$ is determined up to gauge transformations:

$$|\phi(R(t))\rangle \to |\phi'(R(t))\rangle = e^{i\zeta(R(t))}|\phi(R(t))\rangle, \quad \text{with} \quad e^{i\zeta(R(\tau))} = e^{i\zeta(0)}. \tag{9.182}$$

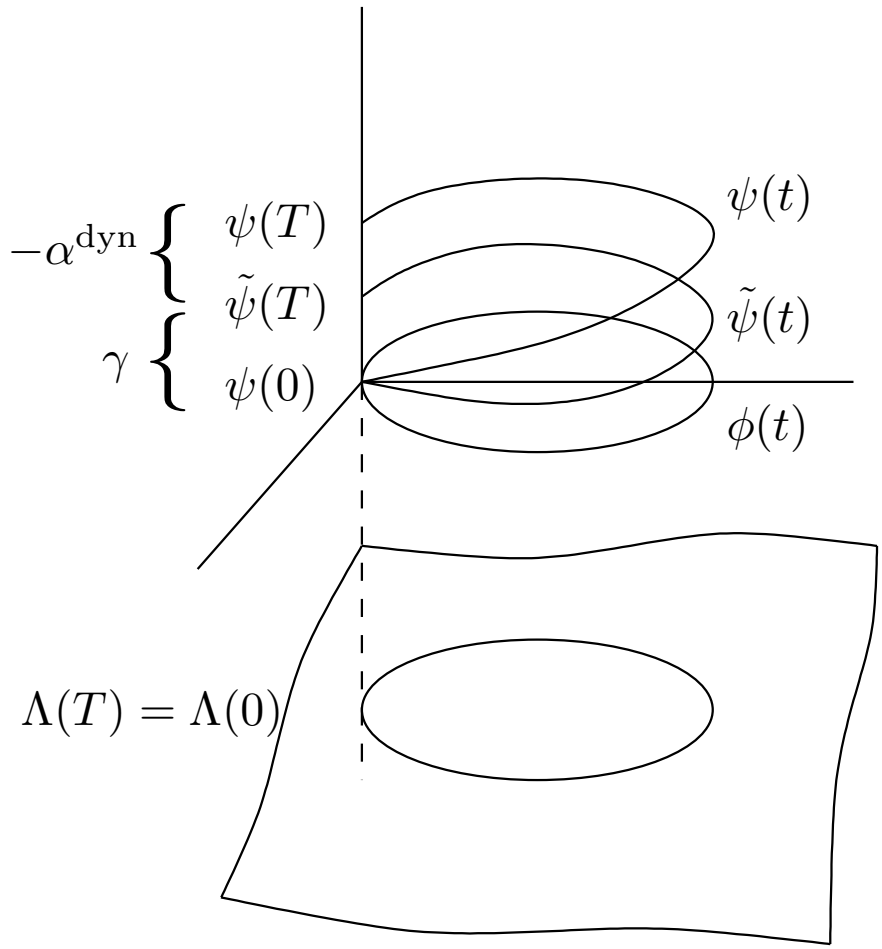

Figure 9.5: Closed path in the space of physical states and its lifts.

In our example (9.62) the closed curve in $\mathcal{H}$ associated with the curve $\mathcal{C}_k$ of (9.179) is given by

$$C_k^{\text{closed}} : |\phi_k(0)\rangle \to |\phi_k(t)\rangle = |k, \tilde{\theta}, \omega t\rangle \to |\phi_k(T)\rangle = |\phi_k(0)\rangle, \tag{9.183}$$

where the vectors $|\phi_k(t)\rangle$ are those of (9.156) and the gauge transformation (9.182) is the one in (9.155). The curve (9.180) in our example is given by the vectors (9.175).

3. The curve

$$\tilde{C} : |\tilde{\psi}(0)\rangle \to |\tilde{\psi}(t)\rangle := e^{i\int_0^t \langle\psi(t')|H(t')|\psi(t')\rangle dt'} |\psi(t)\rangle \to |\psi(\tau)\rangle, \tag{9.184}$$

where $|\psi(t)\rangle$ is the solution of the Schrödinger equation.

These three curves C, C^{closed} and $\tilde{C}$ have the property that under the projection of $\mathcal{H}$ onto $\mathcal{P}(\mathcal{H})$ (state vectors onto states) they project onto the closed curve $\mathcal{C}$ of (9.178), i.e.,

$$|\psi(t)\rangle\langle\psi(t)| = |\phi(t)\rangle\langle\phi(t)| = |\tilde{\psi}(t)\rangle\langle\tilde{\psi}(t)| = W(t) \in \mathcal{P}(\mathcal{H}). \tag{9.185}$$

For this reason we call these three curves *lifts* of $\mathcal{C}$. Figure 9.5 offers a schematic illustration of the situation. The curves C, C^{closed} and $\tilde{C}$ will be called the *dynamical lift*, the *closed lift* and the *Aharonov-Anandan* (A-A) *lift* of the closed curve $\mathcal{C}$, respectively. An important property of the A-A lift $\tilde{C}$ is that unlike the closed lift C^{closed} and the dynamical lift C, the A-A lift $\tilde{C}$ is uniquely determined by $\mathcal{C}$. The non-uniqueness of the closed lift is due to the fact that the single-valued state vectors $|\phi(R(t))\rangle$ are only defined up to gauge transformations (9.182). We shall discuss the non-uniqueness of the dynamical lift and the uniqueness of the A-A lift directly. The A-A lift is also called the *horizontal lift*.

In our example (9.62) the A-A lift is given by

$$|\tilde{\psi}(t)\rangle := e^{i\int_0^t \langle\psi(t')|H(t')|\psi(t')\rangle dt'} |\psi(t)\rangle = e^{i\Omega k(1+\frac{\omega}{\Omega}\cos\tilde{\theta})t} |\psi(t)\rangle. \tag{9.186}$$

It is not a closed curve in $\mathcal{H}$, but has the property

$$\tilde{\mathcal{C}}_k : |\tilde{\psi}(0)\rangle \to |\tilde{\psi}(t)\rangle \to |\tilde{\psi}(T)\rangle = e^{i\gamma_k(T)} |\tilde{\psi}(0)\rangle, \tag{9.187}$$

where $\gamma_k(T) = -\alpha_k^{\text{geom}}$ is the geometrical phase (9.162) or (9.174).

The relation between the A-A lift, the dynamical lift and the closed lift in our example is expressed by

$$|\tilde{\psi}(t)_k\rangle = e^{i\alpha_k^{\text{dyn}}} |\psi(t)\rangle = e^{i\gamma_k(t)} |k, \tilde{\theta}, \varphi(t)\rangle, \tag{9.188}$$

where

$$\alpha_k^{\text{dyn}}(t) := \int_0^t \langle\psi(t')|H(t')|\psi(t')\rangle dt'. \tag{9.189}$$

Provided that $\psi(t)$ is a solution of the Schrödinger equation (9.3), it follows that

$$\begin{aligned} i\frac{d}{dt}|\tilde{\psi}(t)\rangle &= -\langle\psi(t)|H(t)|\psi(t)\rangle|\tilde{\psi}(t)\rangle + ie^{i\int_0^t\langle\psi(t')|H(t')|\psi(t')\rangle dt'}\frac{d}{dt}|\psi(t)\rangle \\ &= -\langle\psi(t)|H(t)|\psi(t)\rangle|\tilde{\psi}(t)\rangle + e^{i\int_0^t\langle\psi(t')|H(t')|\psi(t')\rangle dt'}H(t)|\psi(t)\rangle \\ &= -\langle\psi(t)|H(t)|\psi(t)\rangle|\tilde{\psi}(t)\rangle + H(t)|\tilde{\psi}(t)\rangle \end{aligned}$$

Thus the A-A lift

$$|\tilde{\psi}(t)\rangle := e^{i\int_0^t\langle\psi(t')|H(t')|\psi(t')\rangle dt'}|\psi(t)\rangle \tag{9.190}$$

satisfies the following equation and initial condition:

$$\begin{aligned} i\frac{d}{dt}|\tilde{\psi}(t)\rangle &= [H(t) - \langle\psi(t)|H(t)|\psi(t)\rangle\mathbf{1}]|\tilde{\psi}(t)\rangle, \\ |\tilde{\psi}(0)\rangle &= |\psi(0)\rangle. \end{aligned} \tag{9.191}$$

Taking the inner product of the right-hand side of (9.191) with $|\tilde{\psi}(t)\rangle$ or $|\psi(t)\rangle$, we obtain

$$\begin{aligned} \langle\psi(t)|\frac{d}{dt}|\tilde{\psi}(t)\rangle &= 0 \\ \langle\psi(t)|\frac{d}{dt}|\psi(t)\rangle &= 0 \end{aligned} \tag{9.192}$$

This means that the tangent vector $\frac{d}{dt}|\tilde{\psi}(t)\rangle$ of $|\tilde{\psi}(t)\rangle$ is orthogonal (in the Hilbert space sense) to both $|\psi(t)\rangle$ and $|\tilde{\psi}(t)\rangle$.

Although the dynamical lift C is uniquely determined by the Hamiltonian $H(t)$, it is not uniquely determined by the physical problem. For example, the simple substitution

$$H(t) \to H'(t) = H(t) - \kappa(t)\mathbf{1} \qquad \text{with } \kappa(t) \in \mathbb{R} \tag{9.193}$$

leads to a new Hamiltonian $H'(t)$ which describes the same physics, i.e., it has the same (closed) curves of physical states $t \to W(t) = |\psi(t)\rangle\langle\psi(t)|$ in the projective Hilbert space $\mathcal{P}(\mathcal{H})$ as $H(t)$ does. But $H(t)$ and $H'(t)$ define different dynamical lifts $t \to \psi(t)$ and $t \to \psi'(t)$. Moreover, two Hamiltonians $H(t)$ and $H'(t)$ which have the same curves of physical states $t \to |\psi(t)\rangle\langle\psi(t)|$ and $t' \to |\psi'(t)\rangle\langle\psi'(t)|$ differ by a multiple $\kappa(t)\mathbf{1}$ of the unit operator $\mathbf{1}$. Thus the dynamical lift does not uniquely correspond to the physical problem. A lift that is uniquely associated with the closed curve $\mathcal{C} : t \to |\psi(t)\rangle\langle\psi(t)|$ in $\mathcal{P}(\mathcal{H})$, and therefore reflects the physical effects, is the A-A lift $\tilde{C} : t \to \tilde{\psi}(t)$.

We will now discuss the generalisations of (9.183), i.e., closed lifts (9.181) of the curve $\mathcal{C}$. As seen from (9.173), $|\phi_k(t)\rangle$ can be used to calculate the geometric phase, if one does not have a solution $|\psi(t)\rangle$ of the Schrödinger equation. There

are various ways to obtain these single-valued $|\phi(t)\rangle \in \mathcal{H}$. In general they are curves of *local sections*. A local section is a smooth function of an open patch O of $\mathcal{P}(\mathcal{H})$ into $\mathcal{H}$. We will assume that our curve $\mathcal{C}$ lies in such an open patch O. Then for any closed curve $\mathcal{C} : t \to W(t)$ one has the closed (single-valued) lift

$$t \to |\phi(t)\rangle = |\phi(W(t))\rangle, \tag{9.194}$$

with

$$W(t) = |\phi(t)\rangle\langle\phi(t)|, \text{ and } |\phi(\tau)\rangle = |\phi(0)\rangle. \tag{9.195}$$

This is however determined only up to a gauge transformation (9.182). The importance of the local sections $|\phi\rangle$ or alternatively the closed lifts C^{closed} is due to their utility in the calculation of the geometric phase.

Since $t \to |\psi(t)\rangle$, $t \to |\tilde{\psi}(t)\rangle$ and any $t \to |\phi(t)\rangle$ are lifts of the same closed curve $t \to W(t)$, there must exist a phase factor $\omega(t)$ such that

$$|\tilde{\psi}(t)\rangle = \omega(t)|\phi(t)\rangle. \tag{9.196}$$

Next we calculate $\omega(t)$. Differentiating both sides of (9.196), we obtain

$$\frac{d}{dt}|\tilde{\psi}(t)\rangle = \frac{d\omega(t)}{dt}|\phi(t)\rangle + \omega(t)\frac{d}{dt}|\phi(t)\rangle. \tag{9.197}$$

Taking the scalar product of this expression with $|\tilde{\psi}(t)\rangle$, we have

$$\overline{\omega(t)}\frac{d\omega(t)}{dt} + |\omega(t)|^2\langle\phi(t)|\frac{d}{dt}|\phi(t)\rangle = \langle\tilde{\psi}(t)|\frac{d}{dt}|\tilde{\psi}(t)\rangle = 0, \tag{9.198}$$

where in the last equality we have used (9.192). Next we write (9.198) in the form

$$\frac{1}{\omega(t)}\frac{d\omega(t)}{dt} = -\langle\phi(t)|\frac{d}{dt}|\phi(t)\rangle,$$

which can be integrated to yield

$$\frac{\omega(t)}{\omega(0)} = e^{-\int_0^t \langle\phi(t')|\frac{d}{dt'}|\phi(t')\rangle dt'}. \tag{9.199}$$

We shall denote the phase factor on the right-hand side of (9.199) by $e^{i\gamma(t)}$ and write (9.196) as

$$|\tilde{\psi}(t)\rangle = \omega(0)e^{i\int_0^t i\langle\phi(t')|\frac{d}{dt'}|\phi(t')\rangle dt'}|\phi(t)\rangle =: \omega(0)e^{i\gamma(t)}|\phi(t)\rangle. \tag{9.200}$$

If we chose the arbitrary constant phase $\omega(0)$ equal to 1 such that $|\tilde{\psi}(0)\rangle = |\psi(0)\rangle = |\phi(0)\rangle$, then we have

$$|\tilde{\psi}(t)\rangle = e^{i\gamma(t)}|\phi(t)\rangle. \tag{9.201}$$

This is the generalisation of (9.188). Combining (9.190) and (9.201), we find

$$|\psi(t)\rangle = e^{-i\int_0^t \langle\psi(t')|H(t')|\psi(t')\rangle dt'} e^{i\gamma(t)}|\phi(t)\rangle. \tag{9.202}$$

Equation (9.202) is the general relation between the solution of the Schrödinger equation $|\psi(t)\rangle$ and the closed lift $|\phi(t)\rangle$. Equation (9.40) is the adiabatic approximation of this relation, and (9.158) is its special case for the spinning quantum system in a precessing external magnetic field. The adiabatic approximation uses in place of the closed lifts $|\phi(t)\rangle$ the eigenvectors of $H(R(t))$ which are more easily accessible than $|\phi(t)\rangle$. According to (9.200), for the closed path $\mathcal{C}$ in $\mathcal{P}(\mathcal{H})$ the phase angle $\gamma(\tau)$ is given by

$$\gamma(\tau) = \gamma(\mathcal{C}) = \oint_0^\tau i\langle\phi(t)|\frac{d}{dt}|\phi(t)\rangle dt = \oint i\langle\phi|d|\phi\rangle \quad \text{modulo } 2\pi, \tag{9.203}$$

where $|\phi(t)\rangle$ corresponds to any of the closed lifts of $\mathcal{C}$.

The phase angle $\gamma(\tau)$ is independent of the choice of the time parameterisation of $|\phi(t)\rangle$, i.e., the speed with which $|\phi(t)\rangle$ traverses its closed path. It is gauge invariant. It is independent of the choice of the Hamiltonian as long as these Hamiltonians describe the same closed path $\mathcal{C}$ in $\mathcal{P}(\mathcal{H})$. It depends only on the closed curve $\mathcal{C}$. It is therefore considered to be a "geometric" property of $\mathcal{C}$, thus has the name *geometric phase*.

The one-form appearing in the integrand of (9.203),

$$\mathcal{A} := i\langle\phi|d|\phi\rangle, \tag{9.204}$$

is called the *Aharonov-Anandan connection one-form*. It is the analogue of the Mead-Berry connection one-form (9.36). It satisfies the following transformation rule under gauge the transformation (9.182)

$$\mathcal{A} \to \mathcal{A}' = \mathcal{A} - d\zeta. \tag{9.205}$$

The formula (9.204) for the A-A connection was obtained from the requirement that $\tilde{\psi}(t)$ is the A-A lift, i.e., the lift fulfilling (9.192) (which in turn followed from its definition (9.190)). This was the only possible definition of a lift which depended solely on the physics of the problem.

Equations (9.201) and (9.194) lead to

$$|\tilde{\psi}(\tau)\rangle = e^{i\gamma(\mathcal{C})}|\tilde{\psi}(0)\rangle = e^{i\gamma(\mathcal{C})}|\psi(0)\rangle. \tag{9.206}$$

Then, using (9.190) one obtains for the cyclic evolution of a state vector

$$|\psi(\tau)\rangle = e^{-i\int_0^\tau \langle\psi(t')|H(t')|\psi(t')\rangle dt'} e^{i\gamma(\mathcal{C})}|\psi(0)\rangle. \tag{9.207}$$

This relation is the non-adiabatic generalisation of (9.51).

Figure 9.5 shows a graphical representation of our description of the general cyclic evolution. It shows a *base space* representing the space $\mathcal{P}(\mathcal{H})$ of physical states and including a closed curve $\mathcal{C}$. This curve represents the cyclic evolution of a pure state $W(t)$. Above $\mathcal{C}$ are shown the lifts $C^{\text{closed}}, \tilde{C}$ and C of $\mathcal{C}$ which belong to the Hilbert space $\mathcal{H}$ (depicted in the figure by the three dimensional space). Also shown is a *fibre* above the base point $W(0)$ (depicted by the positive z-axis with the z coordinate representing the phase angle modulo 2π or the element $e^{i\zeta(0)}$ of the (gauge) group U(1). The fibre in this case (though it has been drawn as a straight line) is a copy of the unit circle S^1 or the group U(1). We can attach a copy of this S^1 not only to the point $W(0)$ but to every one-dimensional projection operator $\Lambda \in \mathcal{P}(\mathcal{H})$. In this way we get a *bundle* of U(1) fibres attached to each point of $\mathcal{P}(\mathcal{H})$.

The mathematical structure that we have encountered here is an example of a *principal fibre bundle* (PFB). We shall refer to this PFB as the *Aharonov-Anandan principle bundle*.

Like any fibre bundle the A-A PFB consists of a base space, a set of fibres associated with the points of the base space and forming a larger space called the *total* or *bundle space*, and a *structure group* which acts on the fibres. As the total space consists of fibres over points of the base space, we can define a projection map from the total space to the base space. The fibres are then viewed as the inverse images of points of the base space under this projection.

For the A-A PFB, the base space is the projective Hilbert space $\mathcal{P}(\mathcal{H})$ also denoted by $\mathbb{C}P^{N-1}$ where $N \leq \infty$ is the dimension of the Hilbert space $\mathcal{H}$. The total space $S(\mathcal{H})$ is the set of all normalised state vectors in $\mathcal{H}$, i.e.

$$S(\mathcal{H}) := \{\psi \in \mathcal{H} : \langle\psi|\psi\rangle = 1\} = S^{2N-1}. \tag{9.208}$$

The projection map

$$\pi : S(\mathcal{H}) \to \mathcal{P}(\mathcal{H}) \qquad (\text{or } \pi : S^{2N-1} \to \mathbb{C}P^{N-1}) \tag{9.209}$$

is the obvious projection of the state vectors onto states,

$$\pi(|\psi\rangle) = |\psi\rangle\langle\psi|. \tag{9.210}$$

The fibres are normalised rays in the Hilbert space. They consist of all the normalised state vectors associated with a given pure state and hence differing by a phase factor. Therefore the fibres are copies of the unit circle S^1. Finally the structure group is the Abelian group U(1) which has the manifold structure of S^1 as well. We shall denote the A-A PFB by

$$\begin{array}{ccc} \eta : \mathrm{U}(1) \longrightarrow S(\mathcal{H}) \\ \qquad\qquad \downarrow \pi \\ \qquad\quad \mathcal{P}(\mathcal{H}) \end{array} \qquad \text{or} \qquad \begin{array}{ccc} \mathrm{U}(1) \longrightarrow S^{2N-1} \\ \qquad\quad \downarrow \pi \\ \qquad\quad \mathbb{C}P^{N-1}. \end{array} \tag{9.211}$$

A PFB may be endowed with a geometric structure. The latter provides a notion of *parallel transportation* or alternatively the notion of a *horizontal lift*. A geometric structure on a PFB is also called a *connection*. For an Abelian PFB, i.e., a PFB with U(1) as its structure group, a connection may be expressed by a differential one-form satisfying a set of (gauge) transformations rules. The A-A connection one-form $\mathcal{A}$ of (9.204) defines a particular connection on the A-A PFB η. The A-A phase also has a very well-known mathematical counterpart called *holonomy*.

Exact Cyclic Evolution for Periodic Hamiltonians

If the time-dependent Hamiltonian is periodic, i.e.

$$H(t+T) = H(T), \tag{9.212}$$

for some time period T, then we can use the results of what is known as Floquet theory in mathematics. In particular we next show that the evolution operator for any periodic Hamiltonian has precisely the same form as the evolution operator (9.142) for the spin system (9.62). More precisely we prove that for *any T-periodic Hamiltonian, satisfying (9.212), there exists a time-independent Hermitian operator $\tilde{h}$ and a T-periodic unitary operator $Z(t)$ with $Z(0) = \mathbf{1}$, such that th time-evolution operator is given by*

$$U^\dagger(t) = Z(t)e^{it\tilde{h}}. \tag{9.213}$$

To see this, consider the unitary operator $V(t) := U^\dagger(t+T)$. V satisfies the following Schrödinger equation:

$$\begin{aligned} \frac{d}{dt}V(t) &= -iH(t)V(t) \\ V(0) &= U^\dagger(T) =: V_0, \end{aligned} \tag{9.214}$$

since

$$i\frac{d}{dt}V(t)|\psi(0)\rangle = H(t)V(t)|\psi(0)\rangle, \quad \text{for all } |\psi(0)\rangle.$$

The operator $V'(t) := U^\dagger V_0$ also satisfies (9.214). However we know from the uniqueness theorem for initial value linear differential equations that solution of (9.214) is unique. Therefore we have $V(t) = V'(t)$, i.e.,

$$U^\dagger(t+T) = U^\dagger(t)V_0 = U^\dagger(t)U^\dagger(T). \tag{9.215}$$

This relation is sufficient to construct a pair of operators $(Z(t), \tilde{h})$ which satisfies (9.213). To see this we first write $t = nT + t_0$ for some integer n and $t_0 \in [0, T)$ and then apply (9.215) repeatedly. This yields

$$U^\dagger(t) = U^\dagger(t_0)[U^\dagger(T)]^n = U^\dagger(t_0)V_0^n. \tag{9.216}$$

Next we assume that the unitary operator V_0 can be expressed as the exponential of a Hermitian operator[28], i.e.,

$$V_0 = e^{-it\tilde{h}'}. \tag{9.217}$$

In view of (9.216),(9.217) and $n = \frac{t-t_0}{T}$, we have

$$U^\dagger(t) = U^\dagger(t_0)e^{\frac{-i(t-t_0)}{T}\tilde{h}'} \tag{9.218}$$

$$= U^\dagger(t_0)e^{\frac{it_0}{T}\tilde{h}'}e^{\frac{it}{T}\tilde{h}'} \tag{9.219}$$

$$= Z(t)e^{-it\tilde{h}}, \tag{9.220}$$

where we have defined

$$Z(t) := U^\dagger(t_0)e^{\frac{it_0}{T}\tilde{h}'}, \text{ and } \tilde{h} := \frac{\tilde{h}'}{T}$$

Clearly, $\tilde{h}$ is hermitian and $Z(t)$ is unitary. Furthermore, $Z(t)$ satisfies

$$Z(t+T) = Z(t), \text{ and } Z(0) = U^\dagger(0) = 1. \tag{9.221}$$

For $t = T$, (9.218) reproduces the general result, namely

$$U^\dagger(T) = e^{-iT\tilde{h}}. \tag{9.222}$$

In particular, $\tilde{h}$ yields the exact cyclic states with period $\tau = T$ as its eigenstates.

The pair of operators $(Z(t), \tilde{h})$, so constructed, is not unique. The non-uniqueness of $\tilde{h}$ is reminiscent of the non-uniqueness of the Hamiltonian $H(t)$ discussed previously.

If the Hamiltonian is parameter dependent ($H = H(R)$) and its time dependence is realised by changing the parameters R in time, then the operator $\tilde{h}$ will be a function of the initial parameter, $R_0 = R(t = 0)$. Thus in general it also depends on a set of parameters belonging to the same parameter space M.

As in the case of the spin system of Section 3, the operator $\tilde{h}(R)$ generally differs from the Hamiltonian $H(R)$. In general, the dependence of $\tilde{h}(R)$ on the Hamiltonian is not explicitly known. The only established fact is that for an adiabatic evolution $\tilde{H}(R)$ can be approximated by $H(R)$.

[28]This can always be done if the Hilbert space is finite dimensional. For an infinite dimensional Hilbert space there are unitary operators which cannot be written as the exponent of ($-i$ times) some Hermitian operator. However, the set of unitary operators which are exponentials of Hermitian operators is a dense subset of the set of unitary operators with an appropriate choice of topology on the latter set. This means that one can always find a sequence of unitary operators $\{e^{-i\tilde{h}'_k} : k = 0, 1, 2, \dots\}$ which converges to V_0 in this topology. Therefore, one can approximate V_0 with $e^{-i\tilde{h}'}$ where $\tilde{h}' := \tilde{h}'_k$ for some large value of k.

In the remainder of this section we briefly discuss the relation between the operators $\tilde{h}$ and $Z(t)$ of (9.213) and the geometric phase of Aharonov and Anandan.

Consider the evolution of a cyclic state vector $|\psi(0)\rangle$. By definition $|\psi(0)\rangle$ is an eigenvector of the evolution operator:

$$U^\dagger(\tau)|\psi(0)\rangle = Z(\tau)e^{-i\tau\tilde{h}}|\psi(0)\rangle = e^{-i\alpha(\tau)}|\psi(0)\rangle, \tag{9.223}$$

where we have employed (9.213). On the other hand the evolution of $|\psi(0)\rangle$ is governed by the Schrödinger equation (9.3). In terms of the operators $Z(t)$ and $\tilde{h}$, these equations take the form

$$|\psi(t)\rangle = Z(t)e^{-it\tilde{h}}|\psi(0)\rangle, \tag{9.224}$$

$$H(t) = i\dot{Z}(t)Z^\dagger(t) + Z(t)\tilde{h}Z^\dagger(t), \tag{9.225}$$

where we have used the unitarity of $Z(t)$, and $\dot{Z}(t)$ stands for the time-derivative of $Z(t)$.

Next we compute the dynamical phase angle. Substituting (9.224) and (9.225) in the definition of the dynamical phase angle (9.160)

$$\alpha^{\rm dyn}(\tau) := \int_0^\tau \langle\psi(t')|H(t')|\psi(t')\rangle dt' \quad \text{modulo } 2\pi, \tag{9.226}$$

we have

$$\alpha^{\rm dyn}(\tau) = \int_0^\tau i\langle\psi(0)|e^{it'\tilde{h}}Z^\dagger(t')\dot{Z}(t')e^{-it'\tilde{h}}|\psi(0)\rangle dt' \tag{9.227}$$

$$+ \tau\langle\psi(0)|\tilde{h}|\psi(0)\rangle \quad \text{modulo } 2\pi. \tag{9.228}$$

For a cyclic state with the same period as the Hamiltonian ($\tau = T$), the cyclic state vector $|\psi(0)\rangle$ is an eigenvector of the operator $\tilde{h}$. Hence the second term on the right-hand side of (9.227) is precisely the totally phase angle

$$\tau\langle\psi(0)|\tilde{h}|\psi(0)\rangle = \alpha(T). \tag{9.229}$$

In view of this equation we can directly express the geometric phase in terms of the operator $Z(t)$ and its time derivative:

$$\begin{aligned}\gamma(T) = \gamma(\mathcal{C}) &:= \alpha^{\rm dyn}(T) - \alpha(T) \quad \text{modulo } 2\pi \\ &= \int_0^T i\langle\psi(0)|Z^\dagger(t')\dot{Z}(t')|\psi(0)\rangle dt' \quad \text{modulo } 2\pi.\end{aligned} \tag{9.230}$$

Equation (9.230) is of some practical importance. Since both the Hamiltonian $H(t)$ and the operator $Z(t)$ are periodic with the same period T, one can in principle expand them in Fourier series. There are procedures to relate the Fourier

components of $Z(t)$ to those of $H(t)$ which may be used to yield a series expansion of the geometric phase for arbitrary periodic systems.

The operator $Z(t)$ is also of particular interest since it may be used to yield single-valued vectors $|\phi(t)\rangle$ of (9.194), namely

$$|\phi(t)\rangle = Z(t)|\psi(0)\rangle. \tag{9.231}$$

In view of this identification, we can write (9.230) in the form

$$\begin{aligned}\gamma(T) &= \int_0^T i\langle\psi(0)|Z^\dagger(t')\frac{d}{dt'}[Z(t')|\psi(0)\rangle]dt' \quad \text{modulo } 2\pi \\ &= \int_0^T i\langle\phi(t')|\frac{d}{dt'}|\phi(t')\rangle dt' \quad \text{modulo } 2\pi,\end{aligned}$$

which is identical with (9.203). The non-uniqueness of $Z(t)$, mentioned above, corresponds to the gauge freedom of $|\phi(t)\rangle$.

Furthermore, we can use (9.231) to express the evolution of a cyclic state vector according to

$$\begin{aligned}|\psi(t)\rangle &= Z(t)e^{-it\tilde{h}}|\psi(0)\rangle \\ &= e^{-i\frac{\alpha(T)}{T}t}Z(t)|\psi(0)\rangle \\ &= e^{-i\frac{\alpha(T)}{T}t}|\phi(t)\rangle.\end{aligned} \tag{9.232}$$

Here we have used the fact that $|\psi(0)\rangle$ is an eigenvector of $\tilde{h}$ with eigenvalue $\alpha(T)/T$.

The fact that the evolving state vector $|\psi(t)\rangle$ is expressed as the product of a phase factor and a periodic state vector $|\phi(t)\rangle$ is a direct consequence of the periodicity of the Hamiltonian. The state vectors of the form (9.232) are encountered in almost all physical systems with periodic features. The corresponding wave functions are known as the *Bloch wave functions*.

10 Berry phase II: The Aharonov-Bohm effect

Oliver Pfäffli
Supervisor: Sebastian Pilgram

Interesting phenomena of the electromagnetic potentials in quantum systems will be discussed. In contrast to the conclusion of classical mechanics, potentials cause effects on charged particles, even in regions where all the forces on the particles vanish. The Aharonov-Bohm effect and the Aharonov-Casher effect are examples for this fact. We will see that the A-B phase is a topological phase as well as a Berry phase. That the Aharonov-Casher effect is a variation of the A-B effect will, finally, be demonstrated.

1 Introduction

The time evolution of quantum states is totally different to the time evolution of classical objects. This will be demonstrated with different experimental setups which have in common, that the states do not undergo any forces but that they live in a regime with non-zero potentials. The potentials cause physically relevant effects even if all forces vanish. A well-known example for this is the Aharonov-Bohm (A-B) effect which occurs if electrons move around an area with a magnetic field. The quantum state of the electrons changes its phase when propagating even if the magnetic field is confined to an area where the wave function of the electron is zero. We will see, that the A-B phase is a topological phase and a Berry phase. This means that the A-B phase is invariant under continuous deformations of the electron's path and that the A-B effect can be described by Berry's formalism. His idea was to parameterise the environment of a quantum state. He concluded that under certain conditions, basically the adiabatic assumption, this dependence on the environment results in additional phase shifts, which are caused by the dynamics of the quantum state and the geometry of its path. In the case of the

A-B effect the area, to which the magnetic field is confined, is the environment of the electron moving around it. Furthermore, the Aharonov-Casher (A-C) effect, which is a variation of the A-B effect, will be described. Instead of electrons we analyse magnetic moments, for example neutrons. Classically, Neutrons do not interact with electric fields but, similar to the A-B effect, the phase of the neutrons changes as they propagate in an area with an electric field. There are also short descriptions of experiments which verify the A-B and the A-C effect. These experiments measure interference phenomena, which prove the existence of the change in the phase of quantum states.

Over long passages the text is very close to the references given at the end of the article. Italicized parts relate to main ideas originating from primary sources.

2 The Aharonov-Bohm-Effect

Metal Tube Experiment

In this section I shall discuss the significance of the electromagnetic potentials in quantum systems. These vector and scalar potentials were used in classical electrodynamics as a mathematical aid for calculating the physical relevant fields. However, in classical electrodynamics the equations of motion can be expressed directly in terms of the fields, namely in the Maxwell equations. In quantum mechanics this is not possible because the description of physical phenomenas requires the canonical formalism. The Hamilton operator occurs in the Schrödinger equation, which is the equation of motion in quantum mechanics. In the Hamiltonian the electromagnetic potentials represent the electromagnetic interactions between the particles described. Nevertheless, the Schrödinger equation of an electromagnetic interacting particle is gauge invariant under the transformation

$$\Psi \longrightarrow e^{i\chi(x)}\Psi, \qquad A \longrightarrow A + \nabla\chi. \tag{10.1}$$

Thus, if the electromagnetic fields vanish, it appears as if the potentials could be gauged away and the potentials had no independent significance. That in general this conclusion is incorrect can be shown with several physical systems, which require a further interpretation of the potentials.

The first example is a charged particle inside a 'Faraday cage' connected to an external generator which causes the potential to alternate in time[29]. This external potential $V(x,t)$ will cause an additional term in the Hamiltonian. $V(x,t)$ is constant on the surface of the metallic box in space. Moreover, it is constant in space inside the box since $\nabla^2 V(x,t) = 0$. Hence, the potential is only a function of time and the electric field vanishes. The Hamiltonian of the system is given by $H = H_0 + V(t)$ whereas H_0 is the Hamiltonian of the free particle confined to the box. If $\Psi_0(x,t)$ is a solution of the Hamiltonian H_0, the solution for H will

[29] See [55]

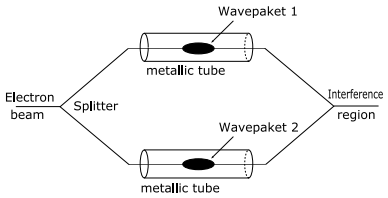

Figure 10.1: Metal tube Experiment

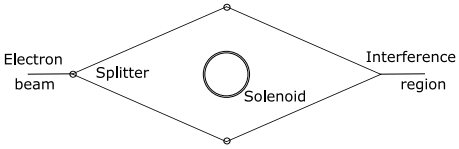

Figure 10.2: A-B Experiment

be[30]

$$\Psi = \Psi_0 e^{-iS/\hbar}, \qquad S = \int_0^t V(t)dt = \int_0^t e\varphi(t)dt, \tag{10.2}$$

which derives from

$$i\hbar\frac{\partial\Psi}{\partial t} = \left(i\hbar\frac{\partial\Psi_0}{\partial t} + \Psi_0\frac{\partial S}{\partial t}\right) = \big(H_0 + V(t)\big)\Psi = H\Psi.$$

The new solution Ψ remains the same as Ψ_0 up to a phase factor which causes no change in the physical result.

The phase factor, however, becomes physically relevant, if we look at the interference phenomena of two wave packets. Therefore, consider an experiment in which a single incoming coherent electron beam is split up into two beams passing through two different metal tubes (Figure 10.1). These metal tubes have to be long in comparison to the width of the wave packets' envelope function. When the beams passed through the tubes they have to be recombined in order to interfere coherently. The moment at which the wave packets are well inside the tubes and far from their openings this system is equal to two 'Faraday cages' of the kind which was mentioned above. A problem occurs if the wave packets come near to the opening of the tube. At this stage, the applied potential causes electric fields. Thus, the potential has to be zero when the wave packets enter or quit the tubes. But if the wave packets are inside the tubes and far from their openings the potential can be changed in time. This arrangement will ensure that the wave packets are never in a field. The potential are changed differently for each tube. Hence, the two wave packets will get different phase factors according to (10.2). The solution at the interference point is then given by the sum of the two splitted electron waves

$$\Psi = \Psi_1^0 e^{-iS_1/\hbar} + \Psi_2^0 e^{-iS_2/\hbar}, \tag{10.3}$$

whereas

$$S_1 = e\int_0^t \varphi_1 dt, \qquad S_2 = e\int_0^t \varphi_2 dt.$$

[30] See [55]

The interference will depend on the phase difference $(S_1 - S_2)/\hbar$, which can be expressed through the integral $e/\hbar \oint \varphi dt$ around a closed curve in space-time evaluating φ at the center of the wave packet. *Thus, there is a physical effect of the potentials even though no force is ever actually exerted on the electron*[31].

Up to now the considerations were non-relativistic. In order to get a covariant phase factor, we could try the following generalization. Replace φ by the relativistic Vierervector (φ, A) and the dt by $\frac{1}{c}(cdt, d\mathbf{x})$. This leads to the phase factor

$$\Delta S = e \oint \left(\varphi dt - \frac{\mathrm{A}}{c} \cdot d\mathbf{x} \right). \tag{10.4}$$

This generalization gives another example. Regard a long closely wound solenoid, which is centered at the origin with the axis in the z direction. It creates a magnetic field H, with $\nabla \times \mathrm{A} = \mathrm{H}$. The field H is confined within the solenoid. However, the potential A is not, since the magnetic flux ϕ_0 through a surface S containing the origin is constant

$$\phi_0 = \int_S \mathrm{H} d\mathbf{s} = \oint_{\partial S} \mathrm{A} d\mathbf{x}. \tag{10.5}$$

Again, let a coherent electron beam, which points in the direction of the solenoid, be splitted in two, so that each part goes along the opposing side of the solenoid (Figure 10.2). However they must not touch the solenoid. In the end, they have to be recombined at a point behind the solenoid. The Hamiltonian of this configuration is

$$H = \frac{\left(\mathbf{p} - (e/c)\mathrm{A}\right)^2}{2m} \tag{10.6}$$

The electron beam, which is now not necessarily divided into wave packets, can be considered as moving along a path in space only (at a constant time t). Hence, equation (10.4) suggests that the associated phase shift of the electron beam is

$$\Delta S = -\frac{e}{c} \oint \mathrm{A} \cdot d\mathbf{x} = -\frac{e}{c} \phi_0. \tag{10.7}$$

Again, the wave function in this case splits up into two parts $\Psi = \Psi_1 + \Psi_2$ whereas Ψ_i represents the beam passing the solenoid on the one or on the opposite side. If Ψ_1^0, Ψ_2^0 are the solutions with magnetic field $\mathrm{H} = 0$, we can write

$$\Psi_1 = \Psi_1^0 e^{-iS_1/\hbar}, \qquad \Psi_2 = \Psi_2^0 e^{-iS_2/\hbar}, \tag{10.8}$$

whereas S_1 and S_2 represent the phase factor $(e/c) \int \mathrm{A} \cdot d\mathbf{x}$ along the paths of the first respectively of the second beam. *The interference between the two beams will evidently depend on the phase difference*[32], $(S_1 - S_2) = \Delta S$ given in equation (10.7).

[31] See [55]
[32] See [55]

This second experiment is called the Aharonov-Bohm effect (A-B effect) and in the following sections we will establish, why the phase shift (10.7) is the correct choice.

In 1985 the group of R.A. Webb et al.[33] confirmed the Aharonov - Bohm effect using minute Au rings. For the first time they measured the prescribed period h/e of the magnetoresistance oscillation with respect to the magnetic flux. The difficulty in this experiment was to manage two rivaling effects: Firstly, the metallic ring has to be small enough in order to avoid randomisation by inelastic scattering while the electrons traverse the ring. Secondly, the smaller the ring is the more difficult it becomes to confine the magnetic field to the area bordered by the ring. If the magnetic field enters the arms of the ring (and in practice this is the case) the phase shift of the electron becomes path dependent as we will see in the following section. Since the wire, which the ring is made of, has an extension, the electrons can move on different paths in the wire. This could destroy the interference effect if the magnetic field is high enough. Webb's group used rings with an average diameter of 825 nm at a temperatures less than 1 K. The oscillations persisted to rather high magnetic fields of around 8 T, which was a quite surprising result.

Relation to Topology

One wishes to investigate a class of geometric phases which are topological in nature. The generic example is the Aharonov-Bohm (A-B) phase. Aharonov and Bohm analysed the quantum mechanics of an electron moving around but not actually penetrating a magnetic flux line[34]. This system has a non trivial topology if we let the magnetic field be confined within an infinitely long solenoid. In this section it will be shown, that the A-B phase is a particular case of the geometric phases[35].

To start the analysis, let us consider a spinless particle of mass m and electric charge e in free space. The coordinate and momentum operators $\hat{x}^i$ and $\hat{p}^i$ satisfy the following commutation relations:

$$[\hat{x}^i, \hat{x}^j] = 0,$$

$$[\hat{p}_i, \hat{p}_j] = 0$$

$$[\hat{x}^i, \hat{p}_j] = i\delta^i_j \hat{1}, \tag{10.9}$$

[33] See [56]

[34] See [57], p. 26

[35] for the definition of the geometric phase see [57] sect. 2.3. or Berry Phase I of this Proseminar

here is $\hat{1}$ the identity operator acting on the Hilbert space $\mathcal{H}$. Now we can find the position representation of these operators which fulfills (10.9). For a state vector $\psi \in \mathcal{H}$ is

$$\langle x|\hat{x}^i|\psi\rangle = x^i\langle x|\psi\rangle = x^i\psi(x), \tag{10.10}$$

$$\langle x|\hat{p}_i|\psi\rangle = \Big(-i\frac{\partial}{\partial x^i} + \omega_i(x)\Big)\psi(x), \tag{10.11}$$

whereas $x = (x^1, \ldots, x^{\mathcal{M}})$ are coordinates of the configuration space M and $\omega_i = \omega_i(x)$ are scalar functions of x. Since

$$\langle x|[\hat{p}_i, \hat{p}_j]|\psi\rangle$$

$$= \Big[\big(-i\partial_i + \omega_i(x)\big)\big(-i\partial_j + \omega_j(x)\big) - \big(-i\partial_j + \omega_j(x)\big)\big(-i\partial_i + \omega_i(x)\big)\Big]\psi(x)$$

$$= i\psi(x)\big(\partial_j\omega_i - \partial_i\omega_j\big) = 0$$

holds for any $\psi(x)$, the following equation results:

$$\partial_i\omega_j - \partial_j\omega_i = 0. \tag{10.12}$$

We will see later on, that since usually the configuration space M is an Euclidean space $\mathbb{R}^{\mathcal{M}}$, the functions ω_i have no physical significance and thus are neglected.

The operator $\hat{p}_i$ behaves well under coordinate transformations. This implies that the $\omega_i's$ transform the same way as the cotangent vectors[36] $\frac{\partial}{\partial x^i}$ do and we can write[37]

$$\omega := \omega_i dx^i, \tag{10.13}$$

which is a one-form on M. If we use (10.12) we find that the exterior derivative of ω vanishes (One says ω is a closed one-form):

$$d\omega = \sum_{i,j} \partial_i\omega_j dx^i \wedge dx^j = \sum_{i,j} \frac{1}{2}(\partial_i\omega_j - \partial_j\omega_i)dx^i \wedge dx^j = 0. \tag{10.14}$$

Here, the asymmetry of the wedge product $dx^i \wedge dx^j = -(dx^j \wedge dx^i)$ was used. An important result of algebraic topology is the Poincaré lemma, which states: *Every closed form is exact provided that the manifold M on which the differential form*

[36] A vector $\vec{\omega}_p$ at a point p of the manifold M is called a *cotangent* or *covariant* vector if its components behave under coordinates transformation as follows: $(\omega'_p)_i = \frac{\partial x^j}{\partial x'^i}(\omega_p)_j$. Since for $\frac{\partial}{\partial x^i}$ the chainrule $\frac{\partial}{\partial x'^i} = \frac{\partial x^j}{\partial x'^i}\frac{\partial}{\partial x^j}$ is valuable, this is indeed a cotangent vector. See Appendix A.2. of [57]

[37] The local basis vectors dx^i of the cotangent space are defined by $dx^i := D(x_p)_i$, whereas D is the usual derivative and $(x_p)_i := \langle \vec{p}, \vec{e_i}\rangle$ the i^{nd} coordinate function.

is defined is (topologically equivalent to) a star-shaped region of some Euclidean space $\mathbb{R}^{\mathcal{M}}$,[38]. Intuitively, 'star-shaped' means there are no holes or cuts in M. An exact one-form is a one-form ω which can be written as

$$\omega = df = \underbrace{\partial_i f(x)}_{\omega_i} dx^i, \tag{10.15}$$

whereas $f = f(x)$ is a function on M. Particularly if $M = \mathbb{R}^{\mathcal{M}}$, the equation (10.15) is valid. Moreover the $\omega_i' s$ may be gauged away in the following way

$$\psi \longrightarrow \psi' = e^{-if(x)}\psi, \tag{10.16}$$

since then

$$\begin{aligned} \langle x|\hat{p}_i|\psi'\rangle &= \big(-i\partial_i + \omega_i(x)\big)\psi'(x) \\ &= \big(\omega_i(x) - \partial_i f(x) - i\partial_i\big)\psi' \\ &= -i\partial_i\psi'. \end{aligned}$$

However, if M is not equivalent to a star-shaped region and in fact the infinitely long solenoid in three dimensional space is a physically relevant example of such an M, then Poincaré's lemma is violated and the $\omega_i' s$ must not be neglected in (10.11). In order to understand what the influence of the functions ω_i on $\psi(x)$ is, an infinitesimal spacial displacement of the state vector ψ has to be considered, for example in the direction $\epsilon = \big(\epsilon^1, \ldots, \epsilon^{\mathcal{M}}\big)$. The Operators $\hat{p}_i$ generate such a displacement in the i-direction. Let us examine it for ϵ in the first-order of ϵ:

$$\begin{aligned} \langle x|\psi\rangle \longrightarrow \langle x|e^{i\epsilon^i\hat{p}_i}|\psi\rangle &= (1 + \epsilon^i\partial_i + i\epsilon^i\omega_i)\psi(x) \\ &= [\psi(x) + \epsilon^i\partial_i\psi(x)](1 + i\epsilon^i\omega_i) \\ &= \psi(x+\epsilon)e^{i\epsilon^i\omega_i}. \end{aligned} \tag{10.17}$$

In order to see, why it is a good thing to investigate infinitesimal displacements of ψ we have to keep in mind that the system we describe consists essentially of free fermions. The wave function ψ describes an electron at the Fermi surface, where the dispersion relation can be linearised within a good approximation (Figure 10.3):

$$p = \pm p_F + \hbar k, \qquad H = \frac{p^2}{2m} \pm \frac{p_F\hbar k}{m} + O(k^2) \approx E_F \pm v_F\hbar k.$$

The system is conservative (i.e. the Hamiltonian is time independent), hence the time evolution of ψ is

$$|\psi(t)\rangle = e^{-iHt}|\psi(0)\rangle \propto e^{-i\hbar k\cdot v_F t}|\psi(0)\rangle.$$

[38] See [57], p. 23

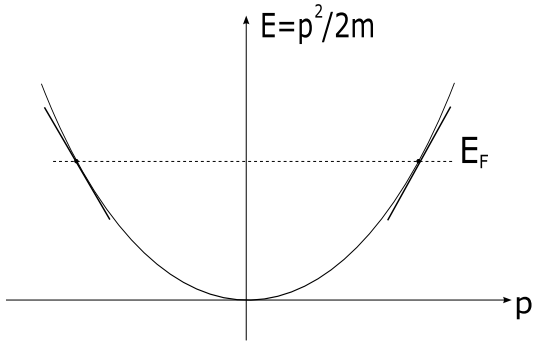

Figure 10.3: Dispersion relation of free electrons

The Fermi-velocity v_F times an infinitesimal t is equivalent to the ϵ^i in equation (10.17).

Because the $\hat{p}_j$ commute among themselves (10.17) can be generalised to large displacements. For example let us displace ψ along a smooth curve

$$\mathrm{C} : [0, T] \to M.$$

Under C the state vector transforms as follows:

$$\langle x|\psi\rangle \longrightarrow \langle x|e^{i\int_\mathrm{C} dx^i \hat{p}_i}|\psi\rangle = \psi(x + \Delta x)e^{i\int_\mathrm{C}\omega}. \tag{10.18}$$

Here is $\Delta x = \mathrm{C}(T) - \mathrm{C}(0)$ and $\omega := \omega_i dx^i$ is the one-form, which appears in the position representation of the momentum operator. We assumed, that the initial and the end point of the curve C lies in a single patch of the manifold M, since otherwise the quantity Δx would not be well defined. If we take C to be closed ($\mathrm{C}(T) = \mathrm{C}(0)$), a path-dependent phase-factor will remain:

$$\langle x|\psi\rangle \longrightarrow \langle x|e^{i\oint_\mathrm{C} dx^i \hat{p}_i}|\psi\rangle = \psi(x)e^{i\oint_\mathrm{C}\omega}. \tag{10.19}$$

This phase-factor $\exp(i\oint_\mathrm{C}\omega)$ will vanish, if M is a star-shaped manifold and ω a closed one-form. One can show this easily by using Pointcaré ($\omega = df$) and by the fact that an integral over the exterior derivative df of a function f is equal to the difference $f(\mathrm{C}(T)) - f(\mathrm{C}(0))$, which for a closed path C is always equal to zero. Alternatively using the Stokes' theorem:

$$\oint_\mathrm{C}\omega = \int_\mathrm{S} d\omega = 0, \tag{10.20}$$

whereas S is a surface bounded by the curve $\mathrm{C}(:= \partial S)$. Stokes' theorem is valid on any manifold and this gives the possibility to generalize the phase-factor derived above to non-trivial manifolds. Let us for example examine a quantum system with an infinitely long solenoid in three dimensional space. Since this system has

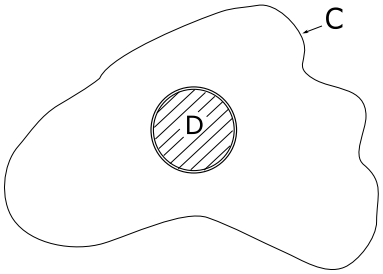

Figure 10.4: Closed path encircling a disk

an translation symmetry along the axis of the solenoid, it is enough to look at a configuration space M consisting of a two-dimensional plane $\mathbb{R}^2$ with a disk D of radius ρ removed. Consider now a path C encircling the disk D and define S' as the surface bounded by the loop C and the boundary ∂D of the disk D (Figure 10.4). Stokes leads to the following expression:

$$\oint_{\mathrm{C}} \omega - \oint_{\partial \mathrm{D}} \omega = \int_{\mathrm{S}'} d\omega = 0, \tag{10.21}$$

since ω is a closed one-form. From this equation one can see, *that the phase does not depend on the particular closed curve used for the displacement, as long as it encircles D once*[39]. The phase factor depends only on how many times the closed curve C winds around D and it is independent of continuous deformations of the curve C. One calls such a phase, since it is totally defined by the topological property of the curve, a *topological phase.*

Let us now treat a system of an electron traversing a closed loop C in the configuration space $\mathbb{R}^3$ with an external magnetic field

$$\mathrm{B}^{(el)} = \nabla \times \mathrm{A}^{(el)}, \tag{10.22}$$

whereas $\mathrm{A}^{(el)} = (A^1, A^2, A^3)$ is the electromagnetic vector potential. It can be expressed in terms of differential forms according to $A^{(el)} = A_a dx^a$, and one gets

$$\begin{aligned} F^{(el)} := dA^{(el)} &= \left(\frac{\partial}{\partial x^b} A_c^{(el)}\right) dx^b \wedge dx^c \\ &= -\frac{1}{2}\epsilon_{abc}\left(\mathrm{B}^{(el)}\right)^a dx^b \wedge dx^c. \end{aligned} \tag{10.23}$$

The minus sign in the last expression comes from the Minkowski metric η with $\eta_{ab} = -\delta_{ab}$ whereas $a, b = 1, 2, 3$ are the space components. Then, the contravariant space coordinates of the electromagnetic space-time vector potential can be shifted to covariant coordinates via: $A_a := \eta_{ab} A^b = -A^b$.

[39] See [57], p. 25

To get the interaction between the electron and the magnetic field into the equations of motion, one has to replace the momentum operator $\hat{\mathrm{p}}$ by its covariant generalisation

$$\hat{\mathrm{p}} \to \hat{\pi} := \hat{\mathrm{p}} - \frac{e}{c}\mathrm{A}^{(el)}, \tag{10.24}$$

which follows, for example, from the derivation of the Hamiltonian of a charged particle in electromagnetic fields via Legendre-Transformation of the Lagrangian $L = \frac{1}{2}m\dot{\mathrm{q}}^2 - e\Phi(\mathrm{q},t) + \frac{e}{c}\dot{\mathrm{q}}\cdot\mathrm{A}(\mathrm{q},t)$ or, alternatively, from field theory by assuming a local $U(1)$ gauge invariance. This means that the Lagrangian is required to be invariant under $\phi(x) \mapsto e^{i\alpha(x)}\phi(x)$, whereas $\alpha(x)$ is an arbitrary function of space and time. The terms involving derivatives of ϕ (e.g. $\partial_\mu\phi$) are not invariant under such transformations. *To remedy this one needs to introduce the electromagnetic gauge potential* $a_\mu(x)$*, with time and space components* (a_0, a),[40]. The gauge covariant derivative of ϕ can then be defined by $D_\mu\phi := \partial_\mu\phi - ia_\mu\phi$, if we postulate that a_μ transforms under the gauge transformation to $a_\mu \mapsto a_\mu + \partial_\mu\alpha$. Calculations show that D_μ transforms the same way as ϕ does: $D_\mu \mapsto e^{i\alpha}D_\mu$. The space coordinates of the covariant derivative can be identified with the covariant momentum

$$\hat{\pi}_i = \hat{\mathrm{p}}_i - \frac{e}{c}\mathrm{A}_i^{(el)} = iD_i = i\partial_i + a_i. \tag{10.25}$$

We now incorporated the effect of the magnetic field in the definition of the covariant momentum operator $\hat{\pi}$ and want to look whether the movement of an electron along a path C may be achieved by using this momentum as the generator of the accordant displacements. The momentum $\hat{\pi}$ in the coordinate representation is

$$\langle x|\hat{\pi}_a|\psi\rangle = \left(-i\frac{\partial}{\partial x^a} - \frac{e}{c}\mathrm{A}_a^{(el)}(x) + \tilde{\omega}_a(x)\right)\psi(x), \tag{10.26}$$

whereas $\tilde{\omega}_a$ are components of a closed one-form $\tilde{\omega}$ on $\mathbb{R}^3$. Since we are considering the configuration space $\mathbb{R}^3$, this one-form must be exact. However, from the field theory point of view we saw that $A_i^{(el)}$ is defined up to addition of a gauge term $\partial_i\alpha(x)$, which is the i-th component of an exact one-form. Hence, we can absorb $\tilde{\omega}$ in the definition of $A^{(el)}$. This leads to the representation

$$\langle x|\hat{\pi}_a|\psi\rangle = \left(-i\frac{\partial}{\partial x^a} - \frac{e}{c}A_a^{(el)}(x)\right)\psi(x). \tag{10.27}$$

Displacing the electron along C gives

$$\langle x|\psi\rangle \to \langle x|e^{i\oint_\mathrm{C} dx^a\hat{\pi}_a}|\psi\rangle = \psi(x)e^{-i\frac{e}{c}\oint_\mathrm{C} A^{(el)}}. \tag{10.28}$$

We receive an electromagnetic phase $e^{i\frac{e}{c}\oint_\mathrm{C} A^{(el)}}$, which is in general *not* independent of the path C. If the magnetic field $\mathrm{B}^{(el)}$ vanishes, then $A^{(el)}$ becomes a

[40] See [58], p. 33

closed one-form and the electromagnetic phase is going to be a topological phase. Hence, in the case of $\mathbb{R}^3$ the closedness of $A^{(el)}$ implies its exactness and the phase angle vanishes. However we can view cases, in which the configuration space M is just a portion of $\mathbb{R}^3$ in which the magnetic field vanishes. Hence, in general M could have a non-trivial topology. *In view of this observation, a comparison of* (10.11) *and* (10.27) *suggests the identification of the closed one-form* ω *of* (10.13) *with the electromagnetic one-form* $A^{(el)}$ [41]

$$\omega = -\frac{e}{c}A^{(el)}. \tag{10.29}$$

Let us now analyse the A-B effect. In the A-B system the magnetic field is confined to an infinitely long solenoid, the electron is circulating around and not allowed to pass through it. The magnetic field vanishes outside the solenoid and the configuration space of the electron can be compared with the system described directly after (10.20). Hence, the topological (A-B) phase associated with a closed curve C is determined by the winding number of C and the fundamental topological phase:

$$e^{\frac{ie}{c}\int_{\mathrm{D}} F^{(el)}},$$

where we used (10.20). This phase can be computed by using the information about the magnetic field, equation (10.23), and Stoke's theorem

$$\begin{aligned} e^{-\frac{ie}{c}\oint_{\partial D} A^{(el)}} &= e^{-\frac{ie}{c}\int_D dA^{(el)}} = e^{\frac{ie}{c}\int_D F^{(el)}} \\ &= e^{-\frac{ie}{c}\int_D \mathrm{B}^{(el)}\cdot d\mathrm{S}} = e^{-\frac{ie}{c}\Phi_B}, \end{aligned} \tag{10.30}$$

whereas Φ_B is the magnetic flux through D. The phase derived in (10.30) is the Aharonov-Bohm (A-B) phase and exactly the same result as we got in (10.7). *Its significance is that although the electron is classically confined to a region where the magnetic field vanishes, it is influenced by the field quantum mechanically*[42].

Relation to the Berry's geometric phase

The A-B phase can be viewed as a special case of the Berry's geometric phase $\gamma_n(t)$, which is defined as follows[43]

$$\gamma_n(t) = \int_{R(0)}^{R(t)} i\langle n; R(t)|d|n; R(t)\rangle = \int_C A^n, \tag{10.31}$$

whereas $|n; R(t)\rangle$ is the Eigenstate to the n-th Eigenvalue of the Hamiltonian $\hat{h}(t)$. This Eigenstate depends on the parameter $R(t)$, which is a point in the parameter space describing the environment of the quantal system under consideration. We

[41] See [57], p. 27
[42] See [57], p. 28
[43] See [57], p. 16

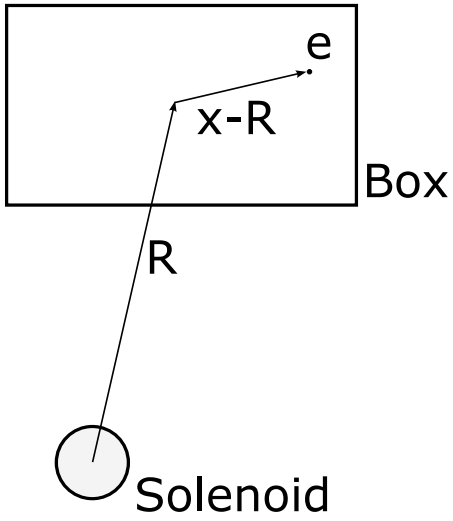

Figure 10.5: A-B system with the electron confined to a box.

want to show that under an adequate description of $|n; R(t)\rangle$ the Mead-Berry connection one-form A^n is proportional to the electromagnetic vector potential $A^{(el)}$ of the A-B system. To see this, let the electron be confined to a box placed at a point R of space, with $|R| \gg \rho$, whereas ρ is the radius of the solenoid centered in the origin (Figure 10.5). The Hamiltonian of the system depends on the space coordinate and the covariant momentum $\hat{\pi}$

$$\hat{h} = \hat{h}\Big(\hat{\pi}, \hat{x} - R\Big). \tag{10.32}$$

Here we have switched to a coordinate frame centered inside the box. The location R of the box plays in this description the role of the parameter which parameterize the Hamiltonian $h = h(R)$. We assume that there is one single Hilbert space $\mathcal{H}$ which is complete for any R of the parameter space. Then the Eigenstates $|n; R\rangle$ are defined by:

$$\hat{h}\Big(\hat{\pi}, \hat{x} - R\Big)|n; R\rangle = E_n(R)|n, R\rangle. \tag{10.33}$$

If we consider ψ_n to be the Eigenvectors of the free Hamiltonian $\hat{h}_0 = \hat{h}_0(\hat{\mathrm{p}}, \hat{x} - R)$ it can be readily shown that

$$\langle x|n; R\rangle = e^{\frac{ie}{\hbar c}\int_R^x A^{(el)}}\psi_n(x - R), \tag{10.34}$$

since

$$\begin{aligned}\hat{h}(\hat{\pi},\hat{x}-R)|n;R\rangle &= \frac{\left(\hat{p}-\frac{e}{c}A^{(el)}\right)^2}{2m}|n;R\rangle \\ &= \left(\frac{-\hbar^2\nabla^2}{2m}+\frac{1}{2m}\Big(\frac{ie\hbar}{c}(\nabla A^{(el)})+2iA^{(el)}\hbar\nabla \right. \\ &\quad \left.+\frac{e^2}{c^2}A^{(el)^2}\Big)\right)e^{\frac{ie}{\hbar c}\int_R^x A^{(el)}}\psi_n(x-R) \\ &= \cdots = E_n e^{\frac{ie}{\hbar c}\int_R^x A^{(el)}}\psi_n(x-R) \\ &= E_n|n;R\rangle,\end{aligned}$$

where the term $\nabla A^{(el)}$ was set to zero using the Coulomb-gauge. From this equation one can also see, that the introduction of the magnetic field does not affect the energy eigenvalues E_n. Furthermore the integration in (10.34) is independent of the choice of the path along which the integral is evaluated as long as the path does not intersect or encircle the solenoid, since the magnetic field outside the tube vanishes.

Having an expression for $|n;R\rangle$, the Mead-Berry connection one-form can be computed

$$\begin{aligned}A^n &:= i\langle n;R|d|n;R\rangle = i\langle n;R|\frac{\partial}{\partial R^i}|n;R\rangle dR^i \\ &= i\int dx^3\psi_n^*(x-R)\Big(-\frac{ie}{c}A^{(el)}(R)\psi_n(x-R)+d\psi_n(x-R)\Big) \\ &= \frac{e}{c}A^{(el)} \qquad (10.35)\end{aligned}$$

The third equality holds, since ψ_n is assumed to be normalized (ψ_n can be choosen to be real since the Hamiltonian is invariant under time-reversal). Equation (10.35) together with the definition of the Berry's phase (10.31) gives us the following identification:

$$e^{i\gamma_n} = e^{\frac{ie}{\hbar c}\oint_C A^{(el)}}. \qquad (10.36)$$

The closed path C in M represents the curve along which the box, containing the electron, is transported. The right hand side of (10.36) is independent of the energy quantum number n. Hence (10.36) is valid for any superposition of the energy eigenvectors and consequently for any wave packet. This point gives a subsequent legitimation to the idea to start the analysis with an electron which is confined to a finite box R.

This derivation shows, that the A-B phase is a particular example of Berry's geometric phase. However, if we consider a regime in which the magnetic field vanishes, the A-B phase is topological in nature unlike the usual geometric phase. If we go to a regime where the magnetic field is nonzero, the A-B phase becomes

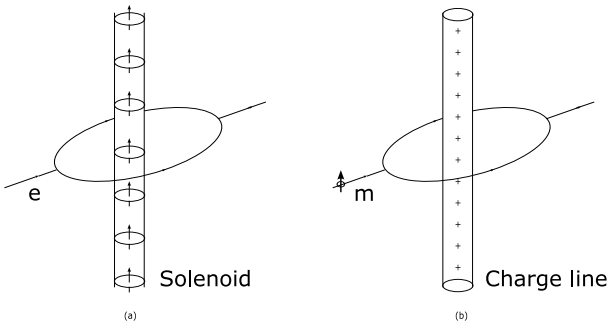

Figure 10.6: a: A-B System, b: A-C System

truly geometric, which means though independent of the details of the dynamics it depends on the geometry of the closed path C.

Furthermore, it should be noted that in this specific example of a Berry's phase, the adiabatic approximation is valid. The adiabatic approximation demands that the physical system which depends on the time evolution of its environment does not jump from the initial n-th eigenstate $|n;R\rangle\langle n;R|$ at $t=0$ into any other eigenstate $|m,R(t)\rangle\langle m,R(t)|, m \neq n$ at any later time t. This compare to the condition that the adiabatic approximation is valid if and only if $\langle m;R(t)|\frac{d}{dt}|n;R(t)\rangle$ can be neglected[44]. Using (10.34) it can be shown that in our case this expression vanishes for $m \neq n$. Hence, the adiabatic approximation is satisfied for our system regardless of the speed with which the electron moves around the solenoid.

3 The Aharonov-Casher-Effect

In their paper[45] Aharonov and Casher thought of an experiment in which neutral particles with a magnetic moment will exhibit the Aharonov-Bohm effect. The general idea is to treat the solenoid in the A-B effect as a straight line of magnetic moments and then in a second step to exchange the role of this moments and the electrons (Figure 10.6). It is the subject of this section, to show how this can be achieved.

The Dual of the A-B Effect

We start with the Lagrangian of an A-B system, which is an electron in a magnetic vector potential (e is positive)

$$\mathcal{L} = \frac{1}{2}\mathrm{m}v^2 - \frac{e}{c}\vec{A}\cdot\vec{v}. \tag{10.37}$$

[44] See [57], p. 14
[45] See [59]

Evaluating the path integral of this system in the semi-classical approximation, this Lagrangian leads to a phase factor in the propagator (and hence in the wavefunction) of the form

$$\exp(\frac{i}{\hbar}S) = \exp(-\frac{ie}{c\hbar}\oint \vec{A}\cdot\vec{v}dt) = \exp(-\frac{ie}{c\hbar}\oint \vec{A}\cdot d\vec{x}), \tag{10.38}$$

whereas $S = S[\bar{x}] := \int_{t_a}^{t_b}\mathcal{L}(x,\dot{x},t)dt$ is the action over the classical path[46] $\bar{x}$ (in the expression (10.38) the kinetic term was disregarded, since it does not produce characteristic phenomena for the A-B effect).

Let us analyse a more detailed Lagrangian which describes not only the dynamics of the electric charged particle at point $\vec{r}$, but also the dynamics of the solenoid located at the point $\vec{R}$ (in the plane). One may suggest that $\mathcal{L}$ is

$$\mathcal{L} = \frac{1}{2}mv^2 + \frac{1}{2}MV^2 - \frac{e}{c}\vec{A}(\vec{r}-\vec{R})\cdot\vec{v}, \tag{10.39}$$

since the solenoid is electrically neutral. However, evaluating the Euler-Lagrange equations, the Lagrangian (10.39) leads to a non-vanishing force on the electron

$$\begin{aligned}\frac{d}{dt}\frac{\partial\mathcal{L}}{\partial\dot{r}_j} - \frac{\partial\mathcal{L}}{\partial r_j} &= m\dot{v}_j - \frac{e}{c}\sum_i\left(\frac{\partial A_j}{\partial r_i}\frac{dr_i}{dt} - \frac{\partial A_j}{\partial R_i}\frac{dR_i}{dt} - \frac{\partial A_i}{\partial r_j}v_j\right)\\ &= m\dot{v}_j - e/c\cdot\underbrace{v_i(\partial_i A_j - \partial_j A_i)}_{(v\wedge(\nabla\wedge A))_j} + e/c\cdot V_i\partial_i A_j = 0\end{aligned}$$

The second term in the second line is the ordinary Lorentz force and vanishes outside the solenoid because $H = 0$. The third therm generates a non-vanishing force which is proportional to the velocity of the solenoid. To avoid this force, Aharonov and Casher proposed an extra term in the Lagrangian (10.39):

$$\mathcal{L} = \frac{1}{2}mv^2 + \frac{1}{2}MV^2 - \frac{e}{c}\vec{A}(\vec{r}-\vec{R})\cdot(\vec{v}-\vec{V}). \tag{10.40}$$

The extra term in (10.40) leads to an extra Term $e/c\cdot V_i\partial_j A_i$ in the equations of motion:

$$m\dot{\vec{v}} = -\frac{e}{c}(\vec{v}-\vec{V})\wedge\vec{B} = -M\dot{\vec{V}}, \tag{10.41}$$

with the magnetic field $\vec{B} = \nabla\wedge\vec{A}(\vec{r}-\vec{R})$. This new Lagrangian is gauge invariant under the transformation $\vec{A}\to\vec{A}+\nabla\chi$. Moreover, it is translation invariant and hence the momentum is conserved.

In the following it will be proved that (10.40) follows from electrodynamics and correctly describes the A-B system. As mentioned above a solenoid can be viewed as a line of magnetic moments which interacts with the electron. Therefore, we

[46] A classical path is a path for which the Variation δS of the action S vanishes.

first want to look at a single magnetic moment $\vec{\mu}$ moving in an external static electric field of an electron. This magnetic moment is generated by a current distribution:

$$\vec{j} = \nabla \wedge \vec{\mathscr{M}}, \qquad \int \vec{\mathscr{M}} = \vec{\mu}. \tag{10.42}$$

The velocity-Vierervector of the moment is $\mathrm{U}^\alpha = (c, \vec{V})$ and the generalized current $\mathrm{J}^\alpha = (c\rho, \vec{j})$. In the inertial system, in which the velocity of the moment vanishes, we have $\mathrm{U}'^\alpha = (c, \vec{0})$ and $\mathrm{J}'^\alpha = (0, \vec{j}')$. The Minkovski scalar product of two Vierervectors is invariant, hence

$$c^2\rho - \vec{V} \cdot \vec{j} = J^\alpha U_\alpha = J'^\alpha U'_\alpha = 0$$

and we get

$$c^2\rho = \vec{V} \cdot \vec{j}. \tag{10.43}$$

Equation (10.43) states that a moving magnetic moment generates a charge density ρ. Thus, the Lagrangian of the magnetic moment is

$$\begin{aligned} \mathcal{L} = \frac{1}{2}MV^2 - \int \rho A_0 \quad &= \tfrac{1}{2}MV^2 - \tfrac{1}{c^2}\int A_0 \vec{V} \cdot \nabla \wedge \vec{\mathscr{M}} \\ &= \tfrac{1}{2}MV^2 - \tfrac{1}{c^2}\vec{V} \cdot \vec{E} \wedge \vec{\mu}, \end{aligned} \tag{10.44}$$

whereas $\vec{E} = -\nabla A_0$ is the electric field at the position of the magnetic moment. The last identity holds, because if we use Stokes, we get

$$0 = \int \nabla \wedge (A_0 \vec{\mathscr{M}}) = \int (\nabla A_0) \wedge \vec{\mathscr{M}} + A_0(\nabla \wedge \vec{\mathscr{M}})$$

and the magnetisation is basically given by $\vec{\mathscr{M}}(\vec{x}) = \vec{\mu}\delta(\vec{x} - \vec{R})$. The electric field $\vec{E}$ is nothing else but the Coulomb field of the electron, therefore

$$\vec{E} \wedge \vec{\mu} = -\frac{e}{4\pi}\frac{(\vec{R} - \vec{r}) \wedge \vec{\mu}}{|R - r|^3} = -e\vec{A}(\vec{r} - \vec{R}), \tag{10.45}$$

whereas $\vec{A}$ is the vector potential of a magnetic dipole[47] whose source is the magnetic moment $\vec{\mu}$ at $\vec{R}$. Now we are ready to add the Lagrangian of the electron (10.37) and recognize immediately that this combination is equal to equation (10.40).

Next we analyse a system of more than one electric charged particle interacting with more than one magnetic moment. In the Lagrangian of this system we include the interaction between charged particles and magnetic moments but

[47] See also J. D. Jackson, Klassische Elektrodynamik, sect. 5.6.

interactions among charged particles or magnetic moments itself are excluded because we are not interested in their dynamics. The Lagrangian is then:

$$\begin{aligned}\mathcal{L} &= \frac{1}{2}\sum_e m_e v_e^2 + \frac{1}{2}\sum_m M_m V_m^2 \\ &\quad + \sum_{e,m}(\vec{v}_e - \vec{V}_m)\cdot e\vec{A}(\vec{r}_e - \vec{R}_m)\end{aligned} \tag{10.46}$$

Encouraged by this derivation of (10.40) for a many particle system, we may dare an interpretation: *Because of the dependence of A on* $(\vec{r} - \vec{R})$, *the system possesses a kind of duality when the roles of* $\vec{r}_e$ *and* $\vec{R}_m$ *are reversed*[48]. This statement leads in particular to the fact, that though a magnetic moment which moves in the electric field of a straight homogeneously charged line feels no force, it undergoes an A-B effect with the following phase shift

$$\Delta S = -\frac{e}{c}\oint \mathrm{A}(\vec{r} - \vec{R})\cdot d\vec{R}. \tag{10.47}$$

This phenomena is the Aharonov-Casher Effect (A-C Effect). We assume the magnetic moment to be polarized along the z-axis and calculate the electrostatic field of the charge line with Gauss' law. Expression (10.45) for the vector potential A leads to[49]

$$\Delta S = \pm\frac{4\pi\mu\Lambda}{\hbar c}, \tag{10.48}$$

depending on whether the neutron has spin up or down. Thus the phase shift is proportional to the lineal charge density Λ and the magnetic moment μ.

The group of A. Cimmino et al. verified in 1989 the existence of the A-C Effect[50]. They used a neutron interferometer containing an electrode system which was prism-shaped to amplify the expected phase shift. Since the A-C phase is a topological phase, this generates the same effect as if they had used a line charge. An experimental problem was the stability of the interferometer (the measurements took several month). A polarized neutron beam would have been disturbed so strong that the sensitivity of the experiment would have been destroyed. Therefore, an unpolarised neutron beam was used. In order to get a interference effect with an unpolarised beam, they introduced an additional and spin-independent phase shift. This phase shift was maintained using the gravitational potential. The interferometer was tilted about the incident beam direction. Neutrons traveling along two opposing paths around the prism-shaped center electrode experience different gravitational potentials. The result is a spin-independent phase shift. This experiment shows, that not only electromagnetic

[48] See [59]
[49] See [60]
[50] See [60]

potentials can cause phase shifts but also for instance the gravitational potential. The ratio of the experimental result compared to the theoretically predicted value is

$$\frac{(\Delta\phi_{AC})_{exp}}{(\Delta\phi_{AC})_{theor}} = 1.46 \pm 0.35.$$

Derivation of the A-C-Effect via Dirac Equation

In order to strengthen the a bit dirty foundation of (10.40), in which we used a relativistic argument to explain the generation of a charge density of a moving neutron, (10.40) is to be rederived from the Dirac equation. The Dirac Lagrangian of a purely magnetic particle without electric charge though in an external electric field is (we set $\hbar = c = 1$)

$$\mathscr{L} = \bar{\psi}\big(i\partial_\mu\gamma^\mu - m - \frac{1}{2}\mu F^{\mu\nu}\sigma_{\mu\nu}\big)\psi, \tag{10.49}$$

where $\bar{\psi} = \psi^\dagger\gamma^0$, m the mass of the particle, μ the magnetic moment, $F^{\mu\nu}$ the electromagnetic field tensor and $\sigma_{\mu\nu} = \frac{1}{2}i[\gamma_\mu, \gamma_\nu]$,

$$F^{\mu\nu} = \begin{pmatrix} 0 & E_x & E_y & E_z \\ -E_x & 0 & B_z & -B_y \\ -E_y & -B_z & 0 & B_x \\ -E_z & B_y & -B_x & 0 \end{pmatrix}.$$

In equation (10.49) we used the following representation

$$\gamma^0 = \beta = \begin{pmatrix} 1 & 0 \\ 0 & -1 \end{pmatrix}, \qquad \alpha^k = \begin{pmatrix} 0 & \sigma^k \\ \sigma^k & 0 \end{pmatrix}, \tag{10.50}$$

with $k \in \{1, 2, 3\}$ the space components and $\gamma^k = \beta\alpha^k$.

Afterwards, we analyse the nonrelativistic limit of the Euler-Lagrange-Equations of the Lagrangian given in (10.49). Therefore, we write the field ψ, which describes the four-component vector-field of the particle, as a vector $\psi = \begin{pmatrix} \varphi \\ \chi \end{pmatrix}$ with u and v a two-component vector-field per each representing the particle with positive energy and the antiparticle with negative energy. With the Euler-Lagrange equations

$$\partial_\mu \frac{\partial\mathscr{L}}{\partial(\partial_\mu\psi^*)} - \frac{\partial\mathscr{L}}{\partial\psi^*} = 0,$$

we get

$$-\gamma_0\Big(i\gamma_\mu\partial_\mu - m - \frac{1}{4}i\mu F^{\mu\nu}[\gamma_\mu, \gamma_\nu]\Big)\psi = 0 \tag{10.51}$$

Since we consider a neutral particle, we can set the electric charge $e = 0$. The external magnetic field though we will take along to check whether the Lagrangian

(10.49) produces the correct interaction term between the magnetic moment μ and the magnetic field B . With this assumptions equation (10.51) can be simplified to

$$\Big(-i\partial_0 - i\alpha_k\partial^k + \gamma_0 m + \gamma_0 i\mu(\vec{E}\cdot\vec{\alpha}) + \gamma_0\mu\vec{B}\cdot\vec{\sigma}\Big)\begin{pmatrix}\varphi\\ \chi\end{pmatrix} = 0. \tag{10.52}$$

This leads to the following equation of motion which will be the starting point for subsequent non-relativistic approximations:

$$i\partial_0\begin{pmatrix}\varphi\\ \chi\end{pmatrix} = -i\vec{\sigma}\vec{\nabla}\begin{pmatrix}\chi\\ \varphi\end{pmatrix} + m\begin{pmatrix}\varphi\\ -\chi\end{pmatrix} + i\mu\vec{\sigma}\cdot\vec{E}\begin{pmatrix}\chi\\ -\varphi\end{pmatrix} + \mu\vec{B}\cdot\vec{\sigma}\begin{pmatrix}\varphi\\ -\chi\end{pmatrix} \tag{10.53}$$

In the case of the non-relativistic limit the rest energy of our particle is much larger than the other terms and the field φ can be separated in a part carrying the time evolution and a part which varies slowly in time:

$$\begin{pmatrix}\varphi\\ \chi\end{pmatrix} = e^{-imt}\begin{pmatrix}\tilde{\varphi}\\ \tilde{\chi}\end{pmatrix}. \tag{10.54}$$

This Ansatz will generate a solution with positive energy. Inserting it into (10.53) leads to an equation for the slowly varying $\tilde{\psi}$

$$i\hbar\frac{\partial}{\partial t}\begin{pmatrix}\tilde{\varphi}\\ \tilde{\chi}\end{pmatrix} = -i\vec{\sigma}\cdot\vec{\nabla}\begin{pmatrix}\tilde{\chi}\\ \tilde{\varphi}\end{pmatrix} + i\mu\vec{\sigma}\cdot\vec{E}\begin{pmatrix}\tilde{\chi}\\ -\tilde{\varphi}\end{pmatrix} + \mu\vec{B}\cdot\vec{\sigma}\begin{pmatrix}\tilde{\varphi}\\ -\tilde{\chi}\end{pmatrix} - 2m\begin{pmatrix}0\\ \tilde{\chi}\end{pmatrix}. \tag{10.55}$$

In the second equation of (10.55) the terms $\dot{\tilde{\chi}}$ and $\mu\vec{B}\cdot\vec{\sigma}\tilde{\chi}$ can be neglected compared to $2m\tilde{\chi}$ and we get approximately[51]

$$\tilde{\chi} = \frac{1}{2m}\big(-i\vec{\sigma}\cdot\vec{\nabla} - i\mu\vec{\sigma}\cdot\vec{E}\big)\tilde{\varphi} \tag{10.56}$$

Since $-i\vec{\nabla}$ can be identified with the momentum $\vec{p}\sim m\vec{v}$ one can see, that in our approximation $\tilde{\chi}$ is of the order $\sim v/c$ smaller than $\tilde{\varphi}$. Inserting (10.56) into the first equation of (10.55) we get

$$\begin{aligned} i\partial_0\tilde{\varphi} &= \frac{1}{2m}\Big(\big(\vec{\sigma}(-i\vec{\nabla})\big)\big(\vec{\sigma}(-i\vec{\nabla}) - i\mu\vec{E}\vec{\sigma}\big) + i\mu\big(\vec{\sigma}\vec{E}\big)\big(-i\vec{\nabla}\vec{\sigma} - i\mu\vec{E}\vec{\sigma}\big)\Big)\tilde{\varphi} \\ &\quad +\mu(\vec{B}\cdot\vec{\sigma})\tilde{\varphi} \\ &= \frac{1}{2m}\Big(\vec{p}^2 + \mu^2\vec{E}^2 - 2\mu\vec{\sigma}\cdot(\vec{p}\wedge\vec{E})\Big)\tilde{\varphi} + \mu(\vec{B}\cdot\vec{\sigma})\tilde{\varphi}, \end{aligned} \tag{10.57}$$

whereas the following identity was used: $(\vec{\sigma}\cdot\vec{a})(\vec{\sigma}\cdot\vec{b}) = \vec{a}\cdot\vec{b} + i\vec{\sigma}\cdot(\vec{a}\wedge\vec{b})$. The second term in (10.57) describes the interaction of the magnetic moment with

[51] See [61], p. 129

the external magnetic field $\vec{B}$. This term occurs also in the Pauli Equation for a non-relativistic particle with Spin 1/2. Hence, the Lagrangian (10.49) seems to describe the system correctly. Finally, by using $(\mu\vec{E} \wedge \vec{\sigma})^2 = \mu^2\vec{E}^2$ we have the nonrelativistic Hamiltonian (the magnetic field is now neglected)

$$H_{NR} = \frac{1}{2m}\left(\left(\vec{p} - (\mu\vec{E} \wedge \vec{\sigma})\right)^2 - \mu^2\vec{E}^2\right). \tag{10.58}$$

If we identify $\mu\vec{\sigma} = \vec{\mu}$ with the magnetic moment (and this identification makes sense, since $\vec{\sigma}$ is proportional to the Spin $\vec{S}$), *the first term in* (10.58) *is precisely the Hamiltonian which corresponds to* equation (10.44)[52]. The second term in (10.58) can be neglected if we assume that $\mu\vec{E}$ is small compared to $m\vec{v}$. Therefore, the derivation which started from the Dirac Equation (10.51) leads to the Lagrangian (10.46) and we are done.

4 Summary

The investigation on the Aharonov-Bohm effect, then, resulted that there are several experimentally realisable quantum systems in which electrons or neutrons undertake interference effects even if they don't feel a force. For example an electron, which moves around a solenoid feels no magnetic field. However, the electron picks up a phase shift. This phase shift is proportional to the magnetic flux through a surface which is bounded by the closed path of the electron. A possible explanation for this phenomenon is that the electromagnetic potential, which does not vanish outside the solenoid, evokes the phase shift. This means that in quantum mechanics the potentials become physically relevant whereas in classical mechanics they were not. The A-B phase is purely topological in nature if the magnetic field is confined to an area which is not penetrated by the electrons. This means that the phase shift depends only on how many times the electron winds around the solenoid and it does not depend on the actual shape of the electron's path. However, if the magnetic field extends into the area of the electron, the A-B phase becomes a geometric phase and path-dependent. In the experiments it is quite difficult to suppress this path dependence which destroys the interference effects. It could be done further investigations on this topic. For example, the group of Yang Ji et al.[53] made an experiment with electrons which are forced to move on a single path using the quantum hall effect. The result was a very pure interference pattern. In the section about the relation between A-B effect and Berry's phase the fact that the electrons in the A-B effect evolve adiabatically showed that they can be well described by Berry's formalism. The introduction of the Aharonov-Casher effect illustrated that the A-C effect is a dual of the A-B effect since the roles of electrons and magnetic moments can be

[52] See [59]
[53] See [62]

reversed. The idea is to analyse the Lagrangian of the A-B system by including the dynamics of the electron as well as the dynamics of the solenoid. After some calculations we saw that this Lagrangian is invariant under the exchange of the coordinates of electrons and magnetic moments. Hence, we can describe a neutron moving around an electric charged line with the A-B-Lagrangian. Though electrically neutral, the magnetic moment of the neutron causes a phase shift. The first derivation uses a classical Lagrangian but a relativistic argument to explain the interaction of the magnetic moment with the electric field. This derivation is inconsistent and has to be redone using a relativistic Lagrangian. A neutron is a fermion and, therefore, it has to be described by the Dirac equation. With interest in the particle part of the Dirac equation, we looked at the non-relativistic limit of positive energy and derived the same Lagrangian as in the first place.

Finally, I would like to thank Dr. Sebastian Pilgram for many inspiring discussions and his competent support. Lars Steffen's contribution on various irking Latex and computer problems were very helpful and many thanks go to my younger brother Roman for patiently brushing up on my English.

11 Berry phase III: Berry phase and Bloch states

Juan Carlos Andresen
Supervisor: Sebastian Pilgram

The base for understanding the dynamics of electrons in a periodic crystal, is given by the Bloch theory for periodic systems. In this text the dynamics of electrons in a crystal under perturbations is derived (up to the first order gradient correction). The semi-classical equations are derived by describing the system with the Bloch theory for perturbated crystals and then passing to the semi-classical limit under some simple assumptions. In this equations new terms arise. For the specific case of electromagnetic perturbations on crystals this new terms can be interpreted as the anomalous velocity, which gives rise to the anomalous Hall effect, and the magnetization energy. Applying the quantization rule of Einstein, Brillouin and Keller in the obtained semiclassical equations, new kins of Berry phases emerge.

1 Introduction

In this text, the dynamics of electrons in crystals under slowly varying perturbations are presented. In the development of the dynamics the Bloch theory for periodic systems will play an important role, as the electron wave packet will be expanded in a basis which is spanned by the Bloch wave eigenstates.

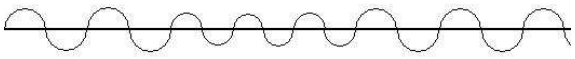

Figure 11.1: Perturbation of the periodicity of the crystal potential.

It will be then presented how, through some assumptions (spread of the wave packet centered at $\mathbf{x}_c$ and the distribution of the expectation value of the wave vector $\mathbf{q}$) the motion of the electron in a perturbated crystal can be described in the semi-classical limit. For this purpose, a Lagrangian given by a time-dependent variational principle is computed. Taking into account the assumptions that made possible to see the electron dynamics in the semi-classical limit, the Lagrangian function can be rearranged in a simple form. This rearranged Lagrangian can be handled as in classical mechanics to derive the semi-classical equations of motion of the electron in the perturbated crystal. By computing these equations of motion new terms arises in a natural form. These new terms can be seen as a correction to the known semi-classical equations of motion for a Bloch electron.

These equations can be "re-quantized" and through this re-quantization a Berry phase emerges as a correction to the quantization condition.

Structure

These text is structured as following:

1. A brief review of the Bloch theory, the semi-classical dynamics and quantization theory.
2. A derivation of the semi-classical equations of electron for different Hamiltonians (a general one and one for an electromagnetic field applied on the crystal).
3. A discussion for the extra terms that arise from the derivation of the semi-classical equations.
4. The quantization of the semi-classical equations and the Berry phase acquired by a wave packet (upon going round a closed orbit once) under a uniform magnetic field and under a uniform electromagnetic field.

2 Review

Bloch Theory

In a perfect crystal, a free electron sees a periodic potential acting on it, i.e. $U(\boldsymbol{r})=U(\boldsymbol{r}+\boldsymbol{R})$, where $\mathbf{R}$ is a Bravais lattice vector. With this assumption the Schrödinger equation for a single electron is

$$H\Psi = \left(-\frac{\hbar^2}{2m}\nabla^2 + U(r)\right)\Psi = E\Psi. \tag{11.1}$$

The electrons that obey this Schrödinger equation are called the *Bloch electrons*.

Bloch Theorem *The solution of the given Schrödinger equation with periodic potential can be written as a modulated plane wave* $\Psi_{nk}(\mathbf{r}) = e^{ikr}u_{nk}(\mathbf{r})$ *with* $u_{nk}(\mathbf{r}) = u_{nk}(\mathbf{r}+\mathbf{R})$ *for all* $\boldsymbol{R}$ *in the Bravais lattice.*[63]

The strong periodicity postulation in the potential has other consequences that follow immediately from the Bloch states. The Bloch waves, for which the wave vector differ only by a reciprocal lattice are equal, this means

$$\Psi_{\mathbf{k}+\mathbf{K}}(\mathbf{r}) = \Psi_{\mathbf{k}}(\mathbf{r}) \tag{11.2}$$

with $\mathbf{K}$ being a reciprocal lattice vector. This result combined with the eigenvalue equation

$$H\Psi_{\mathbf{k}}(\mathbf{r}) = \epsilon(\mathbf{k})\Psi_{\mathbf{k}}(\mathbf{r}) \tag{11.3}$$

gives the periodicity of the energy as a function of the wave vector $\mathbf{k}$, i.e.

$$\epsilon(\mathbf{k}) = \epsilon(\mathbf{k}+\mathbf{K}). \tag{11.4}$$

Semi-classical equations

The behavior of a free electron gas can be calculated using the classical equations, provided that there is no need to localize an electron in a scale comparable to the inter-electronic distance[63]. For a free electron with momentum $\hbar\mathbf{k}$ and energy $E(\mathbf{k}) = \frac{\hbar^2k^2}{2m}$ in a electromagnetic field, the equations of motion are (between collisions)

$$\begin{aligned} v(k) &= \frac{\hbar\mathbf{k}}{m} = \frac{1}{\hbar}\frac{\partial E(\mathbf{k})}{\partial \mathbf{k}} \\ \hbar\dot{\mathbf{k}} &= -e\left(\mathbf{E} + \frac{1}{c}\mathbf{v}\times\mathbf{H}\right) \end{aligned} \tag{11.5}$$

For the Bloch electrons the equations are very similar. In this case the explicit function of the energy is not given, but the periodicity, i.e. $E(\mathbf{k}) = E(\mathbf{k}+\mathbf{K})$. It is assumed that the band index n is a constant of the motion and that there are no inter-band transitions. The semi-classical equations of motion of the Bloch electrons in a electromagnetic field are[63]:

$$\begin{aligned} \dot{\mathbf{r}} &= \mathbf{v_n}(\mathbf{k}) = \frac{1}{\hbar}\frac{\partial E_n(\mathbf{k})}{\partial \mathbf{k}} \\ \hbar\dot{\mathbf{k}} &= -e\left(\mathbf{E} + \frac{1}{c}\mathbf{v_n}\times\mathbf{H}\right) \end{aligned} \tag{11.6}$$

Note: *The momentum $\hbar\mathbf{k}$ is not the momentum of the Bloch electron, it is the crystal momentum, i.e. only external forces apply on the electrons, not the periodic ones.*

Bohr - Sommerfeld quantization rule

Semi-classical Limit for Time-Independent Problems In stationary quantum mechanical states the wave function is separable in the form of $\Psi(\mathbf{q},k) = \Psi(\mathbf{q})\, e^{i\frac{Et}{\hbar}}$, where E is the energy of the stationary state. With the ansatz $\Psi(\mathbf{q}) = e^{i\frac{S(\mathbf{q})}{\hbar}}$, the wave function is $\Psi(\mathbf{q},t) = e^{i\frac{S(\mathbf{q})}{\hbar}-i\frac{Et}{\hbar}}$ substituting this expression to the Schroedinger equation gives

$$\frac{1}{2m}(\nabla S\cdot\nabla S) + V(\mathbf{q}) - E - \frac{i\hbar}{2m}\nabla^2 S = 0 \tag{11.7}$$

Taking it to the classical limit $\hbar \longrightarrow 0$ gives the time independent Hamilton - Jacobi equation

$$\frac{1}{2m}(\nabla S_0)^2 + V(\mathbf{q}) = E \tag{11.8}$$

where $S_0(\mathbf{q}) = \int_{\mathbf{q}_0}^{\mathbf{q}} \mathbf{p}\cdot\mathbf{dq}$ with $\mathbf{q}_0$ being some initial point on a given trajectory.

Wentzel-Krammers-Brillouin approximation Using the Wentzel-Krammers-Brillouin (WKB) approximation, i.e. expansion of the solution for the above differential equation in the form $y(x) = \exp\left\{\frac{1}{\hbar}\sum_{n=0}^{\infty}\hbar^n S_n(x)\right\}$, and solving the Schroedinger equation with the ansatz

$$\Psi(\mathbf{x}) = e^{i\frac{S(x)}{\hbar}} \tag{11.9}$$

where $S(x) = S_0 + \hbar S_1 + \hbar^2 S_2 + ...$ and solving (as in perturbation theory) recursively form lower correction order to higher ones, leads us to the solution of S_0 and S_1

$$S_0(x) = \pm\int_{x_0}^{x} p(x')\,dx' = \pm\int_{x_0}^{x}\sqrt{2m(E-V(x'))}dx' \tag{11.10}$$

and

$$S_1(x) = -\ln\sqrt{p(x)} + \ln c. \tag{11.11}$$

The general approximation to first order of $\hbar$ for the wave function is

$$\Psi(x) = \frac{A}{\sqrt{p}}\exp\left\{+\frac{i}{\hbar}\int_{x_0}^{x} p(x')\,dx'\right\} + \frac{B}{\sqrt{p}}\exp\left\{-\frac{i}{\hbar}\int_{x_0}^{x} p(x')\,dx'\right\}. \tag{11.12}$$

For the classical allowed regions the solution must be real. The two exponentials are chosen to give a real expression

$$\Psi(x) = \frac{A}{\sqrt{p}} \sin\left\{\frac{1}{\hbar}\int_{x_0}^{x} p(x')\,dx' + \alpha\right\} \tag{11.13}$$

being α a phase factor. Requiring that the solution has to join smoothly the form to the left of a classical returning point x_0, the phase α must be $\frac{\pi}{4}$.

Bohr-Sommerfeld quantization The quantization rule of Bohr-Sommerfeld

$$\oint p(x')\,dx' = 2\pi\hbar\left(n + \frac{1}{2}\right) \tag{11.14}$$

comes assuming the situation where the motion is bounded between the two classical turning points $a \leq x \leq b$ and requiring Ψ to be single valued, therefore

$$\Psi(x) = \frac{A}{\sqrt{p}} \sin\left\{\frac{1}{\hbar}\int_{a}^{x} p(x')\,dx' + \frac{\pi}{4}\right\} \tag{11.15}$$

must be the same as

$$\Psi(x) = \frac{B}{\sqrt{p}} \sin\left\{\frac{1}{\hbar}\int_{x}^{b} p(x')\,dx' + \frac{\pi}{4}\right\} \tag{11.16}$$

and writing the first wave function as

$$\Psi(x) = -\frac{A}{\sqrt{p}} \sin\left\{\frac{1}{\hbar}\int_{x}^{b} p(x')\,dx' + \frac{\pi}{4} + \frac{1}{\hbar}\int_{b}^{a} p(x')\,dx' - \frac{\pi}{2}\right\} \tag{11.17}$$

The generalization for many degrees of freedom is[64]

$$I_k = \oint_{C_k} \mathbf{p}\cdot\mathbf{dq} = 2\pi\hbar\left(n_k + \frac{\alpha_k}{4}\right) \tag{11.18}$$

where α_k is the number of caustics traversed.These is the EBK quantization procedure (Einstein, Brillouin and Keller).

3 Semi-classical Dynamics and Berry Curvature

In this section the semi-classical equations of motion for an electron in a perturbed crystal will be derived. The dynamics for the wave packet in a crystal can be derived from the Schrödinger equation, we will not follow this line as it is not convenient. The method used here will be a time -dependent variational principle using the Lagrangian L given by[65]

$$L = \langle\Psi|i\frac{d}{dt} - \hat{H}|\Psi\rangle. \tag{11.19}$$

It can be seen, that by varying this Lagrangian independently in respect to $|\Psi\rangle$ and $\langle\Psi|$ we get the Schrödinger equation.

$$\delta S = \delta \int dt L\left(\Psi, \Psi^*\right) \longrightarrow i\frac{\partial}{\partial t}|\Psi\rangle = \hat{H}|\Psi\rangle \tag{11.20}$$

using the convention $\hbar = 1$.

The first step to get the motion equations is to compute these Lagrangian with the Hamiltonian given by the system. The second is to consider the wave packet expanded in a basis of Bloch eigenstates from a given band, i.e.

$$|\Psi\rangle = \int d^3k a\left(\mathbf{k}, t\right)|\psi_{\mathbf{k}}\left(\mathbf{x}_c, t\right)\rangle. \tag{11.21}$$

Having this, we assume that the spread of the wave packet in the wave vector is small compared with the dimensions of the Brillouin zone and we assume that the spread of the wave packet centered at $\mathbf{x}_c$ is small compared with the length scale of the perturbations.

Under the above assumptions the Lagrangian can be written as a function of the position $\mathbf{x}_c$, the wave vector $\mathbf{k}_c$ and their time derivatives and t. That means, that the system can be seen as a semi-classical one, and the motion of the electrons will be described by the semi-classical equations derived from the Lagrangian.

Mean position and mean wave vector

As mentioned above, the Lagrangian will become a function of the mean position, the mean wave vector and their time derivatives and of t, so that it is convenient to know the expression of these variables, ($\mathbf{x}_c$ and $\mathbf{k}_c$). For the mean wave vector we have this expression, with the narrow distribution $|a\left(\mathbf{k}, t\right)|^2$ compared with the Brillouin zone,

$$\mathbf{k}_c = \int d^3k \mathbf{k}|a\left(\mathbf{k}, t\right)|^2 \tag{11.22}$$

and for the mean position we have this other expression

$$\begin{aligned}
\mathbf{x}_c = \langle\Psi|\hat{\mathbf{x}}|\Psi\rangle &= \int\int\int d^3x\ d^3k\ d^3k'\ a^*_{\mathbf{k}}\psi^*_{\mathbf{k}}\ \mathbf{x}\ a_{\mathbf{k}'}\psi_{\mathbf{k}'} \\
&= \int\int\int d^3x\ d^3k\ d^3k'\ a^*_{\mathbf{k}}u^*_{\mathbf{k}}\ e^{-i\mathbf{k}\mathbf{x}}\ a_{\mathbf{k}'}u_{\mathbf{k}'}\frac{1}{i}\frac{\partial}{\partial\mathbf{k}'}e^{i\mathbf{k}'\mathbf{x}} \\
= i\int\int\int d^3x\ d^3k\ d^3k'\ a^*_{\mathbf{k}}\psi^*_{\mathbf{k}}\ a_{\mathbf{k}'}&\left\{-\frac{\partial}{\partial\mathbf{k}'}\psi_{\mathbf{k}'} + e^{i\mathbf{k}'\mathbf{x}}\frac{\partial}{\partial\mathbf{k}'}u\right\}
\end{aligned} \tag{11.23}$$

with $|u_{\mathbf{k}}\rangle = |u(\mathbf{k}.\mathbf{x},t)\rangle = e^{-i\mathbf{k}\hat{\mathbf{x}}}|\psi_{\mathbf{k}}(\mathbf{x},t)\rangle$ being the periodic part of the Bloch wave, normalizing the amplitude $a(\mathbf{k},t)$ as

$$\int d^3k|a(\mathbf{k},t)|^2 = \langle\Psi|\Psi\rangle = 1$$

and writing the amplitude as

$$a(\mathbf{k},t) = |a(\mathbf{k},t)|\exp\{-i\gamma(\mathbf{q},t)\} \tag{11.24}$$

integrate by parts

$$\mathbf{x}_c = \int d^3k\ |a|^2\left\{\frac{\partial\gamma}{\partial\mathbf{k}} + \langle u|i\frac{\partial u}{\partial\mathbf{k}}\rangle\right\}$$

finally being $|a|^2$ a narrow packet $\mathbf{x}_c$ is

$$\mathbf{x}_c = \frac{\partial\gamma_c}{\partial\mathbf{k}_c} + \langle u|i\frac{\partial u}{\partial\mathbf{q}_c}\rangle. \tag{11.25}$$

The Lagrangian with a general Hamiltonian

Now having the expressions for $\mathbf{x}_c$ and $\mathbf{k}_c$ the Lagrangian can be calculated for a given Hamiltonian $\hat{H}$. The general Hamiltonian can be approximated up to first order perturbations

$$\hat{H} \approx \hat{H}_c + (\hat{\mathbf{x}} - \mathbf{x}_c)\cdot\mathrm{grad}_{\mathbf{x}_c}\beta_i(\mathbf{x}_c,t) \tag{11.26}$$

where the $\hat{H}_c \equiv H(\hat{\mathbf{x}},\hat{\mathbf{p}};\{\beta_i(\mathbf{x}_c,t)\})$ has the periodicity of the perfect crystal and $\beta_i(\mathbf{x},t)$ are the modulation functions characterizing the perturbations[66], for example under an electromagnetic field, the Hamiltonian will have the form

$$\begin{aligned}\hat{H} &= H_0(\hat{\mathbf{x}}+\beta_1,\hat{\mathbf{p}}+\beta_2)+\beta_3\\ \rightarrow \hat{H} &= H_0(\mathbf{k}+A(\hat{\mathbf{x}},t)) - e\Phi(\hat{\mathbf{x}})\end{aligned} \tag{11.27}$$

with $\beta_1(\hat{\mathbf{x}},t) = 0$. The energy spectrum of the periodic part are the Bloch bands and the wave functions are the Bloch states

$$\hat{H}_c(\mathbf{x}_c,t)|\psi_{\mathbf{k}}(\mathbf{x}_c,t)\rangle = \epsilon_c(\mathbf{x}_c,\mathbf{k},t)|\psi_{\mathbf{k}}(\mathbf{x}_c,t)\rangle. \tag{11.28}$$

The band index is omitted as only one single band will be treated, i.e. the transition probabilities to other bands are negligible.

To compute the Lagrangian $L(\Psi,\Psi^*)=\langle\Psi|i\frac{d}{dt}-\hat{H}|\Psi\rangle$ we first take the first term and compute it

$$\begin{aligned}|\frac{d\Psi}{dt}\rangle &= \int d^3\mathbf{k}a(\mathbf{k},t)\frac{d}{dt}\psi_{\mathbf{k}}(\mathbf{x}_c,t)+\int d^3\mathbf{k}\frac{d}{dt}\left\{a(\mathbf{k},t)\right\}\psi_{\mathbf{k}}(\mathbf{x}_c,t)\\ =\int d^3\mathbf{k}a(\mathbf{k},t)\frac{d}{dt}\left(u_{\mathbf{k}}(\mathbf{x}_c,t)\right)e^{i\mathbf{k}\hat{\mathbf{x}}}&+\int d^3\mathbf{k}a(\mathbf{k},t)\left(u_{\mathbf{k}}(\mathbf{x}_c,t)\right)\frac{d}{dt}e^{i\mathbf{k}\hat{\mathbf{x}}}+\\ &\int d^3\mathbf{k}a(\mathbf{k},t)(-i)\frac{d}{dt}\left\{\gamma\right\}\psi_{\mathbf{k}}(\mathbf{x}_c,t)\\ \Longrightarrow\langle\Psi|i\frac{d}{dt}\Psi\rangle &= \langle u|i\frac{d}{dt}u\rangle-\dot{\mathbf{k}}_c\mathbf{x}_c+\frac{d\gamma_c}{dt}=\\ \frac{d\gamma_c}{dt}-\dot{\mathbf{k}}_c\mathbf{x}_c+\dot{\mathbf{q}}_c\cdot\langle u|i\frac{\partial u}{\partial\mathbf{k}_c}\rangle&+\dot{\mathbf{x}}_c\langle u|i\frac{\partial u}{\partial\mathbf{x}_c}\rangle+\langle u|i\frac{\partial u}{\partial t}\rangle\end{aligned} \tag{11.29}$$

The second part of the Lagrangian can be computed up to first order with the linearized Hamiltonian given above.

$$\epsilon=\langle\Psi|\hat{H}|\Psi\rangle\approx\langle\Psi|\hat{H}_c|\Psi\rangle+\langle\Psi|\Delta\hat{H}|\Psi\rangle \tag{11.30}$$

The expectation value of the Hamiltonian $\hat{H}$ is $\epsilon=\epsilon_c+\Delta\epsilon$ where ϵ_c is the expectation value of the unperturbed Hamiltonian $\hat{H}_c$ and $\Delta\epsilon$ after some calculation can be brought to this expression

$$\Delta\epsilon=-\Im\left\{\langle\frac{\partial u}{\partial\mathbf{x}_c}|\cdot\left(\epsilon_c-\hat{H}_c\right)|\frac{\partial u}{\partial\mathbf{k}}\rangle\right\}|_{\mathbf{k}=\mathbf{k}_c} \tag{11.31}$$

Calculation of the perturbation energy $\Delta\epsilon$ *For the calculation of $\Delta\epsilon$ the expression of the perturbation of the Hamiltonian is needed, this is*

$$\Delta\hat{H}=\frac{1}{2}\left\{(\hat{\mathbf{x}}-\mathbf{x}_c)\frac{\partial\hat{H}}{\partial\mathbf{x}_c}+\frac{\partial\hat{H}}{\partial\mathbf{x}_c}(\hat{\mathbf{x}}-\mathbf{x}_c)\right\}$$

we begin with the matrix elements of the position operator

$$\langle\psi_{n\mathbf{k}}|\hat{\mathbf{x}}|\psi_{n'\mathbf{k}'}\rangle=\left\{i\frac{\partial}{\partial\mathbf{k}}\delta_{nn'}+\langle u_n|i\frac{\partial u_{n'}}{\partial\mathbf{k}}\rangle\right\}\delta(\mathbf{k}-\mathbf{k}') \tag{11.32}$$

and from the derivation of the eigenvalue equation in relation to the position $\mathbf{x}_c$ and the completeness relation

$$\sum_n\int d^3k|\psi_{n\mathbf{k}}\rangle\langle\psi_{n\mathbf{k}}|=1$$

the gradient of the Hamiltonian-operator can be written as follows

$$\begin{aligned}
\frac{\partial \hat{H}_c}{\partial \mathbf{x}_c}|\psi_{n'\mathbf{k}'}\rangle &= \left(\epsilon_{n'} - \hat{H}_c\right)|\frac{\partial}{\partial \mathbf{x}_c}\psi_{n'\mathbf{k}'}\rangle + \frac{\partial \epsilon_{n'}}{\partial \mathbf{x}_c}|\psi_{n'\mathbf{k}'}\rangle \\
\Longleftrightarrow \langle\psi_{n\mathbf{k}}|\frac{\partial \hat{H}_c}{\partial \mathbf{x}_c} &= \langle\frac{\partial}{\partial \mathbf{x}_c}\psi_{n\mathbf{k}}|\left(\epsilon_n - \hat{H}_c\right) + \langle\psi_{n\mathbf{k}}|\frac{\partial \epsilon_n}{\partial \mathbf{x}_c} \\
\Rightarrow \frac{\partial \hat{H}_c}{\partial \mathbf{x}_c} &= |\psi_{n\mathbf{k}}\rangle\langle\frac{\partial}{\partial \mathbf{x}_c}\psi_{n\mathbf{k}}|\left(\epsilon_n - \hat{H}_c\right) + |\psi_{n\mathbf{k}}\rangle\langle\psi_{n\mathbf{k}}|\frac{\partial \epsilon_n}{\partial \mathbf{x}_c}
\end{aligned} \tag{11.33}$$

with the former expression for the gradient of the operator, the matrix elements of the gradient take this form

$$\begin{aligned}
\langle\psi_{n\mathbf{k}}|\frac{\partial \hat{H}_c}{\partial \mathbf{x}_c}|\psi_{n'\mathbf{k}'}\rangle = \delta\left(\mathbf{k}-\mathbf{k}'\right)\langle u_n|\frac{\partial \hat{H}_c}{\partial \mathbf{x}_c}|u_{n'}\rangle = \\
\delta\left(\mathbf{k}-\mathbf{k}'\right)\left\{\left(\epsilon_{cn}-\epsilon_{cn'}\right)\langle\frac{\partial u_{n\mathbf{k}}}{\partial \mathbf{x}_c}|u_{n'\mathbf{k}}\rangle + \frac{\partial \epsilon_{cn}}{\partial \mathbf{x}_c}\delta_{nn'}\right\}
\end{aligned} \tag{11.34}$$

In the last equation the first term does not contribute to the expectation value as the wave packet is expanded only in Bloch states of a given band n. Having this, the next step is to calculate the matrix elements of $\frac{\partial \hat{H}_c}{\partial \mathbf{x}_c}\cdot\hat{\mathbf{x}}$

$$\langle\psi_{n\mathbf{k}}|\frac{\partial \hat{H}_c}{\partial \mathbf{x}_c}\cdot\hat{\mathbf{x}}|\psi_{n\mathbf{k}'}\rangle = \frac{\partial \epsilon_{cn}}{\partial \mathbf{x}_c}\langle\psi_{n\mathbf{k}}|\hat{\mathbf{x}}|\psi_{n\mathbf{k}'}\rangle + i\langle\frac{\partial u_{n\mathbf{k}}}{\partial \mathbf{x}_c}|\cdot\left(\epsilon_{cn}-\hat{H}_c\right)|\frac{\partial u_{n\mathbf{k}}}{\partial \mathbf{k}}\rangle\delta\left(\mathbf{k}-\mathbf{k}'\right)$$

Now we can finally calculate the expectation value of the perturbation

$$\begin{aligned}
\langle\Psi|\frac{\partial \hat{H}_c}{\partial \mathbf{x}_c}\cdot\left(\hat{\mathbf{x}}-\mathbf{x}_c\right)|\Psi\rangle &= i\langle\frac{\partial u_{n\mathbf{k}}}{\partial \mathbf{x}_c}|\cdot\left(\epsilon_{cn}-\hat{H}_c\right)|\frac{\partial u_{n\mathbf{k}}}{\partial \mathbf{k}}|_{\mathbf{k}=\mathbf{k}_c} \\
\Longrightarrow \langle\Psi|\Delta\hat{H}|\Psi\rangle &= -Im\left\{\langle\frac{\partial u}{\partial \mathbf{x}_c}|\cdot\left(\epsilon_c-\hat{H}_c\right)|\frac{\partial u}{\partial \mathbf{k}}\rangle\right\}|_{\mathbf{k}=\mathbf{k}_c}\,.
\end{aligned} \tag{11.35}$$

Now with the expectation value of the Hamiltonian and neglecting the total time derivatives, as it does not affect the equations of motion, the Lagrangian can be written as

$$L = -\epsilon + \mathbf{k}_c\dot{\mathbf{x}}_c + \dot{\mathbf{k}}_c\langle u|i\frac{\partial u}{\partial \mathbf{k}_c}\rangle + \dot{\mathbf{x}}_c\langle u|i\frac{\partial u}{\partial \mathbf{x}_c}\rangle + \langle u|i\frac{\partial u}{\partial t}\rangle. \tag{11.36}$$

The Lagrangian is invariant under gauge transformations and under the displacement of a reciprocal lattice vector. In the expression of the Lagrangian can be seen, that under the taken assumptions (semi-classical limit) this function can be seen as "classical one", i.e. a Lagrangian that depends on the "generalized coordinates and velocities". The Lagrangian will be now be handled as a classical one with the generalized coordinates $\mathbf{x}_c$ and $\mathbf{k}_c$ and the generalized velocities $\dot{\mathbf{x}}_c$ and $\dot{\mathbf{k}}_c$. This is in some sense unusual as now the crystal momentum stands as a general coordinate next to the position, and the general velocities are their time derivatives. This will not be a problem in the computations, one has only to put the general coordinates as a vector consisting of $(\mathbf{x}_c, \mathbf{k}_c)$ and the general velocities as a vector consisting of $\left(\dot{\mathbf{x}}_c, \dot{\mathbf{k}}_c\right)$.

With this considerations from the Lagrangian that was computed, the semi-classical equations can be obtained by variation. This gives

$$\dot{\mathbf{x}}_c = \frac{\partial \epsilon}{\partial \mathbf{k}_c} - \left(\bar{\mathbf{\Omega}}_{\mathbf{kx}}\dot{\mathbf{x}}_{\mathbf{c}} + \bar{\mathbf{\Omega}}_{\mathbf{kk}}\dot{\mathbf{k}}_{\mathbf{c}}\right) + \mathbf{\Omega}_{t\mathbf{k}} \tag{11.37}$$

$$\dot{\mathbf{k}}_c = -\frac{\partial \epsilon}{\partial \mathbf{x}_c} + \left(\bar{\mathbf{\Omega}}_{\mathbf{xx}}\dot{\mathbf{x}}_{\mathbf{c}} + \bar{\mathbf{\Omega}}_{\mathbf{xk}}\dot{\mathbf{k}}_{\mathbf{c}}\right) - \mathbf{\Omega}_{t\mathbf{x}} \tag{11.38}$$

where the components of the tensor $\bar{\mathbf{\Omega}}_{\mathbf{xx}}$ are defined by

$$\left(\bar{\mathbf{\Omega}}_{\mathbf{xx}}\right)_{\alpha\beta} \equiv \Omega_{x_\alpha x_\beta} \equiv i\left(\langle\frac{\partial u}{\partial k_{c\alpha}}|\frac{\partial u}{\partial k_{c\beta}}\rangle - \langle\frac{\partial u}{\partial k_{c\beta}}|\frac{\partial u}{\partial k_{c\alpha}}\rangle\right) \tag{11.39}$$

and the vector $\mathbf{\Omega}_{t\mathbf{x}}$ by

$$\left(\mathbf{\Omega}_{t\mathbf{x}}\right)_{\alpha} \equiv \Omega_{tx_\alpha} \equiv i\left(\langle\frac{\partial u}{\partial t}|\frac{\partial u}{\partial x_{c\alpha}}\rangle - \langle\frac{\partial u}{\partial x_{c\alpha}}|\frac{\partial u}{\partial t}\rangle\right). \tag{11.40}$$

These tensors are known as the Berry curvatures.

These equations have an extra term in the velocity and in the energy. If the crystal lies under electromagnetic perturbations the extra term in the velocity will become the anomalous velocity, which gives rise to a spontaneous hall effect in ferromagnetic materials and the extra term in the energy this will be the orbital magnetization energy.

Berry curvatures in electromagnetic fields

Now the general semi-classical equations of motion for the Bloch electrons in a crystal under weak perturbations are known. To illustrate what the Berry curvatures are under "real" perturbations we take an electromagnetic field acting on

the crystal. With this example the equations will be brought from a abstract form to a more physical form. In this case, under electromagnetic field perturbation, one of the two extra terms in the semi-classical equations will become the anomalous velocity, that predicts a spontaneous Hall effect in ferromagnetic materials and the second will be the orbital magnetization energy. Under some symmetry properties these two terms vanish and become the usual known semi-classical equations of motion.

For a class of perturbations for which the Hamiltonian is of the special form

$$H_0 \left\{ \hat{\mathbf{x}} + \beta_1 \left(\hat{\mathbf{x}}, t \right), \hat{\mathbf{p}} + \beta_2 \left(\hat{\mathbf{x}}, t \right) \right\} + \beta_3 \left(\hat{\mathbf{x}}, t \right)$$

all the results can be expressed in terms of the unperturbed Bloch wave bases. In this section, we shall consider electromagnetic perturbations for which $\beta_1 \left(\hat{\mathbf{x}}, t \right) = 0$[66]. An example for a Hamiltonian with $\beta_1 \left(\hat{\mathbf{x}}, t \right) \neq 0$ would be the deformation of the crystal potential due to a deformation of the crystal.

Let $\hat{H}_0 \left(\mathbf{k} \right)$ denote the Hamiltonian for the bare crystal, with the eigenstate $|u \left(\mathbf{k} \right)\rangle$ (the periodic part of the Bloch wave) and the band energy $\epsilon_0 \left(\mathbf{k} \right)$ for a particular band. The Hamiltonian gets modified by the slowly varying gauge potentials $\left[\mathbf{A} \left(\mathbf{x}, t \right), \Phi \left(\mathbf{x}, t \right) \right]$ of an electromagnetic field to

$$\hat{H} = H_0 \left\{ \mathbf{k} + e\mathbf{A} \left(\hat{\mathbf{x}}, t \right) \right\} - e\Phi \left(\mathbf{x}_c, t \right) \tag{11.41}$$

This has the above form, with the gauge potentials playing the role of the modulation functions, and hence the local Hamiltonian $\hat{H}_c$ must have the form

$$\hat{H}_c = H_0 \left\{ \mathbf{k} + e\mathbf{A} \left(\mathbf{x}_c, t \right) \right\} - e\Phi \left(\mathbf{x}_c, t \right). \tag{11.42}$$

As $e\mathbf{A} \left(\mathbf{x}_c, t \right)$ is fly an additive constant to the crystal momentum $\mathbf{k}$, the basis states have the form $|u \left(\mathbf{x}_c, \mathbf{k}, t \right)\rangle = |u \left(\mathbf{K} \right)$, where $\mathbf{K} = \mathbf{k} + e\mathbf{A} \left(\mathbf{x}_c, t \right)$ is the gauge invariant or mechanical crystal momentum[66].

From the crystal momentum $\mathbf{K}$ that is gauge invariant, some simplifications can be achieved. The expectation value of the local Hamiltonian $\hat{H}_c$ can be written as

$$\epsilon_c \left(\mathbf{x}_c, \mathbf{K}, t \right) = \epsilon_0 \left(\mathbf{K} \right) + e\Phi \left(\mathbf{x}_c, t \right). \tag{11.43}$$

Therefore the total energy can be written as

$$\epsilon = \epsilon_c \left(\mathbf{x}_c, \mathbf{K}, t \right) + \Delta\epsilon = \epsilon_0 \left(\mathbf{K} \right) + e\Phi \left(\mathbf{x}_c, t \right) + \Delta\epsilon. \tag{11.44}$$

At this point, we have to know the expression for the perturbation energy, i.e. for $\Delta\epsilon$, this becomes the orbital magnetization energy of the wave packet,

$$\Delta\epsilon = -\mathbf{M} \cdot \mathbf{B} \tag{11.45}$$

where $\mathbf{B} = \mathrm{curl}_{\mathbf{x}_c}\mathbf{A}\left(\mathbf{x}_c, t\right)$ is the magnetic field, and $\mathbf{M}$ is the magnetic field

$$\mathbf{M} = e\Im\left\{\langle\frac{\partial u}{\partial \mathbf{K}}| \times \left(\epsilon_0 - \hat{H}_0\left(\mathbf{K}\right)\right)|\frac{\partial u}{\partial \mathbf{k}}\rangle\right\}|_{\mathbf{k}=\mathbf{k}_c} \tag{11.46}$$

is the orbital magnetic moment of Bloch electrons.[66] This expression comes from the general one, derived above, and substituting the mechanical crystal momentum in the equation.

Now, following the same schema as above, for the general derivation, the Lagrangian can be written explicitly and takes the final form of

$$L = -\epsilon_M + e\Phi\left(\mathbf{x}_c, t\right) + \dot{\mathbf{x}}_c\mathbf{K}_c - e\dot{\mathbf{x}}_\mathbf{c}\mathbf{A}\left(\mathbf{x}_c, t\right) + \dot{\mathbf{K}}_c \cdot \langle u|i\frac{\partial u}{\partial \mathbf{K}_c}\rangle \tag{11.47}$$

where $\epsilon_M = \epsilon_0\left(\mathbf{K}_c\right) - \mathbf{MB}$.

To get the semi-classical equations of motion for the Bloch electrons in a crystal under an electromagnetic field, one can use the general equations derived above and only substitute with the new values, or with the special Lagrangian the equations can be obtained variationally. This equations get the form of

$$\begin{aligned}\dot{\mathbf{x}}_c &= \frac{\partial \epsilon_M}{\partial \mathbf{K}_c} - \dot{\mathbf{K}}_c \times \mathbf{\Omega} \\ \dot{\mathbf{K}}_c &= -e\mathbf{E} - e\dot{\mathbf{x}}_c \times \mathbf{B}\end{aligned} \tag{11.48}$$

where $\mathbf{E} = \mathrm{grad}_{\mathbf{x}_c}\Phi\left(\mathbf{x}_c, t\right) - \partial\mathbf{A}\left(\mathbf{x}_c, t\right)/\partial t$ is the electric field and

$$\left(\mathbf{\Omega}\right)_\alpha = \frac{1}{2}\epsilon_{\alpha\beta\gamma}\left(\bar{\Omega}_{\mathbf{KK}}\right)_{\beta\gamma} \tag{11.49}$$

are the components of the vector form of the antisymmetric tensor $\bar{\Omega}_{\mathbf{KK}}$ given in the general formulation of the semi-classical equations. Here repeated Cartesian indices are taken to be summed[66].

Here we have the new equations of motion, if these are compared with the ones given in the review (11.6), two terms clearly differ from these two equations. The first one, as mentioned above, in the energy, is the orbital magnetization energy, the other one, also mentioned above, is an extra term in the velocity, which is called anomalous velocity. This term, has an analogous presentation as the magnetic field dependent term in the Lorentz force. That means that the vector of the antisymmetric tensor can be viewed as a magnetic field acting on the reciprocal space. This vector will be called *reciprocal magnetic field* and has some interesting properties. Some of this properties will be mentioned later, it is more convenient to analyze the equations under some symmetries and see how this new terms behave under these symmetries.

Symmetry	$\mathbf{k}_c$	$\dot{\mathbf{k}}_c$	$\mathbf{x}_c$	$\dot{\mathbf{x}}_c$	$\mathbf{B}$	$\mathbf{E}$
time reversal	-	+	+	-	-	+
spatial inversion	-	-	-	-	+	-

Table 11.1: Behavior of the reciprocal magnetic field and magnetic moment under Spatial inversion and time reversal symmetries.

The reciprocal magnetic field and the magnetic moment in presence of crystal symmetries If a crystal has a specific symmetry, then the derived equations must have the same symmetries. These type of conditions imposed to the equations restrict severely the possible form of the Berry curvature (reciprocal magnetic field) and of the magnetic moment as function of $\mathbf{K}$.

Under time reversal transformation, $\mathbf{K}_c$, $\dot{\mathbf{x}}_c$, and $\mathbf{B}$ change sign, while $\mathbf{x}_c$, $\dot{\mathbf{K}}_c$ and $\mathbf{E}$ are fixed. Under spacial inversion, $\mathbf{E}$, $\mathbf{x}_c$, $\dot{\mathbf{K}}_c$, $\mathbf{K}_c$ and $\dot{\mathbf{x}}_c$ change sign, while $\mathbf{B}$ is fixed (table 11.1). Under pure rotations, all of these quantities behave as vectors. The presence of these symmetries has the following consequences. If the unperturbed system has time-reversal symmetry, the symmetry condition on the velocity formula requires that $\epsilon(-\mathbf{K}) = \epsilon(\mathbf{K})$, $\Omega(-\mathbf{K}) = -\Omega(\mathbf{K})$ and $\mathbf{M}(-\mathbf{K}) = -\mathbf{M}(\mathbf{K})$. If the unperturbed system is invariant under spatial inversion the symmetry condition on the velocity formula gives rise to $\epsilon(-\mathbf{K}) = \epsilon(\mathbf{K})$, $\Omega(-\mathbf{K}) = \Omega(\mathbf{K})$ and $\mathbf{M}(-\mathbf{K}) = \mathbf{M}(\mathbf{K})$. Therefore, with either time-reversal or spatial-inversion symmetry, the band energy is an even function of $\mathbf{K}$, whereas the reciprocal magnetic field and the magnetic moment behave differently in the two situations; odd with time-reversal symmetry and even with spatial-inversion symmetry[67].

This analysis shows that if a crystal has simultaneously time-reversal symmetry and spatial inversion symmetry, both, the reciprocal magnetic field and the magnetic moment vanish identically throughout the Brillouin zone. In this case the velocity equation reduces to the usually known expression. In many cases in solid state physics both symmetries are present, so that the usually known equation is valid for a large number of situations. But there are many cases where one of these symmetries are not present. For example, in ferromagnetic or anti-ferromagnetic materials the crystal breaks the time-reversal symmetry.

Anomalous Velocity and Magnetic Monopoles in Momentum Space

In this section, some properties of the extra term in the velocity equation, namely the anomalous velocity, are presented. This term does not vanish in a metallic ferromagnet and in this case an anomalous Hall effect can be measured. This effect is a phenomenon in which the transverse resistivity ρ_{xy} in ferro-magnets

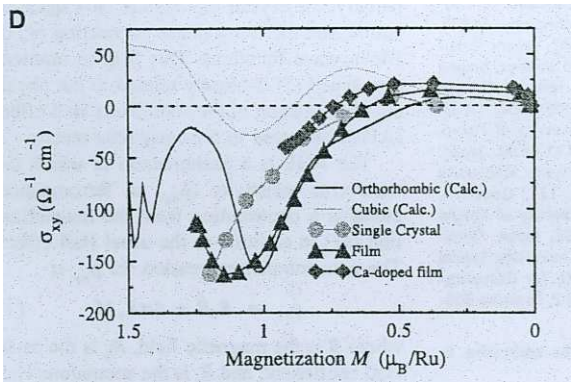

Figure 11.2: The transverse conductivity σ_{xy} is shown as a function of $\mathbf{M}'$, together with the calculated results[68].

contains a contribution from the magnetization $\mathbf{M}'$ (this is not the same magnetization as the one given above, this magnetization is the one which leads to the ferromagnetic properties of the crystal) in addition to the usual Hall effect. The conventional expression for ρ_{xy} is

$$\rho_{xy} = R_0\mathbf{B} + 4\pi R_s\mathbf{M}'$$

where R_0 is the usual Hall coefficient and R_s the anomalous Hall coefficient[68]. This conventional expression says that the extra term in the Hall conductivity is proportional to $\mathbf{M}'$. The conventional expression is not always supported by experimental data, the experimental data shows, in contradiction to the conventional expression, for the conductivity a non-monotonous dependence of $\mathbf{M}'$ (figure 11.2). Here we see clearly a limit of the conventional expression, it can only be applied in a region where the extra term is proportional to $\mathbf{M}'$. But if the extra term that gives rise to the AHE is seen as a consequence of the new term that arose in the velocity equations (11.48) and calculate this with the Berry curvature given above, then the samples measured follow the same rule qualitatively[68], as seen in the figure 11.2

To continue the discussion of the anomalous Hall effect (AHE) it is convenient to examine the Berry curvature, i.e. the reciprocal magnetic field more in detail. As mentioned above, this extra term has the form of a magnetic field acting on the momentum space, therefore we expect that this reciprocal magnetic field has similar properties as a normal magnetic field. As known form electromagnetics, the divergence of a magnetic field is equal zero, in the case of the reciprocal magnetic field we have

$$\nabla \cdot \mathbf{\Omega}\left(\mathbf{K}\right) = \sum_i q_{ni}\delta^3\left(\mathbf{K} - \mathbf{K}_{ni}\right)$$

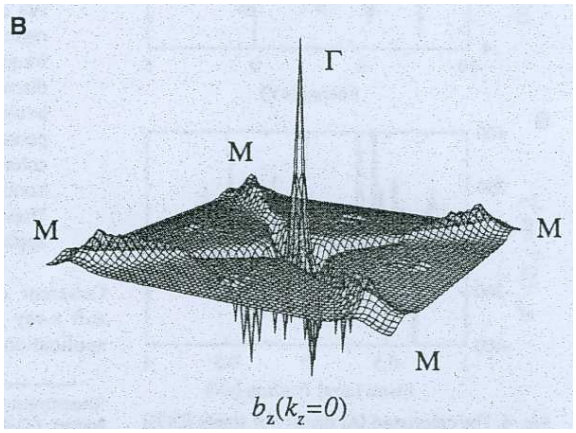

Figure 11.3: Calculated flux distribution in **k**-space, The sharp peak around $k_x = k_y = 0$ and the ridges along $k_x = \pm k_y$ are due a to the near degeneracy[68].

with $q_{ni} = \pm 2\pi$, and we have restored the band index n[69].This means that it is divergence free except for quantized monopoles sources with a charge quantum 2π, which are associated with band degeneracies. These occur at isolated **K** points[69]. This result can be interpreted as magnetic monopoles corresponding to the source or sink of the curvature defined by the Berry phase connection[68](figure11.3).

At this point it is useful to make a small summary of the AHE, to give the last results for the AHE calculated with the Berry curvature. The reciprocal magnetic field acting on the momentum space, can be seen as a field which sources are magnetic monopoles in the momentum space, these monopoles arise in the band degeneracies. Now to see that the AHE is given by the shape of the Berry curvature, and to illustrate the dependence of $\mathbf{M}'$ of the transverse resistivity, we write the transverse conductivity σ_{xy} as the sum of the anomalous velocity over the occupied states[68]

$$\sigma_{xy} = \sum_{n,\mathbf{K}} n_F \left\{\epsilon_n \left(\mathbf{K}\right)\right\} \left(\bar{\Omega}_{\mathbf{K}K}\right)_{xy}$$

with the Fermi distribution $n_F\left(\epsilon\right) = 1/\left(e^{\frac{(\epsilon-\mu)}{T}} - 1\right)$. Here a the transverse conductivity has a Temperature dependence, if the magnetization $\mathbf{M}'$ is calculated in dependence of Temperature, we can combine these two and get the magnetization dependence $\mathbf{M}'$ for the transverse conductivity. As said before, this method results to describe the experiments non-monotonous dependence of $\mathbf{M}'$ qualitatively (figure 11.2).

4 Semi-classical quantization

Now we will proceed with the last part, namely, the "re-quantization". Now the equations of motion in the semi-classical limit are known, and the dynamics of the electron are given. As we are in the limit of a classical system and a quantum system we can proceed to quantize the equations derived by before. First the general equations will be quantized, and then separately when an uniform electric field is present and when an uniform magnetic field is present.

Semi-classical quantization for a general Hamiltonian

First of all we need to compute the canonical momenta conjugate to the generalized coordinates, these are given by the partial derivative of the Lagrangian in respect to the generalized velocities

$$\mathbf{P}_1 = \frac{\partial L}{\partial \dot{\mathbf{x}}_c} = \mathbf{k}_c + \langle u | i \frac{\partial u}{\partial \mathbf{x}_c} \rangle \tag{11.50}$$

$$\mathbf{P}_2 = \frac{\partial L}{\partial \dot{\mathbf{k}}_c} = \langle u | i \frac{\partial u}{\partial \mathbf{k}_c} \rangle \tag{11.51}$$

and the semi-classical Hamiltonian is given by the Legendre transformation

$$\mathbf{H} = \dot{\mathbf{x}}_c \cdot \mathbf{P}_1 + \dot{\mathbf{k}}_c \cdot \mathbf{P}_2 - L = \epsilon \left(\mathbf{x}_c, \mathbf{k}_c, t \right) - \langle u | i \frac{\partial u}{\partial t} \rangle \tag{11.52}$$

The semi-classical Hamiltonian is independent of $\mathbf{P}_1$ and $\mathbf{P}_2$, and the canonical momenta do not depend on the generalized velocities. Therefore, one cannot obtain the equations of motion from the Hamilton equations if the Berry-phase terms are nonzero and the formal quantization procedure cannot be applied.

If we make the restriction of static perturbations, the semi-classical quantization can be applied, and for a wave packet motion that is regular and is described by closed orbit in the phase space $(\mathbf{x}_c, \mathbf{k}_c)$, semi-classical energy levels are obtained using the quantization procedure due to Einstein, Brillouin and Keller[66]. This procedure gives the quantized energy values as

$$\oint_C \mathbf{P}_1 \, d\mathbf{x}_c + \oint_C \mathbf{P}_2 \, d\mathbf{k}_c = 2\pi \left(m + \frac{\nu}{4} \right) \tag{11.53}$$

where C denotes an orbit of constant energy ϵ, m is an integer that labels the eigenvalue and ν the number of caustics traversed. Inserting in this quantization the canonical momenta the above quantization is

$$\oint_C \mathbf{k}_c \, d\mathbf{x}_c = 2\pi \left(m + \frac{\nu}{4} - \frac{\Gamma \left(C \right)}{2\pi} \right) \tag{11.54}$$

with

$$\Gamma(C) = \oint_C d\mathbf{x}_c \cdot \langle u|i\frac{\partial u}{\partial \mathbf{x}_c}\rangle + \oint_C d\mathbf{k}_c \cdot \langle u|i\frac{\partial u}{\partial \mathbf{k}_c}\rangle \tag{11.55}$$

being the Berry phase acquired by the wave packet upon going round the closed orbit once.

Here we have seen, how in an easy way to of re-quantization the Berry phase arises as a "correction" to the quantized energy levels.

Semi-classical quantization in presence of an uniform magnetic field

In presence of only an uniform magnetic field the equations of motion simplify as

$$\begin{aligned} \dot{\mathbf{x}}_c &= \frac{\partial \epsilon}{\partial \mathbf{K}_c} \\ \dot{\mathbf{K}}_c &= -e\dot{\mathbf{x}}_c \times \mathbf{B} \end{aligned} \tag{11.56}$$

These two equations can be combined in a single one for the $\mathbf{K}$-motion. It follows from the equations that the component of $\mathbf{K}$ along the magnetic field and the electronic energy $\epsilon(\mathbf{K})$ are both constants of the motion. With these two conservations laws the orbit of the motion is completely determined in $\mathbf{K}$-space: Electrons move along curves given by the intersection of surfaces of constant energy with planes perpendicular to the magnetic field[63]. Such a closed orbit is known as a cyclotron orbit. As the motion over the $\mathbf{K}$-space is closed the quantization formula of EBK can be applied. For this we need the canonical momenta which is given by

$$\begin{aligned} \mathbf{P}_1 &= \mathbf{K}_c - e\mathbf{A}(\mathbf{x}_c, t) \\ \mathbf{P}_2 &= \langle u|i\frac{\partial u}{\partial \mathbf{K}_c}\rangle \end{aligned} \tag{11.57}$$

and the quantization yields

$$\frac{1}{2}\hat{\mathbf{B}} \cdot \oint_C \mathbf{K}_c \times d\mathbf{K}_c = \frac{e|\mathbf{B}|}{\hbar}\left(m + \frac{1}{2} - \frac{\Gamma(C)}{2\pi}\right)$$

where

$$\Gamma(C) = \oint_C d\mathbf{K} \cdot \langle u|i\frac{\partial u}{\partial \mathbf{K}_c}\rangle$$

is the Berry phase acquired by the wave packet upon going around the orbit C. This phase influences energy levels, and affects the density of states[66].

Semi-classical quantization in presence of an uniform electric field

In presence of an uniform electric field, the general solution of the equations are

$$\mathbf{K}(t) = \mathbf{K}(0) - \frac{e\mathbf{E}}{\hbar}$$

All electrons change their wave vector in a time t by the same amount. We note that this is not a current-carrying configuration, which may not be intuitive in a classical form. The current carried by an electron is proportional to its velocity, which in this case is not proportional to the wave vector $\mathbf{K}$

$$v(\mathbf{K}(t)) = v\left(\mathbf{K}(0) - \frac{e\mathbf{E}}{\hbar}\right)$$

Since $v(\mathbf{K})$ is periodic in the reciprocal lattice, the velocity is a bounded function of time and, when the field $\mathbf{E}$ is parallel to a reciprocal lattice vector, oscillatory[63]. This behavior is a consequence of the additional force exerted by the periodic potential, which , though no longer explicit in the semi-classical model, lies buried in it (through the functional form of $\epsilon(\mathbf{K})$)[63].

For simplification we will restrict the discussion to one dimension, this will guaranties that the electric field will be parallel to a reciprocal lattice vector, so that the motion in real space will be bounded and periodic. So in the reduced zone scheme, the motion is closed in the phase space $(\mathbf{x}_c, \mathbf{K}_c)$. The Hamiltonian for the presence of a uniform electric field is

$$H = \epsilon_0(K_c) + eEx_c$$

Following the semi-classical quantization of EBK the formula yields

$$-\int_{-\frac{\pi}{a}}^{\frac{\pi}{a}} dK_c x_c(K_c) = 2\pi\left(m + \frac{\nu}{4} - \frac{\Gamma}{2\pi}\right) \tag{11.58}$$

where a stands for the lattice constant, and

$$\Gamma = \int_{-\frac{\pi}{a}}^{\frac{\pi}{a}} dK \langle u | i \frac{\partial u}{\partial K} \rangle$$

is known as the Zak phase, $x_c(K_c)$ is the constant energy curve for the mth energy level defined by $W_m = \epsilon_0(K_c) + eEx_c$. Averaging this expression over the orbit, we obtain

$$W_m = \bar{\epsilon}_0 + eEa\left(-m - \frac{\nu}{4} + \frac{\Gamma}{2\pi}\right) \tag{11.59}$$

where $\bar{\epsilon}_0$ is the average of the band energy over the Brillouin zone. This spectrum is known as the Wannier-Stark ladder.[66]

12 Superfluidity and winding numbers

Barbara Theiler
Supervisor: Lode Pollet

After a brief introduction on the phenomenon of superfluidity and on its macroscopic description known as the two-fluid model, the quantum-classical isomorphism will be introduced. In the path integral the thermodynamic properties of a Bose system are mapped onto those of a classical system of interacting ring polymers. An explicit formula for the superfluid density ρ_s can be derived in terms of the winding number, a topological invariant of the polymer system. As for most many-body problems it is impossible to treat this problem analytically. By use of Monte Carlo simulations however, numerical results for ρ_s are obtained which are in good agreement with experimental measurements.

1 Introduction

Superfluidity is a phase of matter which is characterized by the total absence of viscosity and is related to the behavior of quantum liquids at low temperatures. The first observations of this phase were made in 1937 in liquid ^{4}He which is the classic example of a superfluid. Below a characteristic temperature some properties of the system change abruptly. For instance, the heat flow is no longer proportional to the temperature gradient, and the liquid is able to flow without apparent friction. This sudden change implies that a phase transition has taken place which divides the liquid phase into He-I and He-II. While He-I behaves like a normal fluid, He-II exhibits superfluid behavior.
This second-order transition to the superfluid state is known as the λ-transition due to the λ-shaped anomaly in the specific heat curve. Along the vapor pressure

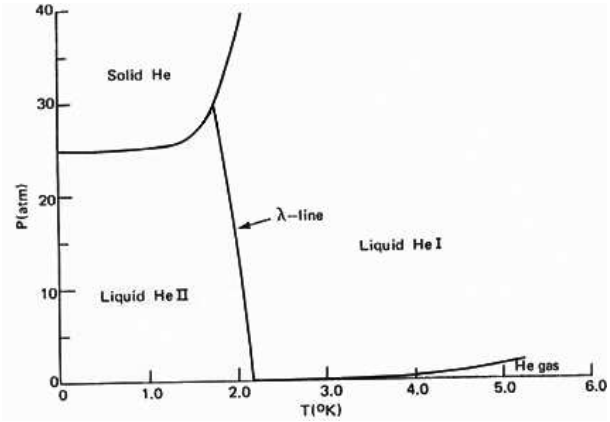

Figure 12.1: Phase diagram of ^{4}He near the transition temperature.

curve, the λ-transition occurs at the λ-point

$$\begin{aligned} T_\lambda &= 2.17\text{K}, \\ V_\lambda &= 46.2\,\text{Å}^3/\text{atom}. \end{aligned}$$

Near T_λ, the specific heat c is of the form

$$c(T) \propto A_\pm |T - T_\lambda|^{-\alpha},$$

where $A_\pm$ is the amplitude for positive/negative $|T - T_\lambda|$, and α the critical exponent. The theory of Ginzburg-Landau predicts $\alpha = 0$. Recent measurements [70] however obtain $\alpha = -0.0127 \pm 0.0003$. This implies that the heat capacity does not diverge at $T = T_\lambda$ but stays finite.

A remarkable property of helium is that it does not solidify under its own vapor pressure down to the absolute zero of temperature. Solidification occurs at external pressure of at least 25bar. Qualitatively, this may be understood as follows [71]: As a noble gas, its only molecular interaction is a weak Van der Waals attraction. In addition, the mass of He is smallest among the noble gases. These circumstances result in a large zero-point motion which inhibits the localization of the atoms at well-defined lattice sites.
The fact that helium is liquid down to zero temperature makes it a nearly perfect system for studying macroscopic quantum effects. Since the atoms are delocalized, the indistinguishability of the particle becomes very important. Furthermore, as helium has two isotopes, ^{3}He ($= 2p + 1n + 2e \Rightarrow$ Fermion) and ^{4}He ($= 2p + 2n + 2e \Rightarrow$ Boson), one can experimentally distinguish the effects of correlation from those of statistics.
^{3}He and ^{4}He behave quite differently at low temperatures; ^{3}He does not undergo a phase transition to a superfluid state near $T_\lambda = 2.17$K. Apart form a difference in atomic masses, the only difference between these two isotopes is that ^{4}He

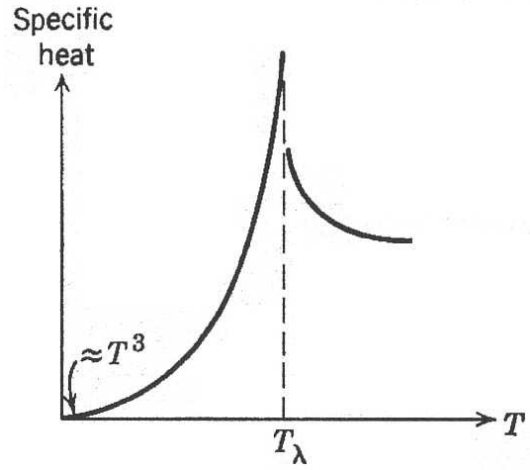

Figure 12.2: Experimental specific heat of liquid ^{4}He along the vapor pressure curve. The low-temperature behavior implies a linear dispersion relation (phonon-excitations).

atoms obey Bose statistics, whereas ^{3}He atoms follow the statistic of Fermi-Dirac. The lower the temperature, the more impact do quantum statistics have on the system. It is therefore natural to assume that the phenomenon of superfluidity is a quantum statistical effect. But before we study the properties of an interacting many-Boson system such as liquid ^{4}He, we have a look at the macroscopic description of superfluidity.

The Two-Fluid Model

Below a critical velocity, He-II can be observed to flow through a thin capillary ("superleak") with zero resistance, a phenomenon which implies zero viscosity. On the other hand, if a cylinder is rotated in a He-II-bath, there is a momentum transfer from the rotating body to the liquid, indicating that the viscosity is not zero. This apparent contradiction gives rise to the idea of the two-fluid model.
Macroscopically, the anomalous flow behavior of the He-II phase can be understood in terms of this model; He-II is assumed to be made up of two components called the normal and the superfluid component. Between these two components there is no friction, i.e., no transfer of momentum, and they cannot actually be separated. Experimentally, the two fluids are distinguished through their behavior in the presence of moving boundaries as the example of the rotating cylinder shows; the normal component gets accelerated by the external motion, whereas the superfluid component stays at rest.
A first quantitative theory of the flow properties of He-II is due to Landau (1941). It provides an explicit construction of the two-fluid model near absolute zero

([71], [72]): The superfluid component is identified with the part of the liquid that remains in its ground state, while the normal component corresponds to low-temperature excitations. Assuming that there are no other excitations near the ground state except elementary excitations (whose spectrum, illustrated in Figure 12.3, is found experimentally by neutron scattering [73]), it is possible to describe the normal component as an ideal gas of Boson-like quasiparticles with energy

$$E_n = E_0 + \sum_k \hbar\omega_k n_k,$$

where $\hbar\omega_k$ is the energy of the elementary excitation of wave number k, and $\{n_k\}$ a set of occupation numbers. For T sufficiently low, one can assume the n_k's to be independent and their thermodynamic average to be given by $\langle n_k\rangle = [e^{\hbar\omega_k\beta}-1]^{-1}$. The internal energy of the liquid of volume V is then

$$U = E_0 + \sum_k \hbar\omega_k\langle n_k\rangle = E_0 + \frac{V}{2\pi^2}\int_0^\infty dk \frac{k^2\hbar\omega_k}{e^{\hbar\omega_k\beta}-1}. \tag{12.1}$$

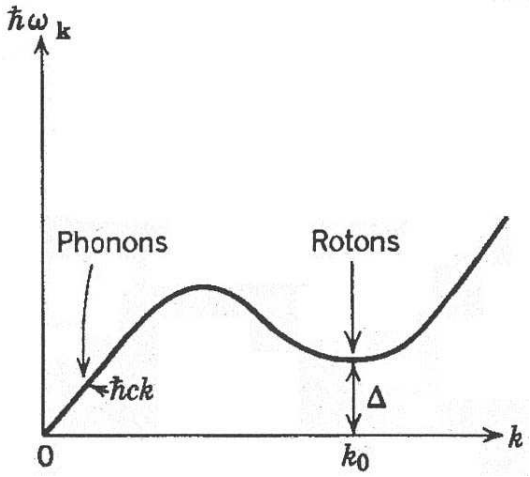

Figure 12.3: Energy spectrum of elementary excitations in liquid ^{4}He.

According to [72], the excitation spectrum can be derived from the structure factor $S(k)$ by the formula

$$\epsilon(k) = \frac{\hbar^2k^2}{2mS(k)}.$$

A typical form of the structure factor of a compressible system is shown in Figure 5. For $k \to 0$, $S(k)$ behaves approximately linear which implies $\epsilon(k) \propto \hbar k$, whereas the peak of $S(k)$ leads to the roton minimum near $k = 2\pi/d$, where d is the particle distance.

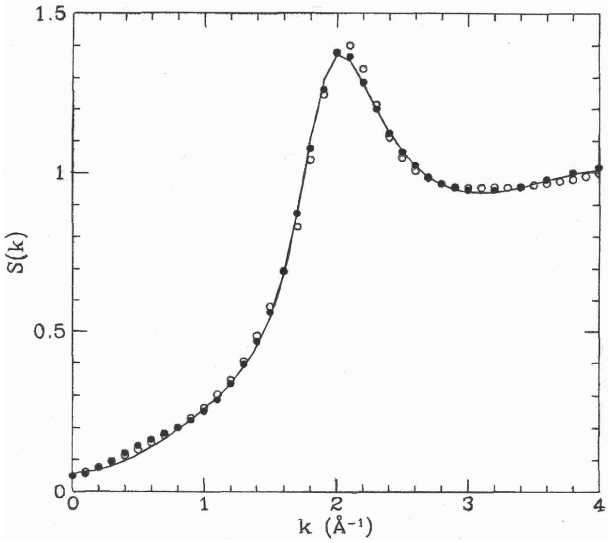

Figure 12.4: The structure factor of ^{4}He at 1.38K and saturated vapor pressure: solid line, calculated by PIMC; •, measured by neutron scattering (Sears et al., 1979); ∘, measured by x-ray scattering (Robkoff and Hallock, 1981).

At low temperatures, there are two types of quasiparticles which contribute significantly to the integral in (12.1): phonons with spectrum $\epsilon(k) = c\hbar k$ and rotons, which are regarded as quantized rotational motion with spectrum $\epsilon(k) = \Delta + \frac{\hbar^2(k-k_0)^2}{2\mu}$. The parameters are experimentally found [71]:

$$c = 239\,\frac{\mathrm{m}}{\mathrm{s}}, \quad \Delta = 8.65\,\mathrm{K}, \quad k_0 = 1.9\,\mathrm{\AA}^{-1}, \quad \mu = 0.16 m_{\mathrm{He}}.$$

The specific heat $c_V = \frac{\partial U}{\partial T}$ can be approximated as the sum of the contribution of the phonons and the one of the rotons

$$c_V = c_{\mathrm{phonon}} + c_{\mathrm{roton}}.$$

The phenomenon of frictionless flow for a velocity less than a critical velocity $v_c = \min_p \frac{\epsilon(p)}{p}$ may be understood in terms of the gas of quasiparticles: Consider an external object with mass m moving with velocity $\vec{v}$ through the stationary liquid. The only way of transferring momentum and energy to the liquid is by creating an excitation. Let $\vec{p}$ be the momentum of the new quasiparticle. Then, by conservation of momentum, $m\vec{v} = m\vec{v'} + \vec{p}$, where $\vec{v'}$ is the remaining velocity of the object. Its kinetic energy is

$$\frac{1}{2}mv'^2 = \frac{1}{2}mv^2 - \vec{v}\cdot\vec{p} + \frac{p^2}{2m}.$$

The creation of an excitation with energy $\epsilon(p)$ requires $\frac{1}{2}mv^2 > \frac{1}{2}mv'^2 + \epsilon(p)$ which for large m leads to the criterion

$$\epsilon(p) < \vec{v}\cdot\vec{p} - \frac{p^2}{2m} \approx \vec{v}\cdot\vec{p} \approx vp. \tag{12.2}$$

Therefore, in order to transfer energy to the liquid it must hold: $v > v_c$. v_c is determined by drawing the tangent with smallest slope from the origin to the curve of the energy spectrum (Figure 12.3). The critical velocity for ^{4}He obtained in this way is $\frac{\Delta}{\hbar k_0} \approx 60\,\frac{\mathrm{m}}{\mathrm{s}}$. The experimental value however is only about $1\frac{\mathrm{cm}}{\mathrm{s}}$. This implies that there are other excitations at small velocity (Vortices, see [72]).
Nevertheless, from (12.2) one can conclude: Any spectrum in which sufficiently small excitations are phonons may lead to superfluidity, as $\frac{\partial \epsilon(p)}{\partial p} > 0$ near $p = 0$. The dispersion relation for a massive particle satisfies $\frac{\partial \epsilon(p)}{\partial p} \to 0$ as $p \to 0$. Hence, such a system cannot be superfluid. In particular, there is no superfluid phase in an ideal Bose gas.
Besides the ground state property, the superfluid component is conceived as carrying zero entropy and flowing irrotationally; by contrast, the normal component behaves like any other viscous fluid. From these apparently minimal postulates Landau was able to derive a complete, quantitative theory of two-fluid dynamics. While this two-fluid hydrodynamics provides a conceptual basis for superfluidity, which still stands today, it is phenomenological in the sense that both properties of the superfluid and the nature of the excitation spectrum are postulated in an intuitive way rather than being explicitly demonstrated to be a consequence of the Bose statistics obeyed by the atoms.

Bose-Einstein Condensation

An ideal Bose gas below a characteristic temperature, which depends on the mass and density, exhibits Bose-Einstein condensation (BEC, see [74]); A finite fraction of all the particles (and at zero temperature, all of them) occupies a *single* one-particle state. For the usual case of periodic boundary conditions and translational invariance, this is the zero momentum state.
In a noninteracting gas with the mass and density of ^{4}He, the phenomenon of BEC would occur at 3.1K: The critical temperature for an ideal Bose gas with specific volume V is given by

$$T_c = \frac{2\pi}{\zeta(\frac{3}{2})^{\frac{2}{3}}} \frac{\hbar^2}{k_B m V^{\frac{2}{3}}},$$

where k_B is the Boltzmann constant and $\zeta(\frac{3}{2}) = 2.612$, where $\zeta(x)$ for $x > 1$ is the Riemannian Zeta-function. For ^{4}He with $V = 46.2\,\text{Å}^3/\text{atom}$, $T_c = 3.1\text{K}$.
In order to generalize this notion to interacting many-Boson systems, we introduce the one-body density matrix

$$\rho^{(1)}(\vec{r}_i, \vec{r}_j) = \langle \hat{\Psi}^\dagger(\vec{r}_i)\hat{\Psi}(\vec{r}_j)\rangle,$$

where $\hat{\Psi}(\vec{r})$ is the field operator that annihilates a single particle at $\vec{r}$ in the system. The eigenvectors and eigenvalues of $\rho^{(1)}(\vec{r}_i, \vec{r}_j)$ describe the so-called

natural orbitals and the corresponding occupation numbers. BEC is present if one of the natural orbitals is *macroscopically* occupied. This means that the condensate fraction $f_c = \frac{N_c}{N}$ remains finite in the thermodynamical limit. Here, N_c is the number of condensate particles which is given by the occupation number of the orbital providing the condensate wave function χ_c.
The presence of BEC is equivalent to the existence of off-diagonal long-range order (ODLRO), i.e., the matrix elements of the one-body density matrix do not go to zero far off the diagonal but remain finite:

$$\rho^{(1)}(\vec{r}_i, \vec{r}_j) \not\to 0, \quad |\vec{r}_i - \vec{r}_j| \to \infty.$$

For a translationally invariant system

$$\begin{aligned} \rho^{(1)}(\vec{r}_i, \vec{r}_j) = \langle \hat{\Psi}^\dagger(\vec{r}_i)\hat{\Psi}(\vec{r}_j)\rangle &= \frac{1}{\Omega}\sum_{\vec{k}} e^{i\vec{k}\cdot(\vec{r}_i-\vec{r}_j)}\langle n_{\vec{k}}\rangle \\ &= \frac{\langle n_{\vec{0}}\rangle}{\Omega} + \int \frac{d^3k}{(2\pi)^3} e^{i\vec{k}\cdot(\vec{r}_i-\vec{r}_j)}\langle n_{\vec{k}}\rangle, \end{aligned}$$

and in the limit $|\vec{r}_i - \vec{r}_j| \to \infty$, the second term (all $\vec{k} \neq 0$) vanishes by cancellation.

BEC and Superfluidity

Macroscopic occupation implies phase coherence which means that all properties of the condensate wave function may be expressed in terms of the single-particle wave function $\chi_c(\vec{r}) = \phi(\vec{r})e^{i\varphi(\vec{r})}$. The condensate density is independent of the phase: $\rho_c(\vec{r}) = |\phi(\vec{r})|^2$. The current density of the condensate on the other hand is

$$\vec{j}_c(\vec{r}) = \frac{\hbar}{2mi}\big(\chi_c^*(\vec{r})\nabla\chi_c(\vec{r}) - \chi_c(\vec{r})\nabla\chi_c^*(\vec{r})\big) = |\phi(\vec{r})|^2\frac{\hbar}{m}\nabla\varphi(\vec{r}).$$

This suggests the definition of the condensate velocity as

$$\vec{v}_c(\vec{r}) \equiv \frac{\hbar}{m}\nabla\varphi(\vec{r}).$$

The flow described by this velocity field is irrotational, $\nabla \times \vec{v}_c = 0$. Moreover, the state of the condensate is well-defined and thus the entropy must be carried entirely by the particles occupying other single-particles states than χ_c.
These two observations provide the basis for Landau's two-fluid hydro-dynamics. One might leap to a false conclusion by identifying the phenomenon of superfluidity with the one of BEC. Note however, that the only assumption necessary in order to derive the velocity field $\vec{v}_c(\vec{r})$ is the existence of phase coherence. Macroscopically, the superfluid density is defined through the response of the system to an external potential while the condensate fraction is an equilibrium quantity. The Mermin-Wagner theorem tells us that in a 2-dimensional system at non-zero temperature, spontaneous continuous symmetry breaking is not possible

and thus, ODLRO does not exist. The one-body density matrix however decays algebraically (BKT-transition). This quasi long-range-order is sufficient for a superfluid state to be established showing that BEC and superfluidity can be observed one without the other. In addition, in liquid ^{4}He the superfluid density ρ_s tends to the total density $\rho = \frac{N}{V}$ in the limit $T \to 0$, whereas the condensate fraction remains only about 10%.

2 Imaginary-Time Path Integrals

In this section we consider a quantum system with fixed particle number N, temperature T, and volume Ω (canonical ensemble). Using the path-integral method we will see that the thermodynamic properties of Bose systems are equivalent to those of classical systems of interacting ring polymers. This will give us a classical picture which is not only simple but also exact for all thermodynamic properties, including superfluidity.
We will first develop the formalism of imaginary-time path integrals for the general case of a many-body system which obeys Boltzmann statistics. Later on, Bose statistics will be taken into account.

The Thermal Density Matrix

According to the theory of thermodynamics, all information about the statistical properties of a many-body system is contained in the density matrix $\hat{\rho}$. At high temperature, quantum systems reduce to classical systems, and one may obtain $\hat{\rho}$ by classical calculation. But as temperature decreases quantum effects must be accounted for. This is where the path-integral method enters.
The density matrix can be defined in terms of the exact eigenvalues and eigenfunctions of the Hamiltonian $\hat{H}$

$$\hat{\rho} \equiv e^{-\beta\hat{H}} = \sum_i |\phi_i\rangle e^{-\beta E_i} \langle\phi_i|, \quad \beta \equiv \frac{1}{k_B T}.$$

The equilibrium value of an operator $\hat{O}$ is

$$\langle\hat{O}\rangle = Z^{-1}\mathrm{tr}(\hat{O}\hat{\rho}) = Z^{-1}\sum_i \langle\phi_i|\hat{O}|\phi_i\rangle e^{-\beta E_i},$$

where Z is the partition function

$$Z \equiv \mathrm{tr}(\hat{\rho}) = \sum_i e^{-\beta E_i}.$$

In the following, we will work exclusively in position representation where the particles are labeled. In configuration space a density matrix element is given by

$$\rho(R, R'; \beta) \equiv \langle R|e^{-\beta\hat{H}}|R'\rangle = \sum_i \phi_i^*(R) e^{-\beta E_i} \phi_i(R'),$$

where $R = (\vec{r}_1, ..., \vec{r}_N)$, and $\vec{r}_k$ represents the position of the k^{th} particle. In space dimension 3, ρ is a function of $6N + 1$ variables.
From the definition of $\hat{\rho}(\beta)$ one derives the Bloch Equation

$$-\frac{\partial \hat{\rho}}{\partial \beta} = \hat{H}\hat{\rho},$$

with initial conditions $\hat{\rho}(0) = Id$, or $\rho(R, R'; 0) = \delta(R - R')$ in position representation.

Basis of Path Integral

The basis for the path integral representation is the identity

$$e^{-(\beta_1+\beta_2)\hat{H}} = e^{-\beta_1\hat{H}}e^{-\beta_2\hat{H}}.$$

It gives a way to express the density matrix at temperature T as a product of density matrices at temperature MT with $M \in \mathbf{N}$, i.e., for $\tau \equiv \frac{\beta}{M}$

$$e^{-\beta\hat{H}} = (e^{-\tau\hat{H}})^M.$$

In position representation one finds

$$\rho(R_0, R_M; \beta) = \int ... \int dR_1...dR_{M-1}\rho(R_0, R_1; \tau)\rho(R_1, R_2; \tau)...\rho(R_{M-1}, R_M; \tau), \tag{12.3}$$

where $R_k = (\vec{r}_{1,k}, ..., \vec{r}_{N,k}) \in \mathbf{R}^{3N}$ is the configuration of the N particles at link k. The succession of the points $(R_0, R_1, ...R_M)$ is called a path. Expression (12.3) is the sum over all discretized paths. Note that it is exact for any $M > 0$. In the limit $M \to \infty$, the path becomes continuous, but its derivative will be discontinuous at almost all points of the path. Nevertheless, for small τ it provides sufficiently accurate analytical approximations of the density matrix. This is due to the fact that for sufficiently large M, each density matrix of the right-hand side of equation (12.3) can be computed in the high-temperature limit for which the so-called primitive approximation holds:

$$e^{-\tau(\hat{T}+\hat{V})} \approx e^{-\tau\hat{T}}e^{-\tau\hat{V}}.$$

The error is of order τ^2 which may be seen by the Baker-Campbell-Hausdorff formula

$$e^{-\tau\hat{T}}e^{-\tau\hat{V}} = e^{-\tau(\hat{T}+\hat{V})}e^{\tau^2 C_1 - \tau^3 C_2 + ...}$$

with $C_1 = \frac{1}{2}[\hat{T}, \hat{V}]$ and $C_2 = \frac{1}{12}[\hat{T} - \hat{V}, [\hat{T}, \hat{V}]]$. The Trotter formula (which holds for operators that are bounded from below)

$$e^{-\beta(\hat{T}+\hat{V})} = \lim_{M\to\infty}[e^{-\tau\hat{T}}e^{-\tau\hat{V}}]^M$$

guarantees a well-controlled process as the number of time steps increases.
Suppose the interaction of the many-body system is well-described by a non-relativistic Hamiltonian of atoms interacting by a pair potential,

$$\hat{H} = \hat{T} + \hat{V} = -\lambda \sum_{i=1}^{N} \nabla_i^2 + \sum_{i<j} v(|\vec{r_i} - \vec{r_j}|),$$

with $\lambda \equiv \frac{\hbar^2}{2m}$.
In the primitive approximation the discrete path-integral formula (12.3) for the density matrix in configuration representation is

$$\begin{aligned} \rho(R_0, R_M; \beta) &= \int ... \int dR_1 ... dR_{M-1} (4\pi\lambda\tau)^{-\frac{3NM}{2}} \\ &\exp\big(-\sum_{m=1}^{M} \big[\frac{(R_{m-1} - R_m)^2}{4\lambda\tau} + \tau V(R_m)\big]\big). \end{aligned} \tag{12.4}$$

According to the primitive approximation in position space, the potential and the kinetic part can be treated separately:

$$\rho(R_0, R_1; \tau) \approx \int dR < R_0|e^{-\tau\hat{T}}|R >< R|e^{-\tau\hat{V}}|R_1 > .$$

From $\hat{V}|R >= V|R >$ it follows directly that

$$< R|e^{-\tau\hat{V}}|R_1 >= e^{-\tau V(R_1)} < R|R_1 >= e^{-\tau V(R_1)}\delta(R_1 - R).$$

For the kinetic part consider N free, distinguishable particles in a cube of side L with periodic boundary conditions. The eigenfunctions and eigenvalues are $\varphi_n(R) = L^{-\frac{3N}{2}} e^{-iK_{\vec{n}}R}$ and $E_{\vec{n}} = -\lambda K_{\vec{n}}^2$ with $K_{\vec{n}} = \frac{2\pi\vec{n}}{L}, \vec{n} \in \mathbf{Z}^{3N}$. Then

$$\begin{aligned} < R_0|e^{-\tau\hat{T}}|R > &= \sum_{\vec{n},\vec{m}} < R_0|\varphi_n >< \varphi_n|e^{-\tau\hat{T}}|\varphi_m >< \varphi_m|R > \\ &= \frac{1}{L^{3N}} \sum_{\vec{n}} e^{-iK_{\vec{n}}R_0} e^{-\tau\lambda K_{\vec{n}}^2} e^{iK_{\vec{n}}R} \\ &= e^{-\frac{(R_0-R)^2}{4\lambda\tau}} \frac{1}{L^{3N}} \sum_{\vec{n}} e^{-(\sqrt{\tau\lambda}2\pi\frac{\vec{n}}{L} + i\frac{(R_0-R)}{2\sqrt{\tau\lambda}})^2} \\ &= (4\pi\lambda\tau)^{-\frac{3N}{2}} e^{-\frac{(R_0-R)^2}{4\lambda\tau}}. \end{aligned} \tag{12.5}$$

The last step follows by approximating the sum by an integral. This requires that $\lambda\tau \ll L^2$ which will always be assumed.
The density matrix can thus be calculated at any temperature from an integral over the intermediate configurations $R_1, ..., R_{M-1}$. Such an integral looks like a partition function of some classical system. In particular, the integrand is always non-negative and can be interpreted as a probability; an essential property for Monte Carlo simulations.

The Classical Isomorphism

In quantum mechanics, matrix elements of the time evolution operator $e^{-\frac{i}{\hbar}\hat{H}(t_f-t_i)}$ in terms of path-integrals [75] yield the expression

$$U(x_f t_f, x_i t_i) = \int_{(x_i,t_i)}^{(x_f,t_f)} \mathcal{D}[x(t)] e^{\frac{i}{\hbar}S[x(t)]}.$$

Analogously one interprets the exponent in formula (12.4) as an action $S \equiv \sum_{m=1}^{M} S_m \equiv -\sum_{m=1}^{M} \ln[\rho(R_{m-1}, R_m; \tau)]$. Since it has the form of a classical potential-energy function multiplied by τ, τ plays the role of imaginary time, $t = \frac{it}{\hbar}$.
Now let us have a look at a single particle where V is some external potential. The path consists of a list of points $\vec{r}_0, ..., \vec{r}_M$. The kinetic action for the k^{th} link in equation (12.4) is

$$\frac{3N}{2} \ln(4\pi\lambda\tau) + \frac{(\vec{r}_{i,k-1} - \vec{r}_{i,k})^2}{4\lambda\tau}.$$

The second term can be interpreted as a spring potential. A path corresponds to a polymer where only next neighbors in the chain are connected with springs. Each bead on the chain represents the particle at different times $t_k = k\tau$. Hence, moving a quantum particle is equivalent to evolve the polymer.
The same interpretation can be applied to the many-body system since

$$\sum_{k=1}^{M} (R_{k-1} - R_k)^2 = \sum_{k=1}^{M} \sum_{j=1}^{N} (\vec{r}_{j,k-1} - \vec{r}_{j,k})^2 = \sum_{j=1}^{N} \sum_{k=1}^{M} (\vec{r}_{j,k-1} - \vec{r}_{j,k})^2.$$

Quantum particles may be represented by a classical system of polymers. By adding the potential interaction, this picture only changes to a system of interacting polymers. But contrary to real-time polymers, these polymers interact only at the same time and only between beads on different chains.
Thermodynamical properties, or static properties diagonal in position space, are determined by the trace of the density matrix, i.e., the integral of (12.4) over R_0 with $R_0 = R_M$. This involves all possible paths that return to their starting point after M steps. In the classical analog, these correspond to closed chains, to ring polymers.

Bose Symmetry

Thus far only systems of distinguishable particles have been considered. Now we want to introduce Bose statistics to our path-integral method.
For Bose systems only totally symmetric eigenfunctions $\varphi_i(R)$ contribute to the density matrix - those such that $\varphi_i(PR) = \varphi_i(R)$ for all permutations P with

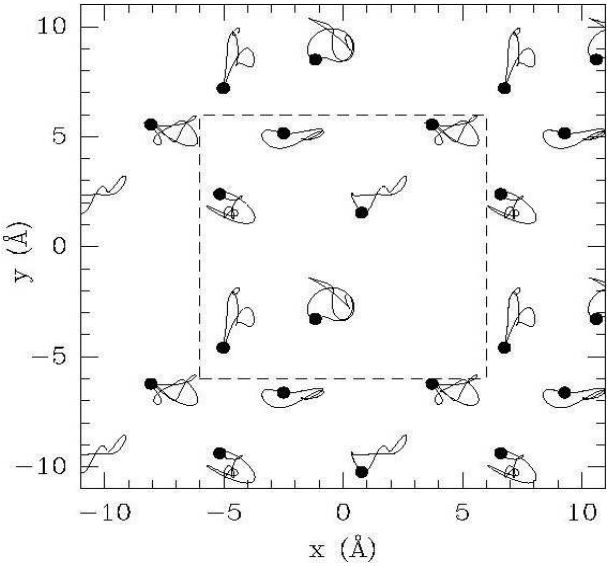

Figure 12.5: Trace of the paths of six helium atoms in the extended cell view at 2K with 80 time slices.

$PR = (\vec{r}_{P_1}, ..., \vec{r}_{P_N})$. The Bosonic density matrix is obtained by summing over all possible symmetrized states in configuration space, i.e.,

$$\rho_B(R_0, R_1; \beta) = \frac{1}{N!} \sum_P \rho(R_0, PR_1; \beta),$$

where ρ is the Boltzmann density matrix element which we have been considering up to this point.
A Bosonic simulation consists of a random walk through the path space and the permutation space. The partition function for a Bose system has the form

$$\begin{aligned} Z_B &= \frac{1}{N!} \sum_P \int ... \int dR_0 ... dR_{M-1} (4\pi\lambda\tau)^{-\frac{3NM}{2}} \\ &\qquad \exp\big(- \sum_{m=1}^{M} \big[\frac{(R_{m-1} - R_m)^2}{4\lambda\tau} + \tau V(R_m) \big] \big), \end{aligned}$$

with new boundary conditions on path closure: $PR_M = R_0$. Thus the partition function includes contributions from $N!$ closures, and the allowed paths can close on any permutation of their starting position. At high temperature the identity permutation dominates, while at zero temperature all permutations have equal contributions (see section 3).
As a consequence of the paths closing at any permutation, ring polymers can cross-link. A two-atom system of M links can be in two possible permutation states: either two separate ring polymers, each with M links, or one larger polymer with $2M$ links.

Any permutation can be broken into a product of cyclic permutations. Each cycle corresponds to several polymers cross-linking and forming a larger ring polymer. According to Feynman's 1953 theory [76], the superfluid transition is represented in the classical system by the formation of macroscopic polymers, i.e., those stretching across an entire system and involving on the order of N atoms. Paths of atoms involved in cyclic exchanges wrap around the periodic boundary conditions. They are called winding paths and are a direct manifestation of superfluidity.

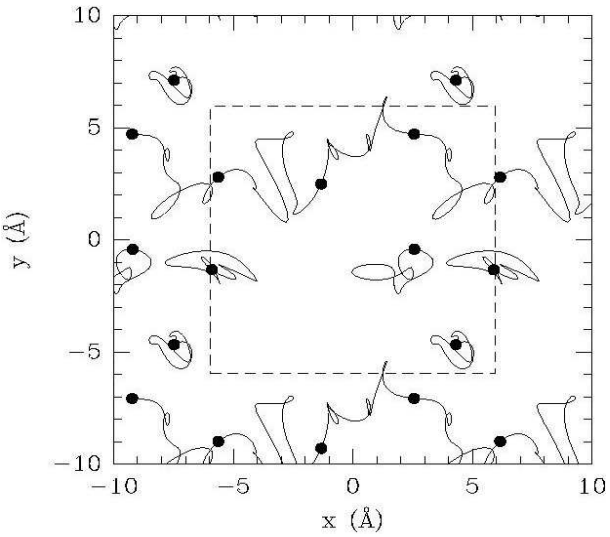

Figure 12.6: The extended trace of six helium atoms at a temperature of 0.75K. Three of the atoms are involved in an exchange which winds around the periodic cell in the x direction.

In thermodynamics one may assign to any system its thermal wavelength Λ_β. Let d be the interatomic distance. In the limit $d \ll \Lambda_\beta$ quantum statistics can be neglected and the system treated classically. For $d \simeq \Lambda_\beta$ quantum statistics may have a great impact on the system and must be taken into account.
Analogously we want to find a criterion for the polymer system to decide whether quantum statistics are important. In the absence of interaction, the size of a path (or polymer) is of the order of its thermal wavelength Λ_β; The path-length $\langle s \rangle$ of the i^{th} particle (using equation (12.5)) is given by $\langle s \rangle^2 \leq \langle s^2 \rangle = \langle (\vec{r}_{i,\beta} - \vec{r}_{i,0})^2 \rangle = \langle \big(\sum_{k=1}^{M} (\vec{r}_{i,k} - \vec{r}_{i,k-1}) \big)^2 \rangle = \langle \sum_{k=1}^{M} (\vec{r}_{i,k} - \vec{r}_{i,k-1})^2 \rangle = M \langle (\vec{r}_{i,1} - \vec{r}_{i,0})^2 \rangle = M 2\lambda\tau = 2\lambda\beta = \Lambda_\beta^2$. When Λ_β equals the interpolymer spacing, roughly $\rho^{-\frac{1}{3}}$ where ρ is the particle density, it is at least possible for the polymers to link up by exchanging end points. This relationship $\Lambda_\beta = \rho^{-\frac{1}{3}}$, defines the degeneracy temperature

$$T_D = \frac{\rho^{-\frac{2}{3}} \hbar^2}{m k_B}.$$

For temperatures higher than T_D, quantum statistics are not very important. In a liquid state, T_D gives a surprisingly good estimate of the transition temperature: For ideal Bose condensation in three dimension, $\frac{T_c}{T_D} = 3.31$, for liquid ^{4}He at saturated-vapor-pressure conditions, $\frac{T_\lambda}{T_D} = 2.32$.

3 The Superfluid Transition

A typical feature of the superfluid transition is the anomalous shape of the specific heat curve near the transition temperature. Feynman showed that it is the formation of macroscopic polymers which leads to this $\lambda-$peak. A qualitative argument may be given as follows ([77],[76],[72]); The effect of interaction can be taken into account by replacing the mass of the atoms by an effective mass, i.e., $\lambda \to \lambda^*$, and the partition function simplifies to

$$\begin{aligned} Z_B \;\propto\; & \frac{1}{N!}\sum_P \int ... \int dR_0 ... dR_{M-1} (4\pi\lambda^*\tau)^{-\frac{3NM}{2}} \\ & \exp\big(-\sum_{m=1}^{M}\big[\frac{(R_{m-1}-R_m)^2}{4\lambda^*\tau}\big]\big) \\ \propto\; & \frac{1}{N!}\sum_P \int dR \exp\big(-\frac{(R-PR)^2}{4\lambda^*\beta}\big). \end{aligned}$$

Not all particle configurations are equally probable; Configurations with well-separated atoms are important while configurations where atoms overlap can be neglected (due to the hard-core pair-potential of helium). This is taken into account by introducing a normalized configuration distribution $f(R)$ into the partition function

$$Z_B \approx \frac{K_\beta}{N!}\int dR f(R) \sum_P \exp\big(-\frac{(R-PR)^2}{4\lambda^*\beta}\big).$$

As the pair-correlation function of liquid helium does not change much in the region of λ-transition [77], one may assume $f(R)$ to be independent of temperature and write $f(R) = \frac{1}{N!}\sum_P \delta(R-PR_0)$ where R_0 is a typical configuration of atoms.

In contrast to ideal Bosons which tend to attract each other to maximize exchange, the interatomic potential of liquid helium does not allow regions of high density. Thus, we may choose R_0 to be a perfect cubic lattice with spacing d ($\approx 3.6\mathring{A}$). Permutations among particles can be visualized as polygons with arrows on the lattice. The sum over all permutation is therefore equivalent to the sum over all possible polygon patterns. At 2.2K, $\exp\big(-\frac{d^2}{4\lambda\beta}\big) \approx 0.3$, which shows that a side of a polygon longer than d is not important, and that the sides of all

polygons that contribute have length of order d, i.e.,

$$\sum_P \exp\big(-\frac{(R_0 - PR_0)^2}{4\lambda^*\beta}\big) \to \widetilde{\sum}_P \exp\big(-\frac{s(P)d^2}{4\lambda^*\beta}\big),$$

where $\widetilde{\sum}_P$ is the sum over all polygons made up of lines joining near neighbors, and $s(P)$ is the total number of sides. With these assumptions, an r-sided polygon contributes to Z roughly with the weight y^r where $y = \exp\big(-\frac{d^2}{4\lambda^*\beta}\big)$, and an r-cycle contributes with $n_r y^r$ where n_r is the number of polygons with r sides which increases with r. y depends essentially on the temperature. While at high temperature long exchanges may be neglected as $y \ll 1$, they become more important as the critical temperature is approached, $y \approx 1$. This yields the phase transition.
According to thermodynamics, the internal energy U of our system is

$$U \propto -\frac{T^2\langle x\rangle}{N},$$

as the relation between the internal energy and the partition function is given by $U = -\frac{\partial}{\partial\beta}\ln(Z)$. Therefore, one obtains for the specific heat

$$c_V \propto -2\frac{T\langle x\rangle}{N} + \frac{T^2\langle(x - \langle x\rangle)^2\rangle}{N}.$$

The specific heat depends crucially on the mean-squared fluctuation of the exchange distance. Its anomaly at the λ-point is due to the fact that in this region both short and long exchanges contribute significantly to Z.

4 Path Integral and Superfluidity

In section 2 we have seen that certain properties of liquid helium can be related to path integrals. We will now explicitly do so for the momentum distribution and for the superfluid density.

The Momentum Distribution

The probability density of finding a particle with momentum $\hbar\vec{k}_1$ is defined as

$$n_{\vec{k}_1} = (2\pi)^{-3N}\int d\vec{k}_2 ... d\vec{k}_N \Big|\int dR\phi(R)e^{-iKR}\Big|^2,$$

where $\phi(R)$ is the many-body wave function, $R = (\vec{r}_1, ..., \vec{r}_N)$, and $K = (\vec{k}_1, ..., \vec{k}_N)$. By expressing the one-body density matrix in configuration space

$$\rho^{(1)}(\vec{r}_1, \vec{r}_1') = \frac{\Omega}{Z}\int d\vec{r}_2 ... d\vec{r}_N \rho(\vec{r}_1, \vec{r}_2, ..., \vec{r}_N, \vec{r}_1', \vec{r}_2, ..., \vec{r}_N; \beta),$$

the momentum distribution simplifies to

$$n_{\vec{k}} = \frac{1}{\Omega(2\pi)^3} \int d\vec{r} d\vec{r}' e^{-i\vec{k}(\vec{r}-\vec{r}')} \rho^{(1)}(\vec{r}, \vec{r}'). \tag{12.6}$$

The normalization factors in the last two expressions are such that $\int d\vec{r} \rho^{(1)}(\vec{r}, \vec{r}) = \Omega$ and $\int d\vec{k} n_{\vec{k}} = 1$, where Ω is the volume of the periodic cell. In terms of $n_{\vec{k}}$ the condensate fraction which is the probability of finding a particle with zero momentum is given by $f_c = \frac{(2\pi)^3}{\Omega} n_{\vec{0}}$.
From equation (12.6) follows that $n_{\vec{k}}$ is the Fourier transform of $\rho^{(1)}(\vec{r}, \vec{r}')$, which itself is the contraction of an off-diagonal element of the density matrix. In the classical analog, such a density matrix element is represented by a possibly cross-linked configuration of $(N-1)$ ring polymers and 1 linear polymer (worm). A cross-link of the linear with a ring polymer results in the destruction of the ring polymer and the worm gets longer, i.e., the worm eats up the ring polymer.

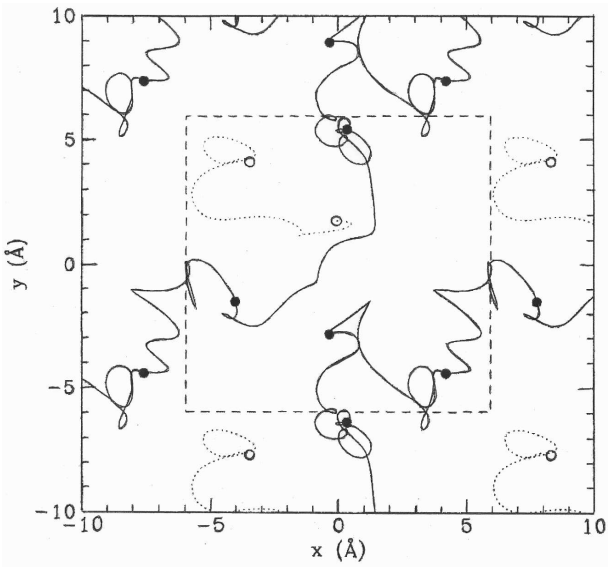

Figure 12.7: Extended trace of five ^{4}He atoms at $T = 0.75$K. The dotted path is that of the cut polymer, the one that is not periodic in time.

In the high-temperature limit, $n_{\vec{k}}$ results in the Maxwellian momentum distribution $\propto \exp\big(-\beta\lambda\vec{k}^2\big)$; As quantum effects are not important (no macroscopic exchange), the end-to-end distribution of the linear polymer is almost free-particle like, i.e., $\rho^{(1)}(\vec{r}, \vec{r}') \propto \exp\big(-\frac{(\vec{r}-\vec{r}')^2}{4\lambda\beta}\big)$.
Note that in the presence of macroscopic exchanges, the two ends of the linear polymer can become much more separated than a thermal wave length as they may be involved in a permutation cycle as well. This separation however depends not only on the statistical mechanics of the system, but also on its dimension.
The one-body density matrix of a 3D bulk liquid in the superfluid state tends to

a constant as r gets large [77], and the momentum distribution shows a peak at the origin which implies the existence of a condensate. For a homogeneous liquid, we get the condensate fraction

$$\begin{aligned} f_c = \frac{(2\pi)^3}{\Omega} n_{\vec{0}} &= \frac{1}{\Omega^2} \int d\vec{r} d\vec{r}' \rho^{(1)}(\vec{r}, \vec{r}') \\ &= \frac{1}{\Omega} \int d\vec{r} \rho^{(1)}(r). \end{aligned}$$

In the thermodynamical limit ($\Omega, N \to \infty$, $\frac{N}{\Omega}$ =const.), one sees that the condensate fraction is the large-distance limit of the one-body density matrix

$$f_c = \lim_{r \to \infty} \rho^{(1)}(r).$$

Thus the condensate fraction can be interpreted as the probability of finding a configuration where the worm-ends have attached themselves to a macroscopic exchange and the worm stretches across the whole system.

The Superfluid Density

As mentioned in section 1, the normal and the superfluid components can be determined experimentally by their different response to boundary motion. In particular, one finds an explicit expression for the superfluid density ρ_s in a periodic system in terms of a nonclassical free-energy change due to this motion [78]. Note that in this section the energy is measured with respect to the center of mass.

Consider a system enclosed between two cylinders of radii R and $R + d$ which rotate with angular frequency ω. For $\frac{d}{R} \ll 1$ centrifugal effects can be neglected and this set-up is equivalent to a system between two planes moving with velocity $v = \omega R$ which has periodic boundary conditions in one dimension ($L \equiv 2\pi R$). The density-matrix operator in the moving frame is

$$\hat{\rho}_v = e^{-\beta \hat{H}_v},$$

where

$$\hat{H}_v = \sum_j \frac{(\vec{p}_j - m\vec{v})^2}{2m} + V.$$

$\vec{p}_j$ denotes the momentum of the j^{th} particle in the lab frame.

Since the superfluid component is viscous-free, the part of the liquid which responds to the boundary motion is exactly the normal component,

$$\frac{\rho_n}{\rho} N m \vec{v} = \langle \vec{P} \rangle = \frac{\mathrm{tr}(\vec{P}\hat{\rho}_v)}{\mathrm{tr}\hat{\rho}_v},$$

where $\vec{P}$ is the total momentum of the liquid in the lab frame and $\rho = \rho_n + \rho_s$ the total particle density. This equation may also be written in terms of the free energy $F_v = -\frac{1}{\beta}\ln(Z) = -\frac{1}{\beta}\ln(\mathrm{tr}\hat{\rho}_v)$ of the system with moving walls:

$$\begin{aligned}\frac{\rho_n}{\rho}Nm\vec{v} &= \frac{\partial}{\beta\partial\vec{v}}\ln(\mathrm{tr}\hat{\rho}_v) + Nm\vec{v} \\ &= -\frac{\partial F_v}{\partial\vec{v}} + Nm\vec{v}.\end{aligned}$$

The free-energy change due to the boundary motion is for small velocities

$$\frac{\Delta F_v}{N} = \frac{F_v - F_{v=0}}{N} = \frac{1}{2}mv^2\frac{\rho_s}{\rho} + O(v^4). \tag{12.7}$$

The last step follows by the Taylor series expansion of $\frac{F_v}{N}$ in $\frac{1}{2}mv^2$ around $v = 0$ using $\frac{\partial\frac{F_v}{N}}{\partial\vec{v}} = m\vec{v}\frac{\partial F_v}{\partial(\frac{1}{2}mv^2)}$. This free-energy change ΔF_v depends on the superfluid component and does not occur for a classical fluid ($\rho_s = 0$).
In the following, we generalize our considerations to a system which is periodic in all spatial directions. For the computation of ΔF_v and hence ρ_s by the path-integral algorithm we switch to the system of stationary walls. ρ_v satisfies the Bloch equation

$$-\frac{\partial\rho_v(R,R';\beta)}{\partial\beta} = \big[\frac{1}{2m}\sum_j(-i\hbar\nabla_j - m\vec{v})^2 + V\big]\rho_v(R,R';\beta),$$

with periodic boundary conditions

$$\rho_v(\vec{r}_1,...,\vec{r}_N,\vec{r}'_1,...,\vec{r}'_j+\vec{L},...\vec{r}'_N;\beta) = \rho_v(\vec{r}_1,...,\vec{r}_N,\vec{r}'_1...,\vec{r}'_j,...\vec{r}'_N;\beta).$$

By introducing the gauge transformation $\phi(R) \to e^{-i\frac{m}{\hbar}\vec{v}\cdot\sum_j\vec{r}_j}\phi(R)$, we get the equivalent system

$$-\frac{\partial\tilde{\rho}(R,R';\beta)}{\partial\beta} = \big[\frac{1}{2m}\sum_j(-i\hbar\nabla_j)^2 + V\big]\tilde{\rho}(R,R';\beta),$$

with boundary conditions

$$\tilde{\rho}(\vec{r}_1,...,\vec{r}_N,\vec{r}'_1,...,\vec{r}'_j+\vec{L},...\vec{r}'_N;\beta) = e^{i\frac{m}{\hbar}\vec{v}\cdot\vec{L}}\tilde{\rho}(\vec{r}_1,...,\vec{r}_N,\vec{r}'_1...,\vec{r}'_j,...\vec{r}'_N;\beta).$$

Hence $\tilde{\rho}$ satisfies the usual Bloch equation in the system with stationary walls. Note, in addition, that $\rho_v(R,R';\beta) = e^{i\frac{m}{\hbar}\vec{v}\cdot\sum_j(\vec{r}_j-\vec{r}'_j)}\tilde{\rho}(R,R';\beta)$. The calculation of the density matrix $\hat{\rho}_{\vec{v}}$ can therefore be done by use of the usual density matrix if an additional phase factor is included as a weight. In particular, in a path-integral calculation the contribution to the density matrix from a path ending

on a periodic image of its initial point must include the factor $e^{i\frac{m}{\hbar}\vec{v}\cdot\vec{L}}$. The fact that the density matrix element depends now on the actual trajectories of the particles suggests the definition of the winding number $\vec{W}$:

$$\vec{W}L \equiv \sum_j (\vec{r}_{P(j)} - \vec{r}_j), \quad P \in S_N.$$

The winding number is obtained by tracing the path of each single particle from its initial position $\vec{r}_i$ to its final position $\vec{r}_{P(i)}$ a time β later and counting the number of times periodic boundary conditions have been invoked. Usually there are periodic boundary conditions in all spatial direction and the winding number is a vector which is given in units of the box length. The winding number is a topological invariant of a given path; It can be determined by counting the flux of paths across any plane, no matter where it is inserted. As we will see, paths with a nonzero winding are the signal for superfluidity.
The free-energy change is related to the winding number by

$$e^{-\beta\Delta F_v} = \frac{\mathrm{tr}\hat{\rho}_v}{\mathrm{tr}\hat{\rho}_{v=0}} = \frac{\mathrm{tr}(e^{i\frac{m}{\hbar}\vec{v}\cdot\sum_j(\vec{r}_j - \vec{r}'_j)}\tilde{\rho})}{\mathrm{tr}\tilde{\rho}} = \langle e^{i\frac{m}{\hbar}\vec{v}\cdot\vec{W}L}\rangle.$$

Thus ΔF_v is the Fourier transform of the winding number distribution and is $\frac{h}{mL}$-periodic in v. By symmetry, the average value of $\vec{W}$ vanishes, and for small velocities

$$\beta\Delta F_v = \frac{m^2v^2}{2\hbar^2}\frac{\langle W^2\rangle L^2}{3} + O(v^4),$$

where the factor $\frac{1}{3}$ comes from symmetrizing over the three equivalent axis assuming a cubic periodic cell. By comparison with equation (12.7) one obtains the winding number formula for the superfluid density

$$\frac{\rho_s}{\rho} = \frac{m}{\hbar^2}\frac{\langle W^2\rangle L^2}{3\beta N}.$$

The analogous derivation in d spatial dimensions results in the formula

$$\frac{\rho_s}{\rho} = \frac{m}{\hbar^2}\frac{\langle W^2\rangle L^{2-d}}{d\beta\rho}.$$

The superfluid density is essentially given by the mean-squared winding number, i.e., a nonvanishing probability for winding paths implies that the system is in the superfluid state. This formula provides a very elegant way to evaluate ρ_s. The tricky part about it is the computation of $\langle W^2\rangle$ which cannot be done in an analytical way but must be solved numerically, by Monte Carlo simulations.

5 Path-Integral Monte Carlo Simulations

Monte Carlo simulations play a very important role in the theoretical investigation of complex systems such as quantum many-body systems. In addition to accurate results, they may also improve our conceptual understanding of certain phenomena.

For Bose systems, the most powerful method is the path-integral Monte Carlo simulation (PIMC) which is a computational technique for simulating quantum systems at $T \neq 0$K, and which is exact in the sense that all approximations are controllable. PIMC is based on the quantum-classical isomorphism introduced in section 2. The explicit expression for the density matrix (12.3) requires altogether $3N(M-1)$ integrations. Without introducing very severe approximations, the only way of doing the integrals as N gets large is stochastically, i.e., by sampling the integrand. In a few words, certain values of the input random variables in a simulation have more impact on the parameter being estimated than others.

The Monte Carlo evaluation for the given problem consists of generating a large set of independent paths-configurations $X^s \equiv [R_0^s, ..., R_M^s]$, $s = 1, ...S$ statistically sampled from a probability density proportional to $\rho(R_0, R_M; \beta)$. The thermal average of any operator $\hat{O}$ can then be estimated as a statistical average over the set of values $\{O(X^s)\}$,

$$\langle O \rangle = \frac{1}{S} \sum_{s=1}^{S} O(X^s).$$

Importance sampling is mostly based on the Metropolis algorithm, which is a Markov chain Monte Carlo sampling algorithm for generating an arbitrary given distribution $\pi(s)$. A Markov chain is characterized by a transition rule $P(s \to s') = T(s \to s')A(s \to s')$ and generates a reversible random walk $\{s_0, s_1, ...\}$, where $s = [P, R_0, ..., R_M]$ with $R_M = PR_0$ is an element of the total configuration space. At each point on the walk a random trial move from the current position in configuration space is selected. This trial move is then either accepted or rejected according to a simple probabilistic rule.

If the transition rule is ergodic and fulfills the condition of detailed balance

$$\pi(s)P(s \to s') = \pi(s')P(s' \to s), \tag{12.8}$$

then the probability distribution converges to an equilibrium state satisfying

$$\sum_s \pi(s)P(s \to s') = \pi(s'),$$

and the Markov process samples $\pi(s)$ (see [75]). Note that detailed balance is not a necessary, but for practical use a very convenient condition. Ergodicity means that one can move from any state to any other state in a finite number of steps with a nonzero probability.

In the Metropolis method the transition probability is split into an "a priori" sampling distribution $T(s \to s')$ and an acceptance probability $A(s \to s')$,

$$P(s \to s') = T(s \to s')A(s \to s'),$$

where

$$A(s \to s') \equiv \min\left\{1, \frac{T(s' \to s)\pi(s')}{T(s \to s')\pi(s)}\right\}.$$

If $A(s \to s') > \epsilon$, where ϵ is a randomly drawn number between zero and one then the move is accepted, otherwise rejected. This $P(s \to s')$ satisfies by definition (12.8) which ensures asymptotic convergence.
Note that the acceptance rate is not unique, there are many possible choices. Another choice that also satisfies the detailed balance equation is for example

$$A(s \to s') = \frac{\frac{\pi(s')}{\pi(s)}}{1 + \frac{\pi(s')}{\pi(s)}}.$$

This is known as the heat-bath algorithm and will be used in the next subsection.

Monte Carlo Simulation on a Lattice in One Dimension

In order to understand the basic concepts of PIMC, we consider a one-dimensional system of N hard-core Bosons which occupy arbitrary sites of a finite spatial lattice. We work at finite β and impose periodic boundary conditions. The term hard-core refers to the fact that the particles are not allowed to overlap and therefore cannot occupy the same lattice site at equal times.
Suppose the Hamiltonian of our system can be written in the form

$$\hat{H} = \hat{H}_1 + \hat{H}_2,$$

with $\hat{H}_1$ and $\hat{H}_2$ each being diagonalizable. In the primitive approximation we find for the partition function

$$\begin{aligned} Z &= \sum_{i_1 \ldots i_M} \langle i_1|e^{-\tau\hat{H}}|i_L\rangle\langle i_M|e^{-\tau\hat{H}}|i_{M-1}\rangle \ldots \langle i_2|e^{-\tau\hat{H}}|i_1\rangle \\ &\approx \sum_{i_1 \ldots i_{2M}} \langle i_1|\hat{U}_1|i_{2M}\rangle\langle i_{2M}|\hat{U}_2|i_{2M-1}\rangle\langle i_{2M-1}|\hat{U}_1|i_{2M-2}\rangle \ldots \langle i_2|\hat{U}_2|i_1\rangle, \quad (12.9) \end{aligned}$$

with $\hat{U}_j = e^{-\tau\hat{H}_j}$ and $\tau = \frac{\beta}{M}$. By choosing the intermediate state $|i_k\rangle$ in a convenient way, e.g. as an eigenstate of $\hat{H}_1$ for k odd, and as an eigenstate of $\hat{H}_2$ for k even, one obtains a quite simple expression for the partition function Z.
In the following, we study a system with nearest-neighbor interactions described by the Hamiltonian

$$\hat{H} = \sum_{i=1}^{N} \hat{H}_{i,i+1},$$

with periodic boundary conditions $\hat{H}_{N,N+1} = \hat{H}_{N,1}$. By defining

$$\begin{aligned} \hat{H}_1 &= \sum_{i\,\text{odd}} \hat{H}_{i,i+1}, \\ \hat{H}_2 &= \sum_{i\,\text{even}} \hat{H}_{i,i+1}, \end{aligned}$$

we get operators given by the sum of $\frac{N}{2}$ mutually commutating operators (as they act between different pairs of particles) and hence,

$$\hat{U}_{1(2)} = e^{-\tau \hat{H}_{1(2)}} = \prod_{i\,\text{odd(even)}} e^{-\tau \hat{H}_{i,i+1}}.$$

Let the Hamiltonian be given by

$$\hat{H} = \sum_{i=1}^{N} -t(\hat{C}_{i+1}^{\dagger}\hat{C}_i + \hat{C}_i^{\dagger}\hat{C}_{i+1}) + V(\hat{n}_i - \frac{1}{2})(\hat{n}_{i+1} - \frac{1}{2}),$$

where $\hat{C}_i^{\dagger}$ and $\hat{C}_i$ are the creation and annihilation operators and $\hat{n}_i = \hat{C}_i^{\dagger}\hat{C}_i$ the particle number operator. We denote the state in which n_i particles are on the i^{th} lattice site and n_{i+1} on the $(i+1)^{th}$ by $|n_i, n_{i+1}\rangle$, where $n_i, n_{i+1} \in \{0, 1\}$. By applying the commutation relations $[\hat{C}_i, \hat{C}_j^{\dagger}] = \delta_{ij}$ and $[\hat{C}_i, \hat{C}_j] = [\hat{C}_i^{\dagger}, \hat{C}_j^{\dagger}] = 0$, and taking into account that no site can be occupied by more than one particle, one may verify that the two terms of $\hat{H}_{i,i+1}$ commute. Thus $e^{-\tau \hat{H}_{i,i+1}} = e^{\tau t(\hat{C}_{i+1}^{\dagger}\hat{C}_i + \hat{C}_i^{\dagger}\hat{C}_{i+1})} e^{-\tau V(\hat{n}_i - \frac{1}{2})(\hat{n}_{i+1} - \frac{1}{2})}$ and

$$\begin{aligned} e^{-\tau \hat{H}_{i,i+1}}|0,0\rangle &= |0,0\rangle e^{-\tau \frac{V}{4}}, \\ e^{-\tau \hat{H}_{i,i+1}}|1,1\rangle &= |1,1\rangle e^{-\tau \frac{V}{4}}, \\ e^{-\tau \hat{H}_{i,i+1}}|1,0\rangle &= \big(\cosh(\tau t)|1,0\rangle + \sinh(\tau t)|0,1\rangle\big) e^{\tau \frac{V}{4}}, \\ e^{-\tau \hat{H}_{i,i+1}}|0,1\rangle &= \big(\cosh(\tau t)|0,1\rangle + \sinh(\tau t)|1,0\rangle\big) e^{\tau \frac{V}{4}}. \end{aligned} \tag{12.10}$$

These equations follow by expanding $e^{\tau t(\hat{C}_{i+1}^{\dagger}\hat{C}_i + \hat{C}_i^{\dagger}\hat{C}_{i+1})}$ into its Taylor series and noting that $(\hat{C}_{i+1}^{\dagger}\hat{C}_i + \hat{C}_i^{\dagger}\hat{C}_{i+1})|1,0\rangle = |0,1\rangle$ and $(\hat{C}_{i+1}^{\dagger}\hat{C}_i + \hat{C}_i^{\dagger}\hat{C}_{i+1})^2|1,0\rangle = |1,0\rangle$.

The world-line perspective is very suitable for depicting this process. The x-axis represents the periodic spatial lattice of sites, the y-axis shows the imaginary-time evolution. Each time step τ is divided further into two steps. In the first step $\hat{U}_1$ acts on the system, in the second step $\hat{U}_2$. This results in a checkerboard pattern where the shaded boxes correspond to the areas of space and time in which particle exchange can take place, that is, on which world-lines may be drawn across.

We want to develop an algorithm for generating all allowed world-line configurations. This is achieved by successive local changes of the world-line. As we work

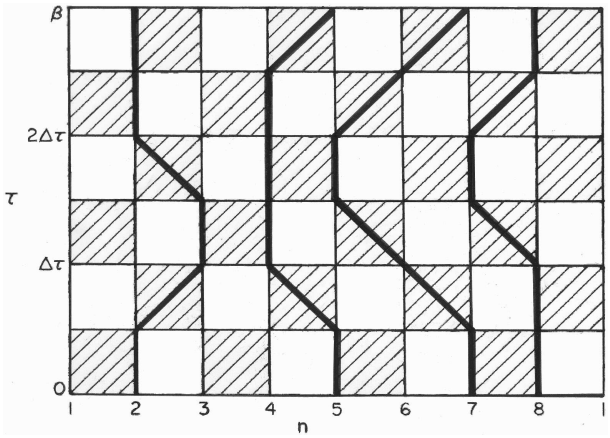

Figure 12.8: Checkerboard pattern for the one-dimensional system. The world lines represent the particles which may interact in the shaded squares.

in the canonical ensemble where particle number N is fixed, these local changes must conserve N in each intermediate state, i.e., within each shaded box. Otherwise, the move must be rejected. After creating new configurations at random, the algorithm accepts or rejects the configurations according to a sample probability which is proportional to the product of amplitudes in equation (12.9).
To derive an explicit expression for the acceptance probability, we designate each lattice site by (i, j), where i denotes the spatial and j the temporal position, $i = 1, ..., N$ and $j = 1, ..., 2M$. As particle number must be conserved within each shaded box, a permitted change always involves a move across an unshaded box (Figure 12.9). In addition, the occupation number $n(i, j)$ at each site can only be 0 or 1. Thus, a move across a box, whose lower left-hand corner is at (i, j), is possible if and only if $|s| = 2$, where

$$s \equiv n(i, j) + n(i, j + 1) - n(i + 1, j) - n(i + 1, j + 1).$$

$s = +2$ corresponds to a move from left to right, whereas $s = -2$ to one from right to left.
By using the heat bath algorithm, the probability of acceptance for a proposed new configuration is given by

$$P = \frac{R}{1 + R},$$

where R is defined as the ratio of the configurations before and after the move. This ratio depends on the actual form of the world-line as well as on the direct neighborhood of the local change. The occupation numbers $n(i + 1, j - 1)$ and $n(i+1, j+2)$ determine whether the world-line to be moved is vertical or diagonal, and $n(i-1, j)$ and $n(i+2, j)$ provide information about the existence of additional world-lines in the boxes to the left and right of our unshaded one. One finds

$$R = \big[\tanh(\tau t)\big]^{su} \big[\cosh(\tau t)\big]^{sv} e^{\tau V \frac{sv}{2}},$$

where

$$\begin{aligned} u &\equiv 1 - n(i+1, j-1) - n(i+1, j+2), \\ v &\equiv n(i-1, j) - n(i+2, j). \end{aligned}$$

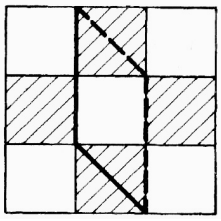

Figure 12.9: Example of a local change in the world line where the solid line show the world line before, the dashed line after the move.

Note that with these local updates, the winding number never changes during the whole process. This means in particular that increasing the number of time steps (i.e., cooling down our system) will not result in an increase of the macroscopic exchanges. Thus, this algorithm is not very appropriate in order to study systems which manifest superfluidity.

The Worm Algorithm

A rather novel computational model which is also based on PIMC is the worm algorithm (WA). It allows efficient calculations of winding numbers and one-body density matrices for systems up to various thousand particles. The main difference to the conventional MC algorithms is that it operates on the extended configuration space, containing both closed world-line configurations which contribute to the partition function Z, and configurations containing one open line (worm). The worm-configurations contribute to the one-body density matrix and are referred to as off-diagonal configurations. All topologically non-trivial modifications of the paths occur in the off-diagonal configurational space; When the system arrives at a diagonal configuration (all world-lines closed), the number of particles and the winding number are updated.
Consider the discrete paths $X \equiv (R_0, R_2, ..., R_M)$, periodic in the imaginary time interval $\beta = M\tau$. The probability density is given by

$$\rho(X) = e^{-U(X)} \prod_{j=0}^{M} \rho_0(R_j, R_{j+1}; \tau), \tag{12.11}$$

where $\rho_0(R_j, R_{j+1}; \tau) = \prod_{i=1}^{N} \rho_0(\vec{r}_{i,j}, \vec{r}_{i,j+1}; \tau)$ is the product of N free-particle propagators. According to equation (12.5), $\rho_0(\vec{r}_{i,j}, \vec{r}_{i,j+1}; \tau)$ are Gaussian for all

i, j and can be used as probability weights. U describes the spatial and imaginary-time interactions between the particles and is chosen such that $\rho(X) \to \rho(R, R; \beta)$ as $\tau \to 0$.

With the WA it is possible to perform simulations in the grand-canonical ensemble where the number of particle N is not fixed; An off-diagonal configuration contains a worm, i.e., a world line with two ends which we denote by I and M. These two points are localized in the space-time at $(\vec{r}_I, t_I)$ and $(\vec{r}_M, t_M)$. As usual, the paths are sampled by a Metropolis random walk but the local updates result exclusively in stochastic movements in space-time of I and M. At times t_I and t_M the conservation of the particle number N is violated and therefore, N is both configuration- and time-dependent.

The set of local updates consists of complementary pairs which switch between diagonal and off-diagonal configurations, as well as local changes which are self-complementary as they preserve the number of variables. Possible worm-movements are:

1a) Open. In diagonal configuration X, three numbers i, j, m are selected at random. i denotes the world line to be altered and j defines the position $(\vec{r}_{i,j}, t_j)$ of I. M is placed on the same line a time mt later, $(\vec{r}_{i,j+m}, t_{j+m})$, and the beads in between are removed. This process thus splits an arbitrarily chosen world line i into two independent world lines i and i_0; The first ending at I, the second starting at M. Let us denote the configuration after the move by X'. The acceptance probability is

$$A_{\text{open}} = \min\big\{1, \frac{N_X}{V} \frac{e^{\Delta U - \mu m \tau}}{\rho_0(\vec{r}_{i,j}, \vec{r}_{i,j+m}, m\tau)}\big\},$$

where $\Delta U = U(X) - U(X')$, V is the volume of the system, N_X is the number of particles before the move, and the input parameter μ represents the chemical potential.

The expression for A_{open} can be derived as follows:

$$\begin{aligned}
\rho(X) &= e^{-U(X)+\mu m\tau} \prod_{k=j}^{k=j+m-1} \rho_0(\vec{r}_{i,k}, \vec{r}_{i,k+1}; \tau), \\
\rho(X') &= C e^{-U(X')} \\
T(X \to X') &= p_{\text{open}} \frac{1}{N_X M \bar{m}}, \\
T(X' \to X) &= p_{\text{close}} \frac{\prod_{k=j}^{k=j+m-1} \rho_0(\vec{r}_{i,k}, \vec{r}_{i,k+1}; \tau)}{\rho_0(\vec{r}_{i,j}, \vec{r}_{i,j+m}, m\tau)}.
\end{aligned}$$

p_{open} and p_{close} denote the probabilities that the algorithm implements the move *Open* or *Close*. C is a constant controlling the relative statistics of the diagonal and off-diagonal configurations and is here set to $C = \frac{1}{VM\bar{m}}$, where $\bar{m} < M$ is a fixed number defining the maximal time interval. The factor $\frac{1}{N_X M \bar{m}}$ is the probability for selecting an arbitrary triplet i, j, m. In order to connect world line

i with world line i_0, one must generate a path with fixed initial and end points, $\vec{r}_{i,j}$ and $\vec{r}_{i_0,j+m}$. But not each of these paths is equally probable. This leads to the quotient in the expression of $T(X' \to X)$.
1b) Close. Consider the off-diagonal configuration with I being the j^{th} bead on world line i and M the $(j+m)^{th}$ bead on i_0. The move consists in generating a world line of $m-1$ beads connecting the two worm ends. It eliminates the world line i_0 along with the worm and creates a diagonal configuration. If $m > \bar{m}$, the update is rejected. For $m \leq \bar{m}$ the acceptance probability is

$$A_{\text{close}} = \min\left\{1, \frac{V}{N_{X'}} e^{\Delta U + \mu m \tau} \rho_0(\vec{r}_{i,j}, \vec{r}_{i,j+m}, m\tau)\right\}.$$

2a) Insert. A worm of length m is created out of the vacuum in diagonal configuration. Its starting position M as well as the number of beads $m \geq \bar{m}$ are picked at random and it is accepted with probability

$$A_{\text{insert}} = \min\left\{1, e^{\Delta U + \mu m \tau}\right\}.$$

2b) Remove. If the existing worm is of length $m \leq \bar{m}$, it is proposed to remove the whole world line connecting M and I and accepted with

$$A_{\text{remove}} = \min\left\{1, e^{\Delta U - \mu m \tau}\right\}.$$

3a) Advance. An simple modification of the configuration is done by advancing I forward in time by a random number m of slices which has acceptance rate

$$A_{\text{advance}} = \min\left\{1, e^{\Delta U + \mu m \tau}\right\}.$$

In this move, I may advance past M.
3b) Recede. By erasing m consecutive beads, I may also move backwards in time with probability of acceptance

$$A_{\text{recede}} = \min\left\{1, e^{\Delta U - \mu m \tau}\right\}.$$

The number of beads to be eliminated should not exceed the number of beads of the worm. Otherwise, the move is "a priori" rejected.
4) Swap. This move operates on the off-diagonal configuration. Let $(r_{i,j}, t_j)$ be the position of I and select a world line k with probability $T_k = \frac{\rho_0(\vec{r}_{i,j}, \vec{r}_{k,j+\bar{m}}, \bar{m}\tau)}{\Sigma_i}$ where $\Sigma_i \equiv \sum_l \rho_0(\vec{r}_{i,j}, \vec{r}_{l,j+\bar{m}}, \bar{m}\tau)$ is the normalization factor. If k contains M at a time slice in $[j, j+\bar{m}]$ the move is rejected. The beads $\vec{r}_{k,j+1}, ..., \vec{r}_{k,j+\bar{m}-1}$ are removed and the position of I is connected to the bead $\vec{r}_{k,j+\bar{m}}$ by a randomly generated piece of world line $\vec{r}_{i,j+1}, ..., \vec{r}_{i,j+\bar{m}-1}$. The new end point I is now localized at $r_{k,j}$. The final configuration, which is again off-diagonal, may possess a winding number that does not agree with the one of the initial configuration.

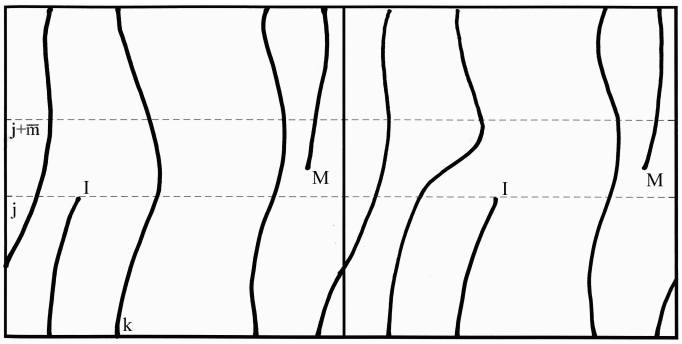

Figure 12.10: Illustration of the *Swap* move: left before, right after the move.

Thus, with repeated application of the Swap move it is possible to generate all permutations of the particles. This move is accepted with probability

$$A_{\text{swap}} = \min\left\{1, e^{\Delta U}\frac{\Sigma_i}{\Sigma_k}\right\}.$$

Note that there is a high acceptance probability for the moves $3a, b$ and 4 as they do not require the particles to be close together (within the region of repulsive potential) and therefore, macroscopic exchanges occur rather frequently in this algorithm.

6 Conclusion

Experimentally it is rather easy to find out whether a system is in the superfluid state, e.g., by examine its response to moving boundaries. With the winding number formula from section 4 we have found a way to theoretically predict the behavior of our system.
The results for ρ_s obtained by PIMC simulations agree with the experimental values within the statistical uncertainties (see Figure 12.11, taken from [78]). The discrepancy above the experimental transition temperature is due to finite-size effects. The worm algorithm from section 5 overcomes this limitation of previous PIMC technology allowing simulations for systems of several thousand particles and affords efficient large-scale computations of thermodynamic properties for many-body systems.

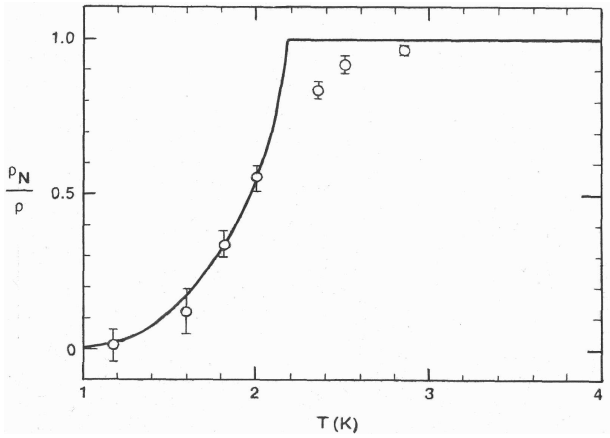

Figure 12.11: Normal-component fraction along the vapor pressure curve for bulk ^{4}He. Solid line is the experimental data, the open circle are obtained by PIMC simulations for 64 atoms.

13 Introduction to quantum computing

Lukas Gamper
Supervisor: Lode Pollet

This chapter starts with the basic concepts and operations of quantum computing. Afterwards the most important algorithm known in quantum computing, the factorization algorithm, is derived. In the last part the basic concepts of cryptography are introduced and the most widely used quantum key distribution protocols are presented.

1 Introduction

Classical Computers

Classical computers work with bits. A bit is like a coin: there is either head or tail, so one bit can store *one* binary decision. Operations are performed with so called gates. One of the most important gates is the XOR (exclusive or) gate. The XOR gate implements the operation $x + y \pmod 2 \equiv x \oplus y$. If the inputs have more than one bit, the operation is performed bitwise. The XOR operation is it's own inverse: $x \oplus x \oplus y \equiv y$. An other important gate is the NAND gate (not and gate). The NAND gate is 0 if both input bits are set to 1, 1 otherwise. The NAND gate is universal, which means, that every other gate can be implemented as a combination of NAND. E.g. $x \oplus y \equiv (x \text{ NAND } (y \text{ NAND } y)) \text{ NAND } ((x \text{ NAND } x) \text{ NAND } y)$.

What is a Qubit?

A qubit is the analogous concept for *quantum computation*. A qubit has two eigenstates $|0\rangle$ and $|1\rangle$, which correspond to the states 0 and 1 for a classical bit.

In contrast to classical bits, qubits can store a *superposition* of $|0\rangle$ and $|1\rangle$:

$$|\psi\rangle = \alpha|0\rangle + \beta|1\rangle, \tag{13.1}$$

where α and β are *complex numbers* normalized to 1 ($|\alpha|^2 + |\beta|^2 = 1$). The special states $|0\rangle$ and $|1\rangle$ are known as *computational basis states*, and form an orthogonal basis for vector spaces.

A possible realization of qubits are two orthogonal polarisations of a photon.

We can express $|\psi\rangle$ as a point(θ, φ) on a unit sphere:

$$|\psi\rangle = (\cos\theta|0\rangle + e^{i\varphi}, \sin\theta|1\rangle) \tag{13.2}$$

where θ and φ are real numbers. This representation is called the Bloch sphere representation.

If we do a binary extension of φ

$$|\varphi\rangle = \pi \sum_{k=0}^{\infty} a_i 2^{-i}, \tag{13.3}$$

we see, that we can store an *infinite number of classical bits* in one *qubit*.
This conclusion turns out to be misleading, because in a measurement of a qubit we will only get one of the eigenvalues $|0\rangle$ or $|1\rangle$. It turns out that only if infinitely many identically prepared qubits were measured, we would be able to determine α and β for such a qubit.

Suppose we have two qubits. Then the *computational basis states* are $|00\rangle$, $|01\rangle$, $|10\rangle$ and $|11\rangle$. Thus the state vector describing the two qubits is

$$|\varphi\rangle = a_{00}|00\rangle + a_{01}|01\rangle + a_{10}|10\rangle + a_{11}|11\rangle, \tag{13.4}$$

with

$$\sum_{i,j\in\{0,1\}} |a_{ij}|^2 = 1. \tag{13.5}$$

Quantum gates

A quantum gate must fulfill the normalization condition. If $U(\alpha|0\rangle + \beta|1\rangle) = \alpha'|0\rangle + \beta'|1\rangle$, then $\alpha'^2 + \beta'^2 = 1$ must hold!

Single qubit gates

Pauli-X	$\mathcal{X}$	$\begin{pmatrix} 0 & 1 \\ 1 & 0 \end{pmatrix}$
Pauli-Y	$\mathcal{Y}$	$\begin{pmatrix} 0 & -i \\ i & 0 \end{pmatrix}$
Pauli-Z	$\mathcal{Z}$	$\begin{pmatrix} 1 & 0 \\ 0 & -1 \end{pmatrix}$
Hadamard gate	$\mathcal{H}$	$\frac{1}{\sqrt{2}}\begin{pmatrix} 1 & 1 \\ 1 & -1 \end{pmatrix}$
Phase gate	$\mathcal{S}$	$\begin{pmatrix} 1 & 0 \\ 0 & i \end{pmatrix}$
$\pi/8$ gate	$\mathcal{T}$	$\begin{pmatrix} 1 & 0 \\ 0 & e^{i\pi/4} \end{pmatrix}$

Pauli-X gate The Pauli-X gate is the quantum mechanical analogy to the classical NOT gate:

$$\mathcal{X}\begin{pmatrix} \alpha \\ \beta \end{pmatrix} = \begin{pmatrix} \beta \\ \alpha \end{pmatrix}. \tag{13.6}$$

Pauli-Z gate The Pauli-Z gate leaves $|0\rangle$ unchanged and flips the sign of $|1\rangle$ to $-|1\rangle$.

Hadamard gate Note that $\mathcal{H} = (\mathcal{X} + \mathcal{Z})/\sqrt{2}$ and $H^2 = I$. On the *Bloch sphere*, the *Hadamard gate* is a rotation on the sphere about the x axis by 90^o, followed by a reflection at the $x - y$ plane.

$\pi/8$ **gate** The $\pi/8$ gate is called $\pi/8$ for historical reasons. It can be written as

$$\mathcal{T} = e^{i\pi/8}\begin{pmatrix} e^{-i\pi/8} & 0 \\ 0 & e^{i\pi/8} \end{pmatrix}. \tag{13.7}$$

and the global phase is unimportant, so both entries of the Matrix have a phase of $\pi/8$.

Multi qubit gates

The standard base of an n qubits system is given by $|\{0,1\}^n\rangle$, where the basis states are mapped to a vector space of dimension 2^n.

Example 2. A system of two qubits is usually represented as follows:

$$|00\rangle = \begin{pmatrix} 1 \\ 0 \\ 0 \\ 0 \end{pmatrix}, |01\rangle = \begin{pmatrix} 0 \\ 1 \\ 0 \\ 0 \end{pmatrix}, |10\rangle = \begin{pmatrix} 0 \\ 0 \\ 1 \\ 0 \end{pmatrix}, |11\rangle = \begin{pmatrix} 0 \\ 0 \\ 0 \\ 1 \end{pmatrix}. \tag{13.8}$$

Controlled gate Out of any gate described above, a controlled gate can be constructed. It consists of two qubits labeled as *control qubit*, $|c\rangle$, and *target qubit*, $|t\rangle$. The action of a single qubit gate is only performed if the *control qubit* is set to $|1\rangle$. The quantum scheme of the gate is:

The matrix representation of the controlled gate in the basis described above is:

$$\left(\begin{array}{cc|cc} 1 & 0 & 0 & 0 \\ 0 & 1 & 0 & 0 \\ \hline 0 & 0 & \multicolumn{2}{c}{\multirow{2}{*}{$\mathcal{U}$}} \\ 0 & 0 & & \end{array}\right).$$

CNOT The controlled-NOT-gate is a quantum two qubits gate. The action of the $CNOT$ is given by $|c\rangle|t\rangle to|c\rangle|t \oplus c\rangle$, i.e., if the control qubit is set to $|1\rangle$, then the target qubit is flipped, otherwise the target qubit is left unchanged. The quantum scheme of the gate is

The matrix representation is

$$\left(\begin{array}{cccc} 1 & 0 & 0 & 0 \\ 0 & 1 & 0 & 0 \\ 0 & 0 & 0 & 1 \\ 0 & 0 & 1 & 0 \end{array}\right).$$

Swap gate The swap gate swaps the states of two qubits. The sequence of gates has the following sequence of effects on a computational basis state $|a, b\rangle$

$$\begin{aligned} |a, b\rangle &\rightarrow |a, a \oplus b\rangle && (13.9) \\ &\rightarrow |a \oplus (a \oplus b), a \oplus b\rangle = |b, a \oplus b\rangle && (13.10) \\ &\rightarrow |b, (a \oplus b) \oplus b\rangle = |b, a\rangle. && (13.11) \end{aligned}$$

where the $\oplus$ is the XOR operator. The quantum scheme reads

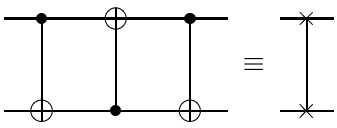

Copying qubits

Is it possible to make a copy of an unknown quantum state? Suppose we have a quantum machine with two slots, the *data slot* and the *target slot*:

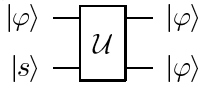

The *data slot* starts in an unknown but pure quantum state, $|\varphi\rangle$. This is the state which is to be copied into the *target slot*. We assume that the *target slot* starts in some standard pure state, $|s\rangle$. Thus the initial state of the copying machine is

$$|\varphi\rangle \otimes |s\rangle. \tag{13.12}$$

Some unitary evolution U now affects the copying procedure. Ideally,

$$|\varphi\rangle \otimes |s\rangle \rightarrow^{\mathcal{U}} \mathcal{U}(|\varphi\rangle) \otimes |s\rangle) = |\varphi\rangle \otimes |\varphi\rangle. \tag{13.13}$$

Suppose this copying procedure works for two particular pure states, $|\psi\rangle$ and $|\varphi\rangle$. Then we have

$$\mathcal{U}(|\psi\rangle) \otimes |s\rangle) = |\psi\rangle \otimes |\varphi\rangle \tag{13.14}$$

$$\mathcal{U}(|\varphi\rangle) \otimes |s\rangle) = |\varphi\rangle \otimes |\varphi\rangle. \tag{13.15}$$

Taking the inner product of these two equations gives

$$\langle\psi|\varphi\rangle = (\langle\psi|\varphi\rangle)^2. \tag{13.16}$$

But $x = x^2$ has only two solutions, $x = 0$ and $x = 1$, so either $|\psi\rangle = |\varphi\rangle$ or $|\varphi\rangle$ and $|\psi\rangle$ are orthogonal. Thus a cloning device can only clone states which are orthogonal to one another, and therefore a general quantum cloning device is impossible. A potential quantum cloner cannot, for example, clone the qubit states $|\varphi\rangle = |0\rangle$ and $|\varphi\rangle = (|0\rangle + |1\rangle)/\sqrt{2}$, since these states are not orthogonal.

EPR, Bell states

The name *EPR pairs* or *Bell states* comes from the people who first pointed out the strange properties of this state: Einstein, Podolsky, Rosen and Bell. The states are produced by the following circuit:

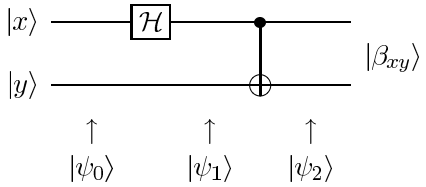

In	Out
$\|00\rangle$	$(\|00\rangle + \|11\rangle)/\sqrt{2} \equiv \|\beta 00\rangle$
$\|01\rangle$	$(\|01\rangle + \|10\rangle)/\sqrt{2} \equiv \|\beta 01\rangle$
$\|10\rangle$	$(\|00\rangle - \|11\rangle)/\sqrt{2} \equiv \|\beta 10\rangle$
$\|11\rangle$	$(\|01\rangle - \|10\rangle)/\sqrt{2} \equiv \|\beta 11\rangle$

The circuit has the following internal states:

$$|\psi_0\rangle = |x\rangle|y\rangle \tag{13.17}$$

$$|\psi_1\rangle = \frac{a_x(|0\rangle + |1\rangle) + b_x(|0\rangle - |1\rangle)}{\sqrt{2}}|y\rangle \tag{13.18}$$

$$|\psi_2\rangle = |\beta_{xy}\rangle \equiv \frac{|0, y\rangle + (-1)^x|1, -y\rangle}{\sqrt{2}}. \tag{13.19}$$

The states are called β_{00}, β_{01}, β_{10} and β_{11} because of the notation

$$|\beta_{xy}\rangle \equiv \frac{|0, y\rangle + (-1)^x|1, -y\rangle}{\sqrt{2}} \tag{13.20}$$

.

Quantum teleportation

Suppose Alice and Bob share an *EPR pair*, each having one qubit of the EPR pair. Alice can only communicate over a *classical wire* with Bob. How can Alice deliver a qubit $|\psi\rangle$ to Bob?

Alice can modulate the qubit $|\psi\rangle = \alpha|0\rangle + \beta|1\rangle$ with her half of the *EPR pair* with the following circuit:

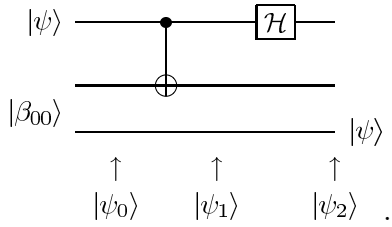

.

It has the following states:

$$|\psi_0\rangle = |\psi\rangle|\beta_{00}\rangle \tag{13.21}$$

$$= \frac{1}{\sqrt{2}}\left[\alpha|0\rangle(|00\rangle + |11\rangle) + \beta|1\rangle(|00\rangle + |11\rangle)\right] \tag{13.22}$$

$$|\psi_1\rangle = \frac{1}{\sqrt{2}}\left[\alpha|0\rangle(|00\rangle + |11\rangle) + \beta|1\rangle(|10\rangle + |01\rangle)\right] \tag{13.23}$$

$$|\psi_2\rangle = \frac{1}{2}\left[\alpha(|0\rangle + |1\rangle)(|00\rangle + |11\rangle) + \beta(|0\rangle - |1\rangle)(|10\rangle + |01\rangle)\right] \tag{13.24}$$

$$= \frac{1}{2}\left[|00\rangle(\alpha|0\rangle + \beta|1\rangle) + |01\rangle(\alpha|1\rangle + \beta|0\rangle)\right. \tag{13.25}$$

$$+ \left.|10\rangle(\alpha|0\rangle - \beta|1\rangle) + |11\rangle(\alpha|1\rangle - \beta|0\rangle)\right]. \tag{13.26}$$

Then Alice performs a measurement and sends the result, one out of $|00\rangle$, $|01\rangle$, $|10\rangle$ and $|11\rangle$, to Bob. Depending on Alice's measurement, Bob has one of the

following states:

$$\begin{aligned} 00 &\rightarrow \alpha|0\rangle + \beta|1\rangle && (13.27)\\ 01 &\rightarrow \alpha|1\rangle + \beta|0\rangle && (13.28)\\ 10 &\rightarrow \alpha|0\rangle - \beta|1\rangle && (13.29)\\ 11 &\rightarrow \alpha|1\rangle - \beta|0\rangle. && (13.30) \end{aligned}$$

This fact prevents Alice and Bob from communicating faster than the speed of light. If Bob does not know the result of Alice's measurement, his qubit does not contain any information.

2 Algorithms

In this chapter we will derive an algorithm to factorize with a *quantum computer*. To achieve this, we will extend the *quantum Fourier transformation algorithm* to a *phase estimation algorithm*. This will lead us to a solution of the *order finding problem*. The order finding algorithm can be used as the core of a factorizing algorithm.

In this chapter the following notation is used:

$$|0\cdots 0\rangle, \ldots, |1\cdots 1\rangle \equiv |0\rangle, \ldots, |2^n - 1\rangle \tag{13.31}$$

Quantum Fourier transformation

The classical *discrete Fourier transformation* takes as input a vector of complex numbers, $x_0, \ldots, x_{N-1}$, with length of the vector N. The output is a vector of complex numbers $y_0, \ldots, y_{N-1}$, defined by

$$y_k \equiv \frac{1}{\sqrt{N}} \sum_{j=0}^{N-1} x_j e^{2\pi i j k/N}. \tag{13.32}$$

The *quantum Fourier transformation* is exactly the same. It is defined on an orthonormal basis $|0\rangle, \ldots, |N-1\rangle$ as a linear operator acting as follows:

$$|j\rangle \rightarrow \frac{1}{\sqrt{N}} \sum_{k=0}^{N-1} e^{2\pi i j k/N} |k\rangle. \tag{13.33}$$

The action on an arbitrary state may be written as a base transformation,

$$\sum_{j=0}^{N-1} x_j |j\rangle \rightarrow \sum_{k=0}^{N-1} y_k |k\rangle, \tag{13.34}$$

where the amplitudes y_k are the discrete Fourier transforms of the amplitudes x_j.

In the following we take $N = 2^n$, where n is some integer, and the basis $|0\rangle, \ldots, |2^n - 1\rangle$ is the computational basis for an n qubit quantum computer. It is helpful to write the state $|j\rangle$ using the binary representation $j = j_1 2^{n-1} + j_2 2^{n-2} + \ldots + j_n 2^0$. It is also convenient to adopt the notation $0.j_l j_{l+1} \ldots j_m$ to represent the binary fraction $j_l 2^{-1} + j_{l+1} 2^{-2} + \ldots + j_m 2^{-m+l-1}$. This leads to the product representation

$$|j_1, \ldots, j_n\rangle \rightarrow \frac{(|0\rangle + e^{2\pi i 0.j_n}|1\rangle)(|0\rangle + e^{2\pi i 0.j_{n-1}j_n}|1\rangle) \cdots (|0\rangle + e^{2\pi i 0.j_1 j_2 \ldots j_n}|1\rangle)}{2^{n/2}}. \tag{13.35}$$

The product representation makes it easy to derive an efficient circuit for the quantum Fourier transform. We need the Hadamard gate and the gate R_k

$$\mathcal{R}_k \equiv \begin{pmatrix} 0 & 1 \\ 1 & e^{2\pi i/2^k} \end{pmatrix}. \tag{13.36}$$

The resulting circuit is shown below:

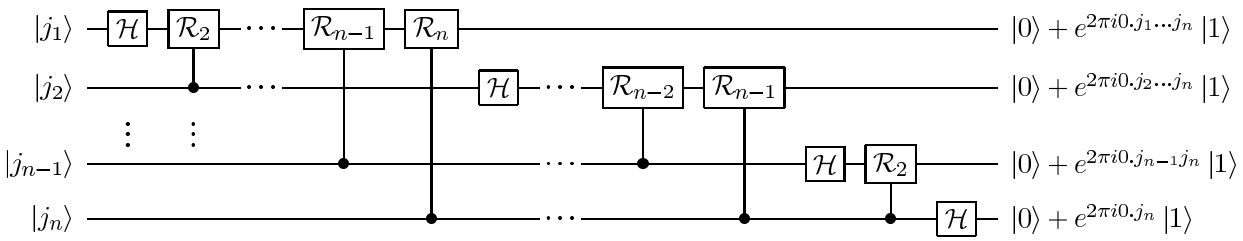

The swap operations, used to reverse the order of the circuit, are omitted from the circuit for clarity.

On the first wire we use n gates, on the second we use $n-1$ gates, up to 1 gate in the last wire. In this way we get $n+(n-1)+\ldots+1 = n(n+1)/2$ required gates plus the gates involved in the swap. At most $n/2$ swaps are required, and each swap can be accomplished using three controlled NOT gates, as described in the introduction. Therefore, the circuit provides a $\Theta(n^2)$ algorithm for performing the quantum Fourier transformation.

In contrary to the *quantum Fourier transformation*, a classical algorithm for computing the *discrete Fourier transformation* on 2^n elements such as the Fast Fourier transformation, needs $\Theta(n2^n)$ gates to compute the *discrete Fourier transformation*. This is an exponential speedup! But there is no way of determining the Fourier transform amplitudes of the original state by measurements.

Example: Three-qubit quantum Fourier transform. The circuit of the three qubit quantum Fourier transformation:

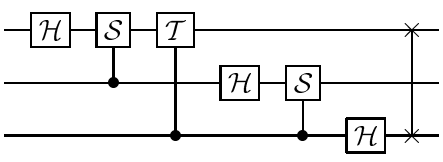

Here $\mathcal{S}$ is the phase gate and $\mathcal{T}$ the $\pi/8$ gate. As a matrix the *quantum Fourier transformation* in this instance may be written out explicitly, using $\omega = e^{2\pi i/8} = \sqrt{i}$, as

$$\frac{1}{\sqrt{8}} \begin{pmatrix} 1 & 1 & 1 & 1 & 1 & 1 & 1 & 1 \\ 1 & \omega & \omega^2 & \omega^3 & \omega^4 & \omega^5 & \omega^6 & \omega^7 \\ 1 & \omega^2 & \omega^4 & \omega^6 & 1 & \omega^2 & \omega^4 & \omega^6 \\ 1 & \omega^3 & \omega^6 & \omega & \omega^4 & \omega^7 & \omega^2 & \omega^5 \\ 1 & \omega^4 & 1 & \omega^4 & 1 & \omega^4 & 1 & \omega^4 \\ 1 & \omega^5 & \omega^2 & \omega^7 & \omega^4 & \omega & \omega^6 & \omega^3 \\ 1 & \omega^6 & \omega^4 & \omega^2 & 1 & \omega^6 & \omega^4 & \omega^2 \\ 1 & \omega^7 & \omega^6 & \omega^5 & \omega^4 & \omega^3 & \omega^2 & \omega \end{pmatrix}. \tag{13.37}$$

Phase estimation

Suppose $|u\rangle$ is an eigenvector for the unitary operator U with the eigenvalue $e^{2\pi i\varphi}$, where φ is unknown. The goal of the phase estimation algorithm is to estimate φ.

The quantum phase estimation procedure uses two registers. The first contains t qubits initially in the state $|0\rangle$. How to choose t depends on two things: the accuracy we want to achieve for our estimate for φ and the probability we want the phase estimation procedure to be successful. The second register starts with the state $|u\rangle$, and contains as many qubits as necessary to store $|u\rangle$.
The overall scheme of the algorithm is

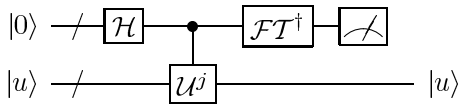

The phase estimation is performed in three stages. First, we apply the Hadamard transformation to the first register, followed by an application of controlled-U operation on the second register, with U raised successively to higher powers of two. The final state of the first register is

$$\frac{1}{2^{t/2}}(|0\rangle + e^{2\pi i 2^{t-1}\varphi}|1\rangle)(|0\rangle + e^{2\pi i 2^{t-2}\varphi}|1\rangle)\cdots(|0\rangle + e^{2\pi i 2^{0}\varphi}|1\rangle) = \frac{1}{2^{t/2}}\sum_{k=0}^{N-1} e^{2\pi i\varphi k}|k\rangle. \tag{13.38}$$

The second state of the phase estimation is to apply the inverse quantum Fourier transformation on the first register. This can be done in $\Theta(t^2)$ steps.
The third and final stage of the phase estimation is to read out the state of the first register by doing a measurement in the computational basis.
The heart of this procedure is the ability of the inverse Fourier transformation to

perform the transformation

$$\frac{1}{2^{t/2}} \sum_{j=0}^{2^t-1} e^{2\pi i \varphi j} |j\rangle |u\rangle \rightarrow |\tilde{\varphi}\rangle |u\rangle, \tag{13.39}$$

where $|\tilde{\varphi}\rangle$ denotes a state which is a good estimate for φ when measured.

Example 3. Suppose φ may be expressed exactly in t bits, as $\varphi = 0.\varphi_1 \ldots \varphi_t$. The first register after the first step may be rewritten as

$$\frac{1}{2^{t/2}} (|0\rangle + e^{2\pi i 0.\varphi_t} |1\rangle)(|0\rangle + e^{2\pi i 0.\varphi_{t-1}\varphi_t} |1\rangle) \cdots (|0\rangle + e^{2\pi i 0.\varphi_1 \varphi_1 \cdots \varphi_t} |1\rangle). \tag{13.40}$$

Comparing this equation with the product representation of the Fourier transform, we see that the output state of the second stage is the product state $|\varphi_1 \ldots \varphi_t\rangle$. A measurement in the computational basis therefore gives us φ exactly.

Order - finding

For positive integers x and N, $x < N$, with no common factor, the order of x modulo N is defined to be the least positive integer r, such that $x^r = 1 \pmod N$.

Example 4. Let $x = 5$ and $N = 21$. Then $5^6 = 15625 = 744 * 21 + 1$, and thus the order of x modulo N is 6.

The quantum algorithm for order finding is just the phase estimation algorithm applied to the unitary operator

$$\mathcal{U}|y\rangle \equiv |xy \bmod N\rangle, \tag{13.41}$$

with $y \in \{0,1\}^L$. The states

$$|u_s\rangle \equiv \frac{1}{\sqrt{r}} \sum_{k=0}^{r-1} e^{-2\pi i s k/r} \big|x^k \bmod N\big\rangle, \tag{13.42}$$

for an integer $0 \leq s \leq r-1$ are eigenstates of $\mathcal{U}$, since

$$\mathcal{U}|u_s\rangle \equiv \frac{1}{\sqrt{r}} \sum_{k=0}^{r-1} e^{-2\pi i s k/r} \big|x^{k+1} \bmod N\big\rangle = e^{2\pi i s/r} |u_s\rangle. \tag{13.43}$$

The phase estimation procedure allows us to obtain the corresponding eigenvalue $exp(2\pi i s/r)$.

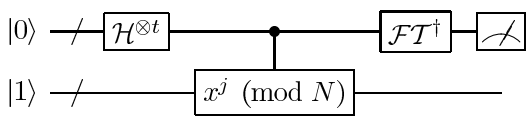

There are two important requirements for us to be able to use the phase estimation procedure: we must have efficient procedures to implement a controlled-u^{2^j} operation for any integer j, and we must be able to efficiently prepare an eigenstate $|u_s\rangle$ with a non-trivial eigenvalue, or at least a superposition of such eigenstates.

The first requirement is satisfied by using a procedure known as modular exponentiation. We want to compute the transformation

$$\begin{aligned} |z\rangle|y\rangle &\rightarrow |z\rangle U^{z_t 2^{t-1}} \dots U^{z_1 2^0}|y\rangle && (13.44)\\ &= |z\rangle\left|x^{z_t 2^{t-1}} \times \cdots \times x^{z_1 2^0} y \bmod N\right\rangle && (13.45)\\ &= |z\rangle|x^z y \bmod N\rangle. && (13.46) \end{aligned}$$

The second requirement is a little trickier: preparing $|u_s\rangle$ requires that we know r, so this is out of question. Fortunately, there is a clever observation which allows us to circumvent the problem of preparing $|u_s\rangle$, which is that

$$\frac{1}{\sqrt{r}} \sum_{s=0}^{r-1} |u_s\rangle = |1\rangle, \tag{13.47}$$

so we get to $|u_s\rangle$ for free.

The continued fraction expansion The reduction of order-finding to phase estimation is completed by describing how to obtain the desired answer, r, from the result of the phase estimation algorithm, $\varphi \approx s/r$. We only know φ to a finite number of bits, but we know *a priori* that it is a *rational* number.

The idea of the *continued fraction algorithm* is to describe real numbers in terms of integers alone, using expressions of the form

$$[a_0, \dots, a_M] \equiv a_0 + \cfrac{1}{a_1 + \cfrac{1}{a_2 + \cfrac{1}{\dots + \cfrac{1}{a_M}}}}, \tag{13.48}$$

where $a_0, \dots, a_M$ are positive integers. It is clear that the *continued fraction algorithm* terminates after a finite number of 'split and invert' steps for any rational number, since the numerators are strictly decreasing (e.g 31, 5, 3, 2, 1 in the example below). The decomposition can be done in $O(L^3)$ operations.

Example 5. Suppose we are trying to decompose 31/12 as a continued fraction. The first step of the continued fraction algorithms is to split 31/13 into its integer and fractional part

$$\frac{31}{13} = 2 + \frac{5}{13}. \tag{13.49}$$

Next, we invert the fractional part, obtaining

$$\frac{31}{13} = 2 + \frac{1}{\frac{13}{5}} = 2 + \frac{1}{2 + \frac{3}{5}}. \tag{13.50}$$

Continuing in this way, we come to the final continued fraction representation of 31/13:

$$\frac{31}{13} = 2 + \frac{1}{2 + \frac{1}{1 + \frac{1}{1 + \frac{1}{2}}}}. \tag{13.51}$$

Performance There are two possibilities for the order-finding algorithm to fail: First, the phase estimation procedure might produce a bad estimate for s/r, or, s and t might have a common factor, in which case the number r' returned by a continued fraction algorithm is a factor of r, and not r itself. This can be solved by repeating the *phase estimation continuous fraction procedure* several times.

Factorizing

The *factorizing problem* tuns out to be equivalent to the order-fining problem. The reduction of factorizing to order finding proceeds in two steps: First, we show that we can compute a factor of N, if we can find a non-trivial solution to $x^2 \neq \pm 1 \pmod N$ to the equation $x^2 = 1 \pmod N$. The second step is to show that a randomly chosen y co-prime to N is quite likely to have an order r which is even, and such that $y^{r/2} \neq \pm 1 \pmod N$, and thus $x \equiv y^{r/2}$ is a non-trivial solution to $x^2 = 1 \pmod N$. These two steps are embodied in the following theorems (for proof see [81]).

Theorem 6. *Suppose N is an L bit composite number, and x is a non-trivial solution for the equation $x^2 = 1 \pmod N$ in the range $1 \leq x \leq N$, that is, neither $x = 1 \pmod N$ nor $x = N - 1 = -1 \pmod N$. Then at least one of $\gcd(x-1, N)$ and $\gcd(x+1, N)$ is a non-trivial factor of N that can be computed using $O(L^3)$ operations.*

Theorem 7. *Suppose $N = p_1^{\alpha_1} \dots p_m^{\alpha_m}$ is the prime factorization of an odd composite positive integer. Let x be an integer chosen from a uniform distribution, with the restriction that $1 \leq x \leq N - 1$ and x is co-prime to N. Let r be the order of x modulo N. Then*

$$p(r \text{ is even and } x^{r/2} \neq -1 \pmod N) \geq 1 - \frac{1}{2^m}. \tag{13.52}$$

Now we can give an algorithm which returns a non-trivial factor of any composite N with high probability. All steps in the algorithm can be performed efficiently on a classical computer except an order-finding 'subroutine'. By repeating the procedure we may find a complete factorization of N.

The factorizing algorithm The algorithm takes a composite number N as input and returns in $O((\log N)^3)$ a non trivial factor of N with probability $O(1)$.

1. If N is even, **return the factor 2**
2. Determine whether $N = a^b$ for integers $a \geq 1$ and $b \geq 2$, and if so **return the factor a**
3. Randomly choose x in the range 1 to $N-1$. If $\gcd(x, N) > 1$ then **return the factor** $\gcd(x, N)$
4. Use the order-finding subroutine to find the order r of x modulo N
5. If r is even and $x^{r/2} \neq -1 \pmod{N}$ then compute $\gcd(x^{r/2} - 1, N)$ and $\gcd(x^{r/2} + 1, N)$, and test if one of these is a nontrivial factor, **returning the factor if so**. **Otherwise the algorithm fails**.

Example: Factorizing 15. The use of order-finding, phase estimation, and continued fraction expansion in the quantum factorizing algorithm is illustrated by applying it to factorizing $N = 15$. First we choose a random number which has no common factors with N; suppose we choose $x = 7$. Next we compute the order r of x with respect to N, using the quantum order-finding algorithm. Begin with the state $|0\rangle|0\rangle$ and create the state

$$\frac{1}{\sqrt{2^t}} \sum_{k=0}^{2^t-1} |k\rangle|0\rangle = \frac{1}{\sqrt{2^t}} \left(|0\rangle + |1\rangle + |2\rangle + \ldots + \left|2^t - 1\right\rangle\right) |0\rangle, \tag{13.53}$$

by applying $t = 11$ Hadamard transformations on the first register. Next, compute $f(k) = x^k \pmod{N}$. Leaving the result in the second register, we get

$$\frac{1}{\sqrt{2^t}} \sum_{k=0}^{2^t-1} |k\rangle\left|x^k \bmod N\right\rangle = \frac{1}{\sqrt{2^t}} \left(|0\rangle|1\rangle + |1\rangle|7\rangle + |2\rangle|4\rangle + |3\rangle|13\rangle + \ldots\right). \tag{13.54}$$

We now apply the inverse Fourier transformation $FT^\dagger$ to the first register and measure it. Since no further operation is applied to the second register, we can assume that the second register is measured, obtaining a *random* result from 1, 7, 4 or 13. Suppose we get 4; this means the state input to $FT^\dagger$ would have been $\sqrt{\frac{1}{2^t}} \left(|2\rangle + |4\rangle + |10\rangle + |14\rangle + \ldots\right) |4\rangle$ (from the equation above we take the states where the second bit is in the state $|4\rangle$). After applying $FT^\dagger$, we obtain some state $\sum_l \alpha_l |l\rangle$, with the possible measurements 0, 512, 1024, 1536, each

with probability almost exactly 1/4. Suppose we obtain $l = 1536$ from the measurement; Computing the continued fraction expansion thus gives

$$\frac{1536}{(2^t \equiv 2048)} = \frac{1}{1+\frac{1}{3}}, \tag{13.55}$$

so that 3/4 occurs as a convergent in the expansion giving $r = 4$ as the order of $x = 7$. By chance r is even, and moreover

$$x^{r/2} = 7^2 \neq -1 \pmod{15}, \tag{13.56}$$

so the algorithm works; computing the greatest common divisor $\gcd(x^2-1, 15) = 3$ and $\gcd(x^2+1, 15) = 5$ tells us that $15 = 3 \times 5$.

3 Cryptography

In cryptography a fixed terminology is used: The communication parties are always called Alice and Bob, where Alice sends a message to Bob and Eve tries to eavesdrop the communication between.

Cryptography is the art of enabling two parties to communicate in private. In our days nearly everybody is using cryptographic methods by using *ssh*, managing a bank account by the internet or doing *e-commerce*. First, the classical cryptographic methods are described:

One Time Pad

Alice and Bob have an n-bit secret key string. Alice encodes her n-bit message by *adding* message and key together, and Bob decodes by *subtracting* the key to invert the encoding. Normally the bitwise XOR is used to add and subtract, because XOR is it's own inverse. The *One Time Pad* can be demonstrated in the following scheme:

Alice		**Bob**
	$\overset{y}{\longrightarrow}$	
$y = x + e$		$x = y - e$

Example 6. Encode the word 'QUANTUM' with the key 'GQYRWAD'. We use only upper case letters, so we can encode our letters in numbers from 1 to 26. The letter A has the code 1, the letter Z has the code 26. All operations are done in a *Cyclic Group* with 26 elements (that means that $X + D = 24 + 4 = 2 = B$). So the encoding can be done as:

Original message	Q	U	A	N	T	U	M
	+	+	+	+	+	+	+
Encryption key	G	Q	Y	R	W	A	D
	⇓	⇓	⇓	⇓	⇓	⇓	⇓
Encrypted message	W	L	Y	F	Q	U	P
		⇓	Public Channel				
Received message	W	L	Y	F	Q	U	P
	-	-	-	-	-	-	-
Decryption key	G	Q	Y	R	W	A	D
	⇓	⇓	⇓	⇓	⇓	⇓	⇓
Decrypted message	Q	U	A	N	T	U	M

Even if Eve has an infinite amount of *computation power* she cannot decrypt the message. She is able to get all messages with 7 characters, but she is not able to get any informations out of it.

The major problem of the *One Time Pad* is the distribution of the key bits. In particular, the *One Time Pad* is only secure if the number of key bits is at least as large as the size of the message being encoded, and the key can not be reused, else there will be a correlation between the messages!
Suppose we have a community of n people, which want to communicate pairwise. Then everybody needs $n-1$ keys!

This method is used if security is very important, for example in the *Cold War* to encrypt the telephone hot line between *Moscow* and *Washington*. But there where whole airplanes full of hard disks to provide the keys.

Public Key Cryptography

The main idea of the public key cryptosystem is to have two keys, a *public key* and a *secret key*.

Example of Public Key Cryptography. A very easy example of a *public key cryptosystem* is the postbox in front of your house. Everybody can leave you a message, but only you (or anybody, who owns a key to the box) can get the messages. This shows that the concept of a *public key cryptosystem* is not restricted to the computer technology.

The most used cryptosystem, the *RSA*, is now introduced.

RSA

RSA is the most widely used cryptosystem, named by the initials of its creators: Rivest, Shamir and Adelman. The security of RSA is based on the difficulty of factorizing on a classical computer. The scheme of RSA cryptography:

1. Select two large prime numbers, p and q
2. Compute the product $n \equiv pq$
3. Select randomly a small odd integer, e, that is co-prime to $\varphi(n) = (p-1)(q-1)$
4. Compute d, the multiplicative inverse of e, modulo $\varphi(n)$
5. The *RSA* public key is the pair $P = (e, n)$. The *RSA* secret key is the pair $S = (d, n)$

. This leads to the following scheme:

Alice		**Bob**
Generate primes p and q $n \equiv p \cdot q$ $\varphi(n) \equiv (p-1)(q-1)$		
Select e co-prime to $\varphi(n)$ $d \equiv e^{-1} \pmod{\varphi(n)}$	n, e $\longrightarrow$	Plaintext $M \in \{1, \ldots, m-1\}$
$D(E(M)) \equiv E(M)^d \pmod{n}$	$E(M)$ $\longleftarrow$	$E(M) \equiv M^e \pmod{n}$

Suppose we have two parties Alice and Bob. Bob wants to send the message M to Alice using the *RSA* scheme. Assume that M has only $\lfloor \log n \rfloor$ bits, as longer messages may be encrypted by breaking M up into blocks of most $\lfloor \log n \rfloor$ bits and then encrypt the blocks separately. Bob encrypts the message with

$$M \to E(M) = M^e \pmod{n}. \tag{13.57}$$

Now Bob can transmit $E(M)$ to Alice. Alice can quickly decrypt the message with

$$E(M) \to M = D(E(M)) = E(M)^d \pmod{n}. \tag{13.58}$$

To verify this, note that $ed = 1 \pmod{\varphi n}$ and thus $ed = 1 + k\varphi(n)$ with $k \in \mathbb{N}$.

To proof RSA, we need the following theorems (for proof see [82]):

Euler's generalization of Fermat's little theorem.

$$\text{if } a \text{ is co-prime to } n \Rightarrow a^{\varphi(n)} = 1 \pmod{n}. \tag{13.59}$$

proof of RSA. If M is co-prime to n, then from *Euler's generalization of Fermat's little theorem* follows that $M^{k\varphi(n)} = 1 \pmod{n}$ and thus

$$\begin{aligned} D(E(M)) &= E(M)^d \pmod{n} && (13.60)\\ &= M^{ed} \pmod{n} && (13.61)\\ &= M^{1+k\varphi(n)} \pmod{n} && (13.62)\\ &= M \cdot M^{k\varphi(n)} \pmod{n} && (13.63)\\ &= M \pmod{n}. && (13.64) \end{aligned}$$

If M is not co-prime to n, assume p divides M and q does not divide M (the other cases are analogous). Because p divides M, we have $M = 0 \pmod{n}$ and thus $M^{ed} = 0 = M \pmod{n}$. Because q does not divide M we have $M^{q-1} = 1 \pmod{n}$ by the theorem above and thus $M^{\varphi(n)} = 1 \pmod{n}$, since $\varphi(n) = (p-1)(q-1)$. Using $ed = 1 + k\varphi(n)$, we see that $M^{ed} = M \pmod{q}$ and it follows that we must have $M^{ed} = M \pmod{n}$. □

For further informations look also at [83]

Example 7. Encode the letter 'Q' using $p = 3$ and $q = 11$, thus $n = pq = 33$ and $\varphi(n) = (p-1)(q-1) = 20$. We choose a random odd integer $e \equiv 7$ that is co-prime to 20. The multiplicative inverse of 7 is 3 (mod 20). So the *public key* is $P = (7, 33)$ and the *secret key* is $S = (3, 33)$.

If we encode our letters in numbers from 1 to 26, the letter 'Q' has the representations 17. So

$$\begin{aligned} E(17) &= 17^7 = 8 \pmod{33} && (13.65)\\ D(20) &= 20^3 = 17 \pmod{33}. && (13.66) \end{aligned}$$

So if we use the *quantum factorizing algorithm* to factorize n we can now break *RSA*:

Suppose Eve could factorize $n = pq$, extracting p and q, and thus is given a means for efficiently computing $\varphi(n) = (p-1)(q-1)$. It is then an easy matter for Eve to compute d, the inverse of e modulo $\varphi(n)$, and thus completely determine the secret key (d, n).

Quantum cryptorgraphy

Quantum cryptography is only used to distribute the keys for a classical cryptographic protocol. Quantum key distribution is *provably* secure, and therefore private key bits can be created between two parties over a public channel. The key bits can then be used to implement a classical private key cryptosystem.

The basic idea of *quantum key distribution* is the fundamental observation that Eve cannot gain any information from the qubits transmitted from Alice to Bob without disturbing their state and because of the following

Proposition 18. *Information gain implies disturbance in any attempt to distinguish between two non-orthogonal quantum states, information gain is only possible at the expense of introducing disturbance to the signal.*

Proof. Let $|\psi\rangle$ and $|\varphi\rangle$ be the non-orthogonal quantum states Eve is trying to obtain information about. She uses unitary intersections of the states $|\psi\rangle$ and $|\varphi\rangle$ with a prepared state $|u\rangle$. Assuming that this process does not disturb the states, in the two cases one obtains

$$|\psi\rangle|u\rangle \rightarrow |\psi\rangle|v\rangle \tag{13.67}$$
$$|\varphi\rangle|u\rangle \rightarrow |\varphi\rangle|v'\rangle. \tag{13.68}$$

Eve would like $|v\rangle$ and $|v'\rangle$ to be different so that she can acquire information about the identity of the state. However, since inner products are preserved under unitary transformations, it must be that

$$\langle v|v'\rangle \langle\psi|\varphi\rangle = \langle u|u\rangle \langle\psi|\varphi\rangle . \tag{13.69}$$

and since u and v are unitary

$$\langle v|v'\rangle = \langle u|u\rangle = 1, \tag{13.70}$$

which implies that $|v\rangle$ and $|v'\rangle$ must be identical up to a global phase. Thus, distinguishing between $|\psi\rangle$ and $|\varphi\rangle$ must inevitably disturb at least one of these states. □

This is a weaker statement of the fact that copying of qubits is not possible! The proposition leads to the following three *quantum key distribution* protocols:

The protocol from Bennett and Brassard (BB84) Alice generates two strings a and b, each of $(4+\delta)n$ random classical bits. She then encodes these strings as a block of $(4+\delta)n$ qubits,

$$|\varphi\rangle = \bigotimes_{k=1}^{(4+\delta)n} |\varphi_{a_k b_k}\rangle, \tag{13.71}$$

where a_k is the k^{th} bit of a (and similarly for b), and each qubit is one of the four states

$$|\varphi_{00}\rangle = |0\rangle \tag{13.72}$$
$$|\varphi_{10}\rangle = |1\rangle \tag{13.73}$$
$$|\varphi_{01}\rangle = |+\rangle = (|0\rangle + |1\rangle)/\sqrt{2} \tag{13.74}$$
$$|\varphi_{11}\rangle = |-\rangle = (|0\rangle - |1\rangle)/\sqrt{2}. \tag{13.75}$$

The protocol is described in the following scheme:

Alice		**Bob**
$a, b =$ rnd $2n$-bit strings		
$\|\varphi\rangle = \bigotimes_{k=1}^{2n} \|\varphi_{a_k b_k}\rangle$	$\|\varphi\rangle$	Generate $2n$-bit string b'
$(a_k = k^{th}$ bit of $a)$	$\longrightarrow$	Measure each qubit in
	ACK	X or Z bases determined by b'
	$\longleftarrow$	$a' \equiv$ measurement $\in \{0, 1\}$
	b	
Publish b	$\longrightarrow$	
Keep only those $\{a, a'\}$ for which $b = b'$		
Select n-bits at random	$\longrightarrow$	Check if too many are wrong, if so, retry
Use the One Time Pad with the remaining n-bits		

The effect of this resource is to encode a in the basis X or Z, as determined by b. Alice then sends $|\varphi\rangle$ to Bob, over their *public quantum communication channel*. Bob receives $\mathcal{E}(|\varphi\rangle\langle\varphi|)$, where $\mathcal{E}$ describes the *quantum operation* due to the combined effect of the channel and Eve's actions. He then acknowledges that he has received the message. At this point, Eve has no knowledge of what basis she should have measured in to eavesdrop on the communication; she can only guess, and if her guess was wrong, then she disturbed the state received by Bob.

For Bob $\mathcal{E}(|\varphi\rangle\langle\varphi|)$ contains also no information at this point, because he does not know anything about b either. Nevertheless, he creates a random $(4+\delta)n$ bit string b' and measures each qubit in the X or Z basis determined my b'. He saves the measurement in the classical bit string a'. After that, Alice publishes b, and by discussion over a public channel, Bob and Alice discard all bits in $\{a', a\}$ except those for which corresponding bits of b' and b are equal. Their remaining bits satisfy $a' = a$, since for these bits Bob measured in the same basis Alice prepared in. It is important, that Alice does not publish b until after Bob has confirmed the reception of Alice's qubits. For simplicity in the following explanation, let Alice and Bob keep just 2 n bits of their result.

Now Alice selects n bits (of their $2n$ bits) randomly and publicly announces the selection. Bob and Alice then publish and compare the values of these check bits. If more than t disagree, then they abort and retry the protocol from start.

t is selected such that if the test passes, then they can apply information reconciliation on privacy amplification algorithms to obtain m acceptably secret key bits from the remaining n bits.

If the bits are accepted, the n bits can be used as a key in a *classical decrypting protocol* like the *One Time Pad*.

The protocol from Bennett (B92) The BB84 protocol can be generalized by using other states and bases. In fact, a particular simple protocol exists in which only two states are used. The scheme reads:

Alice		**Bob**
$a =$ rnd $2n$-bit string		
$\|\varphi\rangle = \bigotimes_{k=1}^{2n} \|\varphi_{a_k}\rangle$	$\|\varphi\rangle$	Generate $2n$-bit string a'
$(a_k = k^{th}$ bit of $a)$	$\longrightarrow$	Measure each qubit in
	b	X or Z bases determined by a'
	$\longleftarrow$	$b \equiv$ measurement $\in \{0, 1\}$
Keep only those $\{a, a'\}$ for which $b = 1$		
Alice's key is a		Bob's key is $1 - a'$
Select n-bits at random	$\longrightarrow$	Check if too many are wrong, if so, retry
Use the One Time Pad with the generated key		

To understand the differences to the protocol before, it is sufficient to consider what happens to a single bit at a time.

Suppose Alice prepares one random classical bit a, and, depending on the result, sends Bob

$$|\varphi\rangle = \begin{cases} |0\rangle & \text{if } a = 0 \\ \frac{|0\rangle + |1\rangle}{\sqrt{2}} & \text{if } a = 1 \end{cases} \tag{13.76}$$

Depending on a random classical bit a' generated by Bob, he measures in the Z basis ($|0\rangle$, $|1\rangle$) if $a' = 0$, or in the X basis ($|\pm\rangle = (|0\rangle \pm |1\rangle/\sqrt{2})$ if $a' = 1$. From this measurement, he obtains the result b', which he publicly announces. Alice and Bob then conduct a public discussion and keep only those pairs $\{a, a'\}$ for which $b = 1$. Note that when $a = a'$, then b=0 always. Only if $a' = a - 1$ Bob will obtain $b = 1$, which occurs with probability 1/2. The final key for Alice is a and $1 - a'$ for Bob.

One possible physical implementation of this two protocols are polarized pho-

tons in two orthogonal directions.

The EPR protocol (Eckert 93) Suppose Alice and Bob share a set of n entangled pairs of EPR pairs in the state

$$\frac{|00\rangle + |11\rangle}{\sqrt{2}} \tag{13.77}$$

The scheme reads:

Alice		**Bob**
Alice and Bob share a set of $2n$ EPR pairs in the state $\|\beta_{00}\rangle$		
b = rnd $2n$-bit string		b' = rnd $2n$-bit string
Measure each half of		Measure each half of
the EPR pairs in X or Z		the EPR pairs in X or Z
bases determined by b	b, b'	bases determined by b'
$a \equiv$ measurement $\in \{0,1\}$	$\Longleftrightarrow$	$a' \equiv$ measurement $\in \{0,1\}$
Keep only those $\{a, a'\}$ for which $b = b'$		
Select n-bits at random	$\Longleftrightarrow$	Check if too many are wrong, if so, retry
Use the One Time Pad with the remaining $a = a'$ as key		

Alice and Bob then select a random subset of the EPR pairs, and test to see if they are real EPR states.

Since the EPR protocol is symmetric, Alice and Bob perform identical tasks on their qubits. Suppose that Alice prepares a random classical bit b, and according to it, measures her half of the EPR pair in either the $|0\rangle$, $|1\rangle$ basis, or in the basis $|\pm\rangle = (|0\rangle \pm |1\rangle)/\sqrt{2}$, and obtains a. Let Bob identically measure in his randomly chosen basis b', where he obtains a'. Now they exchange b and b' over a public classical channel, and keep as their key only those $\{a, a'\}$ for which $b = b'$.

4 Conclusion

We have seen that quantum computers work with quantum bits (qubits), an analogous concept to the classical bit. A qubit can not be copied, but as long as you do not disturb the qubit, it is possible to save a tremendous amount of information in *one* qubit. Furthermore we saw an algorithm to factorize a composed

number, with an exponential speedup with respect to the classical algorithm. In the last part, cryptographic protocols and the algorithms for quantum key distribution were introduced.

14 Topologically protected quantum computing

Bojan Skerlak
Supervisor: Helmut Katzgraber

The two main problems arising in quantum computation are preparation of a coherent state and accurate interaction with a qubit. These problems appear due to decoherence and the fragile nature of any quantum mechanical system. Instead of fighting those problems with clever circuit design and error correction software, one can theoretically build hardware that exploits topology in order to protect information. Systems with Abelian anyons allow us to encode robust qubits and braiding non-Abelian anyons allows us to process quantum information safely. Theory is far ahead in this field and experiments have not been realised yet. Still, it is a very interesting and promising field as fractional statistics have been observed in the context of strongly correlated systems such as fractional quantum hall liquids and proposed implementations promise very high fidelity.

Introduction

Richard Feynman stated in 1982 that quantum systems cannot be efficiently simulated on classical computers, i.e, without exponential slowdown [84]. Three years later, David Deutsch described the universal quantum computer as a totally new kind of computer with higher computational power [85]. In 1994, Peter Shor developed his famous factoring algorithm [86] which theoretically allows to break most cryptographic systems easily, because the factoring problem scales algebraically instead of exponentially with the number of digits. As an example, a 1024-bit RSA code can be cracked in reasonable time using 2051 qubits (generally: an L bit code needs $2L + 3$ qubits and $O[L^3\ln(\mathrm{L})]$ gates using the

circuit described in Refs. [87, 88]). This attracted considerable attention to the relatively new field of quantum computing. From then on, it was certain that quantum computer process certain algorithms far faster than any classical computer and that they can be of great use. New algorithms that profit from the special features of quantum computers were found [89] and first experiments were successfully made [90]. On the theoretical side, error correction codes were developed that allow to improve the reliability of given hardware. Those codes were found to demand an accuracy of the hardware that is not reachable even today. In the search for fundamentally better hardware which is intrinsically protected against errors, topology plays an important role. Therefore, we have to find systems that show topological behaviour such as ones with fractionalized excitations. Those excitations, which are only possible in two dimensions, are called anyons and can be mathematically described using the braid group. We then also find a way to not only protect our qubits against errors, which is done with Abelian anyons, but also protect them during the computation. For this, we need non-Abelian anyons that have been shown to exist theoretically but lack experimental verification.

Quantum computers: the standard model

The fundamental reason why quantum computers are more powerful than classical computers is that they do not use the classical bits that are restricted to being in state 0 or 1 but quantum bits (qubits), which can also be in a quantum superposition of the two states: any superposition $\alpha|0\rangle + \beta|1\rangle$ with $\alpha, \beta \in \mathbb{C}$ and $|\alpha|^2 + |\beta|^2 = 1$ is allowed. A quantum computer thus consists of n qubits that correspond to a 2^n-dimensional Hilbert space. Before the calculation, the qubits are prepared in some well-known state $|0\rangle^{\otimes n}$ and afterwards, they are measured in the computational basis $|0\rangle, |1\rangle$. Any computation consists of a sequence of gates acting on the n qubits. All possible gates can be approximated with arbitrary accuracy using a dense subgroup of $SU(2^n)$. Such a set of gates is called universal for quantum computation. A popular choice for an universal set consists of the two one-qubit gates $NOT \in SU(2)$, $S \in GL(2, \mathbb{C})$ [91] and of a special two-qubit gate, the controlled-not gate $CNOT \in SU(4)$ [92]. The latter flips the target qubit if and only if the control qubit is in state $|1\rangle$.

$$NOT := \begin{pmatrix} 0 & 1 \\ 1 & 0 \end{pmatrix}, S := \begin{pmatrix} 1 & 0 \\ 0 & i \end{pmatrix}, Z := \begin{pmatrix} 1 & 0 \\ 0 & -1 \end{pmatrix}, CNOT := \begin{pmatrix} 1 & 0 & 0 & 0 \\ 0 & 1 & 0 & 0 \\ 0 & 0 & 0 & 1 \\ 0 & 0 & 1 & 0 \end{pmatrix}$$

Experimental approaches to non-topological quantum computation

Up to date, no quantum computer with more than ten qubits has been operated. The three most promising and successful approaches to traditional quantum computation as well as their main problems are shortly presented here.

NMR quantum computing

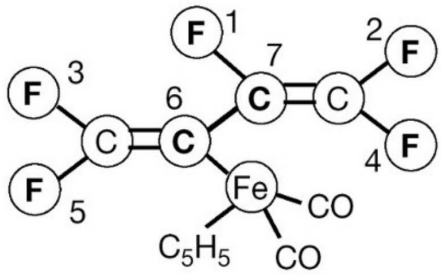

Figure 14.1: The molecule used by IBM research [93]: qubits are encoded in the spin states of nuclei.

The nuclear magnetic resonance (NMR) approach uses the spin states of nuclei within a molecule in an external magnetic field as qubits. As the atoms can be distinguished by their resonance frequencies due to the different chemical environment, every spin-1/2 nucleus acts as a qubit. One-qubit operations are easily implemented with radio frequency fields. The coupling between qubits is achieved via the naturally occurring spin-spin coupling. The main advantage of this system is that NMR technology is relatively mature so the precision of those interactions is very high (error rate $\lesssim 10^{-3}$). In 2001, IBM researchers implemented Shor's algorithm in a 7-qubit NMR quantum computer using 10^{18} molecules [93]. After preparing the molecules, they factored $15 = 3 \cdot 5$ in four hours of computation. The big problem is that one has to create a pure state of many molecules as the signal coming from one molecule is too small. The system is operated at room temperature and therefore, thermal fluctuations cause a very small signal to noise ratio. Preparing large numbers of molecules in a desired configuration is hard to achieve using appropriate pulse sequences. Distillation processes [94] are used to deal with that problem but are believed not to work with large molecules [95]. The number of qubits is limited by the size of the molecule as each nucleus represents a qubit. The spin-spin interaction is short-ranged and thus very distant spins cannot be entangled. As a consequence of those problems, NMR implementations will not scale beyond 100 qubits [96].

Trapped ion quantum computers

Ions or charged atomic particles are confined using electromagnetic fields and cooled down so that their motion is governed by quantum mechanics. Different states of the ions are used as qubits. Lasers are used for both single-qubit operations and two-qubit logical gates. As the ions interact via the Coulomb force, collective motion states are available. These can be excited and de-excited to entangle different qubits. Creating arrays of ion traps, one could in principle scale the system to large number of qubits. Trapped ion quantum computing already has had some successes: the first CNOT gate has been realised this way in 1995 [90] and in 2000, four particles have been entangled [97]. Controlling the motion of ion traps is very difficult, they are very susceptible to decoherence errors. These systems are also not likely to work with more than ~ 100 qubits [96], which at the moment still is out of reach.

Solid state quantum computing: Quantum Dots

By creating quantum wells with semiconductor hetero-structures [98], electrons can be confined to a very small region ($\sim 2 - 10\,nm$). Their spin degrees of freedom, which have very long decoherence times ($\sim$ ns [99]), are used as qubits. Interactions between qubits can either be achieved by changing the tunneling amplitude between neighbouring electrons or using lasers. The latter version needs the structure to be built inside a cavity whose modes can in principle be used to entangle even distant qubits [100]. Those interactions can be performed quickly ($\sim$ THz) [101]. Although fully controlling a qubit and performing accurate gates still is a formidable task, solid-state implementations are thought to be scalable to more than 100 qubits [96].

What is the problem?

The last section shows that the scalability is a crucial feature in the search for useful approaches [95]. But not only the number of qubits is important, we also have to control them well. Controlling qubits includes preparation of a coherent state, performing accurate operations and reliable read out of the result. Each step is susceptible to errors because of the very nature of quantum mechanics. A qubit is, as all quantum mechanical systems are, very sensitive to disturbance by the environment. We cannot hope to completely isolate the qubits which means that they interact with the environment and thus suffer from decoherence. On the other hand, we have to be able to perform accurate interactions without introducing additional errors during calculation. Implementation of non-destructive measurement brings several additional problems such as the need for a supply of qubits in a well-known state. All these effects can accumulate and end up in making the calculation intractable.

On classical computers instead, we are able to both store and process information with a remarkable reliability. The mean time to failure for common hard-disks is $\sim 10^6\,h$ and processors operate easily with GHz frequencies. This is the result of decades of development of both soft- and hardware but also due to material properties that allow us to build such reliable hardware. Therefore, we assume that we are able to store classical information perfectly and are able to perform classical gates with arbitrary accuracy and sufficiently high speed. Moore's law supports this assumption [102] but it will not hold forever: a limit on classical computer speed is visible since the hardware cannot be scaled to arbitrary small size.

The aforementioned implementations show much higher error rates ($\epsilon \sim 10^{-3}$) which means that after 1000 operations, the information is most certainly lost. We therefore have to find a way to operate a system albeit its vulnerability to errors.

Fault-tolerant quantum computation

"A device that works effectively even when its elementary components are imperfect is said to be fault-tolerant" [103].

Building such a system can in principle be done on either a software or hardware level. Classical hardware is very reliable and error correction software that further improves the accuracy can be implemented with reasonable overhead. Using qubits, the situation is far more complicated: creating quantum mechanical hardware that works in a noisy environment is a subtle task. The types of errors occurring is not only restricted to flipping bits but can be an entanglement with any state of the environment. Thus, correcting such errors is far more difficult. We have to know what kind of error occurred without actually measuring the encoded information which would lead to a collapse of the state. Albeit those problems, quantum error correction codes (QECC) that protect the qubits and the operations on them exist [104].

Quantum error correction

Suppose we have n qubits, described by a Hilbert space of dimension $\dim\mathbb{H} = 2^{\mathrm{n}}$. The "Pauli group" is the group of operators

$$X := \begin{pmatrix} 0 & 1 \\ 1 & 0 \end{pmatrix}, Y := \begin{pmatrix} 0 & -i \\ i & 0 \end{pmatrix}, Z := \begin{pmatrix} 1 & 0 \\ 0 & -1 \end{pmatrix}.$$

The "n-qubit Pauli group" G_n is then defined as the "Pauli group" acting on the tensor product: $G_n := \{I, X, Y, Z\}^{\otimes n}$. Let $\{M_1, M_2, ..., M_{n-k}\} \in G_n$ be inde-

pendent mutually commuting Pauli operators ($[M_i, M_j] = 0\ \forall i, j$). They satisfy $M_i^2 = I$ and define an Abelian subgroup $S \subset G_n$ called the stabilizer group. We then define a subspace of $k < n$ logical qubits with $\dim\mathbb{H}_{\text{code}} = 2^k$ as the simultaneous eigenspace of the $n - k$ operators in S: $M_i|\Psi\rangle = |\Psi\rangle\ \forall i$. These logical qubits are no more located at one physical qubit but are entangled states of multiple physical qubits. The stabilizer operators are chosen in a way that every error operator that we want to be able to correct anticommutes with at least one M_i. Thus such an error $E \in G_n$ takes $\mathbb{H}_{\text{code}}$ unambiguously to mutually orthogonal subspaces, namely the eigenspaces corresponding to the eigenvalue -1 of the corresponding M_i's. We then measure all stabilizer operators, which is called syndrome measurement, and obtain all information needed about the error E. By performing E^{-1} we can correct our data.
We have to keep in mind that measurement of an operator acting on the qubits destroys our computational state so we want to measure the syndrome without measuring the data. This is possible and is accomplished by cleverly entangling the state with ancillary qubits. If we measure them, the code subspace is preserved and we get all information needed about E without acquiring any information about the quantum information encoded in our device [105]. A similar procedure is used to protect operations on encoded qubits. If we can construct a set of fault-tolerant universal gates, we can overcome the deficiencies of the hardware [106].

Example: 2 qubit "code"

Suppose we want to protect one logical state using two qubits. Define two stabilizer operators $M_1 := X \otimes X$ and $M_2 := Z \otimes Z$. The protected space is the simultaneous eigenspace consisting of $|\Psi\rangle^+ := \frac{1}{\sqrt{2}}(|00\rangle + |11\rangle)$. Thus, the protected subspace has dimension $2^{n-2} = 1$. We see that this is not really a code in the sense described above since we cannot encode a qubit but it shows the main ideas. The kind of errors we can correct is restricted: only one qubit is allowed to

	$I \otimes I$	$X \otimes I$	$Y \otimes I$	$Z \otimes I$
M_X	$+$	$-$	$-$	$+$
M_Z	$+$	$+$	$-$	$-$

Table 14.1: Syndrome measurement detects the error unambiguously.

be damaged. Assume we damage the first qubit with an error $E \in \{I, X, Y, Z\} \otimes I$. Measuring the operators of the stabilizer group, M_1 and M_2, via ancillary states, we obtain the syndrome (see Table 14.1), can distinguish between different errors and are therefore able to repair the state by performing E^{-1}.

Limits of quantum error correction

We are only able to correct certain errors. In most codes, the stabilizer operators are constructed in a way that lets the code correct errors up to a weight t. We define the weight t of an error E as the number of qubits on which the error acts non-trivially. If all errors up to weight t are distinguishable and thus correctable, we say the code corrects t errors. All errors with weight greater than t will destroy our data. As errors arise from local physics, we expect them to be not strongly correlated, meaning that errors are not likely to hit multiple qubits at a time. It is therefore exponentially less probable that an uncorrectable error occurs if we can correct large t.

The effect of QECC on decoherence errors can be described using the density matrix ρ of a given state. Its fidelity is defined as $F := \mathrm{tr}(\rho^2)$ and describes how coherent a state is. A perfectly coherent state has fidelity 1. If we want to prepare a certain state but due to imperfections we just reach fidelity $F = 1 - \epsilon$, using Steane's 7-qubit code [107], which uses 7 qubits to protect one against errors up to weight 1, we can enhance the fidelity to $F = 1 - O(\epsilon^2)$. Better quantum error correction codes [108] which correct t errors so that an uncorrectable error only occurs if at least $t + 1$ independent errors occur in a single block, result in a fidelity of $F = 1 - O(\epsilon^{t+1})$.

This sounds very promising but we have to face another problem: if we raise t, our code uses more qubits and gets more complicated, therefore it takes more time to perform error correction as we have to perform more gates. This lack of speed and the big number of gates result in a rising probability of another error occurring during correction of the first one, making the code useless. This leads to a limit on the accuracy needed when performing gates. The estimates for the threshold differ but the order of magnitude is $\epsilon \sim 10^{-5}$ (most recent value: $3.61 \cdot 10^{-5}$ [109]), which of course is a very restrictive condition on the hardware. Once we build hardware that is sufficiently accurate, we can theoretically improve the fidelity as much as we want and thus perform arbitrarily reliable quantum computation for an arbitrary duration using concatenated codes [105]. Technical problems such as the system size growing by a factor $10^2 - 10^3$ [110] (assuming $\epsilon = 10^{-6}$) and the need for a support of each qubit by more than ten ancillary qubits in a low-entropy state [95] remain unsolved.

Topologically protected quantum computation

Another approach to the problem is to build far better hardware. Using todays techniques, we cannot reach $\epsilon \lesssim 10^{-5}$. The key to better hardware is the locality of errors. We are therefore looking for systems with states that are not changed by local interaction which protects them from local errors. This principle is a

particular feature of topology: topological parameters are not measurable locally and can thus not be changed by local errors. So the idea behind topologically protected quantum computation is to encode information in topological properties of the hardware. Such hardware protects encoded qubits passively from errors and is thus intrinsically fault-tolerant.

Figure 14.2: The states $|\text{left}\rangle$ and $|\text{right}\rangle$ are topologically different.

As an example, consider a plane with a hole in it. Draw a path passing the hole on the left site and another one passing it on the right with fixed endpoints: see Fig. 14.2. Away from the hole, one cannot decide on which side the path observed passes it. Errors that deform the path smoothly cannot change the information $|0\rangle := |\text{left}\rangle$ into $|1\rangle := |\text{right}\rangle$ or vice versa as seen in Fig. 14.3. If we allow our path to be in a superposition of $|0\rangle$ and $|1\rangle$, we have a topologically protected qubit.

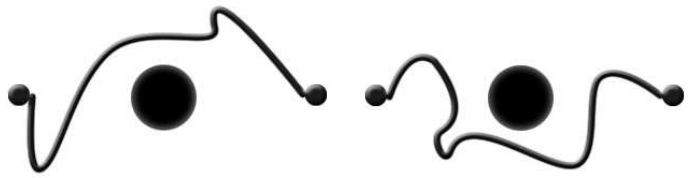

Figure 14.3: Smooth deformation of the path does not change the state.

Kitaev's toric code

A possible way to build such intrinsically fault-tolerant hardware is described by a spin model introduced by Kitaev in 1997 [111].

Setup

Consider a $k \times k$ square lattice with spin-1/2 particles placed on the links of the lattice (see Fig. 14.4). This gives us $n = 2k^2$ spins. Here, we choose $|1\rangle := (1, 0)^T$

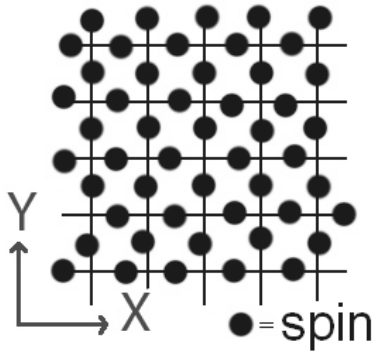

Figure 14.4: There is one spin on each link of the lattice.

and $|0\rangle := (0,1)^T$, the eigenvectors of σ^z, as the states of each spin. Denote by s a site, i.e, a point connected by four links and by p a plaquette, i.e, a square surrounded by four links.
We define the following operators:

$$A_s := \prod_{j \in \text{Star(s)}} \sigma_j^z \qquad B_p := \prod_{j \in \partial p} \sigma_j^x.$$

A_s counts the parity of $|0\rangle$'s around a site and B_p flips the spins located on the border of the plaquette. These operators are Hermitian $A_s^\dagger = A_s$, $B_p^\dagger = B_p$ with eigenvalues $+1, -1$ and satisfy the following commutation rules:

$$[A_s, A_{s'}] = [A_s, B_p] = [B_p, B_{p'}] = 0.$$

Thus we can define a protected subspace $\mathbb{H}_{\text{code}} \subset \mathbb{H}$ as the simultaneous eigenspace of all operators A_s and B_p to the eigenvalue 1:

$$\mathbb{H}_{\text{code}} := \{|\psi\rangle \in \mathbb{H} : A_s|\psi\rangle = |\psi\rangle, B_p|\psi\rangle = |\psi\rangle \quad \forall s, p \in \text{lattice}\}.$$

We see that A_s and B_p have the function of stabilizer operators as discussed in QECC's. In order to have the lattice live on a topologically non-trivial manifold (for reasons that are discussed in the section on topological order), we choose a torus by imposing periodic boundary conditions (see Fig. 14.5). This yields two additional relations, $\prod_s A_s = \prod_p B_p = 1$, which reduce the number of independent stabilizer operators to $m = 2k^2 - 2$. From the general theory on QECC's [105] we therefore know that $\dim(\mathbb{H}_{\text{code}}) = 2^{n-m} = 2^2 = 4$. Each state $|\psi\rangle \in \mathbb{H}_{\text{code}}$ corresponds to a state of 2 qubits: we have encoded 2 qubits using m stabilizer operators in a n dimensional Hilbert space.

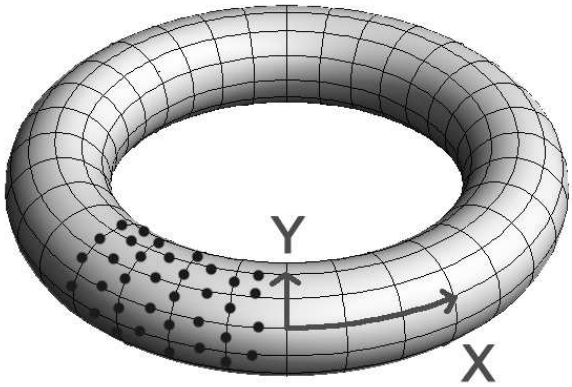

Figure 14.5: Toroidal geometry is chosen by imposing periodic boundary conditions.

Ground state

The model Hamiltonian is

$$H_0 := -\sum_s A_s - \sum_p B_p$$

so the protected subspace $\mathbb{H}_{\text{code}}$ is the ground state of the system. We chose classical spin configurations as a basis from which our quantum ground state configurations will be constructed. The former can be represented by pictures as plotted in Fig. 14.6. Connections between lattice sites correspond to qubits in

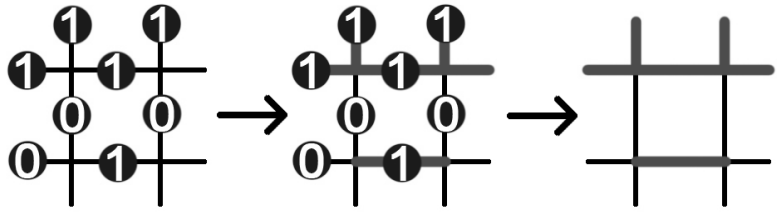

Figure 14.6: Pictorial representation of configurations: the spin states are mapped to connections.

$|1\rangle$ whereas qubits in $|0\rangle$ are represented by no connection. The operators A_s and B_p also have a pictorial counterpart: see Figs. 14.7 and 14.8, respectively.
The ground state constraint $A_s|\psi\rangle = |\psi\rangle$ demands an even number of $|0\rangle$'s and thus connections at every site. This requires our connections to form closed loops as they cannot terminate at any site. Those closed loops can move around the torus by the action of the B_p operator.

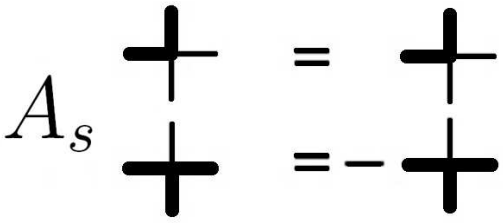

Figure 14.7: The operator A_s counts the parity of $|0\rangle$'s, which correspond to links without a connection. This is the same as the parity of $|1\rangle$'s, which correspond to links with a connection.

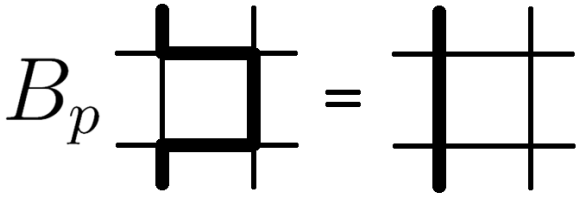

Figure 14.8: The operator B_p flips all spins around a plaquette resulting in exchanging connection and no connection.

Loop gas

Possible operations on the loops by flipping plaquettes are:

- deform loops "smoothly" (i.e, without cutting them open)
- create/annihilate contractible loops
- surgery operation (connect two loops or cut a loop into two).

The motion of the loops is given by the time evolution operator $U(t) = e^{iH_0 t/\hbar}$ which includes the operators B_p. Our ground state can thus be visualized as a gas consisting of loops that transform according to the operations listed above. This is what we refer to as "the quantum loop gas".
All loops that can be obtained from each other by flipping plaquettes form an equivalence class. Flipping any plaquette must not change the ground state: $B_p|\psi\rangle = |\psi\rangle$. This constrains ground states to equal amplitude superpositions of all loops in the same class. Although this loop gas does not look like a sorted system, there are conserved quantities that allow us to distinguish different ground states.

Topological quantum numbers

As our model is defined on a topologically nontrivial manifold, a genus $g = 1$ torus, loops can wind along two non-contractible paths (along x and along y). The parity (even or odd) of the winding numbers along those two paths is conserved by the loop gas operations as can be seen in Figs. 14.9, 14.10 and 14.11.

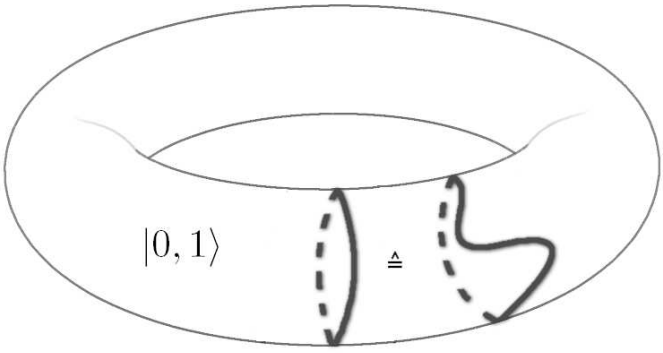

Figure 14.9: Smooth deformation of loops does not change the winding number.

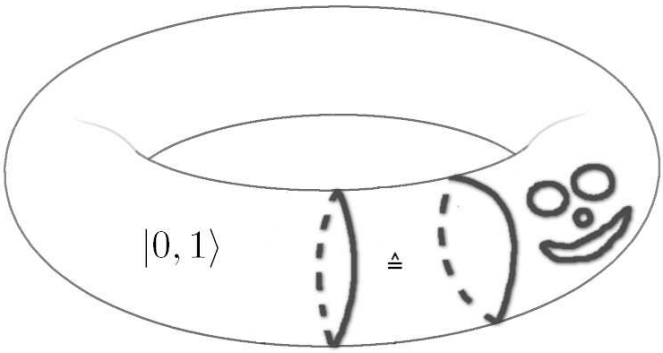

Figure 14.10: Creating/annihilating does not change the winding number.

This gives four different combinations which correspond to the equivalence classes mentioned before. Our ground state thus splits in four topological sectors with an unique ground state in each class (equal amplitude superposition):

$$|0,0\rangle,\ |0,1\rangle,\ |1,0\rangle,\ |1,1\rangle$$

where $0 :=$ even, $1 :=$ odd and $|\Omega_x, \Omega_y\rangle$ with Ω_x, Ω_y denoting the winding number parity around x and y axis, respectively. We can use those four sectors to encode two logical qubits:

$$|0\rangle_1 := |0,0\rangle,\ |1\rangle_1 := |0,1\rangle,\ |0\rangle_2 := |1,0\rangle,\ |1\rangle_2 := |1,1\rangle.$$

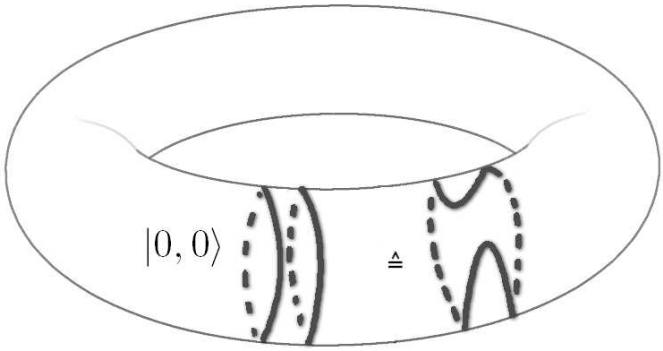

Figure 14.11: The surgery operation changes the winding number by two and thus does not change its parity.

Two qubits are not much and scalability is an important issue. In the section on topological order, the scalability of this model is discussed. The robustness of those encoded qubits becomes visible when we investigate the action of errors.

Errors

Suppose an error $E \in L(\mathbb{H}_{\text{code}})$ occurs. One can show [111] that each such error E can be written as Pauli matrices acting along a closed loops:

$$S^x(t) := \prod_{j \in t} \sigma_j^x$$

$$S^z(t') := \prod_{j \in t'} \sigma_j^z.$$

$S^x(t)$ flips spin along a closed loop t on the lattice and $S^z(t')$ gives the parity of the spins along a closed loop t' on the dual lattice (see Fig. 14.12). Since we want the operators to preserve the ground state, they have to commute with all stabilizer operators. This is the case if and only if the error paths are closed loops. If the loop is contractible, it can be written as a product of the stabilizer operators and thus is no error at all: see Fig. 14.13. An error that changes the value of the logical qubits only occurs if the loop is non-contractible i.e, it has to wind around the torus at least once: see Fig. 14.15. The crucial point is that as the errors are assumed to be uncorrelated, the probability for such an error is $\propto e^{-k}$ where k is the lattice size because at least k qubits have to be affected. Thus, topology protects the logical qubit exponentially in system size against decoherence errors.

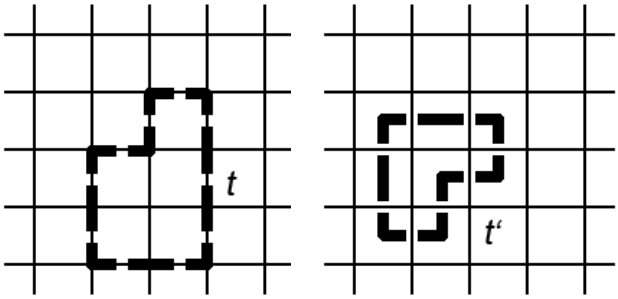

Figure 14.12: A closed path t on the lattice and a closed path t' on the dual lattice. Those paths do not denote states of spins but the action of the error operators.

Excitations

When implementing such qubits, we have to work at finite temperature which means that thermal fluctuations introduce transitions to excited states. Leaving the ground state is only possible if at least one of the constraints $A_s|\psi\rangle = |\psi\rangle$ or $B_p|\psi\rangle = |\psi\rangle$ is violated. Because of $\prod_s A_s = \prod_p B_p = 1$ we are not allowed to do this at only one site or plaquette: we can only violate the ground state constraint at an even number of sites or plaquettes. Using the known error operators, we define the excited states:

$$|\psi_{\text{charge}}(t)\rangle := S^x(t)|\psi\rangle,$$

$$|\psi_{\text{flux}}(t')\rangle := S^z(t')|\psi\rangle.$$

Every pair of violated conditions can be connected via a string on the lattice or the dual lattice. The excited states do not depend on the exact path taken but on its homotopy class. The endpoints of that string can be though of as quasi-particle excitations. A charge-type error causes the loops of the ground state to break up and form strings with the same endpoints as the path in the error operator. We say "charges" live on those two sites (endpoints of t). A flux-type error creates minus signs at certain configurations in the coherent superposition, namely at those connected by a plaquette flip at one of the "fluxes" (endpoints of t'): see Fig. 14.16.

Interestingly, these quasi-particle excitations interact topologically: we calculate what happens when we move a "charge" counterclockwise around a "flux." $|\psi_{\text{initial}}\rangle = S^z(t')|\psi^x(q)\rangle$ is our initial state where $|\psi^x(q)\rangle$ denotes the state with a pair of charges at the endpoints of the path q. $S^z(t')$ creates a pair of fluxes.

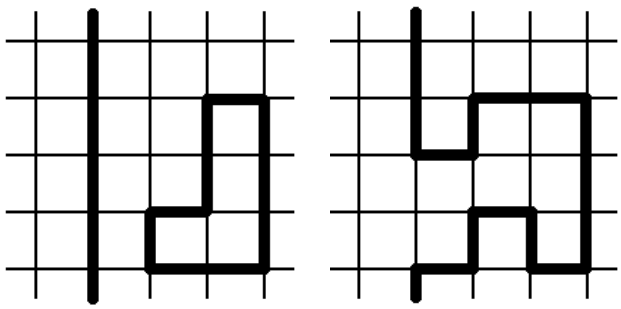

Figure 14.13: The left configuration is affected by the $S^x(t)$ error with t being the path in Fig. 14.12. The result is plotted on the right side. The error thus transforms one configuration of loops into another one in the same equivalence class, i.e, it does not change the winding number parities and the encoded qubit is not affected.

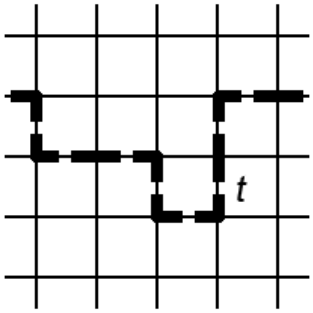

Figure 14.14: A non-contractible path t on the lattice.

We move one charge around one flux:

$$|\psi_{\text{final}}\rangle = S^x(c)S^z(t')|\psi^z(q)\rangle = -S^z(t')S^x(c)|\psi^x(q)\rangle = -S^z(t')|\psi^x(q)\rangle = -|\psi_{\text{initial}}\rangle,$$

because σ^x and σ^z anticommute. Winding two excitations of different type around each other results in the global wave function picking up a phase of -1. The familiar Aharonov-Bohm effect [55] explains the choice of the names for the quasiparticles.

These excitations can also be used to jump from one topological sector to another one. Creating a pair of charges, winding one around the torus and then re-annihilating the pair corresponds to a non-contractible error path t which changes the winding number parities of the configuration. We can thus interact

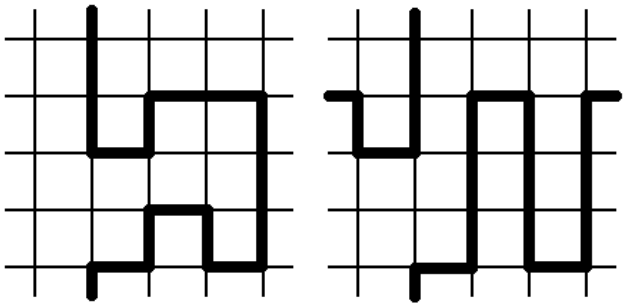

Figure 14.15: The configuration on the left side is transformed into the one on the right side by $S^x(t)$ acting along the non-contractible loop from Fig. 14.15. The winding number parity along the x-direction is changed and this corresponds to a non-trivial operation on the encoded qubit.

with our logical qubits using quasi-particle excitations. The energy cost for creating a pair of excitations is $2U$ where U is some energy scale in the Hamiltonian. If U is big compared to the operating temperature, such processes will be exponentially suppressed $\sim e^{-2U/T}$.

Kitaev's model describes thus how topology can help reliably storing quantum information by exponentially eliminating the effects of both thermal and quantum noise.

Quantum Dimer Model

In order to implement Kitaev's model for topologically protected qubits, one has to find microscopic Hamiltonians that show the same effective behaviour. A promising candidate is a more realistic model called the quantum dimer model (QDM). It was first introduced in 1988 in the context of superconductivity of cuprates [112] and has been thoroughly investigated [113, 114, 115, 116, 117] on several lattices. The triangular lattice is the simplest one that supports a resonating valence bond (RVB) phase [118] for a finite range of parameters with deconfined, gapped excitations [114], see Fig. 14.18.

Setup of the QDM

Each site of the lattice, whose boundary conditions are chosen periodic, is connected to exactly one other site, thus forming dimers. The connections are restricted to next neighbour bonds because, assuming a spin gap, such configurations have proved to be good low-energy variational states [112]. As this condition, called the hard-core condition, has to hold for all sites, the lattice is

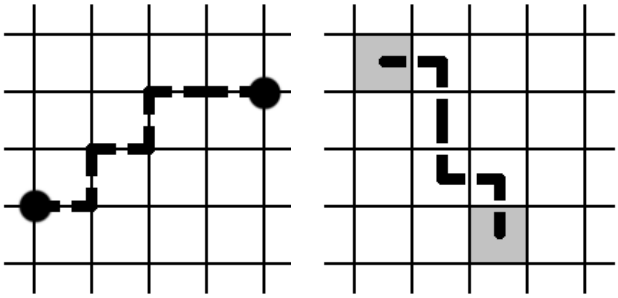

Figure 14.16: A charge-type error acting along a string on the lattice and a flux-type error acting along a string on the dual lattice. Disks represent "charges" and filled plaquettes "fluxes."

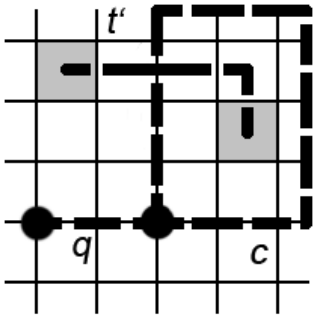

Figure 14.17: Moving a "charge" along the path c counterclockwise around a "flux" gives a phase -1.

completely covered with dimers that do not touch each other. Classical configurations are again taken as a basis and superimposed in order to find the quantum states. The Hamiltonian of the model can be written in terms of dimers:

$$H = -tT + vV = \sum -t(|\_^{-}\rangle\langle\!/\!/| + |/\!/\rangle\langle\_^{-}|) + v(|/\!/\rangle\langle\!/\!/| + |\_^{-}\rangle\langle\_^{-}|).$$

The kinetic term T lets the configuration gain an energy t by flipping pairs of parallel dimers while the potential term V acts as a repulsion between flippable dimer pairs since it punishes such configurations with an energy v. For $t \sim v$ one gets a highly frustrated and unordered phase called dimer liquid phase according to its similarity with other liquid phases. This special phase, that has been shown to be stable for $0.7 \lesssim v/t \leq 1$ [114, 119], corresponds to Anderson's RVB phase [118] and has interesting quasi-particle excitations.

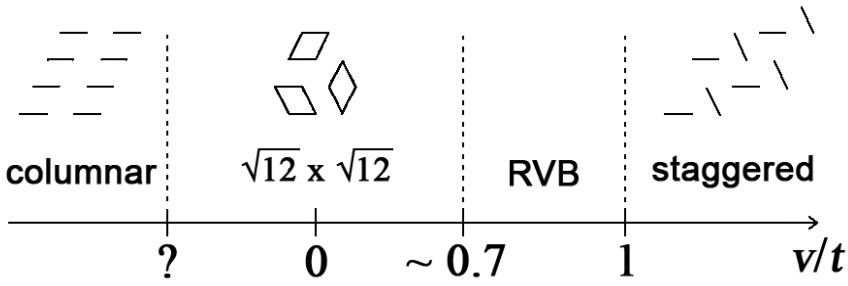

Figure 14.18: The phase diagram for the QDM on a triangular lattice calculated by A. Ralko *et al.* in 2005. [119] It shows, that the RVB phase persists for a finite range of parameters and not just at one point as on the square lattice.

Transition graph

QDM states can be mapped onto the loop gas: choose one specific dimer configuration C_0 as background. This can in principle be any configuration but usually the columnar state is chosen. Superimposing a given configuration C with C_0 yields a set of closed loops called the transition graph of C relative to C_0, see Fig. 14.19. The effect of the operators in the Hamiltonian of the QDM on those loops

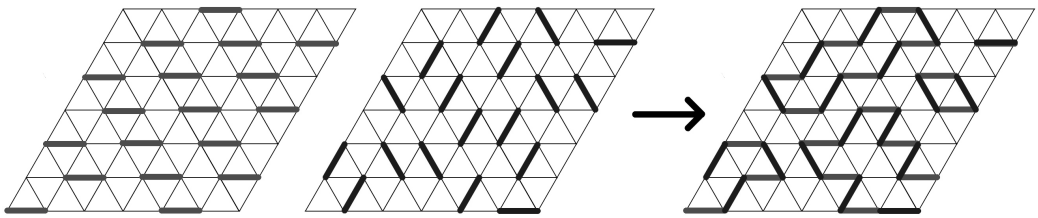

Figure 14.19: Superimposing the hard-core dimer configuration on the left side with the reference columnar configuration in the middle yields the transition graph on the right side. It consists of closed loops that can be used to describe the configuration.

correspond to the loop gas operations: see Figs. 14.20, 14.21 and 14.22. As in the Kitaev model, there are conserved quantities that allow us to distinguish different configurations. Instead of the winding number parity, the dimer count parity along a non-contractible loop is chosen. It is left invariant by dimer flips (see Fig. 14.23) so the Hilbert space splits into topological sectors corresponding to different parities.

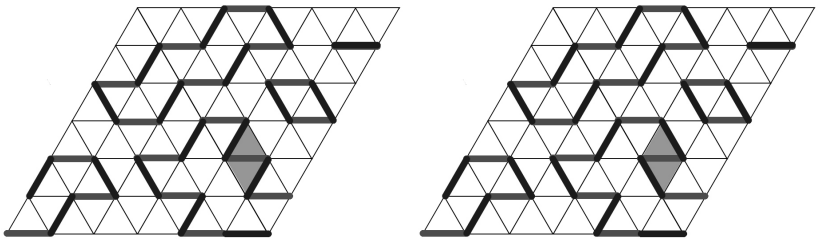

Figure 14.20: The isotopy move.

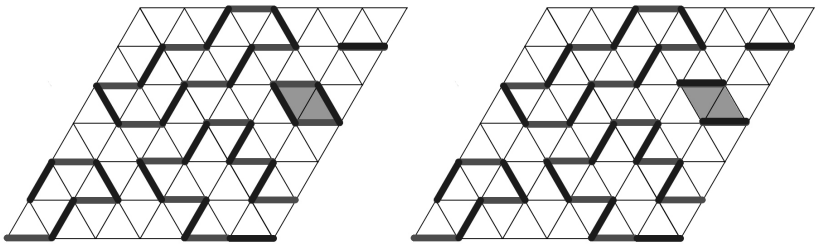

Figure 14.21: Create/annihilate contractible loops.

Implementation using Josephson junction arrays

This idea is used in an implementation of such qubits proposed by L. B. Ioffe et al. in 2002 [110]. Josephson Junction arrays are used on a hexagonal lattice with binding states of cooper pairs representing dimers between islands of hexagons of such junctions. These dimers thus live on the dual lattice which is the triangular one. By clever design, they meet the hardcore condition, periodic boundary conditions and short ranged interaction between dimers so this system shows the same behaviour as the QDM on a triangular lattice. Instead of a two-dimensional torus in three dimensions, they use a annulus in the plane. The dimer count parity along a line from the inner to the outer boundary acts as topological order parameter and splits the Hilbert space into $\mathbb{H}_{\text{even}} \oplus \mathbb{H}_{\text{odd}}$. The two sectors are not connected by local operators in the Hamiltonian and can be used to encode a logical qubit. Operating on the qubit is achieved using one controllable link. This implementation is treated in more detail in the next chapter.

Topological order and fractionalization

In both the Kitaev model and the QDM, non-local properties of the system are used to hide quantum information. This is achieved by associating topological quantum numbers such as winding numbers with states of qubits. The reason for a system to have such non-locally encoded quantum numbers is a concept

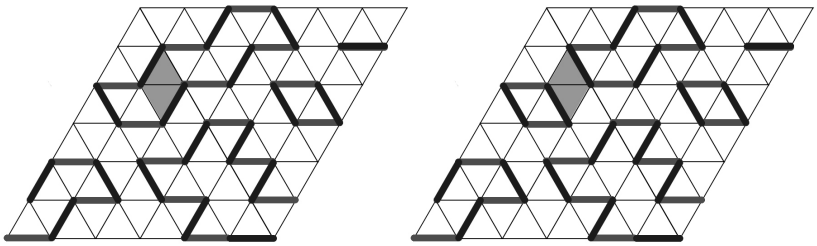

Figure 14.22: Surgery operation.

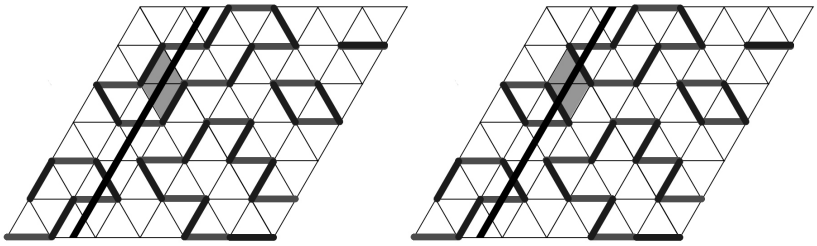

Figure 14.23: The dimer count along the line is changed only by the surgery operation which changes it by two thus preserving the dimer count parity.

called topological order. Conventional order is described by Landau symmetry breaking and conservation laws come from symmetries in the Hamiltonian via the Noether theorem. However, systems with topological order can have conserved quantities without requiring a corresponding symmetry in the Hamiltonian. This kind of order can not be understood using correlation functions and local order parameters.
Quasi-particle excitations in topologically ordered systems interact topologically, i.e, rotating them around each other has a non-trivial effect on the wave function of the system. In the chapter about anyons we see that this is of great importance for quantum computation.
Recently, it has been shown [120] that topological order is a necessary condition for fractionalization which is defined as quasi-particle excitations carrying fractions of the quantum numbers in the system. Systems that show fractionalization are thus interesting candidates for quantum computation.
A further hallmark of topological order is a ground-state degeneracy depending on the topology of the system instead of being caused by spontaneous symmetry breaking. This is the reason why the boundary conditions in the Kitaev model are chosen periodic: the system then lives on a torus, which is a non-trivial genus $g = 1$ manifold and allows us to encode two robust qubits. More general, the ground state degeneracy in the Kitaev model is 4^g and allows us thus to encode 2^g

qubits. This permits to scale the number of encoded qubits exponentially: a torus with 10 holes hosts 1024 robust qubits. Systems that show topological order can be seen in reality, although it is hard to detect this kind of order experimentally. The best-understood example is the fractional quantum hall effect.

Fractional quantum hall effect

We measure a voltage in the direction perpendicular to the current flowing when putting a conductor into a magnetic field. This is the well-known classical Hall effect:

$$U_H = R_H \frac{IB}{d}.$$

R_H is the Hall constant, and for a single type of charge carriers, $R_H = 1/(ne)$. [54] The usual measurement setup is to fix the current and record the Hall resistance $\rho_H = U_H/I$. The latter is supposed to grow linearly in B as seen from the formula above. But in a two-dimensional electron system such as a GaAs - GaAlAs heterostructure, we see plateaus at low temperatures ($\sim 10mK$) and strong magnetic fields $\sim 5T$ at $\rho_H = 1/m \cdot h/e^2$ where m is an integer. This is the integer quantum hall effect (IQHE) [121, 122, 123], which can be measured incredibly precisely ($\pm 10^{-9}$) independent of the material.

When thoroughly investigating such systems with even higher magnetic fields and lower temperatures, extra plateaus appear in addition to the integer ones, namely at

$$\rho_H = 1/\nu \cdot h/e^2$$

with $\nu = p/q$ and where p and q are integers, q being odd. The parameter ν, which is the filling factor of the Landau levels, describes the density of electrons with reference to the present magnetic flux: $\nu = n_{\text{electrons}} hc/(eB)$. This phenomena is called the fractional quantum hall effect (FQHE) [125]. It originates from many electron correlations, and cannot be explained the same way IQHE is (using Landau Levels). Quasi-particle excitations in fractional quantum hall states with filling factor $\nu = q/(2q+1)$ (main FQH sequence) carry a fractional charge [126]:

$$\tilde{e} = \frac{e}{2q+1}. \tag{14.1}$$

The ground state of such strongly correlated electron systems has been found to have a degeneracy depending on the genus g of the manifold it is defined on [127]:

$$q^g, \tag{14.2}$$

where q is the denominator of ν. The quasi-particles have fractionalized statistics [128]: exchanging two excitations in a ν state counterclockwise (ccw) results in

[54] I=current, B=magnetic flux density, q=charge of carrier, d=thickness of the conductor parallel to the B-field and n=density of carrier particles

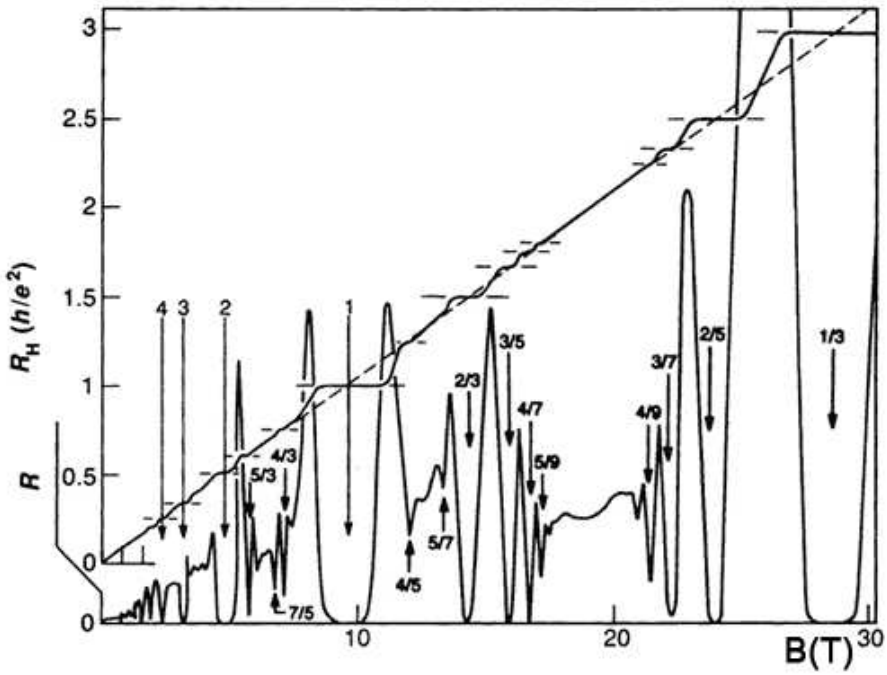

Figure 14.24: The fractional quantum hall effect: plateaus appear in the transversal Hall resistivity at fractional Landau level filling factors. Picture adopted from Ref. [124].

the wave function picking up a phase

$$e^{-i\pi\nu}. \tag{14.3}$$

As the integer q resp. the fraction ν appear in Eqns. (1), (2) and (3), the existence of a common background, which is topological order, is visible.
Besides the very important FQHE and the QDM [114, 129, 130, 119], there are other examples for fractionalization and thus topological order:

$\mathbb{Z}_2$ gauge theory and high-T_c superconductors

The Ising gauge theory is a more general concept which has a limit that describes the QDM [116]. The field has been extensively studied on various lattices in the context of frustrated Heisenberg antiferromagnets and high-T_c superconductors [115, 131]. The electron breaks into fractional particles and furthermore, there are non-trivial, gapped topological excitations [132]. The electron splits up into a "chargeon" that carries its charge and a "spinon" that carries its spin. The flux of the $\mathbb{Z}_2$ gauge field is a gapped excitation dubbed the "vison"[133, 134]. So topological order in the form of a RVB state is also a possible explanation for

high-T_c superconductivity. An experiment in 2001 [135] has shown that if visons exist, they are very unstable.

Rotating BEC's

The important parameter is the filling fraction $\nu = N/N_v$ where N denotes the number of Bosons and N_v the number of vortices. There is a zero-temperature phase transition as a function of ν between a triangular vortex lattice phase and a strongly correlated vortex liquid phase, which is quite similar to the incompressible liquid phase in FQHE, and is thought to be governed by topological order [136].

Frustrated magnets

Experiments carried out in 2003 have shown that the quasi-2D spin 1/2 frustrated Heisenberg antiferromagnet Cs_2CuCl_4 is very likely to have spin 1 waves which fractionalize into two spin-1/2 excitations ("spinons") [137]. Those experiments also showed that the quantum fluctuations dominate the mean field effect, which would prefer order, indicating an RVB spin liquid state.

Quantum computation by anyons

Topological order can be used to hide quantum information: encoding qubits in the global properties of the system protects them from local influences. Excitations that interact topologically such as Abelian anyons, can be used to jump from one topological sector to another by moving them along topologically non-trivial paths and thus perform one-qubit operations. Before we can further investigate the idea of quasi-particles performing operations, we have to describe those excitations emerging in systems governed by topological order in a well-defined way.

Anyons

In three spatial dimensions, the statistics of identical particles is restricted to Fermi-Dirac and Bose-Einstein statistics because a path that describes two counterclockwise (ccw) exchanges can be smoothly deformed into no exchange at all. This is not possible in two dimensions therefore statistics change drastically. A ccw exchange of two identical particles cannot only result in a phase of -1 or none but also in any other phase $e^{i\theta}$. Anyons can also consist of more than one "real" particle. As an example of an anyon, consider a flux-charge composite with flux Φ and charge q, sometimes called "cyon." It acquires a phase $e^{iq\Phi}$ when counterclockwise rotated by 2π as an Aharonov-Bohm effect [55]. $q\Phi = \theta$ is also referred to as topological spin of the object. The ccw exchange of two such composites results in a phase: $e^{i(\frac{q\Phi}{2}+\frac{q\Phi}{2})} = e^{iq\Phi} = e^{i\theta}$. The topological spin is the same as the

exchange phase. Therefore we have a similar connection between spin and statistics as in 3D (exchange phase $= e^{2\pi i s}$ where s =spin). We can state the following hand-waving argument: half-integer or integer spin correspond to Fermions or Bosons and fractionalized spin thus corresponds to fractionalized statistics. Further details are presented in the last chapter.

The permutation group S_n does not suffice to describe anyons. Instead, we draw the two-dimensional (2 d) world in which our anyons live in the x-y plane and chose the time axis along z. The time evolution of the system lets the anyon world lines form braids in 2+1 d. The braids are in distinct topological

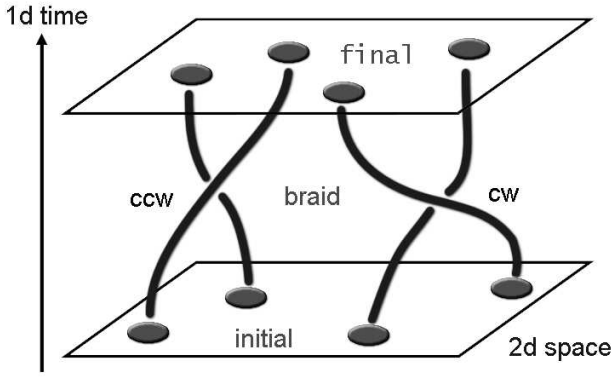

Figure 14.25: Exchanging ccw and cw is not the same in 2d: the world lines of such processes in 2+1 d are topologically different. Therefore we do not investigate the permutation group to classify particles but the braid group, which takes this difference into account.

classes. A ccw exchange is not the same as an clockwise (cw) exchange of two particles because they cannot be smoothly deformed into each other. As a further simplification, we usually do not draw 2+1 d but 1+1 d with a new relation "over" and "underneath." If the left particle goes over the right one, this corresponds to a ccw exchange while the right going over the left is a cw exchange. So the topological interactions between particles in 2+1 d are described in a well-defined way by drawing braids in 1+1 d and the latter are mathematically described by the braid group.

Unitary representations of the braid group B_n

The objects of the braid group act on lined up particles by moving them in topologically different ways to another configuration of the same particles. We call the n particles $(1, ..., n)$ and let $\sigma_i,\ i = 1, ..., n-1$ denote a ccw exchange

of the particles at positions i and $i+1$. The σ_i are the generators of the braid group and they satisfy the following two rules:

$$\sigma_j \sigma_k = \sigma_k \sigma_j, \ |j-k| \geq 2$$

and the Yang-Baxter relation:

$$\sigma_j \sigma_{j+1} \sigma_j = \sigma_{j+1} \sigma_j \sigma_{j+1} \quad j = 1, ..., n-2.$$

The braid group is infinite and has thus an infinite number of unitary irreducible representations. These representations are "carried" by the anyons in the sense that braiding anyons of type ρ with some braid $b \in B_n$ results in $\rho(b)$ acting on the Hilbert space. This leads us to a definition for anyons:

Abelian anyons := Indistinguishable particles that transform as a one-dimensional representation of the braid group.

Each braid group generator thus corresponds to a phase $\rho(\sigma_j) := e^{i\theta_j}$ and with the Yang-Baxter relation, we see that all the phases have to be the same:

$$e^{i\theta_j} e^{i\theta_{j+1}} e^{i\theta_j} = e^{i\theta_{j+1}} e^{i\theta_j} e^{i\theta_{j+1}} \Rightarrow e^{i\theta_j} = e^{i\theta_{j+1}} =: e^{i\theta}.$$

All ccw exchanges are represented by the same phase, which tells us that a phase is enough to fully characterize Abelian anyons. The special cases $\theta = 0$ and $\theta = \pi$ correspond to Bosons and Fermions, respectively. The effect of braiding Abelian anyons on the system is restricted to picking up phases. Those operations are not sufficient for universal quantum computation. However, the mere existence of Abelian anyons in a system implies topological sectors in the ground state that can be used to encode robust qubits. To perform universal quantum computation with those robust qubits, we need to be able to perform one- and two-qubit gates which are matrices. The idea presented by M. Freedman *et al.* in 2000 [138, 139] is to use non-Abelian representations to perform such gates.

Non-Abelian anyons := Indistinguishable particles that transform as higher-dimensional representations of the braid group.

Braiding them results in performing gates on a topological Hilbert space because the representation has dimension greater than one and is thus a matrix:

$$|\Psi\rangle_{\text{final}} = \rho(\text{braid})|\Psi\rangle_{\text{initial}}.$$

The gate performed by a braid only depends on the topological class of the braid but not on the exact form of the world lines. The environment is allowed to disturb the anyons during calculation as long as it does not affect the topological properties of the braid.

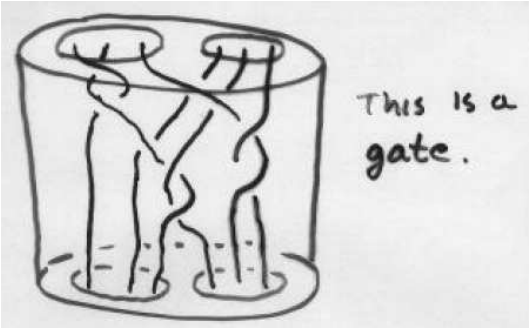

Figure 14.26: Braiding particles that carry higher-dimensional representations of the braid group results in matrices acting on the Hilbert space via $|\Psi\rangle_{\text{final}} = \rho(\text{braid})|\Psi\rangle_{\text{initial}}$ and can thus be used for quantum computation [139]. Picture adopted from Ref. [140]

If we keep the anyons far apart, it is exponentially improbable that such errors occur. Another source of errors are virtually created anyon anti-anyon pairs that interfere with our computational braid before re-annihilating. Such processes can be suppressed by low operating temperatures. For certain anyon models, the representation is dense in all reversible, unitary operations and therefore, braiding such anyons can approximate any operation with arbitrary fidelity: they have the capability of simulating universal topologically protected quantum computation [139] .

Non-Abelian anyon models

Before we can give an example, we introduce some concepts. All details can be found in Ref. [103].

A general non-Abelian anyon model describes particles in a two-dimensional surface that carry locally conserved charges. It has three defining properties:

- **Labels**: They specify what charges the different particles carry.
- **Fusion rules**: They specify the possible values of the charge that can be obtained when two particles of known charge are fused together and analogous for splitting.
- **Braiding rules**: They define the phase picked up when rotating a particle by 2π and the result of an exchange of two particles.

When we combine two particles, the resulting compound also has a charge. The possible charges obtained are defined by the fusion rules. As the fusion is

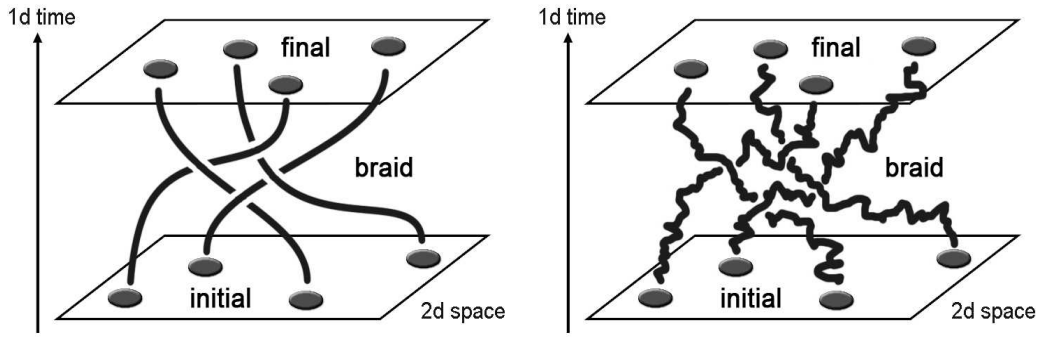

Figure 14.27: Non-Abelian anyons provide a topologically protected way to perform gates. Noise that alters the world lines does not change the gate executed as long as the braid stays in the same homotopy class.

associative, there are different ways to fuse to a given total charge. These correspond to different bases which are related by an unitary transformation called the F-matrix. An anyon model is non-Abelian if at least one pair of charges has more than one possibility to fuse into another charge. The Hilbert space spanned by the different possible fusion results is called fusion space of that pair of charges. The Hilbert space of n anyons with given total charge c is a sum of fusion spaces and one can define a standard basis for it [103]. Often, this Hilbert space is referred to as the "topological Hilbert space" to emphasize that the information is encoded non-locally: the state is defined by its fusion result but if the particles are far apart, one cannot access this information. This explains that we have to fuse the result of our computation in order to measure the calculation output.

Counterclockwise exchanging particles with charges a and b does not change their total charge c. Therefore the exchange operator, which is called R, acts on their fusion space. If the latter is multidimensional, the former is a matrix dubbed the R-matrix. Furthermore, the eigenvalues of the monodromy operator R^2 are determined by the topological spins of the particles.
To fully specify the representation of any braid on the topological Hilbert space, it suffices to investigate the effect of the generators of the braid group: using the F-matrix, one can move from the standard basis to a block diagonal basis for R, apply R and then transform back. Thus, the representation of the braid group realised by n anyons is completely determined by the F-matrix and the R-matrix, which have to fulfill consistency relations called the pentagon and the hexagon relation [103].

Since R^2 defines the topological spin, the constructed representation is defined on a larger group, "the mapping class group for the sphere with n punctures"

which can be visualized by extending world lines to ribbons that can twist [111]. All those rules together define a mathematical structure called a "unitary topological modular functor" which is closely related to quantum field theories in 2+1 d and conformal field theories in 1+1 d [141, 91, 105, 139, 142].

Fibonacci anyons

To illustrate the ideas, the simplest non-Abelian anyon model that is universal for quantum computation is briefly presented here: the Fibonacci anyon model [103, 143].

Defining properties of Fibonacci anyons:

- There is only one charge called the q-spin. It can take the values 0 and 1.
- The fusing rules are: $0 \times 0 = 0$, $0 \times 1 = 1$, $1 \times 1 = 0 + 1$.

A $q = 0$ anyon is the same as no anyon at all. The two-dimensional fusion space of two qubits thus consists of the state where two $q = 1$ anyons fuse to $q = 0$ and to $q = 1$, denoted by $|(11)_0\rangle$ and $|(11)_1\rangle$, respectively. Two $q = 1$ qubits can be in a superposition $|\psi\rangle = \alpha|(11)_0\rangle + \beta|(11)_1\rangle$. Adding further anyons to the system obeying the fusion rules enlarges the number of possible combinations for a cluster of anyons to fuse to total q-spin 0 or 1. For n anyons, the dimension of the topological Hilbert space is the $(n + 1)$'th Fibonacci number, hence the name. The consistency relations for braiding and fusing yield the R-matrix and the F-matrix in an unambiguously way up to an unimportant global phase:

$$R := \begin{pmatrix} e^{i4\pi/5} & 0 & 0 \\ 0 & -e^{i2\pi/5} & 0 \\ 0 & 0 & -e^{i2\pi/5} \end{pmatrix}$$

$$F := \begin{pmatrix} \tau & \sqrt{\tau} & 0 \\ \sqrt{\tau} & -\tau & 0 \\ 0 & 0 & 1 \end{pmatrix} \quad \tau := \frac{\sqrt{5}-1}{2}.$$

Following [138], we encode a qubit in the three dimensional topological Hilbert space of three Fibonacci anyons.

$$|0\rangle := |(((11)_0)1)_1\rangle,\ |1\rangle := |(((11)_1)1)_1\rangle,\ |NC\rangle := |(((11)_1)1)_0\rangle$$

The q-spin of the two leftmost particles thus determines the state of the encoded qubit. $|NC\rangle$ is not used as computational state and transitions into this states correspond to unwanted leakage errors (decoherence). Braiding within the qubit does not change its total charge so as long as we perform only single-qubit operations, we do not face decoherence problems. One-qubit operations are here

described by the braid group of three particles, B_3. The representation of the generators σ_1 and σ_2 can be calculated using the R-matrix and the F-matrix:

$$\rho(\sigma_1) = R = \begin{pmatrix} e^{i4\pi/5} & 0 & 0 \\ 0 & -e^{i2\pi/5} & 0 \\ 0 & 0 & -e^{i2\pi/5} \end{pmatrix}$$

$$\rho(\sigma_2) = F^{-1}RF = \begin{pmatrix} -\tau e^{i\pi/5} & i\sqrt{\tau}e^{i\pi/10} & 0 \\ i\sqrt{\tau}e^{i\pi/10} & -\tau & 0 \\ 0 & 0 & -e^{-i2\pi/5} \end{pmatrix}.$$

Each braid $b \in B_3$ can be written as product of σ_1 and σ_2 and therefore we can calculate the matrix corresponding to all possible braids by multiplying the matching powers of $\rho(\sigma_1)$ and $\rho(\sigma_2)$. For example, the braid $b = \sigma_2\,\sigma_1^{-1}\,\sigma_2\,\sigma_1^{-1}$ results in $|\psi_{\text{final}}\rangle = \rho(b)|\psi_{\text{initial}}\rangle = \rho(\sigma_2)\rho(\sigma_1)^{-1}\rho(\sigma_2)\rho(\sigma_1)^{-1}|\psi_{\text{initial}}\rangle$
Finding the braid that simulates a given gate $U \in SU(2)$ with desired accuracy is the more interesting task. It can be done by brute force, which is very hard and scales exponentially, but Solovay and Kitaev found an algorithm [144] that allows systematic improvement of a braid. With this algorithm, the braid length used to achieve error rates smaller than ϵ grows as $|\ln(\epsilon)|^c$, where $c \approx 4$.
The real challenge is to implement the CNOT gate or another multi-qubit gate that is universal for quantum computation. With more than one qubit involved, we have to face the problem of leakage errors but clever weaving techniques (injection weaving) deal with that. Bonesteel *et al.* have proposed a CNOT gate using six Fibonacci anyons (three for each qubit) that reaches an error rate of $\epsilon \sim 10^{-3}$ [143].

The effective operations executed by the braid are single qubit operations in $SU(2)$ that can be improved using the Solovay-Kitaev algorithm and therefore, that CNOT can theoretically be carried out with arbitrary accuracy. Thus, we can theoretically build a universal topological quantum computer using Fibonacci anyons: see Ref. 14.30.

Anyons in real life?

Fractional quantum hall states are the most promising candidates for systems with anyons, i.e., theoretically, quasi-particles emerging from a ν state have braiding statistics of $\theta = -\pi\nu$: see [128, 146] and references therein. But until 2005, experimental proof was lacking. F. E. Camino *et al.* [146] have measured interference patterns when sending a $\tilde{e} = 1/3$ quasi-particle around an island containing a $\nu = 2/5$ FQH fluid which agree with the assumption that they are Abelian anyons that interact topologically. Still, the results are not excessively explained by this assumption which lets many scientists doubt that this experiment can be seen as a proof for the existence of anyons.
Theory also predicts non-Abelian statistics for certain filling factors ν. The most

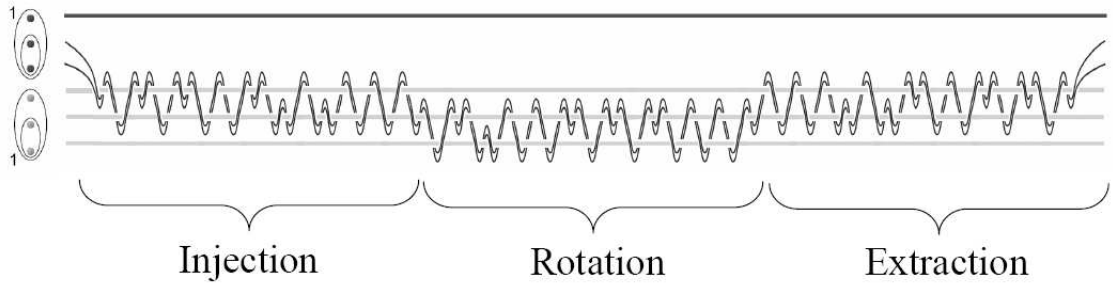

Figure 14.28: A CNOT gate is approximated up to an error of $\epsilon \sim 10^{-3}$ using six Fibonacci anyons. With the first part (Injection), identity is approximated resulting in a permutation of two anyons of the control qubit with two anyons of the target qubit. This ensures that the next part (Rotation) is carried out within one qubit thus preventing leakage errors. The last step (Extraction) is the inverse of the injection braid and permutes the anyons again. If the control qubit is in state $|0\rangle$, the effect of this braid is identity which makes it a controlled-NOT gate. Picture adopted from Ref. [145]

important two are $\nu = 5/2$ and $\nu = 12/5$. Although the non-Abelian statistics describing quasi-particles in the $\nu = 5/2$ state are not sufficient for universal computation, one can simulate a universal set of gates with a very modest error threshold of $\epsilon > 0.14$ [147]. M. Freedman *et al.* [148] have proposed another way to extend the $\nu = 5/2$ statistics to universal quantum computation and their estimate for the error rate is $\epsilon \lesssim 10^{-30}$! The $\nu = 12/5$ state is believed to have non-Abelian anyons that can be described using a $SU(2)_3$ Chern-Simons gauge theory [149] and thus are universal for quantum computation [139].

It is not yet clear whether quantum error correction or topologically protected quantum computation will be the future standard of quantum computation but the beautiful topology involved gives the latter an "intrinsic coolness factor" [148].

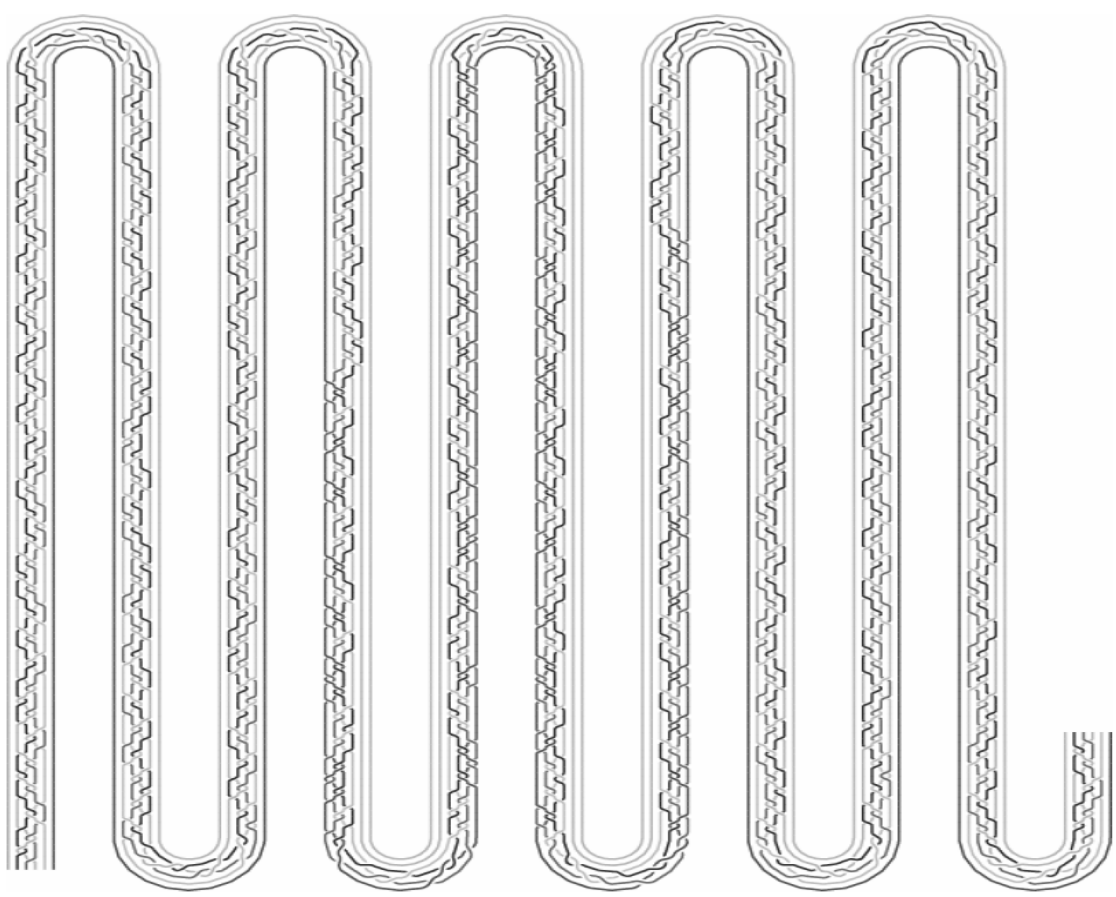

Figure 14.29: Improved version of the CNOT with an error of $\sim 10^{-4}$. The braid length used to achieve a ten times better accuracy grows by a factor of ≈ 4. Picture adopted from Ref. [145].

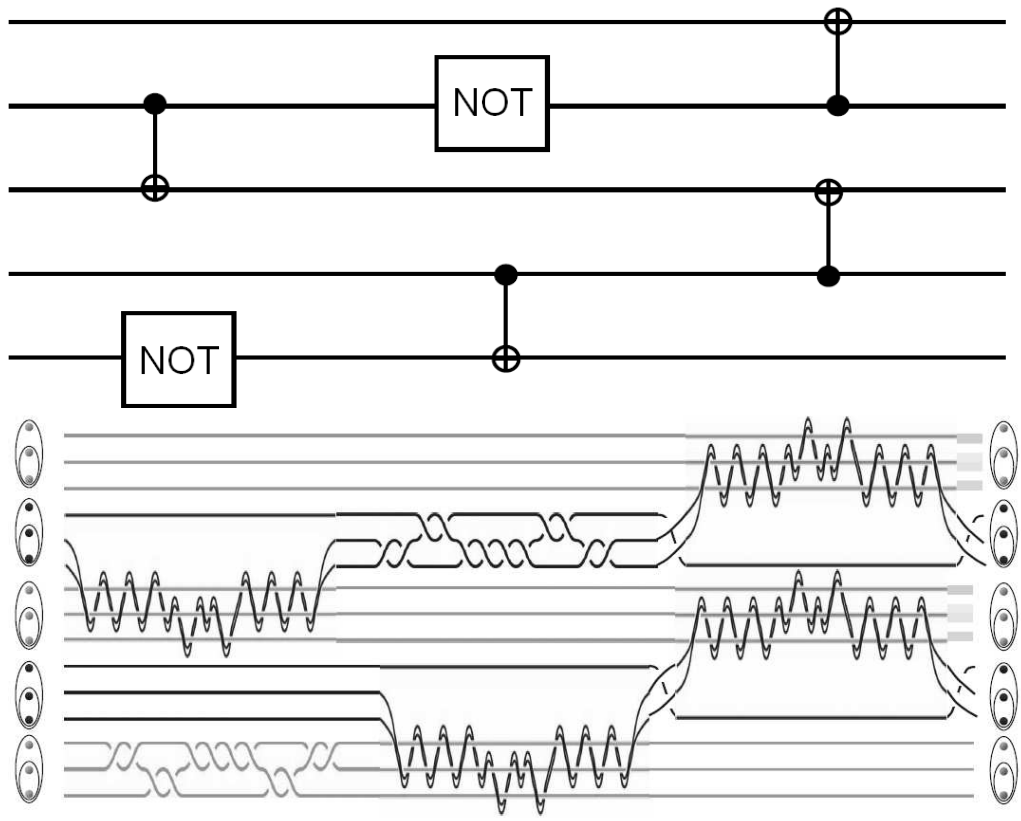

Figure 14.30: A possible quantum computing circuit approximated by braiding non-Abelian Fibonacci anyons. Error rate $\epsilon \gtrsim 10^{-3}$. Picture adopted from Ref. [145].

15 Topological quantum computing implementations

Mario Berta
Supervisor: Fabricio Albuquerque

For any implementation of a quantum computer one can not eliminate every source of decoherence. We show in this chapter how one can use the ideas of topological quantum computing [150] to implement quantum bits that are topologically protected and therefore stable against decoherence. We discuss a possible implementation, introduced by Ioffe and collaborators [110], based upon quantum simulators built from Josephson junction arrays for the triangular lattice quantum dimer model in its liquid phase.

1 Introduction

If we want to implement quantum bits (henceforth dubbed qubits) for a quantum computer we have to overcome conflicting requirements. On one hand the qubits should be manipulable through externals signals and on the other hand the qubit should be screened as much as possible from its neighbourhood. As an example we can think of an electron spin as a qubit (i.e. spin up and spin down are the qubit states). We need to isolate this electron spin from everything except the measurement and manipulation mechanism. Furthermore we need to be able to turn off the coupling of the qubit to the measurement so as to not decohere the qubit while performing an operation on it. Because of the very quantum mechanical nature of the qubits these requirements are difficult to achieve.
Hence any quantum computer has to incorporate some fault tolerance. It is impossible to eliminate every source of decoherence. There exist quantum error-correction schemes [151] to deal with this problem and to scale down the number of errors. These schemes require active interference with the system during runtime. Quantum error-correction schemes spread one qubit onto several qubits and

then the encoded quantum information is protected against errors of a limited form. The problem is that the system increases by a factor of 10^2 to 10^3 when such schemes are applied. Moreover, we require an accuracy about one error in 10^4 operations that it is useful to apply quantum error-correction schemes. This implies that each gate must perform its task 10'000 times faster than the decoherence time of the system. Up today it is not possible to achieve this.
Recapitulating we can say that decoherence is one of the biggest problem we have to face when we want to build a quantum computer. Topological protection of qubits offers a promising possibility to solve this difficulty. Kitaev's idea [150] of topological quantum computing is to bring the stabilization against decoherence to the hardware level. This means that the desired quantum computer is coherent because of its physical nature and the stabilisation against decoherence is achieved passively.
For a physical implementation of a topologically protected qubit we need a many body quantum system which fulfils the following constraints: (i) The Hilbert space of the system splits into two orthogonal sectors. (ii) Each of these sectors remains isolated under the action of local perturbations. (iii) The ground state in both sector has the same energy (i.e. the ground state is twofold degenerate). (iv) The excitation spectrum is gapped in sectors.
If we choose the two states of a qubit as the two ground states in the different sectors, these states are stable under external disturbance and hence are stable against decoherence. Furthermore the ground states within each sector are secured through a gapped excitation spectrum. To manipulate such qubits in order to build a topologically protected quantum computer we have to find and implement global operators which can switch the qubits between the distinct sectors of the Hilbert space.
A many body quantum system that displays all these desired properties is the Quantum Dimer Model [112] [152] [153] [154]. Ioffe et al. [110] proposed to emulate such a Quantum Dimer Model in a Josephson junction array. It is the main goal of this report to review and explain the ideas of this paper.
This report is organized as follows. In the next section we introduce the Quantum Dimer Model and discuss its properties on the square and triangular lattice. Moreover, we present an exact solvable Quantum Dimer Model for the Kagome lattice. Afterwards we describe the Josephson effect and arrays of Josephson junctions. Finally we discuss the idea of implementing topologically protected qubits in a Josephson junction array (Ioffe et al. [110]).

2 Quantum Dimer Model

Motivation of the Quantum Dimer Model

Two dimensional (2D) antiferromagnetic spin systems are well described by the 2D Heisenberg model whose Hamiltonian reads:

$$H = J \sum_{\langle i,k \rangle} \mathbf{S_i} \cdot \mathbf{S_k} \tag{15.1}$$

where $\mathbf{S_i}$ is the spin operator of the electron on site i and the sum runs just over nearest neighbours. J stands for a super exchange coupling between two spins on nearest neighbour sites.

After extensive and intense research it is known today that the ground state of

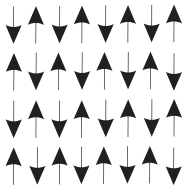

Figure 15.1: For classical spins the ground state is the ordered Néel state. In this configuration the spins are alternating pointing up and down.

the antiferromagnetic Heisenberg model in the square [155] and triangular lattice [156] is Néel-ordered (see Fig. 15.1) at $T = 0$ and hence displays long-ranged order with spontaneous symmetry breaking.

Because of the work of Anderson [118] people got interested in other possible quantum phases without magnetic long-ranged order as well. Conditions that favour unconventional states are low dimensional lattices with significant geometrical frustration (see Fig. 15.2) and strong quantum mechanical fluctuations (they are maximal in the extreme quantum limit $S = \frac{1}{2}$) [157]. Spins can lower

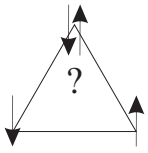

Figure 15.2: Geometrical frustration in a lattice with triangular symmetry: It is not obvious how to orient the spins in a Néel-ordered way. The spin on the third site can point up or down equal likely, because both of the states have the same energy.

their energy if they build singlets and the most likely state in such a regime is a state with all spins paired into singlets [118].

The state of two spins that are paired, sitting on sites i, j, is given by an anti-symmetric combination of up and down spins:

$$|(ij)\rangle = \frac{1}{\sqrt{2}}(|\uparrow_i\downarrow_j\rangle - |\downarrow_i\uparrow_j\rangle) \tag{15.2}$$

where $\uparrow_i$ denotes a spin up at site i and $\downarrow_j$ a spin down at site j. These singlet states are called valence bonds (see Fig. 15.3). We can get a state for the whole

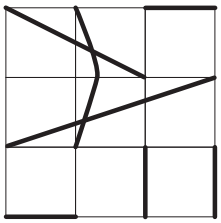

Figure 15.3: A valence bond state for a 4×4 square lattice.

lattice if we assign valence bonds to all vertices and write the product state as a tensor product of all the singlets:

$$|VB\rangle = \prod_{\text{pairs}} |(i_k j_k)\rangle. \tag{15.3}$$

Since there are a lot of ways to pair the spins, a possible ground state without long-ranged magnetic order will be a superposition of such valence bond (VB) states. VB states can be long-ranged, i.e. any two spins can pair (Fig. 15.3) or short ranged, i.e. just spins that are nearest neighbours can pair (Fig. 15.4). Note that in the last case the valence bonds are non-intersecting and we can therefore think of hardcore dimer coverings instead of short ranged VB states. For extremely frustrated spin systems we expect short ranged VB states. One

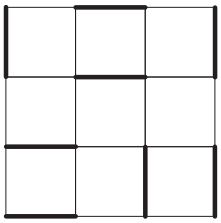

Figure 15.4: A short-range resonating valence bond state on a 4×4 square lattice. The bold lines represent dimers.

can find that the short ranged VB states form a basis for the spin zero sector of the Hilbert space of a given system. Furthermore they are linearly independent for all lattices which are discussed in this text [158]. Quantum Dimer Models

(QDM) are defined in the Hilbert space of short ranged VB states and try to describe phases without long-ranged magnetic order. So QDM do not operate in the σ^z spin basis anymore, but in a new basis: The dimer basis.
Given the basis we need to find an effective Hamiltonian from the Heisenberg model that describes the dimer degrees of freedom. Because the short ranged VB states are highly non-orthogonal we need to calculate the overlap-matrix $\Omega_{a,b} = \langle\Psi_a|\Psi_b\rangle$ for any two short ranged VB states $|\Psi_a\rangle$ and $|\Psi_b\rangle$. To do this it is necessary to establish the concept of transition graphs. The transition graph of two dimer coverings C, C' is constructed by drawing C and C' on the same lattice. The result is a covering with non-intersecting loops. Trivial loops are obtained

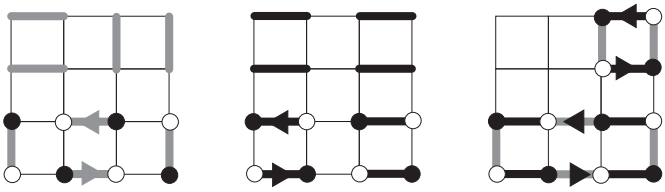

Figure 15.5: Two dimer coverings C, C' and their corresponding transition graph (trivial loops are skipped because we are not interested in them).

when the dimers are in the same positions in both coverings. For non-matching bonds the loops get larger, although they are always closed.
Now let's first have a look at the square lattice. Since the square lattice is bipartite[55] every bond connects one sub lattice W with the other sub lattice B and the transition graph is orientable. A dimer from covering C is oriented from W to B and one from C' from B to W. This results in oriented loops $W \to B \to W \to B$ etc. in the transition graph (see Fig. 15.5).
Sutherland [159] derived the result $\Omega_{a,b} = 2^{1-\frac{L}{2}}$ where L is the length of the loops of the transition graph between $|\Psi_a\rangle$ and $|\Psi_b\rangle$. So an orthogonalized valence bond state takes the form: $|\hat{a}\rangle = \sum_a (\Omega^{-\frac{1}{2}})_{a,a'}|a\rangle$ and we can write the matrix elements of the effective Hamiltonian that describes the situation in the dimer basis as:

$$\mathcal{H}^{\text{eff}}_{a,b} = \sum_{a',b'} (\Omega^{-\frac{1}{2}})_{a,a'} \langle a'|H|b'\rangle (\Omega^{-\frac{1}{2}})_{b,b'}. \tag{15.4}$$

In general this is a difficult expression, but Rokhsar and Kivelson [112] introduced a simplification. They considered a formal overlap expansion parameter x and replaced $\langle\Psi_a|\Psi_b\rangle$ by $2x^L$. Their idea is to expand the effective Hamiltonian in the parameter x [112]. For physical $SU(2)$ spin systems we have $x = \frac{1}{\sqrt{2}}$ and for an expansion up to order n we can get an effective Hamiltonian which may lead

[55] It is possible to break down the lattice in two sub lattices (white W and black B).

to a good approximate model.
There are many ways to choose such Hamiltonians but convenient choices are much simpler than their original spin Hamiltonians and are often accessible to numerical and analytical calculations [158]. In particular it is possible to write down some simple QDM in a Kagome lattice which is solvable and all excited state wave functions are known [130].
QDM can be good approaches to the phases of antiferromagnets which are dominated by short range valence bonds, as in an extreme quantum limit of a $SU(2)$ spin model [160]. Even if QDM are toy models in some way, they lead to many nontrivial results and are interesting objects. As we will see in the next two sections, these models offer simple descriptions of unconventional orders as Valence Bond Crystals (VBC) [112] as well as resonating valence bond (RVB) liquids [114] [130].
Moreover, Ioffe et al. [110] realised that QDM can be used to implement topologically protected qubits.

Quantum Dimer Model on the square lattice

The first QDM was introduced by Rokhsar and Kivelson [112]. The model is defined on the square lattice, and the Hamiltonian reads:

$$\mathcal{H} = -t\hat{T} + v\hat{V} = \sum_{i=1}^{N_p}(-t(|=\rangle\langle ||+||\rangle\langle =|) + v(|=\rangle\langle =|+||\rangle\langle ||)) \tag{15.5}$$

where N_p is the number of plaquettes of the lattice. The Hamiltonian contains a potential term and a kinetic term (represented by $\hat{V}$, $\hat{T}$ resp.). We can obtain this Hamiltonian with a formal overlap expansion of the Heisenberg Model in the parameter x, where we just keep the two most local terms (i.e. the lowest order terms[56]). To analyze the Hamiltonian we first discuss the two terms $\hat{T}$ and $\hat{V}$ separately.
The potential term stands for an attractive or repulsive (i.e. negative or positive v) interaction between dimers. This term is diagonal in the dimer basis: $\hat{V}|=\rangle = v|=\rangle$ and analogue for $||\rangle$.
On the other hand the kinetic term represents a dimer move on the lattice. Without lost of generality t can be taken greater or equal zero[57]. The kinetic term rotates parallel dimers and $|\Psi\rangle = ||\rangle + |=\rangle$ is an eigenstate of $\hat{T}$ on a single plaquette system. Thus the kinetic energy maximizes the number of resonating plaquettes. We can say the kinetic term resonates the dimers, what can naturally be associated with kinetic energy. As we can see the two terms of the Hamiltonian counteract each other and favour different phases.

At one end of the diagram, for $\frac{v}{t} > 1$, the system minimizes the number

[56] In fact $t \backsim x^4$ and $v \backsim x^8$. Note that a three dimer kinetic term of order x^6 is not considered because the term is less local [112].

[57] Because a change in the sign would just reverse the orientation of the states of the dimers.

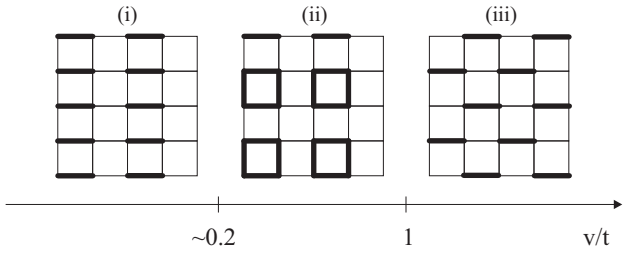

Figure 15.6: Phase diagram of the square lattice QDM: (i) columnar phase (ii) plaquette phase made up resonating plaquettes (iii) staggered phase.

of flippable plaquettes (=plaquettes with two parallel dimers) due to the large repulsive interaction between dimers. The resulting configuration is the staggered one. This configuration is a zero energy eigenstate of the Hamiltonian in general and a ground state for $v \geq t$. We can see this by calculating the expectation value for the energy on one plaquette. A non-flippable plaquette is annihilated by $\mathcal{H}$ and a flippable plaquette has a potential energy of v and a kinetic of t or $-t$. This leads to the following constraint:

$$min(0, N_p(v-t)) \leq E \leq max(0, N_p(v+t)) \tag{15.6}$$

where N_p is the number of plaquettes of the lattice. For $\frac{v}{t} > 1$ this shows that any zero energy eigenstate is the ground state. As we can see the staggered state breaks several lattice symmetries. Such configurations with a long range dimer-dimer order and broken lattice symmetries are called a Valence Bound Crystals (VBC). Note that there is no $SU(2)$-symmetry breaking or long range spin-spin order. We can rotate the state by 90° and obtain the same configuration. Therefore the phase is four-fold degenerate. Furthermore no local dimer move can take place in this regime. We can see this if we apply the Hamiltonian to the staggered state; the state gets annihilated.
For $v < 0$ we realize the other extreme situation. Parallel dimers attract each other and the system maximizes the number of flippable plaquettes. The state that results is the columnar state. For $t = 0$ the columnar state is an exact eigenstate, but not for $t \neq 0$. The excitations in this regime are gapped ($\Delta E = 2\,|v|$) and correspond to a pair of dimers which are rotated by 90° compared to the background configuration. The eigenstate for $t = 0$ is a VBC because we have a broken lattice symmetry. Moreover the VBC will survive a small and finite t term because of the gapped nature of the excitations [113].
In the middle of the phase diagram for $t \gg |v|$ (i.e. a large and dominating kinetic energy) the system builds a resonating plaquettes crystal $|\square\rangle = |=\rangle + |\shortparallel\rangle$. This phase is a VBC too. Leung et al. [113] showed using exact diagonalizations that this plaquette phase is realized for $-0.2 \leq \frac{v}{t} < 1$.
All the phases we discussed up to here are VBC and therefore display conventional order. But moreover there exists another type of phase with no broken lattice

symmetries. In fact, for the square lattice, we have this just for one position in the phase diagram: The point where $t = v$. This is somehow intuitive because the amplitudes of the kinetic and potential terms are exactly equal a this point and the terms can antagonise maximally. A this point (called Rokhsar-Kivelson (RK) point) the Hamiltonian can be written as:

$$\mathcal{H} = \sum_p |\Psi_p\rangle\langle\Psi_p| \tag{15.7}$$

$$|\Psi_p\rangle = |\rangle - |\rangle. \tag{15.8}$$

Even if the system has no broken lattice symmetries at the RK point, this phase can exhibit a kind of order, known as topological order. To analyze the situation at the RK point we need to talk about this topological order.
Considering a lattice on a toroidal geometry (i.e. periodic boundary conditions in x- and y-direction), we can define two winding numbers Ω_x and Ω_y. The winding numbers are the net number of topologically non-trivial loops (clockwise minus counter clockwise) in the transition graph encircling the torus in x and y directions, respectively (see Fig. 15.7). By defining a columnar state as the reference

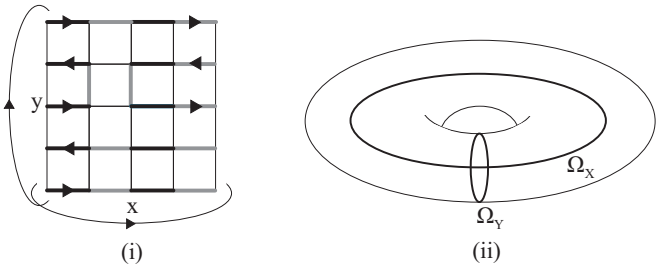

Figure 15.7: (i) Transition graph with winding numbers $\Omega_x = 1$ and $\Omega_y = 0$. (ii) Toroidal geometry with the two possible loops encircling the torus in x- and y-direction, resp.

state it is possible to label any dimer configuration by its winding numbers due to the reference state. Configurations with the same winding numbers can be obtained by local dimer moves (the winding number of the transition graph associated to every local movement is zero). So the coverings can be grouped into topological sectors, labeled by its winding numbers. These topological sectors are disconnected sectors of the Hilbert space since two coverings with the same winding numbers (due to the reference state) can by achieved by repeated application of the Hamiltonian and it is impossible to leave a given topological sector under the action of the Hamiltonian. For the square lattice the Hamiltonian is ergodic (meaning every configuration with the same winding number can be reached under the action of the Hamiltonian). The number of Ω_x and Ω_y is of order $\mathcal{O}(L^2)$, where L is the length of the lattice.

Coming back to the RK point, the equal amplitude linear superposition of all possible coverings $|c\rangle$ in a given topological sector Ω is a ground state. We can write this state as follows:

$$|0\rangle = \frac{1}{\sqrt{N_c}} \sum_{c \in \Omega} |c\rangle \tag{15.9}$$

where N_c is the number of all possible dimer coverings in Ω. $|0\rangle$ is called a RK wave function. It is a ground state because the Hamiltonian annihilates it. We can show this:
Consider one single plaquette in a configuration $|c\rangle$. If $|c\rangle$ is a configuration with no or just one dimer we have $\langle \Psi_p | c \rangle = 0$. For a two dimer configuration there exists a configuration $|c'\rangle$ in the same topological sector which differs from $|c\rangle$ by a two dimer flip. $|c\rangle + |c'\rangle$ is then again orthonormal to $|\Psi_p\rangle$, which implies $\mathcal{H}|0\rangle = 0$.
Rokhsar and Kivelson [112] calculated the excitation spectrum at the RK point using a variational calculation and found a gapless spectrum.
At this special point they were even able to calculate the dimer-dimer correlations. It turns out that the correlation function is algebraically decaying with distance ($\sim \frac{1}{r^2}$) and therefore the dimer-dimer correlations are not truly short ranged.
Recapitulating we notice that the QDM on the square lattice is believed to be ordered (VBC) everywhere except at the RK point. Moreover the QDM exhibits some interesting topological properties at this point. Our goal is to use these properties for the implementation of topologically protected qubits. Unfortunately at least three problems occur. First the number of topological sectors is of order L^2 and unequal to two. Secondly the topological phase is just realized for v exactly equal to t, what is rather difficult to implement. And thirdly the gapless excitation spectrum makes the system susceptible to perturbation. However, on the triangle lattice we can overcome these problems.

Quantum Dimer Model on the triangular lattice

The most local dimer Hamiltonian on the triangular lattice was first discussed by Moessner and Sondhi [114] and reads:

$$\mathcal{H} = \sum_{i=1}^{N_p} \sum_{\alpha=1}^{3} \{-t(|\rangle\langle -| + |-\rangle\langle |) + v(|\rangle\langle | + |-\rangle\langle -|)\} \tag{15.10}$$

where the sum on i runs over all the rhombi of the lattice, the sum on α stands for the three possible orientations of the plaquettes (each rotated by 60 degrees) and N_p is the number of plaquettes. It is possible to give a motivation for this Hamiltonian with an overlap expansion of the Heisenberg model.
As on the square lattice the Hamiltonian contains a kinetic and a potential term

($\hat{T}$ and $\hat{V}$). These terms act exactly as on the square lattice.
The set $\{|c\rangle | c = 1, ..., N_c\}$ corresponds to all possible dimer coverings. Applying $\hat{V}$ to a state $|c\rangle$ we get: $\hat{V}|c\rangle \equiv n_{fl}(c)|c\rangle$ where $n_{fl}(c)$ measures the number of flippable plaquettes of $|c\rangle$.
Like on the square lattice we can have a look at the phase diagram. At the right

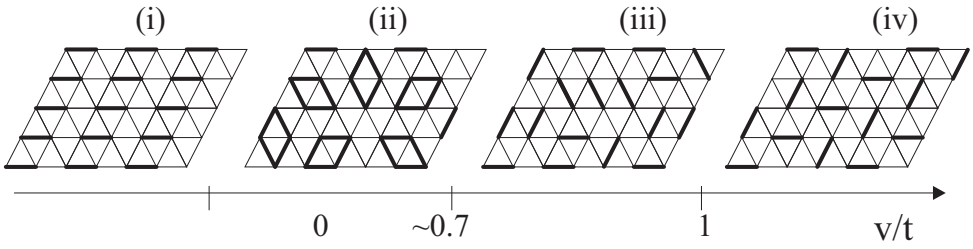

Figure 15.8: Phase diagram of the triangular lattice QDM: (i) columnar phase (ii) $\sqrt{12} \times \sqrt{12}$ phase (iii) liquid phase (iv) staggered phase.

end of the diagram, for $\frac{v}{t} > 1$, the system is in the staggered phase in which the ground state manifold consists of all non-flippable configurations. It is easy to check that equation (15.6) still holds and therefore the ground state is the zero energy eigenstate. The non-flippable configurations actually are these zero energy eigenstates. The staggered phase is a VBC and no local dimer move can take place.
On the other end where $v < 0$ and $t = 0$ the ground states are the maximally flippable states, i.e. those with maximal n_{fl}. This phase is highly degenerate because by shifting all dimers along a straight line in an ordered columnar state, the number of flippable plaquettes is preserved (note that this is not true for the square lattice). The number of such maximally flippable states is exponential in L, the system size. For an infinitesimal t the degeneracy is expect to be lifted. In this case the system gets ordered and favours the columnar state. This phase is a VBC.
In a intermediate situation for v around zero the system favours a so called $\sqrt{12} \times \sqrt{12}$ crystalline phase. The dimers build a triangular super-lattice with a 12 site unit cell out of resonating diamond plaquettes. This phase is a VBC too.
One can calculate using Pfaffian Methods that the system is in a phase without broken lattice symmetries at the RK point [114][161][162]). For a state as in equation (15.9) we can get $\langle 0|\mathcal{H}|0\rangle = (v - t)n_{fl}$. This is zero at the RK point $(v = t)$ and therefore the ground state is an equal amplitude superposition of all states in a given topological sector.
On the square lattice the phase with no broken lattice symmetries is realized just for one disconnected point. The new effect on the triangular lattice is that the phase enlarges to a range $0.7 \approx v_c \leq \frac{v}{t} \leq 1$ and is even a liquid phase (exponentially decaying dimer-dimer correlation function). Moreover Moessner and Sondhi

[114] found from their Monte Carlo simulations (on clusters up to $L_x \times L_y = 36$) that the spectrum is gapped and that the degeneracy of the ground state holds in the thermodynamical limit for the whole sector $v_c \leq \frac{v}{t} \leq 1$. This picture is consistent with the exact diagonalization studies of Ioffe and collaborators [110] (done on clusters up to $L_{x,y} = 6$). This is an interesting situation because the topological properties exist for a finite range for the parameters (t and v) and the topological sectors remain isolated under perturbations because the system is in a liquid phase.

But the topological properties are not the same anymore. Because the triangular lattice is not bipartite it is not possible to orient the transitions graphs. Hence the winding numbers Ω_x, Ω_y (in a toroidal geometry) are defined as the parity of the number of non-trivial loops around the system in x- and y-direction in the transition graph due to the reference columnar state.

The winding numbers are not conserved by local dimer moves; they are conserved modulo two. Therefore they are equal to zero or one. This results in just four topological sectors (Ω_x, Ω_y): (0,1), (1,0), (0,0), (1,1). If we take instead of a torus a cylinder (i.e. periodic boundary conditions in just one direction, let's say x-direction) there is only one winding number Ω_x present. Hence we only have two topological sectors which we can use as the states of a qubit. Ω_x is the conserved topological quantity and $\Omega_x = 0$ corresponds to the state 0 of the qubit (analogue $\Omega_x = 1$ to the state 1 of the qubit).

But if we think of an actual physical implementation a problem occurs: It is non-trivial to measure transition graphs and therefore difficult to determine the state of a given qubit. We can solve this problem when we define the topological conserved quantity in a different but equivalent way. We define it as the parity of the number of dimers intersecting a given line γ. This line has the following two properties: (i) γ ends at the boundaries of the cluster and (ii) γ does not divide the cluster into two disconnected pieces. The first condition ensures that the parity is really conserved when applying the Hamiltonian and the second one guarantees the possibility of constructing configurations with both parities. On a cylinder it is easy to see that the only choice is a straight line in y-direction, going from one end of the system to the other.

Here we can see easily that the qubit states are protected against local disturbance. A local disturbance can just flip flippable plaquettes and this will not change the parity and therefore not decohere the qubit states. The equivalence of these two definitions can be shown as follows:

Consider the columnar reference state. If we shift one dimer to the left in x-direction all dimers along that line have to do so too. Because otherwise there would be vertices with more than one dimer. So we can see that the transition graph of this new dimer covering contains a non trivial loop that encircles the cylinder in x-direction. Hence the two states have different winding numbers $\Omega_x = 0$ and $\Omega_x = 1$. But the parity of counting along the line γ has changed too. For the reference state the parity is even and for the shifted state it is odd.

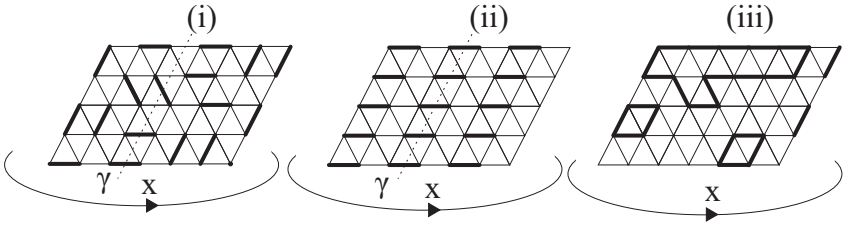

Figure 15.9: Reference line γ: (i) count of 3 $\Rightarrow$ odd parity (ii) count of 5 $\Rightarrow$ odd parity (iii) corresponding transition graph with $\Omega_x = 0$.

Therefore the definitions for the conserved topological quantity are equivalent in this situation. Now consider a state where the dimers are shifted along two lines in x-direction in the same manner. For this covering the winding number is zero (because two non trivial loops encircle the cylinder) and the parity is even. Furthermore it is easy to see that this state and the columnar reference state can be connected by local dimer moves.
As one can check these arguments generalize for any dimer covering of any size triangular lattice. Thus the two topological sectors ($\Omega_x = 0, 1$) can be identified with the sectors of even and odd parity[58].
So on the triangular lattice we find promising properties to implement a topologically protected qubit, but we have to check if the properties concerning the liquid phase and the topology still hold for a potential physical implementation. For that purpose it is necessary that the system is quite tolerant with variations in the parameters (because in any physical system there are always impurities and defects). As mentioned above expensive Monte Carlo Simulations [114] and exact diagonalization [110] studies show that the liquid state is realized for $0.7 \approx v_c \leq \frac{v}{t} \leq 1$. It was also found that there is a weak temperature ($= T$) dependence in the interval $0.25t > T > 0.03t$ and that the gap in the excitation spectrum is of order $\Delta = 0.1t$.
Furthermore the following articles were discussed by Ioffe et al. [110]: (i) The mixing of the two ground states would require the creation of topological defects and that's why the mixing is really weak. The effect is exponentially suppressed in the system size L_x. (ii) The robustness of the degeneracy of the ground-state can be checked by disturbing the system with a quenched disorder potential. This is a mathematical method that varies t and v slightly over the lattice. It was found that the degeneracy is robust to within a factor of 10^{-3} to 10^{-2} of the disorder potential and the results are shown in Fig. 15.10. It is expected that this

[58] On the square lattice it is possible to introduce the same idea. There the parity of counting along γ in a given topological sector is preserved (i.e. the parity is conserved for local dimer moves). But then it is not possible to label the topological sectors by the parity number. This is evident because there are $\mathcal{O}(L)$ topological sectors (for a cylindrical geometry) and just two different parity numbers.

robustness increases exponentially in the system size L_y. (iii) A possible decoher-

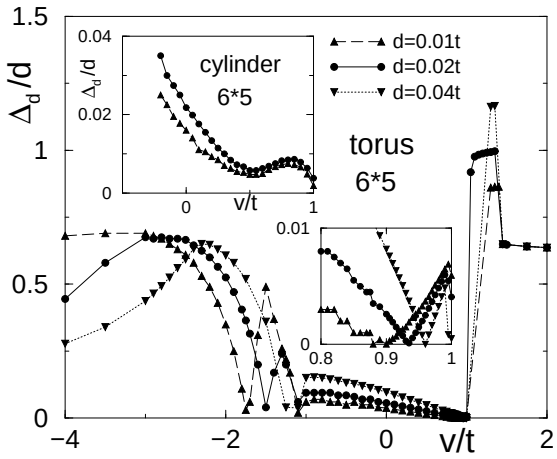

Figure 15.10: Splitting Δ_d of the ground state energies under the action of a disorder potential of strength d. Near $v \approx t$ the disorder splitting for the $6 * 5$ torus is of order 10^{-3} of the disorder energy d.

ence in the relative phase of the two ground states has two different sources. The creation of non-topological excitations in a sector or an adiabatic splitting by an external low-frequency noise. One can eliminate the excitations by setting the operation temperature $T \ll \Delta$. The impact of noise is suppressed for the same reason as the ground-state is robust. (iv) Because an implementation always has finite size they checked if there are low-lying edge states, which would destroy the energy gap in the spectrum. The calculation shows that there are none.
So for a large lattice (i.e. for L_x, L_y large) the system fulfils all requirements to implement topologically protected qubits.
Note that we may also have to consider because of possible higher order dimer flips. Such dimer flips include three or even more dimers on different plaquettes and may destroy the topological order. For any potential implementation this problem has to be analyzed carefully.
Because most of the results on the square and triangular lattice QDM are obtained by numerical calculations it is illustrative to insert here a section about the Kagome lattice. For this model some of the results can be obtained relatively easy.

Quantum Dimer Model on the Kagome lattice

An exactly solvable QDM on the Kagome lattice was introduced by G. Misguich, D. Serban and V. Pasquier [130]. This model offers a very natural and simple framework to illustrate the ideas discussed above. Especially, we will discuss the dimer liquid phase, the topological order, the dimer-dimer correlations, the gap

in the excitation spectrum and the elementary excitations.
Let us first introduce the Kagome lattice. Consider a hexagonal lattice and take the midpoints of the bonds. The Kagome lattice is the lattice of these midpoints[59].
Now let us define the dimer model on the Kagome lattice. For any given hexagon h we define the operator $\sigma^x(h)$ as the sum of all possible kinetic terms involving h only:

$$\sigma^x(h) = \sum_{\alpha=1}^{32} \left\{ |d_\alpha(h)\rangle\langle \bar{d}_\alpha(h)| + H.c. \right\}. \tag{15.11}$$

The sum runs over the 32 loops that enclose a hexagon and around which dimers can be moved. There are 8 inequivalent loops (see Fig. 15.11). The simplest

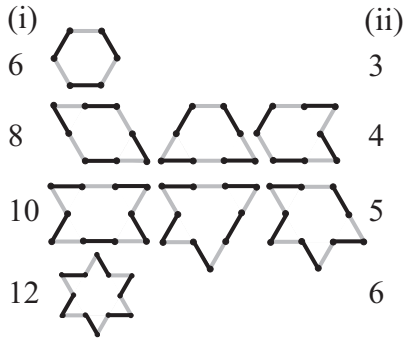

Figure 15.11: Inequivalent loops on the Kagome lattice: (i) loop length (ii) number of dimers involved.

loop is the hexagon itself and it involves 3 dimers. Moves with 4, 5 and 6 dimers are possible as well by including additional triangles to the loop. We find that the loop length has to be even. The largest loop is the star. $|d_\alpha\rangle(h)$ and $|\bar{d}_\alpha\rangle(h)$ are defined as the two ways dimers can be placed along a loop α on a hexagon h. These operators are the kinetic terms, they act like the kinetic terms on the square lattice. Note that for a given dimer covering $|D\rangle$ all kinetic operators but one annihilate $|D\rangle$.
The Hamiltonian for this dimer model introduced in [130] contains only these kinetic terms:

$$\mathcal{H} = -\sum_h \sigma^x(h), \tag{15.12}$$

where the sum runs over all the hexagons h of the lattice[60]. This Hamiltonian is not obviously solvable when written in this form.

[59] In fact all the conclusions in this section can be generalised to any lattice made of corner-sharing triangles.

[60] It is possible to get a similar Hamiltonian with an overlap expansion of the Heisenberg Hamiltonian on the Kagome lattice. But in this picture the kinetic operators $\sigma^x(h)$ have different amplitudes or in a simplification different signs. Including this, the Hamiltonian is

One of the advantages of the Kagome lattice is that there is a correspondence between dimer coverings and arrows sitting on the bonds of the hexagonal lattice. The existence of this arrow representation is a central reason for which the QDM on the Kagome simplifies. This representation was introduced by Elser and Zeng [163] and is illustrated in Fig. 15.12. Each arrow sits on the bonds of a hexagon

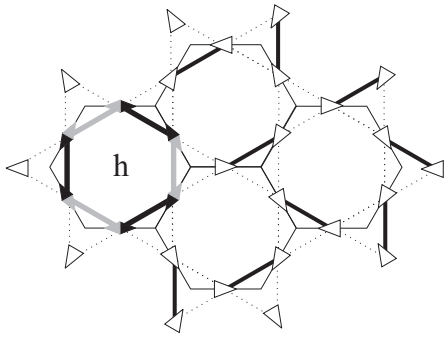

Figure 15.12: Arrow representation on the Kagome lattice.

and has two possible directions: It points toward the interior of one of the two neighbouring triangles. If site i belongs to a dimer (i, j) its arrow must point toward the triangle the site j belongs to. For a triangle without any dimers this rule implies that all arrows are outgoing.
For any given dimer covering it is possible to draw the arrows. Contrariwise a dimer covering can be constructed from any arrow configuration provided that the number of outgoing arrows is one or three (i.e. odd) on every triangle. Hence there is a one-to-one correspondence between the dimer coverings and the arrow configurations that fulfill the constraint above. We can translate the $\sigma^x(h)$-operators into this representation: $\sigma^x(h)$ just flips the 6 arrows sitting on h (see Fig. 15.12). It is easy to see that the $\sigma^x(h)$ conserve the constraint for all triangles. $\sigma^x(h)^2$ flips all arrows twice and thus $\sigma^x(h)^2 = 1$. Furthermore the $\sigma^x(h)$-operators, placed on different hexagons, commute with each other, i.e. $[\sigma^x(h), \sigma^x(h')] = 0$. Note that this is a non-trivial fact in dimer language.
In fact there is even another representation of dimer coverings. Zeng and Elser [163] [164] realised that there is a close correspondence between Ising configurations of pseudospins sitting on hexagons and dimer configurations on the Kagome lattice. The mapping works as follows:
The first step is to take an arbitrary reference dimer configuration $|D_0\rangle$. We can associate to any dimer configuration $|D\rangle$, that lies in the same topological sector as $|D_0\rangle$, a pair of pseudospin configurations $\{\sigma_h^z = \pm 1\}_{h\in\text{hex}}$ in the following way (see Fig. 15.13). (i) Draw the loops of the transition graph of $\langle D_0|D\rangle$. (ii) These loops now divide the areas where the pseudospins are up and where they are

unfortunately not exactly solvable anymore. Note that the Hamiltonian from equation (15.12) is therefore not a good approximation for an antiferromagnetic spin system on a Kagome lattice.

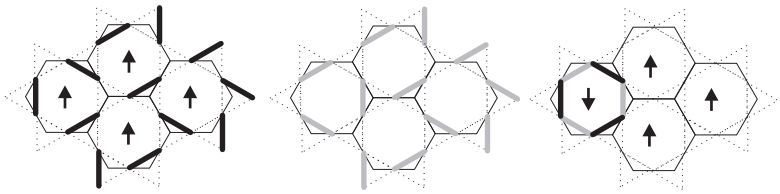

Figure 15.13: Pseudospin representation on the Kagome lattice.

down. Because $|D\rangle$ and $|D_0\rangle$ are in the same topological sector this can be done in a consistent way. (iii) There are two possibilities to assign the pseudospin since there is no natural way to define where is the exterior and interior of a closed loop on a finite sample. Therefore two different pseudospin configurations (related by a global pseudospin flip) represent the same dimer covering. This is a one-to-one correspondence between a dimer covering in a given topological sector and a pair of pseudospin states (with reversed sign). We can proof the uniqueness:
(1) If two dimer coverings $|D\rangle$ and $|D'\rangle$ from the same sector have the same pseudospin state (up to a global sign) they are identical. The transition graph $\langle D|D'\rangle$ is the difference between the transition graphs $\langle D_0|D\rangle$ and $\langle D_0|D'\rangle$. So $\langle D|D'\rangle$ contains the loops that separate the regions where the pseudospins are the same in D and D' and the regions where the pseudospins are different. Because D and D' have the same pseudospin on each hexagon $\langle D|D'\rangle$ contains no loops at all. Therefore D and D' are identical. (2) For any pseudospin state we can associate a corresponding dimer state. For a given reference dimerisation $|D_0\rangle$ the transition graph between the dimer configuration we are looking for and $|D_0\rangle$ will separate hexagons with $\sigma^z = 1$ from hexagons with $\sigma^z = -1$. This path will of course depend on $|D_0\rangle$ but for a fixed $|D_0\rangle$ the path is unique. To see this, consider a single hexagon. Whatever $|D_0\rangle$ is there is only one loop that encircles this hexagon only. We can reconstruct the unique dimer state that corresponds to the pseudospin state by leaving out the part of $|D_0\rangle$ in the transition graph.
The $\sigma^x(h)$-operator just flips the pseudospin sitting on the hexagon h. We can understand this easily:
Consider an arbitrary dimerization $|D\rangle$ and have a look at the hexagon h. All kinetic operators but one annihilate $|D\rangle$ on this hexagon. Applying this operator to $|D\rangle$ gives a state $|D'\rangle$ that differs from $|D\rangle$ only by a single loop around h. In pseudospin language this is exactly the unique state obtained from $|D\rangle$ by flipping the pseudospin at h.
To determine the ground state in a given topological sector we can find that $|\downarrow\rangle = |d_\alpha(h)\rangle + |\bar{d}_\alpha(h)\rangle$ and $|\uparrow\rangle = |d_\alpha(h)\rangle - |\bar{d}_\alpha(h)\rangle$ are the eigenstates of the Hamiltonian on a single plaquette. We can think of a pseudospin in x-direction assigned to these two states. The corresponding energies are 1 for $|\downarrow\rangle$ and -1 for $|\uparrow\rangle$, so the ground state is fully polarized in the pseudopin language in x-direction: $\sigma^x(h) = 1\ \forall h$. If we think of that in the in the σ^z representation, the

ground state the sum of all pseudospin configurations in the σ^z basis. Translated back into dimer language this is nothing but the sum of all dimer coverings in a topological sector; the RK wave-function.
We can derive the dimer-dimer correlations in this state from the arrow representation. If two arrows on two bonds are not on a common triangle they are independent. Therefore dimer-dimer correlations are strictly zero when their corresponding triangles do not touch. So dimers on the Kagome lattice are independent above a finite distance. Because of this absence of long-ranged dimer correlations, the RK state is a dimer liquid and breaks no lattice symmetry. To draw a comparison, on the square lattice the dimer correlation function decays algebraically and on the triangular exponentially. But the correlation always remains finite. Not so on the Kagome lattice, we can say the RK state is a close as possible to a free dimer gas.
We can calculate the whole excitation spectrum too. A said before the $\sigma^x(h)$-operators commute from hexagon to hexagon. $\prod_h \sigma^x(h)$ flips all arrows twice, hence for a setup with periodic boundary conditions and no edges the following constraint has to be fulfilled: $\prod_h \sigma^x(h) = 1$. So the first excited state is not just a single but a pair of flipped hexagons with an energy cost of 4. A $\sigma^x(h) = -1$ hexagon is called a vortex excitation or a vison and excited state consist of two such hexagons a, b with $\sigma^x(a) = -1$ and $\sigma^x(b) = -1$. The excited states are non-local because the flipped hexagons a and b can be arbitrarily far away from each other. We can state the first excited wave-function explicitly. Consider a string going from a hexagon a to a hexagon b (see Fig. 15.14). We define $\Omega(a, b)$ as the operator that measures the parity of the number of dimers crossing that string. $\Omega(a, b)$ commutes with all $\sigma^x(h)$, except for the hexagons a and b at the

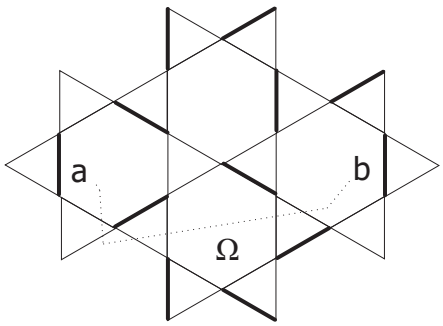

Figure 15.14: Definition of $\Omega(a, b)$.

ends of the string[61]. There we have: $\sigma^x(a)\Omega(a, b) = -\Omega(a, b)\sigma^x(a)$ and analogue for b. Any dimer move changes the sign of $\Omega(a, b)$ if and only if the associated loop crosses the string an odd number of times. So $\Omega(a, b)$ flips $\sigma^x(h)$ in a and b and leaves the rest in the same state[62]. If we apply $\Omega(a, b)$ to the RK wave

[61] Note that we can choose any string going from a to b.
[62] $\Omega(a, b) = \pm\sigma^z(a)\sigma^z(b)$ in the pseudospin language.

function $|0\rangle$ in a given topological sector we get $\Omega(a,b)|0\rangle$ which is still a linear combination of all dimer configurations belonging to that sector. But the amplitudes at hexagons a and b have changed from 1 to -1. $\Omega(a,b)|0\rangle$ is the first excited states of energy 4.

3 Josephson Junctions

The goal of this section is to describe a Josephson junction array. Let's first consider a single junction.
A single Josephson Junction consists of two weakly coupled superconductors. The weak link can be of different types. As an example a thin layer of normal metal between the superconductors. Josephson [165] realised that there is a non-vanishing zero-voltage supercurrent of Cooper pairs through the link between the superconductors. This phenomena is called Josephson effect or Josephson tunneling.
The governing equations for this effect can be derived in many ways. We show here a simply and heuristic derivation first proposed by Feynman [166].
We label the two superconductors with 1 and 2. Now consider a Cooper pair. It can be either in 1 or in 2 and is under the influence of a Hamiltonian $H = H_1 + H_0$, where H_0 is the term that describes the uncoupled system and H_1 is the coupling term. For a weak coupling we can write the wave function of the Cooper pair Ψ as a linear superposition of the two uncoupled states u_1 and u_2. u_1 is the eigenstate of H_0 and E_1 the corresponding energy (analogue for u_2). I.e.

$$H_0 u_{1,2} = E_{1,2} u_{1,2} \tag{15.13}$$

and the time dependent Schroedinger equation reads:

$$i\hbar \frac{\partial \Psi}{\partial t} = H\Psi = (H_0 + H_1)\Psi. \tag{15.14}$$

We take the inner product of the Schroedinger equation with u_2 and use $\Psi = a_1 u_1 + a_2 u_2$:

$$i\hbar \frac{\partial a_1}{\partial t} = E_1 a_1 + a_1 \langle u_1 | H_1 | u_1 \rangle + a_2 \langle u_1 | H_1 | u_2 \rangle. \tag{15.15}$$

We can do the same for u_2 and get:

$$i\hbar \frac{\partial a_2}{\partial t} = E_2 a_2 + a_2 \langle u_2 | H_1 | u_2 \rangle + a_1 \langle u_2 | H_1 | u_1 \rangle. \tag{15.16}$$

The amplitudes a_1 and a_2 are complex numbers and we can therefore write $a_1 = \sqrt{\rho_1}\exp(i\Phi_1)$ and $a_2 = \sqrt{\rho_2}\exp(i\Phi_2)$, where ρ_1 and ρ_2 are the mass density

of Cooper pairs within the superconductors. Φ_1 and Φ_2 are the corresponding phases. We get for the Cooper pair current $I = \dot{\rho_1} = -\dot{\rho_2}$:

$$I = \frac{2H_{12}}{\hbar}\sqrt{\rho_1\rho_2}\sin\left(\Phi_2 - \Phi_1\right) = I_c \sin\Phi, \tag{15.17}$$

where $H_{12} = \langle u_1|H_1|u_2\rangle$, $\Phi = \Phi_2 - \Phi_1$ is the relative phase difference and $I_c = \frac{2H_{12}}{\hbar}\sqrt{\rho_1\rho_2}$ is the critical current. The current of equation (15.17) is the Josephson current that is responsible for the Josephson effect. From the imaginary part of the equations we can get:

$$\Phi(t) = \Phi_0 - \frac{1}{\hbar}\int (E_2' - E_1')dt, \tag{15.18}$$

where Φ_0 is an arbitrary constant and $E_i' = E_i + \langle u_i|H_1|u_i\rangle$. For a macroscopic system $E_2' - E_1'$ is equal to the chemical potential difference $\Delta\mu$ between the two sides. Thus we can write:

$$\frac{d\Phi}{dt} = -\frac{\Delta\mu}{\hbar}. \tag{15.19}$$

Out of the Josephson current we can calculate the coupling free energy F:

$$F = F_0 - E^J \cos\Phi, \tag{15.20}$$

where F_0 is an arbitrary constant and E^J the Josephson coupling energy

$$E^J = \frac{I\Phi_0}{2\pi c}. \tag{15.21}$$

Here $\Phi_0 = \frac{hc}{2e}$ is the flux quantum, h Planck's constant, c the speed of light and e the elementary charge. This energy is a characteristic energy scale for the Josephson effect.
Furthermore, because the probability to find a charge at the edges of the junction is higher than to find one in the middle, there is always a capacitance C associated with the junction. The corresponding Coulomb energy reads:

$$E^C = \frac{(2e)^2}{2C}. \tag{15.22}$$

The next step is to put Josephson junctions together and build a superconducting array. The simplest possible array is the square lattice. To analyze the dynamics of such a system it is useful to calculate the Coulomb energy and its dependence on the differently chosen capacitances. It is illustrative to keep in mind the simple square lattice picture but the generalisation is straightforward.
We can number all the islands and the charge on the i^{th} island is

$$Q_i = C_g V_i + \sum_k C_i^k (V_i - V_{i,k}). \tag{15.23}$$

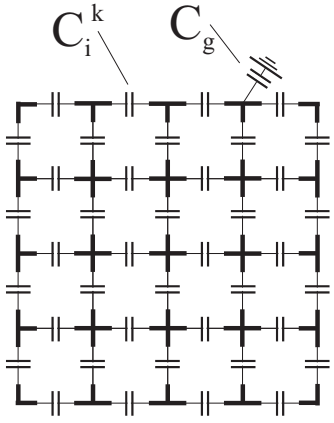

Figure 15.15: Josephson junction square array built from superconducting islands that are coupled through C_i^k and have a ground capacitance of C_g.

Where V_i is the potential the i^{th} island is on, $V_{i,k}$ the potential one of the i^{th} island nearest neighbours is on, C_i^k the capacitance between two neighbouring islands, C_g the ground capacity (which is assumed to be constant for all capacitances) and the sum runs over the nearest neighbours of the i^{th} island. As a next step we can write out the Coulomb energy of the system

$$E = \frac{1}{2}CV^2 = \frac{1}{2}\sum_{ij} V_i C_{ij} V_j = \frac{1}{2}\langle V|C|V\rangle \tag{15.24}$$

and use this as an intrinsic definition for the capacity matrix C_{ij}. So the capacitance matrix for our setup reads:

$$C_{ij} = (C_i^g + \sum_k C_i^k)\delta_{i,j} - \sum_k C_i^k \delta_{j,i+k}. \tag{15.25}$$

The capacitance matrix is regular for nonzero ground capacitance and therefore the inverse of C_{ij} exists. Moreover the matrix is even symmetric: $C = C^T$. Because we do not know the exact potentials all the islands are on we rewrite the energy for the system. For $V = C^{-1}Q$ we get

$$E = \frac{1}{2}\langle Q|C^{-1}|Q\rangle = \frac{1}{2}\sum_{ij} Q_i C_{ij}^{-1} Q_j. \tag{15.26}$$

With this equation we can calculate the Coulomb energy of the lattice in dependence of the charges on the islands. Of course it is in general difficult to find the inverse of the capacitance matrix. For infinite lattices it is useful to transform this calculation into the Fourier space. There analytical calculations can be made [167]. For finite lattices one usually depends on numerical approximations to calculate the inverse.

Until now we are just able to calculate the Coulomb energy of static configurations. To include the tunneling of Cooper pairs from one island to another we have to establish the Bose-Hubbard Model (BHM). A two dimensional BHM is useful to study the effects of interactions between Bosons in a two dimensional lattice. The Hamiltonian looks like:

$$H = H_U + H_T = \sum_{i,j} n_i U_{ij} n_j - \sum_{\langle i,j \rangle} T_{ij}(b_i^\dagger b_j + b_j^\dagger b_i) \tag{15.27}$$

where U contains the Coulomb interaction between the bosons, T_{ij} is the hopping integral, $\langle i,j \rangle$ runs just over the neighbours, $b_i^\dagger$ is the creation operator for a boson at site i, b_i is the annihilation operator for a boson at site i and $n_i = b_i^\dagger b_i$ is the operator that counts the bosons at site i. The operators fulfill the following commutation rules: $[b_i, b_j^\dagger] = \delta_{ij}$, $[b_i, b_j] = 0$ and $[b_i^\dagger, b_j^\dagger] = 0$. Due to the electromagnetic interaction bosons can hop from one site to another. This hopping process is just possible between nearest neighbours and the b-operators exactly represent such dynamics.
For an array of capacitances the U-Term can naturally be identified with the capacitance matrix. The bosons are Cooper pairs in our superconducting lattice (with charge $2e$) and we can insert the Coulomb interaction energy from equation (15.26) into the Hamiltonian. If we understand the $Q_i's$ as operators with $n_i = \frac{Q_i}{2e^2}$ we can write:

$$H_U = \frac{1}{2} \sum_{i,j} 4e^2 n_i C_{ij}^{-1} n_j. \tag{15.28}$$

The T-term is responsible for the hopping of Cooper pairs. Because of the Josephson effect there is a non-vanishing current over every junction and we can understand this as a hopping process. The T-term is therefore proportional to the Josephson coupling energy E^J. Thus our Hamiltonian can be written as:

$$H = H_U + H_T = \frac{1}{2} \sum_{i,j} 4e^2 n_i C_{ij}^{-1} n_j - \sum_{\langle i,j \rangle} E_{ij}^J (b_i^\dagger b_j + b_j^\dagger b_i). \tag{15.29}$$

This Bose-Hubbard Hamiltonian is a good description for a Josephson junction array. Generally one needs to make use of perturbation theory to get some useful results.

4 Implementation

As said before we want to use the triangular lattice QDM for the implementation of topologically protected qubits. We wish to exploit the following features of this model: The topological structure of the Hilbert space and the presence of a liquid ground state with a gap against excitations.
But Ioffe et al. [110] do not use spin systems for the implementation because

there exists no such system which is fully described by a QDM. And even if there would be one, it would still be hard to manipulate the system in a controlled way as it would be necessary for the implementation of qubit operations.
Ioffe and collaborators proposed two different Josephson junction arrays for emulating the quantum dimer liquid state on the triangular lattice; the Josephson junction triangle (JJT) and the Josephson junction Kagome (JJK). The JJT ar-

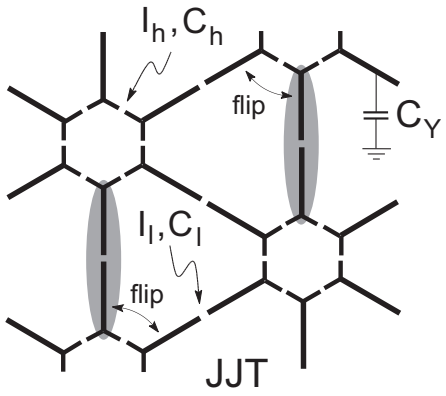

Figure 15.16: Josephson junction triangle (JJT) implementation.

ray is constructed with Y-shaped superconducting islands. One vertex of the triangular lattice consists of six such islands with two ends forming a hexagon and the third end linking to the neighbour hexagons (see Fig. 15.16). All islands are coupled to their neighbours via a capacitance and a Josephson junction. C_Y is the capacitance of the Y-island to the ground, C_h the linking capacity in the hexagon and C_l the capacitance between two adjacent hexagons. I_h is the Josephson current within a hexagon and I_l the current for the linking junction. In sector 2 we derived the corresponding Coulomb energy E^C and the Josephson Coupling energy E^J (see equations (15.22) and (15.21)). We need to find C_Y, C_h and I_l to define the classical dimer states. First we choose C_h to be large for the purpose of joining the hexagons electrically into one vertex. A small capacitance C_Y defines a large charging energy $E_{\text{hex}} \approx \frac{E_Y^C}{6}$ (for C_h large) of a hexagonal vertex. E_{hex} is the basic energy scale of the array and can be calculated by thinking that one vertex (hexagon) is basically nothing more than six capacitances C_Y connected in parallel. We can understand E_{hex} as an approximation for the Coulomb interaction energy between two Cooper pairs sitting on the same hexagon.
The next step is to bias the whole array with a global electric gate to control the number of Cooper pairs in the system. We choose the magnitude of the gate so that there is on average just one Cooper pair for every second vertex. The large charging energy E_{hex} lifts states with two or more Cooper pairs on one hexagon to high energies.
Now, a Cooper pair on a given hexagon can lower its energy via tunneling through the Josephson junction joining two adjacent vertices (involving the I_l coupling).

The bonding state of such a Cooper pair defines the dimer state (valence bond state). Because there is just half a Cooper pair per hexagon, every vertex builds one and only one dimer.
The hopping of dimers comes in due to the vertex junction with small Josephson current $I_h \ll I_l$. The hopping process involves the vertex junction first and proceeds via localisation of one dimer to a vertex (using the I_l Josephson current). Afterwards the located Cooper pair builds a new dimer with another vertex (via the link junction between them). This vertex is now in a virtual state; occupied by the new and the old dimer (i.e. two dimers on one vertex). The large charging energy E_{hex} makes this situation improperly and the old dimer flips in a subsequent hop to another site. This results in the total hopping process predicted from the quantum dimer model on the triangular lattice. The hopping amplitude is of order $t \approx \frac{(E_h^J)^2}{E_l^J}$.
One can furthermore calculate the electrostatic interaction v between parallel dimers by comparing the energy of the staggered and columnar configuration.

The second proposed idea for the implementation is the JJK array. The first

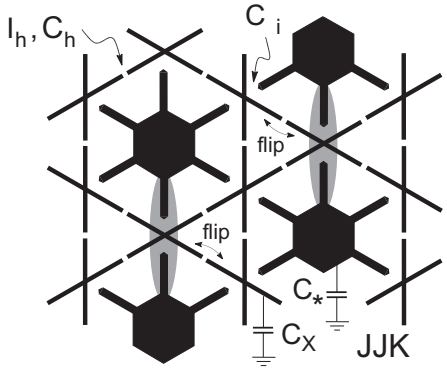

Figure 15.17: Josephson junction Kagome (JJK) implementation.

components are X-shaped islands arranged in a Kagome lattice. They are coupled through capacitances and Josephson junctions with energies E_h^C and E_h^J and their capacitance to the ground is C_X (see Fig. 15.17). A second triangular lattice is laid into the hexagons of the Kagome lattice and consists of star-shaped islands (with ground capacitance C_*). They are capacitively coupled to the six X-islands surrounding each of these star-islands (via C_i). The corresponding Coulomb energy is E_i^C. Note that even we use a Kagome lattice, the QDM implemented in the JJK array is defined on the triangular lattice.
As on the JJT array we introduce a electric gate to bias the Kagome sites to ensure that there is on average just half a Cooper pair for each hexagon. Dimers are defined as Cooper pairs residing on X-islands. To the constraint that no two dimers should touch each other (i.e. two Cooper pairs on the same hexagon

should be forbidden) we need to choose the capacities accordingly.
A small capacitance C_h isolates the hexagons electrically from each other and a large capacitance C_i joins the six X-shaped islands into one island via their strong electric coupling to the star-shaped island in the middle. Next we define the charging energy E_{hex} as the energy required to put two Cooper pairs on the same hexagon. This energy is the basic energy scale of the array and should be large to ensure that there are never two Cooper pairs on the same hexagon ($E_h^J \ll E_{\text{hex}}$). From a perturbative calculation we get $E_{\text{hex}} \approx (\frac{C_i}{C_X})^2 E_*^C$ which shows that E_{hex} is determined by C_X,C_* and C_i. For a good screening on large distances it is furthermore a good idea to choose $C_i < C_*, C_X$. This guarantees that there is no long range interaction between the Cooper pairs.
The dimer dynamics involve the Josephson junction between the X-shaped islands (with energy E_h^J). Due to this coupling one Cooper pair hops to another hexagon which is then double occupied. Because of the large E_{hex} this is just a virtual state and one Cooper pair hops to a further hexagon. This motion of a Cooper pair is the hopping process as predicted from the QDM. Using a perturbative theory we can calculate the the amplitude of this hopping process: $t \approx \frac{(E_h^J)^2}{E_{\text{hex}}}$.
To realise the liquid phase of the QDM we need to satisfy the condition $t \approx v$. It is possible to choose values for the capacitances that this constraint is fulfilled.

We now construct a topologically protected qubit using the Quantum Dimer Model on the triangular lattice with cylindrical boundary conditions. The QDM is emulated in the Josephson junction array as discussed above. The qubit is realised in a ring geometry (see in Fig. 15.18). The reference line γ joins the inner and outer boundary of the array. The qubit states $|e\rangle$ and $|o\rangle$ are defined as the states with odd and even dimer counting parity along the reference line. These two states are the ground states in two distinct topological sectors and are topologically protected. Hence the qubit states are protected too. In order to

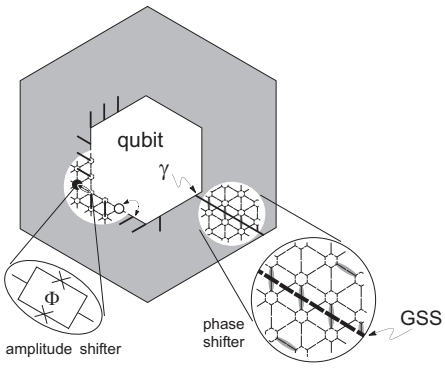

Figure 15.18: Implementation of one qubit and one qubit operations.

manipulate this qubit we need to implement a qubit Hamiltonian. We want to

be able to produce any state of the form:

$$|\alpha, \chi\rangle = \frac{[|e\rangle + \alpha \exp i\chi |o\rangle]}{\sqrt{1+\alpha^2}}, \tag{15.30}$$

i.e. we like to vary the amplitude and the relative phase of the qubit states. The corresponding qubit Hamiltonian reads:

$$H_{\text{qubit}} = h_x \sigma_x + h_z \sigma_z, \tag{15.31}$$

where σ_x and σ_z are the Pauli matrices and h_x, h_y are the parameters that produce the amplitude α and the phase χ from equation (15.30). Thus we need to implement h_x and h_y.

The implementation of h_x requires a mixing of the protected qubit states what results in a reduction of the ground state's topological protection. In the JJT array we place an amplitude shifter at the inner boundary of the ring geometry. This amplitude shifter is a tunable Josephson junction. The tunable junction has a variable Josephson coupling energy $\tilde{E}_l^J$. With an energy cost of $\tilde{E}_l^J$ we can break the dimer over this junction. This creates a virtual particle-hole excitation where one Cooper pair is localised on one hexagon (the particle) and the other hexagon is empty (the hole). While the particle remains at the weak junction the hole is taken around the inner boundary through subsequent dimer flips. After a whole circle the hole is recombined with the particle. Now the qubit state has changed. The amplitude of this process is $h_x \approx E_h^J (\frac{E_h^J}{\tilde{E}_l^J})^M$ where M is the number of links on the inner boundary of the ring. Hence we can change h_x by changing $\tilde{E}_l^J$. On the JJK array the implementation involves a virtual state with two Cooper pairs on one hexagon.

To implement a phase shifter h_y we need to construct a gated superconducting strip (GSS) that lies on the reference line γ, i.e. the GSS joins the inner and outer boundary of the array. The strip should be capacitively coupled to the array and attract dimers onto the reference line γ. When we bias the strip, the energies of the qubit states shifts with respect to another and so does the relative phase χ between the qubit states. The energy u that acts on one dimer due to this process and the duration of this operation τ have to two constraints: (i) $u \approx t \ll E_l^J$ and (ii) $\tau > \frac{\hbar}{\Delta}$. This guarantees that there are no excitations within the dimer liquid. Moreover the fully connected strip represents a global operator and would led to electric fluctuations that would decohere the system. Hence the strip has to break up during idle time. It is possible to construct such a strip out of superconducting Cooper pair transistors [168].

Note that both, the amplitude mixing and the phase shifting are strongly suppressed during idle time. We derived above that amplitude mixing is exponentially small in L_x and phase shifting exponentially small in L_y.

We are now able to implement a single qubit and to manipulate it accordingly.

In order to build a whole quantum computer we need many qubits. We can implement K qubits in a Josephson junction array with K holes (see Fig. 15.19). Around every hole we can visualise the same ring structure from the single qubits. Furthermore we have to implement the qubit Hamiltonian (as in equation (15.31)) for every hole. We can do this in the same way as stated above. The last step is

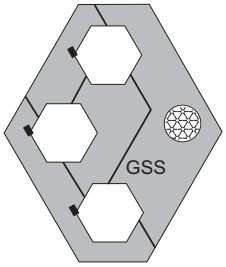

Figure 15.19: Implementation of many qubits and two qubit phase shifters.

the implementation of a two-qubit operation. We use again a GSS, now between two holes that correspond to two qubits. Due to this GSS the phase between the states $|eo\rangle$, $|oe\rangle$ and $|ee\rangle$, $|oo\rangle$ is shifted. With these two qubit phase shifters and the general qubit Hamiltonian for one qubit operations we can construct the controlled-NOT operation [169]. Thus we can perform any n qubit unitary operation [170] and can therefore do all the operations we need for a quantum computer.

5 Conclusions

We introduced the Quantum Dimer Model and showed why it can be used to study disordered spin systems. For the square lattice we were able to describe VBC and found a phase without broken lattice symmetry with an algebraically decaying correlation function, a gapless spectrum and a Hilbert space that splits up into several topological sectors. For the triangular lattice we found VBC and a phase without broken lattice symmetry as well. This phase is realised for a whole range of the parameters, has exponentially decaying correlations (hence is a liquid phase) and a gap in the excitation spectrum. We found that the Hilbert space splits up into four topological sectors on a torus and into two on a cylinder. Moreover we discussed a solvable Quantum Dimer Model on the Kagome lattice and found a liquid phase with finite correlation length and the same topological properties as on the triangular lattice.
Thereafter we explained how to describe Josephson junctions and arrays of Josephson junctions with a generalised Bose-Hubbard Model.
In the next section we reviewed the idea of Ioffe et al. [110] how one can implement a qubit in the triangular lattice Quantum Dimer Model on a cylinder. We showed, if one chooses the two ground states in the two topological sectors

as the two qubit states, that the qubit is topologically protected. In the last point we described how one can build a quantum simulator for the triangular lattice Quantum Dimer Model in its liquid phase in a Josephson junction array and discussed its properties concerning an actual physical implementation.

16 Braid group statistics in quantum mechanics

Klaus Jäger
Supervisor: Walid Abou Salem

We will discuss the configuration spaces of identical particles in different dimensions n. In $n \geq 3$ we will show that there are bosons and fermions only. The situation is totally different in two dimensions, where a continuum of states interpolating the bosonic and the fermionic cases arises. These states are called anyons. We will discuss braid groups as fundamental groups of two-dimensional systems. In the end, we will discuss the cyon system and will give a short introduction into the Chern-Simons theory.

1 Introduction

In this chapter, we will give a short introduction to Abelian braid group statistics, which arise in the context of identical particles in two dimensions.

At the beginning of section 2, we will find the correct configuration manifolds of systems of many identical particles. To understand them better, we will discuss two-particle systems in detail. We will find that the two-two-dimensional case is different from higher dimensional cases [171].

In section 3, we will quantize identical two-particle systems. We will find, that in two dimensions a continuous range of statistics can exist, connecting the bosonic and fermionic cases. Furthermore we will derive in a canonical way that in three and more dimensions only bosons and fermions can exist [171].

In section 4 we will introduce the braid group, the fundamental group of the configuration spaces in two dimensions. We will investigate it and will derive its connection with the statistics [172].

Finally in section 5, we will discuss anyons in a magnetic flux tube, called the cyon system. Afterwards we will give a very short introduction into the Chern-Simons formalism and show, how it is connected with fractional statistics. We can only scratch on the surface of the beautiful issue of the Chern-Simons theory [172].

2 Identical Particles and their configuration spaces

Configuration spaces of systems of many identical particles

We denote the regular coordinate space of a one-particle system by X and we assume N identical particles to be moving in this space. Usually the configuration space of this system is described by X^N, the Cartesian product of N one-particle spaces.

Since the particles are identical, no distinction can be made between points in X^N that differ only in the ordering of the particle coordinates. Thus the two points

$$\begin{cases} \mathbf{x} = (\mathbf{x_1}, ...\mathbf{x_N}) \\ \mathbf{x'} = p(\mathbf{x}) = (\mathbf{x_{p^{-1}(1)}}, ..., \mathbf{x_{p^{-1}(N)}}), \end{cases} \tag{16.1}$$

where p is a permutation of the coordinates, both describe the same physical configuration of the system and therefore must be identified. X^N does not describe our physical configuration. The true configuration manifold is X^N/S_N, where the permutation group S_N is divided out of X^N. This space identifies points which represent the same configuration of the physical system and therefore describes our system well.

X^N/S_N is locally isomorphic to X^N, except at its singular points, where two or more particles coincide in position. The difference between the manifolds lies in their global properties. X^N has only regular points, whereas the singularities give a topological structure to X^N/S_N.

In our discussion we suppose our particles to be hard core, i.e. two or more particles cannot occupy the same position at the same time. Topologically, this means, that we exclude the singular points from the configuration manifold. The excluded points can be written as a generalized diagonal

$$\Delta = \{(\mathbf{x}_1, ..., \mathbf{x}_N) \in X^N | \mathbf{x}_i = \mathbf{x}_j, i \neq j\}. \tag{16.2}$$

Hence, the configuration manifold for a system of N indistinguishable particles in n dimensions is given by

$$\mathcal{M}^{\mathbf{n}}_{\mathbf{N}} = (\mathbf{X^N} - \mathbf{\Delta})/\mathbf{S_N}. \tag{16.3}$$

In the following, we suppose the one particle space X to be the n-dimensional Euclidian manifold $\mathcal{E}^n$ ($\mathcal{E}^n \equiv \mathbb{R}^n$). We can introduce center of mass (c.m.) coor-

dinates

$$\mathbf{X} = \frac{1}{N}\sum_{i=1}^{N}\mathbf{x}_i, \tag{16.4}$$

where $\mathbf{x}_i \in \mathcal{E}^n$ are the coordinates of the i^{th} particle. Now, the configuration manifold of a classical system of N identical hard-core particles can be written as a Cartesian product,

$$\mathcal{M}_N^n = \mathcal{E}^n \times r_N^n \tag{16.5}$$

where $\mathcal{E}^n$ is the c. m. space and r_N^n is a *relative space*, describing the relative motions of the particles. It has got $nN - n$ degrees of freedom.

Configuration spaces of two-particle systems

The relative space r_2^n is the result of identifying $\mathbf{x} = \mathbf{x_1} - \mathbf{x_2}$ with $-\mathbf{x} = \mathbf{x_2} - \mathbf{x_1}$ in $\mathcal{E}^n$. It has one singular point at $\mathbf{x} = 0$, corresponding to a coincidence of the position of the two particles. As the singularity is excluded from $\mathcal{M}_N^n$, the relative space r_2^n can be written as the Cartesian product

$$r_2^n = (0, \infty) \times \mathbb{R}P^{n-1}. \tag{16.6}$$

It consists of the positive real line $(0, \infty)$, giving the length $|\mathbf{x}|$ of a vector $\mathbf{x}$ in $\mathcal{E}^n$, and the real projective space $\mathbb{R}P^{n-1}$. At this point we need to explain some mathematical terms and definitions:

Definition 1. The **Real Projective Space** $\mathbb{R}P^{n-1}$ is the set of lines $p \subset \mathbb{R}^n$ through 0. Its dimension is $\dim \mathbb{R}P^{n-1} = n - 1$ [14].

One can describe the projective space in the following way:

$$\mathbb{R}P^{n-1} = (\mathbb{R}^n - \{0\})/\mathbb{R}^*, \tag{16.7}$$

where $\mathbb{R}^*$ denotes the set $\mathbb{R} - \{0\}$. The elements of $\mathbb{R}P^{n-1}$ are equivalence classes of vectors $\mathbf{v} \neq 0$ in $\mathbb{R}$ under the relation $\mathbf{v} \sim \lambda\mathbf{v}$, $\lambda \in \mathbb{R}^*$. One can visualize $\mathbb{R}P^{n-1}$ as the $n-1$ dimensional sphere S^{n-1} with antipodal points identified.

Definition 2. Two paths $q : [0,1] \to \mathcal{M}$ and q' in a manifold $\mathcal{M}$ are called **homotopic**, if there exists a continuous function $H : [0,1] \times [0,1] \to \mathcal{M}$, such that $H(0,[0,1]) \equiv q([0,1])$ and $H(1,[0,1]) \equiv q'([0,1])$.

If $q(0) = q(1)$, the path is called *closed path* or *loop*. All loops in $\mathcal{M}$ that are homotopic form a class.

Definition 3. The group generated by all equivalence classes of loops in $\mathcal{M}$, is called the **first homotopy group** or **fundamental group** $\pi_1(\mathcal{M})$.

Example 1. In $\mathbb{R}^n$, all loops can be deformed into each other, therefore the fundamental group contains only one element, i.e. it is trivial what we write as

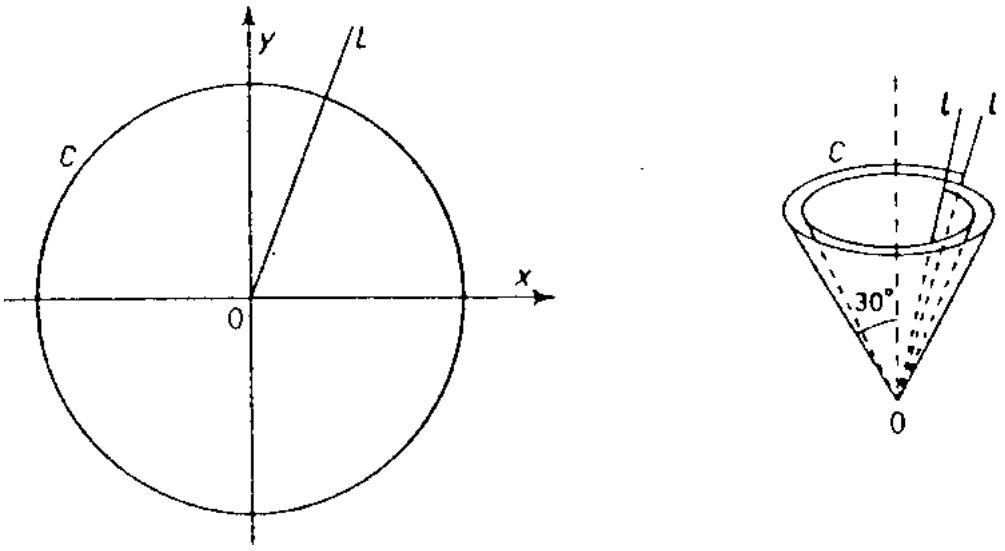

Figure 16.1: The relative space r_2^2 of two two-dimensional particles is the plane with pairs of opposite points $\mathbf{x}$ and $-\mathbf{x}$ identified. The identification may be effected by cutting the plane along a line l from the origin 0 and then folding it into a circular cone.

$\pi_1(\mathbb{R}^n) \simeq \{1\}$. The same is true on the n-dimensional sphere S^n, $n > 1$. All loops can be continuously deformed into each other, $\pi_1(S^n) \simeq \{1\}$.

On S^1 this is not true: If a path encircles S^1 twice, it cannot be continuously deformed into a path that encircles S^1 four times, for example. It is also important, into which direction one walks. So the fundamental group of S^1 is isomorphic to the set of integers with the addition as group action, $\pi_1(S^1) \simeq \{(\mathbb{Z}, +)\}$.

Example 2. $\mathbb{R}P^0$ is a point and has no more structure. $\mathbb{R}P^1$ is a circle, its fundamental group is $\pi_1(\mathbb{R}P^1) \simeq \mathbb{Z}$. It is countably infinite, as we have seen above. For $n > 2$, $\pi_1(\mathbb{R}P^{n-1}) \simeq \mathbb{Z}/2\mathbb{Z}$ and has got two elements. It is often written as $\mathbb{Z}_2$. We will take a closer look at these properties later.

At this point, one can see the essential differences among one-, two- and three- or higher-dimensional Euclidian spaces for the first time. Now we will take a closer look at $\mathcal{M}_2^n$ in different dimensions:

Two identical particles in two dimensions

The configuration manifold of two identical particles moving in $\mathcal{E}^2$ is

$$\mathcal{M}_2^2 = \mathcal{E}^2 \times r_2^2. \tag{16.8}$$

The relative space r_2^2 is the plane $\mathcal{E}^2 - 0$ with the points $\mathbf{x}$ and $-\mathbf{x}$ identified. This manifold can be seen as a circular cone as we see in figure 16.1.

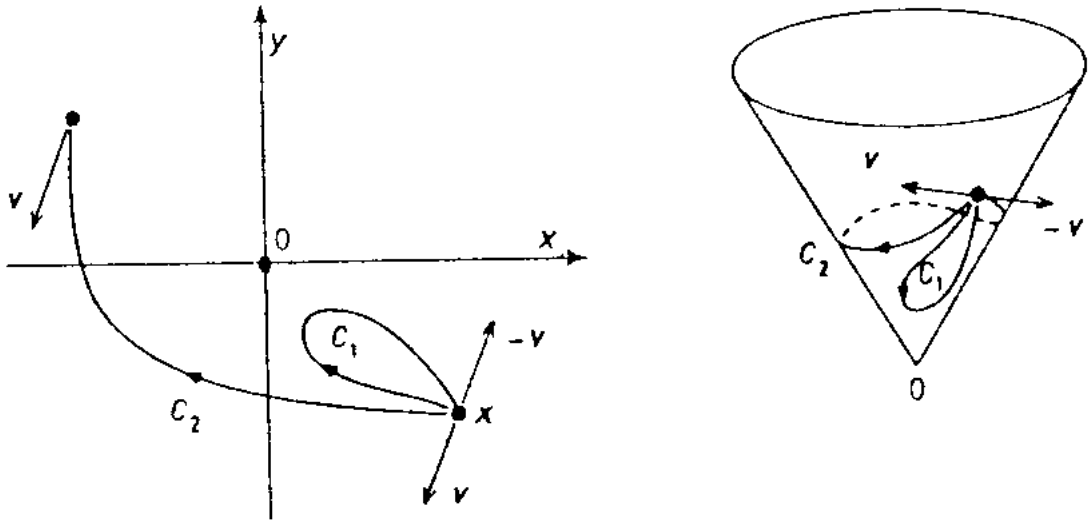

Figure 16.2: The parallel transport of a tangent vector $\mathbf{v}$ around two different closed curves on the cone.

A cone is globally curved, although it is locally flat everywhere except at the singular vertex. Now we watch the parallel transport of a tangent vector. For this we may map back onto the plane. The mapping is isometric (by definition), and parallel transport on the cone becomes the familiar parallel transport in the plane. Note, that a tangent vector $\mathbf{v}$ at the point $x \in \mathcal{E}^2$ is identified with the vector $-\mathbf{v}$ at $-x$. We see in figure 16.2 that the parallel transport around a closed curve on the cone r_2^2 changes $\mathbf{v}$ into $(-1)^m\mathbf{v}$, $m \in \mathbb{Z}$ being the number of revolutions or winding number of the curve around the vertex.

More generally speaking, we see, that in n dimensions, $n \in \mathbb{N}$, there are two classes of equivalent closed curves with respect to the transport of a tangent vector $\mathbf{v}$ in the relative space r_2^2. One class does not change $\mathbf{v}$, while the other class changes $\mathbf{v}$ into $-\mathbf{v}$. A closed curve of the first class connects a point $(x^1, x^2) \in \mathcal{E}^{2n}$ continuously with itself, while a closed curve of the second class connects (x^1, x^2) continuously with (x^2, x^1) in $\mathcal{E}^{2n}$.

Two identical particles in three dimensions

The physically most interesting case is of course $X = \mathcal{E}^3$. We have already seen that $r_2^3 = (0, \infty) \times \mathbb{R}P^2$, where $\mathbb{R}P^2$ is the two-dimensional real projective space. One can get it by identifying antipodal points on the two-dimensional sphere S^2. We get a visualization of $\mathbb{R}P^2$ by dropping the southern hemisphere of S^2 and identifying antipodal points on the equator (figure 16.3).

A tangent vector $\mathbf{v} \in r_2^3$ is changed into $-\mathbf{v}$ by the parallel transport of a closed curve q_2, which is a closed curve in $\mathbb{R}P^2$ connecting opposite points on

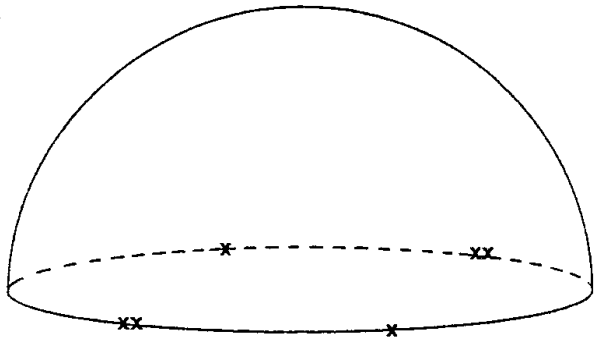

Figure 16.3: The real projective space $\mathbb{R}P^2$ can be represented as the northern hemisphere with opposite points on the equator being identified.

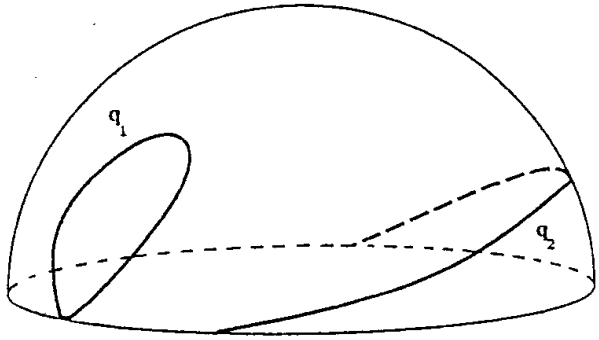

Figure 16.4: Examples of a contractible (q_1) and a non-contractible (q_2) loop on $\mathbb{R}P^2$.

the sphere. Such a curve encircles the singular point $x = 0$ once. If a closed curve q_1 encircles the singularity twice, it can be be continuously contracted to a point without having to pass through the singularity, as we see in figure 16.4. This is a completely different picture as in the two-dimensional case, where loops with different winding numbers can never be continuously deformed into each other. Now we also understand why the fundamental group of $\mathbb{R}P^{n-1}$, $n > 2$ has got only two elements, i.e. $\pi_1(\mathbb{R}P^{n-1}) \simeq \mathbb{Z}_2$, whereas it is countably infinite for $n = 2$.

3 Quantization of two-particle systems

How can we quantize two-particle systems? The configuration space of the identical particles is locally isometric to that of two nonidentical particles, except at the singularity. The difference in global topology of the two systems does not show up, unless we study a situation where the particles may physically inter-

change positions in the course of time evolution. For particles being far apart, it is of no importance whether they are identical or not.

On the other hand, there is no obvious way to quantize a theory with a curved configuration space, which even has singularities. We will try to follow the simplest way, trying not to impose unnecessary restrictions on the theory. We follow the Schrödinger quantization scheme and assume, that the state of the system is given by a quadratically integrable function defined on the configuration space. The problem is to define the free Hamiltonian, by taking properly care of the physical effects of the singular points. As usual, an interaction between particles will be described by adding a potential to the free particle Hamiltonian.

In two and more dimensions, the configuration manifold $\mathcal{M}_2^n$ is not flat, even if all singular points are excluded. The presence of singularities is revealed through a global curvature, which we studied in the section before in terms of the parallel transport of tangent vectors around closed curves. In a similar way we introduce the concept of parallel displacement of state vectors.

First, we introduce for each point $\mathbf{x}$ in the configuration manifold a corresponding, one dimensional Hilbert space h_x, called a fiber. We assume the state of the system to be described by a continuum of vectors $\mathbf{\Psi}(\mathbf{x}) \in h_x$. $\mathbf{\Psi}$ is assumed to be a single-valued function over the configuration manifold, whose function value $\mathbf{\Psi}(\mathbf{x})$ at the point $\mathbf{x}$ is a vector in h_x. If a normed basis vector χ_x is introduced for each space h_x, then the complex-valued wave function $\psi(\mathbf{x})$ is just the coordinate of the vector $\mathbf{\Psi}(\mathbf{x})$ relative to that basis:

$$\mathbf{\Psi}(\mathbf{x}) = \psi(\mathbf{x})\chi_x. \tag{16.9}$$

It is clear that the function $\psi(\mathbf{x})$ will depend on the set of basis vectors, or gauge $\{\chi_x\}$. A change in this set causes a gauge transformation:

$$\chi_x \to \chi'_x = e^{-i\phi(\mathbf{x})}\chi_x \tag{16.10}$$

$$\psi(\mathbf{x}) \to \psi'(\mathbf{x}) = e^{i\phi(\mathbf{x})}\psi(\mathbf{x}) \tag{16.11}$$

In order to define a gauge-invariant derivative of the functions $\psi(\mathbf{x})$ we need the concept of parallel displacement. Let us denote the linear operator which transports the vectors of h_x into $h_{x'}$ parallelly by $P(\mathbf{x}', \mathbf{x})$. The transport is along a continuous curve joining $\mathbf{x}$ to $\mathbf{x}'$. The parallel displacement in general may depend on the curve, but we assume that the infinitesimal parallel displacement $P(\mathbf{x} + d\mathbf{x}, \mathbf{x})$ is uniquely defined. $P(\mathbf{x}', \mathbf{x})$ is assumed to be always a unitary operator. Finally we assume that it is possible, at least locally, to choose the gauge $\{\chi_{\mathbf{x}}\}$ in such a way that the rule of infinitesimal parallel displacement is of the form

$$P(\mathbf{x} + d\mathbf{x}, \mathbf{x})\chi_{\mathbf{x}} = \left(1 + i\, dx^k b_k(\mathbf{x})\right) \chi_{\mathbf{x}+\mathbf{dx}}. \tag{16.12}$$

The covariant derivative is

$$\nabla_k = \frac{\partial}{\partial x^k} - ib_k(\mathbf{x}). \tag{16.13}$$

The functions b_k are determined partly by the dynamics of the systems and partly by the choice of the gauge $\{\chi_{\mathbf{x}}\}$. To make $P(\mathbf{x} + d\mathbf{x}, \mathbf{x})$ unitary, they must be real valued. The noncommutativity of the components of the covariant derivative is measured by the gauge-invariant quantity

$$f_{kl} = i[\nabla_k, \nabla_l] = \frac{\partial b_l}{\partial x_k} - \frac{\partial b_k}{\partial x_l}. \tag{16.14}$$

In the case of parallel transport of tangent vectors, it corresponds to the curvature tensor.

In the quantum theory of a charged particle in a magnetic field, we can find a similar formulation, introduced by Weyl. The force field corresponds to the antisymmetric tensor f_{kl}, the vector potential to $b_k(\mathbf{x})$.

In the present case we do not want f_{kl} to describe a force field. Therefore we assume that $f_{kl}(\mathbf{x}) = 0$ for all $\mathbf{x}$ except at the singular points of the configuration manifold, where f_{kl} is undefined. It follows, that a vector $\mathbf{\Psi} \in h_x$ will be unchanged by the parallel transport around any closed curve not encircling the singularity. If $\mathbf{\Psi}$ is parallely transported around the singularity m times, it will be transformed into $(P_x)^m\mathbf{\Psi}$, where P_x is a linear, unitary operator acting on h_x. Since the Hilbert space is one-dimensional, P_x is just a phase factor,

$$P_x = e^{i\nu\pi}, \tag{16.15}$$

where $\nu \in (\mathbb{R} \mod 2)$. P_x transforms like

$$P_{x'} = P(\mathbf{x}', \mathbf{x}) P_x P(\mathbf{x}', \mathbf{x})^{-1} = e^{i\nu\pi}. \tag{16.16}$$

Therefore, the parameter ν must be independent of the position $\mathbf{x}$, thus it is a *characteristic value of the given two-particle system.*

We call ν the statistics of the system. As we will see below, it describes the many body nature of the system. A system is bosonic or fermionic for $\nu = 0$ or $\nu = 1$ respectively. In two dimensions intermediate states exist, which we call *anyons.*

The field $b_k(\mathbf{x})$ has a dynamical effect through the gauge-invariant differentiation operator ∇_k. In the case we are considering, b_k can be transformed into zero by choosing the basis vectors χ_x in a particular way. When the basis vector χ_x is given at some arbitrary point $\mathbf{x}$, then we define the basis vectors for all other points by parallel displacement of this χ_x. When f_{kl} vanishes, this procedure defines a gauge where b_k vanishes. On the other hand, the complex wave function $\psi(\mathbf{x})$ will be multivalued in this gauge, since all the basis vectors χ_x, $e^{\pm i\nu\pi}\chi_x$,

$e^{\pm 2i\nu\pi}\chi_x$, etc. are generated by parallel transport of χ_x around different closed curves.

We see now that we have managed to transfer the dynamical effect of the singularities from the differentiation operator, and therefore from the Hamiltonian, to the multivalued character of the wave function $\psi(\mathbf{x})$.

In one dimension the topology is trivial. For a solution of two particles moving in one dimension, the interested reader may refer to [171], p. 11f.

An example in two dimensions

To discuss the two-dimensional case, we investigate **two anyons in a harmonic well** [171], p. 15f and [173] p. 958.

The Hamiltonian of two anyons in an harmonic well is given by

$$H = -\frac{\hbar^2}{2m}\left(\frac{\partial^2}{\partial \mathbf{x}_1^2} + \frac{\partial^2}{\partial \mathbf{x}_2^2}\right) + \frac{1}{2}m\omega^2(\mathbf{x}_1^2 + \mathbf{x}_2^2) \tag{16.17}$$

where $\mathbf{x}_1$ and $\mathbf{x}_2$ are the coordinates of the anyons. When we write the Hamiltonian in terms of the center of mass coordinates $\mathbf{X}$ and relative coordinates $\mathbf{x}$, it becomes

$$H = \left(-\frac{\hbar^2}{4m}\frac{\partial^2}{\partial \mathbf{X}^2} + m\omega^2\mathbf{X}^2\right) + \left(-\frac{\hbar^2}{m}\frac{\partial^2}{\partial \mathbf{x}^2} + \frac{1}{4}m\omega^2\mathbf{x}^2\right) \tag{16.18}$$

We observe that the center of mass part and the relative part completely split off and therefore can be treated separately. As the center of mass space is topologically trivial, the motion of the center of mass is the usual harmonic oscillator in two dimensions. The eigenfunctions should be quadratically integrable and nonsingular at the origin. This problem can be solved as in [174], p. 102 ff.

For the discussion of the relative motion, we introduce polar coordinates r and ϕ. The relative space is topologically nontrivial because of the singularity. As we have seen above, the wavefunction obtains an additional phase when the two particles are interchanged:

$$\psi(r, \phi + 2\pi) = e^{i\nu\pi}\psi(r, \phi). \tag{16.19}$$

There is no obvious reason to restrict ν to the bosonic and fermionic cases only. Therefore, we get a continuum of intermediate cases connecting those two. With the gauge transformation

$$\psi(r, \phi) \to \psi'(r, \phi) = e^{-i\frac{\nu}{2}\phi}\psi(r, \phi) \tag{16.20}$$

we find

$$\psi'(r, \phi + 2\pi) = \psi'(r, \phi). \tag{16.21}$$

We can solve the problem, where the wave function behaves as in (16.21) in the usual way. With the transformed Hamiltonian

$$H' = e^{-i\frac{\nu}{2}\phi} H e^{i\frac{\nu}{2}\phi} = -\frac{\hbar^2}{m}\left(\frac{\partial^2}{\partial r^2} + \frac{1}{r}\frac{\partial}{\partial r} + \frac{4}{r^2}\left(\frac{\partial}{\partial \phi} + i\frac{\nu}{2}\right)^2\right) + \frac{1}{4}m\omega^2 r^2 \quad (16.22)$$

the Schrödinger equation for the relative motion becomes

$$E\psi' = H'\psi'. \quad (16.23)$$

We can split off the angular motion by choosing the eigenfunctions as

$$\psi'(r,\phi) = e^{il\phi} R(r), \quad (16.24)$$

where l is an integer. The radial function is then determined by the equation

$$\left(\frac{d^2}{dr^2} + \frac{1}{r}\frac{d}{dr} - \frac{4}{r^2}\left(l + \frac{\nu}{2}\right)^2 - \frac{1}{4}\frac{m^2\omega^2}{\hbar^2}r^2 + \frac{mE}{\hbar^2}\right) R = 0. \quad (16.25)$$

Apart from the values of $l + \nu/2$, this is the ordinary radial equation of the harmonic oscillator in two dimensions which can be solved as above. We find the allowed energies to be

$$E_{n,l} = 2\hbar\omega\left(n + \left|l + \frac{\nu}{2}\right| + \frac{1}{2}\right) \quad (16.26)$$

where $n \in \mathbb{N}$. We see that the value ν influences the energy spectrum of the system. An example is shown in figure 16.5.

The three-dimensional case

We have seen before that a closed curve encircling the singularity twice can be continuously contracted to a point without passing through the singularity. This implies for the operator P_x the additional condition

$$P_x^2 = 1. \quad (16.27)$$

Therefore, $P_x = \pm 1$, and the statistics ν can only take the values 0 and 1. This means, that there can only be fermions and bosons in higher dimensions.

4 Artin's braid groups

So far we have discussed only the cases with two particles. Now we will talk about systems with more than two particles. As we have seen before, the configuration manifold of an Euclidian system of N particles in n dimensions is given by

$$\mathcal{M}_N^n = (\mathcal{E}^{nN} - \Delta)/S_N. \quad (16.28)$$

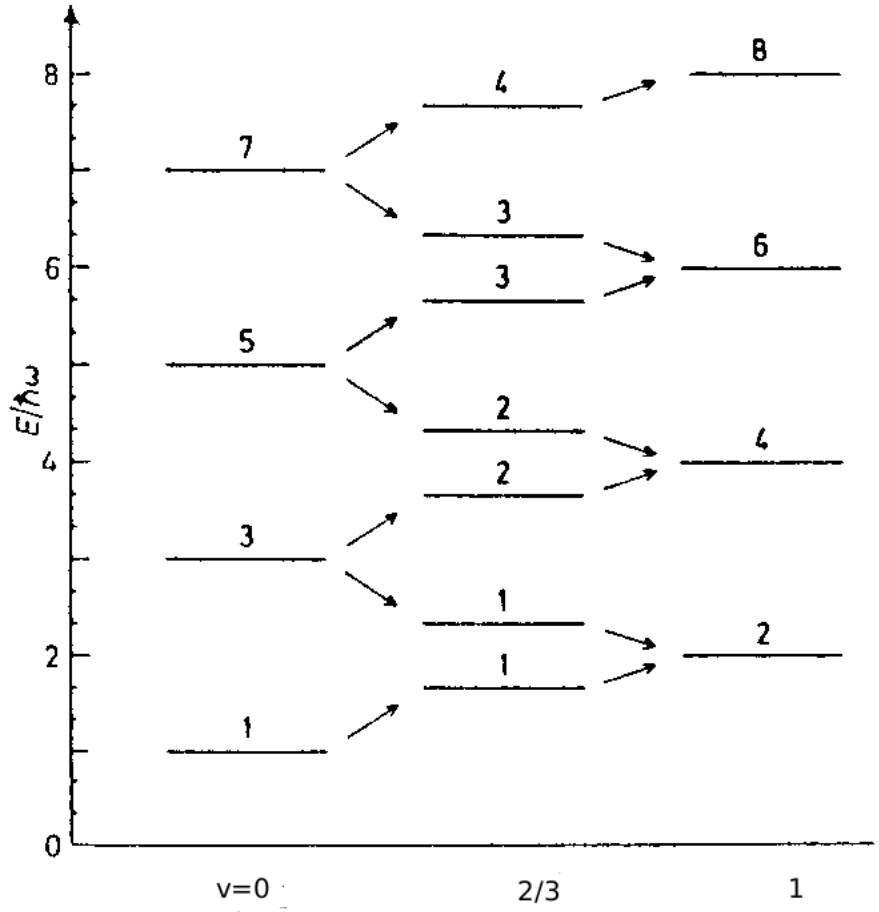

Figure 16.5: The energy spectrum of the relative motion of two anyons in an harmonic well. It is shown for three different statistics, namely the bosonic $\nu = 0$, the fermionic $\nu = 1$ and an intermediate case $\nu = \frac{2}{3}$. The degeneracies of each level are given in the figure.

The calculation of the fundamental groups of manifolds like $\mathcal{M}_N^n$ in different dimensions n is an important topic of algebraic topology. It was solved in the early 1960's [175].

Theorem 1. Let $\mathcal{M}_N^n = (\mathcal{E}^{nN} - \Delta)/S_N$ be the configuration manifold of a system of N particles in n dimensions. Then the fundamental groups of this manifold are

$$\pi_1(\mathcal{M}_N^1) \simeq \{1\}, \tag{16.29}$$
$$\pi_1(\mathcal{M}_N^2) \simeq B_N, \tag{16.30}$$
$$\pi_1(\mathcal{M}_N^{\geq 3}) \simeq S_N, \tag{16.31}$$

where B_N is the braid group of N strands (to be defined later) and S_N is the permutation group.

The result for $n \geq 3$ is the result we expected. The bosonic case is described via totally symmetric one-dimensional representations of the permutation group S_N. The fermionic case is described by totally antisymmetric one-dimensional representations of S_N. We observe that $S_2 \simeq \mathbb{Z}_2$.

The two-dimensional case is totally different from the higher-dimensional case. The fundamental group here is *Artin's braid group* of N strands.

Definition 4. The braid group of N strands, B_N, is an infinite non-Abelian group. It is generated by $N-1$ elementary moves σ_i, satisfying the following properties:

$$\sigma_i \sigma_{i+1} \sigma_i = \sigma_{i+1} \sigma_i \sigma_{i+1} \tag{16.32}$$

for $i = 1, ..., N-2$ and

$$\sigma_i \sigma_j = \sigma_j \sigma_i \tag{16.33}$$

for $|i-j| \geq 2$. The inverse element of σ_i is denoted by σ_i^{-1}, the identity by $\mathbf{1}$.

The elementary moves are best described by a pictorial representation as follows: Given N vertical strands, the generator σ_i acts on them by simply braiding the i^{th} strand around the $(i+1)^{th}$ in a definite way as shown on the left hand side of figure 16.6. On the right hand side we see the move σ_i^{-1}, undoing σ_i. One easily sees, that $B_2 \simeq \mathbb{Z}$.

A generic braid is a word in the generators σ_i and their inverses σ_i^{-1}, which can be arranged using the relations (16.32) and (16.33). The usual convention is that generators on the right act first.

In general $\sigma_i^2 \neq \mathbf{1}$. If $\sigma_i^2 = \mathbf{1}$ for all i, then the braid group reduces simply to the permutation group S_N. Now we will look at an example.

Example 3. We assume a system of three identical particles. At the time t the configuration is the one displayed on the left hand side of figure 16.7. We can describe it by listing the azimuthal angles of all possible pairs of particles measured

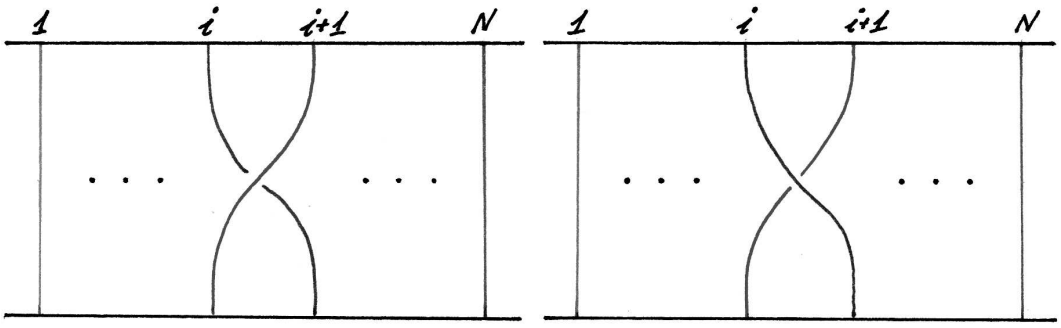

Figure 16.6: Pictorial representation of the elementary moves σ_i and σ_i^{-1} respectively.

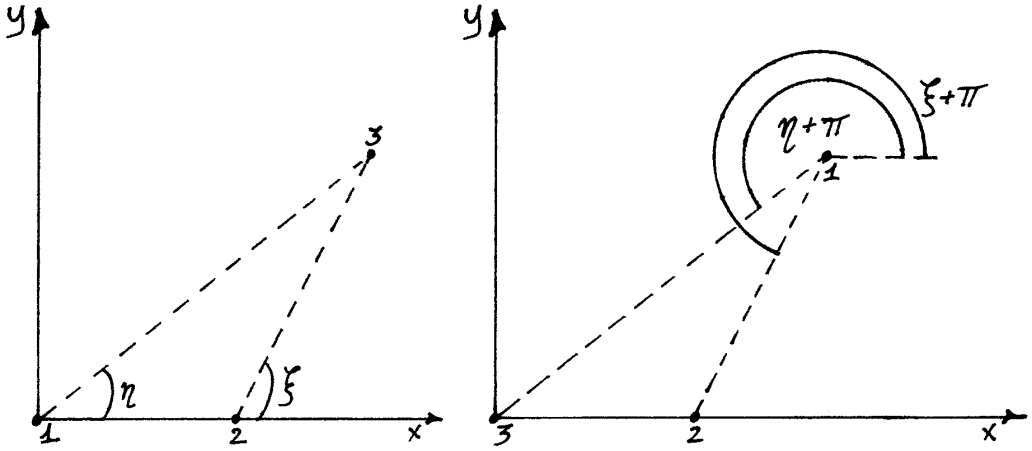

Figure 16.7: Configuration of the three identical particles at times t and t'.

with respect to some arbitrary axes. In our case the angles are

$$\varphi_{12}(t) = 0, \tag{16.34}$$
$$\varphi_{13}(t) = \eta, \tag{16.35}$$
$$\varphi_{23}(t) = \xi, \tag{16.36}$$

where

$$\varphi_{ij} = \arctan\left(\frac{y_j - y_i}{x_j - x_i}\right). \tag{16.37}$$

At a certain time t' the particles should reach the positions shown on the right hand side of figure 16.7. Now, the winding angles are

$$\varphi_{12}(t') = \xi + \pi, \tag{16.38}$$
$$\varphi_{13}(t') = \eta + \pi, \tag{16.39}$$
$$\varphi_{23}(t') = \pi. \tag{16.40}$$

Because of the indistinguishability the positions at times t and t' are in fact the same, even if the particles 1 and 3 have been interchanged. We notice that $\varphi_{ij}(t') - \varphi_{ij}(t)$ is not in general an integer multiple of π. However, the relation

$$\sum_{i<j} \varphi_{ij}(t') - \sum_{i<j} \varphi_{ij}(t) = n\pi \tag{16.41}$$

is always true, where n is an integer, in our example $n = 3$. The evolution from t to t' can be seen as the braiding $\sigma_1\sigma_2\sigma_1$ as shown in figure 16.8. The strands are non intersecting world lines in $[0,1] \times \mathbb{R}^2$ as described in [176], chapter 8.1.

Before we go on, we repeat some facts about path integrals. According to the standard path-integral formulation of quantum mechanics, the amplitude for a two dimensional system which evolves from the configuration q at time t to the configuration q' at time t' is given by the Kernel

$$K(q',t';q,t) = \langle q',t'|q,t\rangle = \int_{q(t)=q}^{q(t')=q'} \mathcal{D}q\, e^{\frac{i}{\hbar}\int_t^{t'} d\tau \mathcal{L}[q(\tau),\dot{q}(\tau)]} \tag{16.42}$$

where $\mathcal{L}(q,\dot{q})$ is the Langrangian of the N-particle system. The symbol $\int_{q(t)=q}^{q(t')=q'} \mathcal{D}q$ denotes the sum over all paths connecting q at time t with q' at time t'. The Kernel $K(q',t';q,t)$ evolves the single-valued wave-function $\psi(q,t)$ according to

$$\psi(q',t') = \int_{\mathcal{M}_N^2} dq\ \langle q',t'|q,t\rangle\, \langle q,t|\psi\rangle \tag{16.43}$$
$$= \int_{\mathcal{M}_N^2} dq\, K(q',t';q,t)\psi(q,t). \tag{16.44}$$

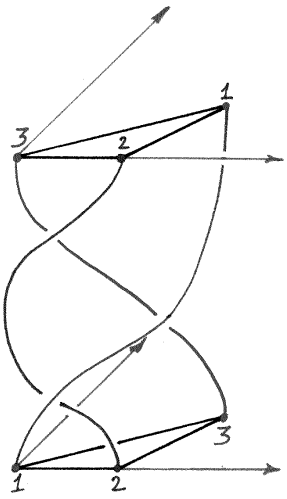

Figure 16.8: The interchange of the particles 1 and 3, seen as braiding $\sigma_1\sigma_2\sigma_1$.

Now, we set $q' = q$ and hence describe loops. As all homotopic loops are equivalent, we can write the sum over all loops in (16.42) into a sum over homotopic classes $\alpha \in \pi_1(\mathcal{M}_N^2)$ and into a path integral in each class. Therefore, (16.42) may be rewritten as

$$K(q,t';q,t) = \sum_{\alpha\in\pi_1(\mathcal{M}_N^2)} K_\alpha(q,t';q,t) \tag{16.45}$$

$$= \sum_{\alpha\in\pi_1(\mathcal{M}_N^2)} \int_{q_\alpha(t)=q}^{q_\alpha(t')=q'} \mathcal{D}q_\alpha \, e^{\frac{i}{\hbar}\int_t^{t'} d\tau \mathcal{L}[q_\alpha(\tau),\dot{q}_\alpha(\tau)]}. \tag{16.46}$$

We can interpret this formula as a decomposition of the amplitude $K(q,t';q,t)$ into the subamplitudes $K_\alpha(q,t';q,t)$ to which only homotopic loops contribute. With such a decomposition it is clear that in principle we can assign different weights to the different subamplitudes $K_\alpha(q,t';q,t)$, provided that we preserve the conventional rules for the composition of probabilities. Thus, instead of (16.46) we can write

$$K(q,t';q,t) = \sum_{\alpha\in\pi_1(\mathcal{M}_N^2)} \chi(\alpha) \int_{q_\alpha(t)=q}^{q_\alpha(t')=q} \mathcal{D}q_\alpha \, e^{\frac{i}{\hbar}\int_t^{t'} d\tau \mathcal{L}[q_\alpha(\tau),\dot{q}_\alpha(\tau)]}, \tag{16.47}$$

where $\chi(\alpha)$ is some complex number. If our amplitude should be a probability amplitude, our weights $\chi(\alpha)$ cannot be arbitrary. In fact, since we want to

maintain the usual rule for combining probabilities,

$$K(q'',t'';q,t) = \langle q'',t''|q,t\rangle \tag{16.48}$$

$$= \int_{\mathcal{M}_N^2} dq' \; \langle q'',t''|q',t'\rangle \, \langle {}'q,'t|q,t\rangle \tag{16.49}$$

$$= \int_{\mathcal{M}_N^2} dq' \, K(q'',t'';q','t)K(q',t';q,t) \tag{16.50}$$

the weight must satisfy

$$\chi(\alpha_1)\chi(\alpha_2) = \chi(\alpha_1\alpha_2) \tag{16.51}$$

for any $\alpha_i \in \pi_1(\mathcal{M}_N^2)$. Statement (16.51) can be read differently as well: **The weights $\chi(\alpha)$ must be one-dimensional representations of B_N.**

They are given by

$$\chi(\sigma_k) = e^{-i\pi\nu} \tag{16.52}$$

for any $k = 1, ..., N-1$, where ν is a real parameter defined mod 2. It will be identified with the statistics. Since in general $\sigma_k^2 \neq \mathbf{1}$, ν is an arbitrary number. In the elementary move σ_k all winding angles φ_{ij} remain constant except for $\varphi_{k,k+1}$ which changes by π. Thus we can rewrite $\chi(\sigma_k)$

$$\chi(\sigma_k) = e^{-i\nu\Delta\varphi_{k,k+1}} = e^{-i\nu\sum_{i<j}\Delta\varphi_{ij}^{(k)}}, \tag{16.53}$$

where we have introduced

$$\Delta\varphi_{ij}^{(k)} := \varphi_{ij}^{(k)}(t') - \varphi_{ij}^{(k)}(t) = \pi\delta_{i,k}\delta_{j,k+1}. \tag{16.54}$$

With this notation, we can easily generalize (16.53) to an arbitrary braiding α. The representation can then be written as

$$\chi(\alpha) = e^{-i\nu\sum_{i<j}\int_t^{t'} d\tau \frac{d}{d\tau}\varphi_{ij}^{(\alpha)}(\tau)}, \tag{16.55}$$

where the increment $\varphi_{ij}^{(\alpha)}(t') - \varphi_{ij}^{(\alpha)}(t)$ has been written as an integral over an evolution parameter τ. In general, the functions $\varphi_{ij}^{(\alpha)}$ are very complicated. They can only be specified when the dynamics of the particle is taken fully into account. If we substitute (16.55) into (16.47) we obtain

$$K(q,t';q,t) = \sum_{\alpha\in\pi_1(\mathcal{M}_N^n)} \int_{q_\alpha(t)=q}^{q_\alpha(t')=q} \mathcal{D}q_\alpha \, e^{\frac{i}{\hbar}\int_t^{t'} d\tau \left\{\mathcal{L}[q_\alpha(\tau),\dot{q}_\alpha(\tau)] - \hbar\nu\sum_{i<j}\frac{d\varphi_{ij}^{(\alpha)}}{d\tau}\right\}}. \tag{16.56}$$

When we define

$$\mathcal{L}' := \mathcal{L} - \hbar\nu\sum_{i<j}\frac{d\varphi_{ij}^{(\alpha)}}{d\tau}, \tag{16.57}$$

we see that the Kernel $K(q,t';q,t)$ is decomposed into subamplitudes of the same weight each with respect to $\mathcal{L}'$. This is as if we were describing bosons:

$$K(q,t';q,t) = \sum_{\alpha\in\pi_1(\mathcal{M}_N^n)} \int_{q_\alpha(t)=q}^{q_\alpha(t')=q} \mathcal{D}q_\alpha \, e^{\frac{i}{\hbar}\int_t^{t'} d\tau \mathcal{L}'}. \tag{16.58}$$

In other words, we can deal with bosons governed by the Langrangian $\mathcal{L}'$ instead of anyons governed by the Langrangian $\mathcal{L}$. We can trade anyonic statistics for some kind of "fictitious" force and describe anyons as ordinary particles (for example bosons) with an additional statistical interaction. This statistical interaction is, of course, very peculiar and intrinsically topological in nature. In our example, it is a total derivative. The addition of a total derivative to $\mathcal{L}$ does not change the equations of motion, but it *does change* the statistical properties of the particle, which is related to the global topological structure of the configuration space.

One can generalize from a system on the plane to systems of N identical particles on compact Riemannian surfaces Σ with the corresponding braid group

$$B_N(\Sigma) \equiv \pi_1\left(\frac{(\Sigma)^N - \Delta}{S_N}\right) \tag{16.59}$$

It has been classified for all kinds of Riemannian surfaces Σ. The topology of Σ plays a very important role because it restricts the possible values of the statistics ν, the number of particles N and the number of components of the wavefunction. The interested reader will find more information about this topics in [172], p. 19 ff.

5 Fractional statistics in the Chern-Simons gauge

In this section we will discuss one example for a system with fractional statistics and give a very short introduction to the Chern-Simons theory.

The cyon system and its symmetries

The cyon system is composed of a non-relativistic particle with mass m and electric charge e and a magnetic flux Φ across the origin. The flux is created by an infinitely long and thin solenoid oriented along the z-axis and passing through the origin. As the motion in z direction is free, the relevant motion happens on the (x,y) plane. The Langrangian of this system is

$$\mathcal{L} = \frac{m\mathbf{v}^2}{2} + \frac{e}{c}\mathbf{v}\mathbf{A}(\mathbf{r}) \tag{16.60}$$

for $|\mathbf{r}| > 0$, where $\mathbf{v} = \dot{\mathbf{r}}$. In a convenient symmetric gauge, the magnetic vector-potential $\mathbf{A}$ is given by

$$\mathbf{A}(\mathbf{r}) = \frac{\Phi}{2\pi}\left(\frac{-y}{x^2+y^2}\hat{x} + \frac{x}{x^2+y^2}\hat{y}\right) \tag{16.61}$$

where Φ is the magnetic flux and $\hat{x}$ and $\hat{y}$ are the unit vectors pointing in x and y direction respectively. In this two-dimensional case, the magnetic field B is a pseudo-scalar. We obtain

$$B = \nabla \wedge \mathbf{A} = \Phi \delta^{(2)}(\mathbf{r}) \tag{16.62}$$

and

$$\int_{\mathbb{C}} d^2 r B = \Phi. \tag{16.63}$$

The canonical momentum is derived from the Langrangian via

$$\mathbf{p} = \frac{\partial \mathcal{L}}{\partial \mathbf{v}} = m\mathbf{v} + \frac{e}{c}\mathbf{A}(\mathbf{r}). \tag{16.64}$$

We note, that the canonical momentum is different from the kinetic momentum $m\mathbf{v}$. With a Legendre transformation we get the Hamiltonian H of the system:

$$H = \mathbf{p} \cdot \mathbf{v} - \mathcal{L} = \frac{1}{2m}\left(\mathbf{p} - \frac{e}{c}\mathbf{r} \wedge \mathbf{A}\right)^2 = \frac{m\mathbf{v}^2}{2} \tag{16.65}$$

The magnetic field and the vector potential are invisible when the Hamiltonian is written in terms of the kinetic momentum. In fact, the Hamiltonian of the cyon is numerically equal to that of the free particle. The non-trivial relationship between the kinetic and canonical momentum is the only effect of the vortex in classical mechanics. The non-trivial features get important in the quantum theory.

As the Lagrangian is rotationally invariant, the canonical orbital angular momentum J_c is a constant of motion,

$$J_c = \mathbf{r} \wedge \mathbf{p} = \mathbf{r} \wedge m\mathbf{v} + \frac{e}{c}\mathbf{r} \wedge \mathbf{A} \tag{16.66}$$

$$= \mathbf{r} \wedge \mathbf{p} = \mathbf{r} \wedge m\mathbf{v} + \frac{e\Phi}{2\pi c} \tag{16.67}$$

$$= J + \frac{e\Phi}{2\pi c}, \tag{16.68}$$

where J is the gauge invariant *kinetic angular momentum*. Formula (16.66) can be written as

$$J_c = J + \frac{e}{c}\mathbf{r} \wedge \mathbf{A} \tag{16.69}$$

$$= J - \frac{1}{c}\int d^2x\, \mathbf{x} \cdot \mathbf{E}(t, \mathbf{x}) B(t, \mathbf{x}) + \frac{1}{c}\int d^2x\, \nabla \cdot [\mathbf{E}(t, \mathbf{x})\, \mathbf{x} \wedge \mathbf{A}] \tag{16.70}$$

where $\mathbf{E}(t, \mathbf{x})$ represents the electric field created by the moving charge. It satisfies the Gauss law $\nabla \mathbf{E}(t, \mathbf{x}) = e\delta^{(2)}(\mathbf{x} - \mathbf{r}(t))$, where $\mathbf{r}(t)$ is the position of the particle

at time t. By substituting (16.62), we find that the second term in the right hand side of (16.70) identically vanishes, so that we are left with

$$J_C = J + \frac{1}{c}\int d^2x\, \nabla \cdot [\mathbf{E}(t,\mathbf{x})\, \mathbf{x} \wedge \mathbf{A}] \tag{16.71}$$

for the cyon system. The second term in (16.71) is a boundary term which is dissipated away to infinity. Therefore only the kinetic angular momentum is present on the cyon.

The spectrum of the canonical angular momentum is represented by the quantum mechanical operator

$$J_c = -i\hbar\frac{\partial}{\partial\phi} \tag{16.72}$$

where ϕ is the polar angle on the plane. When this operator acts on a single valued wave-function with angular dependence $e^{im\phi}$, it becomes simply

$$J_c = \hbar m \tag{16.73}$$

with $m \in \mathbb{Z}$. The spectrum of J_c is always the conventional one.

The kinetic angular momentum operator is given by

$$J = J_c - \frac{e\Phi}{2\pi c} = -i\hbar\frac{\partial}{\partial\phi} - \frac{e\Phi}{2\pi c}. \tag{16.74}$$

When it acts on a single valued wave function with angular dependence $e^{im\phi}$, it becomes

$$J = \hbar\left(m - \frac{e\Phi}{hc}\right), \tag{16.75}$$

$m \in \mathbb{Z}$. Therefore, the spectrum of J consists of integers shifted by $-\frac{e\Phi}{hc}$.

We call the kinetic angular momentum the *spin* of the cyon. More precisely, we have

$$s = \frac{J(m=0)}{\hbar} = -\frac{e\Phi}{hc}. \tag{16.76}$$

In general, s is neither integer nor half-integer. Therefore we should expect the cyon to be an anyon in general, if a connection between spin and statistics exists.

To establish the statistical properties, we consider two identical cyons with a wavefunction $\psi(1,2)$. We assume, that the electric charge and the magnetic flux are tightly bound on each particle. Now we slowly move one cyon around the other by a full loop and neglect both charge-charge and vortex-vortex interactions. As we know from the Aharonov-Bohm effect, the wave function acquires a phase

$$\chi = e^{-i\frac{e}{\hbar c}\int_\Gamma d\mathbf{r}\cdot\mathbf{A}} \tag{16.77}$$

when we move cyon 1 around cyon 2 in a closed loop Γ. We can rewrite (16.77) in terms of the magnetic flux using Stoke's theorem

$$\chi = e^{-i\frac{e}{\hbar c}\int_\Gamma d\mathbf{r}\cdot\mathbf{A}} = e^{-i\frac{e}{\hbar c}\int d^2r\, B} = e^{-2\pi i\frac{e\Phi}{\hbar c}}. \tag{16.78}$$

If one particle is rotated around the other, there are actually *two* contributions to the phase. One is due to the motion of the first particle in the vortex field of the second, and one is due to the motion of the second particle in the vortex field of the first. The total phase acquired by the wavefunction $\psi(1,2)$ under a full 2π rotation is then

$$e^{-2\pi i \frac{2e\Phi}{\hbar c}}. \tag{16.79}$$

Therefore, the statistics of the cyon is

$$\nu = -\frac{2e\Phi}{hc}. \tag{16.80}$$

The spin s and the statistics ν are related in the usual way

$$\nu = 2s. \tag{16.81}$$

The Chern-Simons construction of fractional statistics

Now we will present a simple construction of fractional statistics of many body systems. In the Chern-Simons formulation, fractional statistics is implemented by means of a local, long range, Abelian gauge interaction taking place in a $(2+1)$-dimensional spacetime. Rather than affixing an external vector potential $\mathbf{A}$ to an ordinary particle by hand, one promotes $\mathbf{A}$ to be the space component of a dynamical (2+1) dimensional $U(1)$ gauge field A_α. Its action is the Chern-Simons action

$$S_{CS} = \int dt\, \mathcal{L}_{CS} = \frac{\kappa}{2c} \int d^3x\, \epsilon^{\alpha\beta\gamma} A_\alpha \partial_\beta A_\gamma \tag{16.82}$$

where $\epsilon^{\alpha\beta\gamma}$ is the completely antisymmetric tensor density. We will use the convention that Greek indices take the values $0, 1, 2$ and are contracted with the metric $\eta_{\alpha\beta} = \mathrm{diag}(1, -1, -1)$. The space components are labeled by Latin indices and take the values $1, 2$. We denote the three-vector $x^\alpha \equiv (ct, x^i)$ by x, so that $d^3x = c\, dt\, d^2x$.

The action (16.82) is gauge invariant even if the Langrangian contains an undifferentiated gauge field A_α. Under gauge transformations

$$A_\alpha \longrightarrow A_\alpha + \partial_\alpha \Lambda, \tag{16.83}$$

where Λ is a space-dependent parameter, the Chern-Simons Langrangian changes only by a total derivative

$$\delta \mathcal{L}_{CS} = -\frac{\kappa}{2c} \epsilon^{\alpha\beta\gamma} \partial_\alpha [(\partial_\beta \Lambda) A_\gamma], \tag{16.84}$$

so that the action remains invariant.

Now we will couple the gauge field A_α to a matter system consisting of N non-relativistic point particles of mass m and charge e, whose coordinates $\mathbf{r}_I(t)$ serve

as dynamical variables. Here, the capital Latin indices take the values $1, \ldots, N$ and label the particles. We introduce the current

$$j^\alpha(x) = \sum_{I=1}^{N} e v_I^\alpha(t) \delta^{(2)}(\mathbf{x} - \mathbf{r}_I(t)) \equiv (c\rho, \mathbf{j}), \tag{16.85}$$

with $v_I^\alpha \equiv (c, \mathbf{v}_I(t))$ with the velocity $\mathbf{v}_I(t) = \dot{\mathbf{r}}_I(t)$. It clearly satisfies the continuity equation

$$\partial_\alpha j^\alpha = \partial_t \rho + \nabla \cdot \rho = 0. \tag{16.86}$$

We clearly see the meaning of j^α when we write the time and space components explicitly:

$$\rho(x) = \sum_{I=1}^{N} e\, \delta^{(2)}(\mathbf{x} - \mathbf{r}_I(t)), \tag{16.87}$$

$$\mathbf{j}(x) = \sum_{I=1}^{N} e \mathbf{v}_I(t) \delta^{(2)}(\mathbf{x} - \mathbf{r}_I(t)). \tag{16.88}$$

ρ and $\mathbf{j}$ are the conventional charge and current density for point particles located at $\mathbf{r}_I(t)$ and moving with velocity $\mathbf{v}_I(t)$.

We couple the conserved current j^α to the gauge field A_α in the standard minimal way

$$S_{int} = -\frac{1}{c^2} \int d^3x\, j^\alpha(x) A_\alpha(x) \tag{16.89}$$

$$= \frac{1}{c} \int dt \left\{ \sum_{I=1}^{N} e \left[\mathbf{v}_I(t) \cdot \mathbf{A}(t, \mathbf{r}_I(t)) - \mathbf{A}_0(t, \mathbf{r}_I(t)) \right] \right\}. \tag{16.90}$$

As kinetic term for the N particles, we take the non-relativistic action

$$S_{matter} = \int dt \left(\sum_{I=1}^{N} \frac{1}{2} m \mathbf{v}_I^2 \right). \tag{16.91}$$

Therefore, the total action for our System is

$$S = S_{matter} + S_{int} + S_{CS} = \int dt \mathcal{L} \tag{16.92}$$

with the total Langragian

$$\mathcal{L} = \sum_{I=1}^{N} m \mathbf{v}_I^2 + \frac{1}{c} \int d^2x \left(-j^\alpha A_\alpha + \frac{\kappa c}{2} \epsilon^{\alpha\beta\gamma} A_\alpha \partial_\beta A_\gamma \right). \tag{16.93}$$

The equations of motion of the gauge field A_α are given by

$$\frac{\delta \mathcal{L}}{\delta A_\alpha} - \partial_\gamma \frac{\delta \mathcal{L}}{\delta\, \partial_\gamma A_\alpha} \stackrel{!}{=} 0. \tag{16.94}$$

Hence we find

$$j^\alpha = -\frac{\kappa c}{2}\epsilon^{\alpha\beta\gamma}\left(\partial_\beta A_\gamma - \partial_\gamma A_\beta\right) = \frac{\kappa c}{2}\epsilon^{\alpha\beta\gamma}F_{\beta\gamma}. \tag{16.95}$$

Instead of equations of motion we call them identities, because they relate the fields $\mathbf{E}$ and B to the matter currents $\mathbf{j}$ and ρ. When we write (16.95) in components, we get

$$E^i = \frac{1}{\kappa c}\epsilon^{ij}j^j, \tag{16.96}$$

$$B = -\frac{1}{\kappa}\rho, \tag{16.97}$$

with the Chern-Simons magnetic field

$$B = \nabla \wedge \mathbf{A} = \partial_1 A^2 - \partial_2 A^1 \equiv -F_{12} \tag{16.98}$$

and the Chern-Simons electric field

$$E^i = -\frac{1}{c}\partial_t A^i - \partial_i A_0 \equiv F_{0i}. \tag{16.99}$$

Equations (16.96) and (16.97) are very important because they tell us, that the Chern-Simons field is not arbitrary, but uniquely prescribed. This is a big difference to the cyon system, where we affixed an arbitrary external magnetic flux to the charged particle. Especial equation (16.97) has remarkable consequences.

If we integrate this equation over a small two-dimensional disk C_I which includes only the I-th particle the left hand side yields the magnetic flux attached to that particle, while the right hand side gives its charge, namely

$$\Phi_I = \int_{C_I} d^2x\, B = -\frac{e}{\kappa}\int_{C_I} d^2x \sum_{J=i}^{N} \delta^{(2)}(\mathbf{x} - \mathbf{r}_J(t)) = -\frac{e}{\kappa}. \tag{16.100}$$

Equation (16.100) tells us that a particle possesses a flux $\Phi = -e/\kappa$, whenever it possesses a charge e. The Chern Simons automatically binds charge and flux to the particles.

We want to deepen our understanding with analysing the corresponding Hamiltonian H which we get in the usual way as in [177], p. 153 f.

$$H = \sum_I p_{Ii}v_I^i + \frac{1}{c}\int d^2x, \pi^\alpha A_\alpha - \mathcal{L} \tag{16.101}$$

where π^α is the field, canonical conjugated to the gauge field A^α, namely

$$\pi^\alpha = \frac{\delta \mathcal{L}}{\delta\, \partial_0 A_\alpha} = \frac{\kappa c}{2} \frac{\partial}{\partial\, \partial_0 A_\alpha} \epsilon^{\beta 0 \alpha} A_\beta \partial_0 A_\alpha = \frac{\kappa c}{2} \epsilon^{\beta 0 \alpha} A_\beta. \tag{16.102}$$

. We find, that $\pi^0 = 0$ and $\pi^j = \frac{\kappa c}{2} \epsilon^{ij} A_i$. The canonical conjugated momentum p_{Ii} is

$$p_{Ii} = \frac{\partial \mathcal{L}}{\partial v_I^i} = m v_I^i + \frac{e}{c} A_i(t, \mathbf{r}_I(t)). \tag{16.103}$$

Combining (16.101), (16.102), (16.103) and (16.87) gives us

$$H = \sum_{I=I}^{N} \frac{1}{2} m \mathbf{v}_I^2 + \int d^2x A_0(x) \left(\kappa B(x) + \rho(x)\right). \tag{16.104}$$

We impose $\rho = -\kappa B$ as a constraint. Hence H becomes numerically equal to the Hamiltonian of N non interacting particles

$$H = \sum_{I=1}^{N} \left(\frac{1}{2} m \mathbf{v}_I^2 \right). \tag{16.105}$$

As in the cyon system, the non-trivial dynamics resides entirely in the relation between the canonical and the kinetic momenta.

We fix A_α using the Weyl gauge $A_0 = 0$ and the Coulomb gauge $\partial^i A_i = 0$. We solve the constraint $\rho = -\kappa \epsilon^{ij} \partial_i A_j$ by using equation (16.87) and get

$$\frac{e}{\kappa} \sum_{I=1}^{N} \epsilon^{ji} \delta^{(2)} \left(\mathbf{x} - \mathbf{r}_I(t)\right) = \partial_i A_j. \tag{16.106}$$

Equation (16.106) has the solution

$$A_I^i(\mathbf{r_I}, \ldots, \mathbf{r_N}) = \frac{e}{2\pi\kappa} \sum_{J \neq I} \epsilon^{ij} \frac{r_I^j - r_J^j}{|\mathbf{r_I} - \mathbf{r_J}|^2}. \tag{16.107}$$

The Hamiltonian can be written as

$$H' = \sum_{I=1}^{N} \frac{1}{2m} \left(\mathbf{p}_I - \frac{e}{c} \mathbf{A}_I(\mathbf{r_1}, \ldots, \mathbf{r_N}) \right)^2. \tag{16.108}$$

The prime on H denotes that we used the solution given on (16.107). This effective vector potential is non-local since it depends on the positions of all particles, and in particular, when $N = 1$, it vanishes. The magnetic field associated to $\mathbf{A}(\mathbf{r_1}, \ldots, \mathbf{r_N})$ is

$$B_I = \epsilon^{ij} \frac{\partial}{\partial r_I^i} A_I^j(\mathbf{r_1}, \ldots, \mathbf{r_N}). \tag{16.109}$$

Each particle sees the $(N-1)$ others as vortices carrying a flux $\Phi = -\frac{e}{\kappa}$ (16.100). The non-local potential $\mathbf{A}_I(\mathbf{r_1}, \ldots, \mathbf{r_N})$ seems divergent at first sight. But this is not the case as the coincident points ($\mathbf{r_I} = \mathbf{r_J}$), where the singularities would occur, are excluded from the configuration manifold $\mathcal{M}_N^2$ of the system.

We observe, that the solution (16.107) can be written as

$$A_I^i = \frac{e}{2\pi\kappa}\epsilon^{ij}\frac{\partial}{\partial r_I^j}\sum_{J\neq I}\ln|\mathbf{r_I} - \mathbf{r_J}| \tag{16.110}$$

$$= -\frac{e}{2\pi\kappa}\frac{\partial}{\partial r_I^j}\sum_{J\neq I}\varphi_{IJ} \tag{16.111}$$

as well. φ_{IJ} is the winding angle of particle J with respect to particle I, such that

$$\varphi_{IJ} = \tan^{-1}\left(\frac{x_I^2 - x_J^2}{x_I^1 - x_J^1}\right), \tag{16.112}$$

as we discussed in (16.37). The Langrangian corresponding to (16.108) is then

$$\mathcal{L}' = \sum_{I=1}^{N}\left(\frac{1}{2}m\mathbf{v}_I^2 + \frac{e}{c}\mathbf{v}_I\cdot\mathbf{A}_I(\mathbf{r_1}, \ldots, \mathbf{r_N})\right) \tag{16.113}$$

$$= \sum_{I=1}^{N}\left(\frac{1}{2}m\mathbf{v}_I^2\right) + \frac{e^2}{2\pi c\kappa}\sum_{I=1}^{N}\sum_{I\neq J}v_I^i\frac{\partial}{\partial r_I^i}\varphi_{IJ} \tag{16.114}$$

$$= \sum_{I=1}^{N}\left(\frac{1}{2}m\mathbf{v}_I^2\right) + \frac{e^2}{2\pi c\kappa}\sum_{I<J}(v_I^i - v_J^i)\frac{\partial}{\partial r_I^i}\varphi_{IJ}. \tag{16.115}$$

With

$$\frac{d}{dt}\varphi_{IJ} = \left(v_I^i\frac{\partial}{\partial r_I^i} + v_J^i\frac{\partial}{\partial r_J^i}\right)\varphi_{IJ} = (v_I^i - v_J^i)\frac{\partial}{\partial r_I^i}\varphi_{IJ} \tag{16.116}$$

it becomes simply

$$\mathcal{L}' = \sum_{I=1}^{N}\left(\frac{1}{2}m\mathbf{v}_I^2\right) - \frac{e^2}{2\pi c\kappa}\left(\sum_{I<J}\frac{d}{dt}\varphi_{IJ}\right). \tag{16.117}$$

When we compare (16.117) with (16.57), we can directly read off the statistics of our system

$$\nu = \frac{e^2}{2\pi\hbar c\kappa} = -\frac{e\Phi}{2\pi\hbar c} = \frac{\kappa\Phi^2}{2\pi\hbar c}. \tag{16.118}$$

As in the cyon system, the statistics are not integer in general. Additionally, we mention, that the statistics in the Chern-Simons system is twice the statistics in the cyon system which is explained in detail in [172], p. 34 f.

Bibliography

[1] W. Fulton and J. Harris, *Representation Theory*, Springer, 2004.

[2] H. Georgi, *Lie Algebras in Particle Physics*, Benjamin/Cummings Publishing Company, Inc., 1982.

[3] M. E. Peskin and D. V. Schroeder, *An introduction to quantum field theory*, chapter 15,20, Addison-Wesley, Massachusetts, 1995.

[4] H. Huang, *Quarks, leptons and gauge fields*, chapter 3, 4, World scientific, Singapore, 1992.

[5] P. Goddard and D. I. Olive, *Magnetic monopoles in gauge field theories*, Rep. Prog. Phys. **41**, 1375 (1978).

[6] S. Coleman, *Aspects of Symmetries*, chapter 5.2, Cambridge University Press, Cambridge, 1984.

[7] L. O'Raifeartaigh, *Group structure of gauge theories*, chapter 8, Cambridge University Press, Cambridge, 1987.

[8] W. Greiner, *Eichtheorie der schwachen Wechselwirkung*, chapter 1,2,3,4, Verlag Harri Deutsch, Thun, 1995.

[9] A. A. Abrikosov, *Fundamentals of the Theory of Metals*, chapter 5, Elsevier Science Publishers B.V., Amsterdam, 1998.

[10] J. Jackson, *Klassische Elektrodynamik*, chapter 6, de Gruyter Verlag, 2002.

[11] A. Wachter and H. Hoeber, *Repetitorium Theoretische Physik*, chapter 2, Springer Verlag, 2005.

[12] Goddard, P. and Olive, D. I., *New Developments in the Theory of Magnetic Monopoles*, Rept. Prog. Phys. **41**, 1357 (1978).

[13] Harvey, J. A., *Magnetic monopoles, duality, and supersymmetry*, (1996), hep-th/9603086.

[14] T. Broecker, *Lineare Algebra und Analytische Geometrie*, chapter 3, Birkhäuser Verlag, 2003.

[15] V. Rubakov, *Classical Theory of Gauge Fields*, Princeton University Press, 2002.

[16] N. Manton and P. Sutcliffe, *Topological solitons*, chapter 3,8, Cambridge University Press, 2004.

[17] L. D. Faddeev, *Nonlocal, nonlinear and nonrenormalisable field theories*, Proc. Int. Symp., Alushta (Dubana: Joint Institute for Nuclear Research) , 207 (1976).

[18] S. Coleman, *New Phenomena in Subnuclear Physics*, Proc. 1975 Int. School of Physics 'Ettore Majorana' , 297 (1975), ed Zichichi, A.

[19] A. S. Schwarz, *Magnetic Monopoles in Gauge Theories*, Nucl. Phys. **B112**, 358 (1976).

[20] E. Corrigan, D. I. Olive, D. B. Fairlie, and J. Nuyts, *Magnetic Monopoles in SU(3) Gauge Theories*, Nucl. Phys. **B106**, 475 (1976).

[21] J. Arafune, P. G. O. Freund, and C. J. Goebel, *Topology of Higgs Fields*, J. Math. Phys **16**, 433 (1975).

[22] A. Hatcher, *Algebraic Topology*, chapter 4, Cambridge University Press, 2002.

[23] N. S. Manton, *The Force between 't Hooft-Polyakov Monopoles*, Nucl. Phys. **B126**, 525 (1977).

[24] N. Ashcroft and N. Mermin, *Festkoerperphysik*, Oldenbourg Verlag, 1999.

[25] J. Friedel, *Dislocations*, Pergamon Press, New York, 1964.

[26] A. Cottrell, *Theory of Crystal Dislocations*, Gordon and Breach Science Publishers, New York, 1965.

[27] D. Hull, *Introduction to Dislocations*, Pergamon Press, New York, 1965.

[28] M. Peach and J. Koehler, *The Forces Exerted on Dislocations and the Stress Fields Produced by Them*, Phys. Rev. Lett. **80**, 436 (1950).

[29] F. Nabarro and A. Kosevich, *Dislocations in Solids Vol.1*, North-Holland Publishing Group, Amsterdam, 1979.

[30] P. Rosakis, *Supersonic Dislocation Kinetics from an Augmented Peierls Model*, Phys. Rev. Lett. **86**, 95 (2001).

[31] A. Rosakis, O. Samudrala, and D. Coker, *Cracks Faster than the Shear Wave Speed*, Science **284**, 1337 (1999).

[32] J. Eshelby, *Supersonic Dislocations and Dislocations in Dispersive Media*, Proc. Phys. Soc. (London) **B69**, 1013 (1956).

[33] N. Manton and P. Sutcliffe, *Topological solitons*, chapter 1-5, Cambridge University Press, 2004.

[34] http://maths.dur.ac.uk/ dma0saa/Solitons/solitons.pdf, *Solitons*, 2005.

[35] N. P. Ong, *Transport studies near phase transitions in $NbSe_3$*, Phys. Rev. B **17**, 3243 (1978).

[36] W. Fogle and J. H. Perlstein, *Semiconductor-to-Metal Transition in the Blue Potassium Molybdenum Bronze, $K_{0.30}$ MoO_3; Example of a Possible Excitonic Insulator*, Phys. Rev. B **6**, 1402 (1972).

[37] E. B. Lopes, M. Almeida, and J. Dumas, *Thermal conductivity of the molybdenum blue bronze $Rb_{0.3}MoO_3$*, Phys. Rev. B **42**, 5324 (1990).

[38] G. Grüner, *Density Waves in Solids*, Addison-Wesley, 1994.

[39] A. J. Berlinsky, *One-dimensional metals and charge density wave effects in these materials*, Rep. Prog. Phys. **42**, 1243 (1979).

[40] W. P. Su, J. R. Schrieffer, and A. J. Heeger, *Soliton excitations in polyacetylene*, Phys. Rev. B **22**, 2099 (1980).

[41] W. P. Su, J. R. Schrieffer, and A. J. Heeger, *Erratum: Soliton excitations in polyacetylene*, Phys. Rev. B **28**, 1138 (1983).

[42] W. P. Su and J. R. Schrieffer, *Fractionally Charged Excitations in Charge-Density-Wave Systems with Commensurability 3*, Phys. Rev. Lett. **46**, 738 (1981).

[43] T. L. Einstein and J. R. Schrieffer, *Indirect Interaction between Adatoms on a Tight-Binding Solid*, Phys. Rev. B **7**, 3629 (1973).

[44] V. Ginzburg and L. Landau, *On the theory of superconductivity (in Russian), ZH. Eksp. Teor. Fiz. 20, 1064 (1950): Collected Papers of L.D. Landau (ed. D. ter Haar)*, Gordon and Breach, New York, 1967.

[45] D. R. Tilley and J. Tilley, *Superfluidity and Superconductivity*, chapter 8, Adam Hilger, Bristol, New York, 1990.

[46] G. H. Derick, *Comments on nonlinear wave equations as models for elementary particles*, J. Math. Phys. **5**, 1252 (1964).

[47] R. S. Palais, *The Principle of Symmetric Criticality*, Commun. Math. Phys. **69**, 19 (1979).

[48] N. Manton and P. Sutcliffe, *Topological Solitons*, chapter 1, 2, 3, 4, 7, Cambridge University Press, Cambridge, 2004.

[49] L. Jacobs and C. Rebbi, *Interaction energy of superconducting vortices*, Phys. Rev. **B19**, 4486 (1979).

[50] S. M. Girvin, *Lecture Notes The Kosterlitz-Thouless Phase Transition*, chapter 2, 2000.

[51] P. M. Chaikin and T. C. Lubensky, *Principles of Condensed Matter Physics*, chapter 5, 6, 9, Cambridge University Press, Cambridge, 1995.

[52] A. Tomita and R. Chiao, *Observation of Berry's topological phase by use of an optical fibre*, Phys. Rev. Lett. **57**, 937 (1986).

[53] M. Berry, *Quantal phase factors accompanying adiabatic changes*, Proc. R. Soc. Lond. **A 392**, 45 (1984).

[54] A. Bohm, A. Mostafazadeh, H. Koizumi, Q. Niu, and J. Zwanziger, *The geometric phase in quantum systems*, chapter 2,3,4, Springer, Berlin, 2003.

[55] Y. Aharonov and D. Bohm, *Significance of Electromagnetic Potentials in the Quantum Theory*, Phys. Rev **115**, 485 (1959).

[56] R. A. Webb, S. Washburn, C. Umbach, and R. Laibowitz, *Observation of h/e Aharonov-Bohm Oscillations in Normal-Metal Rings*, Phys. Rev. Lett. **54**, 2696 (1985).

[57] A. Bohm, *The geometric phase in quantum systems*, chapter 2.1-2.4, 4.1-4.3 and A.1, A.2, Springer-Verlag, Berlin, 2003.

[58] N. Manton, *Topological solitons*, chapter 2, Cambridge University Press, 2004.

[59] Y. Aharonov and A. Casher, *Topological Quantum Effects for Neutral Particles*, Phys. Rev. Lett. **53**, 319 (1984).

[60] A. Cimmino, G. Opat, and A. Klein, *Observation of the Topological Aharonov-Casher Phase Shift by Neutron Interferometry*, Phys. Rev. Lett. **63**, 380 (1989).

[61] F. Schwabl, *Quantenmechanik für Fortgeschrittene*, chapter 5.3 and 6.2, Springer-Verlag, Berlin, 2004.

[62] Y. Ji et al., *An elecronic Mach-Zehnder interferometer*, Nature **422**, 415 (2003).

[63] N. W. Ashcroft and N. D. Mermin, *Solid State Physics*, chapter 8,9,10,12, Holt, Rinehart and Winston, Cornell University, 1975.

[64] M. Tabor, *Chaos and Integrability in Nonlinear Dynamics*, chapter 6, Wiley, Columbia University, New York, 1989.

[65] P. Kramer and M. Saraceno, *Geometry of the Time-Dependent Variational Principle in Quantum Mechanics*, chapter 1, Springer-Verlag, Berlin, Heidelberg, New York, 1981.

[66] Q. Sundaram, G. Niu, *Wave-packet dynamics in slowly perturbed crystals:Gradient corrections and Berry-phase effects*, Phys. Rev. **59**, 14915 (1999).

[67] Q. Bohm, A. Niu, *The Geometric Phase in Quantum Systems*, chapter 12, Springer, Berlin Heidelberg New York, 2003.

[68] Z. Fang and N. Nagaosea, *The Anomalous Hall Effect and Magnetic Monopoles in Momentum Space*, Science **302**, 92 (2003).

[69] F. Haldane, *Berry Curvature on the Fermi Surface: Anomalous Hall Effect as a Topological Fermi-Liquid Property*, Physical Review Letters **93**, 206602 (2004).

[70] J. A. Lipa, J. A. Nissen, D. A. Stricker, D. R. Swanson, and T. C. P. Chui, *Specific heat of liquid helium in zero gravity very near the lambda point*, Phys. Rev. B **68**, 174518 (2003).

[71] K. Huang, *Statistical Mechanics*, Wiley and Sons, New York, 1987.

[72] R. P. Feynman, *Statistical Mechanics: A Set of Lectures*, W. A. Benjamin, Massachusets, 1972.

[73] H. Palevsky, K. Otnes, and K. Larsson, *Excitation of Rotons in Helium II by Cold Neutrons*, Phys. Rev. **112**, 11 (1958).

[74] A. J. Legget, *Superfluidity*, Rev. Mod. Phys. **71**, 318 (1999).

[75] J. W. Negele and H. Orland, *Quantum Many-Particle Systems*, Addison Wesley, New York, 1988.

[76] R. P. Feynman, *Atomic Theory of the λ-Transition in Helium*, Phys. Rev. **91**, 1291 (1953).

[77] D. M. Ceperley, *Path Integrals in the Theory of Condensed Helium*, Rev. Mod. Phys. **67**, 279 (1995).

[78] E. L. Pollock and D. M. Ceperley, *Path-Integral Computation of Superfluid Densities*, Phys. Rev. B **36**, 8343 (1987).

[79] J. E. Hirsch, R. L. Sugar, D. J. Scalapino, and R. Blankenbecler, *Monte Carlo Simulations of One-Dimensional Fermion Systems*, Phys. Rev. **26**, 5033 (1982).

[80] M. Boninsegni, N. Prokof'ev, and B. Svistunov, *Worm Algorithm for Continuous-Space Path Integral Monte Carlo Simulations*, Phys. Rev. Lett. **96**, 070601 (2006).

[81] N. A. Nielsen and I. I. Chuang, *Quantum Computation and Quantum Information*, Cambridge University Press, 2004.

[82] E. W. Weisstein, *Euler's Totient Theorem.*, http://mathworld.wolfram.com/EulersTotientTheorem.html **1**, 1 (2003).

[83] U. Maurer, *Vorlesungsskript Informationssicherheit und Kryptographie*, Unpublished, 2004.

[84] R. P. Feynman, *Simulating physics with computers*, Int. J. Theor. Phys. **21**, 467 (1982).

[85] D. Deutsch, *Quantum theory, the Church-Turing principle, and the universal quantum computer*, Proc. Roy. Soc. London **A400**, 97 (1985).

[86] P. W. Shor, *Algorithms for quantum computation: discrete logarighms and factoring*, Proceedings of the 35 Annual Symposium on the Foundations of Computer Science, 1994, pp. 124-134.

[87] J. A. Walter, *Kryptographie: Prinzipien und Anwendungen*, Talk at University Bielefeld, 2003.

[88] S. Beauregard, *Circuit for Shor's algorithm using 2n+3 qubits*, (quant-ph/0205095), 2002.

[89] L. K. Grover, *Quantum mechanics helps in searching for a needle in a haystack*, Phys. Rev. Lett. **79**, 325 (1997).

[90] C. Monroe, D. M. Meekhof, B. E. King, W. M. Itano, and D. J. Wineland, *Demonstration of a fundamental quantum logic gate*, Phys. Rev. Lett. **75**, 4714 (1995).

[91] M. H. Freedman, A. Y. Kitaev, M. J. Larsen, and Z. Wang, *Topological Quantum Computation*, (quant-ph/0101025), 2002.

[92] A. Barenco et al., *Elementary gates for quantum computation*, (quant-ph/9503016), 1995.

[93] L. M. K. Vandersypen et al., *Experimental realization of Shor's quantum factoring algorithm using nuclear magnetic resonance*, (quant-ph/0112176), 2001.

[94] N. A. Gershenfeld and I. L. Chuang, *Quantum computing with molecules*, Science **275**, 350 (1997).

[95] D. P. DiVincenzo, *The Physical Implementation of Quantum Computation*, (quant-ph/0002077), 2000.

[96] A. Imamoglu et al., *Quantum information processing using quantum dot spins and cavity-QED*, (quant-ph/9904096), 1999.

[97] C. A. Sackett et al., *Experimental entanglement of four particles*, Nature **404**, 256 (2000).

[98] R. Vrijen et al., *Electron Spin Resonance Transistors for Quantum Computing in Silicon-Germanium Hetero-structures*, (quant-ph/9904096), 1999.

[99] J. M. Kikkawa, I. P. Smorchkova, N. Samarth, and D. D. Awschalom, *Room-Temperature Spin Memory in Two-Dimensional Electron Gases*, Science **277**, 1284 (1997).

[100] T. Pellizzari, S. A. Gardiner, J. I. Cirac, and P. Zoller, *Decoherence, Continuous Observation, and Quantum Computing: A cavity QED Model*, Phys. Rev. B **71**, 224109 (2005).

[101] M. S. Sherwin, A. Imamoglu, and T. Montroy, *Quantum Computation with Quantum Dots and Terahertz Cavity Quantum Electrodynamics*, (quant-ph/9904096), 1999.

[102] G. E. Moore, *Cramming more components onto integrated circuits*, Electronics **38** (1965).

[103] J. Preskill, *Topological Quantum Computation*, Lecture notes, 2000, chapter 9 of "Quantum Computation" available online: www.theory.caltech.edu/people/preskill/ph229.

[104] P. W. Shor, *Scheme for reducing decoherence in quantum computer memory*, Phys. Rev. A **52**, 2493 (1995).

[105] J. Preskill, *Fault-tolerant quantum computation*, (quant-ph/9712048), 1997.

[106] D. Gottesman, *A theory of fault-tolerant quantum computation*, (quant-ph/9702029), 1997.

[107] A. M. Steane, *Error correcting codes in quantum theory*, Phys. Rev. Lett. **77**, 793 (1996).

[108] A. R. Calderbank and P. W. Shor, *Good quantum error-correction codes exist*, Phys. Rev. A **54**, 1098 (1996).

[109] K. M. Svore, D. P. DiVincenzo, and B. Terhal, *Noise Threshold for a Fault-Tolerant Two-Dimensional Lattice Architecture*, (quant-ph/0604090), 2006.

[110] L. B. Ioffe et al., *Topologically protected quantum bits using Josephson junction arrays*, Nature **415**, 503 (2002).

[111] A. Y. Kitaev, *Fault-tolerant quantum computation by anyons*, (quant-ph/9707021), 2004.

[112] D. S. Rokhsar and S. A. Kivelson, *Superconductivity and the Quantum Hard-Core Dimer Gas*, Phys. Rev. Lett. **61**, 2376 (1988).

[113] P. W. Leung, K. C. Chiu, and K. J. Runge, *Columnar dimer and plaquette resonating-valence-bond orders in the quantum dimer model*, Phys. Rev. B **54**, 12938 (1996).

[114] R. Moessner and S. L. Sondhi, *Resonating Valence Bond Phase in the Traingular Lattice Quantum Dimer Model*, Phys. Rev. Lett. **86**, 1881 (2001).

[115] R. Moessner, S. L. Sondhi, and P. Chandra, *Two-Dimensional Periodic Frustrated Ising Models in a Transverse Field*, Phys. Rev. Lett. **84**, 4457 (2000).

[116] R. Moessner, S. L. Sondhi, and E. Fradkin, *Short-ranged RVB physics, quantum dimer models, and Ising gauge theories*, Phys. Rev. B **65**, 024504 (2001).

[117] K. S. Raman, R. Moessner, and S. L. Sondhi, *SU(2)-invariant spin-1/2 Hamiltonians with RVB and other valence bond phases*, Nature **414**, 887 (2001).

[118] P. W. Anderson, Mater. Res. Bull. **8**, 153 (1973).

[119] A. Ralko, M. Ferrero, F. Becca, D. Ivanov, and F. Mila, *Zero-temperature properties of the quantum dimer model on the triangular lattice*, Phys. Rev. B **71**, 224109 (2005).

[120] M. Oshikawa and T. Senthil, *Fractionalization, topological order, and quasiparticle statistics*, (cond-mat/0506008), 2005.

[121] T. Ando, Y. Matsumoto, and Y. Uemura, *Theory of Hall Effect in a Two-Dimensional Electron System*, J. Phys. Soc. Jpn **39**, 278 (1975).

[122] K. v. Klitzing, G. Dorda, and M. Pepper, *New Method for High-Accuracy Determination of the Fine-Structure Constant Based on Quantized Hall Resistance*, Phys. Rev. Lett **45**, 494 (1980).

[123] R. B. Laughlin, *Quantized Hall conductivity in two dimensions*, Phys. Rev. B **23**, 5623 (1981).

[124] J. P. Eisenstein and H. L. Stormer, *The fractional quantum Hall effect*, Science **248**, 1510 (1990).

[125] D. C. Tsui, H. L. Stormer, and A. C. Gossard, *Two-Dimensional Magnetotransport in the Extreme Quantum Limit*, Phys. Rev. Lett. **48**, 1559 (1982).

[126] R. B. Laughlin, *Anomalous Quantum Hall Effect: An Incompressible Quantum Fluid with Fractionally Charged Excitations*, Phys. Rev. Lett. **50**, 1395 (1983).

[127] X. G. Wen and Q. Niu, *Ground-state degeneracy of the fractional quantum Hall states in the presence of a random potential and on high-genus Riemann surfaces*, Phys. Rev. B **41**, 9377 (1990).

[128] D. Arovas, J. R. Schrieffer, and F. Wilczek, *Fractional Statistics and the Quantum Hall Effect*, Phys. Rev. Lett. **53**, 722 (1984).

[129] O. I. Motrunich and T. Senthil, *Exotic Order in Simple Models of Bosonic Systems*, Phys. Rev. Lett. **89**, 27704 (2002).

[130] G. Misguich, D. Serban, and V. Pasquier, *Quantum Dimer Model on the Kagome Lattice: Solvable Dimer-Liquid and Ising Gauge Theory in strongly correlated systems*, Phys. Rev. Lett. **89**, 137202 (2002).

[131] R. Moessner and S. L. Sondhi, *Ising models of quantum frustration*, Phys. Rev. B **63**, 224401 (2000).

[132] T. Senthil and M. P. A. Fisher, *Fractionalization, topological order, and cuprate superconductivity*, (cond-mat/0008082), 2000.

[133] T. Senthil and M. P. A. Fisher, *Z2 gauge theory of electron fractionalization in strongly correlated systems*, Phys. Rev. B **62**, 7850 (1999).

[134] T. Senthil and M. P. A. Fisher, *Fractionalization in the cuprates: Detecting the topological order*, (cond-mat/0006481), 2000.

[135] D. A. Bonn et al., *A limit on spin-charge separation in thigh T_c superconductors from the absence of a vortex-memory effect*, Nature **414**, 887 (2001).

[136] N. R. Cooper, N. K. Wilkin, and J. M. Gunn, *Quantum Phases of Vortices in Rotating Bose-Einstein Condensates*, Phys. Rev. Lett. **87**, 120405 (2001).

[137] R. Coldea, D. A. Tennant, and Z. Tyczynski, *Extended scattering continua characteristic of spin fractionalization in the two-dimensional frustrated quantum magnet Cs_2CuCl_4 observed by neutron scattering*, Phys. Rev. B **68**, 134424 (2003).

[138] M. H. Freedman, A. Y. Kitaev, M. J. Larsen, and Z. Wang, *Topological quantum computation*, Bull. Amer. Math. Soc. **40**, 31 (2002).

[139] M. H. Freedman, M. J. Larsen, and W. Z., *A modular functor which is universal for quantum computation*, Comm. Math. Phys. **227**, 587 (2002).

[140] M. H. Freedman, *A topological modular functor which is universal for quantum computation*, Talk given at MSRI, 2000, available online: http://www.msri.org/communications/ln/msri/2000/qcomputing/freedman/1/index.html.

[141] A. Y. Kitaev, *A Class of P,T-Invariant Topological Phases of Interacting Electrons*, (cond-mat/0307511), 2003.

[142] M. H. Freedman, C. Nayak, and K. Shtengel, *A Line of Critical Points in 2+1 Dimensions: Quantum Critical Loop Gases and Non-Abelian Gauge Theory*, Phys. Rev. Lett. **94**, 147205 (2005).

[143] N. E. Bonesteel, L. Hormozi, and G. Zikos, *Braid Topologies for Quantum Computation*, Phys. Rev. Lett. **95**, 140503 (2005).

[144] C. M. Dawson and M. A. Nielsen, *The Solovay-Kitaev algorithm*, (quant-ph/0505030), 2005.

[145] N. E. Bonesteel, *Braid Topologies for Quantum Computation*, Talk given at KITP, 2006, available online: http://online.kitp.ucsb.edu/online/qubit06/bonesteel/.

[146] F. E. Camino, W. Zhou, and V. J. Goldman, *Aharonov-Bohm Superperiod in a Laughlin Quasiparticle Interferometer*, Phys. Rev. Lett. **95**, 246802 (2005).

[147] S. Bravyi, *Universal Quantum Computation with the $\nu = 5/2$ Fractional Quantum Hall State*, Phys. Rev. A **73**, 042313 (2006).

[148] M. H. Freedman, C. Nayak, and K. Walker, *Towards Universal Topological Quantum Computation in the $\nu = 5/2$ Fractional Quantum Hall State*, (cond-mat/0512066), 2005.

[149] J. K. Slingerland and F. A. Bais, *Quantum groups and nonabelian braiding in quantum Hall systems*, Nucl. Phys. B **612**, 229 (2001).

[150] A. Y. Kitaev, *Fault-tolerant quantum computation by anyons*, Ann. Phys. **303**, 2 (2003).

[151] J. Preskill, *Introduction to quantum computation and information*, World Scientific, Singapore, 1998.

[152] S. A. Kivelson, D. S. Rokhsar, and J. P. Sethna, *Topology of the resonating valence-bond state: solitons and high-T_c superconductivity*, Phys. Rev. B **35**, 8865 (1987).

[153] X. G. Wen, *Mean-field theory of spin-liquid states with finite energy gap and topological orders*, Phys. Rev. B **44**, 2664 (1991).

[154] L. B. Ioffe and A. I. Larkin, *Superconductivity in the liquid-dimer valence-bond state*, Phys. Rev. B **40**, 6941 (1989).

[155] E. Manousakis, *The spin-1/2 Heisenberg antiferromagnet on a square lattice and its application to the cuprous oxides*, Rev. Mod. Phys. **63**, 1 (1991).

[156] L. Capriotti, A. E. Trumper, and S. Sorella, Phys. Rev. Lett. **82**, 3899 (1999).

[157] W. Marshall, Proc. R. Soc. London, Ser. A **232**, 48 (1955).

[158] G. Misguich and C. Lhuillier, *Frustrated spin systems*, World Scientific, 2005.

[159] B. Sutherland, *Systems with resonating-valence-bond ground states: Correlations and excitations*, Phys. Rev. B **37**, 3786 (1988).

[160] G. Misguich, D. Serban, and V. Pasquier, *Quantum dimer model with extensive ground-state entropy on the Kagome lattice*, Phys. Rev. B **67**, 214413 (2003).

[161] P. Fendley, R. Moessner, and S. L. Sondhi, *Classical dimers on the triangular lattice*, Phys. Rev. B **66**, 214513 (2002).

[162] A. Ioselevich, D. A. Ivanov, and M. V. Feigel'man, *Ground-state properties of the Rokhsar-Kivelson dimer model on the triangular lattice*, Phys. Rev. B **66**, 174405 (2002).

[163] V. Elser and C. Zeng, *Kagome spin-1/2 antiferromagnets in the hyperbolic plane*, Phys. Rev. B **48**, 13647 (1993).

[164] C. Zeng and V. Elser, *Quantum dimer calculations on the spin-1/2 kagome Heisenberg antiferromagnet*, Phys. Rev. B **51**, 8318 (1995).

[165] B. D. Josephson, *Possible new effects in superconductive tunnelling*, Phys. Letters **1**, 251 (1962).

[166] R. P. Feynman, *The Feynman Lectures on Physics Vol. III*, Pearson Addison-Wesley, San Francisco, 2006.

[167] E. Simanek, *Inhomogeneous Superconductors - Granular and Quantum Effects*, International Series of Monographs on Physics, Oxford University Press, 1994.

[168] H. Grabert and M. H. Devoret, *Single charge tunneling: coulomb blockade phenomena in nanostructures*, Plenum Press, New York, 1992.

[169] L. B. Ioffe, V. B. Geshkenbein, M. V. Feigel'man, A. L. Fauchére, and G. Blatter, *Environmentally decoupled s-wave–d-wave–s-wave Josephson junctions for quantum computing*, Nature **398**, 678 (1999).

[170] M. Nielsen and I. Chuang, *Quantum Computation and Quantum Information*, Cambrige University Press, 2000.

[171] J. M. Leinaas and J. Myrheim, *On the Theory of identical particles*, Il Nuovo Cimento **37 B** (1977).

[172] A. Lerda, *Anyons*, volume m14 of *Lecture Notes in Physics*, chapter 2, 3, Springer Verlag, New York, 1992.

[173] F. Wilczek, *Quantum Mechanics of Fractional-Spin Particles*, Phys. Rev. Lett. **49**, 957 (1982).

[174] F. Scheck, *Nichtrelativistische Quantentheorie*, Theoretische Physik 2, Springer Verlag, Berlin, Heidelberg, 2000.

[175] E. Fadell and L. Neuwirth, *Configuration Spaces*, Math. Scand. **10**, 111 (1962).

[176] J. Fröhlich, *Vorlesungsskript Quantenmechanik II*, chapter 8, 2005, given at ETH Zürich.

[177] F. Scheck, *Klassische Feldtheorie*, Theoretische Physik 3, Springer Verlag, Berlin, Heidelberg, 2004.

[178] J. C. Davis and R. E. Packard, *Superfuid He Josephson weak links*, Rev. Mod. Phys. **74**, 741 (2002).

[179] E. Fradkin, *Field Theories of Condensed Matter Systems*, Frontiers in Physics 82, Westview Press, 1991.

[180] L.-P. Levy, *Magnetism and Superconductivity*, Springer Verlag, Berlin, 2000.

[181] J. Blin, *Energie Mutuelle de Deux Dislocations*, Acta Metallurgica **3**, 199 (1955).

[182] D. P. Landau and K. Binder, *A Guide to Monte Carlo Simulations in Statistical Physics*, chapter 2, pages 7–26, Cambridge University Press, Cambridge, 2000.

[183] J. Cardy, *Scaling and Renormalization in Statistical Physics*, chapter 1, 2, 3, 6, Cambridge University Press, Cambridge, 1996.

[184] M. Plischke and B. Bergersen, *Equilibrium Statistical Physics*, chapter 5, pages 206–213, Scientific Publishers, London, 1994.

[185] Y. Aharonov and D. Bohm, *Significance of Electromagnetic Potentials in the Quantum Theory*, Phys. Rev. **115**, 485 (1959).

[186] G. Grüner, *The dynamics of charge-density waves*, Rev. Mod. Phys. **60**, 1129 (1988).

[187] K. Maki, *Creation of Soliton Pairs by Electric Fields in Charge-Density¯Wave Condensates*, Phys. Rev. Lett. **39**, 46 (1977).

[188] G. P. Collins, *Computing with Quantum Knots*, Scientific American **April**, 57 (2006).

[189] A. Y. Kitaev, *Quantum computations: algorithms and error correction*, Russian Math. Survey **52:61**, 1191 (1997).

[190] M. H. Freedman, C. Nayak, and K. Shtengel, *Non-Abelian topological phases in an extended Hubbard model*, (cond-mat/0309120), 2003.